Recycling oceanic crust: Isotopic and elemental constraints from a high pressure terrain

Thesis

Recycling oceanic crust: Isotopic and elemental constraints from a high pressure terrain

A thesis submitted for the degree of

Doctor of Philosophy

by

Christopher Dale, BSc (Hons) (Edinburgh)

Department of Earth Sciences,

The Open University

March 2005

THE OPEN UNIVERSITY

RESEARCH SCHOOL

Library Authorisation Form

Please return this form to the Research School with the two bound copies of your thesis to be deposited with the University Library. All candidates should complete parts one and two of the form. Part three only applies to PhD candidates.

Part One: Candidates Details

Name: CHRISTOPHER DALE PI: U 4902880

Degree: PhD

Thesis title: RECYCLING OCEANIC CRUST: ISOTOPIC AND ELEMENTAL CONSTRAINTS FROM A HIGH-PRESSURE TERRAIN

Part Two: Open University Library Authorisation

I confirm that I am willing for my thesis to be made available to readers by the Open University Library, and that it may be photocopied, subject to the discretion of the Librarian.

Signed: C Dale Date: 21/9/05

Part Three: British Library Authorisation [PhD candidates only]

If you want a copy of your PhD thesis to be available on loan to the British Library Thesis Service as and when it is requested, you must sign a British Library Doctoral Thesis Agreement Form. Please return it to the Research School with this form. The British Library will publicise the details of your thesis and may request a copy on loan from the University Library. Information on the presentation of the thesis is given in the Agreement Form.

Please note the British Library have requested that theses should be printed on one side only to enable them to produce a clear microfilm. The Open University Library sends the fully bound copy of theses to the British Library.

The University has agreed that your participation in the British Library Thesis Service should be voluntary. Please tick either (a) or (b) to indicate your intentions.

☑ I am willing for the Open University to loan the British Library a copy of my thesis.
A signed Agreement Form is attached

☐ I do not wish the Open University to loan the British Library a copy of my thesis.

Signed: C Dale Date: 21/9/05

Abstract

This study investigates the Re-Os and trace element budgets of gabbros, eclogites and metabasalts from subducted oceanic crust, at whole-rock and mineral scales. These data test the hypothesis that elevated $^{187}Os/^{188}Os$ ratios in some OIB evolved from the high Re/Os ratios of subducted oceanic crust recycled into their mantle source.

Re-Os data from metastable gabbros and corresponding eclogites from the Zermatt-Saas ophiolite (ZSO), which have undergone very high-pressure metamorphism (>2.0 GPa), yield a best-fit regression consistent with the crust formation age (164 Ma). ZSO eclogitic metabasalt data lie above this regression line, with a mean Re abundance of 440 ppt, substantially lower than current data for MORB glasses (~1000 ppt). This suggests that Re was lost from the basaltic crust (resulting in lower Re/Os ratios as found in a previous study), while low-strain gabbro bodies remain closed with respect to the Re-Os system during subduction. Re-Os data from pillow basalts of biotite, garnet and kyanite grades from the Sulitjelma ophiolite also indicate substantial Re loss, implying that this process may occur at lower P-T conditions during initial subduction.

Modelling the Os and Pb isotope evolution of a complete section of oceanic crust over 2 Ga implies that HIMU-type OIB can be produced by recycling >40% oceanic crust into the mantle source. Crucially, the effect of the gabbroic portion on the evolution of the whole crust is to considerably reduce $^{206}Pb/^{204}Pb$ ratios without altering the Os isotope evolution significantly. This permits long residence times for recycled crust in the mantle without generating Pb isotopic values higher than known OIB.

For the first time, mineral separates from gabbro and gabbroic eclogite have been analysed for Re and Os. Sulphide dominates the Os budget, while Re is mainly hosted in plagioclase for gabbro, and garnet for gabbroic eclogite.

Trace element measurements on the same mineral and bulk-rock samples are used to assess trace element fluxes during subduction. The most notable conclusion of this work is that U depletion occurs neither in the metabasalts nor metagabbros.

PAGE
MISSING
IN
ORIGINAL

Acknowledgements

Firstly, I would like to thank my original three supervisors, Tom, Kevin and Ian for all their help through the past three years, from hammering very hard rocks in the field to the discussion of the finer points of geochemistry. Mouhcine was added to my group of supervisors and has provided excellent support, particularly in the Re-Os lab, but also in all other areas. The department as a whole has provided a great atmosphere to work in throughout my study. There are also many other staff whom have helped with the acquisition of data, namely: Fatima, Olivier, Nick, Mabs, Peter, Rachael.

The student population has been active and has usually made the best out of the deficiencies of MK. In particular I would like to thank those whom I have shared an office with: Andy R (amongst other things for his rants on bitterness and his explosions), Andy M, Jenny (for her rigid adherence to a 9-6 day, which should perhaps be followed by everyone), Lee, Clive (but not for his obsession with potatoes) and Dave. There are many other people whom I should mention but the following will have to suffice: Jason (for his in-depth discussions about Re-Os chemistry at all hours of the day), Luke, Dan M, Dan C (for his power) and Sam (for often being the sole female social representative). Lunchtime football games have also provided excellent respite during the more laborious parts of doing a PhD.

My parents and siblings have also been constantly supportive and (sometimes even) interested.

Last, but certainly not least, I would like to thank Emily without whom I am sure I would not have eaten in the past few months, let alone enjoyed myself.

PAGE
MISSING
IN
ORIGINAL

Contents

Table of Figures

Table of Tables

Table of Tables - Appendices

1 Introduction

The main focus of this work is the geochemical changes which may occur during subduction-related (high pressure) metamorphism of mafic oceanic crust. The importance of investigating chemical modifications in this tectonic setting is two-fold. Firstly, by understanding changes which occur during subduction, it is possible to more accurately constrain the geochemical signature of oceanic crust which is recycled into the deep mantle. Secondly, knowledge of the mobility and behaviour of elements during high pressure metamorphism provides key information on the processes of arc magma formation. In order to assess the effects of high-pressure (HP) metamorphism on the chemistry of subducting slabs, two suites of samples from metamorphosed ophiolites have been analysed, the nature of which will be expanded upon below. Whole rock Re-Os isotope data are presented, and the distribution of Re and Os before and after metamorphism has been investigated through the analysis of hand-picked mineral separates. In addition, whole rock trace element data are assessed and *in situ* trace and platinum-group element (PGE) data are presented for silicate and sulphide phases respectively.

1.1 Osmium isotopes as a tracer for mantle recycling

The structure and composition of the mantle, being largely beyond direct observation, has been a particular source of debate amongst Earth scientists for several decades. Sampling of mantle lithologies has been possible from orogenic and abyssal peridotites bodies and through xenoliths brought to the surface by mantle melts. However, the most comprehensive sampling of the upper mantle is available, albeit through the modified medium of a melt, from basalts which erupt and crystallise along the extensive network of mid-ocean ridges. The evidence from MORB indicates that the upper mantle is remarkably uniform in terms of isotopic and trace element composition, although large scale regions possessing

anomalous isotopic signatures do exist, e.g. the so-called DUPAL anomaly of Indian Ocean MORB (Dupre and Allegre 1983; Hart 1984). Ocean island basalts (OIB) provide important insights into the geochemical signature of deeper parts of the mantle, and are characterised by geochemically distinct signatures which are thought to reflect differences in the composition of the mantle source.

Through the analysis of oceanic basalts, the mantle has been categorised in terms of several end-member components (DMM, EM-1, EM-2, HIMU, FOZO and C - see Zindler and Hart (1986) and Hofmann (1997) for discussion), which are defined by their isotopic values. Some ocean island basalts (OIB), termed HIMU-type OIB (HIMU = high μ = high $^{238}U/^{206}Pb$), are characterised by their elevated $^{206}Pb/^{204}Pb$ values, with respect to the depleted MORB mantle (DMM) or the primitive mantle (Zindler and Hart 1986). HIMU-type OIB also possess $^{187}Os/^{188}Os$ values which are elevated in comparison with chondritic or DMM values (Hauri and Hart 1993; Marcantonio et al. 1995), and have low $^{87}Sr/^{86}Sr$ ratios. The elevated $^{206}Pb/^{204}Pb$ and $^{187}Os/^{188}Os$ signature of these basalts must be inherited from a mantle component with high $^{238}U/^{204}Pb$ and $^{187}Re/^{188}Os$ ratios. It has been postulated by many authors (initially, Hofmann and White 1982) that the addition of old subducted, recycled oceanic crust to the mantle source of HIMU-type (and other) OIB can result in the isotopic signatures observed.

The behaviour of Re and Os during mantle melting makes the Re-Os system a powerful tool for tracing recycled oceanic crust into the mantle. During partial melting of the mantle, Re behaves as a moderately incompatible element, whereas Os appears to be largely compatible, albeit in sulphide rather than silicate phases. This results in strong fractionation of the two elements and very high Re/Os ratios in oceanic crust. The $^{187}Re/^{188}Os$ ratios of basaltic oceanic crust are typically 200-10,000 times greater than the estimated value for fertile mantle (fertile mantle ~0.4, Meisel et al. 1996; MORB data from Schiano et al. 1997). Over time, the

decay of ^{187}Re will lead to significantly elevated $^{187}Os/^{188}Os$ ratios in MORB, and given recycling timescales of 1 Ga or more, this will lead to very radiogenic Os values. The importance of this observation is that old recycled crustal material within the mantle will have a considerable influence on the Os systematics of a melt produced from that reservoir. Thus, the Re-Os system should be an excellent tracer for recycled oceanic crust within the mantle.

1.2 Assessing the signature of recycled material

While Re-Os and trace element data are readily available for mid-ocean ridge basalt (MORB), what is more difficult to constrain is the precise nature of the recycled component, following the metamorphic changes that occur during the process of subduction. One indirect way to investigate this problem is through the analysis of arc magmatism. However, three main problems arise: Firstly, the fate of material leaving the slab is not well constrained; i.e. some of the material may remain unaccounted for in areas of the mantle wedge not sampled by arc magmatism (e.g. large volumes of water-rich fluids are thought to leave the slab at <40 km depth, Peacock 1990). Secondly, melting processes within the mantle wedge may have a strong influence on the composition of arc magmas, making it more difficult to infer the input from the slab. Finally, some of the observed enrichments in arc magmas may be a result of the stripping of elements from the mantle wedge by slab-derived fluids, and not due to a flux of elements from the slab itself (e.g. Arculus and Powell 1986). An alternative way of assessing the effects of subduction is through the analysis of rocks which have been partially subducted and subsequently exhumed. While this too has its drawbacks (see below) it circumvents the need to assess the role of mantle wedge processes.

Work on rocks from high-pressure terranes undertaken by Becker (2000) suggests that Re may be mobile during subduction, resulting in Re loss from the slab before it is recycled into the mantle (Figure 1.1). This would reduce the potential growth

of radiogenic $^{187}Os/^{188}Os$ in recycled crustal material, and consequently would have important consequences for the models of crustal recycling. Indeed, Becker estimated that if equilibrium mixing in the mantle source is assumed, an unrealistic proportion (80-90%) of MORB is required in the source, to produce observed OIB signatures. However, all samples in that study, except one gabbro, represented *basaltic* ocean crust. In contrast, this study looks at both basaltic and gabbroic lithologies, which have been metamorphosed at eclogite facies. Although gabbros are often considered to be simply the plutonic form of a rock of basaltic composition, there are two important points to be noted: Firstly, Re-Os ratios (and trace element concentrations) in gabbros are generally lower than those of basalts. Secondly, gabbros and basalts may behave differently during subduction due to their notably different petrological structure, differing levels of hydration and hence rheology. This work, therefore, contributes to the knowledge of the Re-Os isotopic composition of recycled, mafic oceanic crust as a whole. In addition, the analysis of trace elements at both a whole rock and mineral grain scale has been used to assess the possible fluxes from the slab which may be transferred to the mantle region which is sourced by arc magmatism.

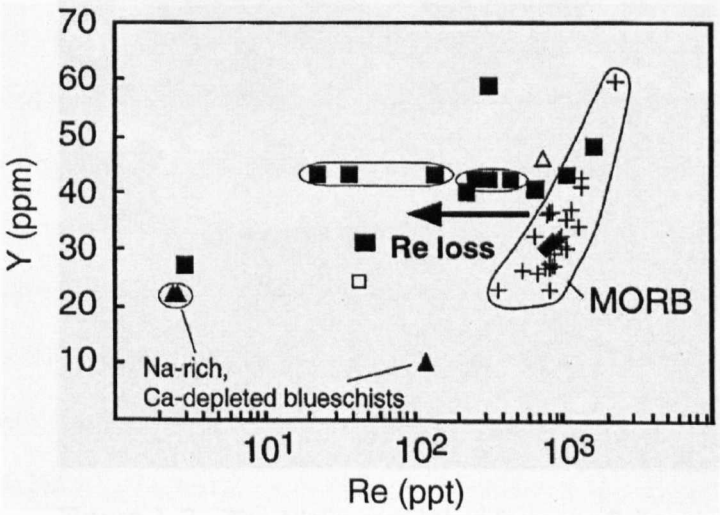

Figure 1.1. Re-Y systematics of metabasalts sampled by Becker (2000) from palaeo-subduction zones, indicating that Re is probably lost from this type of lithology during HP metamorphism. Filled squares: metabasaltic eclogites and blueschists; open square: metagabbroic eclogite; open triangle: low temperature blueschist; filled diamonds: mafic high-pressure granulites.

However, studies of this type are not without drawbacks; four issues seem particularly noteworthy. Firstly, the rocks analysed may only be representative of subducted material which has a similar composition, structure and extent of deformation. Secondly, the depth of burial may not account for the full range of transformations occurring prior to recycling into the deep mantle. Thirdly, it is difficult to ascertain exactly what has been lost during metamorphism because usually the composition of the precursor is not known. In this case, a comparison with a global average rock composition (such as mid-ocean ridge basalt (MORB)) is needed. Finally, care must be taken to ensure that samples preserve peak metamorphic conditions. Without this criterion, it cannot be known whether the effects observed have been caused by metamorphism during the continued subduction and burial of the rocks, or whether they result from metamorphic retrogression during exhumation.

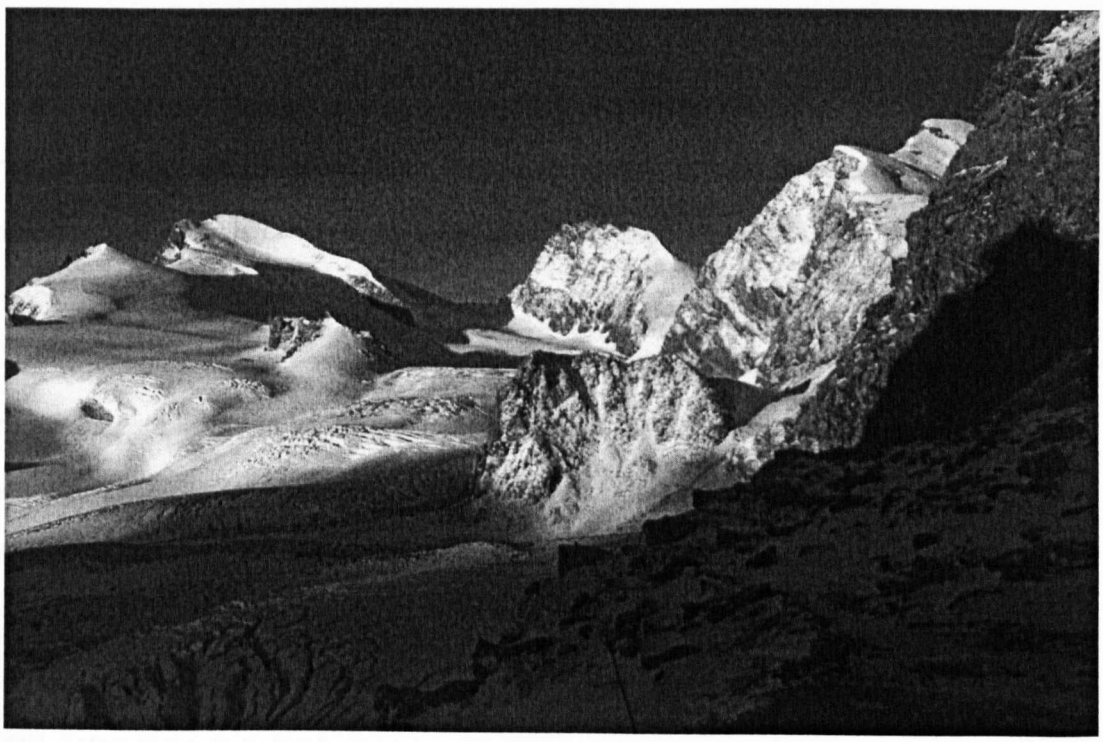

Figure 1.2. The Allalin area taken from the Britannia Hutte, near Saas Fee, Switzerland. The Allalin Gabbro forms the right-hand snow covered peak, and the lower peak in the centre of the photo. Clearly sampling was, at times, rather problematic.

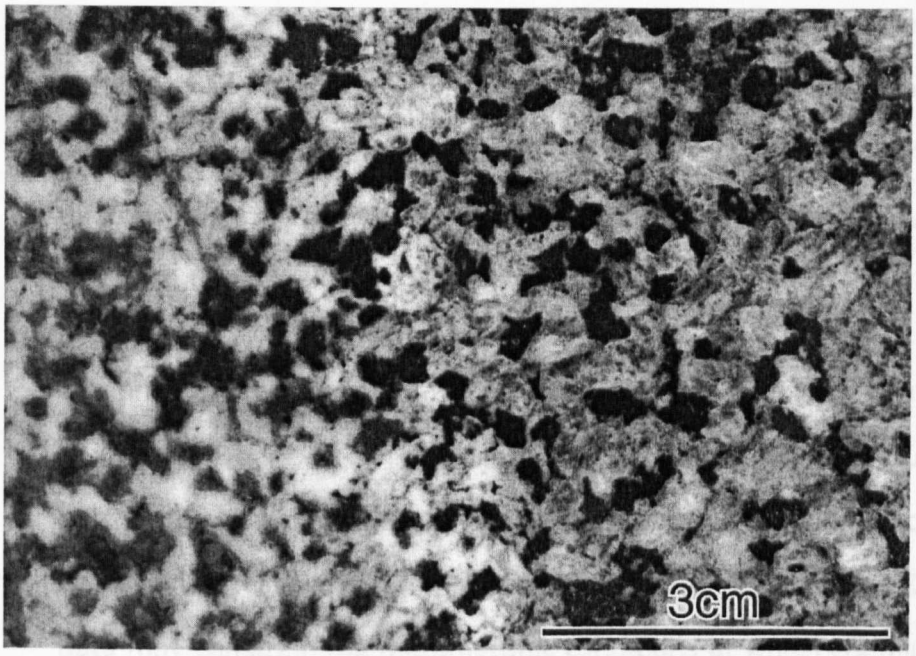

Figure 1.3. The gabbro-eclogite transformation in a single hand-specimen. The right hand portion retains all its igneous mineralogy despite having experienced pressure and temperature conditions of >2.0 GPa and ~600°C. The left-hand side contains garnet, chlorite, zoisite and occasional omphacite, although it still partially retains its igneous mineralogy.

In order to limit the effects of these issues, samples were taken from the metamorphosed gabbros and basalts of the Zermatt-Saas ophiolite, Switzerland, and were chosen on the basis of their well preserved HP assemblages. In particular, gabbros and gabbroic eclogites were sampled from the Allalin Gabbro (Figure 1.2), and basaltic eclogites were collected from Pfulwe pass and the Allalin. Peak metamorphic conditions in these rocks exceeded 2.0 GPa (Meyer 1983a; Barnicoat and Fry 1986; Reinecke 1998), and so these samples represent an exhumed terrane which had previously been subducted to >60 km depth, and possibly as deep as 100 km (Barnicoat 1996). This is probably not a depth equivalent to the typical depth of the slab beneath volcanic arcs (90-150 km, Tatsumi 1986). However, it is likely that much of the dehydration of the slab and consequent hydration of the overlying mantle wedge occurs at shallower levels (<40 km, Peacock 1990; Schmidt and Poli 1998), while hydrated mantle may be transported to a depth and temperature sufficient for melting by the process of

corner flow. Gabbroic mineral assemblages have, in some cases, been metastably preserved and relict igneous mineralogy is observed in these samples (Figure 1.3), allowing a direct comparison of suitable precursor and metamorphosed material and obviating the need for a comparison to be made with an 'average' figure for that rock type.

The findings from the study of the Zermatt-Saas ophiolite (ZSO) samples led to the analysis of a suite of metabasalts and metagabbros from the Sulitjelma ophiolite, northern Norway. These samples have undergone regional metamorphism of the Barrovian type, at lower pressure conditions than those of the ZSO, and thus the data may constrain the metamorphic conditions at which chemical changes begin to occur.

This thesis provides a contribution to the knowledge of the Re-Os system in gabbroic and basaltic lithologies, through whole rock measurements, and particularly through the analysis of mineral separates, which have not been previously studied. By analysing the abundances of Re and Os in mineral phases, an understanding can be gained of the behaviour of these elements during metamorphism, and this might elucidate the processes which may or may not lead to loss of these elements from the slab.

There have been several notable studies over the past ten years which have analysed trace elements in subducted and exhumed mafic rocks in order to assess the loss, or otherwise, of elements from the down-going slab (e.g. Tribuzio et al. 1996; Arculus et al. 1999; Becker et al. 2000; Zack et al. 2002a; Spandler et al. 2003; Spandler et al. 2004). The data presented here provide additional information, from a new suite of rocks. This data, on a whole rock and a mineral scale, lead to some important conclusions on the mobility of certain elements, which have often been assumed to be mobile.

1.3 Thesis structure

The main thrust of this thesis is the behaviour of Re and Os during high pressure metamorphism of oceanic crust. Chapter 2 presents a summary of the issues surrounding the chemical evolution of oceanic crust after crystallisation, with particular reference to trace element behaviour during seafloor alteration and the process of subduction. The geological settings of the Zermatt-Saas (ZSO) and Sulitjelma (SO) ophiolites (the latter also investigated for whole rock Re-Os and trace element data) are outlined in the first part of Chapter 3. Detailed petrographic and mineralogical information and P-T estimates are discussed in the second part of the same chapter. Some of the textures and major element data in this chapter are used to elucidate petrogenetic processes.

In order to assess the mobility and release of elements during subduction, whole rock trace element data for both ophiolite suites (the ZSO and SO) are presented in Chapter 4 and compared with suitable protolith compositions. To permit such an investigation, the likely protoliths of the two ophiolite suites have been ascertained through the analysis of major and trace element data in the first part of Chapter 4. In the case of the gabbroic eclogites, it has been possible to analyse suitable protoliths directly, in the form of the metastably preserved parts of the Allalin gabbro. MORB analyses are used as a baseline for the metabasaltic samples.

To provide a background to the Re-Os data, which forms the basis of much of the work in this thesis, a discussion of the current state of knowledge of the Re-Os system is included in Chapter 5. Whole rock Re-Os data for gabbros, metagabbros and metabasalts from the Zermatt-Saas and Sulitjelma ophiolites are presented and discussed in Chapter 6.

Perhaps the most original data obtained are those of Re and Os abundances and Os isotopic ratios in separate mineral phases from gabbros and gabbroic eclogites of

the Zermatt-Saas ophiolite. These data are presented in Chapter 7 and have been used to calculate a mass balance for the samples involved. *In situ* laser-ablation ICP-MS data for trace elements in silicate phases have been used both qualitatively and quantitatively in a discussion of trace element redistribution, mass balance and possible loss. Preliminary findings from the analysis of PGE in sulphides from gabbroic lithologies also form part of Chapter 7.

In order to provide an overall picture of the chemical modification of mafic crust, a discussion chapter (Chapter 8) brings together lines of evidence from the different datasets and attempts to relate elemental loss to mineralogical changes and deformation. Also of crucial importance, this chapter contains a quantitative assessment of the possible effects of recycling oceanic crust on Re-Os systematics in the mantle source of ocean island basalts. A summary of the conclusions reached in this study are presented in the final chapter.

PAGE
MISSING
IN
ORIGINAL

2 Evolution of oceanic crust

2.1 Pre-subduction evolution of oceanic crust

In order to quantify the effects of recycled oceanic crust in mantle reservoirs, it is necessary to constrain the chemistry of the subducted slab. Several processes modify the chemistry of oceanic crust between its crystallisation at mid-ocean ridges and its eventual recycling into the deep mantle. It is therefore necessary to understand and account for these processes of chemical modification and to use this knowledge to estimate more accurately the composition of recycled crust. This section will include a discussion of the effects of seafloor hydrothermal alteration and subduction on the general trace element chemistry of the oceanic crust. The application of the Re-Os system to mantle geochemistry and subduction zones is discussed in Sections 5.2.2 and 5.2.3 respectively. As the work in this thesis has involved the analysis of rocks of basaltic and gabbroic origin, the following discussion of oceanic crust will concentrate on these lithologies, rather than providing a detailed discussion of the sedimentary cover of oceanic crust or the lithospheric mantle.

2.1.1 Structure of oceanic crust

When considering subduction processes and the recycling of oceanic crust, it is often assumed that the oceanic lithosphere has a uniform structure comprising several clearly defined lithological units: a base of depleted peridotites, a layer of igneous rocks of MORB (mid-ocean ridge basalt) composition, circa 7km thick, and a sedimentary cover of variable thickness. It has been revealed, through studies of both slow and fast spreading centres, that the range of structures of oceanic crust is much more complex. Poli and Schmidt (2002) present two end-member sketches representing oceanic crust formed at fast and slow spreading centres (Figure 2.1). The fast spreading example, (Hekinian et al. 1993; Boudier and Nicolas 1995 and references therein; Constantin 1999), is akin to the 'classic'

layered oceanic crustal section, from top to bottom the units are: mafic volcanics (pillows), mafic intrusives (sheeted dykes and isotropic gabbros), foliated gabbros, layered, differentiated, cumulate gabbros, and depleted harzburgites. In contrast, examples of slow spreading ridges from the Atlantic, Arctic and Indian oceans (e.g. Gente et al. 1995), are not uniformly layered due to extensive extensional faulting and instead can variably expose basalt, gabbro or depleted and serpentinised harzburgite at the seafloor. In a particular section, any one of the igneous units may be absent due to structural omission. Gabbros usually form in small magma chambers, and the various layered, differentiated cumulates that are present in the fast spreading scenario are often absent. On the basis of these two models it may be considered likely that the Allalin Gabbro, a layered cumulate body from the Zermatt-Saas ophiolite which provides the basis for much of this study, was formed at a relatively fast spreading centre. This is consistent with its coherency and the lack of brittle normal faulting and accompanying fluid flow that may be associated with slower spreading rates. The preservation of igneous assemblages through HP metamorphism of the Allalin unit (see Section 3.3.1) is, in part, a result of the lack of seafloor deformation and alteration experienced by the unit.

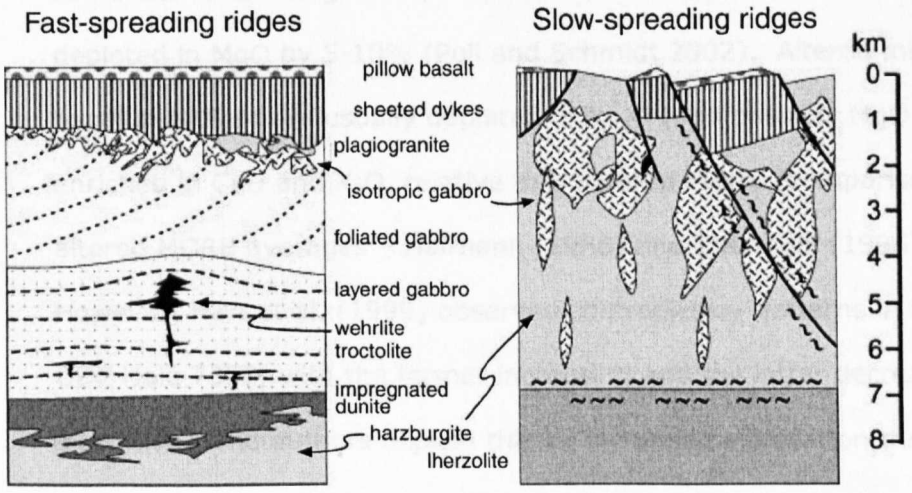

Figure 2.1. The contrast between the structure of oceanic crust formed at fast and at slow spreading ridges, from Poli and Schmidt (2002).

2.1.2 Seafloor hydrothermal alteration

The interaction of rock and fluid during near-ridge hydrothermal circulation modifies the original composition of the oceanic crust. The spatial extent and intensity of alteration is highly variable and is dependent on the thermal regime and the tectonic fabric of the spreading centre (Alt 1995). Thus, hydrothermal alteration at a slow spreading centre is likely to be deep and focussed around fractures and fault zones, whereas the more extreme thermal regime at fast spreading ridges will lead to more uniform and possibly more intense alteration. All parts of the oceanic lithosphere are hydrated to various extents. The upper parts of the slab (sediments and extrusive mafics) are commonly the most extensively hydrated due to their proximity to the seafloor, whereas the deeper gabbroic units are usually less hydrated (Rosenberg et al. 1993; Hart et al. 1994).

Due to the relatively dilute nature of low pressure fluids, the extent of chemical alteration is often limited, particularly when compared to the modification that occurs during subduction related metamorphism and dehydration (Poli and Schmidt 2002). However, fluid-rock ratios are often high resulting in significant changes in some elements. In general, serpentinized ultramafics are enriched in SiO_2 and depleted in MgO by 5-10% (Poli and Schmidt 2002). Altered mid-ocean ridge basalts (MORB) are usually depleted in Na_2O (and possibly MgO and Fe_2O_3) and enriched in CaO and K_2O, relative to unaltered MORB (comparison of unaltered and altered MORB averages – Hofmann (1988) and Staudigel (1996) respectively). However, Hart et al. (1999) observed contradictory patterns in Na_2O and CaO from ODP Hole 735B, with the former increasing and the latter decreasing with alteration. The authors explain this by increased albitisation through either the infiltration of trondhjemite melts or hydrothermal veins.

Elemental loss and gain during seafloor alteration is spatially variable. Cartwright and Barnicoat (1999) summarise the cycling of fluids in oceanic crust (Figure 2.2)

and recognise that rocks in the broad, low temperature, down-flow zones generally experience Ca loss and Mg gain, whereas those in the relatively narrow up-flow zones are enriched in Mn and Ca and depleted in Mg and Na. The most extreme cases of Ca gain in the up-flow zones result in the formation of epidosites. There are numerous occurrences of epidosites in the areas sampled in this study. These are found most notably throughout the Täschalp area, to a moderate extent at Pfulwe and at Egginerjoch, NE of the Allalin unit.

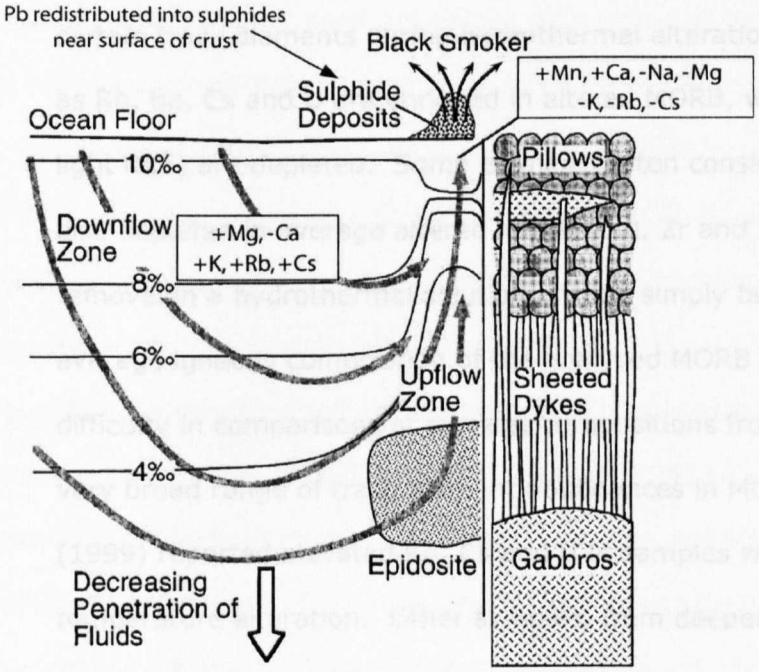

Figure 2.2. Flow of hydrothermal fluids in the oceanic crust and the resulting elemental losses and gains (after Cartwright and Barnicoat 1999), extra elements added from Hart and Staudigel (1982) and Michard and Albarede (1985).

In the case of the fluid mobile elements Na and K, their enrichment in seawater (10770 and 380 ppm respectively) combined with high fluid-rock ratios generally lead to elevated abundances within the rock (although not for Na in the comparison of altered and fresh MORB in the previous paragraph). However, this may not be the case for elements which are less abundant in the circulating fluid.

Trace elements. Hart and Staudigel (1982) investigated alkalis and other large-ion lithophile (LIL) elements in altered oceanic crust and concluded that the large low temperature zones of alteration became enriched in K, Rb, Cs and to a lesser extent, U (Figure 2.2). Uranium was also found to be enriched in altered crust by Michard and Albarede (1985). Conversely, hot lower crust is expected to be a source of these elements, supplying hydrothermal vents above, and thus becoming depleted. Comparison of the average compositions of fresh and altered MORB (Hofmann 1988; Staudigel et al. 1996, respectively) suggests the loss and gain of certain trace elements during hydrothermal alteration. Fluid mobile elements such as Rb, Ba, Cs and U are enriched in altered MORB, while the REE (particularly the light REE) are depleted. Some elements often considered to be fluid *immobile* are also depleted in average altered MORB (e.g. Zr and Nb). This may be the result of removal in a hydrothermal solution or may simply be indicative of a difference in average igneous composition of the analysed MORB suites. There is an inherent difficulty in comparisons of average compositions from different suites due to the very broad range of trace element abundances in MORB samples. Hart et al. (1999) reported elevated Rb, Cs and U in samples which have experienced low temperature alteration. Other samples, from deeper in the core section, display enrichment in Ba relative to Rb. Surprisingly, average Ba, Nb, U and HREE are lower in the upper 500m of the core section of Hart et al. (1999) than in N-MORB (Hofmann 1988), while La, Ce, Pb and Sr all have higher average abundances. Boron was shown to be enriched in altered MORB (Morris et al. 1990), and can be used as a tracer for a flux from altered oceanic crust into the melting regions of subduction zone magmas.

The addition of Cl can be an important process during sea-floor alteration due to its high concentration in seawater (19500 ppm). Chlorine substitutes for OH^- in hydrous minerals and can reach concentrations of ~3% in some amphiboles (Magenheim et al. 1995). The relatively Cl-rich nature of altered lithosphere can

sometimes be traced into subduction zones in the form of highly saline fluid inclusions in mantle wedge ultramafic rocks (Scambelluri et al. 1997; Scambelluri et al. 1998). This observation determines that fluids within the mantle wedge are slab derived, and highlights the importance of hydration of the oceanic lithosphere as a precursor to dehydration and fluid flux into the mantle wedge.

Lead behaviour. A 'lead paradox' between its compatibility during melting and its abundance in continental crust and mantle has long been recognised. Lead concentrations in continental crust are higher than would be expected for an element with its compatibility. Ratios of Ce (a similarly compatible element) against Pb reveal surprisingly low values for the continental crust and higher than bulk earth values in the mantle (e.g. Miller et al. 1994; Chauvel et al. 1995; Muhe et al. 1997). It is clear, through very Pb-rich hydrothermal deposits, that Pb is very mobile during seafloor alteration. The solution to the 'Pb paradox' is that Pb is redistributed in the oceanic crust and concentrated in sulphide precipitates near the surface of the crust (Miller et al. 1994; Chauvel et al. 1995). This surface region is also highly hydrated and therefore undergoes extensive dewatering during dehydration, with concomitant Pb loss. Pb-rich fluids may then infiltrate the melting region of arc magmas, thus preferentially enriching the mantle source in Pb. This is reflected in the low Ce/Pb ratios of arc magmas, and therefore of continental crust.

The behaviour of rhenium and osmium during episodes of oceanic crust alteration is discussed in Section 5.2.4. A discussion of the behaviour of other isotope systems (O, Sr, Nd) is beyond the scope of this work, but information on these systems can be found in Hart et al. (1999) and references therein. One important observation by Stakes et al. (1991) is the relationship between low $\delta^{18}O$ and a high alteration index. Furthermore, samples displaying these characteristics are most common in the top 200m of the core studied, suggesting more alteration in cooler, but more

fluid-rich systems which are in closer proximity to the seafloor. Work by Barnicoat and Cartwright (Barnicoat and Cartwright 1997; Cartwright and Barnicoat 1999) has illustrated that gabbroic eclogites from the Allalin Gabbro have undergone high-temperature hydrothermal alteration through the lower $\delta^{18}O$ values that they possess, in comparison to the unaltered gabbro protoliths. This appears to have been an important mechanism for the introduction of fluids to these samples, and has facilitated their transformation to an eclogite facies assemblage (see Section 3.3.1).

Overall, the bulk oceanic crust that arrives at a subduction zone is chemically similar to that which was crystallised at the mid-ocean ridge, with only small net fluxes between seawater and oceanic crust (Staudigel et al. 1996). However, regions can experience extensive chemical modification in the form of redistribution on a relatively small scale (10-100m), as discussed for Pb above. This does not effect the bulk composition of oceanic crust, but can have important consequences for oceanic crust during subsequent subduction. Infiltration of water into the otherwise largely anhydrous basalts and gabbros is crucial to the process of dehydration (and possibly melting) that occurs during subduction, and provides a medium for transferring elements from the slab into the mantle wedge. Thus the budgets of trace elements may be strongly affected by seafloor alteration, particularly through later processes that occur at subduction zones.

2.2 The subduction zone system

High-pressure metamorphism modifies the composition of oceanic crust during the subduction process, and thus affects the recycling of elements into the deep mantle. It is important to understand the nature and composition of fluids (or melts) released from the slab into the overlying mantle wedge because otherwise the estimation of the slab flux to the deep mantle will be inherently inaccurate, at least for some elements. What follows is a brief summary regarding the current state of knowledge of the composition and nature of the chemical flux from the slab to the mantle wedge, through the indirect evidence of arc magmatism. Amongst other processes, the composition of a fluid will be controlled by the breakdown of different hydrous phases which may house different concentrations of trace elements. A discussion of the stability of hydrous phases and the nature of the slab to wedge transfer of elements is discussed below in Section 2.2.2.

2.2.1 Subduction zone magmatism

In comparison with mid-ocean ridge or ocean island basalts, arc magmas possess some distinct chemical anomalies. It has long been established that this signature is related to a chemical input from the down-going subducting slab. In its simplest geochemical form, the presence of abundant H_2O in many island arc basalts (IAB) is a good indication of the involvement of a hydrous fluid or melt from the subducting slab. However, the exact nature and quantification of the flux from the slab has been more difficult to constrain, particularly given the variety of global subduction settings, which involve different thermal regimes and different inputs and outputs.

There is now a general consensus regarding the key aspects of the physical mechanism of transport into the mantle wedge (Pearce and Peate 1995: see Davies and Stevenson 1992 for details). Firstly, corner flow in the mantle wedge is driven by movement of the subducting slab (e.g. Spiegelman and McKenzie 1987). Secondly, a three stage process is envisaged for the transport of the slab signature

to the site of melt generation: (i) mantle wedge metasomatism by aqueous fluids derived from dehydration of the slab, (ii) aqueous fluid release due to the breakdown of hydrous minerals *within* the mantle wedge (e.g. Tatsumi et al. 1983), and (iii) aqueous fluid (and probably hydrous melt) migration to the site of melt generation; through a combination of diagonally downward transport of volatiles in mantle minerals during the process of corner flow, breakdown of these minerals, and upwards movement of fluid/melt (e.g. Davies and Bickle 1991). In order to generate the observed volumes of melt, it may be necessary to invoke mantle decompression beneath the arc itself (e.g. Ida 1983).

The slab signature. Arc basalts are commonly enriched in non-conservative elements including B and the large ion lithophile elements (LILE): Rb, Sr, Ba, K, U. LILE are known to be particularly mobile in hydrous fluids. For this reason, elevated Ba/La ratios are characteristic of many arc magmas. Two types of arc can be identified by means of their Ce/Yb ratios: one possessing low ratios and the other, high. The high Ce/Yb ratios are due to elevated Ce abundances (Hawkesworth et al. 1993 and references therein), rather than a change in Yb, which is generally considered to be immobile. Arcs with low Ce/Yb have remarkably similar isotopic compositions, indicative of only a small slab input. Arcs with high Ce/Yb tend to also have larger isotope variations and high K abundances, which suggests a greater slab input. Some arc rocks with high Ce/Yb also have elevated Th/U which can be explained by a large sedimentary contribution. Although many arcs possess elevated Ce abundances, low Ce/Pb ratios are common due to the extreme mobility of Pb. In particular, Pb is readily redistributed in the crust and is concentrated in the upper portion during hydrothermal alteration. As such, Pb is prone to being transported in fluids from the slab to the mantle wedge.

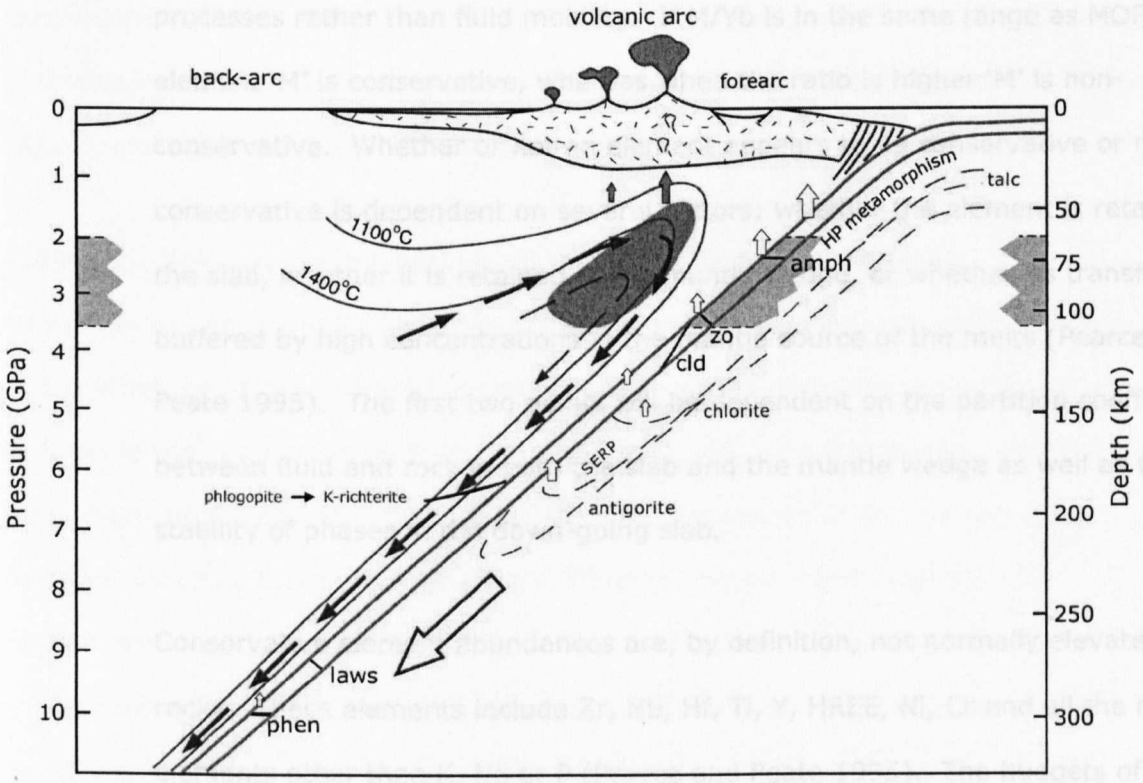

Figure 2.3. A schematic section through a subduction zone system (after Poli and Schmidt 2002). The long, red arrows indicate slab-induced flow within the mantle wedge. Curved grey lines in the mantle wedge are isotherms illustrating the strong negative temperature gradient towards the subducting slab, and the establishment of relatively cool temperatures to deep levels, even in the mantle wedge. The orange zone corresponds to a region where significant, extractable melting will occur. Short unfilled arrows denote fluid flow. Short filled arrows denote the transport of melt. Black lines in the subducting crust, and blue dashed lines in the subducting lithospheric mantle, correspond to the limits of stability of important hydrous phases (although the occurrence of discontinuous breakdown reactions with distinct associated pulses of fluid release is very unlikely due to complex mineralogical solid solutions). The grey shaded areas correspond to the range of pressure estimates for the Allalin Gabbro and other parts of the Zermatt-Saas ophiolite (see Sections 3.2.1.4 and 3.4)

Conservative elements are those for which there is no detectable slab contribution to the source of arc volcanism. *Non-conservative* elements are those for which there is a noticeable contribution (Pearce and Peate 1995). A useful tool in differentiating between conservative and non-conservative elements is to use the ratio 'M'/Yb, and plot this against Nb/Yb (where M is the element under study). By normalising both axes to Yb, the effects of partial melting and fractional crystallisation can be minimised. Niobium is considered a conservative element, and thus the Nb/Yb ratio should be dependent only on melting and magma

processes rather than fluid mobility. If M/Yb is in the same range as MORB, the element 'M' is conservative, whereas when the ratio is higher 'M' is non-conservative. Whether or not an element appears to be conservative or non-conservative is dependent on several factors: whether the element is retained in the slab, whether it is retained in the mantle wedge, or whether its transfer is buffered by high concentrations in the mantle source of the melts (Pearce and Peate 1995). The first two points will be dependent on the partition coefficients between fluid and rock in both the slab and the mantle wedge as well as the stability of phases in the down-going slab.

Conservative element abundances are, by definition, not normally elevated in arc rocks. These elements include Zr, Nb, Hf, Ti, Y, HREE, Ni, Cr and all the major elements other than K, Na or P (Pearce and Peate 1995). The budgets of major elements are controlled by their high abundances in the mantle source region, and so any input from the slab will be buffered. For example, the LILE calcium is likely to be mobile and abundant in slab fluids, but shows no enrichment in arc rocks. McCulloch and Gamble (1991) found that the budgets of the HFSE (e.g. Zr, Nb, Ta) are not consistent with control by a residual phase in the mantle; rather, the systematics of the HFSE can be explained by melting of a depleted mantle source *without* any addition of HFSE from the slab due to the immobile nature of these elements. Brenan et al. (1995) and Stalder et al. (1998) did not experimentally observe any selective depletion of Nb or Ta in a coexisting fluid with garnet, clinopyroxene or amphibole, nor by fluid passage through an amphibole lherzolite (mantle wedge). They therefore concluded that the Nb and Ta budgets must be controlled by the presence of residual rutile in the slab.

Ionic radius is crucial in determining whether or not an element is conservative. Elements with very large (e.g. Cs, Rb, Ba, K) and very small (e.g. B) ionic radii combined with low D (spinel lherzolite/melt) values are the most highly *non-*

conservative. The apparent mobility of some elements increases when the medium of transport is a siliceous melt, rather than a hydrous fluid. This is true of the HFSE (Nb, Zr and Hf) which become non-conservative, rather than conservative.

Isotopes. The only unequivocal slab flux indicator is the ratio $^{10}Be/Be$ (Hawkesworth et al. 1993). This ratio is highly elevated in clay-rich sediments due to the presence of concentrated cosmogenic ^{10}Be in clay minerals. However, only sediments which are younger than 6 Ma can be traced using this system, therefore a flux from older sediments may be recycled into the source of arc melting and there would be no observable increase in $^{10}Be/Be$. Boron is also highly concentrated in sediments and altered MORB, and so is an excellent tracer for inputs from these sources into the arc system. Some B/Be ratios in arc magmas are higher than measured oceanic sediments, and so a contribution from altered oceanic crust is inferred (Morris et al. 1990). The message from long-lived lithophile radiogenic isotope systems is far from clear. Given the large flux of some elements into the mantle wedge, it would be expected that the fluid mobile element Sr, would display significant isotopic variation in arc magmas. However, this is not generally the case, particularly in arcs with low Ce/Yb ratios.

Elevated $[^{238}U/^{232}Th]$ ratios (compared to MORB) are characteristic of many arc rocks, and could represent a high U/Th slab input or a difference in the melting process (Hawkesworth et al. 1993). Experimental work by Brenan et al. (1995) suggests that fluids with elevated $[^{238}U/^{232}Th]$ may be produced by dehydration of basaltic crust. Elliott et al. (1997) studied a wide range of recent volcanics from the Marianas and found that high ^{238}U was broadly correlated with elevations in LILE ratios such as Ba/La, which is consistent with a fluid input, probably from the basaltic crust. It was also concluded that the least radiogenic $^{143}Nd/^{144}Nd$ ratios were found in lavas with the largest negative Nb anomalies and small ^{238}U excesses. The low ^{238}U excesses and unradiogenic $^{143}Nd/^{144}Nd$ ratios can be

explained by a sedimentary input, probably in the form of a melt (Elliott et al. 1997). In general arcs which possess low Ce/Yb ratios also tend to possess higher $^{143}Nd/^{144}Nd$, while those with high Ce/Yb (probably due to a sedimentary input) have lower $^{143}Nd/^{144}Nd$ (as low as 0.5123 in some cases)(Hawkesworth et al. 1993). Plank and Langmuir (1993) stressed the importance of sedimentary input into the source of arc magmas and pointed to a broad global correlation between the enrichment of elements in the subducting sediment and the same enrichments in the associated arc volcanics.

Rhenium and osmium in arc lavas are discussed in Section 5.2.3.

There has been debate over the extent to which the arc budgets of non-conservative elements are derived from the slab. Kay (1980) and Pearce (1983) estimated that up to 70-90% of LILE and Th were derived from the slab. However, the lack of a complementary isotope signature has led some authors to revise this estimate and to suggest that a large part of the 'slab' signature is in fact derived from stripping of the mantle wedge during fluid transport to the source region of melting (Arculus and Powell 1986; Hawkesworth and Ellam 1989). By analysing a depleted mantle wedge (Tonga), which should provide an example of the minimum wedge contribution to the fluid mobile element budget, Hawkesworth and Ellam (1989) estimated that slab fluxes of highly non-conservative elements accounted for approximately 25% of their budgets in the arc magmas. Becker et al. (2000) have more specifically estimated the flux of trace elements, through the analysis of rocks from high-pressure terranes, concluding that large fractions of Rb and K and up to 40% of the U budget of arc magmas may be supplied by the mafic crust. The fluxes of Pb and Sr are thought to be much lower (10 and 5% respectively), which may, at least in part, explain the apparent paradox between enrichments in LILE and the lack of significant Sr isotope variations.

2.2.2 Dehydration of the subducting slab

The major mechanism of element transport into the melting region of the mantle wedge is through the medium of fluids. During hydrothermal seafloor metamorphism, the oceanic lithosphere becomes variably hydrated - that is, it gains a partially hydrous mineral assemblage. During prograde metamorphism of the subducting slab, hydrous phases become unstable and break down, releasing fluid. The vastly differing bulk rock chemistries of the sedimentary pile, the mafic oceanic crust and the ultramafic lithospheric mantle result in different stable hydrous minerals and different depths at which they become unstable and decompose. Dehydration of the serpentinised mantle lithosphere, the mafic crust and the sedimentary unit may all contribute to the fluid released from the slab. The chemical signature from all these different units must be considered, and may well be conflicting rather than complementary.

The mafic system. Simple models, involving limited components, led to the suggestion that discontinuous reactions were common. Consequently, the break down of a particular phase was estimated to occur over a narrow P-T range, and have an associated discrete and sudden fluid release. It became clear in the early 1980s that this common assumption of discontinuous reactions during the dehydration of mafic crust, was inaccurate, and that continuous reactions were dominant (Thompson et al. 1982). For this reason, there will not be discrete episodes of fluid release corresponding to the breakdown of a certain phases at particular P-T conditions. Instead there will be continually changing solid-solution compositions of minerals with gradual dehydration over a range of pressure until a point is reached beyond which the phase is no longer stable.

The P-T stability limits of the important hydrous phases in the mafic system are shown as black lines in the crustal portion of Figure 2.3 and are summarised in Table 2.1. The key hydrous phases in mafic oceanic crust are sodic amphibole,

chlorite and either lawsonite or zoisite (lawsonite is a lower temperature phase). Amphibole becomes unstable by 2.5 GPa in both water and mixed fluid systems (Pawley and Holloway 1993; Poli 1993; Poli and Schmidt 1995; Schmidt and Poli 1998). Amphibole may react with zoisite to form chloritoid + clinopyroxene + quartz + H_2O. Chloritoid may be important in some cases, and may remain stable up to ~4 GPa. Both lawsonite and zoisite may crystallise at shallow levels and can have very large stability fields, beyond the P-T conditions that amphibole is stable (Poli and Schmidt 1995; Ono 1998; Schmidt and Poli 1998; Okamoto and Maruyama 1999). The final hydrous phase to break down is phengite which is ever-present as the lone potassic phase; this phase may be stable up to 10 GPa. However, it is unlikely to be present in sufficient quantities in the mafic crust to transport large volumes of volatiles to these depths. Lawsonite, however, has the capability to store larger amounts of water in its structure and may be more abundant in cool subduction systems. In warmer systems, the final major hydrous phase to break down will be zoisite.

Mineral	Maximum pressure of stability, in subduction zone with average thermal structure
Mafic system	
Amphibole	**2.5 GPa**
Chlorite	**< 2 GPa (T < 600°C)**
Zoisite	**3 GPa**
Lawsonite (in cool subduction regimes)	**~ 9 GPa**
Chloritoid	**< 4 GPa (?)**
Phengite	**~ 10 GPa**

Table 2.1. Summary of the important hydrous phases in basaltic systems during subduction, and their respective stability limits.

Serpentinised mantle lithosphere and the sedimentary unit. The hydrous minerals present in hydrated ultramafic rocks have the capacity to store large

quantities of water. Chlorite and serpentine minerals, particularly antigorite, are important in the transfer of water to depth. Chlorite is stable in most subduction zones to approximately 5 GPa (Figure 2.3), while in certain cases antigorite may be stable to 7 GPa. Beyond this pressure, hydrous Phase A (10 Å) may provide a means of recycling water in to the deep mantle (Fumagalli et al. 2001). In cases where chlorite is the last stable hydrous phase (possibly excepting Phase A), the transformation from an assemblage containing antigorite and chlorite, to one only containing chlorite may involve the loss of 4.5 wt% water. It is possible that fluids derived from dehydrating serpentinite will scavenge elements from the mafic crust and sediment pile during ascent through the slab towards the mantle wedge.

Biotite may be present in HP sediments, and can be stable to 5 GPa in Mg-rich samples (Sobolev and Shatsky 1990). The importance of Topaz-OH and MgMgAl-pumpellyite is unclear at present and requires further investigation, but their presence with phengite at 900°C and 7 GPa (Domanik and Holloway 1996; Ono 1998) suggests that they may provide a mechanism to transport volatiles to even deeper levels than the mafic or ultramafic systems.

The nature of slab fluids. Due to the shallow dP/dT of carbonate reactions, the P-T paths of subduction zone rocks move away from the carbonate saturation surface and so decarbonation of the down-going slab is unlikely to occur (Poli and Schmidt 2002). Conversely, reactions involving hydrous phases have steeper dP/dT and are therefore crossed by the P-T path. As a result, it is likely that fluids created in, and released from the slab will be water rich. Silica and alkalis, together with significant Al and Ca, will be the dominant solutes (Manning 2004). At high P-T conditions the distinction between fluid and hydrous melt becomes blurred, possibly with complete miscibility between the two (Manning 2004). The addition of Cl, and possibly other minor elements, can increase the solubility of many elements in fluids, resulting in solute contents of up to 50% (Brenan et al.

1995; Scambelluri et al. 1997; Scambelluri and Philippot 2001) although the experimental work of Stalder et al. (1998) shows that the partitioning of trace elements may not be strongly affected by fluid composition.

Melting of the subducting slab. Melting of the slab is likely to be the exception rather than the rule due to the cool thermal regime inherent in the subduction system. Melting is unlikely to occur at pressures less than 1 GPa unless there is an unusual subduction scenario, such as ridge subduction (Poli and Schmidt 2002). It is most likely that the sedimentary layer will undergo melting because it has the lowest melting temperature and is situated in a region of closely spaced isotherms (Figure 2.3) where temperatures are most likely to be high due to the close proximity of the mantle wedge. However, Poli and Schmidt (2002) state that estimations of temperatures in subduction zones are inadequate to cause melting of the sedimentary layer, and furthermore, the temperatures required for melting are not consistent with the mechanism for deep earthquakes. Moreover, Poli and Schmidt (2002) suggest that the far greater volume of water in an extensively hydrated basaltic layer, combined with increased (pressure dependent) solubilities of elements in fluids, can explain patterns of elements such as Be and Th through leaching of the sedimentary layer, without the need to invoke melting.

Melting of hydrated mafic oceanic crust will only occur at temperatures of approximately 750°C when P = 1 - 2.5 GPa (Vielzeuf and Schmidt 2001). At this point some melt will be produced, mainly from the breakdown of zoisite, but the quantity is unlikely to be great enough for melt to be extracted from the rock (Poli and Schmidt 2002). It is only at temperatures between 850 and 1000°C that amphibole will decompose to produce enough melt to be extracted from the rock (Vielzeuf and Schmidt 2001). These temperatures are unrealistically high for most subduction zones and so the melting of mafic crust during subduction is very unlikely at pressures less than 3 GPa. Above this pressure, amphibole is unlikely to

remain stable and will break down continuously over a range of depth up to 3 GPa, releasing hydrous fluids and leaving the slab largely anhydrous and therefore not fusible.

2.2.3 Fluid flow during HP metamorphism

The flux of elements from the slab to the mantle wedge requires not only that dehydration or melting reactions occur in the down-going slab, but also that they form a fluid which is coherent and extensive enough to be able to move out of the slab. Much of the fluid formed in the slab may be retained within the slab despite, perhaps, transport over short distances (Miller et al. 2002, and references therein). Modifications of this type do not alter the overall composition of the slab and therefore do not affect the flux to the deep mantle, or indeed to the mantle wedge. It is clear from the compositions of arc magmas that extensive fluid *does* escape from the slab and infiltrate the mantle wedge. The mechanism of this transport is unclear, although it may be aided by volume changes associated with high pressure mineral transformations. On a small scale, stresses induce dislocation creep within crystals, while fracturing is less common (Philippot and van Roermund 1992). The small-scale deformation and recrystallisation of phases is crucial to the development of shear zones. However, despite largely ductile behaviour, the presence of veining in eclogite facies rocks (this study; Pennacchioni 1996) is evidence of brittle behaviour. The low temperature conditions of metamorphism and a scarcity of fluid must inhibit purely ductile behaviour. Pennacchioni (1996) documented that eclogite facies veins provided the nuclei for the development of shear zones. Furthermore, the presence of fluids increases plastic flow rates and also encourages fracturing of minerals (Pennacchioni 1996). Thus, there are complex interactions between stress and fluids which result in the reciprocal promotion of deformation and fluid flow within the down-going slab. Long length-scale transport of fluids (and elements) almost certainly requires the development of shear zones which act as fluid pathways (Miller et al. 2002, and references

therein). This will be discussed further, with respect to the data presented, in Chapter 8.

2.2.4 Constraints on subduction zone trace element fluxes through the examination of high pressure terranes

One consideration of work of this type is the extent to which the samples used are representative. This is true of both the composition of the rocks analysed, and the metamorphic conditions under which they have been transformed. Work by several authors have illustrated that across-arc variations in trace elements exist (e.g. Ishikawa and Nakamura 1994; Ryan et al. 1995) and that mobile element concentrations vary with metamorphic grade (e.g. Moran et al. 1992; Bebout et al. 1993; Bebout 1995). Both of these conclusions emphasise that data from a single set of rocks must be considered as representative only of rocks at that grade/depth and of that particular composition.

Becker et al (1999) analysed high pressure veins (from the Adula nappe, central Alps and the Variscan fold belt, Germany) which were derived from the host eclogites (recognised from isotope data). The authors concluded that the composition of veins were dominated by SiO_2 and Al_2O_3, and were enriched in Cs, Rb, Ba, Pb and K compared to normal MORB (N-MORB). Perhaps surprisingly, the same was not true for Sr, U and Th which were present in the veins in comparable or slightly lower quantities relative to N-MORB. Very low abundances of Nd, Sm, Zr, Nb, Ti and Y were also found. The findings for Ba, Pb, Th and U are consistent with the experimentally determined conclusions of Brenan et al. (1995). A further conclusion of Becker et al. (1999) is that the budgets of incompatible alkalis and possibly Pb may be controlled by the residual mineral phases. However, Spandler et al. (2003; 2004) observed that there is a decoupling between fluid release and trace element release from the slab, at least up to 150km depth, resulting in fluids which are relatively dilute in terms of trace elements. It has been suggested by

Spandler et al. (2003; 2004) that the flux of trace elements from the slab is not directly linked to mineral breakdown (trace elements are merely redistributed in other phases which become stable), and is instead dependent on complex fluid-rock interactions and possibly fluid-assisted partial melting. The formation of dilute subduction zone fluids is confirmed by the modelling of Manning (2004).

Somewhat contradictory bulk rock findings have been published by Becker et al. (2000) and Spandler et al. (2004). Becker and co-authors found that eclogites from various high pressure terranes (including the Zermatt-Saas ophiolite) were strongly depleted in K, Rb and Ba relative to Nb and Th, when compared to fresh and altered MORB, and more mildly depleted in U and Pb. Conversely, Spandler et al. (2004) found that high-grade metamorphic rocks from New Caledonia do not display significant geochemical changes, except for a few samples where B and the LILE are somewhat depleted. At least in part these findings can be explained by differences in P-T conditions. Becker et al. (2000) observed that less than 10-30% of the loss of U and Pb occurred at temperatures below 600°C. Whereas the samples from New Caledonia (Spandler et al. 2004) display an absence of extensive LILE loss, Becker et al. (2000) found that the majority of K and Ba (and presumably Cs and Rb) was lost at temperatures below 600-700°C. Metabasalts from the Catalina Schist terrane (California), analysed by Bebout (1995), retain their enrichments (relative to MORB) in B, K, Rb, Ba and Cs, which are the result of seafloor alteration. However, the peak metamorphic grade of these samples equates to a depth of only 15-45 km (~0.5 - 1.1 GPa, 275-750°C), and thus the lack of trace element mobility may be the consistent with a theory of increasing mobility under increasing P-T conditions. Conversely, Bebout (1995) found that abundances of B, Cs, As, Sb and possibly U were depleted in metasediments from the same region, although an increase in depletion was also observed in these metasedimentary samples. The observation that high-pressure fluids may carry a greater amount of solute has been recognised previously (e.g. Brenan et al. 1995;

Stalder et al. 1998) and is consistent with increasing mobility with increasing P-T conditions.

Arculus et al. (1999) analysed a suite of metamorphosed pelitic schists, mafic and ultramafic rock types from the Raspas complex in Ecuador. The samples have experienced P-T conditions of 1.3 - 2 GPa and ≤ 600°C. The pelitic schists do not display preferential light REE depletion (relative to other REE) when compared to average continental crust. Furthermore, they do not appear to have lost a significant proportion of their Rb, Ba, Pb and U contents. In fact Ba and Pb are relatively enriched compared to the bulk continental crust. Eclogite-facies metabasalts however, display substantial losses of certain elements (namely Rb and Ba) which may amount to 85% of the original budget. This is consistent with the data of Becker et al. (2000) presented above. The lack of loss of U and an enrichment in Pb in the samples of Arculus et al. (1999) is also in agreement with Becker et al. (2000), who concluded that U and Pb loss is minor at temperatures below 600°C.

The trace element data of Messiga et al (1995), Tribuzio et al. (1996) and Spandler et al. (2003) for individual mineral phases from high-pressure rocks will be discussed in Chapter 7, together with the mineral data presented here and other relevant literature.

2.2.5 Summary

The elements that are shown to be non-conservative are lost from the slab to some degree, and therefore will be present in lower abundances in dehydrated, subducted crust in comparison to the original oceanic crust. These include: B, Cs, Rb, Ba, Sr, K, U, Pb and sometimes Th (although the latter is thought to be derived from sediment melts (Hawkesworth et al. 1997)). However, it is not clear by the analysis of arc rocks, how much of the arc signature is derived directly from the

slab and what proportion represents elemental stripping of the mantle wedge. This poses a problem for the estimation of the composition of subducted crust. For this reason, some authors (e.g. Becker et al. 1999; 2000; Spandler et al. 2003; 2004) have analysed trace elements in minerals and veins from high-pressure terranes, in order to better constrain the composition of the oceanic crust after dehydration (discussed in previous section). The work presented in this thesis contributes to this knowledge through the analysis of Re-Os behaviour in bulk rocks, and the distribution of Re, Os and trace elements between high pressure mineral phases from the Zermatt-Saas ophiolite, Switzerland.

3 Geological setting, petrography and P-T estimates

3.1 Sampling areas

The samples collected can be divided, by geographical means, into two suites. The first suite was collected from the Zermatt-Saas ophiolite (ZSO) in the Western Alps and consists of eclogite facies metabasalts from the Pfulwe area and gabbros from the Allalin Gabbro body that display variable metamorphic recrystallisation from fresh igneous assemblages to eclogite facies. The second suite was collected by Alan Boyle (1982), from the Sulitjelma ophiolite of Northern Norway. This suite comprises metamorphosed basalts from the Lomivann unit and metagabbros from the Sulitjelma Gabbro. See Section 3.3 below for a full description of samples.

3.2 Geological setting

3.2.1 Zermatt-Saas ophiolite (ZSO) region, Western Alps

The Alps provided the basis for some pioneering geological work. Notable early work in the Zermatt-Saas Fee area was the mapping by Gerlach for the Karte Schweiz and by the Italian Geological Survey, which dates from the latter part of the 19th century. However, it was the incredibly thorough and detailed work of Peter Bearth in the late 1950s, 1960s and 1970s, that characterised much of the geology of the Zermatt-Saas area (Bearth 1959; 1967a; Bearth 1971; Bearth and Stern 1979).

The Zermatt-Saas ophiolite (ZSO) forms part of the Piemonte zone of the Western Alps, which stretches in an arcuate zone approximately 300km from the Zermatt-Saas Fee area in the north to Genoa in the south (see Figure 3.1). The Piemonte zone consists of meta-ophiolitic material and associated metasediments which represent fragments of Mesozoic Tethyan oceanic crust (see Section 3.2.1.5 for further discussion). To the east of the Piemonte zone (towards the interior), and structurally below, lie continental basement rocks that are thought to be part of the

Briançonnais terrane (e.g. the Monte Rosa nappe) (Figure 3.2) (e.g. Stampfli 1993). To the east of these Briançonnais continental fragments lies the former Adriatic (Apulian) continental margin which is represented by the Sesia zone. In some areas, the Briançonnais continental massifs are not exposed, and the Piemonte zone directly underlies the Sesia zone (Figure 3.1 and Figure 3.2). To the west of the Piemonte zone, and structurally below, lie the Briançonnais cover metasediments.

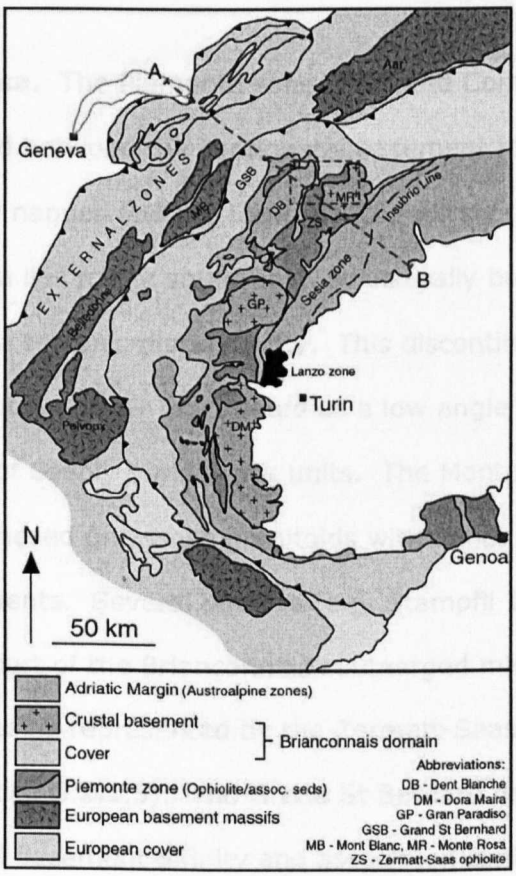

Figure 3.1. Simplified map of the western Alpine geological units (collated from Barnicoat and Fry 1986; Rubatto et al. 1998). Position of cross-section in Figure 3.2 shown by dashed line A-B. Dashed box shows area shown in Figure 3.3.

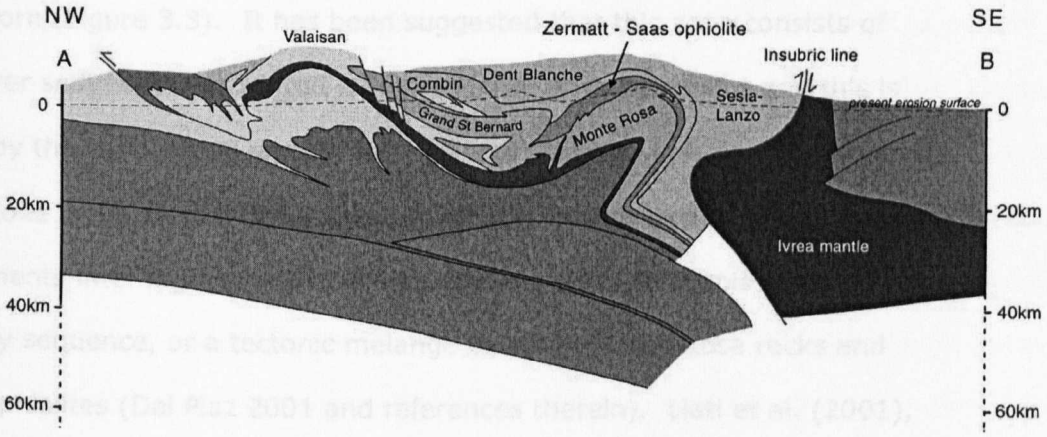

Figure 3.2. Cross section through the central western Alps (from Schmid and Kissling 2000). Line of section is approximately from A to B in Figure 3.1.

Monte Rosa. The Piemonte zone (ZSO and Combin units) in the Zermatt area is sandwiched between the continental basement rocks of the Monte Rosa and Grand St Bernard nappes and the Dent Blanche klippe (Figure 3.1 and Figure 3.2). The Monte Rosa lies to the south-east, structurally below the ZSO, and is separated from it by a tectonic discontinuity. This discontinuity was originally a thrust surface, but was later reactivated as a low angle detachment fault during tectonic unroofing of deeply buried rock units. The Monte Rosa consists of highly metamorphosed gneissose granitoids with minor associated continental shelf metasediments. Several authors (e.g. Stampfli 1993) have suggested that it was originally part of the Briançonnais submerged micro-continent that lay between the Tethyan basins represented by the Zermatt-Saas and Valais ophiolites (see Figure 3.5 in Section 3.2.1.5). The Grand St Bernard nappe consists of rocks of continental basement affinity and associated continental shelf sediments and is also thought to represent part of the Briançonnais terrane (see Figure 3.2).

Within the Monte Rosa nappe lie two zones of disputed origin: the Gornergrat zone and the Furgg zone. The former outcrops on the north western periphery, between the Monte Rosa and Zermatt-Saas nappes, and includes some calc-mica-schists and micaceous marbles which lie adjacent to the Britannia Hutte, a mile north-east of

the Allalinhorn (Figure 3.3). It has been suggested that this zone consists of Triassic cover sediments associated with the Monte Rosa basement and this is confirmed by the U-Pb zircon ages of Rubatto and Gebauer (1999). The origin of the Furgg zone is debated, and it has been variably interpreted as Monte Rosa cover sediments interfingered with Zermatt-Saas rocks, a Mesozoic volcano-sedimentary sequence, or a tectonic melange between Monte Rosa rocks and Piedmont ophiolites (Dal Piaz 2001 and references therein). Liati et al. (2001), found dramatically variable U-Pb SHRIMP magmatic zircon ages which yielded 510 ± 5 Ma for a mafic eclogite and 272 ± 4 Ma for an orthogneiss. From this evidence, and structural arguments previously published, they concluded that the zone was a tectonic melange of very heterogeneous rock types including Variscan basement and mafic intrusions.

The Monte Rosa massif experienced very high-pressure (HP) metamorphism during Alpine subduction / orogeny. Pressure (P) and temperature (T) conditions of peak metamorphism have been estimated by Chopin and Monié (1984), to be 500°C and 16 kbar (1.6 GPa), on the basis of mineral compositions and particularly the very high Mg content of chloritoid, which was the highest reported to that date.

Dent Blanche. This unit lies to the north west, and is structurally above the Zermatt-Saas ophiolite (ZSO) and Combin zone. It consists largely of continental basement gneisses and minor associated calcareous shelf metasediments. It is lithologically very similar to the Sesia zone and is considered to be a klippe of the same unit (e.g. Dal Piaz and Ernst 1978) (see Figure 3.1). Both the Sesia zone and Dent Blanche klippe are parts of what was previously the Adriatic margin. The margin was partially subducted with the down-going oceanic plate and was strongly metamorphosed. However, the Dent Blanche klippe represents a portion of the upper part of the margin, which has been thrust north westwards over the Piemonte and Briançonnais units. As such, it did not experience the very high-

pressure metamorphism (>15kbars (1.5GPa) and 550±50°C) that is evident in the Sesia zone (e.g. Pognante et al. 1987). However, the associated cover sediments in the Dent Blanche have been metamorphosed under blueschist facies conditions. Retrogressive greenschist facies assemblages are generally dominant throughout the gneissose lithologies of the Dent Blanche. It can be inferred from this evidence, that the Dent Blanche and ZSO units were not adjacent during the high-pressure metamorphism of the latter; they were probably juxtaposed by re-structuring of the nappe pile during exhumation. This was most likely accompanied by relaxation of the geotherm and greenschist facies recrystallisation of the Dent Blanche klippe and surrounding units. This may have been linked to the 'Lepontine' thermal overprint event of the Central Alps (e.g. Becker 1993). Despite a lack of high-pressure mineralogy, gneissose textures suggest a previous higher grade metamorphic history for this unit. There is evidence of pre-Alpine amphibolite / granulite metamorphism from inclusions within garnet in the Valpelline gneisses (Gardien et al. 1994).

Combin unit. This unit, together with the ZSO, constitutes the Piemonte zone in this area of the Alps. The Combin (sometimes referred to as the Tsaté nappe, e.g. Stampfli 1993) is the upper tectonic element and the ZSO, the lower. The former unit outcrops discontinuously on the western margin of the ZSO in the Zermatt area (Figure 3.3) and on both the eastern and western margins in the southern part of the ZSO. The zone comprises mica-schists (both calcareous and siliceous), micaceous marbles, and prasinites. Prasinites consist of porphyroblastic albite crystals in a foliated matrix of greenschist facies minerals (actinolite, chlorite, epidote), which probably represent metamorphosed submarine basaltic flows. These lithologies derive from sediments and volcanics which were thought to be peripheral in the oceanic basin and were probably associated with the rifted continental margin of Briançonnais or the Adriatic margin (Dal Piaz and Ernst 1978). Stampfli (1993) proposed that the Combin unit was an accretionary prism

formed as oceanic and continental margin sediments were scraped off the down-going slab.

Eclogite assemblages are absent and the predominant metamorphic grade is greenschist facies. However, peak metamorphism occurred under blueschist facies conditions (Kienast 1973; Cartwright and Barnicoat 2002). Again, this evidence precludes the juxtaposition of the Combin zone and ZSO prior to the high-pressure metamorphism of the latter. The orientations of structural features (schistosity, axial planes, fold hinges) in the Combin have broad similarities to those in the ZSO, although the latter seems to have a previous structural history that has not been pervasively overprinted (unpubl. mapping - Lago di Cignana, Dale 2000).

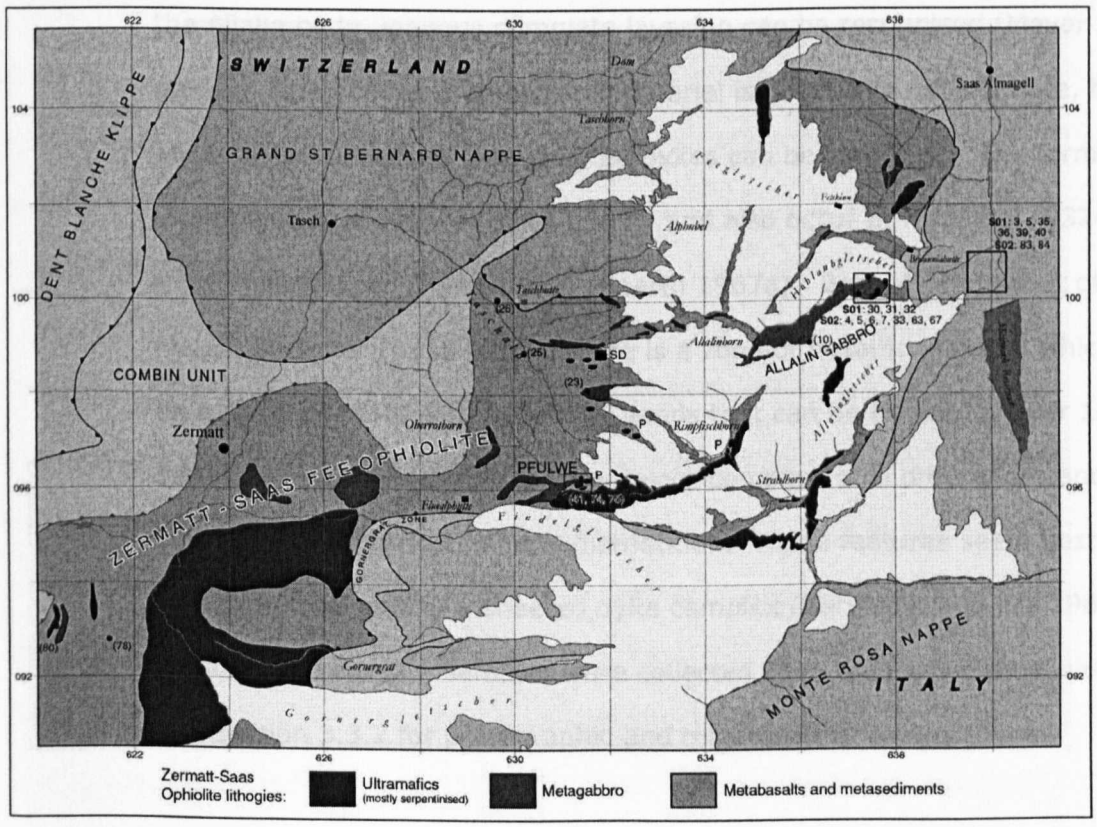

Figure 3.3. Map of northern part of the Zermatt-Saas showing sample localities. Grid lines are based on the Swiss Grid system. P = recognisable pillow basalts. SD = sheeted intrusives.

3.2.1.1 Zermatt-Saas ophiolite (ZSO)

The ZSO lies between Saas Fee in the north east, and Val d'Aosta in the south. It comprises a dismembered ophiolitic sequence of lithologies including ultramafics, metagabbros, metabasalts and associated metasediments. Ultramafic rocks are all but completely serpentinized, with the exception of some diopside and chromite porphyroblasts. Metamorphosed sediments such as manganiferous cherts, typical of ophiolitic sequences, are found and have been recrystallised as piemontite-spessartine-quartzites. However, the lithologies are disrupted and interleaved on a variety of scales from a single metre to hundreds of metres.

Despite the deformed nature of most of the ophiolite, it is possible to identify some original igneous structures indicative of oceanic crust. In the gabbros, particularly the Allalin body, igneous cumulate layering can be recognised (Meyer 1983b; this study). Much of the metabasaltic material is difficult to differentiate, but in some areas pillow structures and sheeted dykes can be identified. The former are unambiguous at Pfulwe (6312 0961), and also occur at Hubeltini (6324 0974) and the Rimpfischhorn (6344 0968) (Bearth 1967a). Beneath the snout of the North Mellichgletscher (6318 0988), there is a zone of basaltic material which is banded on a scale of <1m, with individual bands that can be traced for over 100m. The bands have parallel contacts, only minor compositional differences and have internally symmetrical mineral distribution. These features seem best interpreted as a deformed part of a sheeted dyke complex (Barnicoat and Fry 1986). Metabasaltic eclogite samples were collected from the Pfulwe area within the ZSO see Section 3.3.2 for petrographic and mineralogical observations.

3.2.1.2 Allalin Gabbro

This gabbro body is an overturned but structurally coherent unit which forms a lens of approximately 3 by 2 by 1km that outcrops in the centre of a recumbent fold in the north-eastern part of the ZSO (Meyer 1983a; 1983b). There are two

metamorphic events recorded in this unit. Firstly, the gabbro was metamorphosed by high-temperature (>400°C; Stakes 1993) seafloor hydrothermal alteration. This has been determined by a study of oxygen isotopes which concluded that the fluids present in the hydrated parts of the gabbro have a signature consistent with high temperature seafloor alteration (Barnicoat and Cartwright 1997). Secondly, together with the other lithological units of the Zermatt-Saas ophiolite, the gabbro has been partially subducted and metamorphosed under eclogite-facies conditions.

Despite this history, magmatic structures (e.g. cumulate layering) are commonly observed and magmatic textures are retained in the majority of the body. In places, even magmatic mineralogy has been preserved, in a metastable state, through metamorphism. Ductile deformation and recrystallisation is also common but is not often strongly developed. Much of the eastern edge of the gabbroic body displays eclogitic metamorphic fabrics overprinted by recrystallisation and associated deformation features formed under greenschist facies conditions. The latter is presumably a result of stresses during exhumation and the emplacement of the gabbro body into its current position.

3.2.1.3 Crystallisation age of the Allalin gabbro and ZSO

The igneous crystallisation age of two gabbroic bodies from the ZSO has been determined by SHRIMP U-Pb dating of magmatic zircons. Ages of 164.0 ± 2.7 Ma and 163.5 ± 1.8 Ma have been obtained for the Allalin and Mellichen metagabbros respectively (Rubatto et al. 1998). This dating not only provides an age for the gabbroic bodies, but also suggests an age for the crystallisation of the ophiolite as a whole, assuming the basalts and gabbros are co-genetic (which has not been contested in published literature). It is possible that the basalts *are* derived from a portion of oceanic crust geographically distinct from that of the gabbros, and may have been transported and juxtaposed during subduction and/or orogenesis. However, there is little structural evidence for transport over significant distances

within the ZSO. This evidence, and the coincidence of the gabbro ages from two distinct gabbro units, suggests that the gabbroic and basaltic lithologies in the Zermatt-Saas Fee area may well have formed in the same palaeogeographical area, and most likely concurrently. The age for crystallisation of the ophiolite is consistent with the minimum age of detrital zircons (~150 Ma) extracted from Mn-rich quartzite at Sparrenflue, Täschalp, which places a limit on the maximum age of deposition of the sedimentary cover in the Allalin area (Rubatto et al. 1998). These ages are also in agreement with a Middle to Late Jurassic age for the deposition of Tethyan radiolarites suggested by Baumgartner (1987), on the basis of biostratigraphical evidence.

3.2.1.4 Metamorphism in the ZSO

It has been established for several decades that the ZSO has experienced intense HP metamorphism during partial subduction and the subsequent continental collision that formed the Alpine mountain belt. In 1973, Chinner and Dixon suggested peak metamorphic conditions for the Allalin Gabbro of 1-1.5 GPa and 500-700°C. On the basis of mineral assemblages in the metabasites of the Breuil-St. Jacques area, Ernst and Dal Piaz (1978) estimated eclogite metamorphism at approximately 470 ± 50°C and 10 ± 2 kbar, followed by an overprint of blueschist-facies mineralogy formed at 450 ± 50°C and >7 kbar.

Over the past two decades, the recognised boundaries of metamorphism have been extended by careful petrographic and analytical work, alongside advancements in the understanding of the experimental stability of assemblages. Peak pressure and temperature conditions in the north-east part of the Zermatt-Saas unit have been estimated at approximately 2.0 GPa and 550-600°C from assemblages in metabasalts from the Täschalp area (Barnicoat and Fry 1986) and in the Allalin Gabbro itself (Meyer 1983a; 1983b). In the early 1990s, at Lago di Cignana, near Valtournanche, Val d'Aosta, NW Italy, ultra-high-pressure (UHP) metamorphism

was confirmed by the presence of coesite (UHP is defined as pressure in excess of that required for coesite formation; i.e. >2.8GPa at 700°C (Coleman and Wang 1995)). Coesite, and quartz pseudomorphs after coesite, occur as inclusions in pyrope-rich garnet and in dravitic tourmaline within metamorphosed manganiferous quartzite (Reinecke 1991). Furthermore, coesite relicts have been found in garnet-mica-schist and in metabasalts with MORB affinities in the same area (Reinecke 1998). The peak pressure and temperature recorded by these rocks (which lie about 20 km south-west of Zermatt) is in the range of 2.7-2.9 GPa and 600-630°C (Reinecke 1991; 1998). This equates to a depth of up to 95km, approaching the depth of the Benioff zone beneath modern arcs (Tatsumi 1986).

More recent work by Rebay and Powell (2002) has attempted to unravel the metamorphic history of the petrographically complex Allalin Gabbro (together with other Alpine eclogitic metatroctolites) by the use of pseudosections derived from a complex petrogenetic grid which they have developed from calculated mineral equilibria in the system NCFMASH. The assemblage of chloritoid + talc + garnet + omphacite which is present in the ex-olivine micro-domain corresponds to a peak pressure possibly greater than 27 kbar (2.7 GPa) at temperatures of 570-600°C. For a further discussion of this work, together with P-T estimates presented in this thesis and a discussion of the problems of P-T estimates within the Allalin Gabbro see Section 3.4.

A much higher peak metamorphic pressure for the Allalin Gabbro was estimated, on the basis of the carbonate assemblage, by Barnicoat (1996). He observed the current mineralogy of fine grained aggregates of calcite and much coarser magnesite, and suggested that the former had inverted from its high-pressure form, aragonite. Both aragonite and magnesite appear to have formed from high-pressure metamorphism of dolomite, which may have been originally introduced

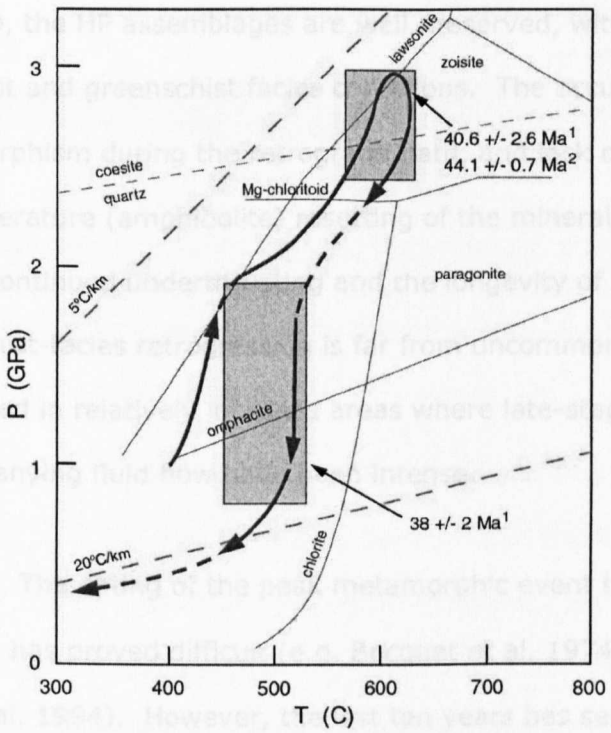

Figure 3.4. P-T path for the Zermatt-Saas ophiolite in the Lago di Cignana area of Val d'Aosta, NW Italy. PT path constructed from garnet zoning profiles by Reinecke (1998) and van der Klauw (1997). Boxes represent geochronological constraints based on the closure temperatures involved with Sm-Nd dating of garnets (peak P-T box) and Rb-Sr dating of micas, from the work of Amato et al. (1999). Ages: 1 Amato et al. (1999), 2 Rubatto et al. (1998). Geotherms corresponding to 5 and 20 degrees C/km are shown together with selected relevant mineral stability fields. The latter are for comparison only and are not necessarily precise for the rock compositions of the Zermatt-Saas ophiolite metabasalts or metagabbros.

into the gabbros during seafloor hydrothermal alteration. Peak pressure estimates for the assemblage (given T = ~600°C) are >3.5GPa; or ~110km of burial.

A 'hairpin' P-T path, illustrating cooling during exhumation, was formulated for the metasediments at Lago di Cignana by van der Klauw (1997) and Reinecke (1998), on the basis of garnet zoning profiles (Figure 3.4). Such P-T paths are dependent on continued underthrusting (subduction) of cold material during the period of exhumation, thereby inhibiting thermal relaxation of the cool geotherm. It is not until the unit has been exhumed to pressures below 2.0 GPa that decompression occurs adiabatically, and even during this stage, fairly rapid exhumation and/or continued underthrusting is required to explain the observed constant temperature during unroofing between 2.0 and 1.0 GPa.

In many parts of the ZSO, the HP assemblages are well preserved, with only minor retrogression at blueschist and greenschist facies conditions. The occurrence of blueschist facies metamorphism during the retrograde path, and lack of relatively low pressure - high temperature (amphibolite) resetting of the mineral assemblage, reinforces the theory of continued underthrusting and the longevity of a relatively cool geotherm. Greenschist-facies retrogression is far from uncommon, but is usually only well-developed in relatively localised areas where late-stage deformation and accompanying fluid flow have been intense.

Age of metamorphism. The dating of the peak metamorphic event in various units throughout the Alps has proved difficult (e.g. Bocquet et al. 1974; Monié and Chopin 1991; Bowtell et al. 1994). However, the last ten years has seen considerable progress in the dating of rocks within the ZSO, and has yielded some fairly precise ages. Amato et al. (1999), with the use of some thorough leaching techniques, obtained a very well constrained Sm-Nd mineral isochron with an age of 40.6 ± 2.6 Ma from a metabasite in the Lago di Cignana area. This value is almost within error of the 44.1 ± 0.7 Ma U-Pb SHRIMP age of metamorphic zircon rims and occasional whole zircon grains, found in an UHP metabasite and two metasediments, also in the Lago di Cignana area (Rubatto et al. 1998).

3.2.1.5 Tectonic Synthesis

Palaeogeography. It has been suggested by many authors that two or three basins existed within the Mesozoic Tethys, but not all concurrently (e.g. Platt 1986; Stampfli 1993; Froitzheim et al. 1996; Schmid et al. 1996). The Meliata-Hallstatt ocean opened to the south-east of the Adriatic margin (the Austroalpine realm) during the mid-Triassic (Kozur 1991, cited in Schmid et al. 1996) and closed during the late Jurassic. Due to its geographical position in the East, this basin has played no part in the evolution of the Western Alps.

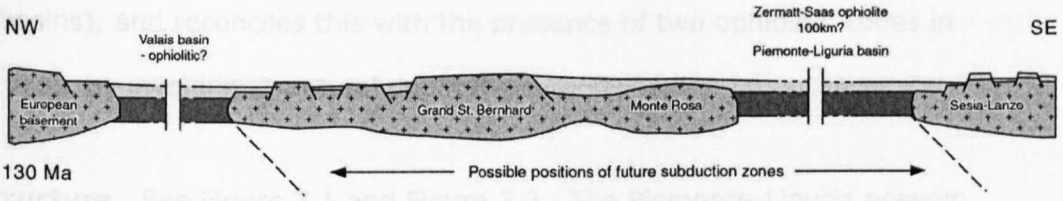

Figure 3.5. Palaeogeography of the Mesozoic Tethys region; after Ernst (1973) and Platt (1986). Modified on the basis of Schmid et al. (1996), who state the presence of only two basins at 130 Ma (the Meliata-Hallstatt basin had closed by this date and the suture lay south-east of the Adriatic margin).

The other two widely recognised palaeo-basins are the Piemonte-Liguria and Valais oceans (see Figure 3.5). The remaining parts of both these ocean basins are major constituents of the current Alpine geological structure. The two basins were separated by thinned basement (Briançonnais microcontinent), with the former lying to the south east between Briançonnais and Sesia (the Adriatic margin) and the latter (Valais) separating Briançonnais from the rifted European margin. The Piemonte-Liguria ocean opened in the mid-Jurassic, as a result of the opening of the central Atlantic (Dewey et al. 1973; Schmid et al. 1996), and closed in the Palaeocene to early Eocene (Froitzheim et al. 1996). The last basin to form was the Valais ocean, which opened in the late Jurassic-early Cretaceous and closed in the Eocene (Frisch 1979; Stampfli 1993; Florineth and Froitzheim 1994).

While the term 'ocean' is used in descriptions of this kind, these basins were by no means of Atlantic proportions. The term merely refers to a basin that is, at least in part, floored by oceanic crust. At its maximum, the Piemonte-Ligurian ocean may have been approximately 100km wide (Platt 1986). It is not altogether clear whether the oceanic units from this ophiolitic series are analogous to MORB, or whether they have a slight back-arc signature. This issue will be addressed using geochemical data presented in *Chapter 4 - Bulk rock chemistry.*

Avigad et al. (1993) proposes a model for the evolution of the Alpine chain which involves the formation of only one ocean basin (instead of the Piemonte-Ligurian

and Valais basins), and reconciles this with the presence of two ophiolitic zones in the current Alps, by invoking structural duplication.

Current structure. See Figure 3.1 and Figure 3.2. The Piemonte-Liguria oceanic crust and associated metasediments manifests itself, in the present day Alpine chain, as the Piemonte zone. This unit lies structurally below and to the east of the Briançonnais domain. However, the internal massifs of Monte Rosa, Gran Paradiso and Dora Maira are thought to represent basement of the Briançonnais microcontinent, and the Piemonte zone lies structurally above and to the west of these Briançonnais units. This can be reconciled by the fact that the formation of the Monte Rosa back-fold has aided the exhumation of the internal basement massifs and brought them to the surface, where they are currently exposed to the east of the Piemonte zone (see Figure 3.2).

The Valais ophiolitic zone outcrops to the north west of the Piemonte and Briançonnais domains. The most south-easterly unit on the Alpine side of the Insubric line is the Sesia zone, which lies structurally highest in the nappe pile and was previously part of the Adriatic margin. South-east of the Insubric line lie the ultramafic mantle rocks of the Ivrea zone. There is a crude progression of increasing metamorphic grade within the Alpine chain from the External zones in the north-west to the Internal zones in the south-east.

Timing of metamorphism. The understanding of the development of the Alpine chain depends strongly on evidence from field relations, calculated P-T conditions and accurate geochronological data. Throughout the Alps, there have been widely disparate estimates of the age of metamorphism by various authors (e.g. Bocquet et al. 1974; Chopin and Monié 1984; Bowtell et al. 1994; Rubatto et al. 1998; Rubatto and Gebauer 1999). While this may, to some extent, be due to actual variation in the timing of metamorphism in different units, there have been

discrepancies between dates obtained from rocks in the same units, and also difficulty in attaining sufficiently precise ages. The latter problem was illustrated by the Sm-Nd study of garnets by Bowtell et al. (1994). They found that small Nd-rich epidote inclusions in garnet led to vastly increased errors and an estimated age of 52 ± 18Ma.

The timing of metamorphism in the Monte Rosa nappe has been difficult to unravel, and provides an example of the variation in estimates from a single unit. Chopin and Monié (1984) published an ^{40}Ar-^{39}Ar plateau age for phengitic mica of 110 ± 3 Ma. However, they also calculated an age of approximately 37 Ma, from phengite in the Gornergrat cover, which they interpreted to be the timing of the 'Lepontine' thermal overprint. High-precision U-Pb dating of metamorphic zircon domains and some precise Sm-Nd ages, have led to the re-evaluation of ^{40}Ar-^{39}Ar dates from parts of the Alps and the conclusion that many of the ages are erroneously old due to the retention of excess argon which was incorporated during the high-pressure event (Arnaud and Kelley 1995). Rubatto and Gebauer (1999) have dated the metamorphic rims of zircons from a high-pressure assemblage in the Gornergrat zone (which is thought to have been structurally coherent with the rest of the Monte Rosa nappe throughout metamorphism) at 34.9 ± 1.4 Ma, using the U-Pb SHRIMP technique. This is consistent with a mid to late Eocene peak metamorphic event in this region (Rubatto et al. 1998; Amato et al. 1999).

Subduction and collision. Froitzheim et al. (1996) and Schmid et al. (1996) envisage a scenario of two pulses of subduction, collision and metamorphism. The earlier phase involved the closure of the Meliata-Hallstatt ocean in the area of the current Eastern Alps and did not, therefore, affect the evolution of the Western Alps. It is known that this phase did not commence prior to ~90 Ma because there was continued sedimentation until this point (Caron et al. 1982).

Despite the problems outlined above (in *Timing of metamorphism*), it is now (fairly) clear that the age of peak metamorphism differs between units. This variation is not random; indeed ages appear to decrease from south-east to north-west (Rubatto et al. 1998). Austroalpine units have the oldest age of peak HP metamorphism, between 100 and 150 Ma (Thoni and Jagoutz 1993). The Sesia zone underwent eclogite-facies metamorphism around 65 Ma (Ramsbotham et al. 1994; Inger et al. 1996; Rubatto et al. 1999). The internal basement massifs (e.g. Monte Rosa), the Piemonte zone ophiolites and cover (ZSO and Combin units) and the Briançonnais cover all have peak metamorphic ages between ~50 and 34 Ma (see ZSO section, and *Timing of metamorphism*, above). Finally, the Valais and distal European margin units are thought to have been subducted and metamorphosed around 35Ma (Rubatto et al. 1998).

An example of an apparent metamorphic dating paradox is presented here. The 35 Ma metamorphic age for the Gornergrat zone stated above is younger than the 38 ± 2 Ma Rb-Sr age of greenschist-facies metamorphism reported by Amato (1999) from the Lago di Cignana area of the ZSO, yet one would expect peak metamorphism to occur before greenschist-facies retrogression. However, as these two dates are from different nappe units, this discrepancy may be explained by simultaneous subduction of one unit and exhumation of another.

This systematic change in age of peak metamorphism is consistent with the closure of the Piemonte-Ligurian and Valais oceans by south-eastward subduction (e.g. Rubatto et al. 1998). Units lying furthest south-east prior to the formation of the Alps would have been subducted and metamorphosed first, followed by units which lay progressively further north-west. With the development of a type of accretionary prism, it would be possible to concurrently subduct one unit while another was being exhumed through the erosion and tectonic reworking of the wedge. Indeed, this type of erosive and tectonic unroofing is driven by continued

underthrusting of material which results in an increase in prism thickness, leading to surface uplift and a decrease in stability which promotes tectonic exhumation (see Platt 1986; 1993). While this system works for plate material of oceanic origin and perhaps ultra-thinned continental material, continued subduction and underthrusting after the attempted subduction of substantial continental fragments is less viable. Opinion is divided on the number of active subduction zones. Some favour a single location at the south-eastern edge of the Piemonte-Ligurian ocean, while others envisage both the presence of this subduction zone, and another zone forming later at the south-eastern edge of the Valais ocean. Perhaps the presence of a second zone of subduction is necessary in order to facilitate continued subduction after the initial zone may have ceased following the attempted subduction of some substantial fragments of lower density continental crust.

3.2.2 Sulitjelma ophiolite, Northern Norway

The Sulitjelma igneous complex lies on the border between Norway and Sweden, just north of the Arctic circle. It forms part of the Köli Nappes of the Upper Allochthon (Stephens et al. 1985; cited in Boyle 1989). The unit consists of an ophiolite-like sequence including ultramafics, layered and isotropic gabbros, a sheeted intrusive complex (hereafter referred to as the 'dyke complex'), and an extrusive zone of pillow basalts and undifferentiated volcanics.

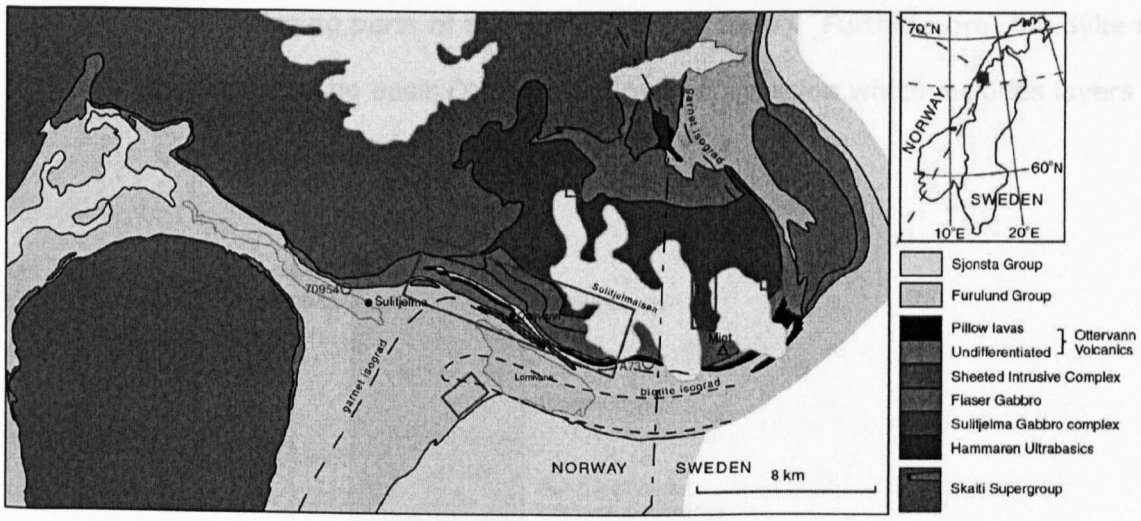

Figure 3.6. Geological map of the Sulitjelma area. Red boxes illustrate areas from which samples were collected. Garnet and biotite isograds are also shown.

3.2.2.1 Field relations

A summary of the major geological relationships follows and is illustrated in Figure 3.6 and Figure 3.7. The oldest unit in the area is the Skaiti Supergroup (Precambrian to Lower Palaeozoic; Westhead and Boyle 1995) consisting of metavolcanics and metasediments, into which the Sulitjelma Gabbro was intruded. The Hammeren ultrabasic harzburgites are deformed and tectonically emplaced but they are considered part of the same igneous sequence as the Sulitjelma Gabbro (Cooper et al. 1979). The majority of the gabbro preserves igneous textures and also some igneous mineralogy. Modal layering is also evident. However in some areas, particularly adjacent to the dyke complex in the Otervann area, the gabbro

has experienced deformation and formed a flaser structure. The flaser gabbro and dyke complex are collectively known as the Sulitjelma amphibolites. The existence of this zone of deformation and an apparent tectonic contact between the dyke complex and the gabbro has led to the suggestion that the Sulitjelma amphibolites and gabbro belonged to different tectonic units, namely the Vasten nappe and the Gasak nappe respectively (Kollung 1989). However, in the Mietjerpakte area the dyke complex and gabbro have a primary igneous relationship, with the former being intruded by the latter (Pedersen et al. 1991), but also with dykes intruding and enclosing parts of the gabbro (Boyle 1980). Furthermore, the dyke complex grades into the basic Otervann volcanic succession which includes layers with unambiguous pillow structures.

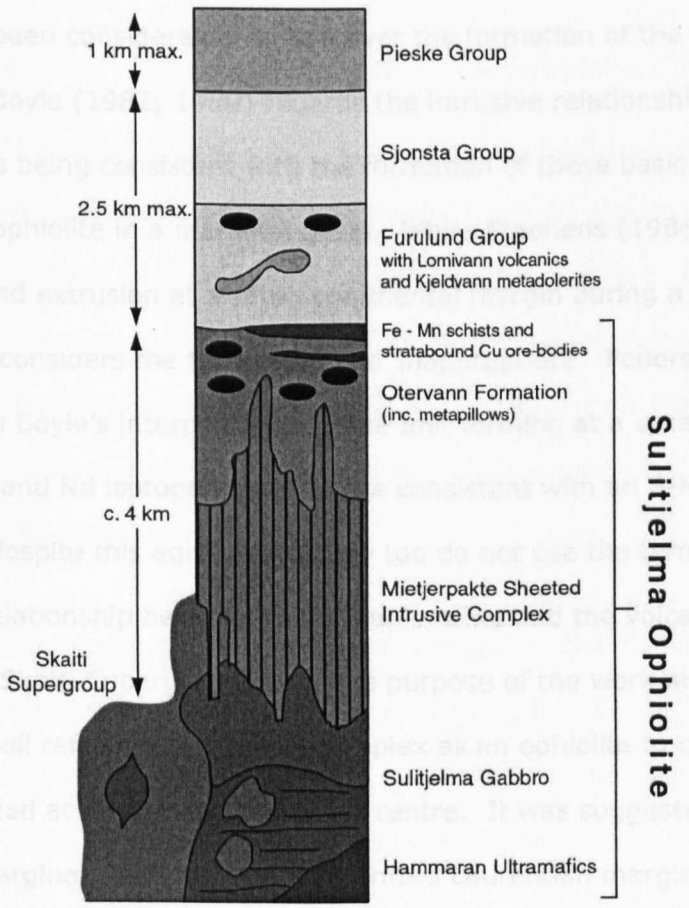

Figure 3.7. Stylised log section illustrating the inferred primary igneous relationships between the units, after Boyle (1989).

In summary, the Sulitjelma igneous complex comprises the Hammeren Ultrabasics, Sulitjelma Gabbro, flaser gabbro, Mietjerpakte dyke complex and the Otervann basic volcanics (including pillow lavas). This sequence is stratigraphically overlain by the Furulund and Sjonsta Group which consist of metasediments and less voluminous meta-igneous rocks. The main sedimentary types of the Furulund group are metamorphosed graphitic shales and calcareous greywackes and represent flysch-like deposits (Boyle and Westhead 1992). The Furulund unit contains the MORB-like Kjeldvann metadolerites and, in the upper part, the Lomivann volcanics, which have some calc-alkaline geochemical affinities indicative of formation in a back-arc setting.

3.2.2.2 Origin

There has been considerable debate over the formation of the Sulitjelma igneous complex. Boyle (1982; 1989) regards the intrusive relationships and geochemical evidence as being consistent with the formation of these basic igneous rocks as part of an ophiolite in a marginal basin. While Stephens (1986) agrees with their intrusion and extrusion at a rifted continental margin during a "major extensional event", he considers the term 'ophiolite' inappropriate. Pederson et al (1991) concur with Boyle's interpretation of the unit forming at a spreading centre and present Sr and Nd isotope data that are consistent with an E-MORB-like protolith. However, despite this agreement, they too do not use the term *ophiolite* due to the intrusive relationship between the plutonic rocks and the volcano-sedimentary sequence (Skaiti Supergroup). For the purpose of the work presented in this thesis, I shall refer to the igneous complex as an ophiolite to convey the point that it was formed at an oceanic spreading centre. It was suggested by Boyle (1989) that the marginal basin formed at the rifted Laurentian margin of the Iapetus Ocean, and was separated from the latter by a volcanic arc system. Their trace element data, in particular the negative Nb anomalies which they display, suggest formation in the initial stages of back-arc spreading. The Furulund and Sjonsta

Groups are considered to represent the infill of this marginal basin, and the meta-igneous rocks which they contain (Lomivann Volcanics) illustrate the progression from MORB-type magmatism to that which has a distinctly back-arc signature.

Crystallisation age. Zircons and titanite from the ophiolite have been dated, using the conventional dissolution U-Pb technique, at 437 ± 2 Ma (Pedersen et al. 1991). This date is interpreted to be the age of magmatic crystallisation, and corresponds well with a conventional dissolution zircon age of 443 ± 3 Ma for the Solund-Stavfjord ophiolite of western Norway (Dunning and Pedersen 1988). The coincidence of these ages for spreading-related magmatism, suggests that the margin of the Iapetus experienced considerable extension at this time and resulted in the formation of marginal basins.

3.2.2.3 Emplacement and metamorphism.

The ophiolite and associated units were obducted and emplaced onto the margin of Baltica shortly after their formation, during the Scandian phase of the Caledonian orogeny (420-440 Ma) (Roberts and Sturt 1980). During emplacement, overshearing in an easterly direction resulted in the formation of what has been termed the Sulitjelma fold-nappe (Burton et al. 1989). The section exposed in the Sulitjelma region represents the lower, overturned limb of this nappe, and thus the sequence is inverted.

The metamorphic history experienced by the ophiolite has been inferred from the study of the stratigraphically overlying Furulund group (Boyle and Westhead 1992). Metamorphic isograds have been mapped out over the area by various workers, using mineral assemblages in metasedimentary rocks from the Furulund group and also layers within the ophiolitic rocks themselves (see Figure 3.6). It is apparent from this work that there is an overall increase in metamorphic grade from east to west across the area. Burton and O'Nions (1992) published peak metamorphic

conditions of 458 ± 20°C and 6.5 ± 1.0 kbar (0.65 GPa) for a sample in the east of the area shown in Figure 3.6 (A73). This sample derives from a unit near the base of the Furulund group (and therefore directly above the Otervann volcanics), and is situated near the garnet isograd between the village of Otervann and the peak of Mietjerpakte. Pressures and temperatures of samples from further west (e.g. 70954), lying in the garnet/kyanite zone have been estimated to be approximately 8 kbar (0.8 GPa) and 500-550°C by Boyle and Westhead (1992). All the metabasaltic and metagabbroic samples analysed and presented in this thesis lie in the biotite, garnet and kyanite zones and most have been collected from the area lying between samples A73 and 70954 (shown by the large red rectangle in Figure 3.6), while the Lomivann volcanics were collected from the small red rectangle in the southern portion of the map. Several metagabbros were sampled in the areas to the east and north of the Sulitjelmaisen ice cap (the three small red rectangles marked). The peak conditions of their metamorphism falls between the values stated above, and increases from east to west. The analysis of these samples has allowed an assessment of Re-Os systematics during the prograde metamorphism of basic oceanic crustal rocks.

The age of metamorphism has been estimated by Burton and O'Nions (1992). Sample A73 contains the assemblage: garnet + amphibole + biotite + chalcopyrite, and these minerals have been analysed using both the U-Pb and the Sm-Nd systems. The resulting regression lines correspond to ages of 432.1 ± 1.5 Ma (U-Pb) and 432.9 ± 1.8 Ma (Sm-Nd).

3.3 Petrography and mineralogy of the Zermatt-Saas ophiolite (ZSO) – Allalin gabbro and Pfulwe metabasalts

A suite of formerly gabbroic samples from the Allalin gabbro has been analysed, encompassing the range from almost entirely unmetamorphosed gabbros to completely recrystallised eclogites. Due to the inaccessibility of much of the Allalin unit, many of the samples were collected from the terminal moraine of the Hohlaub- and Allalin-gletschers close to Mattmark, as well as from the lateral moraines at the foot of the Allalinhorn. Coronitic samples were also collected from the ridge at G.R. 6372 1001. In addition to these samples, a number of metabasaltic eclogites have been analysed which were collected from Pfulwe (G.R. 6315 0962) and Täschalp, east of Zermatt. The easily identifiable pillow lava structures at the former locality allowed sampling from both pillow cores and rims. Figure 3.3 marks all the locations from which samples were collected. The main three sampling areas are marked by blue boxes, from west to east these are: Pfulwe, the eastern extremity of the Allalinhorn, and the terminal moraine near Mattmark.

3.3.1 Allalin Gabbro

The entire Allalin gabbro, as part of the Zermatt-Saas zone, has experienced very high pressures and temperatures during partial subduction and the subsequent Alpine collision (see Section 3.2.1.4 and Section 3.4). However, the assemblages in the unit vary markedly and display an apparent difference in metamorphic grade. The assemblages form a range which represents almost entirely unaltered gabbro (which has been preserved in a metastable state, despite the metamorphic conditions it has experienced), seafloor metamorphism, the subsequent very HP eclogite facies event, and retrogression under blueschist and greenschist facies conditions. Furthermore, there is mineralogical variety *within* the high-pressure assemblages as a result of equilibration at different points on the PT path. The

great variety of assemblages is characterised thoroughly in the PhD thesis of Meyer (1983b) which examines the petrology of the Allalin Gabbro, and should be a reference point for those wishing to examine the rocks of the Allalin in more detail. The occurrence of two metamorphic recrystallisation episodes complicates the ultimate mineralogy and petrography of these rocks – requiring the need for the effects of seafloor and subduction metamorphism to be unravelled and separated.

Several samples were collected which display both unaltered gabbro and partial seafloor metamorphism/eclogite recrystallisation within the same hand specimen (Figure 3.8) (S01/5, S02/10iiix, S02/83viiix). In these cases, the samples have been split and analysed separately with the added notation of G for gabbro and T for transitional. The crystallisation front (marked as a blue dashed line in Figure 3.8) is reminiscent of a fluid percolation boundary, suggesting that the presence or absence of fluid may control the extent of metamorphic recrystallisation. Fluid flow at high pressures in the Allalin Gabbro is evident through veins containing garnet and occasionally omphacite, actinolite, talc, chlorite and carbonate.

Other samples were chosen that represent both ends of the metamorphic spectrum: those which contain only igneous mineralogy (Figure 3.9a), and those which have been entirely recrystallised under eclogite-facies conditions (Figure 3.9d, e & f). Blueschist retrogression is evident in some samples (S02/84viix and S02/84viiix), by the presence of abundant glaucophane in the matrix (Figure 3.9g). Further retrogression at lower grades is rare in the gabbroic eclogites. However, some samples have undergone more extensive retrogression at upper-greenschist facies conditions, and this is accompanied by fairly pervasive deformation (Figure 3.9h shows a moderately deformed retrogressed sample).

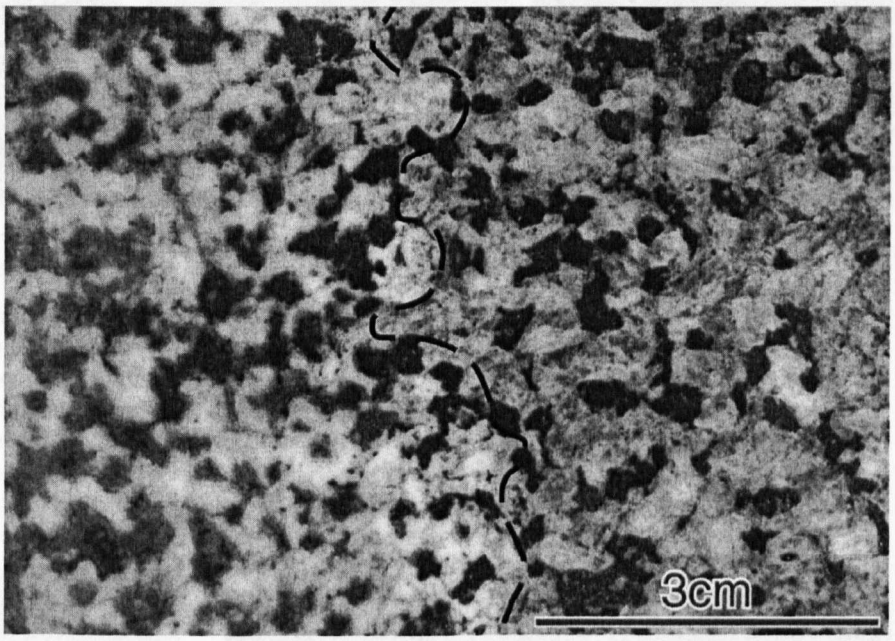

Figure 3.8. The gabbro-eclogite transition preserved within a single sample (S01/5G and T). The right-hand portion of the photo contains unaltered igneous mineralogy. The crystallisation front (marked as a blue dashed line) is suggestive of fluid controlled recrystallisation - with the growth of metamorphic minerals (including some hydrous phases) only occurring on the left-hand side. Also note the high-pressure veins containing garnet and omphacite, on the left-hand side.

Some such samples have been analysed (see *Other Allalin metagabbros* below) but the data must be treated with caution because any geochemical changes observed may represent the effects of retrogression during exhumation as well as prograde metamorphism during subduction.

Table 3.1 summarises the mineralogy of the main Allalin lithologies (both igneous and metamorphic), together with metabasaltic eclogites from Pfulwe. Representative mineral analyses for gabbro, transitional samples and gabbroic eclogites are presented in Table 3.2, Table 3.3 and Table 3.4 respectively.

3.3.1.1 Olivine Gabbro

As previously mentioned, some gabbro with minimal recrystallisation can be found in the Allalin unit. These samples have not been affected by seafloor hydrothermal alteration, and they have been preserved, in a metastable state, through very HP

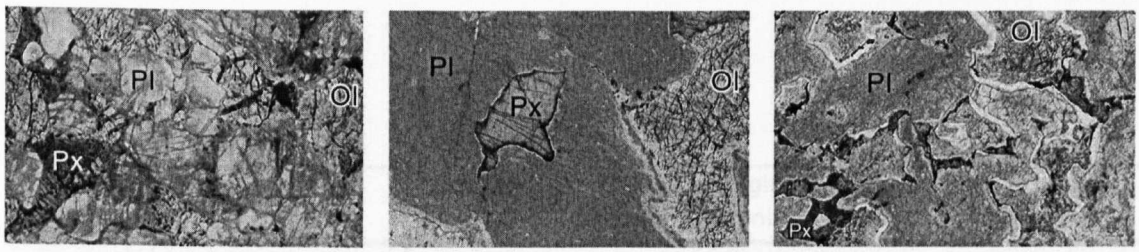

Magmatic textures and mineralogy with increasing recrystallisation, left to right.

A: the only phase to exhibit recrystallisation is the plagioclase, which is turbid in parts. **B:** the plagioclase has largely been replaced by a fine grained 'saussurite' assemblage: zoisite, omphacite/jadeite, ± kyanite, ± quartz. Olivine has begun to break down to chlorite. Augite is almost unaffected. A discontinuous garnet corona is present between the olivine and plagioclase magmatic domains. **C:** olivine relicts exist at the cores of olivine domains, but the outer parts have recrystallised to coronas of enstatite and chlorite, a result, primarily, of sea floor metamorphism. The plagioclase domains are now composed of a coarser grained saussurite. Augite has not undergone recrystallisation. Extensive garnet coronas have formed between plagioclase and olivine domains.

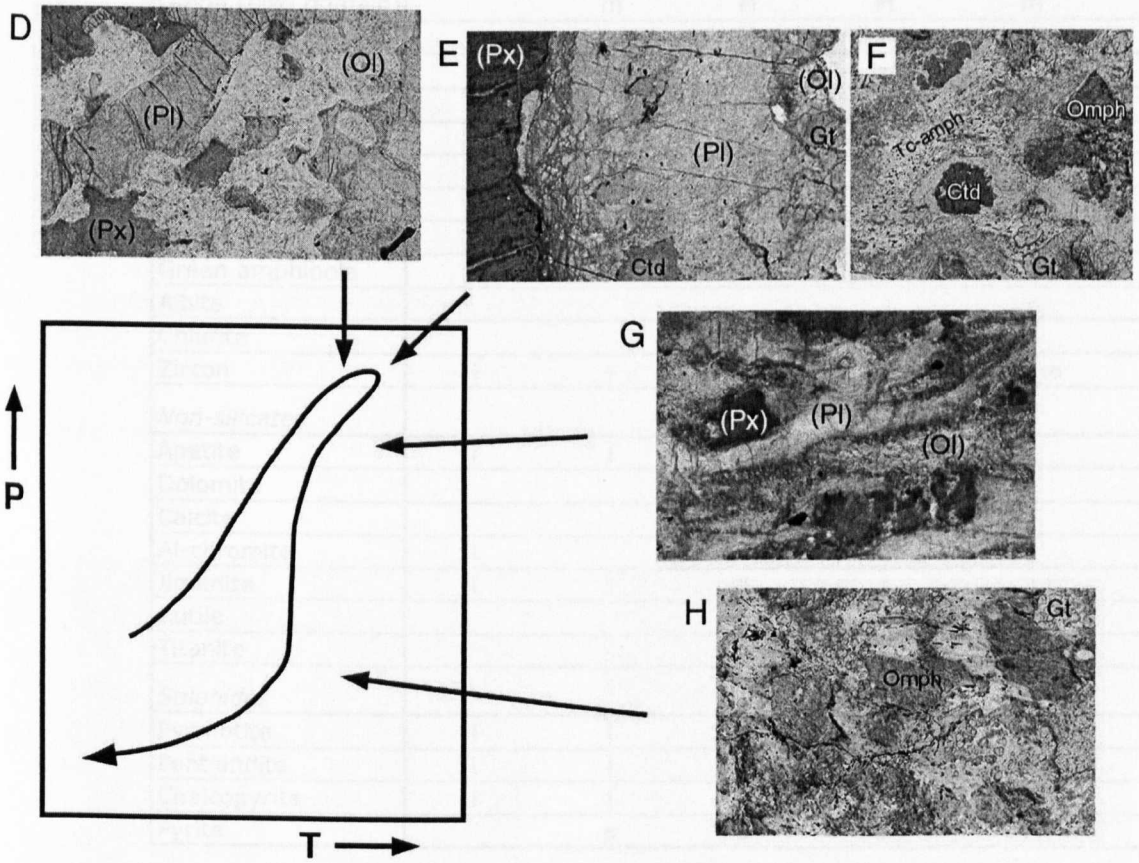

Metamorphic mineralogy and textures displayed by the Allalin gabbro. Field relations indicate all rocks have experienced the same metamorphic history. However, the metamorphic mineralogy and extent of deformation varies markedly. P-T path is purely schematic (see Meyer 1983b for a more precise assessment).

D clearly preserves magmatic domains but complete recrystallisation has occurred. In **E** & **F**, garnet coronas have developed further, growing into the surrounding domains. Chloritoid (grey/blue) is also a major phase. **G** displays abundant glaucophane in the matrix, indicating blueschist facies retrogression, accompanied by deformation. Greenschist facies retrogression is shown in **H**. Garnet has partially broken down to chlorite, Cr-omphacite has been replaced, in part, by green amphibole.

Figure 3.9. Illustration of the progressive stages of recrystallisation of the Allalin gabbro at different pressure and temperature conditions.

Mineral	Gabbro	Transitional gabbro	Eclogitic coronite	Gabbroic eclogite	Retrogressed metagabbro	Metabasalt
Silicates						
Chrysolitic Olivine	I	i				
Augite	I	I				
Plag (Labrad.)	I					
Chlorite		S	s			
Enstatite		S				
Garnet	m	M	M	M	M	M
Zoisite		M	M	M	M	M
Talc			M	M	m	
Glaucophane/actin.			M	M		M
Omph (plag domain)		m	M	M	m	M
Omph (cpx domain)			M	M	M	
Kyanite		m	m	m		
Paragonite				m	M	M
Phengite						M
Quartz		m?	m	m	m	
Chloritoid				M	M	
Epidote						M
Green amphibole					R	r
Albite					r	r
Chlorite				r	r	r
Zircon	i	i	i + m	i + m	i + m	i + m
Non-silicates						
Apatite	i	i	i?	i?	?	i + m?
Dolomite			m/s	m/s		m
Calcite			m/s	m/s		m
Al-chromite	i					
Ilmenite	i	i	i	i		
Rutile			m	m		m
Titanite					r	r
Sulphides						
Pyrrhotite	i	i	i	i	n.k.	n.k.
Pentlandite	i	i	i	?	n.k.	n.k.
Chalcopyrite	i	i	i	i	n.k.	n.k.
Pyrite		s	*s*	*s*	n.k.	n.k.

Table 3.1. Mineral assemblages of the rocks of the Allalin Gabbro and the Pfulwe metabasaltic eclogites. Zircon, dolomite and calcite not found in the Allalin Gabbro in this study, but presence of zircon confirmed by Rubatto et al. (1998) and dolomite and calcite by Barnicoat (1996). Capital letter denotes major constituent. Lower case denotes minor component. I = Igneous crystallisation (black), S = Seafloor metamorphism (blue), M = HP metamorphic crystallisation (red), R = Greenschist retrograde metamorphism (green), n.k. - not known.

metamorphism (this is discussed further in Section 3.3.3). There are three major phases: chrysolitic olivine (Fo_{80-85}), Mg-rich augite (also often Cr and Ti rich) and labradoritic plagioclase ($\sim An_{60}$) (see Figure 3.10). Bytownite plagioclase compositions occur in some samples (An_{75-80}). The Allalin gabbro is a layered igneous intrusion (Meyer 1983b; this study), and thus samples vary in their mineralogical proportions. The olivine abundance, in different samples sectioned, ranges from as little as 5% (S02/83viix) to approximately 35% (S01/5G). Similarly, augite can vary even more markedly from <5% (S01/5G) to as much as 60% (S01/30iiix). Plagioclase abundance is somewhat more consistent and has a range between ~50% and ~70%. Olivine and plagioclase are both coarse grained in all sections (>3mm) and appear to have crystallised first. The former has grown in the form of roughly equidimensional crystals while plagioclase forms interlocking masses of coarse crystals. The pyroxene, by contrast, has an interstitial habit. Even in samples where pyroxene is relatively abundant, its habit is anhedral and it has clearly grown later than the olivine and plagioclase. However, very large (several cm), subhedral pyroxenes do occur in certain layers.

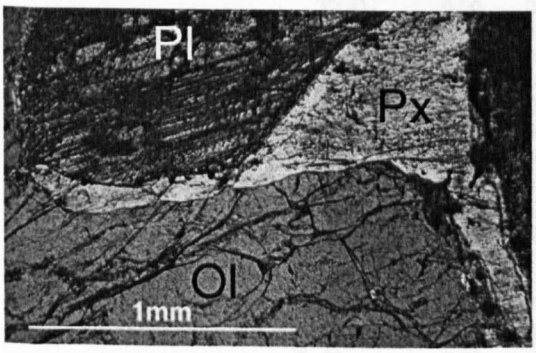

Figure 3.10. Pristine magmatic mineralogy of plagioclase, olivine and augite (Px). There is no evidence of metamorphism.

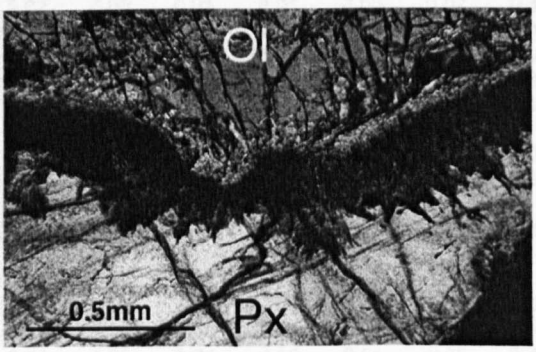

Figure 3.11. The interface between olivine (Ol) and augite shown in a thick-cut section. Unusually, in this case the pyroxene appears to be have recrystallised (perhaps as omphacite) to a greater extent than the olivine.

		Silicates and oxides						Sulphides		
		Ol	Aug	Pl(Lab)	Al-Chr	Ilm		Po	Pn	Cp
Wt %	SiO_2	39.63	50.07	51.44	0.05	0.14	S	36.53	32.48	34.81
	TiO_2	0.01	1.65	0.09	1.37	52.26	Fe	63.29	40.51	30.82
	Al_2O_3	0.01	4.90	30.11	23.91	0.16	Co	0.04	1.62	0.01
	Cr_2O_3	0.00	0.92	0.00	30.01	0.71	Ni	0.03	25.69	0.02
	MgO	43.85	15.21	0.00	2.61	1.56	Zn	0.00	0.00	0.00
	CaO	0.03	21.22	13.01	0.01	0.11	Cu	0.00	0.07	32.70
	MnO	0.24	0.15	0.00	0.56	0.26	Cr	0.01	0.02	0.00
	FeO	15.77	4.40	0.22	41.23	44.78				
	Fe_2O_3	-	-	-	-	-				
	Na_2O	0.03	0.81	4.29	0.00	0.00				
	K_2O	-	0.00	0.06	0.00	0.00				
	H_2O	-	-	-	-	-				
	Total	99.56	99.33	99.22	99.75	99.98	Total	99.89	100.39	98.37
	No. of O	4	6	8	4	3	No. of S	8	8	2
Ions per formula unit	Si	1.00	1.84	2.36	0.00	0.00	S	8.03	7.82	2.02
	Ti	0.00	0.05	0.00	0.03	0.98	Fe	7.98	5.60	1.03
	Al	0.00	0.21	1.63	0.95	0.00	Ni	0.00	0.21	0.00
	Cr	0.00	0.03	0.00	0.80	0.01	Co	0.00	3.38	0.00
	Mg	1.65	0.83	0.00	0.13	0.06	Cu	0.00	0.00	0.00
	Ca	0.00	0.83	0.64	0.00	0.00	Cr	0.00	0.01	0.96
	Mn	0.01	0.01	0.00	0.02	0.01		0.00	0.00	0.00
	Fe^{2+}	0.33	0.05	0.01	0.93	0.92		0.00	0.00	0.00
	Fe^{3+}	-	0.09	-	0.23	0.02				
	Na	0.00	0.06	0.38	0.00	0.00				
	K	-	0.00	0.00	0.00	0.00				
	Total	3.00	4.00	5.02	3.09	2.01	Total	16.02	17.02	4.01

Table 3.2. Representative magmatic mineral analyses for the Allalin gabbro (no recrystallisation). For key to abbreviations see Table 3.4.

		Silicates and oxides								
		En	Ath	Tr	Chl	Tlc	Grt	Omp	Zo	Rt
Wt %	SiO_2	57.68	55.27	56.83	32.26	61.90	38.51	56.83	41.97	0.09
	TiO_2	0.00	0.01	0.05	0.03	0.01	0.07	0.06	0.04	99.76
	Al_2O_3	0.05	1.01	1.68	19.14	1.62	22.07	12.30	31.54	0.02
	Cr_2O_3	0.00	0.00	0.02	0.00	0.01	0.01	0.00	0.02	0.37
	MgO	33.09	31.60	22.78	31.30	27.49	4.79	8.73	0.03	0.03
	CaO	0.04	0.05	12.90	0.02	0.02	11.85	13.29	21.98	0.01
	MnO	0.07	0.10	0.05	0.01	0.00	0.43	0.01	0.00	0.00
	FeO	8.74	0.74	0.95	3.84	2.96	22.09	1.90	0.48	0.10
	Fe_2O_3	-	9.67	1.56	-	-	0.00	-	-	-
	Na_2O	0.01	0.02	0.67	0.01	0.75	0.02	7.33	1.05	0.02
	K_2O	0.00	0.00	0.02	0.02	0.00	0.00	0.00	0.02	0.00
	H_2O	-	2.23	2.19	-	4.66	-	-	-	-
	Total	99.67	100.69	99.69	86.61	99.42	99.83	100.44	97.14	100.40
	No. of O	6	23	23	28	22	12	6	12.5	2
Ions per formula unit	Si	2.01	7.43	7.79	6.09	7.97	2.98	1.99	3.18	0.00
	Ti	0.00	0.16	0.27	0.00	0.00	0.00	0.00	0.00	0.99
	Al	0.00	0.00	0.01	4.25	0.24	2.02	0.51	2.82	0.00
	Cr	0.00	0.00	0.00	0.00	0.00	0.00	0.01	0.00	0.00
	Mg	1.72	6.33	4.66	8.80	5.28	0.55	0.45	0.00	0.00
	Ca	0.00	0.01	1.90	0.00	0.00	0.98	0.50	1.79	0.00
	Mn	0.00	0.01	0.01	0.00	0.00	0.03	0.00	0.00	0.00
	Fe^{2+}	0.25	0.08	0.11	0.61	0.32	1.43	0.04	0.03	0.00
	Fe^{3+}	-	0.98	0.16	-	-	0.00	0.01	-	-
	Na	0.00	0.00	0.18	0.00	0.19	0.00	0.50	0.15	0.00
	K	0.00	0.00	0.00	0.00	0.00	0.00	0.00	0.00	0.00
	Total	3.99	15.00	15.08	19.77	14.00	8.00	4.01	7.98	1.00

Table 3.3. Representative mineral analyses for the transitional samples. For relict igneous phases and sulphides see Table 3.2. For key to abbreviations see Table 3.4.

	Silicates and oxides											Sulphides		
	Grt	Omp	Gln	Tr	Tlc	Zo	Pg	Cld	Ky	Rt		Py	Po	Cp
SiO_2	37.99	56.07	58.58	56.83	61.90	39.26	47.00	25.98	36.26	0.09	S	53.18	38.92	34.99
TiO_2	0.05	0.03	0.01	0.05	0.01	0.04	0.04	0.01	0.00	99.76	Fe	46.55	60.06	30.71
Al_2O_3	21.69	10.89	12.39	1.68	1.62	32.13	39.55	43.33	61.57	0.02	Co	0.66	0.06	0.02
Cr_2O_3	0.01	0.11	0.01	0.02	0.01	0.00	0.07	0.01	0.01	0.37	Ni	0.00	0.65	0.01
MgO	5.82	9.38	13.81	22.78	27.49	0.03	0.08	10.00	0.02	0.03	Zn	0.00	0.00	0.00
CaO	9.03	14.20	0.84	12.90	0.02	24.36	0.17	0.00	0.10	0.01	Cu	0.00	0.16	32.55
MnO	0.69	0.02	0.01	0.05	0.00	0.00	0.01	0.13	0.00	0.00	Cr	0.00	0.00	0.00
FeO	23.54	2.24	1.98	0.95	2.96	0.75	0.28	13.30	0.15	0.10				
Fe_2O_3	0.37	-	2.09	1.56	-	-	-	-	-	-				
Na_2O	0.03	6.84	7.27	0.67	0.75	0.14	7.53	0.01	0.01	0.02				
K_2O	0.00	0.00	0.01	0.02	0.00	0.00	0.36	0.00	0.00	0.00				
H_2O	-	-	2.24	2.19	-	-	4.69	-	-	-				
Total	99.22	99.77	99.24	99.69	94.76	96.71	99.78	92.77	98.12	100.40	Total	100.39	99.85	98.27
Wt %														
No.of O	12	6	23	23	22	12.5	22	12	5	2	No.of S	2	8	2
Si	2.97	1.98	7.88	7.79	7.97	3.02	5.98	2.01	1.00	0.00	S	1.99	7.91	2.03
Ti	0.00	0.00	0.00	0.27	0.00	0.00	0.00	0.00	0.00	0.99	Fe	1.00	7.00	1.02
Al	2.00	0.45	1.96	0.01	0.24	2.92	5.98	3.96	2.00	0.00	Co	0.01	0.01	0.00
Cr	0.00	0.00	0.00	0.00	0.00	0.00	0.00	0.00	0.00	0.00	Ni	0.00	0.07	0.00
Mg	0.68	0.49	2.77	4.66	5.28	0.00	0.06	1.16	0.00	0.00	Zn	0.00	0.00	0.00
Ca	0.76	0.54	0.12	1.90	0.00	2.01	0.03	0.00	0.00	0.00	Cu	0.00	0.02	0.95
Mn	0.05	0.00	0.00	0.01	0.00	0.00	0.00	0.01	0.00	0.00	Cr	0.00	0.00	0.00
Fe^{2+}	1.54	0.01	0.22	0.11	0.32	0.01	0.05	0.86	0.00	0.00				
Fe^{3+}	0.02	0.05	0.21	0.16	-	0.04	-	-						
Na	0.00	0.47	1.90	0.18	0.19	0.02	1.78	0.00	0.00	0.00				
K	0.00	0.00	0.00	0.00	0.00	0.00	0.07	0.00	0.00	0.00				
Total	8.02	4.00	15.06	15.08	14.00	8.02	13.95	8.01	3.00	1.00	Total	3.00	15.01	4.00
Ions per formula unit														

Table 3.4. Representative mineral analyses for a gabbroic eclogite.

Abbreviations from Kretz (1983): Ol - olivine, Aug - augite, Lab - labradorite, Al-Chr - aluminium chromite, Ilm - ilmenite. Po - pyrrhotite, Pn - pentlandite, Cp – chalcopyrite, Py - pyrite, En - enstatite, Ath - anthophyllite, Tr - tremolite, Chl - chlorite, Tc - talc, Gnt - garnet, Om - omphacite, Zo - zoisite, Gln - glaucophane, Pg - paragonite, Cld - chloritoid, Ky - kyanite, Rt - rutile.

In addition to the major phases, there are oxide and sulphide accessory phases, which constitute less than 2% of the rock. Al-chromite, ilmenite, pyrrhotite, pentlandite and very minor chalcopyrite were all present in most sections analysed.

The sulphides form small (<200μm) composite grains, at intra-granular sites within olivine crystals, and at grain boundaries both between two plagioclases and at the interfaces between different phases. Pyrrhotite is almost always present, together with either pentlandite, or more rarely, chalcopyrite. Olivine crystals have numerous tiny opaque inclusions (<2um) which lie along planes within the crystals (Figure 3.12). These may be sulphide, ilmenite or possibly chromite but they have proved impossible to identify due to their extremely small dimensions.

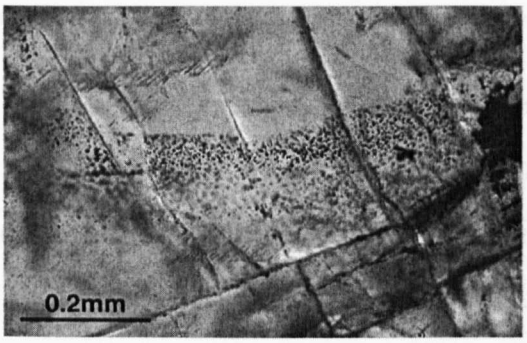

Figure 3.12. Opaque inclusions in olivine. These may be sulphide, ilmenite or Al-chromite.

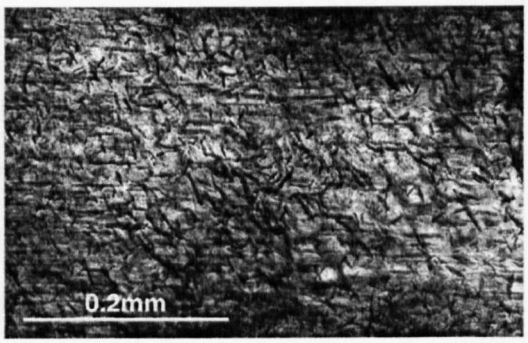

Figure 3.13. Tiny needles of (clino?)zoisite ± kyanite in labradoritic plagioclase (see text for discussion).

In samples showing least recrystallisation the only metamorphic mineral present forms tiny (20 x 2 μm) needles within plagioclase (Figure 3.13). The needles tend to grow in two orientations, at an angle approximately 70° to one another. The identity of this mineral cannot be conclusively determined petrographically or analytically by use of an electron microprobe, although from the evidence of further recrystallised samples it is very likely to be zoisite or clinozoisite ± kyanite. The identification of these inclusions as clinozoisite has been confirmed by the transmission electron microscopy of Wayte et al. (1989). That study concluded that during the initial, sub-microscopic stages of clinozoisite formation, there was only one preferred orientation for the crystals and that was as follows:

$$(100)_{Czo}//(101)_{Pl} \text{ and } [012]_{Czo}//[010]_{Pl}$$

Presumably the second orientation developed as the extent of crystallisation increased. It is interesting to note that this phase change probably requires the addition of small quantities of water to the anhydrous plagioclase - yet the clinozoisite forms intragranular needles with no obvious petrographic evidence for the infiltration of water into the cores of the plagioclase crystals. However, data given in Deer, Howie and Zussman's *Rock-forming minerals* (1992) actually show minor amounts of water in the composition of an anorthite crystal from a gabbro and very limited amounts of water (<1 wt%) in some zoisite compositions.

3.3.1.2 Transitional samples

Due to the variable manifestations of metamorphism in the Allalin gabbro it is possible to study a spatially distributed group of samples which span a broad range of metamorphic recrystallisation, and from this deduce a relative chronology of events and the progressive steps that developed during metamorphism. However, it is not clear whether a sample displaying blue- or greenschist-facies retrogression will have experienced all the previous steps of metamorphism, or whether the presence of greater fluid input close to peak P-T conditions and again during decompression led to relatively rapid complete recrystallisation, without the intervening steps outlined in this section and in Figure 3.9. Photo C (Figure 3.9) contains olivine domains which still retain relict magmatic olivine, while garnet coronas are comparatively well developed (up to 2 mm in thickness). This is in contrast to the sample in photo D (Figure 3.9) which displays much narrower garnet coronas. This would intuitively suggest a lesser extent of recrystallisation, but conversely all magmatic domains are now composed entirely of metamorphic mineralogy. Many of the petrographic textures and assemblages differ slightly from sample to sample and this suggests that it is unlikely that any one sample experienced precisely the same history of crystallisation that is spatially evident throughout the Allalin unit. This is despite the fact that the whole unit experienced the same *P-T* history. However, it is likely that completely recrystallised eclogites experienced an early introduction of water, perhaps during seafloor metamorphism, and this would have been accompanied by some recrystallisation. This cannot, however, be conclusively shown by petrographic studies due to subsequent pervasive recrystallisation of the eclogites. Moreover, the fact that some samples retain some of the seafloor metamorphic assemblage (e.g. enstatite and chlorite in the olivine site) without recrystallisation under peak P-T conditions is somewhat surprising. The evidence for infiltration of water into the eclogitic samples during low-pressure seafloor metamorphism is summarised in the following paragraphs.

High temperature sea-floor metamorphism is evident through both the sulphide mineralogy and oxygen isotope work published by Barnicoat and Cartwright (1997). This latter work observed a lower average $\delta^{18}O$ value in fully recrystallised eclogites than in gabbros with only partial recrystallisation. Barnicoat and Cartwright (1997) stated that these values are consistent with the occurrence of high-temperature alteration (>400°C, Stakes 1993) in the eclogitised samples. However, the spread of $\delta^{18}O$ values for the eclogites was large and some were in fact *higher* than the highest values measured for the partially altered gabbros. The authors suggest that these values may be the result of seafloor alteration at a lower temperature. The preservation of oxygen isotope values that are indicative of seafloor alteration, precludes significant 'flushing' of the gabbros by high-pressure fluids. This is consistent with the retention of metastable igneous assemblages. However, the loss of fluid derived from seafloor alteration / metamorphism, is not precluded.

Sulphides. An important distinction between the sulphide mineralogy of unaltered gabbro and that of the gabbroic eclogites is the predominance of pyrite in the latter lithology. Pyrrhotite and chalcopyrite are also present but much less abundant (pentlandite has not been found in this study). Conversely, pyrite has not been observed in gabbroic samples with little or no metamorphic recrystallisation. Furthermore, the sulphides in the gabbroic eclogites are considerably larger than their igneous counterparts, although less numerous. The sulphur content of eclogitic samples (average: ~100 ppm) is approximately half that of unaltered gabbro (~200 ppm) data, illustrating that despite the larger size of the sulphides in the eclogites, the metamorphosed samples actually contain less sulphide. These observations can be explained by the post-magmatic loss of a relatively nickel-rich, sulphurous fluid from recrystallised samples. The most likely setting for this loss is during hydrothermal seafloor alteration as suggested by Barnicoat and Cartwright (1997). The result of hydrothermal alteration, in this case, has been the reworking of sulphide, coupled with the loss of pentlandite and to a large extent, chalcopyrite.

When unravelling the metamorphic history of these samples, both the relatively high temperature/low pressure (HT/LP) and high pressure/low temperature (HP) events need to be considered. It is not petrographically clear whether the assemblages observed, particularly in the former olivine sites, are the result of LP/HT seafloor metamorphism or HP metamorphism with low rates of diffusion playing a key limiting role. This is discussed in more detail in this section and the following sections. A further, but perhaps more straightforward complication is that some samples display retrogressive recrystallisation under blueschist and/or greenschist-facies conditions.

Plagioclase. Plagioclase is the first of the major igneous phases to break down at HP - LT metamorphic conditions. In samples with <10% plagioclase recrystallisation, the initial product is zoisite, in the form of tiny, aligned needles (as discussed above). More advanced recrystallisation (~10% in plagioclase domains, usually along cracks and grain boundaries) occurs via the reaction:

$$\text{labradorite} + H_2O = \text{zoisite} + \text{kyanite} + \text{quartz} + (NaSiCa_{-1}Al_{-1})_{Pl} \qquad \text{(R1)}$$

(Wayte et al. 1989)

whereby the plagioclase composition becomes more sodic (albitic) as the reaction progresses (Wayte et al. 1989; this study). After a greater extent of reaction, with approximately 50% plagioclase remaining, the metamorphic assemblage is the same but the crystals are now randomly orientated. Eventually, when recrystallisation is almost complete (only 10-20% plagioclase (Wayte et al. 1989)), jadeite is found, together with zoisite, kyanite and quartz. In samples where recrystallisation of the plagioclase has continued to completion, the igneous precursor has been completely replaced by a very fine grained, turbid, randomly orientated assemblage of zoisite + clinopyroxene (now generally omphacitic, illustrating influx of Fe and Mg into the plagioclase domain) + kyanite + quartz. This assemblage is termed 'saussurite' and becomes coarser grained as the extent of recrystallisation increases.

Wayte et al. (1989) pointed out that if equilibrium were maintained throughout the breakdown of plagioclase, then the products would depend only upon the final P-T conditions reached (given sufficient water activities). This is contrary to the observed assemblages that, despite pressures of over 2.0 GPa, contain both jadeite and plagioclase of varying composition. It is also clear that in order to retain large proportions of relict labradoritic plagioclase, there must have been a large extent of overstepping on some reactions (metastability) and this is not consistent with an equilibrium model. Therefore Wayte et al. (1989) suggested two possible disequilibrium models.

The first involves a single stage reaction, whereby the plagioclase exists metastably until pressures exceed 17 kbar (1.7 GPa) and overstep the jadeite-forming reaction (resulting in the assemblage: jadeite + kyanite + zoisite + quartz). The extent of reaction would have been strongly controlled by water movement along grain boundaries and fractures, so that in core regions of crystals, reaction would have been minimal. The activation energies for nucleation of jadeite, kyanite and quartz may have been too high in these areas for these phases to form. In regions where only jadeite failed to crystallise (R1), the extent of reaction may have been controlled by the rate of NaSi – CaAl diffusion in the plagioclase. This can be extremely slow at the temperatures involved (Wayte et al. 1989 extrapolated from diffusion at 900-1100°C of Yund (1986)).

The second model involves a multi-stage reaction, whereby several pulses of infiltration of water occurred at various pressures on the prograde path. This would have resulted in a limited amount of crystallisation at that pressure, dependent on fluid availability. Equilibrium may have been attained within each small zone where reaction took place. If this model is realistic, the existence of regions with mineralogy corresponding to lower pressure conditions (e.g. zo + ky + qtz + pl) suggests that later reaction, at higher pressures, was limited to areas which had

not previously undergone any reaction. This is possible as there would be a greater degree of overstepping of the stability fields of anorthite compared to those of the phases in previously reacted areas. Again, the rate of NaSi – CaAl diffusion may have been a limiting factor for reaction, particularly once recrystallisation had commenced and a greater density of grain boundaries existed, along which transport of ions could take place. In the case of equilibrium reaction (R1) or the second, multi-stage, reaction outlined above, Wayte et al (1989) calculated that the slow rate of NaSi – CaAl diffusion would severely limit the extent of reaction in settings where the subduction rate was rapid. In such cases, pressures would exceed 17 kbar before extensive recrystallisation had occurred.

What is clear, irrespective of the model used, is that the extent of reaction and distribution of more recrystallised zones along cracks and grain boundaries suggests that reaction was controlled by the infiltration of fluid (e.g. Figure 3.21). However, these sites would also provide a greater number of nucleation sites such that the kinetic 'hurdle' may have been lower. On balance it seems necessary to invoke the infiltration of at least a small amount of fluid – particularly as reaction R1 requires the addition of water. For a further discussion of the role of kinetics in reactions of this type see Rubie (1990; 1998) and references therein.

The oxygen isotope data of Barnicoat and Cartwright (1997) suggest a single, earlier introduction of fluid during seafloor metamorphism. This appears to contradict the evidence of reaction, particularly in the plagioclase sites. However, it could be envisaged that most of the water was consumed in hydration reactions within the olivine sites, producing abundant chlorite and sometimes anthophyllite. The transformation during prograde metamorphism from a dominant olivine domain assemblage of enstatite + chlorite to glaucophane + talc would have led to lower water contents in the olivine domains, perhaps leading to fluid influx into the plagioclase domains. The petrographic evidence would suggest that this reaction

did not occur progressively over a large range of P-T conditions (there are few samples which contain chlorite, glaucophane and talc, and no recognisable reaction textures indicating breakdown of chlorite and formation of glaucophane/talc). This supports the model of a single stage reaction triggered by the occurrence, during the very high pressure stage, of an episode of water influx into metastable labradorite domains. A remaining question, however, is whether it is reasonable to assume that no significant alteration of plagioclase occurred during the seafloor metamorphism, or whether there *was* reaction, but it has since been obliterated by recrystallisation at high pressure. One line of evidence to support the alteration of plagioclase at an early stage, is the need for this domain to supply aluminium to the olivine domain in order to produce chlorite (see under *Olivine* later in this section).

The plagioclase reaction products vary considerably in metagabbroic rocks, from different geographical areas, which have undergone little deformation. This variation seems to be dependent on several key factors: composition (of the whole rock, but probably also of the plagioclase), P-T conditions and water availability. An example from the Rocciavré Gabbro in the western Italian Alps illustrates the control of bulk composition. Pognante (1985) examined plagioclase domains from olivine gabbros and norites, and from Fe-Ti-rich gabbros, both of which have undergone the same peak metamorphic conditions (450 ± 50°C, 12-15 kbar (1.2-1.5 GPa)) . In the case of olivine gabbro, the plagioclase had broken down to zoisite + jadeite + quartz, whereas in the Fe-Ti-rich gabbros the reaction products were garnet + omphacite. The latter reaction requires a greater degree (and therefore faster rate) of element transfer between domains. Pognante suggested that the difference in bulk composition may affect the rates of diffusion, perhaps through differing oxygen fugacity.

Plagioclase domains within metagabbros from Flemsøy, Sunnmøre, western Norway, were found by Mørk (1985) to have reacted initially to sodic plagioclase and spinel and then, at a greater degree of recrystallisation, to almandine-rich garnet, Na-plagioclase and spinel, and eventually result in the assemblage garnet + omphacite. The production of grossular + kyanite + quartz + Na-plagioclase is given by Rubie (1990) as the equilibrium anhydrous reaction for the breakdown of calcic plagioclase. However, this reaction may require a high activation energy for nucleation. The introduction of Fe and Mg into the plagioclase domain may reduce the required activation energy and encourage growth of a Fe-Mg-Ca garnet as found in the metagabbros from Flemsøy. The temperatures experienced by the gabbros at Flemsøy are considerably higher than those of the western Alps. This may explain the development of garnet in these rocks and its absence *within* the plagioclase assemblage of the Allalin and Rocciavré units. The pseudosections produced by Rebay and Powell (2002), for rocks of this composition, confirm that garnet is only a stable part of the plagioclase domain assemblage at higher temperatures (>600°C).

Water availability will almost certainly also affect the resulting assemblage. At low temperatures (400-600°C), water will be required as a catalyst and when present will increase the stability of the products of the hydrous reaction (R1), as opposed to the anhydrous reaction involving garnet (Rubie 1990). Small quantities of water may be necessary as a catalyst for the anhydrous reaction also, but petrographic evidence from Flemsøy, Norway, suggests a lack of fluid infiltration into samples which retain igneous domains. Garnet is sometimes found along cracks and veins through the plagioclase domains in the Allalin metagabbros (e.g. Figure 3.21), indicating the catalytic role of fluid in the formation of different assemblages in the plagioclase domain. One major effect of fluid infiltration would be the increased supply of ions required for new mineral growth. This is achieved both by advection in the fluid flow and relatively rapid diffusion *through* the fluid. It is also likely that

the addition of significant amounts of magnesium and iron in these areas led to a reduced activation energy for nucleation of garnet, as discussed in the previous paragraph.

Rebay and Powell (2002) concluded that lawsonite would have been part of the stable plagioclase-domain assemblage in the latter stages of prograde metamorphism and at actual peak P-T conditions. Its stability in systems with this bulk composition is such that its breakdown to kyanite + clinozoisite + quartz would have occurred during the early stages of exhumation at around 20 kbar (2.0 GPa), and hence it would not been preserved in the assemblage. However, no relict lawsonite has been found and there is no petrographic evidence in the literature, or in this study, for the prior existence of lawsonite in the assemblages of the Allalin Gabbro (this work; Meyer 1983b; Wayte et al. 1989). While Rebay and Powell state that on the grounds of mineral equilibria, 'the original presence of lawsonite is hard to avoid', and suggest that the fine grained nature of the plagioclase sites makes identification difficult, the variably recrystallised samples studied by Wayte et al. (1989) using TEM (transmission electron microscopy) do not contain lawsonite, or evidence of its prior existence. The lack of sufficient water within the plagioclase domain may have been a barrier to the crystallisation of lawsonite, resulting in the disequilibrium models of Wayte et al. (1989) which have been outlined above.

Olivine. In samples with partially to completely recrystallised plagioclase, olivine has also undergone considerable recrystallisation (Figure 3.14), and commonly begins to break down around the grain boundaries and forms an outer corona of chlorite. Further into the domain enstatite crystallises, while a metastable core of largely unaltered olivine often remains at the centre. The recrystallisation of the olivine site is controlled by the availability of certain elements, otherwise an assemblage dominated by talc and amphibole would be present, as observed in

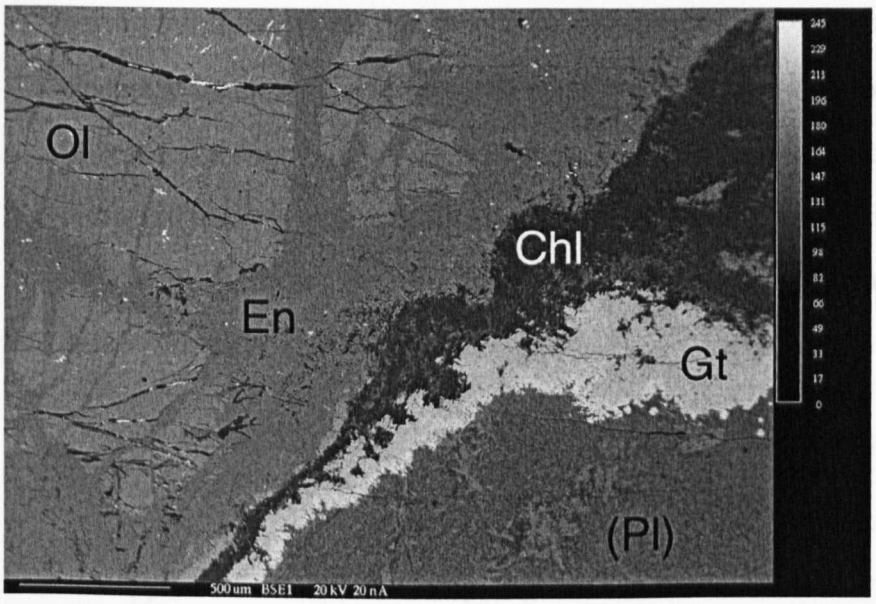

Figure 3.14. Backscattered electron image (BSE) of an olivine domain (left) containing relict olivine (top left) which has been partially recrystallised with zones of enstatite (mid grey, nearest to olivine relict) and chlorite (dark grey, outer zone). The entire domain is enveloped by a garnet corona (brightest region). Zoning, presumably of Fe composition, can be seen in the garnet corona which is brightest adjacent to the plagioclase domain (bottom right) – see discussion of coronas under *Gabbroic eclogites* below.

samples with greater recrystallisation. The transport of these elements is limited due to moderate temperatures, low fluid presence, and the lack of deformation. The transformation of olivine to chlorite, however, which would take place on thermodynamic grounds due to increased pressure, is dependent on the addition of aluminium and water to the otherwise Al-free olivine site. Therefore, the amount of chlorite formation is controlled by the extent of aluminium diffusion (and water infiltration) from the plagioclase domain into the olivine domain, either in the solid state or by intergranular fluid. The control by element availability on the extent and nature of transformations is evident in Figure 3.15.

It is not immediately apparent whether the chlorite/enstatite coronas observed are the result of limited seafloor metamorphism, or the result of very limited element exchange between domains at high pressure. The latter could result in an olivine domain chemistry which allows chlorite to remain stable in transitional samples, even at high pressures. However, from oxygen isotope data, elemental data and

petrographic evidence, it is almost certain that much of the recrystallisation of olivine to coronas of enstatite and chlorite ± anthophyllite took place during hydrous sea floor metamorphism, and not as a result of limited element availability during HP metamorphism. In this case, the assemblage of chlorite and enstatite in transitional samples has been preserved, in a metastable state, through HP metamorphism.

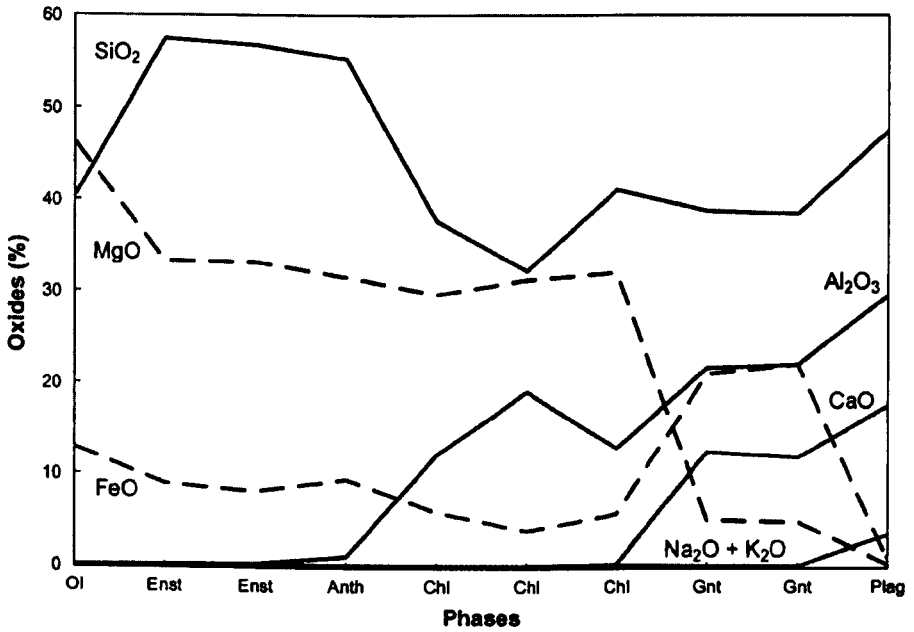

Figure 3.15. Electron microprobe traverse across an olivine domain, from relict olivine to relict plagioclase, illustrating the control of element availability (and therefore diffusion) on the products of reaction. This data suggests that mineral formation in the olivine site was controlled by Al and Ca availability (which would be dependent on diffusion or fluid assisted infiltration). The movement of Ca seems to have been particularly limited. Likewise, any new mineral formation in the plagioclase domain would have been limited by a lack of Mg.

Clinopyroxene. Augite is the last phase to be affected and can be preserved despite complete recrystallisation of the other two major phases. This apparent 'stability' during the transitional corona stage may be due to extremely slow diffusion of Ca and Al within clinopyroxene (Freer et al. 1982; Brady and McCallister 1983). Therefore, the recrystallisation of large grains over the timescales and temperatures of HP metamorphism is unlikely by lattice diffusion alone (Rubie 1990). Otten and Buseck (1987, cited in Rubie 1990) identified two reaction

mechanisms in an eclogitised metagabbro in the western Alps. The first is a topotactic mechanism operating at intracrystalline sites whereby sodic pyroxene is produced and orientated within the host augite. The second is a non-topotactic mechanism operating at grain boundaries – this produced randomly orientated crystals such as those seen in Figure 3.11. The former seems to be an important mechanism in Allalin rocks, with the reaction products being largely aligned with the long axis of the augite crystals (see Section 3.3.1.3).

Garnet is present in all but the least recrystallised samples, and forms coronas at the interfaces between olivine, augite and plagioclase pseudomorphs. The major element zoning of these coronas is discussed below in the *Gabbroic eclogites* section. Trace element zoning is addressed in Chapter 7. One consequence of the formation of garnet coronas is the shielding effect that they have between different igneous domains. It is the rate of exchange by diffusion or fluid transport through the corona that limits the rate of some of the reactions within the domains (e.g. chloritisation which requires aluminium from the plagioclase domain). However, much of the initial element transport may have occurred during seafloor metamorphism, almost certainly before any garnet corona was formed.

3.3.1.3 Gabbroic eclogites

The most pervasively recrystallised eclogites comprise omphacite, garnet (generally almandine-rich but of variable composition), glaucophane or actinolite, talc, zoisite, paragonite and chloritoid, with minor kyanite and quartz. One important difference between transitional coronitic samples and gabbroic eclogites is the approach to larger scale equilibria that is evident in the latter. Igneous mineral domains are no longer clearly zoned, and the compositions of phases throughout the sample show a much greater degree of similarity, despite their different structural positions. This is clear from the garnet compositions shown in Figure 3.18 and has also been noted by Chinner and Dixon (1973), for chloritoid from within and without the olivine site.

Plagioclase domains. The saussurite assemblage remains the predominant mineralogy for the ex-plagioclase domains throughout HP metamorphism and is only replaced at lower pressures by albite, epidote and quartz. However, chloritoid becomes an additional phase which appears to grow on both sides of garnet coronas at the interface between magmatic olivine and plagioclase domains (Figure 3.16). Paragonite also becomes more abundant as the saussurite becomes coarser grained, as high-pressure crystallisation continues. Meyer (1983b) concludes that this phase has grown during a second high-pressure crystallisation event which took place at slightly lower pressure conditions (~1.4-1.8 GPa, 500-550°C). The petrogenetic grids and pseudosections created by Carson et al. (1999) and Rebay and Powell (2002) (the latter is discussed below in Section 2.3.4) also indicate that crystallisation of paragonite will occur during the early stages of exhumation (~600°C, ≤ 2.0 GPa). As recrystallisation progresses, there is a marked increase in grain size within the plagioclase domain, although the average grain size still remains much smaller than that of the olivine domain. Figure 3.21 (backscattered electron (BSE) image) shows a garnet vein running through the saussurite assemblage of the plagioclase. It is only at these sites *within* the plagioclase domain that garnet crystallisation occurs, presumably because Mg and Fe are more readily available and the fluid may act as a catalyst for the reaction.

The importance of veins in the development of high-pressure minerals is also clear from Figure 3.8 where a transitional sample displays crystallisation of garnet along a vein. The presence of fluid was a crucial factor in promoting the gabbro to eclogite transformation. Furthermore, the presence of veining suggests the transport of elements over longer distances may be possible, which may have a bearing on the chemical signatures seen in these rocks.

Olivine domains. Olivine sites in the gabbroic eclogites are not clearly zoned and now comprise an assemblage which consists of varying proportions of talc, glaucophane/actinolite, chloritoid, kyanite and omphacite (Figure 3.16 and Figure

3.17), with talc and the Mg-rich amphibole being ever-present. Despite the lack of clear zoning, the Al-rich minerals chloritoid and kyanite are generally only found close to the margins of the olivine domain in samples which retain their coronitic structure. Chinner and Dixon (1973) suggested that the formation of kyanite was either the result of the breakdown of chlorite with the addition of silica (R2), or the result of interaction between olivine and a fluid saturated in zoisite and jadeite (R3):

$$\text{chlorite} + SiO_2 \rightarrow \text{talc} + \text{kyanite} + \text{chloritoid} + H_2O \quad \text{(R2)}$$

$$6\ \text{zoisite} + \text{olivine} + 12\ \text{jadeite} + \text{quartz} \rightarrow 9\ \text{kyanite} + 12\ \text{omphacite} + \text{talc} \quad \text{(R3)}$$

Chinner and Dixon postulated that the presence of a silica-rich fluid was unlikely and therefore deduced that insufficient quantities of kyanite would be produced by reaction 2. Reaction 3 assumes that olivine is still present as a relict phase prior to

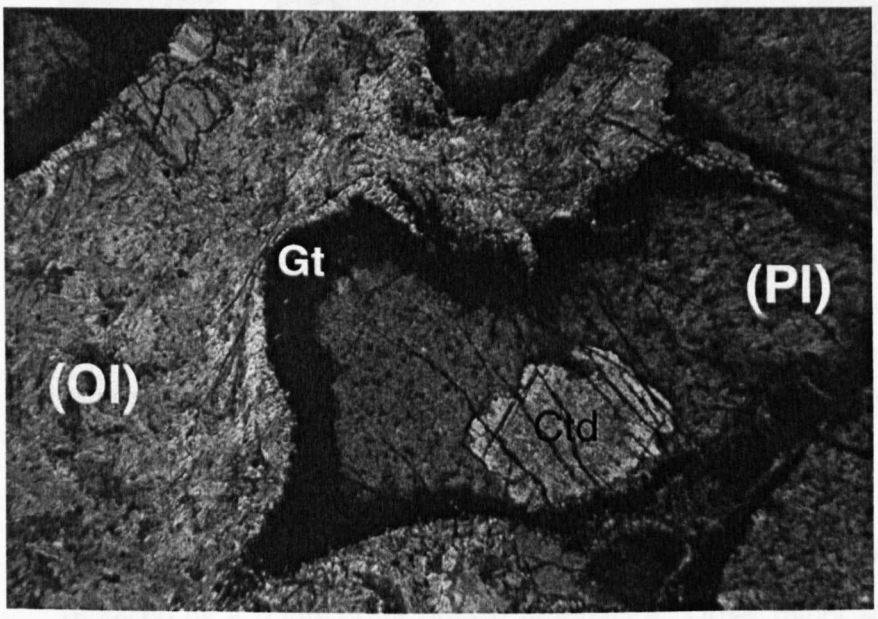

Figure 3.16. Sample S01/40viix. Olivine domains (Ol) are largely composed of talc and zones of saussurite pseudomorph the magmatic plagioclase sites (Pl). Chloritoid (Ctd) occurs as bright, twinned crystals (due to the 100μm thickness of the section), crystallising in both the olivine and plagioclase domains, where major element diffusion (Al from plagioclase, Mg + Fe from olivine) has been sufficient to facilitate its growth. The turbid mass on the bottom right is a recrystallised clinopyroxene with clearer overgrowths of omphacite.

the formation of kyanite. It seems more likely perhaps, on the basis of oxygen isotope data and kinetic arguments, that most of the olivine in samples which have undergone complete HP recrystallisation would have been affected by the transitional stage with the development of extensive chlorite coronas during seafloor metamorphism. Therefore, this would suggest that R2 is perhaps the more likely mechanism for the formation of kyanite within the olivine domains.

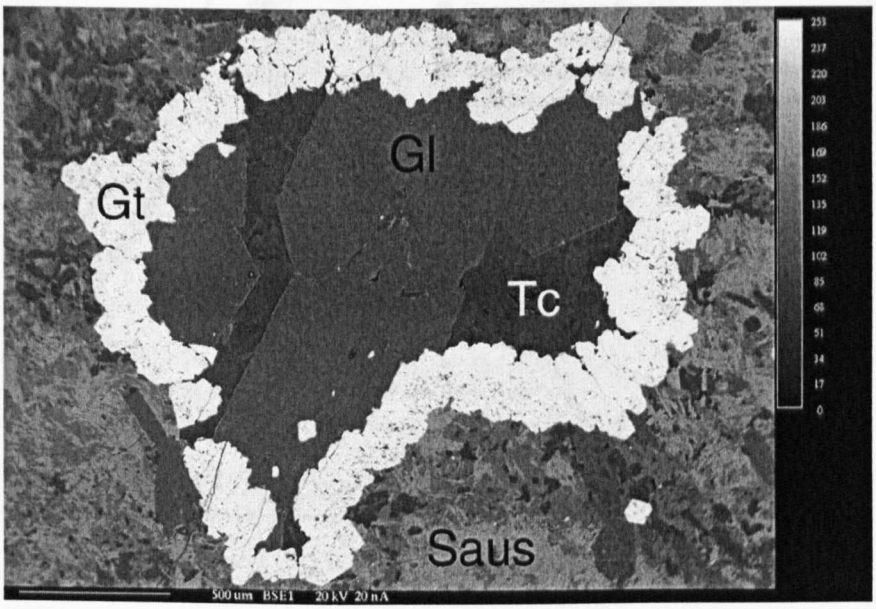

Figure 3.17. Backscattered electron image of a classic coronitic structure of a gabbroic eclogite (S01/3iix). Glaucophane and talc have replaced olivine (and possibly other phases from previous metamorphism, i.e. enstatite). The olivine domain is enclosed by the garnet corona. The surrounding matrix is the plagioclase domain and consists of the saussurite assemblage (Zo + Omp + Ky + Qtz ± Pg).

Clinopyroxene domains. Unlike plagioclase and olivine, pyroxene is largely replaced by a single other phase: omphacite. Other minor phases include talc and rutile. The compositions of all types of pyroxene from the Allalin gabbro are shown in Figure 3.18. The compositions of omphacite form a line on a trend between two end-members: igneous augite and a HP high jadeite clinopyroxene. The analyses from the most augitic part of this group tend to be from omphacite which has crystallised in the augite domain, whereas the more jadeitic compositions are from the plagioclase domain. The presence of a variety of compositions illustrates the

lack of equilibrium between domains, but there is, however, solid-solution across a range of compositions rather than two distinct groups, suggesting an approach to larger scale equilibrium.

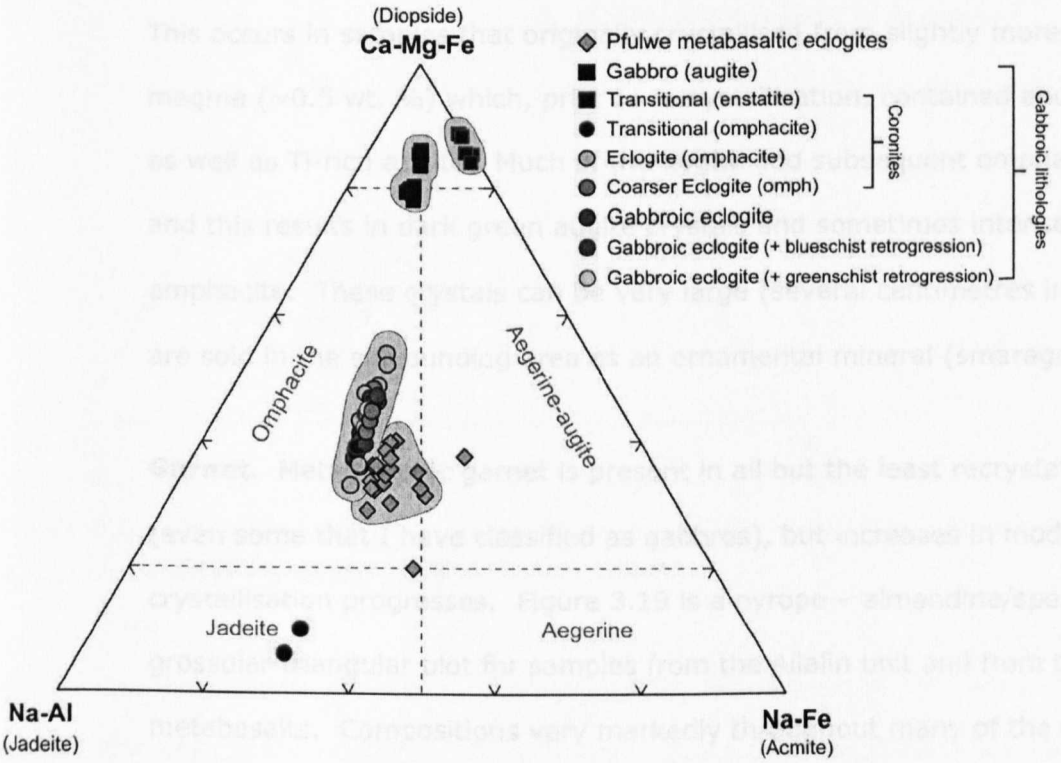

Figure 3.18. Triangular plot of pyroxene compositions for Allalin and metabasaltic samples in augite-jadeite-acmite space.

When omphacite crystallises, it does so with a strongly defined orientation with its long axis parallel to the host augite. In samples with complete reaction, the whole domain can appear to be a single large omphacite crystal due to the consistent extinction under crossed polars. The compositions of magmatic augite, where preserved, are quite Ti-rich (TiO_2 = 0.7-1.7 wt %), but following metamorphic recrystallisation, not all the titanium can be incorporated into the omphacite lattice (TiO_2 in omphacite = <0.1 wt %). As a result, numerous small rutile inclusions occur within the large mass of omphacite crystals. This is analogous to the breakdown of biotite to form chlorite, in which Ti cannot be incorporated (Henry and Guidott 2002). In general, these inclusions are elongate and aligned with the

long-axis of the omphacite crystals, perhaps nucleating, together with omphacite, along the [1 1 0] or [1 $\bar{1}$ 0] cleavage planes of the relict augite. Talc also forms in this orientation. Sometimes large masses of rutile exist around the edges of crystals (particularly omphacite) and can constitute several percent of the rock in parts. This occurs in samples that originally crystallised from slightly more titanium-rich magma (~0.5 wt. %) which, prior to recrystallisation, contained abundant ilmenite as well as Ti-rich augite. Much of the augite and subsequent omphacite is Cr-rich and this results in dark green augite crystals and sometimes intensely green Cr-omphacite. These crystals can be very large (several centimetres in length) and are sold in the surrounding area as an ornamental mineral (smaragdite).

Garnet. Metamorphic garnet is present in all but the least recrystallised samples (even some that I have classified as gabbros), but increases in modal abundance as crystallisation progresses. Figure 3.19 is a pyrope – almandine/spessartine – grossular triangular plot for samples from the Allalin unit and from the Pfulwe metabasalts. Compositions vary markedly throughout many of the samples but are generally almandine rich (the Fe – Mn component almost entirely consists of the almandine end-member in the case of samples of gabbroic origin). There is more compositional variety in samples with only a small extent of HP recrystallisation (gabbro, transitional coronite). This is likely to be a consequence of the strong control of diffusion and element availability on the growth and chemistry of minerals in samples which display limited recrystallisation. In samples that are more pervasively recrystallised, the compositions of the garnets are more homogenous (and more Fe-rich) reflecting the increase in element transport and the establishment of larger equilibrium domains. In the case of the completely transformed gabbroic eclogites, the garnet compositions form a relatively tight cluster of compositions.

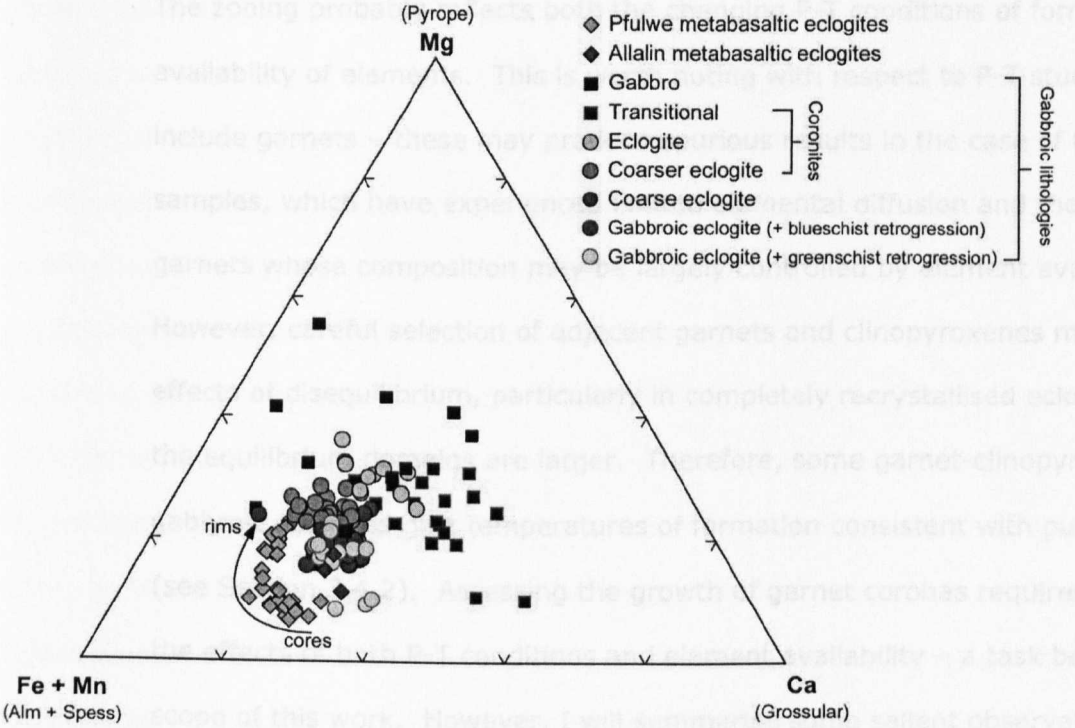

Figure 3.19. Triangular plot of garnet compositions for Allalin and metabasaltic samples in pyrope - almandine - grossular space.

Garnet compositions in gabbros are highly variable, but in general they are more pyrope-rich than in the eclogites. Transitional samples seem to show an overall enrichment in the grossular component, while compositions become more Fe-rich as the extent of recrystallisation increases. This pattern is not consistent with major element chemistry of the host rock, nor does it tally with models for the formation of garnet coronas (discussed below) which suggest the initial formation of Fe-rich coronas due to the loss of this element from olivine domains. It is unlikely to have been purely dependent on changing P-T conditions, although this cannot be ruled out.

Garnet forms coronas between domains of igneous minerals. The coronas increase in thickness as recrystallisation progresses, growing into the olivine domain particularly. The variability of garnet compositions shown in Figure 3.19 manifests itself in the asymmetrical chemical zonation of the coronas, which often display strong zoning from the edge of one igneous domain to the other (not core to rim).

The zoning probably reflects both the changing P-T conditions of formation and the availability of elements. This is worth noting with respect to P-T studies that include garnets – these may produce spurious results in the case of transitional samples, which have experienced limited elemental diffusion and therefore contain garnets whose composition may be largely controlled by element availability. However, careful selection of adjacent garnets and clinopyroxenes may avoid the effects of disequilibrium, particularly in completely recrystallised eclogites where the equilibrium domains are larger. Therefore, some garnet-clinopyroxene pairs in gabbroic eclogites give temperatures of formation consistent with published values (see Section 3.4.2). Assessing the growth of garnet coronas requires unravelling the effects of both P-T conditions and element availability – a task beyond the scope of this work. However, I will summarise some salient observations and attempt to explain their formation.

In some cases, particularly in samples with an incomplete transformation to eclogite, coronas consist of two different generations of garnet. Sample S01/36iiix provides a good example of a composite corona that consists of two texturally different garnet populations (Figure 3.20). A finer-grained, subhedral, turbid corona (with many fine inclusions) borders the former plagioclase domain, while a coarser, clearer corona, with much coarser inclusions lies within the precursor olivine site. Analysis of other coronas, such as those in Figure 3.21, shows the same bimodal pattern. I would tentatively suggest that the finer-grained corona in Figure 3.20 formed first, during the initial stages of HP recrystallisation, while the coarser corona formed later, perhaps at slightly higher temperatures and with more fluid present. This is consistent with greater Mn contents in the two sides of the finer, more turbid corona (albeit at very low levels), which suggests that this part grew earlier. This theory is discussed further in the following paragraphs.

Unlike the textural pattern of the coronas, chemical zonation in the garnet does not follow a consistent trend. The corona in Figure 3.20 displays more chemical

variation within the turbid plagioclase-adjacent portion than the olivine-adjacent part, but in Figure 3.21 the plagioclase-adjacent parts do not display strong zonation. Furthermore, the compositional zoning does not always display enrichment in elements which are abundant in the closest domain (this is contrary to the observation of Ca-rich garnet adjacent to plagioclase domains in the Flemsøy metagabbros (Mørk 1985; 1986)). Nearly all garnet compositions are Fe-rich, but relative to each other, garnets adjacent to olivine domains are commonly Mg-rich while those adjacent to augite are more Ca-rich, but there are exceptions. Plagioclase-adjacent garnets may be more calcic, magnesian or Fe-rich than garnet at the opposite side of the corona. Some of the compositional variation is likely to reflect changing P-T conditions, but in many cases it is difficult to imagine sufficient element supply to allow a purely P-T driven zonation to develop.

In assessing the zonation of these garnet coronas, I have taken into account element transport in fluid, mineralogical transformations and P-T conditions. Note that I have all but omitted a discussion of the effects of differing rates of solid state diffusion of Ca, Mg and Fe. This is due to the complexities involved, which lead to dramatically variable literature values. Modelling by Loomis (1978) implies that rates for solid-state diffusion in garnets at around 700°C, follow this order: Fe > Mg > Ca > Mn. However, experimental work on pelitic garnets summarised in Chakraborty and Ganguly (1991) suggests the order: Mn > Mg ≈ Fe. Ganguly et al. (1998) have added to this work with a study of a pyrope-almandine diffusion couple, and their summary of the current data supersedes that of the previous two publications. These authors conclude that diffusion of Mg is more rapid than Fe, which in turn is similar to both Mn and Ca for samples with little spessartine component. However, they also emphasise the dependency of diffusion rates on temperature, pressure, composition and oxygen fugacity. Moreover, the rates of grain-boundary diffusion, assuming (perhaps erroneously!) the presence of at least a small quantity of fluid, are likely to be much greater than solid-state diffusion.

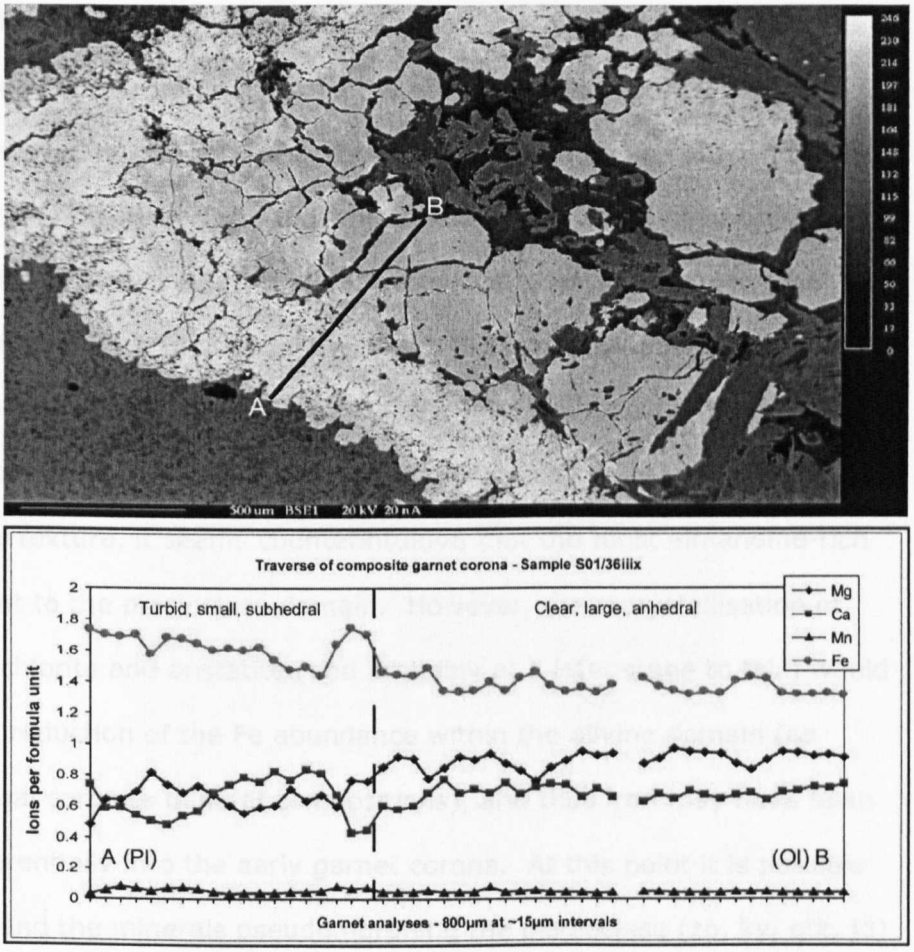

Figure 3.20. Backscattered electron image of a composite garnet corona and an electron microprobe traverse of the corona between a plagioclase domain (A) and an olivine domain (B).

Interestingly, after the initial formation of a garnet corona, elemental transfer between domains may be even more limited. The formation of a corona increases the distance between the domains and acts as a barrier through which diffusion (whether it be solid state or grain boundary) must take place. The development of a second corona is somewhat surprising given the necessary transfer of elements for its formation (Ca and Al from the plagioclase domain or Mg and Fe from the olivine site). What follows is a tentative model for the development of the corona seen in Figure 3.20.

One solution to this problem is the substantial transport of Al (and possibly Ca, but in what olivine domain mineral does it reside?) into the olivine domain, prior to the

crystallisation of the first corona. The aluminium forms a major component of the chlorite which forms another corona around the edges of olivine domains (Figure 3.14). Given the very slow diffusion rates of Al compared to Fe and Mg for instance (e.g. Mørk 1986) it seems most likely that the transfer of Al would have occurred before the formation of a corona, as fluid infiltration led to chlorite growth (the solubility of Al may have been increased by certain fluid compositions). Subsequently, the first garnet corona formed at the interface between the olivine and plagioclase domains - this was of an iron-rich composition. Initially, when looking at the final texture, it seems counterintuitive that the most almandine-rich garnet lies adjacent to the plagioclase domain. However, the recrystallisation of the olivine site to chlorite and enstatite (and probably at a later stage to talc) would have resulted in a reduction of the Fe abundance within the olivine domain (as shown in transitional coronite mineral compositions), and thus iron may have been incorporated preferentially into the early garnet corona. At this point it is possible that both chlorite and the minerals pseudomorphing the plagioclase (zo, ky, qtz, jd) are stable (or at least *meta*stable) and crystallisation of the garnet is relatively slow and forms only at the interface between the two domains.

The second part of the corona crystallised later, and grew into the chlorite – enstatite – talc dominated olivine site and therefore had a higher pyrope content. The breakdown of chlorite would have resulted in the formation of free fluid which would have encouraged more rapid growth of garnet through greater element mobility. This may explain the coarser nature of both the garnets, and the inclusions around which it may have rapidly grown. Another possibility is that the second corona formed under different, probably higher, P-T conditions (greater Mg content as opposed to Fe).

The traverse of a corona between an olivine and plagioclase domain shown in Figure 3.21 (b) displays a much flatter profile of iron content and, unlike the

previous example, the most pyrope-rich part is adjacent to the plagioclase site. It is possible that the pressure of formation may have been higher, but given its textural affinity with the low-Mg corona of Figure 3.20, this seems unlikely. There is evidence for large scale transfer of Mg away from the olivine domain in this area,

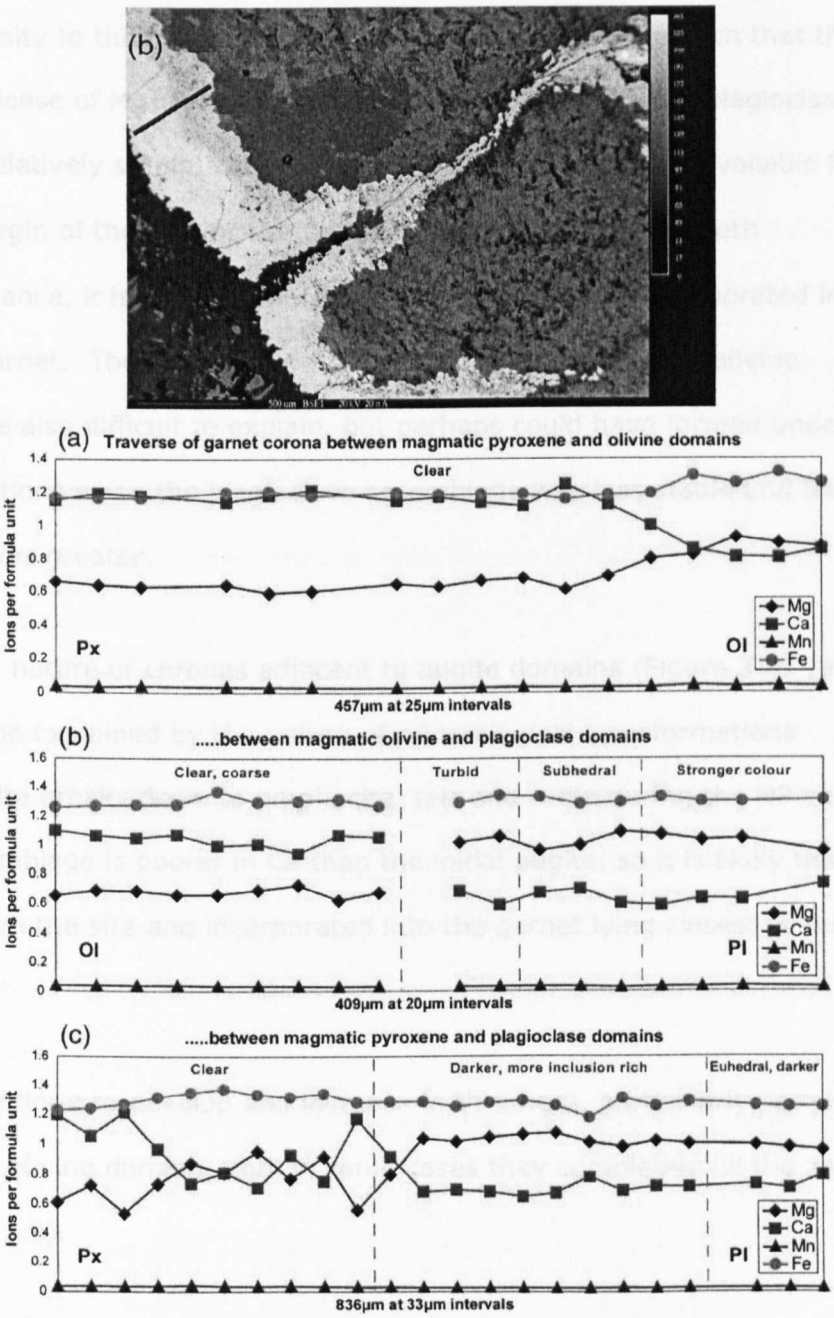

Figure 3.21. Three electron microprobe traverses of garnet coronas from sample S01/40viix. The three coronas have formed between different igneous domains (Px- augite domain, Ol – olivine, Pl – plagioclase). Note the different scales. The BSE image shows the line of traverse for (b), and also illustrates the fluid controlled crystallisation of garnet, along a vein in the plagioclase domain.

by the growth of chloritoid at the margin of the plagioclase domain, close to the end of the garnet traverse (Figure 3.21 - BSE image). This corresponds with a protrusion of the olivine site, the continuation of which is a vein running into the plagioclase domain along which garnet has crystallised (Figure 3.21), indicating the catalytic effect of the fluid and its function as a flux of elements. So it is possible that despite proximity to the plagioclase domain, the reactions were such that there was substantial release of Mg-rich fluid from the olivine site, while the plagioclase assemblage was relatively stable, with the result that there was more available Mg than Ca at the margin of the plagioclase domain. Furthermore, given both elements in abundance, it is perhaps more likely for the Mg to be incorporated into a high-pressure garnet. The calcic nature of the corona nearest to the olivine (Figure 3.21 (b)) is also difficult to explain, but perhaps could have formed under different P-T conditions when the plagioclase assemblage was less stable and the availability of Ca was greater.

The grossular–rich nature of coronas adjacent to augite domains (Figure 3.21 (a) and (c)) can also be explained by the nature of mineralogical transformations taking place. Augite breaks down to omphacite, talc and rutile during the HP stage. The resulting assemblage is poorer in Ca than the initial augite, so it is likely that Ca may be lost from the site and incorporated into the garnet lying closest to the domain.

Garnet coronas continue to develop and increase in thickness, particularly growing into the magmatic olivine domain, until in some cases they completely fill the zone (Photo F in Figure 3.9).

Sulphides. As previously discussed under *Transitional Samples*, gabbroic eclogites contain a greater abundance of sulphide than unaltered gabbro. This is usually in the form of large pyrite dominated grains which often also include minor pyrrhotite and chalcopyrite (but no pentlandite has been found in this study). This is likely to

be the result of infiltration of a fluid during seafloor hydrothermal alteration which was presumably sulphur-rich and nickel-poor.

Other Allalin metagabbros

Several samples have been analysed that display a pervasive episode of deformation which is associated with recrystallisation on the retrograde path. The extent of deformation in these samples is greater than that of the samples with coronitic textures, but comparable to those samples which I have termed 'gabbroic eclogites'. Parts of the Allalin unit display clear evidence of recrystallisation during deformation under blueschist facies on the retrograde path. This has resulted in the formation of abundant and strongly orientated glaucophane in the matrix as shown in G in Figure 3.9. As discussed in Section 3.2.1.4, the occurrence of blueschist facies conditions during unroofing of the unit is evidence of continued subduction in the vicinity, and the preservation of a cool geotherm during the early stages of exhumation.

Other samples, particularly those collected from the eastern periphery of the gabbroic body, display some deformation and accompanied recrystallisation under greenschist facies conditions. In these samples, garnet is unstable and has partially broken down (Photo H in Figure 3.9) and is replaced commonly by chlorite and sometimes by blue-green amphibole. Despite probable recrystallisation during sea-floor metamorphism, HP metamorphism and during retrogression, igneous pyroxene domains are often still recognisable. In contrast, plagioclase and olivine domains are not recognisable to the same extent after deformation. This is probably because they consist of finer grained aggregates that deform more readily, and contain some hydrous minerals which may dehydrate, providing fluid that encourages further recrystallisation under subsequent deformation. The pyroxene domain has undergone a transformation from igneous augite which has

been pseudomorphed by omphacite, talc and rutile and then, during retrogression, has recrystallised to a green amphibole of actinolitic composition.

Although several samples with extensive greenschist retrogression have been analysed, the data do not provide the basis for the results and conclusions presented in this thesis. This is because they do not solely represent the effects of prograde and peak metamorphism, but also may display the results of the retrogressive stage, which is not relevant when considering the process of continuing subduction.

3.3.2 Pfulwe metabasaltic eclogites

As stated previously, the metabasaltic samples were collected from Pfulwe and Täschalp, west of Zermatt. All of the samples used for isotope work were collected at or near Pfulwe (G.R. 6315 0962), except the Allalin dyke metabasalts that are described at the end of this section. Pillow structures are clearly evident in many outcrops close to the Pfulwe pass. This has enabled samples to be taken separately from pillow cores and rims, and ensures that the original nature of the protoliths is well defined. In cases where the rim or core was specifically sampled, the sample number is suffixed by R or C respectively. Several undifferentiated metabasaltic samples were taken from near Pfulwe.

The metabasalts of the Zermatt-Saas Fee area have undergone very high-pressure (HP) metamorphism at approximately 2.0 GPa and 600°C, the same as estimates from the Allalin Gabbro (see Section 2.2.1 and Section 2.3). In stark contrast to the gabbros of the Allalin unit, no magmatic relics of minerals or textures are evident in the metabasaltic eclogites of the Pfulwe region (or any other part of the ZSO). This is almost certainly due to the greater degree of deformation and accompanying fluid flow that the metabasalts have experienced. However, igneous structures in the form of pillows and dykes are still identifiable. The Pfulwe area

has some excellent examples of fully recrystallised pillow basalts that now contain HP eclogitic assemblages, but retain their igneous structure including coarser cores and finer rims which seems to reflect original grain size variations in the pillows (Figure 3.22). Some of these samples have fairly well developed schistosity, which is defined by the orientation of amphibole, epidote and omphacite, but are still clearly recognisable as pillows. There is evidence, in the form of epidosites, of seafloor hydrothermal alteration at Pfulwe and in the surrounding area. Epidosites form by extreme Ca enrichment, usually in the high-temperature, up-flow zones of hydrothermal systems.

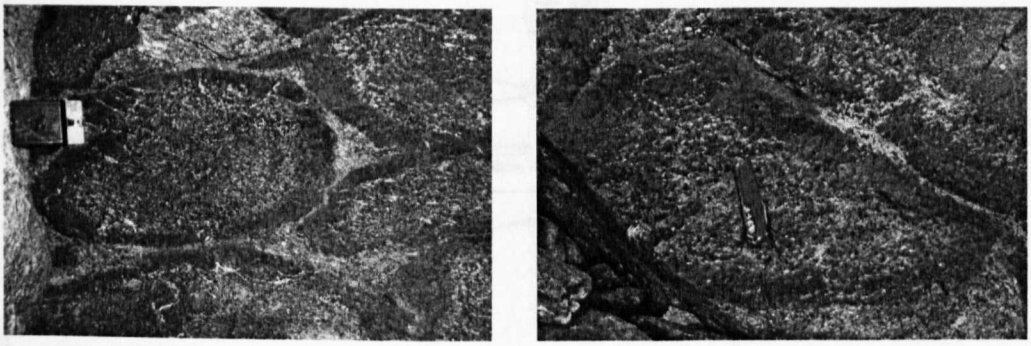

Figure 3.22. Metamorphosed pillow basalts near Pfulwe, east of Zermatt. Pillows preserved despite complete recrystallisation at very HP conditions (~2.0 GPa, 600°C), and considerable deformation which is evident in some samples as a fairly pervasive schistosity.

The mineral assemblage in both pillows and in the undifferentiated samples consists predominately of garnet, omphacite, glaucophane, epidote and paragonite, with a minor quantity of phengite. Chloritoid has been documented by Bearth (1963) and Barnicoat and Fry (1986) from the metabasalts of the Täschalp, but it was not found in the samples collected for this study. Accessory phases include rutile, calcite, dolomite, apatite and zircon. Albite and blue-green amphibole occur as retrogressive reaction products, but their extent is limited; most samples display very little retrogression.

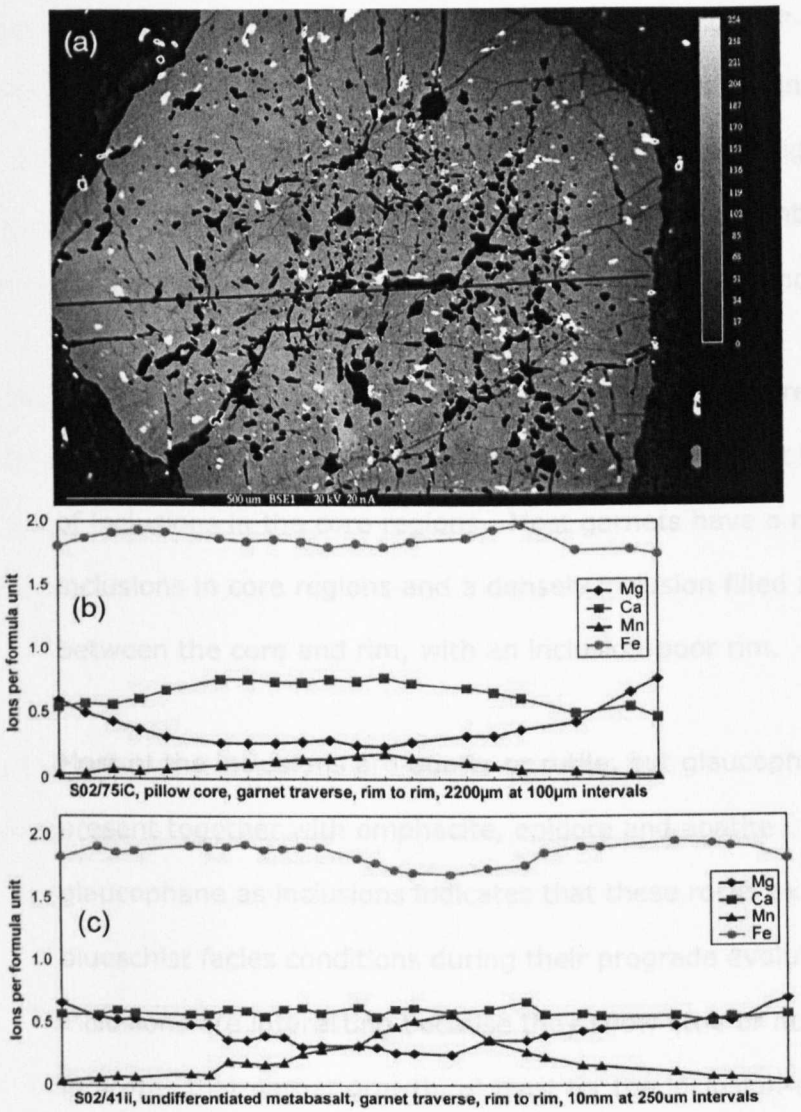

Figure 3.23. (a) BSE image of garnet from S02/75iC, a metapillow core. Blue line: approximate position of the traverse. Zoning only faintly evident due to relatively constant Fe content and high Mn in the core, creating a brighter backscatter in this region. Darker rims due to high pyrope content. Most inclusions are quartz (black) or rutile (white), but occasional omphacite, epidote and glaucophane can be found.

(b) Electron microprobe traverse of garnet porphyroblast from S02/75iC, shown in (a).

(c) Electron microprobe traverse of garnet porphyroblast from S02/41ii, and undifferentiated metabasalt. Note different scales in (b) and (c). Missing analyses due to inclusions which are particularly abundant in S02/41ii.

Garnet occurs as very large porphyroblasts (up to 1cm across in some samples). These are commonly inclusion-rich and display classic chemical zoning with significant amounts of Mn in the cores (nearly 20% spessartine end-member) and pyrope-rich rims (see Figure 3.23). In contrast to the garnet coronas from the

Allalin Gabbro, this chemical zoning reflects changing P-T conditions, with a grossular-spessartine rich garnet crystallising first during prograde metamorphism, followed by increasingly pyrope-rich compositions at higher pressures, probably around peak P-T conditions. The almandine component first increases and then decreases towards the rim as the pyrope component increases rapidly.

The inclusion textures shown in the BSE image in Figure 3.23 are fairly typical of those found in metabasaltic samples, except that most have a lower concentration of inclusions in the core regions. Most garnets have a moderate number of inclusions in core regions and a densely inclusion filled zone approximately half-way between the core and rim, with an inclusion-poor rim.

Most of the inclusions are quartz or rutile, but glaucophane is also sometimes present together with omphacite, epidote and apatite. The presence of glaucophane as inclusions indicates that these rocks experienced relatively cool, blueschist facies conditions during their prograde evolution. Texturally, the inclusions are interesting because they show little or no preferred orientation. This indicates that garnet growth, at least for the inclusion-rich core parts, was apparently pre-tectonic (i.e. it occurred prior to deformation and the formation of a schistosity as defined by amphibole, omphacite and epidote alignment).

In the Täschalp area, but less commonly near Pfulwe, many metabasaltic lithologies contain rhombic masses of clinozoisite + paragonite ± quartz, interpreted as pseudomorphs after lawsonite. Lawsonite is only stable in high-pressure rocks at comparatively low temperatures (e.g. <580°C at 2 GPa; Barnicoat and Fry 1986). The presence of these phenocrysts in the groundmass of the rock is of particular interest because they indicate that these lithologies have experienced low-temperature, blueschist-facies crystallisation during exhumation. Barnicoat and Fry (1986) formulated a P-T path for the metabasalts of Täschalp that suggested substantial cooling during the first stages of exhumation, resulting in the retrograde

path crossing to the lower temperature side of the prograde path. The blueschist-facies retrograde event is also evident from the presence of glaucophane in the matrix. More commonly, blueschist-facies mineralogy is only present as inclusions in strong, buffering phases such as garnet, indicating blueschist-facies conditions on the prograde P-T path.

After exhumation to shallower levels, greenschist-facies conditions prevailed. There was deformation during this period, which led to sometimes intense, but fairly localised retrogressive recrystallisation (e.g. Cartwright and Barnicoat 2002). Blue-green amphibole (barroisite), chlorite and albite were all developed during this stage.

For a further discussion on petrological aspects of the Pfulwe and Täschalp metabasalts, see Bearth (1963; 1967a), Bearth and Schwandler (1967b), Bearth and Stern (1971; 1979), Barnicoat and Fry (1986) and Barnicoat (1988).

Allalin intrusive metabasalts/dolerites

Several metabasaltic samples were taken from dykes within the Allalin gabbro. These dykes are found at the eastern extremity of the Allalinhorn and thus are subject to extensive greenschist retrogression that has occurred in this section of the unit. However, an eclogitic assemblage of omphacite and garnet is still present, together with zoisite and paragonite, which may represent recrystallised products of reaction during the early stages of exhumation. Garnet exists as small, anhedral grains which may be the products of deformation and decay of larger grains, although individually they do not appear to be strongly retrogressed. The groundmass consists of omphacite and retrograde barroisite, which now constitutes a considerable proportion of the rock. Chlorite and albite are both present as the retrogression products of breakdown of omphacite, garnet and possibly Na-amphibole, although there is no petrographic evidence in these rocks for the

presence of the latter. In the main, these samples have experienced pervasive deformation and accompanying fluid flow at greenschist-facies conditions on the retrograde path, and this should be taken into account when analysing the data.

3.3.3 Factors affecting the preservation of igneous assemblages

Occasional relics of igneous minerals are found in the metabasalts of the Sulitjelma area (see Section 2.3.2.2) but in general basaltic lithologies which have undergone metamorphism do not display original igneous mineralogy (or textures) – their recrystallisation is usually complete. Conversely, gabbros often display relics of igneous mineralogy and, even more commonly, textures. These features have been well documented in the Allalin unit (e.g. Chinner and Dixon 1973; Meyer 1983b; this study), the Rocciavré and Monviso gabbros in the Italian western Alps (e.g. Pognante 1985; Kienast and Messiga 1987, respectively) and from a gabbro body in western Norway (Mørk 1985). Parts of the Allalin unit display both magmatic textures and mineralogy (in rare cases >95%) despite having undergone two episodes of metamorphism.

In 1975, Ahrens and Schubert investigated the rate of the gabbro-eclogite transition. Their work found that solid-state diffusion under completely dry conditions was not sufficiently rapid to complete the transition within geologically meaningful timescales at temperatures below 600° – 800°C. Therefore, in dry systems with no deformation incomplete recrystallisation will occur at the relatively cool temperatures associated with subduction (≤600°C in the case of the ZSO). However, diffusion rates increase greatly with the introduction of even a small amount of free interstitial fluid, leading to more rapid eclogitisation despite relatively low temperatures.

However, gabbroic bodies are inherently massive, often isotropic and lack strong internal structure and discordances, so deformation does not develop easily.

Furthermore, the coarse grain size gives rise to greater competence, increases the necessary distances (and therefore times) of diffusion and limits the surface area of the grains on which exchange and nucleation can take place, thus discouraging a complete transition. Deformation creates crystal defects and dislocations which encourage nucleation and fluid flow (Pognante 1985) and thus, without deformation it is difficult to envisage that infiltration of sufficient water could take place to facilitate more rapid diffusion in a grain boundary fluid. Therefore, gabbroic mineralogy may be preserved in a metastable state, throughout the metamorphic episode. In contrast, basaltic units do not have the same internal competence and therefore are more susceptible to deformation and pervasive fluid flow than gabbros. Their smaller grain size also decreases competence, aids more rapid diffusion and provides a greater surface area on which exchange and nucleation can occur. Furthermore, hydrated parts of the basaltic crust, formed during seafloor hydrothermal processes, will undergo dehydration during subduction-related prograde metamorphism, producing a free fluid phase.

Prior to the very HP event, the Allalin Gabbro underwent ocean-floor metamorphism. But perhaps again due to its coherent, competent form, some parts did not experience the introduction of substantial amounts of fluid and the resulting pervasive recrystallisation. In general, the extent of hydrothermal circulation at depths associated with gabbroic bodies is thought to be considerably less than throughout the basaltic domain (Rosenberg et al. 1993; Hart et al. 1994), so consequently gabbros are, on average, less hydrated than basalts prior to subduction.

In summary, the rate and extent of eclogitisation depends particularly on temperature, the presence or lack of a free fluid phase and grain size. In turn, the extent of fluid flow and the grain size are strongly affected by deformation, which is dependent on regional tectonics and the internal structure of the gabbroic body. To

some extent fluid flow may facilitate deformation and therefore create a feedback mechanism – greater fluid flow, and therefore recrystallisation, leads to more pervasive/extensive deformation which in turn provides pathways for greater fluid flow. If the system remains dry and undeformed, then preservation of igneous mineralogy is likely to occur.

In the case of the Allalin Gabbro, only very minor parts display igneous mineralogy. A greater part preserves magmatic domains which have been pseudomorphed by ocean-floor metamorphic and eclogitic assemblages. A similar proportion of the unit has been more pervasively deformed to the extent that the fabrics observed are purely metamorphic. The sample suite represents all of these divisions.

3.4 Zermatt-Saas ophiolite P-T estimates

3.4.1 P-T estimates in the literature

Numerous studies have assessed the P-T conditions of the ZSO (e.g. Chinner and Dixon 1973; Ernst and Dal Piaz 1978; Meyer 1983a, 1983b; Barnicoat and Fry 1986; Reinecke 1991, 1998; Barnicoat 1996; Rebay and Powell 2002). These have been discussed previously in the *geological setting* section (*Metamorphism in the ZSO* within Section 2.2.1.1). In summary, it was recognised by Meyer (1983b) that peak metamorphism of the Allalin unit took place at approximately 2.0 GPa and 550-600°C. Work nearby in the Täschalp area found similar peak P-T conditions (Barnicoat and Fry 1986). The discovery of coesite relics in garnets in the southern part of the ZSO revealed peak pressure conditions in this area of approximately 2.9 GPa (Reinecke 1991; 1998). The work of Rebay and Powell (2002) suggests peak pressures nearly as high as this for the Allalin unit (2.7 GPa).

3.4.2 Conventional geo-thermo-barometry

Garnet-clinopyroxene thermometry. Omphacite – garnet pairs from metabasaltic eclogites give temperatures of equilibration of 600-630°C using the thermometer of Krogh Ravna (2000) and estimating the pressure to be 2.0 GPa. For gabbroic eclogites from the Allalin unit, temperatures are considerably lower, lying between 475°C and 575°C. The large range probably reflects disequilibria between the two phases, although equilibration at different points on the P-T path cannot be ruled out. It is worth noting that depending on which calibration is used (those from: Ellis and Green 1979; Krogh 1988; Pattison and Newton 1989; Krogh Ravna et al. 2000) the calculated temperature may vary up to 90°C either side of the Krogh Ravna (2000) value.

Jadeite in clinopyroxene barometry. The jadeite component in omphacites from the Allalin gabbro and the Pfulwe metabasalts is commonly lower than

expected for the pressure conditions under which they formed, giving rise to pressure estimates of approximately 1.5 GPa and a rare maximum value of ~1.7 GPa (sample S01/5E). However, the nature of the barometer is such that at a given temperature of 600°C, the maximum pressure for Jd_{100} is around 1.7 GPa without considering the effects of ordering or disordering. An unusually high calcium Tschermak component has been found in jadeite analyses from a quartz diorite from the Sesia zone by Koons et al. (1987) and in the Allalin unit by Wayte et al. (1989). While the former authors state the possibility of a small contribution from zoisite, due to very small grain size, Wayte et al. analysed larger grains and do not consider this to be a possibility. One possibility is that the jadeite (or omphacite in the case of this study) actually crystallised at the calculated pressure (~1.5 GPa) and did not subsequently re-equilibrate, but according to Wayte et al. (1989) the plagioclase reaction involving jadeite only occurs above 17 kbar (1.7 GPa). Another possibility is that the composition is somehow affected by the anorthite-rich nature of the original plagioclase during disequilibrium reaction.

3.4.3 THERMOCALC estimates

The THERMOCALC program of Holland and Powell (version 3.1, 2001) based on their internally consistent dataset (Holland and Powell 1985, 1990, 1998; Powell and Holland 1985, 1988) was used to obtain average P-T, using a number of independent reactions. However, as with all geothermobarometers, the acquisition of good data is reliant upon the attainment of equilibrium between the phases used. From the previous petrological discussions of gabbroic eclogites (Section 3.3.1.3) it is clear that many of the samples that have been most extensively studied petrographically, are those which have only attained equilibrium on a very local scale – confined within igneous domains. By restricting the mineral data used to those of a single olivine domain, equilibrium can be all but assured, but the result is an assemblage with too few end-members for THERMOCALC to perform an average P-T calculation.

However, by carefully selecting minerals which lie close to one another and in apparent equilibrium, some reasonably precise results can be obtained, and these values are consistent with previously published estimates. Furthermore, many of the samples analysed belong to the gabbroic eclogite group which exhibit, at least to some extent, an approach to equilibrium, and in some cases recrystallisation associated with deformation has occurred, resulting in the breakdown of the igneous domains and the attainment of large scale equilibrium. The more reliable and precise P-T estimates are presented in Figure 3.24.

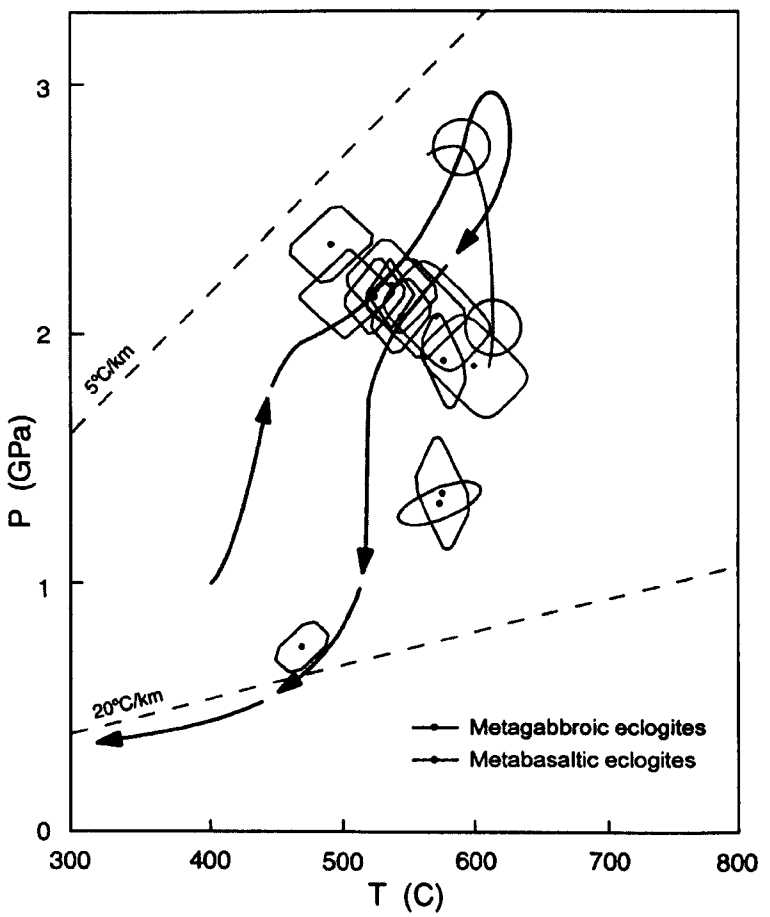

Figure 3.24. P-T estimates from the Allalin metagabbros and the Pfulwe metabasalts, obtained from average P-T calculations in the THERMOCALC program (THERMOCALC v3.1, derived from Powell and Holland 1988). Blue P-T path is for samples at Lago di Cignana, Val d'Aosta, NW Italy (Reinecke 1998). Red circles and P-T path is taken from Rebay and Powell (2002) and is an estimation from eclogite facies metatroctolites from the Western Alps.

Sample S01/40viix has been classed as a coronitic eclogite. This means that complete recrystallisation has occurred, but garnet coronas remain well defined, with little or no growth into surrounding domains. The grainsize within the plagioclase domain has remained very small (<0.1mm). Using the assemblage: garnet + omphacite + talc + chloritoid + zoisite + quartz with the presence of a H_2O-rich fluid ($x(H_2O) = 0.9$), a temperature of equilibration of 621 ± 23°C (1 s.d.) was calculated. The pressure estimates for assemblages from coronitic samples are unfortunately subject to much greater errors, and thus provide a much poorer constraint, in this case: 17.7 ± 6.6 kbar (1.77 GPa). Sample S01/40ix is also a coronitic eclogite and, using the same assemblage but with the addition of kyanite, gives a pressure of 13.5 ± 4.6 kbar and a temperature of 576 ± 11°C. Again the pressure estimate is poor and the large error on this part of the calculation must cast doubt on the reliability of the temperature estimates. However, as can be seen below, gabbroic eclogites provide a more reliable estimation of P-T conditions.

Samples S01/39ix and S01/40vx are gabbroic eclogites (i.e. their mineralogy is completely composed of eclogite facies minerals), they are coarse grained, and metamorphic textures dominate over igneous ones. Sample S01/39ix contains an assemblage of garnet, omphacite, clinozoisite, actinolite, talc and chloritoid, which gives a THERMOCALC P-T estimate of 21.1 ± 1.4 kbar and 536 ± 17°C. Inclusions within chloritoid from sample S01/40vx, comprise garnet, omphacite, talc and paragonite. This assemblage corresponds to P-T conditions of 20.7 ± 1.2 kbar and 544 ± 18°C. The matrix assemblage in this same sample (garnet, omphacite, talc, chloritoid and paragonite) gave a considerably different estimate: 13.6 ± 1.8 kbar and 575 ± 16°C. This probably reflects re-equilibration at lower pressures during exhumation. But somewhat surprisingly, the temperature is similar which is in contrast to the hair-pin P-T path of Reinecke (1998). It is possible that the P-T estimates shown on Figure 3.24 correspond to a P-T path which has much lower peak conditions than that of the Lago di Cignana rocks (Reinecke 1998), and a

slower and hotter exhumation, at least in the early stages. However, it is also possible that the estimates do not represent the true peak conditions of metamorphism (see below) and thus the true P-T path could approximate that of Reinecke (1998). The P-T path of Rebay and Powell (2002) is shown in Figure 3.24 and is consistent with a slower, hotter early exhumation history, but this path is a general path for Alpine metatroctolites, and not specific to the Allalin unit.

By varying fluid composition during the THERMOCALC P-T calculations, it was observed that the errors generated were lowest for fluid compositions which were water-rich, as opposed to CO_2-rich. For this reason, the presence of a water-rich fluid (X_{H2O} = 0.9) has been assumed. While changes in the composition of the fluid do not have dramatic effects on the results produced, the P-T estimates are considerably lower if it is assumed that the rock did not have any free fluid present, and therefore had a much lower water activity. For example, temperature estimates for sample S01/40vx vary from 391 to 495 to 544°C for water activities of 0.1, 0.5 and 0.9 respectively. Petrographically, the evidence from reaction textures and the mineralogy involved in reactions would suggest the presence of at least a small quantity of fluid.

A sample which has undergone greenschist-facies retrogression (during which garnet became unstable) yielded a P-T estimate of 7.4 ± 0.8 kbar and 469 ± 16°C for the assemblage: garnet + chlorite + blue-green amphibole + zoisite + albite + quartz + rutile + titanite.

The accurate assessment of P-T conditions in micro-domains requires analysis of assemblages through the construction of a petrogenetic grid, and the use of pseudosections corresponding to the composition of the individual domain. This is discussed in the following section.

3.4.4 Mineral equilibria in micro-domains

What follows is a summary of the work of Rebay and Powell (2002) which has provided a potentially more rigorous means of analysing the pressure and temperature conditions of the formation of the assemblages seen in the eclogitic metagabbros of the Allalinhorn, particularly in the strongly domainal coronites. This work involved the formulation of a petrogenetic grid for Alpine metatroctolites, through calculation of mineral equilibria in the system NCFMASH. Using this as a base, pseudosections were created which correspond to individual compositional micro-domains within the rock (which are retained from the igneous protolith) rather than an overall bulk composition. This is particularly useful for samples with strong coronite textures, which retain their original igneous domains, as studies which assume large scale equilibrium or involve the bulk composition of the rock will probably result in inaccuracies or at least considerable errors. In addition to pressure and temperature, pseudosections can be contoured for water content or even plotted with P or T (or the P-T path) versus the water content in order to emphasise the crucial role that water content plays in the development of assemblages and their preservation.

An important observation was that the pseudosections for former plagioclase and olivine micro-domains recorded different P-T conditions. The assemblage of chloritoid + talc + garnet + omphacite which is present in the ex-olivine micro-domain corresponds to a peak pressure possibly greater than 27 kbar (2.7 GPa) at temperatures of 570-600°C. However, the clinozoisite + omphacite + garnet + kyanite + paragonite + quartz assemblage, typical of the ex-plagioclase domain, indicates pressures of formation of approximately 20 kbar (2.0 GPa). As prograde metamorphism progresses, the P-T path crosses contours of decreasing water content in both domains. When the pressure begins to decrease, at around 2.7 GPa, the P-T path crosses contours of increasing water content in the olivine domain. The olivine domain becomes H_2O undersaturated and without the influx of

fluid no hydration reactions will take place and therefore the assemblage at 2.7 GPa will be preserved. In the plagioclase domain, the initial stage of exhumation continues to involve dehydration and thus, the assemblage continues to change. By 2.0 GPa, lawsonite breakdown has occurred, resulting in a less hydrous assemblage, while the path crosses into a zone of increasingly H_2O-rich assemblages. Therefore, reactions cease at this pressure, without the addition of fluid. One major uncertainty in work of this nature, is the determination of the bulk chemistry of the domains. Rebay and Powell (2002) estimated the compositions of the olivine and plagioclase domains to be, respectively:

90% Fo_{70} + 10% An_{60}

10% Fo_{70} + 90% An_{60}

However, the authors recognised that the assemblage within the olivine domain was considerably richer in silica and alumina, than the original olivine, and therefore a greater addition of these two elements was required. It was assumed that both domains were at least close to silica saturation, while alumina was added until chloritoid + talc was produced at high pressure (although whether extra addition of Al, above and beyond the estimated concentration, makes a difference to the estimates is not clear). Conversely, the work of Chinner and Dixon (1973) actually concluded that the formation of the olivine assemblage occurred under conditions of silica saturation. The uncertainty of bulk composition of the domains could result in inaccuracies in the calculated stability of phases, which in turn may lead to significant errors for the estimated P-T conditions. Moreover, the olivine domains in the Allalin Gabbro are commonly more forsteritic (~Fo_{80}) than those used in the estimate of microdomain composition. However, the variation between the P-T conditions preserved by the olivine and the plagioclase domains seems robust, as do the observations regarding water content and the preservation of assemblages.

3.5 Petrography and mineralogy of the Sulitjelma ophiolite

The Sulitjelma ophiolite has experienced regional metamorphism which increases in grade in a north-westerly direction, from the biotite to the kyanite zone, as described in Section 3.2.2. The lithologies are now composed of metamorphic mineral assemblages dominated by amphibole, epidote and plagioclase. However, relict igneous textures are found in the gabbros and the pillow lavas, while the gabbros also retain some relict igneous mineralogy. This textural information provides evidence for the precise nature of formation and igneous crystallisation of some of the units. A more comprehensive discussion of textures and mineralogy is given by Boyle (1982). What follows is merely a summary of this work, focussing on the salient points which are relevant to the work presented in this thesis. All samples were collected by A. P. Boyle during fieldwork towards his PhD thesis (1982) and subsequent fieldwork.

3.5.1 Sulitjelma gabbro complex (SGC)

Sixteen gabbroic samples were taken from the Sulitjelma gabbros: eight from the volumetrically dominant Sulitjelma gabbro complex (SGC) and eight from the flaser gabbro. All were collected from the area marked by the large red box in Figure 3.6. The samples from the SGC are largely undeformed and preserve igneous textures and to a large extent, mineralogy. Samples from the flaser gabbro are variably deformed and retain very little, if any, igneous mineralogy.

The Sulitjelma gabbro complex consists of two distinct units: the Sulitjelma Gabbro and the flaser gabbro. It is considered from evidence outlined below, that these two units are co-genetic, but they have experienced different degrees of deformation during metamorphism, resulting in different extents of reaction, different textures and also mineralogy. The flaser gabbro is named as such due to the metamorphic fabric that it displays - the result of a more pervasive deformation event.

Igneous cumulate layering can be observed in the Sulitjelma gabbro complex, and has been described by Mason (1966; 1971). The unit as a whole displays rare earth element (REE) patterns with variable, but positive, Europium anomalies (see *Chapter 4: Bulk rock chemistry*), indicating the overall importance of plagioclase accumulation in their genesis. The original igneous mineralogy of the gabbroic units is partially evident petrographically due to common relicts of igneous minerals, which are found in the flaser gabbros and particularly in the Sulitjelma gabbro complex. Clinopyroxene (augite), orthopyroxene (ferro-enstatite) and a brown hornblende are all present in some samples. Olivine and igneous plagioclase relicts have not been found in any of the units, but Mason (1966; 1971) has shown that both olivine (Fo_{51-82}) and plagioclase (An_{60-75}) were ubiquitous. Hornblende is a minor component, forming rims on the augite and opaque minerals. The similarity in compositions of augite, ferro-enstatite and hornblende between the undeformed Sulitjelma gabbro and the structurally adjacent flaser gabbro has led some authors to conclude that the two units were co-genetic (e.g. Boyle 1982).

Porphyritic textures are common in the Sulitjelma Gabbro complex. Ophitic textures can be seen in the isotropic gabbro and the less deformed parts of the flaser gabbro. In these samples, pseudomorphic laths after plagioclase are enclosed by clinopyroxene (augite), which itself has been partially pseudomorphed by Ca-amphibole (either blue-green hornblende or pale-green actinolite). The gabbros display a range of textures and metamorphic mineralogies, both between the flaser and Sulitjelma gabbros and within each unit. The variations seen are dependent on the extent of deformation and syntectonic recrystallisation. In many ways these variations are similar to those seen in the Allalin Gabbro, although in this case, the overstepping of mineral stabilities is somewhat less remarkable.

Some samples retain their igneous textures and mineralogy, with the exception of olivine and plagioclase which are never preserved. In other samples coronas of Ca-

amphibole form around the rims of igneous pyroxene domains. With increasing recrystallisation, whole grains of pyroxene are pseudomorphed by Ca-amphibole. With increasing deformation, those amphiboles begin to align, defining a schistosity. However, even at this stage, large augen can exist which locally preserve relicts of the igneous assemblage.

In samples with pervasive deformation and complete recrystallisation, metamorphic fabrics have completely obliterated igneous textures. The schistosity that has developed is largely defined by the consistent orientation of calcic amphibole.

3.5.2 Metabasalts – Otervann formation, Mietjerpakte sheeted intrusive complex and Lomivann volcanics

Approximately half (14) of the analysed metabasaltic samples were collected from the Otervann formation - from the area marked by the large red box in Figure 3.6. Nine samples were derived from the Mietjerpakte sheeted intrusive complex from the same area, while three more were collected from the Lomivann volcanics, part of the Furulund group, from within the area marked by the small red box in the southern portion of the same diagram.

The Sulitjelma Ophiolite has experienced less pervasive deformation than the ZSO, and as a result, the precise igneous nature of all metabasaltic samples could be ascertained. Samples with full metamorphic textures are common in parts of the Otervann formation, illustrating the inhomogeneous nature of deformation. However, these samples were not used in this study due to the uncertainty in constraining their exact origin. Pillow basalts were collected from the Otervann formation and the Lomivann volcanics, while dykes were sampled from the Mietjerpakte sheeted intrusive complex.

Pillow basalts generally exhibit an elongation parallel to the regional mineral lineation, but are well preserved. Due to their excellent preservation, both core

and rim portions could be sampled. Vesicles have been retained, but have been filled by either quartz or carbonate. Pillow selvages rich in epidote and quartz-epidote are common, indicating, according to Boyle (1982), submarine alteration that took place prior to regional metamorphism. Occasionally, metabasalts partially preserve igneous textures at the mineral scale. In particular, pseudomorphs after plagioclase exist, with a recrystallised assemblage dominated by metamorphic plagioclase and epidote, but also including muscovite, biotite, Ca-amphibole and quartz. The ophitic textures evident in gabbros are also sometimes present in the basaltic lithologies, particularly within the sheeted intrusive complex. These textures are preserved in the form of pseudomorphs after plagioclase (see above) enclosed by Ca-amphibole which pseudomorphs the igneous clinopyroxene. Other igneous textures include xenocrystic crystal clots within the sheeted intrusive complex, and variolitic texture with fence-like Ca-amphibole textures in pillows.

The metabasalts of both pillow and dyke origin comprise mainly Ca-amphibole, plagioclase, epidote group minerals and chlorite but also contain minor amounts of quartz, carbonate, titanite, biotite, muscovite and opaque minerals. No relict igneous phases exist. More deformed pillows display a schistosity defined by Ca-amphibole orientation. Samples with no remaining igneous structure (i.e. a well-developed schistosity or compositional banding) were not used in this study and therefore shall not be discussed here. In rocks without a schistosity, the Ca-amphiboles have a random orientation. The P-T conditions indicated by the mineral assemblage, has been discussed previously in Section 3.2.2.3).

4 Bulk rock chemistry of metagabbros and metabasalts from the Zermatt-Saas and Sulitjelma ophiolites

Samples of gabbroic and basaltic origin were collected from both the Zermatt-Saas ophiolite (ZSO) and the Sulitjelma ophiolite (SO). There has been some debate over the tectonic setting in which these ophiolites were generated. The ZSO formed in a relatively narrow basin at the edge of the Tethys (e.g. Ernst 1973; Platt 1986). However, the geochemical nature of this marginal basin is poorly defined and there is a paucity of literature on the subject. For most authors the issue is not a crucial one, but for this study it is important to constrain the initial composition of the samples in order to determine a reference point from which to identify possible changes. The Sulitjelma ophiolite was also formed in a marginal basin and is associated with some arc-like magmatic rocks suggesting its formation in a back-arc basin. The classification of the samples through major element chemistry may shed light on this issue and also, as a result, give important information on the likely trace element compositions of the basaltic protoliths. The trace element compositions of the gabbroic eclogite protoliths (i.e. the gabbro suite) can be measured directly due to their metastable preservation through the subduction process. However, it is still important to assess whether the gabbros and corresponding gabbroic eclogites have the same range of major element composition and therefore similar protolith trace element concentrations.

4.1 Major elements in metagabbros and metabasalts from the Zermatt-Saas ophiolite (ZSO), Western Alps

The metagabbros and metabasalts of the Zermatt region, Switzerland, have long been identified as an ophiolite sequence (e.g. Bearth 1963; 1967a; Bearth 1971, and see Section 3.2.1). The ocean in which the ZSO formed, the Piemonte-Liguria basin, was almost certainly a narrow basin at the margins of the Tethys (Ernst

1973; Platt 1986; Schmid et al. 1996; and see Section 3.2.1.5), but it is not altogether clear whether the oceanic crust that formed there had a MORB signature or a different, perhaps arc-related signature. This is an important point for this study, as comparisons of trace element abundances in the metabasalts need to be made with a particular reference material, and this may be N-MORB, E-MORB or a back-arc basin dataset. Beccaluva et al. (1984) provided a (rare) assessment of the geochemical characteristics of the ZSO, and concluded that the ophiolite had transitional to normal MORB characteristics. This is consistent with the absence of significant arc magmatics in the Alpine chain, and was also a conclusion of Bowtell (1991). The question of the magmatic signature will be revisited in the following sections on major and trace elements in the ZSO metabasalts.

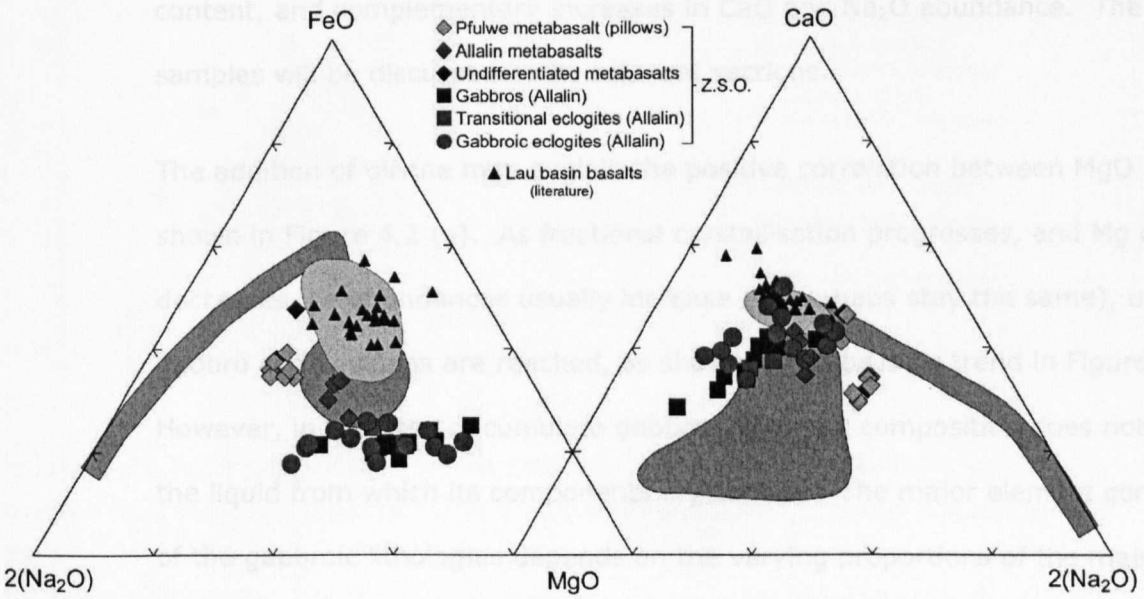

Figure 4.1. Triangular Fe-Na-Mg and Ca-Mg-Na plots of major element compositions of the main suites of samples from the Zermatt-Saas ophiolite. See text for discussion. The Lau basin is an example of a back-arc spreading centre; data from Falloon et al. (1992) and Pearce et al. (1995). Grey field: fresh MORB. Grey/blue: altered MORB. MORB field drawn from data from *Petrological database of the ocean floor* (2004) and A. Gannoun, unpublished data. Dark grey line: fractionation trend for MORB. The MORB fractionation trend and the altered MORB field are taken from Spandler et al. (2004) and references therein. Major element abundances, determined by XRF analysis, are presented in Appendix B, Tables B1 and B2.

4.1.1 Allalin gabbros and gabbroic eclogites

The Allalin Gabbro is a cumulate unit, as discussed in Sections 3.2.1.2 and 3.3.1. The samples have varying proportions of the three major phases: olivine, augite and plagioclase (see Section 3.3.1.1 for details). As a result, plots of the major elements in the gabbro suite display a large range in composition. The left-hand plot in Figure 4.1 (Fe-Na-Mg) illustrates the co-variation of Na and Mg (left-right trend) in the Allalin gabbros and gabbroic eclogites, while the proportion of Fe remains relatively constant. However, this is an artefact of the plot and Figure 4.2 reveals that Fe_2O_3 abundance decreases (from 8.2 to 1.2 wt %) as MgO decreases, although the range in MgO is much larger (18 to 1.5 wt %). In the second plot (Ca-Mg-Na), the gabbros, transitional gabbros and gabbroic eclogites (from this point forward termed 'gabbroic lithologies') form a rough trend of decreasing MgO content, and complementary increases in CaO and Na_2O abundance. The basaltic samples will be discussed in the relevant sections.

The addition of olivine may explain the positive correlation between MgO and Fe_2O_3 shown in Figure 4.2 (a). As fractional crystallisation progresses, and Mg content decreases, Fe abundances usually increase (or perhaps stay the same), until Fe-Ti gabbro compositions are reached, as shown in the basaltic trend in Figure 4.2. However, in the case of cumulate gabbros, the rock composition does not represent the liquid from which its components crystallised. The major element composition of the gabbroic lithologies depends on the varying proportions of the major cumulate minerals (usually plagioclase and olivine). Consequently, a sample with low MgO will have correspondingly low Fe_2O_3 as a result of plagioclase being the principal component. As Al is not partitioned into olivine, the Al content of a sample will increase as MgO decreases (Figure 4.2 b), due to a decrease in the modal abundance of olivine. The small cluster of several metagabbros which lie below the general trend in Figure 4.2 b (to Al-poor compositions) appear to correspond to samples which have a greater modal abundance of augite, thus

producing rocks that are poorer in Al_2O_3 and/or MgO (and richer in Ca), relative to samples which are predominantly troctolitic.

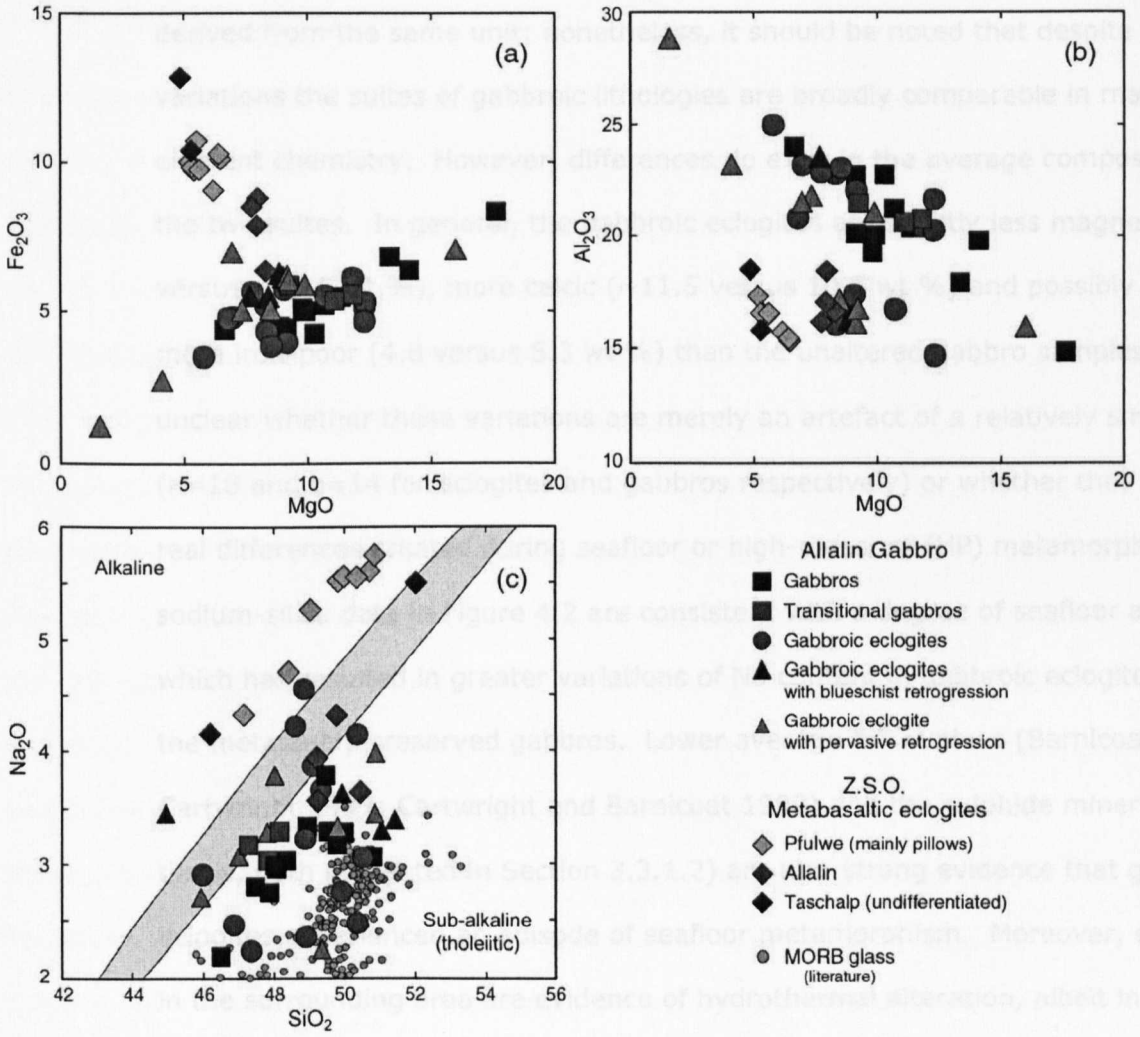

Figure 4.2. Major element plots for the gabbroic lithologies of the Allalin and metabasaltic samples from the ZSO. **(a)** Note the very well-defined positive correlation between Fe and Mg for gabbroic lithologies. Conversely, metabasaltic samples display a positive trend. See the text for discussion. The absence of a correlated decrease of Fe and MgO in the basaltic trend in (a) suggests that the point of crystallisation of an Fe-Ti phase has not been reached. Ilmenite is, however, present in many gabbroic samples. **(b)** Al is negatively correlated with MgO in gabbroic lithologies. This trend is essentially due to mixing between Al-rich plagioclase and MgO-rich olivine endmembers, during accumulation. Some metagabbros plot below the trend line due to the greater abundance of augite in these samples. Metabasalts display little correlation. **(c)** Metabasalts plot in the alkaline field, although this is due to elevated Na content and not K, and so perhaps suggests seafloor alteration as a source. Field for alkaline basalts in (c) is from Boyle (1989). MORB data from *Petrological database of the ocean floor* (2004) and A. Gannoun, unpublished data.

The gabbros, transitional samples and gabbroic eclogites have broadly the same compositional range, but considerable variation exists within each suite (Figure 4.1). A similarity between the Allalin suites is hardly surprising given that they are derived from the same unit; nonetheless, it should be noted that despite cumulate variations the suites of gabbroic lithologies are broadly comparable in major element chemistry. However, differences do exist in the average composition of the two suites. In general, the gabbroic eclogites are slightly less magnesian (~9.5 versus ~10.5 wt %), more calcic (~11.5 versus 10.5 wt %) and possibly slightly more iron-poor (4.8 versus 5.3 wt %) than the unaltered gabbro samples. It is unclear whether these variations are merely an artefact of a relatively small dataset (n=18 and n=14 for eclogites and gabbros respectively) or whether they reflect real differences created during seafloor or high-pressure (HP) metamorphism. The sodium-silica data in Figure 4.2 are consistent with a degree of seafloor alteration which has resulted in greater variations of Na content in gabbroic eclogites than in the metastably preserved gabbros. Lower average $\delta^{18}O$ values (Barnicoat and Cartwright 1997; Cartwright and Barnicoat 1999) and the sulphide mineralogy (this thesis, both presented in Section 3.3.1.2) are also strong evidence that gabbroic eclogites experienced an episode of seafloor metamorphism. Moreover, epidosites in the surrounding area are evidence of hydrothermal alteration, albeit in units which may not necessarily have been in close proximity to the Allalin Gabbro during its seafloor history. The oxygen isotope data, depletion in Mg, enrichment in Ca and variable Na are consistent with alteration in the high-temperature up-flow zones of hydrothermal systems (e.g. Cartwright and Barnicoat 1999).

To summarise, in comparison with average compositions of oceanic crustal gabbros (Poli and Schmidt 2002 and references therein) and data from the Rocciavrè metagabbro, Western Alps (Pognante 1985), the Allalin gabbros can be classified as Si-rich, Al-poor troctolitic compositions and Al-rich olivine gabbros. This reflects

the predominance of plagioclase and olivine in the rocks, but with the addition of a variable quantity of augitic pyroxene.

4.1.2 Basaltic eclogites

The silica contents (48.5 – 51 wt. %) of the (originally) fine grained metabasites collected from Pfulwe, Täschalp and the Allalin unit are consistent with average MORB (50.45%, Hofmann 1988), with the exception of two samples (SiO_2 = 46.2 and 47.1 wt. %). When displayed on a Na-Fe-Mg triangular plot (Figure 4.1), the ZSO metabasalts plot towards more sodic (and less iron-rich) compositions than fresh MORB, perhaps suggesting seafloor alteration entailing sodium addition. Some data for back-arc basalts from the Lau basin are also plotted to provide a comparison with rocks from this tectonic setting. In terms of major elements, the Lau basin samples do not deviate from the average MORB field and thus it is likely that the enrichment in Na is the result of either greater differentiation or seafloor alteration. Furthermore, on the second triangular plot (Ca-Mg-Na) the metabasalts plot in two groups, one close to the MORB differentiation trend, and the other towards lower relative Ca and higher Na. The latter group lie between the fractionation trend for MORB and the field of seafloor altered MORB suggesting that perhaps both processes have a role in determining the observed major element patterns. Figure 4.2 (c) illustrates the Na enrichment of the Pfulwe metabasalts while also displaying silica contents, with the result that Na (but not K) appears to be enriched above the level expected for a given silica content in a tholeiitic sample. Therefore, it seems most probable that the sodium enrichment is largely due to seafloor alteration processes. The data do, however, plot in a fairly well-defined trend, which would not normally be consistent with variable seafloor alteration, except for the fact that this group of samples was collected from a relatively small area. The metabasaltic and metagabbroic samples from the Allalin do not display Na enrichment to the same extent (gabbroic eclogites display variable Na including some depleted samples). This observation is consistent with

a lesser degree of hydrothermal alteration, due to their position at deeper levels in the crust. In addition, if gabbroic samples had been extensively altered, they may have been more prone to subsequent HP deformation, which is inconsistent with a large part of the unit being remarkably undeformed.

The presence of epidosites in the area around Pfulwe is definitive evidence of high temperature seafloor alteration. It is, however, often suggested that rocks in the high temperature up-flow zones are depleted in Na, rather than enriched *(see* Section 2.1.2*)*. Whether the ZSO metabasalts possess a degree of back-arc basin signature will be discussed further in the light of trace element data presented below (Section 4.3.2).

The fractionation trend for MORB forms a negative slope on an MgO-Fe_2O_3 plot (Figure 4.2 a), until the stage at which magnetite (or perhaps Fe-Ti oxides) crystallises, at which point, the trend becomes positively correlated (Fe decreases as Mg decreases). The absence of a downturn in the basaltic trend in either Figure 4.1 (a) suggests that the point of magnetite (± other Fe-Ti oxides) crystallisation has not been reached. However, Figure 4.1 and Figure 4.2 (a) suggest that the metabasalts are significantly fractionated, and that the extent of fractionation increases from the Allalin samples, through the pillows to the undifferentiated Pfulwe samples and finally to the other undifferentiated Täschalp samples.

4.2 Major elements in the metagabbros and metabasalts of the Sulitjelma ophiolite, northern Norway

The major and trace element chemistry of the Sulitjelma ophiolite samples has been described previously by Boyle (1982; 1989), but I will outline some of the key features in the following sections.

4.2.1 Metagabbros

The metagabbros of the Sulitjelma ophiolite are clearly chemically complex and varied, as illustrated in Figure 4.3 and Figure 4.4. Some of the samples are cumulates (Mason 1966; 1971; Boyle 1982) and as such display large major element variations. Unlike the Allalin samples there is no correlation between MgO and Al_2O_3 (Figure 4.4), which precludes control of major element chemistry by plagioclase and olivine. Indeed, clinopyroxene (augite), orthopyroxene (ferro-enstatite) and a brown hornblende are all present in some samples, and for this reason there are no simple cumulate mixing lines.

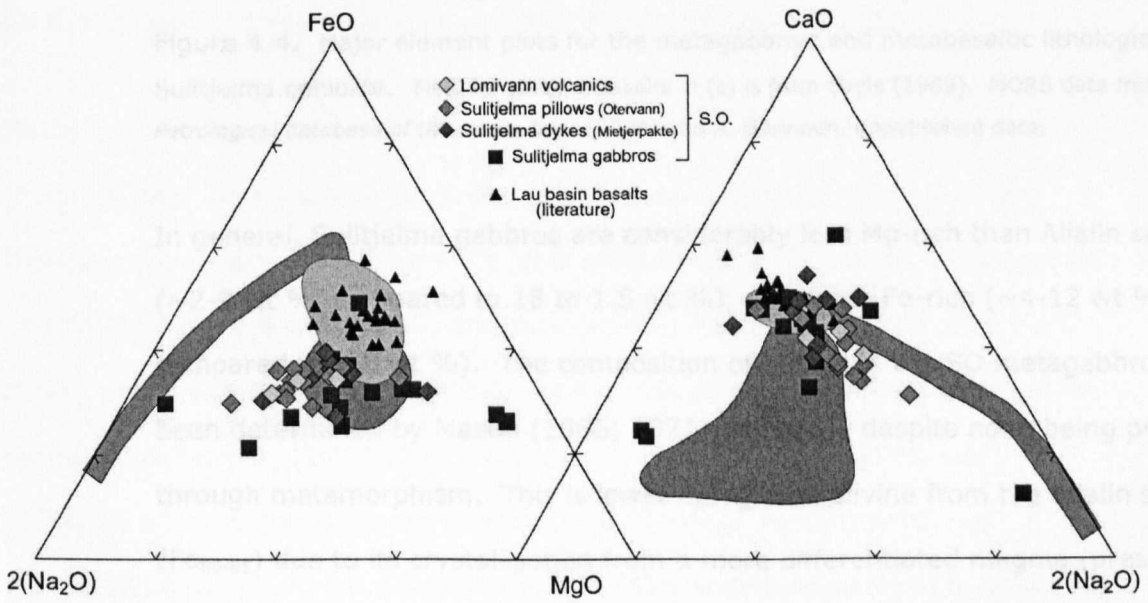

Figure 4.3. Triangular Fe-Na-Mg and Ca-Mg-Na plots of major element compositions of the main suites of samples from the Sulitjelma ophiolite. See text for discussion. Literature data and fields referenced in Figure 4.1. Major element abundances are presented in Appendix B, Tables B3 and B4.

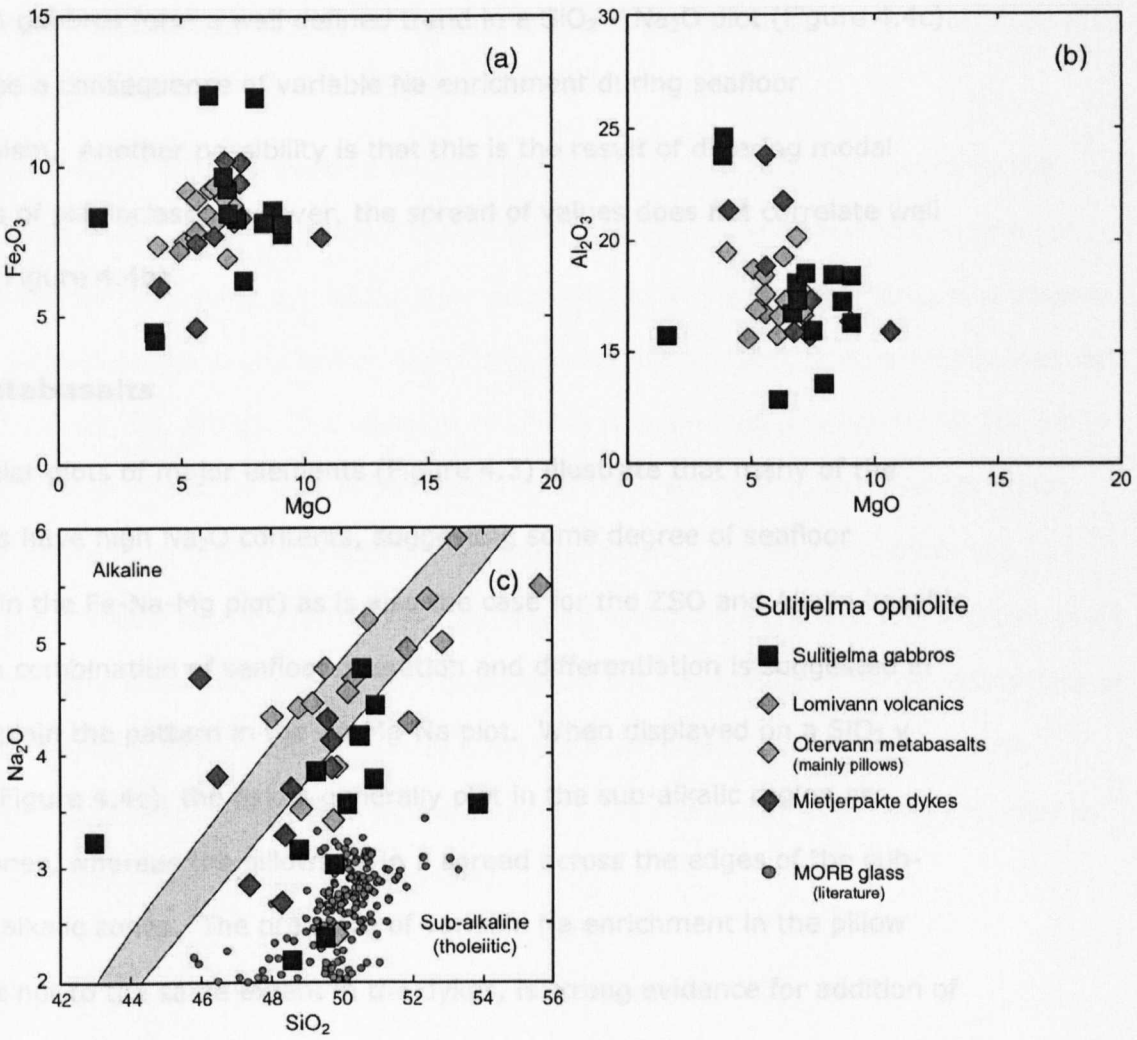

Figure 4.4. Major element plots for the metagabbroic and metabasaltic lithologies of the Sulitjelma ophiolite. Field for alkaline basalts in (c) is from Boyle (1989). MORB data from *Petrological database of the ocean floor* (2004) and A. Gannoun, unpublished data.

In general, Sulitjelma gabbros are considerably less Mg-rich than Allalin samples (~2-9 wt %, compared to 18 to 1.5 wt %), and more Fe-rich (~4-12 wt %, compared to 1-8 wt %). The composition of olivine in the SO metagabbros has been determined by Mason (1966; 1971) as Fo_{50-80}, despite none being preserved through metamorphism. This is lower in Mg than olivine from the Allalin samples (Fo_{80-85}) due to its crystallisation from a more differentiated magma (presumably after extraction of some Allalin type cumulates). The larger range in Al_2O_3 content than MgO is indicative of a greater role of plagioclase accumulation than olivine.

With the exception of two samples (one with very high and one with very low

values), the gabbros form a well defined trend in a SiO_2 – Na_2O plot (Figure 4.4c). This could be a consequence of variable Na enrichment during seafloor metamorphism. Another possibility is that this is the result of differing modal abundances of plagioclase; however, the spread of values does not correlate well with Al_2O_3 (Figure 4.4b).

4.2.2 Metabasalts

The triangular plots of major elements (Figure 4.3) illustrate that many of the metabasalts have high Na_2O contents, suggesting some degree of seafloor alteration (in the Fe-Na-Mg plot) as is also the case for the ZSO and Allalin basaltic samples. A combination of seafloor alteration and differentiation is suggested in order to explain the pattern in the Ca-Mg-Na plot. When displayed on a SiO_2 v Na_2O plot (Figure 4.4c), the dykes generally plot in the sub-alkalic region or between zones, whereas the pillows lie in a spread across the edges of the sub-alkalic and alkalic zones. The presence of variable Na enrichment in the pillow basalts, but not to the same extent in the dykes, is strong evidence for addition of Na during seafloor alteration (discussed further in Section 4.2.2.3).

There is no well defined trend in iron content in any of the metabasaltic suites (Figure 4.4a). No trend can be picked out for pillows from the Lomivann and Otervann formations, while there is a very weak positive correlation between MgO and Fe_2O_3 in the dyke samples, perhaps indicating the crystallisation of an Fe-Ti oxide, which leads to decreasing Fe_2O_3 as MgO decreases. However, a plot of Mg number against TiO_2 (not shown) does not display a decrease in TiO_2 which is indicative of insubstantial crystallisation of Fe-Ti oxide. Furthermore, the metabasaltic samples from Sulitjelma form a fairly well-defined trend in an Mg number versus Fe_2O_3 plot (not shown).

4.3 Trace elements in gabbros, metagabbros and metabasalts of the Zermatt-Saas ophiolite

One aspect of trace element analysis in this study is to determine whether the ophiolites in question possess typical N-MORB-type trace element signatures, or whether, like many ophiolites, they were formed in a back-arc setting and possess corresponding trace element signatures which are enriched in fluid-mobile elements (e.g. Rb, Ba, Sr, U). The importance of this is to provide a 'baseline' for the main thrust of this work, which is the analysis of trace element budgets within mafic oceanic crust during high-pressure metamorphism. In order to identify the geochemical starting point and to compare the current data with that starting point, the data have been plotted on a spidergram and normalised to the N-MORB data of Hofmann (1988), rather than the standard normalisation to primitive mantle composition. Data were determined by ICP-MS except Zr, which was analysed by XRF (see Section A.4.1 for rationale).

4.3.1 Allalin gabbros and gabbroic eclogites

The cumulate nature of the Allalin unit has led to distinct and varied trace element patterns. As the samples do not represent the composition of a single magma from which they formed, the data cannot be used to determine the tectonic setting of formation. Instead, their trace element patterns are dominated by the variable modal abundance of plagioclase (approximately 50-70%), which produces strong positive anomalies in Ba, Sr and Eu (Figure 4.5). With the exception of these elements, and Cs and K, most of the gabbroic lithologies contain very low abundances of most trace elements (less than half the N-MORB value). Samples with higher concentrations of HREE are, for the most part, those samples which plot below the main trend (lower Al_2O_3) in the Al_2O_3-MgO plot (Figure 4.2b), due to a greater modal abundance of augite (Section 4.1.1). The higher abundances of HREE in these samples are most likely due to their high augite content.

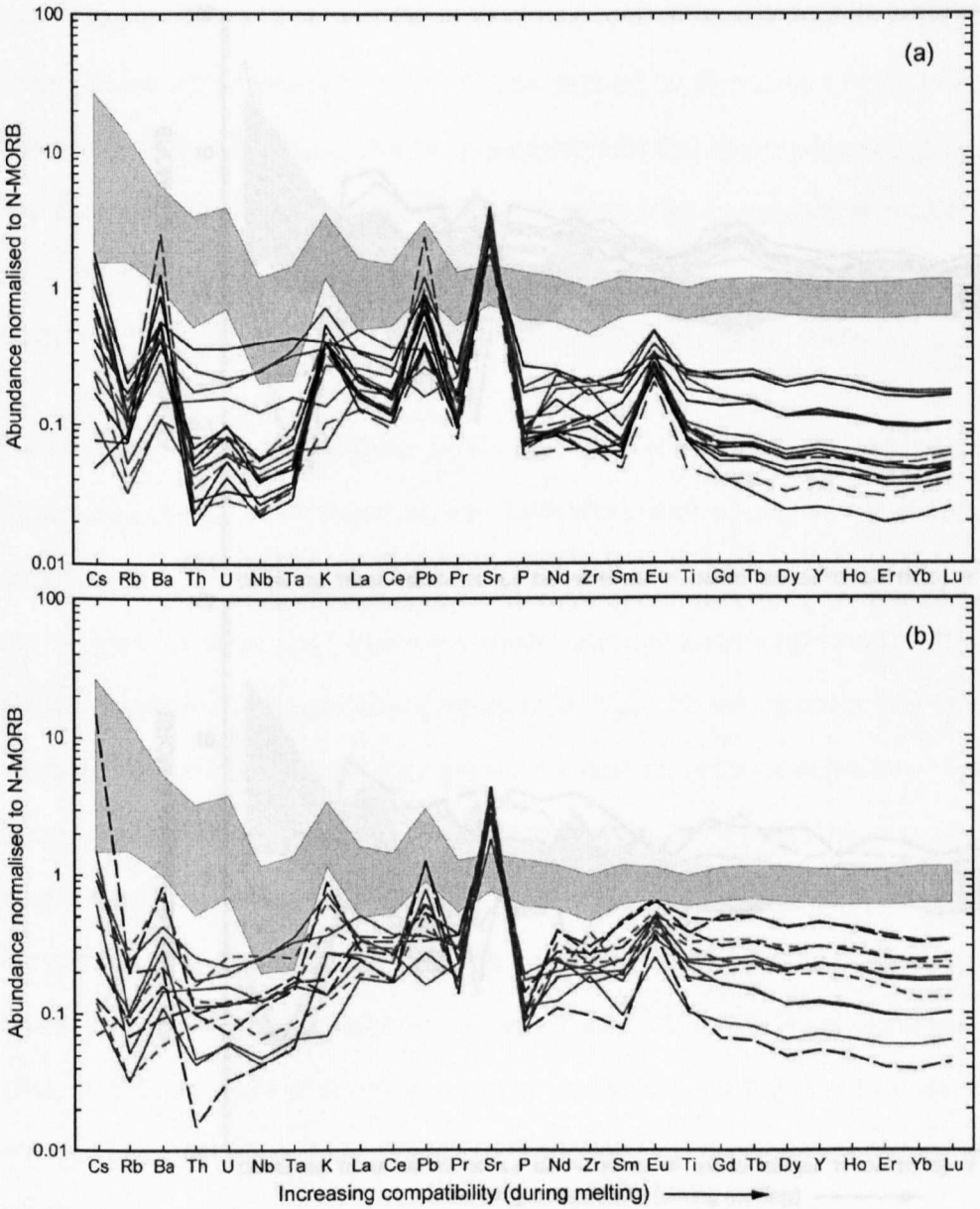

Figure 4.5. N-MORB normalised spidergram for gabbroic lithologies from the Allalin unit, ZSO (N-MORB data from Hofmann (1988)). See text for discussion. (a) very dark blue denotes largely unaltered gabbro, red dashed lines denote transitional eclogites and red unbroken lines denote gabbroic eclogites. (b) Gabbroic eclogites shown for reference by red lines, eclogites with blueschist retrogression shown by blue long-dashed lines, eclogites with greenschist retrogression shown by green short-dashed lines. Back-arc basin basalts shown by light grey field (Lau basin data from Sun et al. 2003c). Trace element abundances are presented in Appendix B, Table B1.

4.3.2 Basaltic eclogites

The patterns of trace elements on the N-MORB normalised multi-element plot in Figure 4.6 are similar in shape to MORB, although somewhat displaced to higher abundances. Unlike the plotted Lau basin field and the Sulitjelma samples

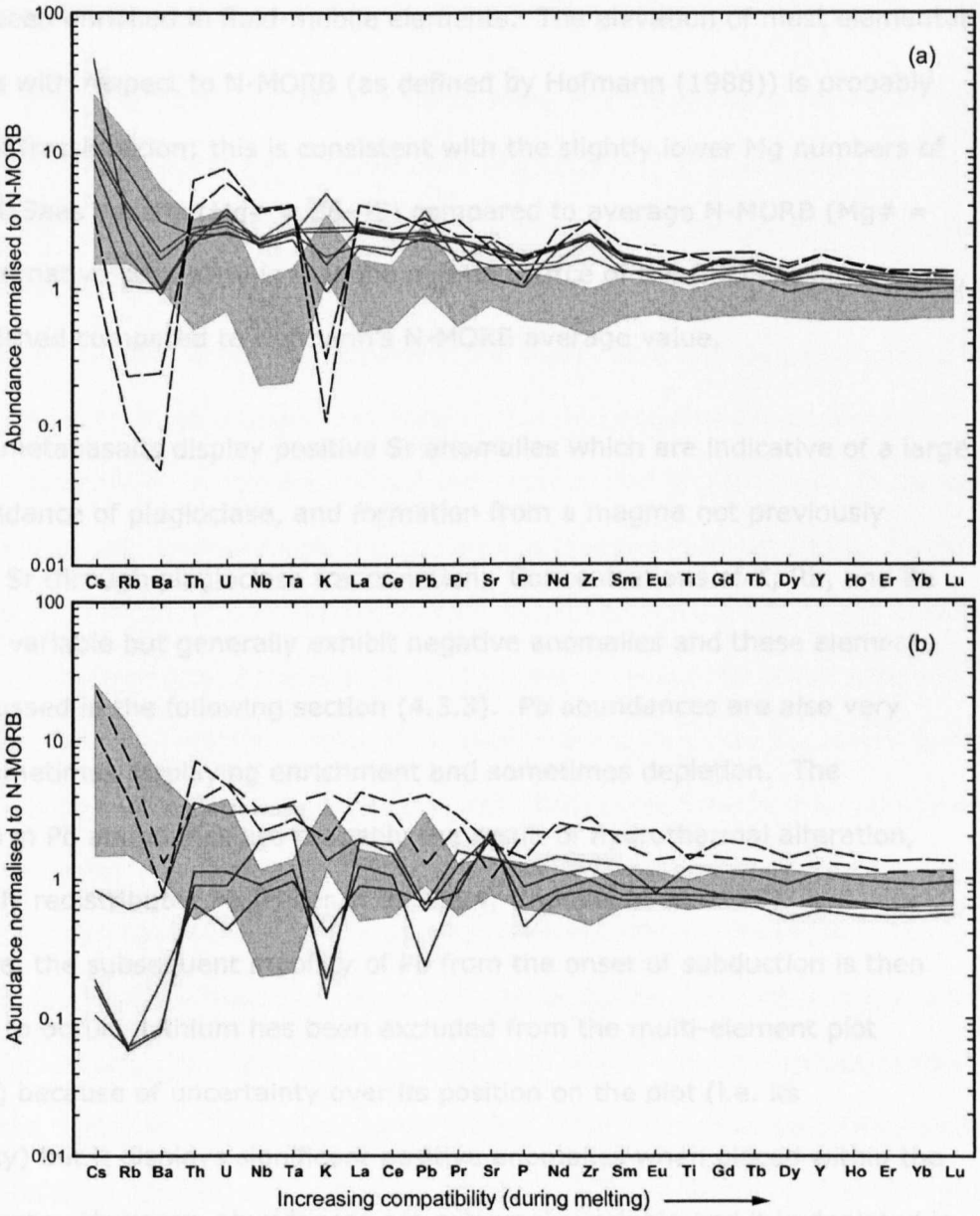

Figure 4.6. N-MORB normalised spidergram for metabasaltic samples from the Zermatt-Saas ophiolite (N-MORB data from Hofmann (1988)). See text for discussion. (a) Pfulwe metabasalts – green lines for pillows, black dashed lines for undifferentiated metabasalts. (b) Allalin basalts (green lines) and undifferentiated metabasalts from Täschalp (black dashed lines. Back-arc basin basalts shown by light grey field (Lau basin data from Sun et al. 2003c). Trace element abundances are presented in Appendix B, Table B2.

(discussed in Section 4.4), ZSO metabasalts do not possess distinct negative Nb, Ta or Zr anomalies (the latter actually has a slightly positive anomaly), and Ti can be slightly enriched or depleted with respect to similarly compatible elements. The lack of negative HFSE anomalies (Nb, Ta, Zr) is strong evidence for a typical MORB source for these basalts, rather than a supra-subduction mantle wedge source

which has been enriched in fluid-mobile elements. The elevation of most elemental abundances with respect to N-MORB (as defined by Hofmann (1988)) is probably the result of fractionation; this is consistent with the slightly lower Mg numbers of the Zermatt-Saas basalts (Mg# = 36-43) compared to average N-MORB (Mg# = 42). An alternative possibility is that the mantle source of the ZSO basalts was slightly enriched compared to Hofmann's N-MORB average value.

Two Allalin metabasalts display positive Sr anomalies which are indicative of a large modal abundance of plagioclase, and formation from a magma not previously depleted in Sr through plagioclase fractionation. Concentrations of K, Rb, and Ba are all very variable but generally exhibit negative anomalies and these elements will be discussed in the following section (4.3.3). Pb abundances are also very variable, sometimes displaying enrichment and sometimes depletion. The fluctuations in Pb abundance are probably the result of hydrothermal alteration, which readily redistributes Pb (Miller et al. 1994; Chauvel et al. 1995). Furthermore, the subsequent mobility of Pb from the onset of subduction is then more likely to occur. Lithium has been excluded from the multi-element plot (Figure 4.6) because of uncertainty over its position on the plot (i.e. its compatibility) but it displays significant positive anomalies when placed within the HREE elements. However, abundances are extremely variable and it is depleted in some samples with respect to N-MORB. Interestingly, all the samples which appear to be depleted in Li also have anomalously low abundances of Rb, Ba and K, although conversely, some samples depleted in Rb, Ba and K do not display depletion in Li. These data suggest that Li may be mobile during high-pressure metamorphism, as is inferred from high Li concentrations and an isotopically light lithium signature in many arc basalts (e.g. Tomascak et al. 2002).

4.3.3 Element mobility in ZSO metagabbros and metabasalts

Some fluid mobile element concentrations are presented in Figure 4.7, normalised to the Yb abundance (a non-mobile element) and plotted against Nb/Yb in order to take into account the effects of partial melting and fractional crystallisation. The field for MORB forms well-defined linear trends (on log-log plots). Data from gabbroic lithologies, particularly in the Allalin unit, cannot be compared to MORB values as trace element concentrations in the gabbros are dependent on accumulation processes and not the fractionation of a magma. In the case of the Allalin unit, unaltered gabbro has been preserved in a metastable state throughout both seafloor and HP metamorphism, providing the opportunity to directly measure the composition of the protoliths. In order to gauge the occurrence and magnitude of elemental mobility during HP metamorphism, it is also necessary to consider the effects of seafloor metamorphism, which may also include the mobility of certain elements, resulting in possible enrichments or depletions when compared to protolith compositions. The data for altered MORB of Staudigel (1996) suggest that fluid mobile elements are more likely to be added than lost during seafloor alteration. Other authors (e.g. Hart et al. 1999) concur with this observation. For the purposes of the following discussion, I have assumed that any elemental *loss* from the eclogitic samples is the result of mobility during HP metamorphism and not through seafloor alteration, although clearly the reality may be more complex. If one assumes that seafloor alteration generally results in the enrichment of fluid-mobile elements, the elemental loss estimated from the HP metamorphic rocks of the ZSO will be a *minimum* value, conversely, if alteration results in element depletions, overestimates of the HP losses will occur.

It should be noted, prior to examining the 'M'/Yb – Nb/Yb plots, that one gabbro and one gabbroic eclogite have anomalously high Nb abundances (>1 ppm) relative to the other gabbroic samples and thus may plot to the lower right of the rest of

the gabbro field due to an elevated Nb/Yb and not due to a lower 'M'/Yb ratio (both samples do consistently plot to the lower right of the rest of the gabbro field).

The high Nb abundance in these cases is most likely due to the accumulation of ilmenite into which Nb is preferentially partitioned (e.g. Pearce 1990). The use of such discrimination diagrams as a means of estimating element mobility and loss assumes the immobility of both Nb and Yb. If Yb is lost, because it is used to normalise both axes, both ratios will increase and consequently the estimates will not be affected greatly. However, if Nb is gained or lost, the Nb/Yb ratio will either increase or decrease leading to, respectively, an overestimate or an underestimate of element loss. This is due to the compatibility controlled slopes of the trends in igneous systems (Figure 4.7). Losses quoted may be minimum estimates as the protolith composition used as a reference point was assumed to plot at the low 'M'/Yb ratio side of the MORB field.

Metagabbros.

Lanthanum data are plotted in Figure 4.7f, and provide a reference with which to compare the other data. La is thought to be moderately mobile, as illustrated by LREE enrichments in arc magmas, but its mobility is less extreme than the LILE. As can be seen in this plot, most of the gabbroic eclogites, including those with retrogression, plot in the same field as the gabbros. Allowing for the two samples with unusually high Nb concentrations, there are possibly three well preserved eclogites and three eclogites with pervasive retrogression (termed 'metagabbro' from this point) that *may* have experienced La loss, although the field for gabbroic lithologies appears to be reasonably broad and the outer limits may not be defined well by a dataset of this size. If the field was broader, then no observable La loss would have occurred.

Similarly, the plot involving uranium (Figure 4.7e), illustrates the well constrained nature of U/Yb ratios in the gabbroic lithologies and there appears to have been no

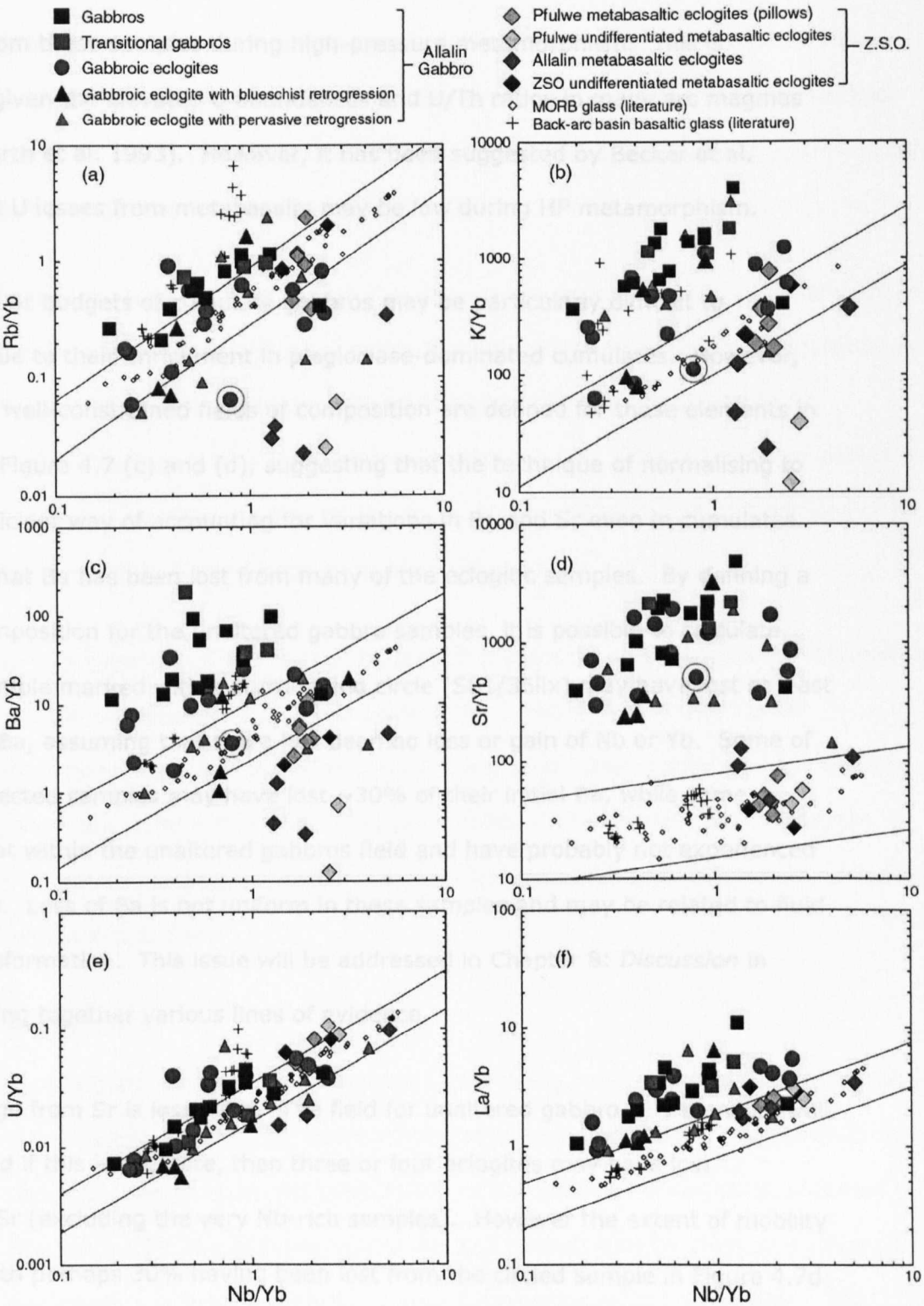

Figure 4.7. Non-conservative element discrimination plots (after Pearce 1983) for ZSO samples. M/Yb v Nb/Yb plots where M is the 'fluid mobile' element under examination and Nb is a non-fluid mobile element, with each normalised to Yb to minimise the effects of partial melting and fractionation. La and (surprisingly) U do not appear to have been mobile in either metagabbros or metabasalts. Rb, K and Ba display variable loss in both metagabbros and basaltic lithologies. The behaviour of Sr is unclear in these plots, possibly showing enrichments in two metabasalts. The parallel lines indicate the MORB field, as defined by data from Sun et al. (2003c), and A. Gannoun (unpublished). The circled gabbroic eclogite is S01/36iix and is referred to in the text.

loss of U from these samples during high-pressure metamorphism. This is surprising given the elevated U abundances and U/Th ratios in many arc magmas (Hawkesworth et al. 1993). However, it has been suggested by Becker et al. (2000) that U losses from metabasalts may be low during HP metamorphism.

The Ba and Sr budgets of cumulate gabbros may be particularly difficult to ascertain due to their enrichment in plagioclase-dominated cumulates. However, reasonably well-constrained fields of composition are defined for these elements in gabbros in Figure 4.7 (c) and (d), suggesting that the technique of normalising to Yb is an efficient way of accounting for variations in Ba and Sr even in cumulates. It is clear that Ba has been lost from many of the eclogitic samples. By defining a zone of composition for the unaltered gabbro samples, it is possible to calculate that the sample marked with a surrounding circle (S01/36iix) may have lost at least 80% of its Ba, assuming that there has been no loss or gain of Nb or Yb. Some of the less affected samples may have lost ~30% of their initial Ba, while some samples plot within the unaltered gabbros field and have probably not experienced any Ba loss. Loss of Ba is not uniform in these samples and may be related to fluid flow and deformation. This issue will be addressed in Chapter 8: *Discussion* in order to bring together various lines of evidence.

The message from Sr is less clear. The field for unaltered gabbro is reasonably well defined, and if this is accurate, then three or four eclogites may have lost significant Sr (excluding the very Nb-rich samples). However the extent of mobility is lower, with perhaps 30% having been lost from the circled sample in Figure 4.7d (the same sample that may have lost 80% of its Ba).

Rubidium and potassium both appear to have been mobile during HP metamorphism. Six gabbroic eclogites (out of 12 samples with normal Nb abundances), two of the eclogites with blueschist retrogression and half of the samples with pervasive greenschist retrogression have experienced K loss. The lost

K, as a proportion of the original composition, may be up to 70-80% in some samples, including the sample S01/36iix previously mentioned. Rubidium loss occurs on the same scale (~70-90% in some samples), and affects approximately half of the analysed gabbroic eclogites.

Losses of LILE from transitional samples are not clearly evident, especially not in the case of K and Sr. The transitional samples have primarily only undergone an episode of seafloor metamorphism/alteration, although considerable HP recrystallisation is also present (see Section 3.3.1.2). These two observations are consistent with the mobility of Ba, Rb, K, and possibly Sr, under conditions of HP metamorphism and not during seafloor alteration.

In summary, Rb, K and Ba can be lost from gabbroic samples in proportions of up to 90% of the original protolith composition, probably as a result of HP metamorphism. The message from Sr data is not clear, partly perhaps because of the strong control of plagioclase accumulation on Sr abundances in gabbroic cumulates. Lanthanum does not appear to be mobile, and surprisingly, U does not exhibit loss either.

Metabasalts.

The Zermatt-Saas ophiolite contains no surviving relics of igneous basaltic material. (The reasons behind the incomplete transformation of gabbros compared to the complete metamorphic recrystallisation of the basaltic lithologies is discussed in Section 3.3.3) For this reason, comparison of metabasaltic chemistry must be made with a reference material, rather than the protolith composition. The arguments laid out in previous sections of this chapter conclude that the ZSO has geochemical characteristics which are consistent with a N-MORB type mantle source, and thus comparison has been made with this reservoir. A field for MORB is plotted on the diagrams in Figure 4.7, based on data from Sun et al. (2003c) and unpublished data from A. Gannoun.

In the metabasalts, neither U nor La appears to deviate from the range of MORB (Figure 4.7, e and f respectively). Several basalts plot just above the upper limit for the drawn MORB range; however, two actual measured MORB glasses also plot outside this average field. Two samples from the Allalin unit plot clearly below the MORB zone, but U loss from these samples may be as little as 10-20%.

Rubidium is lost to a great extent from the undifferentiated metabasaltic eclogites of Pfulwe and the Allalin metabasalts. Although it is probable that most of the loss of Rb, and other fluid mobile elements, occurred during prograde and peak HP metamorphism (concomitant with dehydration reactions), it is also possible that the retrogression of the Allalin samples may have affected the budget of fluid mobile elements. Retrogression was accompanied by some fluid flow as is apparent from the more hydrous assemblage of the retrogressed samples compared with purely eclogitic samples. For this reason, estimates of element loss will be based on the undifferentiated and pillow basalts of the Pfulwe pass area.

Barium and K display similar patterns of elemental loss as those for Rb. For all three of these elements, there are several pillow samples that do not appear to have undergone significant loss. This is almost certainly a reflection of the lower degree of deformation and accompanying fluid flow that these samples have experienced. As a result, estimates of Ba loss range from 98% in the most extreme case (one of the undifferentiated Pfulwe metabasalts) through 50% in some of the pillows, to zero in at least one pillow sample. For Rb, estimates range from ~95% in undifferentiated samples, to between 60% and 0% in pillows. In the case of Rb, several pillow samples plot within the MORB field, indicating that loss has not occurred. Losses of K range from 85-95% in the undifferentiated samples, through 25% to zero loss in the pillow basalts.

The message from Sr is again not clear (Figure 4.7d). Several basaltic samples plot above the MORB field, presumably due to a high modal abundance of plagioclase.

In Figure 4.7 (d), no Sr loss is apparent. In an attempt to see through the effects of plagioclase accumulation I have compared the concentrations of Eu and Sr in metabasalts and gabbroic lithologies.

Figure 4.8 illustrates the enrichment and depletion of Eu and Sr in ZSO gabbros and metabasalts respectively. These enrichments and depletions are largely the result of crystallisation processes with Sr and Eu being preferentially partitioned into plagioclase which is particularly abundant in the cumulate gabbros of the Allalin. In an attempt to assess the possible mobility of Sr during HP metamorphism, Sr/Sr* and Eu/Eu* ratios have been used which compare measured Sr and Eu abundances with those extrapolated from adjacent elements on the spidergram (see Figure 4.8 caption for explanation of ratios). The negative Eu/Eu* and Sr/Sr* anomalies of the metabasalts indicate the extraction of plagioclase from the magma at an earlier stage. However, Eu/Eu* values are consistently ~0.8 - 0.95, whereas, with the exception of basalts displaying positive anomalies (which must have a high modal abundance of plagioclase), Sr/Sr* varies from 0.4 -0.98, suggesting that metabasalts are variably depleted in Sr, over and above that expected from Sr partitioning into cumulate plagioclase. These data suggest the mobility of Sr in high-pressure metamorphic fluids. However, some of this effect may be related to the greater enrichment of Sr in the gabbros (and therefore extraction from the melt) over Eu (Sr/Sr* <24 and Eu/Eu* < 7). This argument depends on whether the gabbros and basalts were co-genetic, although presumably the greater enrichment of Sr observed in these cumulate gabbros, may also be found in other cumulate bodies. Nonetheless, the variability of Sr is far greater than Eu in the metabasalts, and this is consistent with some loss of Sr from the metabasalts. The Sr/Yb – Nb/Yb plot in Figure 4.7d also indicates that some loss of Sr may also occur from gabbroic eclogites, although most of the samples do not appear to have experienced Sr loss. Overall, the evidence suggests variable loss of Sr, with some samples perhaps losing a moderate proportion (30%?) of their initial abundance.

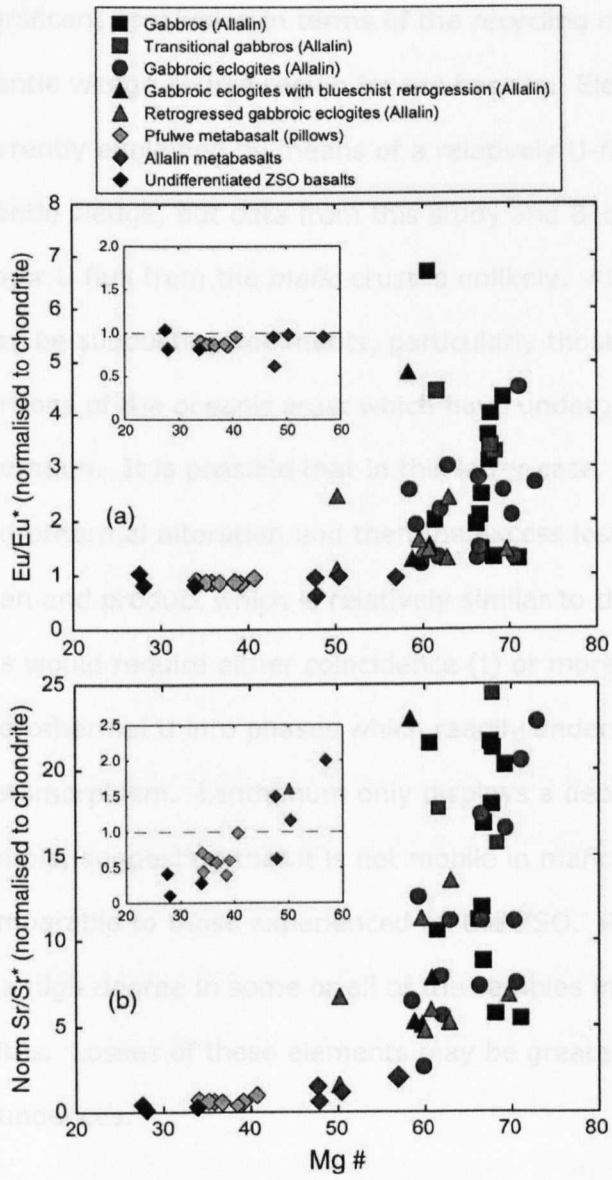

Figure 4.8. Illustration of Eu and Sr enrichment and depletion in ZSO gabbros and metabasalts respectively, by comparison of measured and expected Eu and Sr abundances. Eu/Eu* negative anomalies are consistently ~0.8 - 0.95, whereas Sr/Sr* varies from 0.4 - 0.98, suggesting that metabasalts are variably depleted in Sr, over and above that expected from Sr partitioning into the gabbros. However, some of this effect may be related to the greater enrichment of Sr in the gabbros over Eu (Sr/Sr* up to 24 and Eu/Eu* only up to 7) Sr/Sr*: Sr is the chondrite-normalised measured abundance of Sr, Sr* is the chondrite-normalised calculated expected abundance of Sr, using the normalised abundances of Ce and Nd (which bracket Sr in terms of compatibility). The use of chondrite-normalised values eliminates the discrepancies in natural abundance of the elements used. The calculation of Eu* uses Sm and Gd chondrite-normalised abundances.

In summary, although slight variations exist in U/Yb ratios compared to the range of MORB, there is no significant loss of U from the ZSO metabasalts. This is a

significant conclusion in terms of the recycling of slab-derived elements into the mantle wedge source region for arc basalts. Elevated U/Th ratios in arc basalts are currently explained by means of a relatively U-rich flux from the slab into the mantle wedge, but data from this study and Becker et al. (2000) suggest that a major U flux from the *mafic* crust is unlikely. Alternative sources of a U-rich fluid may be subducting sediments, particularly those of pelagic origin, or possibly portions of the oceanic crust which have undergone intense hydrothermal alteration. It is possible that in this latter case, U may be enriched during hydrothermal alteration and then the excess lost upon HP metamorphism, resulting in an end product which is relatively similar to the original composition. However, this would require either coincidence (!) or more likely, the incorporation of hydrothermal U into phases which readily undergo reactions during HP metamorphism. Lanthanum only displays a departure from MORB values in one sample, suggesting that it is not mobile in mafic systems under HP conditions comparable to those experienced by the ZSO. Rubidium, Ba and K are all depleted to a high degree in some or all of the samples in all the different metabasaltic suites. Losses of these elements may be greater than 90% of the original protolith abundances.

The plots for Rb and K (Figure 4.7 a and b) show at least one pillow sample that plots to the high end of, or above, the MORB field suggesting Rb and K gain in these samples (Rb abundance may be ~160% of the protolith composition). This enrichment may be the result of seafloor alteration, or may be due to infiltration of high-Rb-K fluids during high-pressure metamorphism. If the latter scenario is correct, it suggests elemental loss from one sample may enrich another. If this is commonly the case, estimates of elemental fluxes from the slab need to take into account not only the fact that slab fluids may be unable to move along pathways out of the slab, but also the fact that fluid may react with slab rocks during

transport and lead to enrichment in different parts of the slab, without net loss or gain for the slab.

4.3.4 Summary of trace element information from ZSO samples

The Zermatt-Saas ophiolite appears, from basaltic trace element data, to have affinities with N-MORB, although most of the metabasalts analysed have higher than average trace element abundances. This is due to a greater extent of differentiation (as deduced from the low Mg#), and possibly due to enrichment of fluid-mobile elements during hydrothermal alteration. The trace element concentrations in the Allalin Gabbro samples are indicative of their cumulate nature and do not provide any information on the tectonic setting of formation.

Both gabbroic and basaltic eclogites appear, in at least some cases, to have lost a significant proportion (perhaps as high as 70-95%) of their inferred original inventories of Rb, K and Ba. Interestingly, pillow samples, which have undergone less pervasive deformation, seem to have lost a lower proportion of Rb, K and Ba. The message from Sr is complicated by the strong enrichment of this element in accumulated plagioclase, and the corresponding depletion in basaltic magmas which have previously undergone fractional crystallisation. However, some samples may have lost up to 30% of their original Sr. Neither U nor La display depletion in either the gabbroic or basaltic suites. A lack of U loss from examples of subducted mafic oceanic crust has been previously observed by Arculus et al. (1999) and Becker et al. (2000), and this may be significant considering the U excesses that are observed in many arc basalts. This suggests an alternative source for the extra U in arc magmas; this is likely to be from subducted sediment, although stripping of U from the mantle wedge cannot be ruled out (e.g. Arculus and Powell 1986).

4.4 Trace elements in the metagabbros and metabasalts of the Sulitjelma ophiolite (SO), Northern Norway

4.4.1 Metagabbros

The cumulate nature of the Sulitjelma gabbros is reflected in the broad range of trace element abundances (Figure 4.9 and Figure 4.11). Europium, for the most part, is positively anomalous with respect to similarly compatible elements (Eu/Eu* = 0.94–5.3 and see Figure 4.9). This enrichment is the result of plagioclase accumulation into which Eu is preferentially partitioned. Strontium and Ba also both display positive anomalies in most samples, which is also the result of plagioclase accumulation. The magnitude of these peaks is not as great as those of the Allalin gabbros, although this is in part a result of the greater abundance of most trace elements in the Sulitjelma gabbros, reflecting their more differentiated nature. A strong positive anomaly in Pb abundance is evident, as is depletion in Nb and Zr.

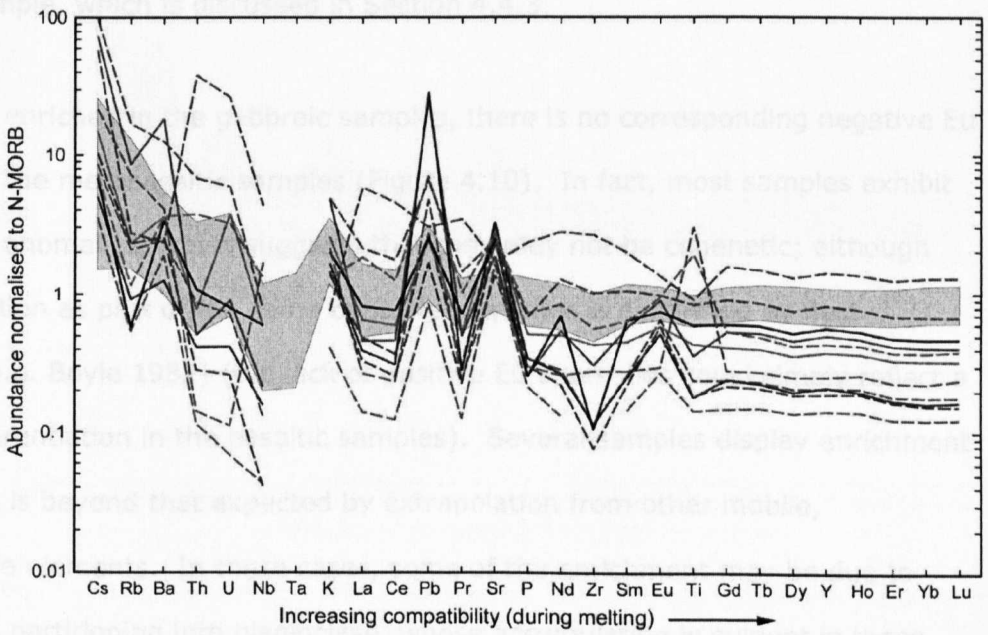

Figure 4.9. N-MORB normalised spidergram for metagabbroic samples from the Sulitjelma ophiolite (N-MORB data from Hofmann (1988)). Broken green lines denote metagabbros, unbroken shades of grey-black denote coarser, less recrystallised metagabbros. Field for back-arc basin basalts shown in grey, data from (Sun et al. 2003c). Tantalum data not plotted due to contamination by milling process. Trace element abundances are presented in Appendix B, Table B4.

With the exception of three of the samples, the trace element patterns presented in Figure 4.9 have similar shapes to the field for Lau Basin back-arc basalts. There is a degree of enrichment in the fluid mobile elements (Cs, Ba, U and sometimes Rb (see discussion in Section 4.4.4)), and crucially Nb is depleted relative to U, and Zr is anomalously low. The environment of formation of the gabbros will be discussed further in Section 4.4.3.

4.4.2 Metabasalts

A field for Lau basin back-arc basalts is drawn on the MORB-normalised spidergram in Figure 4.10. The trace element patterns of the Sulitjelma basalts (and gabbros) have broadly similar shapes, with enrichments in fluid-mobile elements (Cs, Rb, Ba, U, K) and negative anomalies in the high field-strength elements (HFSE) such as Nb and Ti (although not usually Zr). Rubidium displays a negative anomaly in many of the samples, in comparison with the similarly compatible and fluid mobile elements (e.g. Ba). The most striking feature of the patterns is the positive Pb anomaly in all but one sample, which is discussed in Section 4.4.3.

While Eu is enriched in the gabbroic samples, there is no corresponding negative Eu anomaly in the metabasaltic samples (Figure 4.10). In fact, most samples exhibit positive Eu anomalies, which suggests that they may not be cogenetic; although their formation as part of the same ophiolite sequence is confirmed by field evidence (e.g. Boyle 1982) (the lack of positive Eu anomalies could simply reflect a lack of differentiation in the basaltic samples). Several samples display enrichment in Ba which is beyond that expected by extrapolation from other mobile, incompatible elements. In these cases, some of the enrichment may be due to preferential partitioning into plagioclase, whose accumulation is evident in these samples from their positive Eu anomalies.

The three samples which are most enriched in the highly incompatible elements (left side of spidergram in Figure 4.10 a) belong to the Lomivann volcanic group and display a more strongly arc-like signature with extreme enrichment in the more mobile elements (Cs, Rb, Ba, Th? and U). Furthermore, these samples are enriched

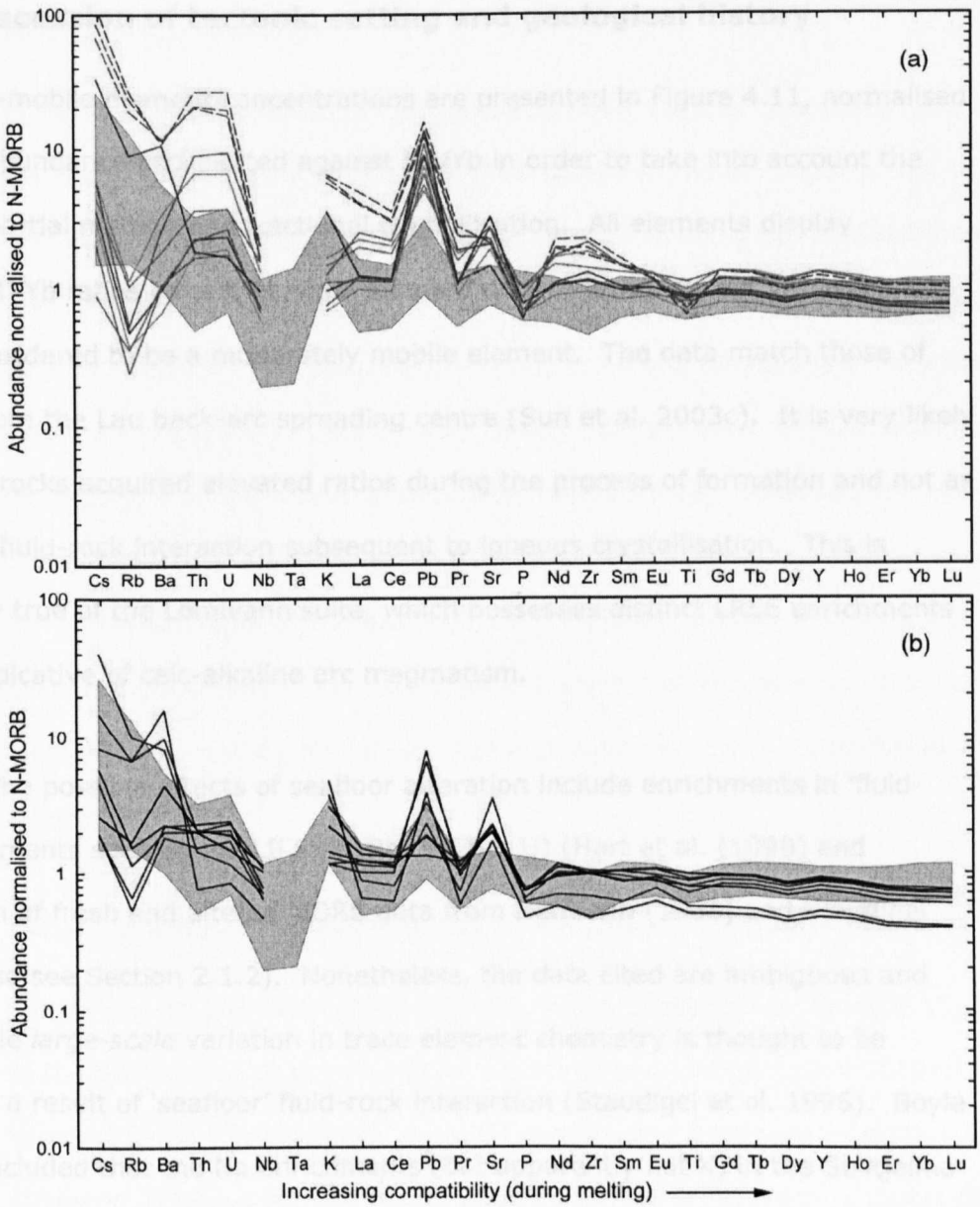

Figure 4.10. MORB normalised spidergram for metabasaltic samples from the Sulitjelma ophiolite (N-MORB data from Hofmann (1988)). (a) Lomivann volcanics are shown as blue dashed lines, with most extreme enrichments in fluid-mobile elements, Otervann metabasalts are all the other unbroken lines. (b) Mietjerpakte dykes. Field for back-arc basin basalts shown in grey, data from (Sun et al. 2003c). Tantalum data not plotted due to contamination during the milling process. Trace element abundances are presented in Appendix B, Table B3.

in the light REE (La, Ce, Pr, Nd) to a degree not seen in the other metabasaltic suites; such enrichment is commonly assigned to a significant slab flux into the mantle source. The environment of formation will be discussed in the following section.

4.4.3 Discussion of tectonic setting and geological history

Some fluid-mobile element concentrations are presented in Figure 4.11, normalised to the Yb abundance and plotted against Nb/Yb in order to take into account the effects of partial melting and fractional crystallisation. All elements display elevated 'M'/Yb ratios (where M is the element under study), except La, which is usually considered to be a moderately mobile element. The data match those of samples from the Lau back-arc spreading centre (Sun et al. 2003c). It is very likely that these rocks acquired elevated ratios during the process of formation and not as a result of fluid-rock interaction subsequent to igneous crystallisation. This is particularly true of the Lomivann suite, which possesses distinct LREE enrichments that are indicative of calc-alkaline arc magmatism.

However, the possible effects of seafloor alteration include enrichments in 'fluid-mobile' elements such as the LILE (K, Rb, Sr, Ba, U) (Hart et al. (1999) and comparison of fresh and altered MORB data from Hofmann (1988) and Staudigel (1996); also see Section 2.1.2). Nonetheless, the data cited are ambiguous and considerable *large-scale* variation in trace element chemistry is thought to be unlikely as a result of 'seafloor' fluid-rock interaction (Staudigel et al. 1996). Boyle (1989) concluded that the Na enrichments (but apparently not K) in the Sulitjelma complex, *were* evidence of fluid enrichment in Na by seawater. This is certainly possible, although K seems to display a positive anomaly when normalised to N-MORB (Figure 4.9 and Figure 4.10), at least in comparison with the non-fluid-mobile element Nb. Boyle (1989) also cites large variations in Cu and Zn contents as powerful evidence of seafloor alteration. Negative Nb (and Ti) anomalies (shown

in Figure 4.9 and Figure 4.10) are usually associated with arc-related magmatism, because Nb is not transferred from the slab to the mantle wedge and so, in comparison with fluid-mobile elements, its budget is controlled by the depleted nature of the mantle wedge. Contrary to expectation Zr, another immobile HFSE, is not depleted. Unfortunately, Ta data could not be used due to contamination during sample preparation.

While it is entirely plausible (and probable) that seafloor processes have affected the chemistry of many of the Sulitjelma samples, I would suggest that the source of *most* of the elevation of fluid-mobile element abundances is enrichment in the mantle source, probably as a result of the infiltration of slab-derived fluids in a back-arc setting. The enrichments of Pb, K, Rb and Ba shown in the field for the Lau basin (Figure 4.10) are broadly comparable to those of the Sulitjelma samples suggesting a similar tectonic setting for their genesis. However, it is unlikely that the extreme positive Pb anomalies (Figure 4.9 and Figure 4.10) are a result only of partial melting and crystallisation. It is probable that fluid-rock interaction after igneous crystallisation has played an important role in elevating Pb abundances, most probably during a seafloor alteration episode, but also possibly during metamorphism.

4.4.4 Element mobility in SO metagabbros and metabasalts

Some fluid-mobile element concentrations are presented in Figure 4.11, normalised to the Yb abundance (a non-mobile element) and plotted against Nb/Yb in order to take into account the effects of partial melting and fractional crystallisation. All elements display elevated 'M'/Yb ratios (where M is the element under study). As discussed in the section above, I have concluded that these elevations are due to enrichments in the mantle source, through the addition of a slab flux. As a result, determining whether the samples have subsequently lost or gained elements during metamorphism is very difficult.

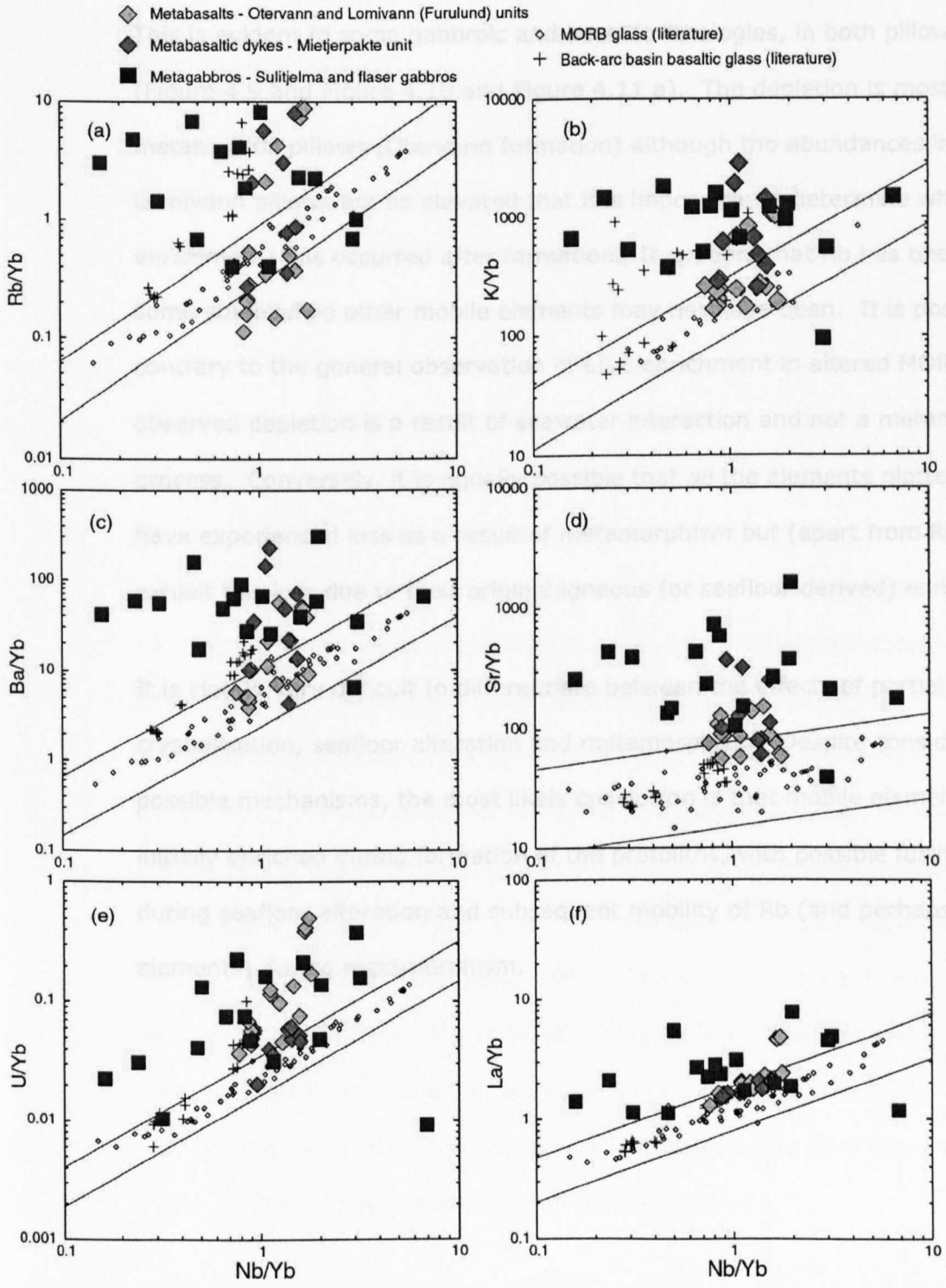

Figure 4.11. Non-conservative element discrimination plots (after Pearce 1983) for Sulitjelma ophiolite samples. M/Yb v Nb/Yb plots, where M is the 'fluid-mobile' element under examination and Nb is a non-fluid-mobile element, and each is normalised to Yb to minimise the effects of partial melting and fractionation. K, Ba, Sr and U all appear to be enriched with respect to MORB, probably reflecting input from subducting slab in a back-arc setting of formation. Rb also displays enrichment but also appears to have been lost from metabasalts and possibly metagabbros. La does not display any enrichment or depletion.

The only element to display obvious depletion (beyond the range of MORB) is Rb. This is evident in some gabbroic and basaltic lithologies, in both pillows and dykes (Figure 4.9 and Figure 4.10 and Figure 4.11 a). The depletion is most obvious in metabasaltic pillows (Otervann formation) although the abundances in the Lomivann pillows are so elevated that it is impossible to determine whether loss (or enrichment) has occurred after formation. It appears that Rb has been mobile at some stage while other mobile elements may not have been. It is possible that contrary to the general observation of LILE enrichment in altered MORB, the observed depletion is a result of seawater interaction and not a metamorphic process. Conversely, it is equally possible that *all* the elements plotted (except La) have experienced loss as a result of metamorphism but (apart from Rb) do not exhibit this loss due to their original igneous (or seafloor derived) enrichments.

It is clearly very difficult to differentiate between the effects of partial melting and crystallisation, seafloor alteration and metamorphism. Despite considering several possible mechanisms, the most likely conclusion is that mobile elements were initially enriched during formation of the protoliths, with possible further enrichment during seafloor alteration and subsequent mobility of Rb (and perhaps other elements) during metamorphism.

PAGE
MISSING
IN
ORIGINAL

5 The rhenium-osmium system

5.1 Background

The Re-Os system comprises two siderophile - chalcophile elements, thus rhenium and osmium are preferentially concentrated in metal or sulphide phases. This is unique amongst long-lived radiogenic isotope systems currently used in Earth science. Consequently, this system can provide insight into certain problems that are largely beyond the scope of lithophile isotope systems, such as the investigation of metal phases within meteorites. A second important difference between the Re-Os system and other (lithophile) radiogenic isotope systems is the compatibility of the two elements. A difference in compatibility during melting is an essential feature of all radiogenic isotope systems, without which, useful petrological and chronological information cannot be gleaned. Most radiogenic isotope systems are based on two predominantly incompatible elements, whereas rhenium behaves as a moderately incompatible element during mantle melting and osmium is largely compatible. This has the effect of strongly fractionating the two elements during melting of the mantle; particularly in the case of small to moderate/large melt fractions such as ocean island basalts (1-5%) and mid-ocean ridge basalts (MORB) (~10%, e.g. McKenzie and Bickle 1988). Consequently, oceanic basalts generally have Re/Os ratios which are extremely elevated in comparison with the mantle source. This should make the Re-Os system an excellent tracer for recycled oceanic crust in the mantle - an observation which is crucial to the work in this study. This will be expanded upon in Section 5.2.2.3.

Fundamentals. Osmium (M=~190.2, A=76) is a member of the Ir-group (Ru, Os, Ir) of platinum group elements (PGE) and has seven naturally occurring isotopes. Its predominant natural oxidation states are 0, +III and +IV (Morgan 1997a). Rhenium (M=186.207, Gramlich et al. 1973) has an atomic number (75) which is one less than osmium and occurs in the form of two isotopes. As with osmium, it

occurs in a variety of oxidation states; the most common being +IV and +VI (Morgan 1997b; Ertel et al. 2001). ^{187}Re is unstable and decays by β emission to ^{187}Os. Due to the extremely low emission energy of the decay, it has proved impossible to accurately measure the decay constant of ^{187}Re. In order to determine the decay constant, Lindner et al. (1989) used a purified perrhenic acid spiked with ^{190}Os and ^{192}Os. This was left for two years and then sampled and measured periodically over the following two years. The decay constant was calculated at 1.64^{-11} year^{-1}. High-precision Re-Os isochrons for iron meteorites have been used to indirectly refine the decay constant, resulting in an estimate of approximately 1.666^{-11} year^{-1} (Shen et al. 1996; Smoliar et al. 1996). Figure 5.1 illustrates the isotopic masses of both osmium and rhenium, together with their relative natural abundances.

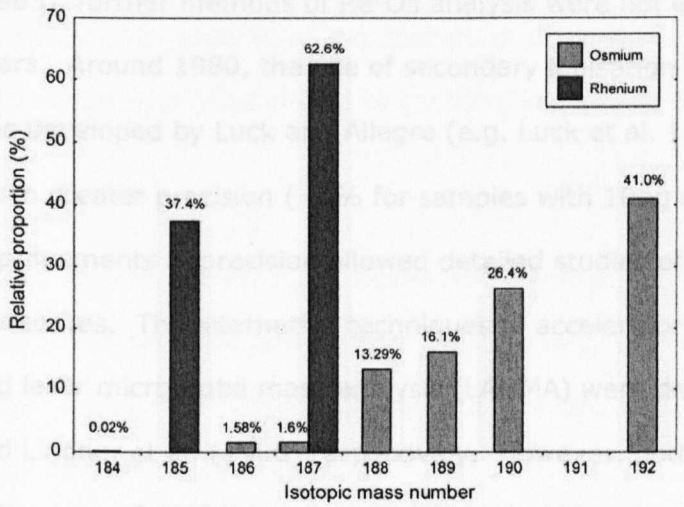

Figure 5.1. Relative natural abundances of the various isotopic masses of osmium and rhenium.

5.1.1 Advancements in Re-Os analysis

It was only at the beginning of the 1990's that the full potential of the rhenium – osmium isotope system, as a geochemical tool, was realised. Previously, the possible benefits of the system had been noted but precise and accurate analysis remained elusive. Furthermore, sample-spike equilibration during sample

dissolution has proved to be problematic due to the numerous oxidation states of both rhenium and osmium.

Mass spectrometry. The earliest rhenium and osmium analysis was performed over four decades ago using a method of gas source mass spectrometry (Hirt et al. 1963). However this technique offered low precision (~10% on very rich samples with 50μg Os). Subsequent methods also suffered from fairly low analytical precision, and this has been the main stumbling block for the development of the system as a common geochemical tool. Advances in the precision and accuracy of rhenium and osmium analysis were sporadic and limited before the development of the N-TIMS technique.

Following the pioneering, but imprecise, work of Herr et al. (1961) and Hirt et al. (1963), further methods of Re-Os analysis were not investigated for the next 15 years. Around 1980, the use of secondary ionisation mass spectrometry (SIMS) was developed by Luck and Allegre (e.g. Luck et al. 1980). This method achieved much greater precision (~1% for samples with 10ng of osmium). The improvements in precision allowed detailed studies of Os-rich samples, such as meteorites. The alternative techniques of accelerator mass spectrometry (AMS) and laser microprobe mass analysis (LAMMA) were developed by Fehn et al. (1986) and Lindner et al. (1986) respectively. However, both suffered from low precision; in the case of AMS this was approximately 10%. An entirely different approach to the ionisation of rhenium and osmium utilises the system of inductively-coupled plasma mass spectrometry (ICP-MS). In this case, ionisation takes place in an argon plasma torch at over 5000°C. However, conventional introduction of the sample through solution nebulisation is inefficient (~10% ionisation), and thus precludes the analysis of small samples through insufficient precision. Resonance ionisation mass spectrometry offered increased precision of ~0.8-2% for samples with sub-nanogram quantities of osmium (Walker and Fassett 1986).

With the advent of N-TIMS (Creaser et al. 1991; Volkening et al. 1991; Walczyk et al. 1991) precision improved dramatically, as did ionisation efficiency, and this development rendered all of the previous methods largely obsolete. The increased efficiency of analysis facilitated the investigation of samples with low osmium abundances such as oceanic basalts (e.g. Pegram and Allegre 1992; Reisberg et al. 1993; Martin et al. 1994; Roy-Barman and Allegre 1994) and therefore allowed the study of the Re-Os system to expand into vast new areas. Subsequent advancements in chemical separation techniques have also helped in the analysis of small quantities of rhenium and osmium due to improved blank levels (e.g. Carius tube digestion (Shirey and Walker 1995), solvent extraction (Cohen and Waters 1996) and Teflon dissolution, bromine extraction and microdistillation (Birck et al. 1997). The methods of sample-spike equilibration have also been scrutinised due to the problems of equilibrating the various oxidation states of rhenium and osmium. This study has mainly used the method of Birck et al. (1997) and has facilitated the analysis of tiny quantities of osmium, even at the mineral scale (<1 ppt Os).

Today, the Re-Os system has provided insight and clarification in systems as diverse as cosmochemistry and weathering. The chemical evolution of the mantle has been another major field of investigation, and it is this area, amongst others, to which this study has strived to contribute.

Convention for reporting osmium data. Hirt et al. (1963) reported osmium isotope data with the ratio $^{187}Os/^{186}Os$, largely due to the convenient natural ratio for chondrites, which is close to 1. This practice was continued by Luck et al. (1980) and subsequent authors. However, ^{186}Os is actually the product of radioactive decay: a rare isotope of platinum, ^{190}Pt, decays to ^{186}Os with a very low decay constant of 1.477^{-12} a^{-1} (McDaniel et al. 2004 and references therein). The ^{186}Os isotope is also, itself, unstable. It decays to ^{182}W, but has an extremely low

decay constant and so can be considered stable. For most applications, the rarity of ^{190}Pt (0.0122% - Walker et al. 1991b), and its long half-life, make any radiogenic contribution to ^{186}Os negligible. However, work on PGE ore deposits can reveal large variations in the $^{186}Os/^{188}Os$ ratio, thus suggesting the ingrowth of substantial ^{186}Os (Walker et al. 1991b) - this is due to the very high Pt/Os ratios of PGE ore deposits. Clearly for work of this nature, normalising the abundance of ^{187}Os to a stable isotope such as ^{188}Os is vastly preferable. Furthermore, the abundance of ^{188}Os is considerably greater than ^{186}Os and so the measurement of $^{187}Os/^{188}Os$ ratios is typically more precise than the measurement of $^{187}Os/^{186}Os$ ratios. For these reasons, normalising ^{187}Os to ^{188}Os has become the preferred convention and all Os isotope compositions quoted in this work are $^{187}Os/^{188}Os$ ratios.

5.2 Applications of the Re-Os system

Due to the particular areas of discussion in this thesis, this summary concentrates on the application of the Re-Os system to mantle geochemistry, crustal recycling and subduction zone settings. For a more in-depth discussion of the use of the Re-Os system in cosmochemistry and mantle geochemistry the reader is referred to the review by Shirey and Walker (1998). Other applications, not discussed here, include weathering and seawater chemistry, and the formation of massive sulphide deposits.

5.2.1 Cosmochemistry and the early Earth

Due to the very high condensation temperatures of rhenium and osmium (1819 and 1814 K respectively at 10^{-4} atm (Wasson 1985)) they were amongst the earliest elements to condense from the solar nebula. As highly siderophile elements (HSE), Re and Os were strongly concentrated in metallic phases during accretion and subsequent melting events. This led to very high abundances (8000-66000 ppb - Morgan et al. 1995; Smoliar et al. 1996) in asteroidal cores, and in the cores of the terrestrial planets, while the bulk silicate Earth contains much lower concentrations (~3 ppb).

The use of the Re-Os system for the analysis of meteorites has helped to develop an understanding of processes which occurred in the very early history of the solar system, and their timescales. The application of the Re-Os system to these problems is particularly fruitful because these elements have relatively high abundances, particularly compared to the elements of lithophile long-lived radiogenic isotope systems which are usually only present in very small amounts, particularly in metallic phases. Moreover, the solid-metal/liquid metal distribution coefficient is greater for Os than for Re, which means that as metal precipitates from a high temperature metal liquid, this leads to increased Re/Os ratios in differentiated material (Morgan et al. 1995; Smoliar et al. 1996). Over time this

will result in varying $^{187}Os/^{188}Os$ ratios throughout the sample suite and therefore may make the calculation of precise isochrons viable. It may then be possible to identify different isochrons, of very similar ages, which relate to different meteorite groups and significant events in the early stages of meteorite formation.

The first studies to glean useful information from the Re-Os system analysed meteorites which are naturally rich in osmium (ranging from ~400 to ~65000 ng/g (ppb)) (e.g. Morgan and Lovering 1967; Luck et al. 1980). Early work documented the Re-Os systematics of iron meteorites using the SIMS technique (Allegre and Luck 1980; Luck et al. 1980; Luck and Allegre 1983). This work defined an isochron for iron meteorites, but the low precision did not allow a precise isochron to be calculated for metal phases within the iron meteorites because the values of $^{187}Re/^{188}Os$, and therefore also $^{187}Os/^{188}Os$, were too tightly clustered. The obtainable precision was also too low to allow the events of the first 50 million years of the solar system to be deciphered. Work in the late 1980s and early 1990s utilised the RIMS technique and produced data for all common types of chondrite e.g. carbonaceous chondrites (Walker and Morgan 1989) and enstatite chondrites (Morgan et al. 1990). The advent of N-TIMS, with its improved precision, led to the attainment of precise isochrons for suites of meteorites with little variability in Re/Os ratios (e.g. for iron meteorites: Horan et al. 1992; Shen et al. 1996; Smoliar et al. 1996).

Smoliar et al. (1996) obtained precise isochrons for two different groups of iron meteorites, IIA and IIIA. This work has shown that the latter group crystallised around 4558 Ma, in agreement with Pb-Pb studies by Lugmair and Galer (1992). The data for the group IIA irons define an isochron of 4537 ± 8 Ma, which despite being close in age to the group IIIA irons, is in fact statistically resolvable to two ages of iron meteorite crystallisation. It is interesting to note that the least evolved material from iron meteorites can have $^{187}Re/^{188}Os$ ratios of up to 1.8, while the

evolved material and chondrite values are consistently around 0.4. This is thought to be the result of the late accretion of chondritic metal to the more evolved iron meteorites.

Some rare Lunar basalts and eucrites have been analysed together with some basaltic and ultramafic Martian meteorites. Samples from both the Moon and Mars contain Os concentrations which are similar, but slightly lower than terrestrial basalts, while rhenium concentrations are considerably lower (Treiman et al. 1986; Birck and Allegre 1994; Warren and Kallemeyn 1996). Birck and Allegre (1994) also obtained Re/Os ratios and found that these are close to the chondritic value. The moon has little or no core and thus it is clear that core segregation of the Earth had occurred prior to the impact which formed the Moon. It may be possible that the thick lunar crust has shielded its mantle from late accretion. However, if this were the case, Re/Os ratios would likely be superchondritic and this does not explain the occurrence of terrestrial-like Os abundances, but considerably lower concentrations of Re. Birck and Allegre (1994) suggest that the lower Re concentrations may be a result of much lower oxygen fugacity in the mantles of the Moon and Mars.

5.2.2 Mantle chemistry and evolution

5.2.2.1 Compatibilities of rhenium and osmium

The details of rhenium and osmium behaviour during melting of different extents and under different conditions are poorly understood. However, there is information to be gleaned from the abundances measured in basic oceanic rocks. Figure 5.2 is a plot of Re and Os abundances in the main basic rock types. The abundance of Re in oceanic basalts is almost always higher than that of the mantle from which it is derived, often by about a factor of 10. This demonstrates the moderately incompatible nature of Re during mantle melting. In the case of osmium, MORB values are usually less than 50 ppt, compared to a depleted mantle

value of ~3 ppb. Clearly Os behaves as a compatible element in situations with moderate melt fractions. Os, together with the other iridium group-platinum group elements (I-PGE) (Ir, Ru), is more compatible than the platinum group (Pd, Rh, Pt) of the PGE (Barnes et al. 1985). This fact is reflected in the greater concentration of the latter in melts. The message from different extents of mantle melting, illustrated in Figure 5.2, is somewhat more complex. Different lithologies, which form from very different melt fractions, do not display strong variation in the concentrations of Re. Komatiites are formed by extensive mantle melting (25-60%, Herzberg and Zhang 1998) yet they have rhenium abundances which are comparable to MORB. With increasing melt fraction, incompatible element concentrations would be expected to decrease. Most ocean island basalts (OIB) are generated from small melt fractions – smaller than MORB generation. However, Re concentrations are lower in the former, which is contrary to expectation.

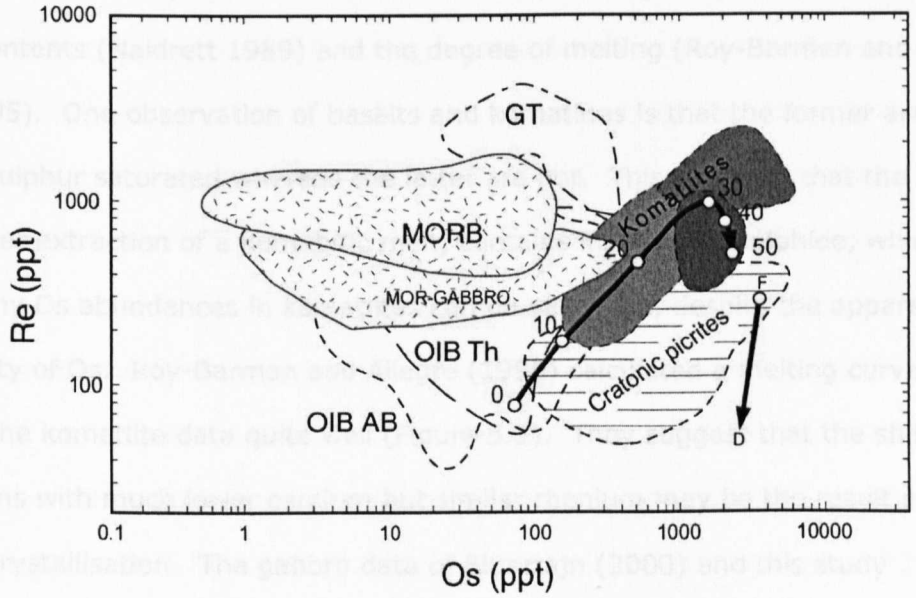

Figure 5.2. Re and Os abundances in basic rocks. Modified from Shirey and Walker (1998) after the addition of data from Schiano et al. (1997) (MORB), Blusztajn et al. (2000) (MORG) and this study (MORG). GT: Gorgona tholeiites, Th: tholeiite, AB: alkali basalt. Curve corresponds to mantle melting increments (%). F: fertile mantle, D: depleted mantle (Morgan 1986).

Moreover, alkali basalts have comparable rhenium abundances to tholeiites in OIB settings, despite the lower melt fraction involved in their formation. Therefore it seems that rhenium does not behave consistently across a broad range of melt fractions. Os concentrations are very low, but extremely variable (0.23 - 250 ppt), in a broad range of OIB and MORB (Roy-Barman and Allegre 1994; Schiano et al. 1997, respectively). Komatiitic abundances are comparable to mantle values.

The inconsistent behaviour of Re and Os is probably dependent on the complex behaviour of sulphide during mantle melting. Sulphide, and associated metallic phases, are likely to contain the vast majority of the osmium in the mantle: perhaps 80-96% of the Os budget resides in sulphide in some Kilbourne Hole xenoliths (Hart and Ravizza 1996). Burton et al (1999) also studied the Os budget in a Kilbourne Hole sample, concluding that approximately 90% of the Os, and 65% of the Re, is housed in sulphide which constitutes only 0.03% of the bulk rock. Sulphide solubility is dependent on various factors including temperature, sulphur and FeO contents (Naldrett 1989) and the degree of melting (Roy-Barman and Allegre 1995). One observation of basalts and komatiites is that the former are generally sulphur saturated whereas the latter are not. This suggests that the mantle, after extraction of a komatiitic melt, contains no residual sulphide, which explains why Os abundances in komatiites can be very high, despite the apparent compatibility of Os. Roy-Barman and Allegre (1995) calculated a melting curve which fits the komatiite data quite well (Figure 5.2). They suggest that the shift to compositions with much lower osmium but similar rhenium may be the result of fractional crystallisation. The gabbro data of Blusztajn (2000) and this study (shown as MOR-G on Figure 5.2), have intermediate osmium abundances and fit well with the theory of fractional crystallisation modification.

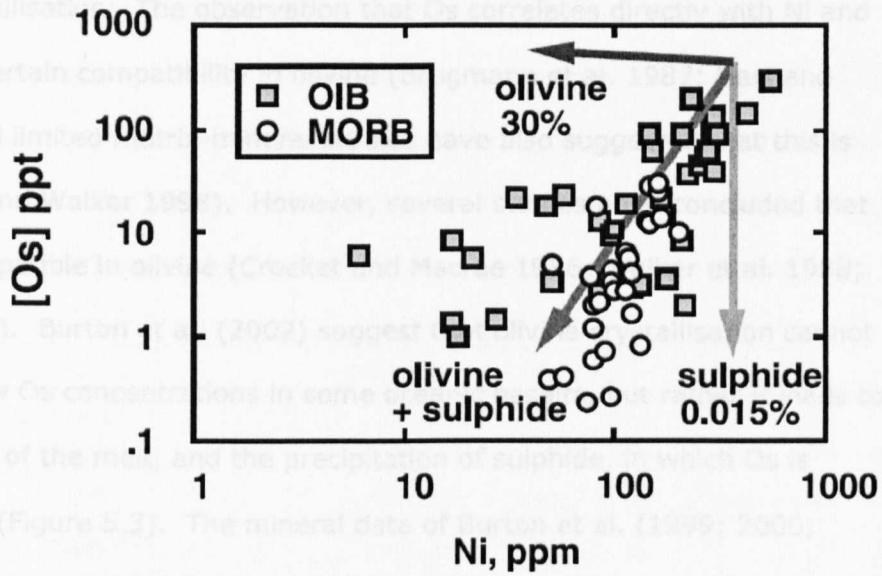

Figure 5.3. Osmium (ppt) plotted against nickel (ppm) for OIB and MORB (from Burton et al. 2002). There is a clear positive correlation between Os and Ni concentrations. Burton et al. (2002) explain this by the co-precipitation of olivine and sulphide from the melt. The observed variations in Ni, but not Os, can be attributed to 30% olivine crystallisation, while the Os variation can be produced by 0.015% sulphide precipitation.

Little is known of the behaviour of Re and Os during crystallisation and so it is likely that processes occurring during magma ascent and differentiation account for some of the variability in Re and Os compositions. The separation of sulphide is likely to lead to an increase in the Re/Os ratio of the remaining melt. This is due to the much higher $^{\text{sulphide melt/silicate melt}}D$ for Os than for Re (Roy-Barman et al. 1998). (Although data published by Gannoun et al. (2004b) have since cast doubt on the reliability of the sulphide-silicate partition coefficient for Re (1000 compared to 43 in the case of the data from Roy-Barman et al. (1998)). Basaltic melts, as previously mentioned, are sulphur saturated and therefore form immiscible sulphide liquids which tend to separate, partitioning much of the osmium from the melt (and some of the rhenium). Other non-silicate phases such as chromite have been shown to have high Os concentrations, at least in mantle rocks (Walker et al. 1996), and may also be important for the Re and Os budgets during crystallisation. Very minor trace phases called PGE clusters may also play a role (Keays 1995). The behaviour of Re and Os in olivine is crucial to the understanding of the effects

of fractional crystallisation. The observation that Os correlates directly with Ni and MgO suggests a certain compatibility in olivine (Brugmann et al. 1987; Hart and Ravizza 1996) and limited matrix-mineral studies have also suggested that this is the case (Shirey and Walker 1998). However, several studies have concluded that Os is highly incompatible in olivine (Crocket and Macrae 1986; Walker et al. 1988; Burton et al. 2002). Burton et al. (2002) suggest that olivine crystallisation cannot account for the low Os concentrations in some oceanic basalts, but rather it leads to sulphur saturation of the melt, and the precipitation of sulphide, in which Os is highly compatible (Figure 5.3). The mineral data of Burton et al. (1999; 2000; 2002) and Gannoun et al. (2004b) (Table 5.1) indicate that there is a wide range of possible Re and Os concentrations in separate mineral phases, and compositions are not only dependent on whole rock chemistry.

Righter et al. (1998) studied a suite of samples, from the Galapagos islands, which formed a fractionation trend. They found that Re concentrations increased during the phase of differentiation when TiO_2 and FeO were increasing in the melt (i.e. in samples from basalt to icelandite), whereas when Ti and Fe contents decreased, Re abundance also decreased from 610 ppt in the icelandite to 36 ppt in the rhyolitic sample. From this evidence, Righter et al. (1998) concluded that Re is relatively compatible in magnetite - an hypothesis that is confirmed by very high (40 ppb) Re concentrations in a magnetite-rich separate.

5.2.2.2 Determining mantle reservoirs.

The determination of rhenium and osmium abundances and the osmium isotopic composition of the mantle is crucial in order to provide a base from which to consider the isotopic variation seen in different oceanic basalts. Three lines of evidence have been used in order to constrain the average rhenium and osmium composition of the mantle: data from chondrites, which represent the bulk composition of the Earth, oceanic basalt chemistry, and direct measurement of the

mantle, through abyssal and orogenic peridotites and mantle xenoliths. Thus far, the dataset is not widespread enough, or free enough from ambiguity, to reveal the homogeneity or possible variation of mantle components. However, the nature of mantle reservoirs is slowly being elucidated. Typical abundances of Re and Os, together with isotopic information, are presented in Table 5.1 and Table 5.2.

		Re (ng/g)	Os (ng/g)	$^{187}Re/^{188}Os$	$^{187}Os/^{188}Os$
Chondrites	Allende[1]	63.23	773.9	0.3935	0.1276
	O,C,E[1]	42.3 - 96.96	47.9 - 1048	0.3731 - 0.4779	0.1272 - 0.1305
Irons	IIAB[2]	0.778 - 4816	8.808 - 65740	0.3526 - 0.9396	0.1232 - 0.1731
Mantle	Fertile[1,3]	0.25 - 0.30	2.8 - 3.4	0.401	0.1290 / 0.1296
	Depleted[4]	0.051 - 0.135	0.8 - 9	0.06 - 1	0.123 - 0.126
	Oceanic lithospheric mantle[5]	0.040 - 0.203	1.2 - 8	0.122 - 0.149	0.123 - 0.128
Komatiite[6]		0.5 - 1.5	0.5 - 6	1 - 6	
MORB[6]		0.5 - 2	0.0005 - 0.04	100 - 5000	0.127 - 0.164
MORB[7]					0.126 - 0.144
MOR gabbro[8]		0.5 - 2	0.001 - 0.05	5 - 1400	0.124 - 0.328
OIB[6]		0.1 - 1	0.01 - 0.5	20 - 3000	0.122 - 0.205
Ave continental crust	[9]	0.2 - 0.4	<0.05	~50	1.2685
	[10]	<2		~300	
Pelagic sediment[11]		0.076 - 1.49			
Black Shale[12]		517	2.46	18,780	high
Molybdenite[13]		0.7 - 160 ppm	only radiogenic	very high	very high
Chromite[14]		0.22 - 0.64	13 - 67	0.02 - 0.2	
Mantle sulphide[15]	E-type	52 - 357	4.7 - 122	5.2 - 104	
	P-type	300 - 2551	6000 - 10000	0.24 - 2	0.104 - 0.121
Mantle minerals[16]	Olivine	0.01 - 0.03	0.05 - 0.15	0.73 - 1.23	0.114 - 0.123
	Cpx	0.01 - 0.14	0.01 - 0.14	1.5 - 9.5	0.114 - 0.123
	Opx	0.04 - 0.08	0.03 - 0.15	1.4 - 13	0.116 - 0.123
	Garnet	0.08 - 0.24	0.01 - 0.02	24 - 96	0.120 - 0.166
	Spinel	0.18 - 0.24	1.01 - 1.23	0.8 - 0.9	0.119 - 0.123
Basaltic minerals[17]	Olivine	0.68 - 4.20	0.002 - 0.012	280 - 5900	0.140 - 0.241
	Cpx	1.15	0.001	4800	0.250
	Plagioclase	0.27 - 1.22	<0.001	1400 - 7200	~ 0.190
	Spinel	1.26	1.20	500	0.187
	Sulphide	700 - 3250	150 - 700	~22	0.130 - 0.132

Table 5.1. Re and Os abundances and $^{187}Re/^{188}Os$ ratios in a variety of geological materials. Modified after Shirey and Walker (1998). References: [1] Meisel et al. (1996), [2] Smoliar et al (1996) & Morgan et al. (1995), [3] Morgan (1986), [4] Pearson et al. (1995), [5] Widom et al. (1999), [6] Shirey and Walker (1998) and references therein, [7] Gannoun et al. (2004a), [8] Blusztajn et al. (2000) [9] Esser and Turekian (1993), [10] Sun et al. (2003a), [11] Peucker-Ehrenbrink (1996), [12] Horan et al. (1994), [13] Suzuki et al. (1996), [14] Walker et al. (1996), [15] Pearson et al. (1998), [16] Burton et al. (1999; 2000; 2002), [17] Gannoun et al. (2004b).

Fertile mantle. Due to the siderophile nature of both Os and Re, it would be expected that abundances in the silicate mantle would be low. Furthermore, the difference in Re and Os partition coefficients between metal and silicate should lead to Re/Os ratios in the mantle that are elevated compared to chondritic values. Direct measurement of suites of xenoliths has been undertaken by Morgan (1986) and Meisel et al. (1996), amongst others. These authors assessed the depletion of the samples through proxies such as S and Se (Morgan) and Lu and Al_2O_3 (Meisel et al.). By extrapolating to a fertile composition, concentrations of Re and Os were estimated at 0.25 - 0.30 and 2.8 - 3.4 ppb respectively. These values are higher than expected for the silicate portion of the Earth (e.g. Jones and Drake 1986). Furthermore, Meisel et al. (1996) concluded that the osmium isotope composition of the fertile mantle was very similar to the chondritic value ($^{187}Os/^{188}Os$ = 0.1290 ± 0.0009 which is the time integrated result of a $^{187}Re/^{188}Os$ ratio of ~0.43, revised to 0.1296 by Meisel et al. (2001)). In fact, it has been recognised for about two decades that both the osmium composition and the $^{187}Re/^{188}Os$ ratio of the mantle lie very close to the chondritic average of 0.1276 and 0.37-0.48 respectively (values from Meisel et al. 1996). Wanke et al. (1984) first recognised that the Earth may have experienced a late episode of accretion of chondritic material after core formation had occurred (termed a 'late veneer'), in order for the mantle to obtain its surprisingly high concentrations of PGE. Os isotope systematics were examined by Morgan (1986) who concurred with the 'late veneer' hypothesis to explain the greater than expected abundances of Re and Os and the low Re/Os and therefore low $^{187}Os/^{188}Os$ signature of the mantle. In this way, the isotopic composition of the mantle would be strongly influenced by the very HSE abundant chondrite signature, thus decreasing its value, while the abundances of Re and Os would both increase. Despite the estimates of primitive mantle composition by Meisel et al. (1996; 2001), the average chondritic $^{187}Os/^{188}Os$ value of 0.1276 ($^{187}Re/^{188}Os$ = 0.39) (e.g. Meisel et al. 1996) is often used as a reference for non-depleted mantle.

Depleted MORB mantle (DMM). The mid-ocean ridge system provides the most widespread sampling of the chemistry of the upper mantle, albeit through the modified medium of melts. Due to MORB melt extraction, the chemistry of a large portion, if not most, of the upper mantle, has been modified with respect to a primitive mantle composition, and has been depleted in elements which are incompatible during melting and thus preferentially partitioned into melts. Rhenium is one such element, leaving the residual mantle depleted in terms of rhenium abundance. As a result, abyssal peridotites, which represent parts of the mantle which have undergone MORB melt depletion, have Re/Os ratios which are generally lower than the fertile mantle component (although variable). The assessment of the osmium signature from such depleted areas is difficult due to the large scale heterogeneity involved, particularly with a fairly small dataset. Snow and Reisberg (1995) combined their data for abyssal peridotites with the previously published values of Roy-Barman and Allegre (1994) and Martin (1991), and concluded that the average Os composition for the DMM was: $^{187}Os/^{188}Os = 0.1246 \pm 0.0014$, with a range of 0.1222 to 0.1276. However, there were many higher values which were dismissed as being contaminated by sea water interaction.

Given a correction to zero age, MORB should have the same isotopic composition as the mantle from which they were derived. However, the average MORB composition is 0.130-0.135 (Gannoun et al. 2004a) or possibly slightly higher (Schiano et al. 1997). This apparent discrepancy may be the result of a marble-cake mantle, such as that proposed by Allegre and Turcotte (1986), whereby pyroxenite layers, possibly formed from previously subducted oceanic crust, are present in the mantle and can have very radiogenic signatures (up to 10, see Reisberg et al. 1991; Kumar et al. 1996; Roy-Barman et al. 1996). These layers are likely to melt preferentially over the surrounding mantle, thus creating a melt which is enriched in radiogenic osmium (see discussion in Schiano et al. 1997). A study of separated mineral phases from two MORB samples by Gannoun et al.

(2004b), revealed that extremely high Re/Os ratios exist in individual phases, and given even short time periods these can generate radiogenic signatures. The mineral data lie on isochronous best-fit lines with initial Os isotope compositions of 0.1265 and 0.129, both of which are consistent with the chondritic mantle value (0.127) and close to the values for fertile and depleted MORB mantle. Therefore, it is necessary to have precise age constraints on the samples in order to accurately correct for radiogenic ingrowth. It is possible that some of the more radiogenic Os isotope signatures from MORB are the result of insufficient age correction rather than a reflection of heterogeneity in the mantle source.

Reservoir	$^{187}Os/^{188}Os$
Fertile convecting mantle	
Chondritic reference	0.127
Fertile mantle (PUM)	0.129
Depleted MORB mantle (DMM)	
Average	0.125
Range	0.123 - 0.128
Subcontinental lithospheric mantle (SCLM)	
Average	0.113
Range	0.105 - 0.129
EP - Enriched plume end member, FOZO?	0.130 - 0.135
HIMU	0.150
EM I - enriched mantle I	0.152
EM II - enriched mantle II	0.136

Table 5.2. Representative osmium ratios for various mantle components. Data from Shirey and Walker (1998) and references therein.

5.2.2.3 Ocean island basalts (OIB) and their insight into mantle reservoirs.

HIMU. Some OIB possess $^{206}Pb/^{204}Pb$ and $^{187}Os/^{188}Os$ isotope ratios that are elevated with respect to known average fertile or depleted mantle components. In certain cases, extremely low Os abundances in these basalts leave them prone to contamination through interaction with lithospheric mantle (which has a sub-chondritic Os signature) or oceanic crust, which, if old, contains a very radiogenic

osmium signature due to ingrowth of ^{187}Os. With careful sampling and analysis of basalts with moderate abundances of Os (e.g. 30-200 ppt), it is unlikely that contamination of this type can produce the observed isotopic ratios. Os isotope compositions of HIMU type OIB are approximately 0.150 ($^{187}Os/^{188}Os$) compared to mantle values below 0.130 (see Table 5.2 and Figure 5.2). Ocean island basalts of this type were first recognised by their high $^{238}U/^{204}Pb$ ratios (= high-μ or HIMU), which over time generate elevated $^{206}Pb^{204}Pb$ ratios (e.g. Hofmann and White 1982). [See Hofmann (1997) for a complete review of the isotopic systematics of OIB.] Hofmann and White (1982) and Zindler et al. (1982) proposed that the observed elevation in Pb isotope composition could be explained by the recycling of ancient oceanic crust into the source of this type of OIB. Elevated Os isotope compositions of HIMU type OIB (e.g. Hauri and Hart 1993; Reisberg et al. 1993; Marcantonio et al. 1995; Roy-Barman and Allegre 1995) are consistent with the model of recycled oceanic crust. As previously noted, oceanic crust generally has very high Re/Os ratios (Figure 5.2 and Table 5.1) and so, over time, will develop very radiogenic Os isotope signatures. By mixing approximately 30-40% of highly radiogenic, ~2 Ga, oceanic crust with unradiogenic mantle, isotopic compositions of HIMU basalts (e.g. from the Austral and Cook islands) can be produced, with the exact proportions depending on the age and U/Pb ratios of the subducted oceanic crust (Hauri and Hart 1993; Reisberg et al. 1993; Marcantonio et al. 1995; Roy-Barman and Allegre 1995; Hauri et al. 1996).

An alternative model for the production of OIB with high $^{187}Os/^{188}Os$ has been proposed. Core-mantle interaction was suggested by Walker et al. (1995) as a means of elevating Os isotopic compositions. During the formation of the inner core, it is thought that Os, rather than Re, would have been preferentially incorporated and so the outer core will have a higher than chondritic Re/Os ratio and thus, a more radiogenic osmium signature over time. However, core-mantle interaction of this type would result in higher Re and Os abundances in OIB, which

is not generally observed. Moreover, the Pb isotope composition of the outer core will be very unradiogenic due to the siderophile nature of Pb, and so the elevated $^{206}Pb^{204}Pb$ signature of HIMU basalts is not consistent with input from the outer core (Shirey and Walker 1998).

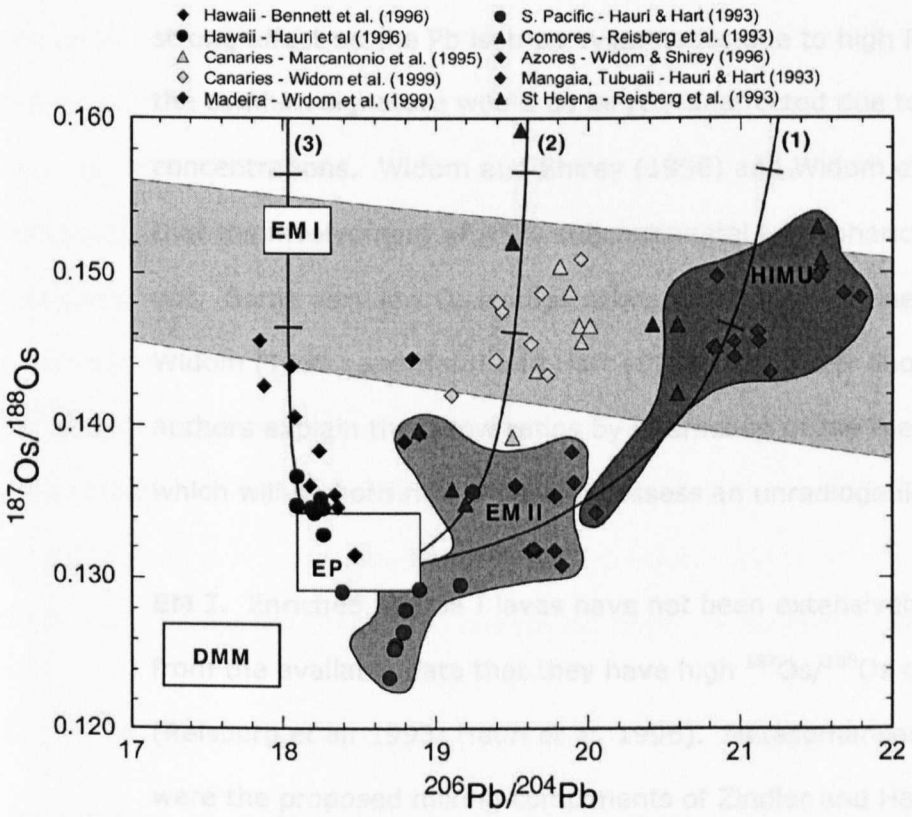

Figure 5.4. Os and $^{206}Pb/^{204}Pb$ isotope compositions of ocean island basalts (OIB) and proposed mantle components, after Shirey and Walker (1998). The grey band corresponds to mixtures of 2 Ga oceanic crust and varying proportions of 2 Ga pelagic sediment (Ben Othman et al. 1989). The mixing lines are taken from Shirey and Walker (1998) and are similar to those used in previous literature (Roy-Barman and Allegre 1995; Bennett et al. 1996; Hauri et al. 1996; Widom 1997). Mixing lines calculated using the following data: (1) Mixing of EP (Os = 3.3ppb, $^{187}Os/^{188}Os$ = 0.130, Pb = 30ppb, $^{206}Pb/^{204}Pb$ = 18.5) with 2 Ga recycled oceanic crust (Os = 0.1ppb, $^{187}Os/^{188}Os$ = 1.78, Pb = 250ppb, $^{206}Pb/^{204}Pb$ = 21.8); (2) Mixing of EP with 2 Ga recycled crust plus 0.6% 2 Ga pelagic sediment (Os = 0.101ppb, $^{187}Os/^{188}Os$ = 1.76, Pb = 447ppb, $^{206}Pb/^{204}Pb$ = 19.72; (3) Mixing of EP with 2 Ga crust plus 3% pelagic sediment (Os = 0.103, $^{187}Os/^{188}Os$ = 1.72, Pb = 1230ppb, $^{206}Pb/^{204}Pb$ = 18.03). Tick marks are at proportions of 25 and 35% recycled material.

EM II. Enriched mantle II (EM II) type OIB have Pb and Os isotope characteristics which are similar, though less extreme, to HIMU basalts. Their Os isotope compositions may be as high as those of the HIMU samples ($^{187}Os/^{188}Os$ of ~0.150)

but their $^{206}Pb/^{204}Pb$ ratios are somewhat lower (19-20). It has been suggested that their formation involves the mixing of a smaller proportion of recycled oceanic crust into the mantle source (or crust with differing age or U/Pb and Re/Os ratios), together with a minor continental sediment input (Zindler and Hart 1986; Hauri and Hart 1993; Marcantonio et al. 1995). The continental sediment input would have a strong effect on the Pb isotope systematics due to high Pb abundances, whereas the osmium signature would be largely unaffected due to very low Os concentrations. Widom and Shirey (1996) and Widom et al. (1999) pointed out that the involvement of <5% subcontinental lithospheric mantle could not be ruled out. Some very low Os isotope ratios have been obtained for EM-II islands by Widom (1996) and Hauri and Hart (1993) (the latter shown in Figure 5.4). The authors explain these low ratios by interaction of the melt with oceanic lithosphere which will be both rich in Os and possess an unradiogenic Os isotope signature.

EM I. Enriched mantle I lavas have not been extensively studied, but it appears from the available data that they have high $^{187}Os/^{188}Os$ coupled with low $^{206}Pb/^{204}Pb$ (Reisberg et al. 1993; Hauri et al. 1996). Metasomatised mantle or lower crust were the proposed mixing components of Zindler and Hart (1986). However, it is difficult to determine whether their composition is consistent with these inputs into the EM I reservoir, due to uncertainty of both the composition of the EM I end-member and the Re-Os systematics of the mixing components. Bennett et al. (1996) analysed picritic lavas from Hawaii and concluded that the isotopic arrays could not be explained with a source solely containing recycled oceanic crust, and therefore proposed a model of mixing between DMM and an oceanic crust - pelagic sediment mix (approx. 3% sediment). This has also been proposed by Roy-Barman and Allegre (1995) and Hauri et al. (1996). The addition of Pb-rich sediments, with low $^{206}Pb/^{204}Pb$ is consistent with the observed unradiogenic ^{206}Pb component of EM I type OIB, while the radiogenic Os concentration is not strongly affected by the signature of the Os-poor sediments.

EP component. With the exception of a some EM II samples analysed by Widom (1996) and Hauri and Hart (1993), all OIB plotted in Figure 5.4 are enriched in radiogenic ^{187}Os with respect to DMM. As previously discussed, this is due to the recycling, in various quantities, of crustal materials into the mantle. However, it is also clear that modelling of OIB compositions does not fit well with mixing between the recycled components and a DMM end-member. Figure 5.4 shows a hypothetical mantle reservoir referred to as an enriched plume component (EP). The presence of a reservoir of this composition is necessary in order to explain the observed OIB compositions by the recycling of crustal materials. It is not at all clear what form this component may take, or indeed, how abundant it is. It is possible that this reservoir lies within the lower mantle, which may be isolated from mixing with the unradiogenic DMM (Shirey and Walker 1998), and is entrained in plumes which pass through the lower mantle (Walker et al. 1995; Widom and Shirey 1996). The EP component may be analogous to the FOZO component used previously in discussions on mantle chemistry (see review paper by Hofmann (1997)).

5.2.3 Rhenium and osmium in subduction settings

The recycling of oceanic crust into the mantle source of some OIB has long been suggested as a means of furnishing OIB with their varied isotopic signatures (e.g. Hofmann and White 1982). As discussed in the previous section, HIMU and probably EM II both appear to have a contribution from ancient, recycled oceanic crust. In order to model the formation of OIB signatures, the compositions of the mixing components must be well constrained. Therefore, the study of subduction processes is crucial to the understanding of the bulk chemistry that is recycled into the deep mantle. Ocean island basalt signatures are defined by their isotopic compositions, and so investigations into the effects of subduction on these isotope systems are particularly important. Furthermore, subduction zone magmatism carries a distinct signature of many elements which indicates fluid and element flux from the slab (see Section 1.2). However, the osmium data so far collected from

arc settings are somewhat inconclusive. The Re-Os system has a distinct advantage over other radiogenic isotope systems in investigations of subduction processes due to the very large fractionation of Re and Os during basalt genesis, which results in much higher Re/Os and, over time, higher $^{187}Os/^{188}Os$ ratios in oceanic crust than in the mantle.

Subduction zone lavas have, until recently, been very difficult to analyse due to their low Os concentrations. The advancements in mass spectrometry and spike-sample chemistry have recently allowed several studies of arc lavas to be performed. Nonetheless, the investigation of subduction zone Re-Os systematics is still in its infancy. It is this field that this study has sought to add to, by the direct measurement of Re and Os in rocks that have been subducted and subsequently exhumed during the Alpine orogeny (Zermatt-Saas ophiolite, western Alps, Switzerland).

5.2.3.1 Osmium

Early studies which investigated Os isotopes in subduction-related rocks include those by Brandon et al. (1996; 1999). Primarily due to problems with blank levels, Re-Os in lavas could not be accurately studied and therefore the work of Brandon et al. (1996; 1999) analysed peridotite xenoliths from the mantle wedge of the Cascades arc and Japan. The latter work led on from the earlier one by analysing a more comprehensive suite of mantle xenoliths from the Simcoe volcano, in the back-arc setting of the Cascades arc. While most of the Os values were chondritic to sub-chondritic, indicating an ancient melting event leaving the samples depleted in Re, several had mildly radiogenic Os signatures (0.1277 – 0.1338) which were explained by the addition of a radiogenic slab component to the mantle wedge (Brandon et al. 1996). Perhaps surprisingly, the back-arc xenoliths are characterised by higher Re/Os and U/Pb ratios than those from the arc itself. The authors postulate that early dehydration of the slab during subduction released a

Pb-rich fluid which left the remaining slab with a high U/Pb signature, which was then imparted to the mantle wedge at a deeper level during subsequent dehydration or melting. Due to the low temperature regimes of most subduction zones, addition of a slab component to the mantle wedge is likely to be in the form of a fluid, but could take the form of a melt (e.g. Peacock et al. 1994; Bourdon et al. 2002; Widom et al. 2003). Either way, the work of Brandon et al. (1996; 1999) suggests that Os can be mobile in oxidised and chlorine-rich fluids or melts (Brandon et al. 1996).

The more recent work of Widom et al. (2003) concurs with this conclusion through the discovery of variably radiogenic mantle wedge xenoliths from the Kamchatka region. The authors suggest that transport of Re and Os varies according to the age and thermal structure of the subducting slab. In the northern part, the slab is hotter (due to slab tearing, Yogodzinski et al. 2001) and consequently highly oxidised adakitic slab melts are produced which effectively transport both Re and Os into the mantle wedge. Further south, where the slab is colder, hydrous, oxidised and possibly Cl-rich fluids transport Os into the overlying mantle wedge. However, in this area Re enrichment is not apparent in the xenoliths and so it is proposed that Re is either not transported or not retained in the fluid over long distances, without reaction with the mantle. The study of a gold deposit and the underlying mantle in Papua New Guinea, elucidated a possible order of fluid mobility for some of the platinum group elements, and Cu and Re, by analysing their respective enrichments in metasomatised mantle harzburgites (McInnes et al. 1999). The order of mobility deduced was: Pd > Au > Pt > Re > Cu > Os. In some samples, concentrations were 2 - 800 times those of harzburgites that had not undergone metasomatism.

Another study of mantle wedge peridotites was published by Parkinson et al. (1998), using samples from a drill core in the Izu-Bonin-Mariana forearc. It is clear

from this very unradiogenic data that, with the possible exception of one sample, none of the spinel-harzburgites have undergone enrichment in Re or Os from slab-derived fluids. In fact, some of the values are amongst the least radiogenic ever reported. However, enrichment of the mantle wedge through the infiltration of slab-derived fluids or melts may be localised, and also may not occur at shallow fore-arc levels, so this data by no means precludes the addition of Os or Re to the mantle wedge. The investigation of subduction zone lavas from Java by Alves et al. (1999) highlighted the heterogeneous nature of slab fluid infiltration by recognising that different initial Os isotope compositions exist within single lava samples which suggest disequilibrium even on a sample scale. Although it seems difficult to envisage how different components of a single lava can inherit variable Os isotope compositions, without being thoroughly mixed in a magma chamber. The Os isotope compositions of the arc lavas from Alves et al. (1999; 2002) form a linear negative correlation with non-radiogenic osmium abundance (i.e. ^{188}Os), and these authors seek to explain this by a binary mixing process between unradiogenic mantle and a different, more radiogenic source. Due to the broad range of basement rocks, it is difficult to explain the mixing in terms of crustal assimilation and contamination (1999; 2002), and therefore the authors invoke a slab-derived mixing component.

A study of primitive calc-alkaline lavas from the Cascades arc concluded that Re and Os abundances and Os isotopes appeared to be dependent on the amount of slab component observed (Borg et al. 2000). This is analogous to the observations of Alves et al. (1999; 2002) whereby Os composition becomes more radiogenic with decreasing Os abundance. However, unlike this latter study, the work of Borg et al. (2000) uses the Sr/P ratio of the lavas to estimate the amount of slab input into these samples. In this way, it has been deduced that samples with a low slab input have higher Re and Os concentrations and less radiogenic Os compositions, whereas those with a greater slab input have lower abundances of Re and Os and

more radiogenic signatures. Unless incompatible element concentrations decrease during differentiation, the authors do not consider that these patterns can be obtained through assimilation and fractional crystallisation. However, in order to explain the variations by involvement of a slab component, the slab input would have to have Os concentrations between 100 and 600 times greater than the slab itself (Borg et al. 2000). In the current light of knowledge of Os mobility, this does not seem plausible. One possibility is that the slab flux into the mantle wedge actually increases the stability of a dominant Os bearing phase and so reduces the Os abundance in melts derived from it (Borg et al. 2000). These melts would then be more susceptible to contamination from the crust.

Chesley et al. (2004) offer a cautionary word to those studying in this field. They suggest that any observations of elevated $^{187}Os/^{188}Os$, which are commonly attributed to a slab component, should be compared more rigorously to well-established slab fluid indicators such as Ba and Rb. Furthermore, these authors cannot see evidence for a mechanism of mantle metasomatism to account for $^{187}Os/^{188}Os$ ratios of over 0.150, either by addition of a radiogenic osmium component or through addition of Re, followed by decay to ^{187}Os. They agree with the findings of Borg et al. (2000), that the observed isotope patterns can only be explained by metasomatism through a slab component that is unrealistically enriched in Os by a factor of 2-4 orders of magnitude. By comparing Ba/Nb and Os ratios of lavas from the Trans-Mexican volcanic arc, Chesley et al. (2002) envisaged their formation through the addition of a Ba-rich slab component to the mantle wedge which then produced melts with high but variable Ba/Nb and low $^{187}Os/^{188}Os$ ratios. The high $^{187}Os/^{188}Os$ ratios are thought to be a result of crustal assimilation.

Despite these many indications that Os mobility may occur in subduction zones settings, there are still many unknowns, particularly for the Re-Os system (see Woodhead and Brauns 2004). Factors such as fractional crystallisation are little

understood and can be corrected for in the case of Re, by normalisation to a similarly compatible element such as Yb, but the same is not true for Os. The Re abundances are, however, complicated by variable degassing which is also poorly understood. Clearly, crustal contamination may be a major contributor to radiogenic Os signatures, particularly in continental arcs where the basement may be very old and possess very radiogenic Os ratios. For this reason Woodhead and Brauns (2004) suggest that investigations are only undertaken on intra-oceanic arcs. Even in cases where most inputs are well-constrained, it may be the accurate estimation of the composition of the mantle wedge that proves to be the limiting factor in the modelling of subduction zone fluxes (Woodhead and Brauns 2004).

5.2.3.2 Rhenium

The average $^{187}Re/^{188}Os$ ratio and Re abundance in the continental crust have been estimated at approximately 50 and 0.4 ppb respectively (Allegre and Luck 1980; Esser and Turekian 1993). As subduction zone magmatism is thought to be the major producer of continental crust, it is interesting to note that Re abundances in arc rocks must be considerably lower than the average for MORB (1-1.5 ppb, Schiano et al. 1997; Peucker-Ehrenbrink et al. 2003). However, Sun et al. (2003a; 2003b; 2004) have measured Re concentrations in glasses from arc settings by LA-ICP-MS (laser ablation inductively-coupled mass spectrometry), and have obtained high values of approximately 2 ppb. These values are comparable to, although in fact actually greater than, the average composition of MORB – perhaps suggesting that Re has been added to the mantle wedge by fluid/melt infiltration from the down-going slab. This is in stark contrast to the findings of Alves et al. (1999; 2002) which identify low Re abundances in arcs (~0.1-0.6 ppb) compared to MORB. Ocean island basalts have also been found to contain low abundances of Re (e.g. Lassiter 2003). It has been suggested previously, that the low measured Re concentrations in arc lavas (and some OIB), are the result of the control of garnet or possibly sulphide in the mantle source of arc basalts and OIB - in experimental

studies, rhenium has been found to be compatible in these phases (Righter and Hauri 1998). However, other trace element patterns involving elements which are compatible in garnet (such as Yb) are not consistent with this model (Lassiter 2003). The explanation for the conflicting estimates of Re concentrations from Sun et al. (2003a; 2003b; 2004) and other studies on arc lavas (e.g. Alves et al. 1999; 2002) is most likely to be the process of degassing. Rhenium is thought to be a volatile element which is commonly lost through degassing during volcanism (Lassiter 2003). The samples in the studies of Alves et al. (1999; 2002) were erupted sub-aerially, whereas the glasses from the publications of Sun et al. (2003a; 2003b; 2004) were clearly from sub-marine eruptions and thus may have escaped the process of degassing. That said, it is difficult to estimate accurately what proportions of the continental crust have been produced by sub-aerial and sub-marine volcanism respectively, and so estimates of the Re concentrations of the continental crust are not without assumption. Furthermore, the varied nature of lithologies in the continental crust makes an estimate extremely difficult. Nonetheless, the study of arc glasses by Sun et al. (2003a; 2003b; 2004) is consistent with significant mobility of Re in subduction zones and its enrichment in some mantle source areas of arc basalts. Woodhead and Brauns (2004) suggest that Re is more mobile in 'fluid-dominated', low K, tholeiite arc settings.

Analyses of PGE and Re have been performed on picritic lavas from Granada and boninitic lavas from the Izu-Bonin arc (Woodland et al. 2002). PGE abundances did not vary appreciably between the two arcs, despite the different major element chemistries, whereas Re was found to be depleted in the Granada samples, but not in the Izu-Bonin arc. Woodland et al. (2002) suggest that this may be due to retention of Re in garnet in the mantle wedge as predicted by Righter and Hauri (1998). However, a different possible explanation for the Re variation in the lavas lies in the fact that the samples from Grenada were erupted sub-aerially and so may have suffered degassing, whereas those from the Izu-Bonin arc were from

submarine eruptions. Another more complex possibility is that the medium for the slab flux is different between the two settings. As suggested by Widom et al. (2003), hydrous melts in hot subduction zones may transport Re more efficiently than silicic fluids, and so it is possible that the low Re abundances in lavas from Grenada are the result of slab-fluid input into the mantle wedge rather than melt. The likelihood of this hypothesis being a major factor depends on the age of subducted crust and the thermal regime at the two different subduction zones. The age of the crust being subducted at the Izu-Bonin arc is older and therefore colder than at Grenada, which would lead to less Re transport in the Grenada setting, which is contrary to the findings of Woodland et al. (2002). However, the mobility of Re may be sensitive to smaller variations in the composition of slab fluids or melts.

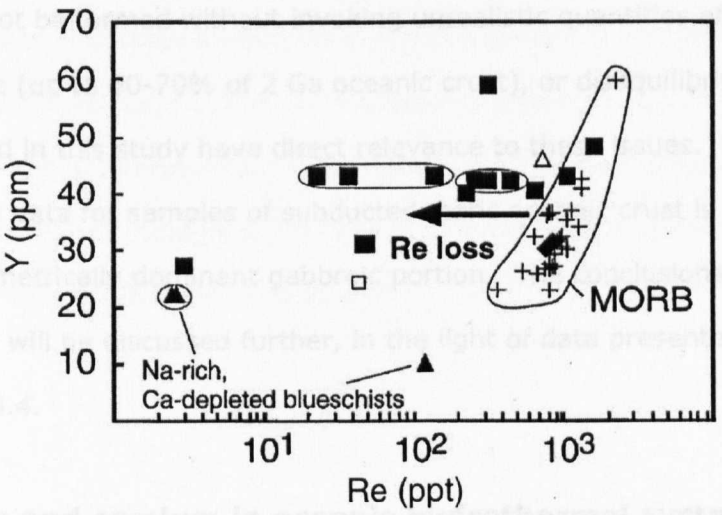

Figure 5.5. Yttrium (ppm) against Re (ppt) for MORB and blueschist and eclogite facies metabasalts (from Becker 2000). Filled squares: metabasaltic eclogites and blueschists; open square: metagabbroic eclogite; open triangle: low-temperature blueschist; filled diamonds: mafic high-pressure granulites.

High-pressure terrane studies

A different line of investigation has been employed by Becker (2000), whereby he analysed a variety of metabasalts that have been subjected to high pressure - low temperature metamorphism during subduction and have been subsequently

exhumed in mountain building events (e.g. Zermatt-Saas ophiolite, Western Alps – see Section 2.2.1). By comparison of Re abundances with a similarly compatible element such as Y or Yb, Becker (2000) estimated that the metabasalts have, in general, undergone Re loss during prograde dehydration (up to 60% Re loss) (Figure 5.5).

The significance of this conclusion is two-fold. Firstly, if the Re-enriched fluids infiltrate the mantle wedge and over time lead to more radiogenic $^{187}Os/^{188}Os$, it may explain the elevated Os isotope signature of some island arc basalts (IAB) and sub-arc mantle xenoliths. Secondly, Becker (2000) recognised that if Re is lost from the slab during subduction, the recycled crustal component will have a lower Re/Os ratio and this will have an effect on the modelling of mixing between recycled components and the mantle. Indeed, he concluded that HIMU type Os signatures could not be formed without invoking unrealistic quantities of oceanic crust in the mantle (up to 60-70% of 2 Ga oceanic crust), or disequilibrium melting. The data presented in this study have direct relevance to these issues. In Chapter 6, bulk rock Re-Os data for samples of subducted mafic oceanic crust is presented, including the volumetrically dominant gabbroic portion. The conclusions of Becker (2000) and others will be discussed further, in the light of data presented in this study, in Section 8.4.

5.2.4 Rhenium and osmium in oceanic hydrothermal systems.

A topic of discussion after the paper by Becker (2000), is whether or not the observed loss of Re in high-pressure (HP) metamorphosed basalts, was the result of the HP stage or an earlier effect from seafloor alteration in a hydrothermal system. There has been little work published addressing this question. Reisberg et al. (2004) proposed that low Re/Os ratios in the Dabie-Sulu UHP terrane may be the result of Re depletion during cold, meteoric water circulation, although whether this is analogous to hotter, oceanic hydrothermal alteration is not clear.

Work on samples from ODP drill cores by Peucker-Ehrenbrink et al. (2003) has provided the most complete assessment of Re concentration throughout the upper oceanic crust. These authors found that Re abundances were highest at depths where most extensive alteration had occurred (e.g. in the transitional / mineralisation zone between volcanics and dykes, and particularly in brecciated zones). This suggests that seafloor hydrothermal alteration is more likely to enrich samples in rhenium. These samples also had corresponding low Os and other PGE concentrations indicating that these elements are more likely to become depleted under these conditions. Overall, however, the authors proposed that Re enrichment is only locally important and does not exceed a few percent for the average oceanic crust. Likewise, any Os depletion cannot account for more than 10% of the crustal budget. While these two effects, taken in tandem, will have the effect of increasing magmatic Re/Os ratios, Peucker-Ehrenbrink et al. (2003) emphasise that fractionation during MORB genesis is the predominant control on Re/Os systematics, possibly with additional processes occurring during subduction. Hydrothermal alteration is not thought to compromise or accentuate the development of radiogenic $^{187}Os/^{188}Os$ signatures during mantle recycling of oceanic crust (Peucker-Ehrenbrink et al. 2003).

5.3 Re-Os system - dissolution, chemistry and mass spectrometry

In order to gain both osmium isotopic ratios and data for osmium and rhenium abundances, it is necessary to spike the sample dissolutions with a known quantity of a very well calibrated solution which is enriched in specific rhenium and osmium isotopes, in this case, ^{190}Os and ^{185}Re. The abundances and osmium isotope ratios of the spike used are shown in Table 5.3 below.

$[^{190}Os]$	37.541 ppt
$[^{185}Re]$	3.665 ppb
$[^{187}Re]$	127.622 ppt
$^{184}Os/^{188}Os$	<0.0085
$^{186}Os/^{188}Os$	0.07157
$^{187}Os/^{188}Os$	0.07368
$^{189}Os/^{188}Os$	2.1749
$^{190}Os/^{188}Os$	126.51
$^{190}Os/^{188}Os$	4.264

Table 5.3. Rhenium and osmium abundances and Os isotope ratios for the spike used.

5.3.1 HBr and HF dissolution, and solvent extraction using bromine and iso-amylol

The dissolution of samples and chemical separation of Re and Os by solvent extraction closely followed the method of Birck et al (1997), and is described below. All acids used were Teflon distilled (TD) unless otherwise stated.

Whole rock powders (0.4g) were placed in 6ml Savillex Teflon pressure vials and digested and equilibrated with ^{185}Re and ^{190}Os mixed spike in 2ml of 9M HBr and 2ml of 29M commercial HF for 3 days at 140°C. At this stage in the chemical procedure, spike and sample equilibration is still not assured. This is due to the various forms in which osmium is present in a rock sample, and therefore the various oxidation states in which it exists. In some samples, Os occurs in the form of metal (iron meteorites and osmiridium alloys) and its oxidation state is 0. More

commonly in basic silicate samples, the oxidation state is +IV, as is the case with sulphides. The following procedure is performed in order to achieve maximum oxidation of all osmium present in the spike-sample solution (i.e. all Os in the form: OsO_4) and therefore be assured of complete equilibration.

The samples were dried and the following reagents added: 1ml of chilled Br_2, 0.4ml CrO_3 in 8M HNO_3 (40% m/v) and 1ml 15M sparged TD HNO_3. The pressure vials were re-sealed and placed on a hotplate at 110°C for at least 3 hours. The CrO_3 solution is a powerful oxidising agent; converting all the Os (which may be present in several oxidation states) to the volatile form OsO_4 which is captured and dissolved in the boiling bromine. A small drop of the aqueous fraction (HNO_3) was added to hydrogen peroxide (H_2O_2) in order to establish that complete oxidation of the osmium had occurred. This was determined by the presence of excess CrO_3 in the aqueous fraction. This could be observed by a vigorous blue reaction between the two solutions. If excess CrO_3 was not observed, an extra 0.2ml of CrO_3 in HNO_3 was added and the vial placed on a hotplate for a further 30 minutes. The oxidation test was repeated, and if negative, more CrO_3 in HNO_3 was added. When the test was positive, the bromine was extracted, placed in a 7ml Teflon vial and dried with 1ml of 9M HBr at ~90°C. The remaining aqueous fraction was used for rhenium chemistry, which is outlined below.

Osmium. The residues that remained after drying the bromine and HBr were micro-distilled in order to ensure maximum purification and oxidation of osmium (see Figure 5.6). This involved re-dissolving the residue in a small drop of HBr, which was then transferred to the lid of a 7ml Teflon conical vial and dried. Two drops of Cr in H_2SO_4 were placed on the residue and a single small drop of HBr was placed in the bottom of the conical vial. The vial was then inverted, screwed onto the lid, completely wrapped in aluminium foil (except for a small hole at the apex) and placed (upside down) on a hotplate at 110°C for at least 3 hours. During this

step, the osmium complex $OsBr_6^{2-}$ is oxidised by CrO_3 to the volatile OsO_4 form. This is transferred in the gas phase to the apex and converted back to $OsBr_6^{2-}$ by the drop of 9M HBr. The osmium solution was then ready for loading and analysis.

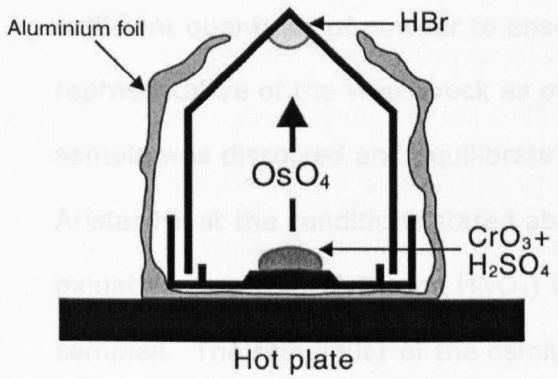

Figure 5.6. Microdistillation technique for osmium purification.

Rhenium. During the capture of OsO_4 by Br_2, the Re is retained in the aqueous phase (15M HNO_3 + CrO_3) and afterwards was reduced by the addition of ethanol and water, and dried in a 15ml Savillex vial. This was re-dissolved in 2ml of 2M HNO_3 and transferred to a transparent FEP Teflon centrifuge tube, to which 2ml of 3-methyl-1-butanol (iso-amylol) was then added. Iso-amylol has a strong affinity for rhenium, and extracts it from the 2M HNO_3. The tube was vigorously shaken for at least 2 minutes in order to mix the two immiscible liquids and subsequently placed in a centrifuge for approximately 5 minutes. Subsequently, the 2M HNO_3 was discarded and the iso-amylol was cleaned at least twice with 2ml of clean 2M HNO_3 repeating the shaking and centrifugation steps on both occasions. Following the cleaning steps, 2ml of Millipore H_2O were added and once again the tubes were shaken and centrifuged. The water was extracted and placed in a 15ml Savillex vial. In the case of samples which had low rhenium concentrations, the water extraction procedure was repeated with a further 2ml of water. The water was then dried and the residue re-dissolved in a single drop of water, ready for loading and analysis.

Larger dissolutions in Teflon. Certain analyses were repeated using large, 30ml Teflon pressure vials for the dissolution, in order to try to limit the so-called 'nugget effect'. This effect is particularly important in the Re-Os system, due to the vastly heterogeneous distribution of both rhenium and osmium. It is vital to analyse sufficient quantities of powder to ensure that the resulting analysis is as representative of the whole rock as possible. In these cases, approximately 2g of sample was dissolved and equilibrated with spike in 2ml of 9M HBr and 10ml of 29M Aristar HF at the conditions stated above. Due to adequate volume in the vials, the oxidation step (Br_2, CrO_3 and HNO_3) was carried out without previously drying the samples. The remainder of the osmium and rhenium separation technique remained unchanged, except for the use of only a 2ml aliquot of the aqueous liquid for the rhenium chemistry, and the use of greater volumes of reagents for the oxidation step: 2ml of bromine, 1.2ml of CrO_3 in HNO_3 and 1.5ml of 15M HNO_3.

Due to vastly increased rhenium blanks, the standard procedure outlined above (using 6ml Teflon pressure vials) was modified for the later analyses. It was ascertained that the oxidation step (either the Br_2 or the CrO_3 in HNO_3) was responsible for increasing the procedural rhenium blank to levels of tens of picograms, while the Os blank remained at a low level (<100fg). Given the small quantity of sample dissolved, this led to an unsatisfactory Re blank correction (upwards of 20% blank contribution). As a consequence, I performed a test on two previously analysed samples, whereby I extracted an aliquot of acid (0.5ml), after dissolution and prior to drying before the oxidation step. This fraction was used for the Re chemistry, while the remaining 3.5ml was dried, oxidised, micro-distilled, and analysed for osmium. Due to the very low abundance and very heterogeneous distribution of Os in rocks of this nature, repeat analyses rarely reproduce exact values. In this case, the test yielded data which had comparable reproducibility to data that were obtained by repeat analyses using the original method alone.

5.3.2 Carius tube dissolution

The HBr and HF dissolution method, outlined above, generally achieved very good results and incomplete digestion was not a common problem. However, complete dissolution may not have been achieved in the case of two gabbros and one sample that had transitional mineralogy between gabbro and coronitic eclogite. The presence of chromite in these rocks, which is difficult to dissolve in HF and HBr at the temperatures used for Teflon dissolution, may explain why complete dissolution was not achieved. In order to ascertain whether incomplete dissolution was an important factor, an alternative digestion method was used on two samples.

The Carius tube procedure followed closely the technique of Shirey and Walker (1995). However, it varied from their method by the use of *inverse* aqua regia (3ml of TD 6M HCl and 9ml of sparged TD 15M HNO_3) in order to achieve dissolution, as opposed to aqua regia. Following dissolution, osmium was separated by the solvent extraction process of Cohen and Waters (1996), while the rhenium procedure followed the iso-amylol extraction technique of Birck et al. (1997).

Approximately 3g of rock powder (weighed accurately to 5 decimal places) was placed in a Pyrex tube, by means of a funnel, and mixed spike was added (see above). Due to the large mass and cumbersome nature of the Carius tubes, spike masses were determined by weighing and reweighing of the spike container. The 3ml of 6M HCl was added and the tubes were placed in the freezer. When sufficiently cold, the 9ml of sparged TD 15M HNO_3 was added and the tubes returned to the freezer. Using an oxygen-propane torch, and with the aid of dry ice to keep the tubes cold, the Pyrex at the opening of the tube was melted and solidified in a small bulb, thus sealing the tubes completely. The tubes were placed in metal jackets and put into an oven at 230 °C for 7 days. This ensures maximum dissolution and also allows leaching of silicate material that would not otherwise be

digested by the inverse aqua regia (i.e. silicate material – HF cannot be used in glass tubes). At this point all osmium from both spike and sample has been oxidised and equilibrated to the OsO_4 form. After seven days, the metal tubes were removed from the oven, allowed to cool, and the Carius tubes removed from within, and placed in the freezer. To avoid explosions during the opening process, the tubes were thoroughly frozen.

In order to open the tubes, the glass was scored approximately half-way round the tube with a piece of tungsten carbide. The oxygen-propane torch was then applied to the score which propagated as a crack in the glass, at which point the top of the glass tube could be broken off. The inverse aqua regia was extracted by pipette (without any residual solids) and placed in a 30ml Teflon vial containing 6ml of carbon tetrachloride (CCl_4). The vial was shaken thoroughly. The CCl_4 extracts OsO_4 from the inverse aqua regia both efficiently and with high selectivity. After leaving overnight, the inverse aqua regia (the upper layer, above the denser organic liquid) was extracted from the vial and placed in a clean 15ml Teflon vial, where it was evaporated to dryness on a hotplate at approximately 130°C. This residue was re-dissolved in 2ml of TD 2M HNO_3 and used for the rhenium chemistry. The rhenium chemistry then followed the iso-amylol solvent extraction and loading method outlined above in Section 5.3.1. Back extraction of the osmium was achieved by placing the CCl_4 in a 30ml vial with 10ml of TD 9M HBr. This was shaken thoroughly and left overnight. The concentrated HBr extracts and reduces the OsO_4 to $OsBr_6^{2-}$. Subsequently, the HBr (which formed the upper layer in the vial) was removed, placed in a clean 15ml Teflon vial, and dried on a hotplate at ~120-130°C. From this point, the osmium chemistry followed the micro-distillation and loading technique outlined above in Section 5.3.1.

5.3.3 Mineral separates

A petrographically representative unaltered gabbro (S01/39iiix) and fully recrystallised coronitic eclogite (S01/3iix) have been hand-picked in order to investigate the redistribution of rhenium and osmium during metamorphic recrystallisation. For the separation process see *Mineral separation* in Appendix A.1.1. All separates were checked twice for purity and cleaned in an ultrasonic bath with acetone, 2M TD HCl and millipore water. They were crushed and ground in a pre-cleaned agate pestle and mortar. The powder was then carefully transferred to a small piece of pre-weighed aluminium foil and then weighed. The dissolution vial was also pre-weighed and re-weighed after the addition of the powder in order to give an indication of the quantity of possible powder lost.

The dissolution and chemical procedure followed the method outlined above in Section 5.3.1. However, as the sample mass was sometimes very small, lower volumes of reagents were used in a (successful) attempt to reduce the total procedural blank (TPB). This is of crucial importance in analyses of this type, where osmium concentrations may be as low as 0.1 pg/g and some sample masses were as little as 40mg. This equates to a possible total osmium content of the analysed sample of only 0.004 pg (4 femtograms). The lowest TPB attained, even for mineral analyses, was approximately 15 fg, so clearly accurate and precise analyses at this level are unobtainable. It is unlikely that this method, or any other, will be able to produce consistently low enough blanks to facilitate analysis of small quantities of certain gabbroic/basaltic minerals. In these cases, much larger quantities, perhaps at least 200 mg would be necessary.

Chemical dissolution and purification for sulphide grains.

Some sulphide grains were sufficiently large to crush roughly in a pre-cleaned agate pestle and mortar and then dissolve in Teflon pressure vials as outlined in Section 5.3.1, only with smaller reagent quantities. However, sulphides from the gabbros

rarely exceed 100 μm in diameter and are often found contained within other grains in the crushate. As well as the difficulty in separation, it is also preferable to analyse single sulphide grains (even though they are in themselves composites of sulphides of several different types). In order to limit blank levels and to ensure efficient dissolution, the sulphide grains were placed on the upside-down lid of a conical vial (used for microdistillation), to which a drop of spike was added and dried. Further drops of 6M TD HBr were added to dissolve the grain, although in two cases the sulphide was not fully dissolved at this stage.

Microdistillation was then performed with a Cr in H_2SO_4 solution which was prepared with more concentrated sulphuric acid. After an extended period of microdistillation, the sulphides were found to have dissolved fully, and the drop of HBr was dried and loaded. The Cr in H_2SO_4 drop on the lid of the up-turned vial was placed in a 15ml Teflon vial and 0.5ml of a 50-50% ethanol-water mixture was added to reduce the Re within the solution. The solution was dried, re-dissolved in 2M TD HNO_3, and purified through the iso-amylol extraction technique outlined above.

5.3.4 Loading and mass spectrometry

The development of negative ionisation mass spectrometry (N-TIMS) as a means of analysing Re and Os was a major breakthrough, and helped to establish the Re-Os system as an important and workable tool in geochemical studies. The methods of N-TIMS have been described previously by Volkening et al. (1991), Walczyk et al (1991) and Creaser et al. (1991). The loading and mass spectrometry technique used here is summarised by Birck et al. (1997), but differs in one respect. Birck et al. (1997) found that the Re loading blank for platinum filaments, despite high purity, was around 1 pg. As a result, that study used Ni filaments for Re analysis. At the Open University, during the period of analysis, the Re loading blanks for Pt

filaments remained below 70 fg, and therefore platinum ribbon was used for both osmium and rhenium analysis.

Loading. Single platinum filaments were made using ultra-pure Pt ribbon (99.999% Pt). These were rinsed with Millipore water and acetone and sonicated in acetone for two minutes. They were then rinsed again with Millipore water and acetone and out-gassed in air for three times 1 minute at approximately 2.3 amps.

For the analysis of osmium, the HBr drop in the conical vial was partially dried (to a volume of between 1 and 10 μm) and loaded slowly, in its entirety, onto a cleaned and out-gassed Pt filament at 0.60 amps. A thin covering of the activator, comprising $Ba(OH)_2$ and NaOH, was added to the filament and the current briefly increased to a point where the load begins to melt. For rhenium analysis, less than 1 μl of water from the remaining drop of water was loaded onto a cleaned and out-gassed Pt filament at 0.5 A, followed by the addition of a thin covering of the same activator, but with no subsequent increase in the current. Without the addition of the activator, the electron work function of the platinum ribbon is too high for efficient generation of negative ions. By using a thin coating of a metal oxide (loaded as hydroxide) such as BaO or Na_2O, (or a combination of the two as in this study) considerably higher ion yields can be produced (Zeininger and Heumann 1983; Volkening et al. 1991).

Mass spectrometry and corrections. The samples were run dynamically on a Thermo-Finnigan Triton using the electron multiplier, measuring negative ions. A small amount of pure oxygen was vented into the source throughout the analysis, in order to encourage the ionisation of both osmium and rhenium. However, generally the vacuum remained below 2.00^{-7} Torr. The filaments were heated slowly (~100mA/minute) to ~850mA; which equates to a filament temperature which is lower than the temperature required for ionisation of Os. At this point, the beam was focussed on the ^{79}Br species, to minimise Re or Os loss during focussing.

The filament was then heated further in 10 or 20mA increments, and focussed several more times before starting measure. All the species to be analysed were peak-centred prior to measurement, and every 4-6 blocks during collection. Blanks were measured for a period of 20 cycles. Depending on beam size, Os samples were run for between eight and fifteen blocks of 10 cycles (80-150 ratios). Rhenium sample ratios were collected for two or three shorter periods of approximately 50 cycles (see following paragraph). As the data was collected dynamically, all data was internally drift corrected to allow for beam variation during the run.

The masses collected for rhenium analysis were 149 ($^{185}Re^{16}O_4^-$) and 151 ($^{187}Re^{16}O_4^-$). These are the only two naturally occurring isotopes of rhenium, of which only ^{185}Re is stable (which is highly enriched in the spike). This unfortunately means that there is no stable isotope pair with which to correct for mass fractionation during N-TIMS analysis. In the absence of a ratio with which to perform a mass fractionation correction calculation, it was necessary to undertake two or three collections at different filament temperatures to try to ensure that the plateau at the highest $^{187}Re/^{185}Re$ ratio was measured (the background-filament $^{187}Re/^{185}Re$ ratio was around 0.6 (i.e. natural abundance), much lower than samples and blanks, and so theoretically the highest value should be the most accurate measurement of the sample).

The masses collected for osmium analysis were 233 ($^{185}Re^{16}O_3^-$), 235 ($^{187}Os^{16}O_3^-$), 236 ($^{188}Os\ ^{16}O_3^-$), 238 ($^{190}Os^{16}O_3^-$) and 240 ($^{192}Os^{16}O_3^-$). Occasionally, when beams were sufficiently large, masses 234 ($^{186}Os^{16}O_3^-$), 237 ($^{189}Os^{16}O_3^-$) and 251 ($^{187}Re^{16}O_4^-$), were also analysed. Without the analysis of ^{186}Os and ^{189}Os, a standard value for $^{186}Os/^{188}Os$ and $^{189}Os/^{188}Os$ was used in the calculations. This value should be constant, after accounting for mass fractionation, but the use of the larger collecting program at regular intervals, confirmed the legitimacy of the

values used. A pre-collection run of 10 cycles was performed in order to determine the $^{192}Os/^{188}Os$ ratio for a given sample or blank. This ratio differed from the true sample value due to an enrichment of ^{192}Os from the spike ($^{192}Os/^{188}Os$ for spike = 4.264 > natural value). The value from the pre-run was used in the method program in order to apply a preliminary on-line correction to the data, based on the variance of the $^{192}Os/^{188}Os$ ratio from the 'true' value. The data were corrected off-line for the effects of mass fractionation, taking into account the $^{192}Os/^{188}Os$ ratio of the analysis and the amount of spike and sample used.

Although $^{187}ReO_4^-$ is the major Re species, some Re takes the form $^{187}Re^{16}O_3^-$ which creates an isobaric interference at mass 235 with $^{187}Os^{16}O_3^-$. Therefore it was necessary to measure $^{185}Re^{16}O_3^-$ and apply a correction to the $^{187}Os^{16}O_3^-$ counts based on the $^{185}Re^{16}O_4$ to $^{187}Re^{16}O_4$ ratio. This latter ratio was monitored prior to collection and the value was entered into the program definition. An automatic on-line correction was applied.

Oxygen correction. As stated above, the osmium isotopes are measured by N-TIMS, in the form of OsO_3^- ions (i.e. masses 235, 236, 237, 238 and 240). However, these masses are not only dependent on the isotopic mass of the osmium, but also on the oxygen isotopes involved. For example, mass 236 would almost entirely consist of $^{188}Os^{16}O_3^-$ ions, but there would also be a small contribution from $^{187}Os^{16}O_2{}^{17}O^-$ ions (~0.1%). A summary of some of these interferences is presented in Table 5.4. An oxygen correction was applied to the data after measurement, by calculating the proportion that each possible species contributes to a given mass measured. This is based on the natural abundances of the three oxygen isotopes, and the number of counts of the different species measured.

Ion mass collected	$^{x}Os^{16}O_3^-$	$^{x}Os^{16}O_2{}^{17}O^-$	$^{x}Os^{16}O_2{}^{18}O^-$
235	187	186	-
236	188	187	186
237	189	188	187
238	190	189	188
240	192	-	190

Table 5.4. A summary of some isobaric interferences that result from variation in oxygen isotopes in the Os ion species measured. Numbers in columns 2-4 refer to Os isotopes that can be substituted for x in the ion species shown to produce total mass shown in column 1.

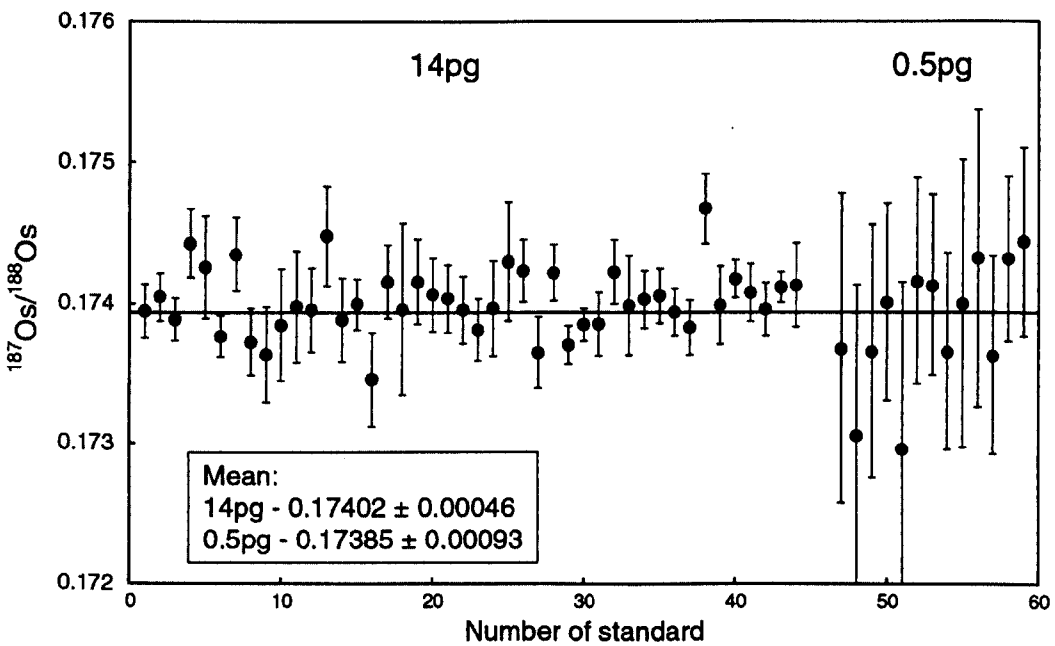

Figure 5.7. Reproducibility of $^{187}Os/^{188}Os$ for Johnson Matthey standard from 11/02 to 11/04: 14 pg and 0.5 pg amounts were loaded for whole rock and mineral analyses respectively. Error bars = 2 standard errors. Quoted error on mean value = 2 s.d. Solid line represents accepted value for the Johnson Matthey standard, collated from various laboratories worldwide.

5.3.4.1 Reproducibility

An aliquot of Johnson Matthey standard solution from the Department of Terrestrial Magnetism, Washington, USA was analysed repeatedly throughout the period of

analyses (11/02 - 11/04). Approximately 14 pg of Os was loaded to be measured with batches of whole rock analyses and 0.5 pg for mineral separates. Between 100 and 150 cycles were measured. The mean $^{187}Os/^{188}Os$ value for the 14 pg standard was 0.17402 ± 0.00046 (2 s.d.), which is in good agreement with the accepted value of 0.17398. The mean for the 0.5pg standard was 0.17385 ± 0.00093 (2 s.d.). Reproducibility is presented graphically in Figure 5.7 and also in Table 5.5.

		Reproducibility (relative 2 s.d.)			
DTM standard	$^{187}Os/^{188}Os$ (n=44, n=13)	*14pg*		*0.5pg*	
		0.26%		0.53%	
Repeat whole rock dissolutions (samples and standards)	Os abundances (n=2-5)	15%			
	Re abundances (n=2-3)	5 - 35%			
	Sample Os abundance	*>70ppt*	*>40ppt*	*<30ppt*	*<10ppt*
	$^{187}Os/^{188}Os$ (n=2-3)	<1%	<4%	~5%	~20%
	$^{187}Re/^{188}Os$ (n=2-3)	<1%	~10%	~10%	-

Table 5.5. Reproducibility of DTM standard and whole rock powder dissolutions.

Repeat analyses of certain samples and the rock standard JB-3 were performed in order to determine the reproducibility of dissolved solid samples (quoted as 2 standard deviations). This varied substantially according to the abundances in the sample. The values are collated below in Table 5.5. Clearly how rigorous these values are is compromised by the low number of analyses and is always likely to result in a lower reproducibility than calculations for much larger populations. It is also important to note that the values quoted for whole rock samples are not only a test of chemical and analytical reproducibility, but also a test of geological homogeneity. This latter factor is particularly important when dealing with the Re-Os system because the distribution of these elements in samples is very

heterogeneous (the so-called 'nugget effect'). Osmium isotope ratios ($^{187}Os/^{188}Os$) were age corrected before reproducibility was calculated, to account for variable ingrowth due to differences in rhenium abundance. No such correction can be applied to abundance values or the $^{187}Re/^{188}Os$ ratio, so the values quoted largely reflect geological variation rather than analytical error.

	Os blanks (pg)		**Re blanks (pg)**	
	Range	Mean	Range	Mean
Whole rock - Teflon diss^{n}	0.04 - 0.35	0.110	2.4 - 15.3	5.12
Whole rock - Large bomb	0.12 - 0.41	0.205	4.7 - 11.0	7.91
Whole rock - Carius tube	2.5 - 7.5	4.98	4.3 - 15.1	9.68
Mineral separates	0.01 - 0.12	0.070	0.7 - 1.4	1.07

Table 5.6. Summary of total procedural blank Re and Os abundances throughout the period of analysis.

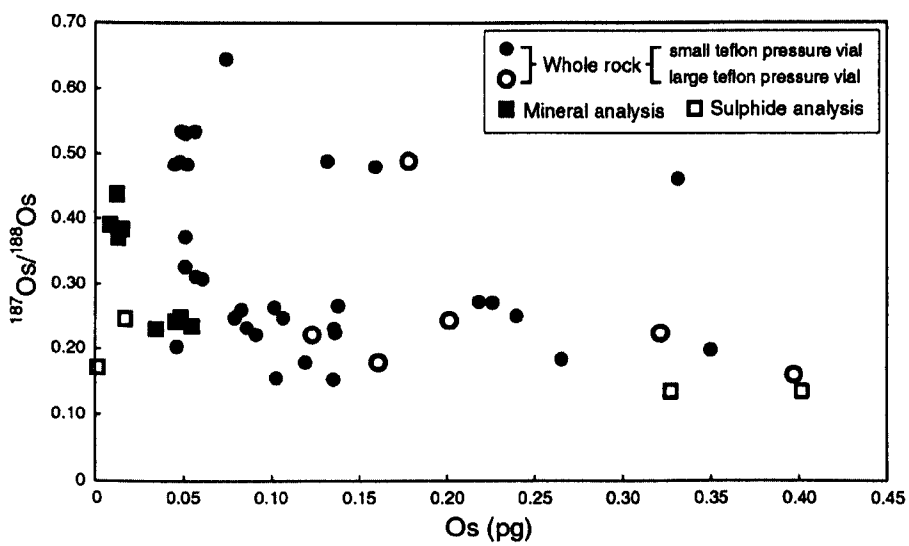

Figure 5.8. Os abundance versus $^{187}Os/^{188}Os$ ratio for all total procedural blanks for Teflon dissolutions from the period of sample analysis.

5.3.4.2 Blanks

Table 5.6 below summarises all total procedural blank values for rhenium and osmium over the period of analysis. Tables presented within Chapters 6 and 7

summarise all rhenium and osmium sample data and include the calculated percentage blank contribution for each analysis. Table 5.7 has a summary of typical reagent blanks for the period. The Os abundances plotted against $^{187}Os/^{188}Os$ ratio are presented in Figure 5.8. Both Os abundance and isotopic ratio vary greatly throughout the period of analysis. These data emphasise the importance of measuring blank values for a given batch of samples and applying a correction which is specific to those analyses.

	Os (pg)	Re (pg)
Loading	0.001 - 0.009	0.03 - 0.07
9M TD HBr	0.008 - 0.016	0.03
29M HF - commercial	0.002 - 0.004	0.05
TD Bromine	0.004 - 0.030	-
Oxidation step (sparged TD HNO_3 + Cr in HNO_3)	0.010 - 0.020	-
Iso-Amylol - cleaned	-	0.02 - 0.10
2M TD HNO_3	-	0.03 - 0.06
Millipore H_2O	-	0.005 - 0.020

Table 5.7. Summary of typical reagent and loading blanks throughout the period of analysis.

6 The behaviour of rhenium and osmium in subducted oceanic crust

The budgets of Os and Re within oceanic crust which passes through the subduction process are of great importance in determining the contribution of recycled oceanic crust to the source of some ocean island basalts. In particular, ocean island basalts that possess a HIMU signature are characterised by high $^{238}U/^{206}Pb$ (μ) and Os isotope compositions that are elevated with respect to other oceanic basalts. Section 5.2 contains a summary of some of the isotopic characteristics of the main mantle reservoirs, particularly with respect to the Re-Os system, and also outlines the state of current knowledge of the behaviour of Re and Os in oceanic crust during alteration and the subduction process.

In this chapter bulk rock Re-Os data are presented for variably metamorphosed gabbroic lithologies from the Allalin Gabbro, and metabasaltic eclogites from the Pfulwe area (Täschalp) both lying within the Zermatt-Saas Fee ophiolite (ZSO). The ZSO is an example of MORB-like oceanic crust (see Section 4.2.1.2) which has been subducted to at least 60 km depth (2.0 GPa or greater) and subsequently exhumed during the Alpine mountain-building event. As such, the majority of samples studied from this ophiolite are eclogite facies metabasalts and metagabbros, although some gabbro has been preserved in a metastable state.

In addition, the findings from the work on ZSO samples led to the investigation of a suite of metabasaltic and metagabbroic samples from the Sulitjelma ophiolite, northern Norway. These samples have been regionally metamorphosed at biotite to kyanite grade during the Caledonian orogeny.

6.1 Zermatt-Saas ophiolite

6.1.1 Abundances of rhenium and osmium in gabbroic and basaltic lithologies

Rhenium and Os abundances and isotopic data, for whole rock gabbroic and basaltic powders, are presented in Table 6.1 and Table 6.2 respectively.

Generally speaking, the concentrations of Re and Os in gabbros are, respectively, slightly lower and higher than in MORB (Figure 6.1 (a) and Figure 6.6). Consequently, many of the Allalin and Sulitjelma gabbros plot below the MORB field, and actually lie in the OIB field in Figure 6.1 (a). Nonetheless, the data for the Allalin and Sulitjelma gabbros are comparable to the published values for gabbros of Blusztajn et al. (2000). The slight displacement of the OIB field, to lower Re/Os relative to MORB, may be the result of Re loss during volcanic degassing, retention of Re in garnet due to differences in the P-T conditions of melting, and the higher Os abundances generally observed in OIB. However, the mantle source of the Allalin Gabbro should be the same as the global MORB source, and clearly degassing cannot be a means of reducing Re contents in a cumulate gabbro body. The reason for the lower Re and higher Os abundance of gabbros is the greater compatibility of Os, relative to Re. The co-variation of Ni and Os has been observed in many oceanic basalt suites and was long assumed to be due to the compatibility of Os in olivine. Burton et al. (2002) demonstrated that Os was not compatible in olivine and the apparent correlation is a result of co-precipitation of olivine and sulphide. Regardless of the mechanism, it is clear from the positive correlation of Os and Ni that Os is most abundant in olivine-rich (and therefore Ni-rich) samples, which correspond to the least fractionated members of mafic crustal sequence. Rhenium, however, does not display a correlation with Ni and behaves less compatibly during fractional crystallisation. Consequently, Re concentrations in gabbros, particularly those of accumulative origin, are lower than in the somewhat more differentiated basalts.

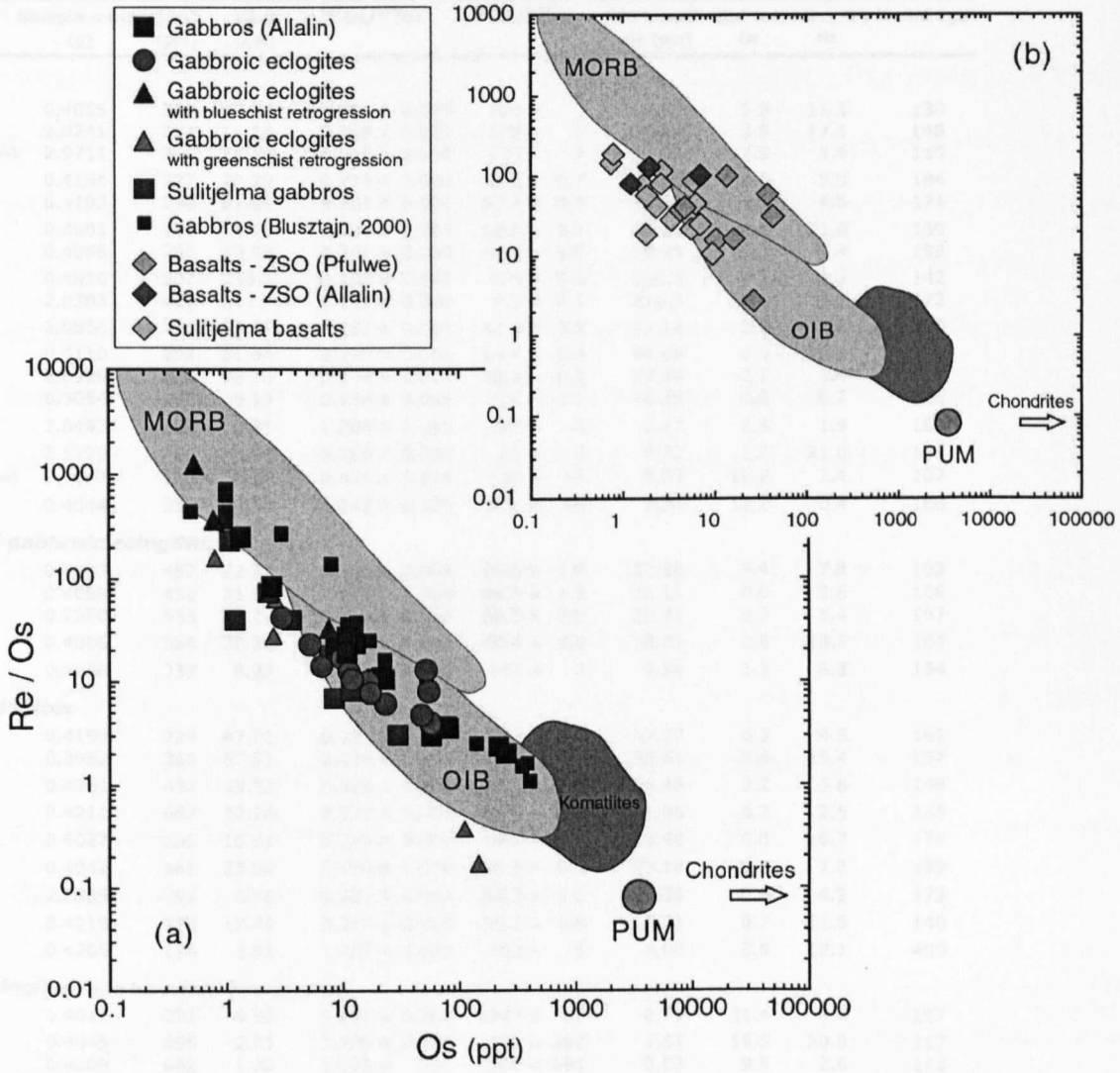

Figure 6.1. Os concentration plotted against Re-Os elemental ratio. The average primitive mantle composition is marked by a large open circle. MORB, OIB and komatiites define the terrestrial fractionation trend. Nearly all gabbroic samples from both ophiolites plot below the MORB field, at lower Re/Os and are coincident with the OIB field. These data are comparable with some of the literature values (Blusztajn et al. 2000). Many of the metabasaltic samples also plot below the MORB field – this shall be discussed further in Section 6.4.

The precise behaviour of Re and Os during crystallisation is not fully understood and therefore there may be more complex processes occurring during crystallisation which have a bearing on the Re-Os systematics of gabbros. Birck and Allegre (1994) suggested that oxygen fugacity has a strong control over Re abundances in planetary basalts, and it is possible that more minor variations in magmatic systems also impose a control on Re, and possibly Os, behaviour.

	Sample mass (g)	[Re] (ppt)	[Os] (ppt)	$^{187}Os/^{188}Os$	$^{187}Re/^{188}Os$	"Common" Os (ppt)	Blank contr. (%) Os	Re	Model age
Gabbros									
S01/5G	0.4055	300	13.22	0.366 ± 0.003	106 ± 3	12.82	5.8	11.3	130
dupl.	2.0241	254	11.25	0.389 ± 0.002	103 ± 5	10.84	2.8	17.1	148
dupl.(Carius tube)	2.9711	307	11.20	0.393 ± 0.010	135 ± 7	10.81	7.5	1.0	115
S01/36ix	0.4164	227	23.29	0.278 ± 0.009	46.5 ± 0.7	22.83	0.6	5.0	184
dupl.	0.4193	240	21.99	0.284 ± 0.001	52.2 ± 0.8	21.53	1.0	4.5	171
S01/39iiix	0.4601	145	11.18	0.334 ± 0.004	62.9 ± 3.1	10.88	6.9	21.0	189
dupl.	0.4066	208	19.93	0.301 ± 0.003	49.9 ± 1.0	19.48	0.7	5.4	199
S02/6ix	0.4016	507	253.4	0.158 ± 0.001	9.5 ± 0.1	252.3	0.1	2.3	142
dupl.	2.0303	422	217.4	0.162 ± 0.000	9.3 ± 0.1	216.3	0.1	1.1	172
S02/10iiixG	2.0854	170	57.57	0.182 ± 0.001	12.6 ± 0.8	57.12	0.4	23.6	225
S02/83vix	0.4110	292	81.44	0.193 ± 0.001	16.4 ± 0.2	80.69	0.9	11.6	210
dupl.	2.0929	315	78.76	0.194 ± 0.000	19.1 ± 0.3	77.99	0.1	1.4	185
dupl.	0.3054	279	79.13	0.194 ± 0.001	16.2 ± 0.3	78.39	0.2	8.2	216
S02/83viix	2.0493	209	2.81	1.204 ± 0.015	392 ± 6	2.47	1.5	1.9	163
S02/83viiixG	2.1229	200	8.97	0.309 ± 0.002	99 ± 6	8.72	1.1	21.0	105
dupl.(Carius tube)	2.9643	234	6.86	0.434 ± 0.018	168 ± 13	6.59	12.2	1.4	107
S02/83viiiix	0.4044	338	2.56	2.742 ± 0.135	978 ± 98	1.34	12.2	0.4	160
Transitional gabbroic eclogites									
S01/5E	0.4007	452	22.77	0.392 ± 0.003	94.8 ± 1.9	22.00	3.4	7.8	163
dupl.	0.4068	438	21.93	0.403 ± 0.004	96.9 ± 1.5	21.16	0.6	2.6	166
dupl.	0.2950	435	21.18	0.412 ± 0.002	98.5 ± 2.0	20.41	0.7	5.4	167
S02/10iiixE	0.4006	324	30.50	0.245 ± 0.001	40.4 ± 4.0	30.01	2.6	18.5	164
S02/83viiixE	0.4056	237	9.87	0.392 ± 0.002	115 ± 2	9.54	1.3	6.8	134
Gabbroic eclogites									
S01/3iix	0.4199	224	47.72	0.194 ± 0.001	22.2 ± 0.3	47.27	0.3	4.5	161
dupl.	0.3982	366	57.01	0.189 ± 0.000	20.6 ± 2.1	56.51	0.6	15.4	157
S01/35iix	0.4361	437	55.22	0.228 ± 0.001	37.7 ± 0.8	54.46	0.2	3.8	148
S01/35iiix	0.4211	667	52.98	0.272 ± 0.001	60.6 ± 0.9	51.96	0.2	2.5	136
S01/40iiix	0.4027	166	16.81	0.274 ± 0.004	46.7 ± 0.9	16.49	0.8	6.7	178
S01/40vx	0.4042	141	23.50	0.228 ± 0.006	28.0 ± 0.6	23.18	0.6	7.8	199
S01/40viix	2.0885	92	6.71	0.327 ± 0.002	66.3 ± 1.0	6.56	0.6	4.2	173
S02/33i	0.4219	133	17.42	0.217 ± 0.001	35.1 ± 0.8	17.21	0.7	11.6	140
S02/85ixE	0.4206	126	3.51	1.437 ± 0.052	190 ± 6	3.00	3.6	12.1	409
Gabbroic eclogites with blueschist retrogression									
S02/84viix	0.4017	291	0.99	5.581 ± 0.382	1747 ± 87	0.79	21.4	3.7	187
S02/84viiix	0.4045	695	2.21	3.709 ± 0.197	1839 ± 202	1.51	15.5	30.8	117
dupl.	0.4209	662	1.30	11.25 ± 1.11	5907 ± 591	0.53	9.8	2.6	113
S01/40iiiix	0.3171	247	8.20	0.765 ± 0.012	146 ± 6	7.57	6.8	11.7	259
Gabbroic eclogites with greenschist retrogression									
S01/30i	0.3232	192	2.98	1.251 ± 0.048	324 ± 23	2.60	12.6	14.6	207
S01/30ii	0.3196	41	110.7	0.157 ± 0.000	1.1 ± 0.4	110.21	0.5	28.2	1181
S01/39iiiix	0.3149	143	0.90	0.952 ± 0.105	750 ± 135	0.81	42.0	18.7	65
S02/5i	0.3369	25	145.7	0.157 ± 0.000	0.3 ± 0.2	145.05	0.4	39.2	3909
S02/7ii	0.3233	132	11.99	0.350 ± 0.003	47.7 ± 0.7	11.65	4.6	19.9	270
S02/85ixR	0.4269	75	2.74	0.757 ± 0.005	130 ± 8	2.53	4.7	18.8	287

Table 6.1. Rhenium and osmium abundances and isotopic data for gabbroic lithologies from the Allalin Gabbro, ZSO. Note the relatively narrow range of model ages for all groups except the samples which have undergone greenschist retrogression. It is likely that a greater extent of deformation within the greenschist samples has facilitated fluid flow, which has enhanced elemental loss. This will be discussed further in Chapter 8. Errors quoted (2 σ) have been propagated from the standard error, assuming 20% uncertainty in blank composition. Model ages have been calculated with a super-chondritic initial composition of $^{187}Os/^{188}Os$ = 0.135, due to the Isoplot calculation of an initial of 0.138. This value is a credible initial, given the average MORB composition of 0.133, while individual MORB compositions are sometimes higher (Gannoun et al. 2004a).

Due to higher Os and lower Re abundances, the Re/Os ratios (and therefore $^{187}Re/^{188}Os$) of gabbros are, on average, lower than in MORB. Therefore, over time, gabbros may not develop such extremely radiogenic Os isotope signatures as is proposed for MORB compositions. This has important implications for the impact of recycled oceanic crust in the mantle. However, on average, osmium is more abundant in gabbros than in basalts, and so the signature of the gabbroic portion of the oceanic crust will have a more marked effect than the basaltic section, in a reservoir predominantely composed of osmium-rich mantle peridotites.

The basaltic eclogites from the ZSO plot over a relatively broad area in Figure 6.1 (b), compared to the narrow range for global MORB, and some are comparable with the OIB field. The displacement of some of the ZSO basalts to lower Re/Os relative to MORB may be the result of Re loss during volcanic degassing, despite their submarine eruption (most samples were taken from recognisable pillow structures). This possibility will be addressed in Section 6.4.

	Sample mass (g)	[Re] (ppt)	[Os] (ppt)	$^{187}Os/^{188}Os$	$^{187}Re/^{188}Os$	"Common" Os (ppt)	Blank contr.(%) Os	Blank contr.(%) Re	Model age
Metabasalts									
Allalin									
S02/4i	0.4057	230	2.41	3.055 ± 0.298	443 ± 44	1.74	18.7	44.9	395
S02/4iiix	0.4165	725	7.58	1.043 ± 0.003	508 ± 8	6.77	1.8	1.4	107
S02/7i	0.4595	93	1.93	6.061 ± 0.232	392 ± 16	1.09	7.2	10.3	900
Pfulwe									
S02/41ii	0.4236	1385	26.43	10.85 ± 0.09	598 ± 12	11.10	1.2	0.5	1065
S02/41v	0.3965	165	4.21	0.795 ± 0.009	200 ± 3	3.87	7.5	3.9	197
S02/74ii	0.4176	233	12.30	0.973 ± 0.003	97.9 ± 1.5	11.08	1.0	6.9	512
S02/75iC	0.4292	632	6.04	0.591 ± 0.002	524 ± 8	5.69	2.1	2.7	52
S02/75iiR	0.4260	147	10.32	0.337 ± 0.001	66.8 ± 1.0	10.03	1.2	10.6	182
S02/75iiiC	0.4082	194	43.08	0.400 ± 0.001	21.9 ± 0.3	41.57	0.7	3.3	722
S02/75iiiR	0.4125	267	13.60	0.644 ± 0.003	98.9 ± 1.5	12.74	2.3	2.4	308
S02/75ivC	0.3986	159	37.82	0.264 ± 0.001	20.1 ± 0.3	37.14	0.8	4.0	384

Table 6.2. Rhenium and osmium abundances and isotopic data for basaltic eclogites from the ZSO. Note the large range of models ages, due to the open system behaviour displayed during metamorphism. See Table 6.1 for details of errors and model ages.

A comparison of Re and Os abundances (Figure 6.2) in gabbroic lithologies (gabbros, transitional samples and gabbroic eclogites) reveals a narrow band of composition (possibly with slightly positive covariation between the two elements.

The gabbroic eclogites form a somewhat broader and steeper trend, at least in the sample set analysed. The range of osmium concentrations in the gabbroic eclogites (3.5-57 ppt) is comparable to, although somewhat smaller than the gabbros (2.5-250 ppt). In contrast, the range of Re abundances in the gabbroic eclogite suite is greater than in the gabbros, although the range for gabbros is bracketed by the gabbroic eclogites (90-670 ppt compared to 170-510 ppt for unaltered gabbros). These observations may indicate a low level of disturbance of the system, possibly with some redistribution, with little overall loss or gain of rhenium or osmium.

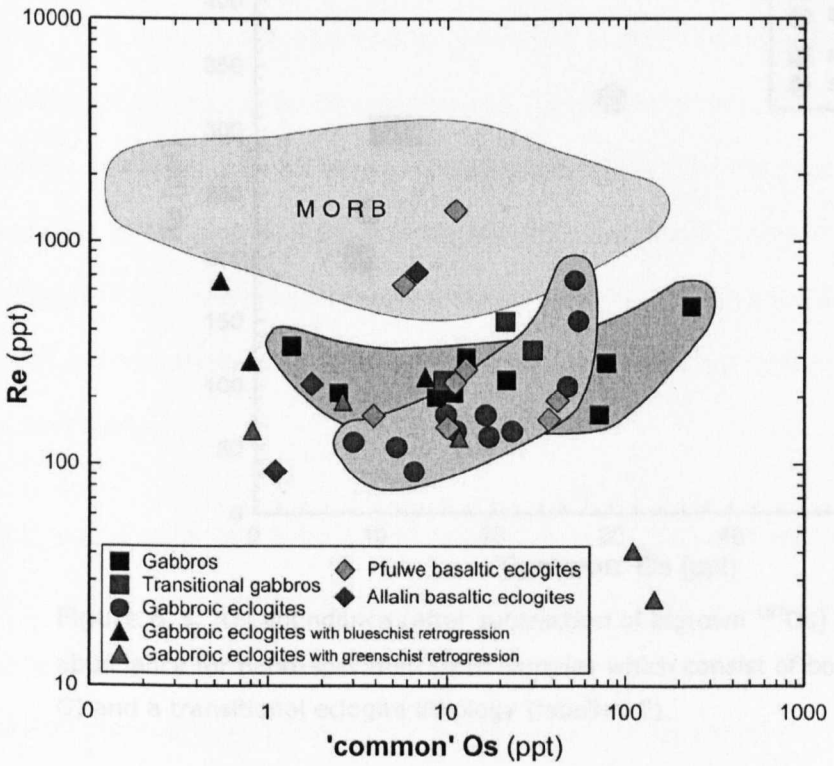

Figure 6.2. Concentrations of Os and Re in metamorphosed gabbros and basalts from the ZSO. Ingrown radiogenic ^{187}Os has been subtracted from the total Os abundance. MORB field after Schiano et al. (1997) and unpublished data from A. Gannoun.

There is a suggestion of lower rhenium abundances in the eclogitic gabbros from Figure 6.2. The mean for the gabbros is 273 ppt (n=9), compared to 233 ppt (n = 9) for the gabbroic eclogites. This difference is not likely to be statistically significant for the small number of samples involved, and is probably more dependent on small overall compositional differences between the suites, which are

commonly observed in cumulate gabbros. The mean concentration of Os in the two suites is 26 and 23 ppt in the gabbros and eclogites respectively (excluding one gabbro which is an order of magnitude richer in Os (~250 ppt) – including this sample the mean is 49 ppt). Considering the extremely heterogeneous distribution of Os, the abundance of Os in the gabbros and eclogites can be considered to be identical.

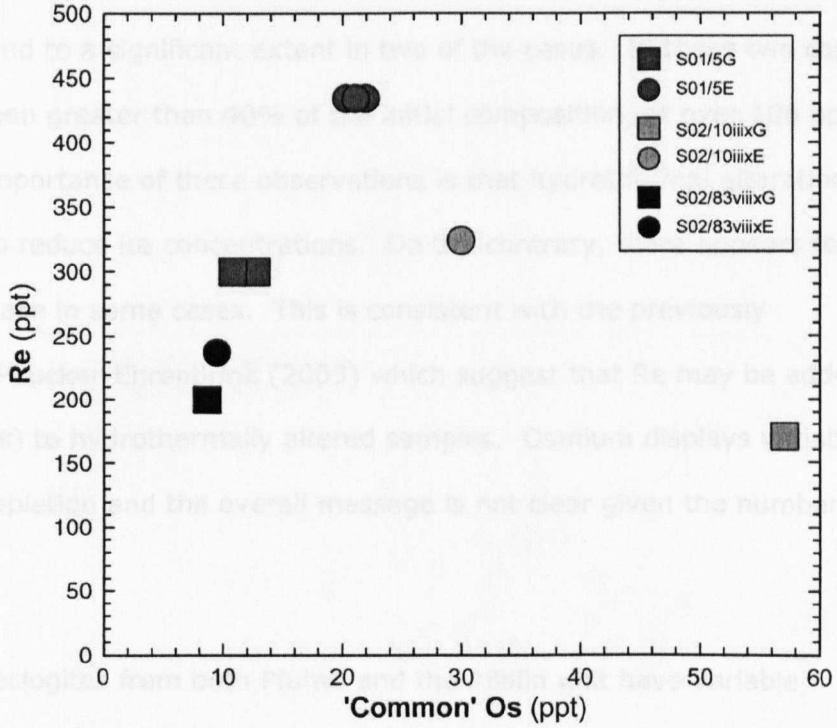

Figure 6.3. Os abundance (after subtraction of ingrown ^{187}Os) plotted against Re abundance for hand-specimen sized samples which consist of both unaltered gabbro (labelled G) and a transitional eclogite lithology (labelled E).

The nature of the Allalin Gabbro is such that some single hand-specimen size samples preserve the transition from unaltered gabbro to a lithology which has been affected by hydrothermal alteration and a degree of high-pressure crystallisation (known in this study as transitional samples). The advantage of studying samples like these is that the protolith composition can be measured directly and therefore differences in composition between the two portions can be assigned to events which are post-magmatic. Data from three such samples are presented in Figure 6.3.

While there is the possibility of some of the variation being dependent on slight sample powder inhomogeneity, the duplicates indicate that this is probably not a major concern. Assuming that the analyses are representative, two of the three transitional samples display increased $^{187}Re/^{188}Os$ ratios compared to their protoliths. Osmium concentrations increase (S01/5), decrease (S02/10iiix) or remain largely the same (S02/83viiix) during the post-magmatic history of the three samples. In comparison, Re abundances increase in all the hydrothermally altered sections, and to a significant extent in two of the cases. In these two cases Re addition has been greater than 40% of the initial composition, or over 100 ppt in real terms. The importance of these observations is that hydrothermal alteration does not appear to reduce Re concentrations. On the contrary, there appears to be a substantial increase in some cases. This is consistent with the previously published data of Peucker-Ehrenbrink (2003) which suggest that Re may be added (in small quantities) to hydrothermally altered samples. Osmium displays variable enrichment and depletion and the overall message is not clear given the number of samples involved.

The metabasaltic eclogites from both Pfulwe and the Allalin unit have variable abundances of Re (93-1400 ppt) and Os (1-42 ppt) (Figure 6.2). The mean Re abundance is low in comparison with most submarine oceanic basalts (385 ppt compared to the average MORB value of ~950 ppt), while the mean osmium abundance is reasonably high (15 ppt compared to 8 ppt for MORB). (MORB values from Schiano et al. (1997).) The samples do not display any co-variation of Re and Os (Figure 6.2).

6.1.2 Rhenium and osmium systematics in gabbroic and basaltic lithologies

It has been previously noted that there is a positive correlation between Os and Ni abundances in many oceanic basalts (e.g. Burton et al. 2002). Figure 6.4 presents

Os and Ni data for ZSO samples. There is a broad scatter of points but there is a moderately well-defined positive correlation within the gabbroic lithologies (particularly the unaltered gabbros, but also many gabbroic eclogites, including the samples retrogressed at blueschist facies, and some of those retrogressed at greenschist-facies conditions). This correlation has commonly been attributed to the compatibility of both Os and Ni in olivine, and therefore the decrease of both elements during fractional crystallisation. However, Burton et al. (2002) concluded that Os is highly incompatible in olivine and as a result, olivine crystallisation alone cannot account for the co-variation of Ni and Os. These authors suggested that olivine crystallisation leads to sulphur saturation of the melt and results in the co-precipitation of olivine (which controls the Ni content) and a sulphide phase, into

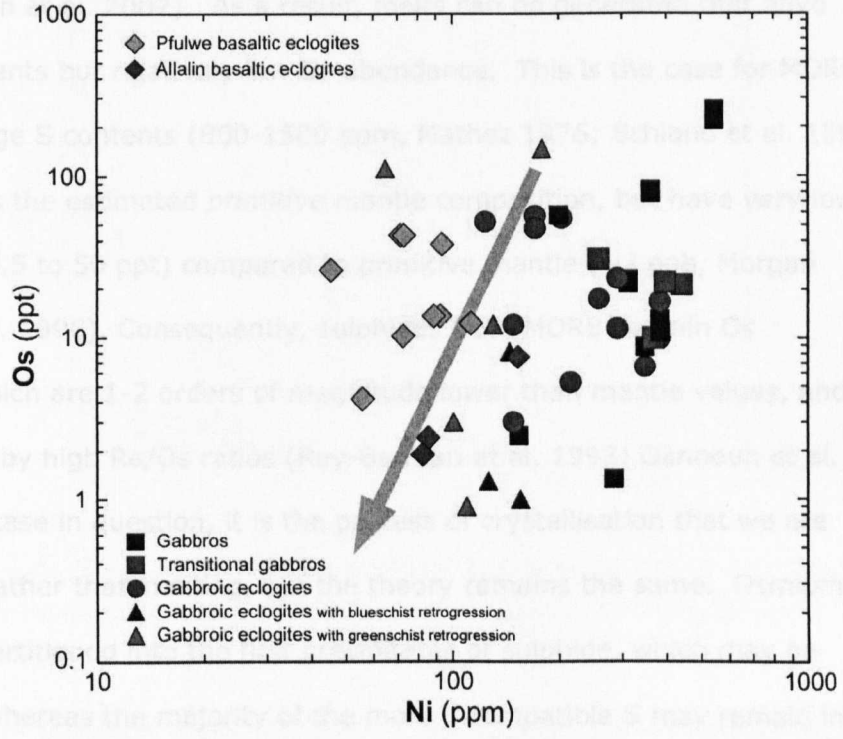

Figure 6.4. Osmium (ppt) plotted against nickel (ppm) for ZSO samples. The gabbroic lithologies display a positive trend, although there is deviation from this trend, particularly in the gabbroic eclogites and retrogressed samples. The grey arrow corresponds to a 'best-fit' line for MORB data (Schiano et al. (1997) and A. Gannoun - unpubl.), orientated with the arrow towards more differentiated samples. The positive correlation between these two elements has often been assigned to the compatibility of Os and Ni in olivine. However, Burton et al. (2002) found Os to be extremely incompatible in olivine and instead envisaged the co-precipitation of olivine and a sulphide phase, the latter controlling the Os abundance, and the olivine, the nickel abundance.

which Os is strongly partitioned. Surprisingly, unlike many oceanic basalts, the ZSO metabasalts do not define a positive correlation between Os and Ni, although they define a narrow range of Ni contents.

Sulphur

As Re and Os are highly chalcophile elements, a correlation between sulphur content and Re and Os abundances may be expected. Figure 6.5 displays Re and Os plotted against sulphur. A good positive correlation is observed between Re and S in all samples, although particularly for the gabbroic lithologies. There is no correlation between Os and S content. The lack of a correlation with Os is dependent on the compatibility of Os. When sulphide melts within the mantle, Os is disproportionately retained in the residual sulphide (Hart and Ravizza 1996; Alard et al. 2000; Burton et al. 2002). As a result, melts can be generated that have high sulphur contents but relatively low Os abundance. This is the case for MORB which have average S contents (800-1500 ppm, Mathez 1976; Schiano et al. 1997) that are 2-3 times the estimated *primitive* mantle composition, but have very low Os abundances (0.5 to 50 ppt) compared to primitive mantle (~3 ppb, Morgan 1986; Meisel et al. 1996). Consequently, sulphides from MORB contain Os concentrations which are 1-2 orders of magnitude lower than mantle values, and are characterised by high Re/Os ratios (Roy-Barman et al. 1998; Gannoun et al. 2004b). For the case in question, it is the process of crystallisation that we are concerned with, rather than melting, but the theory remains the same. Osmium will be strongly partitioned into the first precipitates of sulphide, which may be relatively small, whereas the majority of the more incompatible S may remain in the melt, resulting in a sulphur-rich and osmium-poor magma. The co-variation of Re and S may be consistent with sulphide crystallisation (or the co-precipitation of another phase) exerting the main control on Re concentration, or alternatively it may simply reflect the incompatibility of the two elements.

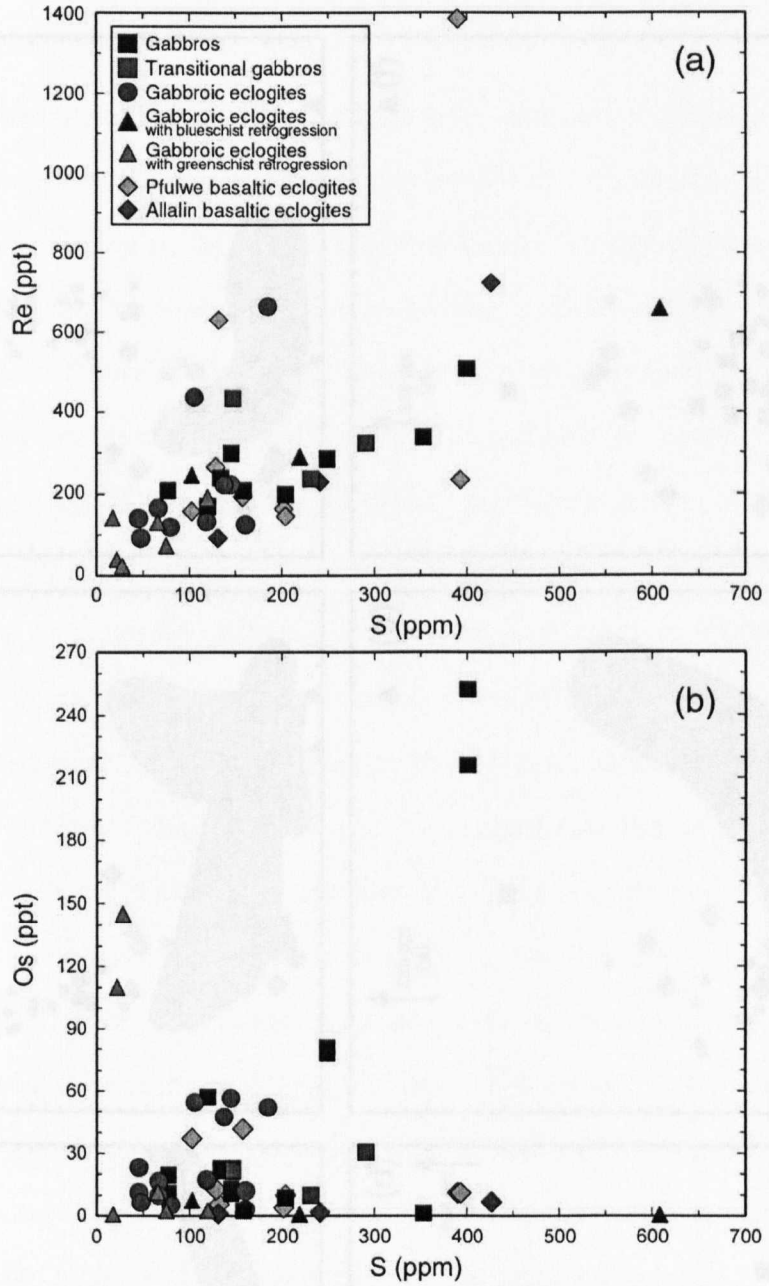

Figure 6.5. Rhenium and osmium abundances plotted against sulphur concentration. Note the good correlation between Re and S, but the lack of correlation between Os and S. Sulphur analysis by XRF (detection limit: ~50ppm).

The sulphur abundances in the ZSO metabasalts (100-450 ppm) are considerably lower than typical MORB values (800-1500 ppm, Mathez 1976; Schiano et al. 1997). Sulphur is known to be particularly prone to loss through volcanic degassing and is also very mobile during hydrothermal alteration (and possibly HP fluids). Thus, any of these three processes may account for the observed low S contents. Volatile loss through degassing will be discussed further, in terms of Re abundances, in Section 6.4.

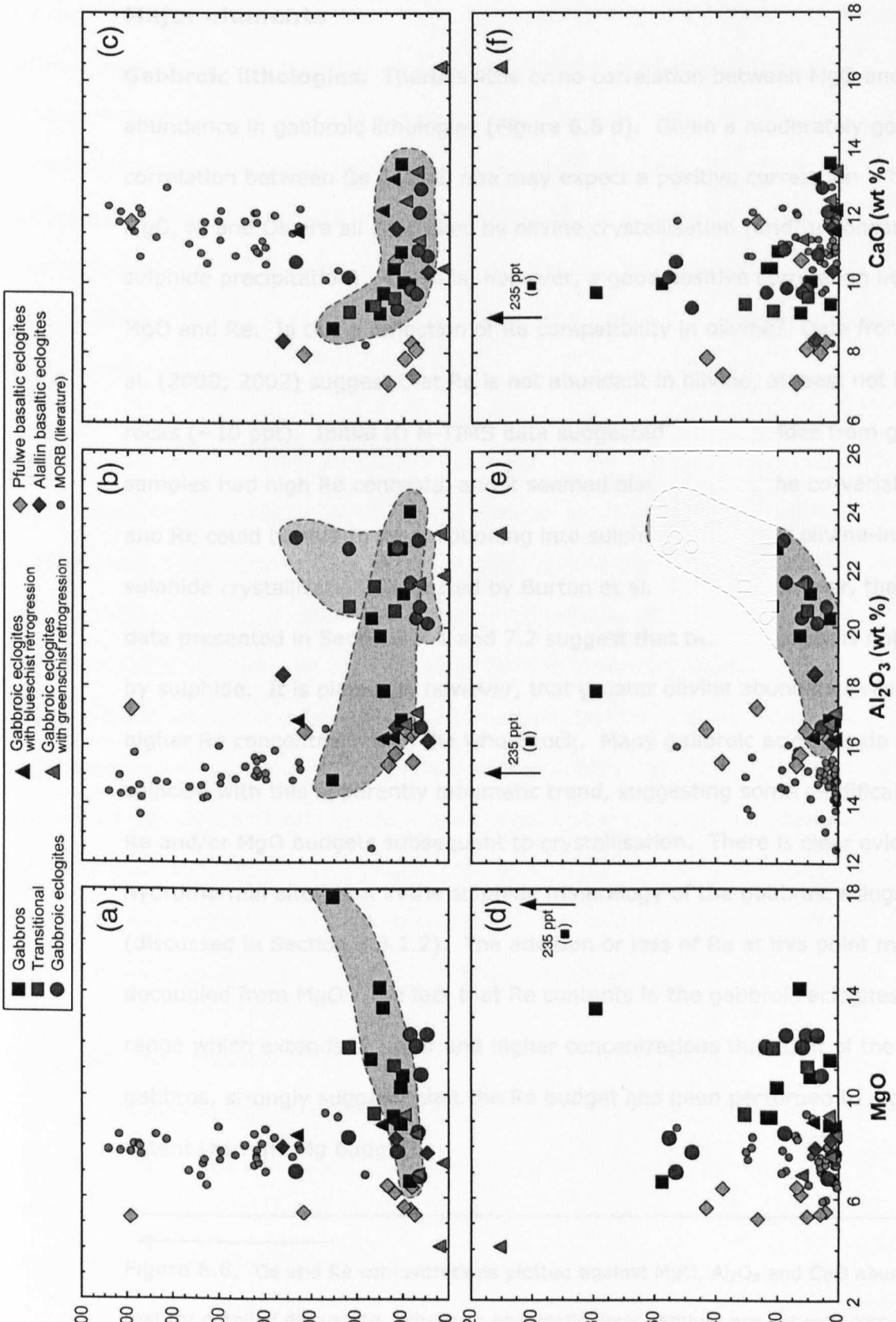
Gabbros
Transitional
Gabbroic eclogites
Gabbroic eclogites with blueschist retrogression
Gabbroic eclogites with greenschist retrogression
Pfulwe basaltic eclogites
Alallin basaltic eclogites
MORB (literature)
(a)
(b)
(c)
(d)
(e)
(f)
Re (ppt)
Os (ppt)
MgO
Al_2O_3 (wt %)
CaO (wt %)
235 ppt

Major elements

Gabbroic lithologies. There is little or no correlation between MgO and Os abundance in gabbroic lithologies (Figure 6.6 d). Given a moderately good correlation between Os and Ni, one may expect a positive correlation with MgO, if MgO, Ni and Os are all controlled by olivine crystallisation (and/or concomitant sulphide precipitation). There is, however, a good positive correlation between MgO and Re. Is this a reflection of Re compatibility in olivine? Data from Burton et al. (2000; 2002) suggest that Re is not abundant in olivine, at least not in mantle rocks (~10 ppt). Initial ID N-TIMS data suggested that sulphides from gabbroic samples had high Re contents, and it seemed plausible that the co-variation of MgO and Re could be due to Re partitioning into sulphide during the olivine-induced sulphide crystallisation suggested by Burton et al. (2002). However, the LA-ICP-MS data presented in Sections 7.1 and 7.2 suggest that the Re budget is not controlled by sulphide. It is plausible, however, that greater olivine abundance results in higher Re concentrations in the whole rock. Many gabbroic eclogites do not coincide with this apparently magmatic trend, suggesting some modification to the Re and/or MgO budgets subsequent to crystallisation. There is clear evidence of hydrothermal alteration in the sulphide mineralogy of the gabbroic eclogites (discussed in Section 3.3.1.2). The addition or loss of Re at this point may be decoupled from MgO. The fact that Re contents in the gabbroic eclogites span a range which extends to lower and higher concentrations than that of the unaltered gabbros, strongly suggests that the Re budget has been perturbed to a greater extent than the Mg budget.

Figure 6.6. Os and Re concentrations plotted against MgO, Al_2O_3 and CaO abundance. See text for detailed discussion. Rhenium and particularly osmium are not well correlated with any of the major elements, reflecting their incompatibility in silicate phases. Grey fields outline trends in unaltered gabbro data, red fields outline gabbroic eclogite trends. MORB data from Schiano et al. (1997) and A. Gannoun (unpublished data).

The most striking plot in Figure 6.6 is (b): Al_2O_3 against Re. The unaltered gabbros define a good negative correlation, as shown by the grey field. Conversely, the gabbroic eclogites do not conform to this trend and exhibit a large range in Re concentrations for their relatively narrow range of Al_2O_3 content. This again suggests that the budgets of Re in these samples are not entirely controlled by magmatic processes. The same observation may be true for CaO versus Re (Figure 6.6 c), although the samples with low Re abundance do not fall, so obviously, below the gabbroic field.

Both CaO and Al_2O_3 contents are largely controlled by the modal abundance of plagioclase in these cumulate samples (see Chapter 4). The fact that Os varies positively with Al_2O_3 content (Figure 6.6 e), but does not display any correlation with CaO (Figure 6.6 f), is rather surprising. Furthermore, given that a positive correlation between MgO and Os is expected (due to olivine crystallisation), a negative trend between Os and Al_2O_3 would be likely, as the gabbroic lithologies are dominated by bimodal variations in the contents of olivine and plagioclase. Yet, the reverse is true: Os abundance appears to increase with greater Al_2O_3 content, and therefore with decreasing olivine abundance. In many of the samples a major host of Ca is augitic pyroxene, which contains little Al. Variable amounts of augite in some samples may account for the decoupling of Os variations with Al_2O_3 and CaO.

The broad positive variation between Os and Al_2O_3 and the negative trend between Re and Al_2O_3 seem counterintuitive as both Re and Os will be most compatible in sulphide phases. The difference in the sense of correlation perhaps suggests that a different phase is controlling the abundance of either Os and Re. Possible candidates could be Al-chromite or ilmenite.

Although some trends can be picked out of the plots in Figure 6.6, it is worth noting that there are usually exceptions. In particular, there are two gabbros that have high Os abundances (~80 and 250 ppt) which do not form part of the trends in the

Os plots (in fact in the plot (e) they are contradictory to the trend), but interestingly they lie within the well defined trends for Re concentrations (a, b and c).

Basaltic eclogites. Trends within the basaltic eclogites samples are difficult to recognise due to the lack of differentiation within the suite. Four or five of the Pfulwe samples form a tight cluster on all plots in Figure 6.6. As a result, there is no clear correlation evident in any of the plots. One point to note, however, is that Os and Re abundances vary dramatically from sample to sample despite little or no difference in major element composition. This observation is a reflection of the siderophile/chalcophile nature of Re and Os and their incompatibility in silicate phases, which contain the majority of the major element budgets. A further complication of the analysis of these data is that far from being primary igneous compositions, the metabasalts may have been affected by elemental mobility in fluids lost during HP metamorphism, volcanic degassing, and/or hydrothermal alteration (either high temperature or low temperature).

There may be a positive correlation between Al_2O_3 and Re, although the number of points, and their similar compositions, are insufficient to confirm this. The same may be true for MgO against Re, although the samples defining the trend are extremely closely clustered, making any conclusion impossible.

Overall, it appears that in some cases unaltered gabbro samples define well-constrained correlations between Re, Os and other major and trace elements. In comparison, gabbroic eclogites often deviate from these trends and plot over a broader range of compositions. The first inference to be taken from this is that the eclogitic samples have undergone modification subsequent to the processes of crystallisation. Whether these modifications took place during seafloor alteration (which is evident from oxygen isotopes and sulphide mineralogy – see Section 3.3.1.2), or high-pressure metamorphism is not clear. Furthermore, apparent

variability on some of the plots is not necessarily reflected in actual mean compositions (e.g. for Re and Os abundances - Figure 6.2 and surrounding text) suggesting that any modification has been minor and localised. The behaviour of Re and Os through seafloor alteration and HP metamorphism will be discussed further in the following section.

Summary. In summary, the salient points from the Re and Os abundance data can be summarised as follows:

(i) Gabbros possess lower Re/Os ratios than co-genetic basalts due to the greater compatibility of Os, over Re. This must be accounted for when modelling mixing of recycled material into the mantle.

(ii) Basaltic samples from both the ZSO and SO have surprisingly low Re contents for submarine erupted basalts.

(iii) The rhenium budgets of gabbroic eclogites appear to have been slightly modified, but with no clear loss or gain, except in transitional eclogite samples where Re enrichment during hydrothermal alteration is observed.

(iv) Os and Ni are positively correlated in gabbroic samples, while the message from basaltic samples is unclear due to a narrow range of Ni content.

(v) Rhenium is positively correlated with sulphur in both gabbroic and basaltic lithologies. Osmium is not.

(vi) Osmium is poorly or not correlated with MgO, Al_2O_3 or CaO.

(vii) In gabbroic samples Re is moderately well correlated with MgO, Al_2O_3 and CaO. The positive co-variation of Re and MgO is suggestive of Re content being controlled by the co-precipitation of sulphide and olivine (or perhaps just olivine).

(viii) The range of basaltic compositions is narrow and does not facilitate the recognition of trends.

6.2 The message from Re-Os isotope systematics in the ZSO

Figure 6.7 illustrates the radiogenic osmium compositions attained in ZSO and SO samples, over 164 Ma and 437 Ma respectively. The more elevated $^{187}Os/^{188}Os$ ratios of the SO are a function of their greater age. It is clear from this plot that $^{187}Os/^{188}Os$ ratios are inversely proportional to the osmium abundance, for a given age. In samples with lower osmium abundances, $^{187}Re/^{188}Os$ ratios tend to be higher, and consequently more radiogenic osmium signatures develop over time. The SO and ZSO metabasalts form steeper, more radiogenic trends than their gabbroic counterparts, due to their higher $^{187}Re/^{188}Os$ ratios compared to gabbros.

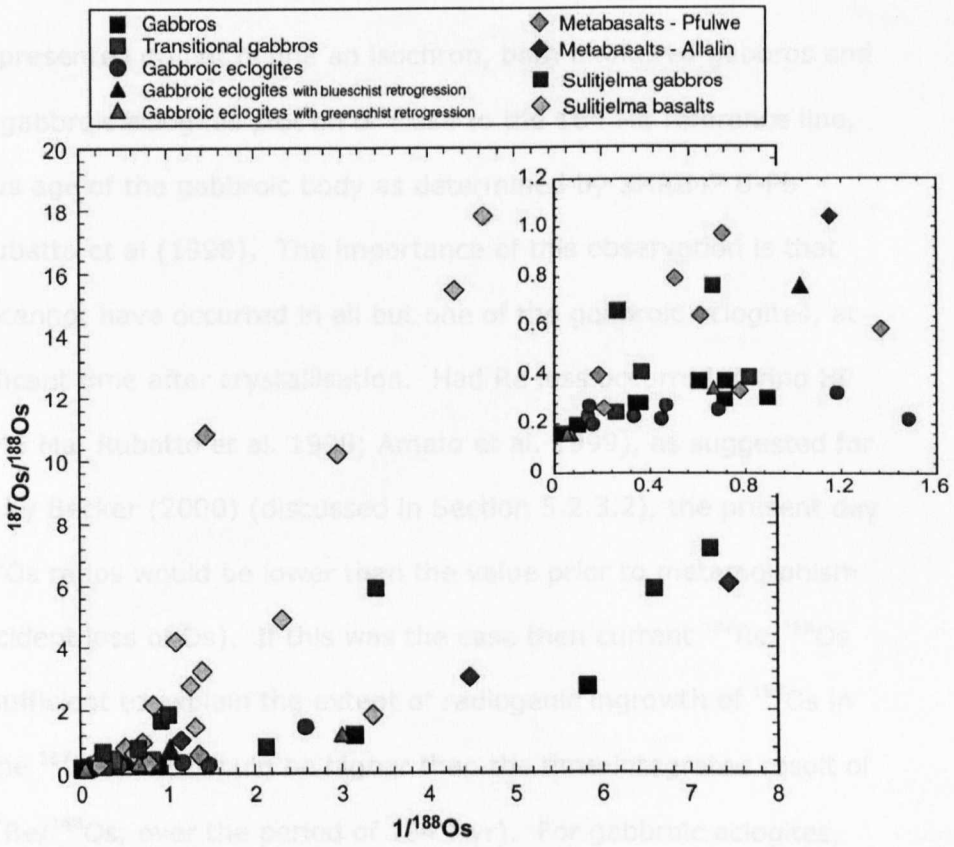

Figure 6.7. Os isotopic composition plotted against $1/^{188}Os$. Osmium-188 is used to discount the increase in Os abundance due to radiogenic ingrowth. The trend is a function of $^{187}Re/^{188}Os$ ratios and age, thus, those samples with low osmium abundances tend to have higher Re/Os ratios and evolve to more radiogenic compositions. Most of the samples in the steep trend are from the much older (~437 Ma - Pedersen et al. 1991) Sulitjelma ophiolite. The inset illustrates the difference in radiogenic osmium generated in metabasalts (generally higher) compared to gabbroic lithologies in the ZSO.

6.2.1 Gabbros and gabbroic eclogites

Although a comparison of Re abundances perhaps suggests the limited loss or redistribution of Re in the gabbroic eclogites, this is by no means a clear message. The abundances of Re, and particularly Os, are very heterogeneous and dependent on individual sample composition and thus may be strongly influenced by sampling bias. A robust means of testing the open or closed system behaviour of Re and Os is through the analysis of ^{187}Re-^{187}Os isotope variations. Figure 6.8 presents a Re-Os isochron diagram ($^{187}Re/^{188}Os$ against $^{187}Os/^{188}Os$) for gabbros (with little alteration) and gabbroic eclogites from within the Allalin Gabbro unit of the ZSO.

Although the data presented do not define an isochron, both unaltered gabbros and fully recrystallised gabbroic eclogites plot on or close to the 164 Ma reference line, which is the igneous age of the gabbroic body as determined by SHRIMP U-Pb zircon dating by Rubatto et al (1998). The importance of this observation is that significant Re loss cannot have occurred in all but one of the gabbroic eclogites, at least not any significant time after crystallisation. Had Re loss occurred during HP metamorphism (~45 Ma, Rubatto et al. 1998; Amato et al. 1999), as suggested for basaltic lithologies by Becker (2000) (discussed in Section 5.2.3.2), the present day measured $^{187}Re/^{188}Os$ ratios would be lower than the value prior to metamorphism (assuming no coincident loss of Os). If this was the case then current $^{187}Re/^{188}Os$ ratios would be insufficient to explain the extent of radiogenic ingrowth of ^{187}Os in the samples (i.e. the $^{187}Os/^{188}Os$ would be higher than the time-integrated result of the present day $^{187}Re/^{188}Os$, over the period of 164 Myr). For gabbroic eclogites, present day $^{187}Re/^{188}Os$ ratios *are* a close approximation to those required to account for the Os isotopic composition observed after 164 Myr.

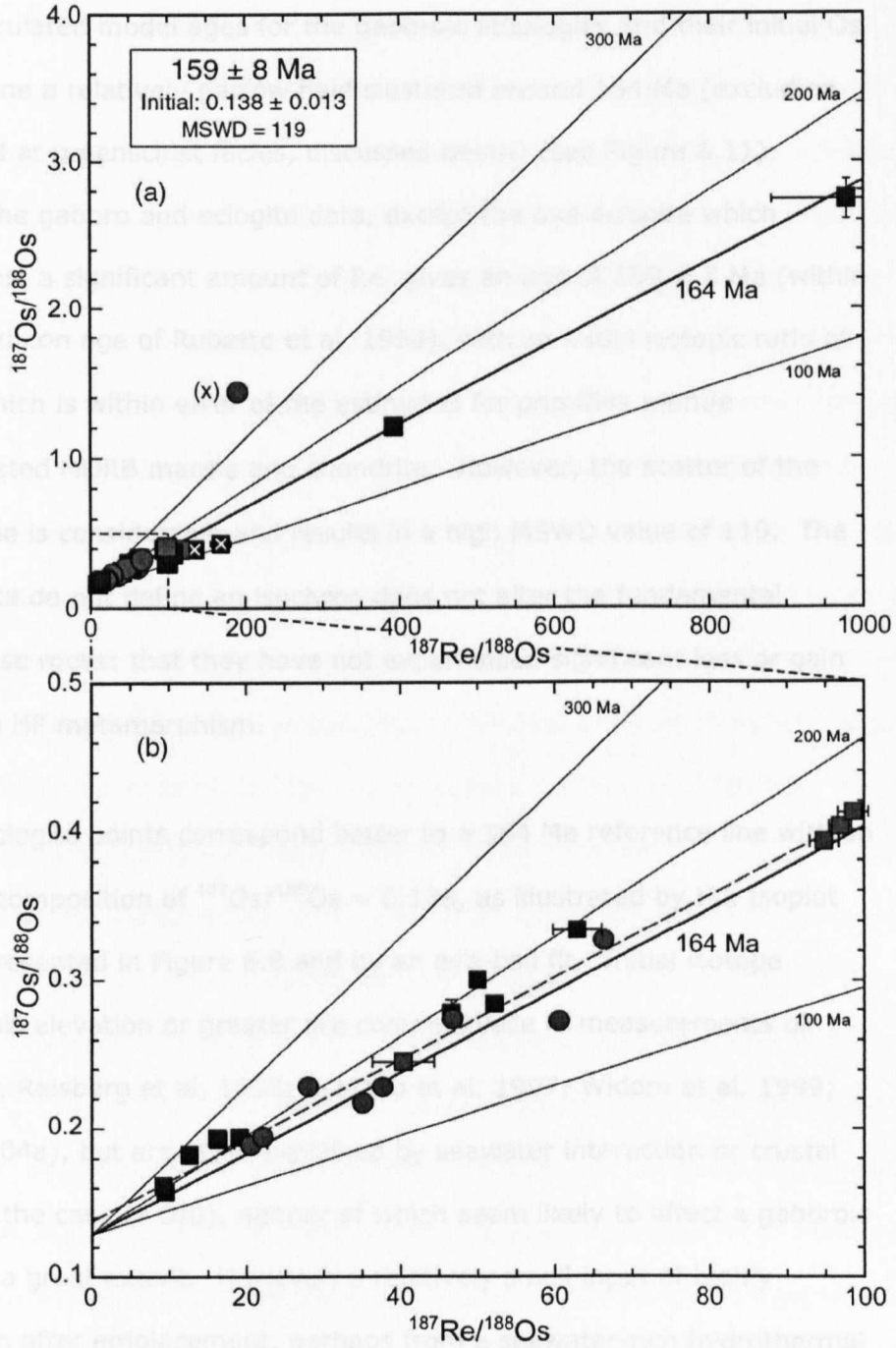

Figure 6.8. Re-Os isochron diagrams for gabbros (navy squares), transitional samples (red squares) and gabbroic eclogites (red circles) from the ZSO. Reference lines corresponding to ages of 164 Ma (thick black line) (age of Allalin body from Rubatto et al. 1998), and 100, 200 and 300 Ma are plotted in (a) and (b). These have an initial Os isotopic composition equal to age corrected PUM ($^{187}Os/^{188}Os$ = 0.128, Meisel et al. 1996), which is a likely initial composition. The Isoplot calculated age of all gabbros and almost all gabbroic eclogites (excluding point 'X') is shown in (a) (159 ± 8 Ma). The result, while not an isochron (MSWD = 119), indicates that significant Re or Os loss or gain has not occurred in any samples except one gabbroic eclogite (X). The initial Os composition (0.138 ± 0.013) of the Isoplot errorchron is just within error of the PUM value for 164 Ma. However, a 164 Ma reference line with an initial isotopic composition of 0.138 is shown in (b) (blue dashed line) and appears to fit the data considerably better than the reference line with a PUM initial composition – this value is not unreasonable given the average modern day MORB isotopic composition (0.133, Gannoun et al. 2004a).

Consequently, calculated model ages for the gabbroic lithologies and their initial Os isotopic ratios define a relatively narrow field clustered around 164 Ma (excluding those retrogressed at greenschist facies, discussed below) (see Figure 6.11). Regression of all the gabbro and eclogite data, except the one eclogite which appears to have lost a significant amount of Re, gives an age of 159 ± 8 Ma (within error of the U-Pb zircon age of Rubatto et al. 1998), with an initial isotopic ratio of 0.138 ± 0.013, which is within error of the estimates for primitive mantle composition, depleted MORB mantle and chondrite. However, the scatter of the points from the line is considerable and results in a high MSWD value of 119. The fact that these data do not define an isochron does not alter the fundamental message from these rocks: that they have not experienced significant loss or gain of Re or Os during HP metamorphism.

The gabbro and eclogite points correspond better to a 164 Ma reference line with an initial Os isotopic composition of $^{187}Os/^{188}Os = 0.138$, as illustrated by the Isoplot calculation data presented in Figure 6.8 and by an eye-ball fit. Initial isotope compositions of this elevation or greater are commonplace in measurements of MORB or OIB (e.g. Reisberg et al. 1993; Schiano et al. 1997; Widom et al. 1999; Gannoun et al. 2004a), but are often explained by seawater interaction or crustal contamination (in the case of OIB), neither of which seem likely to affect a gabbroic cumulate body to a great extent. However, a relatively small input of highly radiogenic Os soon after emplacement, perhaps from a seawater-rich hydrothermal fluid (seawater $^{187}Os/^{188}Os \sim 1$, Sharma et al. 1997; Levasseur et al. 1998) may lead to a significant elevation in the initial $^{187}Os/^{188}Os$ composition of the gabbro. Another seemingly unlikely possibility to explain the positioning of most of the points slightly above the isochron is that most samples could have lost a small percentage of their Re budget during high-pressure (HP) metamorphism. While it is likely, from their deviation from the reference line, that some perturbation of the Re-Os system has occurred, relatively small and uniform percentage losses are not

consistent with the variable loss of elements observed in seafloor and HP metamorphic settings. In addition, the data for unaltered gabbros display greater deviation from the reference line than the transformed eclogite data, which is a strong argument against even a small degree of Re loss from this suite of samples. The deviation of points from the reference line may also be a result of the difficulty in ensuring that the dissolved rock powder was a true representation of the whole rock composition. The use of large Teflon bombs with 2g of sample (rather than 0.4g dissolved in small Teflon bombs) did not facilitate the acquisition of isochronous data points, suggesting that the observed scatter is of geological, rather than analytical origin. Furthermore, Carius tubes were used for duplicate dissolutions of two samples in order to ensure complete yield of Re and Os from acid-resistant phases such as chromite. The data are plotted as navy squares containing a white cross in Figure 6.8, and are included in Table 6.1. Although the Carius tube data plot with slightly higher $^{187}Re/^{188}Os$ and $^{187}Os/^{188}Os$ ratios than their duplicate Teflon dissolutions, these two values are self-consistent and result in the same model age for the sample. The small differences in $^{187}Re/^{188}Os$ and $^{187}Os/^{188}Os$ are likely to be due to a lack of complete homogeneity in the rock powder. The comparable results of Teflon dissolution and the Carius tube technique indicate that incomplete dissolution was probably not the reason for several samples plotting slightly below the reference line. The position of several points at slightly younger ages on the isochron diagram (Figure 6.8) could be explained by small levels of Os loss, but given that none of these samples are completely recrystallised eclogites, this seems unlikely.

While Becker (2000) recognised the implications of Re loss from the basaltic layer of the slab, for the sources of oceanic basalts, he did not take into account the gabbroic lithologies, perhaps because little data exists for this dominant portion of the oceanic crust. The data presented here indicate that, in this case at least, Re is not lost in significant amounts from gabbroic lithologies during HP metamorphism

beyond 2.0 GPa. As a result, oceanic crustal material with $^{187}Re/^{188}Os$ ratios that are comparable to those possessed prior to subduction may be recycled into the deep mantle.

Other metagabbros

The message from other gabbroic eclogites, which have undergone recrystallisation at retrograde P-T conditions, is somewhat different. However, in the case of retrogressed samples, it cannot easily be concluded whether the isotopic information obtained is the result of changes during prograde and peak metamorphism, or during retrogression. Crucially, the effects of retrogression would not impart an effect on the composition of subducted material which is subsequently recycled into the mantle. Consequently, the data from retrogressed gabbroic eclogites must be treated with caution.

Isotope data for samples with either pervasive blueschist or greenschist facies retrogression are presented in Figure 6.9. None of the samples plot directly on the 164 Ma reference line. However, three of the blueschist samples lie within a 50 million year age range of the reference line. The sample with the lowest $^{187}Re/^{188}Os$ ratio actually lies furthest from the line in terms of age (model age of 259 Ma, Table 6.1). The two points which lie below the line are from different dissolutions of the same sample powder, illustrating the extreme heterogeneity of Re and Os distribution. Nonetheless, the model ages are remarkably similar (113 and 117 Ma, Table 6.1), suggesting that both measurements are valid, despite sample inhomogeneity. However, regardless of the coincident ages of the two measurements, analyses using small sample masses and involving low osmium concentrations and abundant Re, may suffer from the so-called 'nugget effect' whereby the extremely heterogeneous distribution of the two elements leads to sample powders that are not fully representative of the whole rock. Nonetheless, it is likely that this sample has experienced a small degree of either Re gain or Os

loss. Overall, blueschist retrogressed gabbroic eclogites do not appear to have lost a substantial proportion of their Re. Of the three samples, it is the one that has undergone least deformation that appears to have experienced Re loss (possibly up to 40%, calculated from the isochron diagram, assuming no Os mobility).

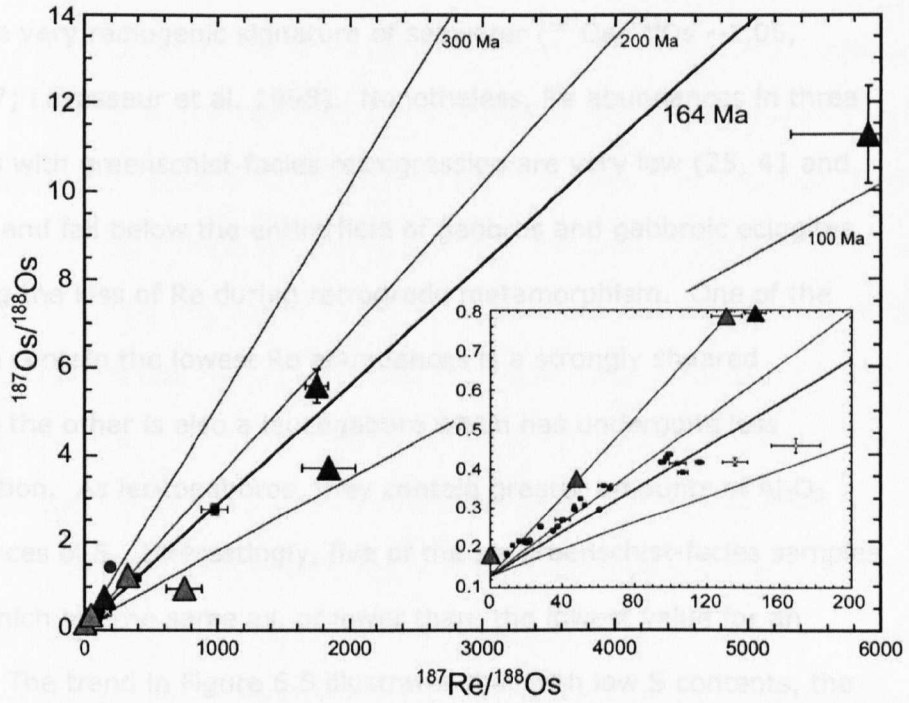

Figure 6.9. Re-Os isochron diagram for gabbroic eclogites with either pervasive blueschist (blue triangles) or greenschist (green triangles) retrogression. Neither group plot precisely on the 164 Ma reference line, however, the extreme $^{187}Re/^{188}Os$ ratios and very low Os abundances in the blueschist samples makes their analysis difficult. Moreover, the heterogeneous distribution of Os and Re in samples can lead to inaccuracies due to the so-called 'nugget effect'. This is illustrated by the fact that both blueschist data points with the highest $^{187}Re/^{188}Os$ were obtained from different dissolutions of the same sample powder. In the case of the greenschist samples, the Re-Os systematics seem to be affected to a greater extent, and in all but one case, the $^{187}Re/^{188}Os$ ratio is insufficient to explain their radiogenic Os signatures for the given age of 164 Ma. This suggests that either Re loss, or Os gain, has occurred in these samples. The data from gabbros and gabbros eclogites from Figure 6.8 is plotted as small symbols, for comparison.

In contrast, the Re-Os systematics for greenschist samples have been significantly altered during the metamorphic process. Three of the five samples display older model ages (i.e. they have $^{187}Re/^{188}Os$ ratios which are insufficient to explain their Os isotopic composition, over 164 million years). However, the two extremely old model ages (1181 and 3909 Ma, Table 6.1) are strongly dependent on the initial

isotopic composition of the gabbro, due to their extremely low $^{187}Re/^{188}Os$ ratios. Thus, with an initial composition of $^{187}Os/^{188}Os$ = 0.150, the model ages of these samples becomes comparable to the 164 Ma reference line. Elevation of the initial isotope composition to this value is unlikely, although localised elevations may occur due to a greater extent of interaction with fluids whose isotopic composition is influenced by the very radiogenic signature of seawater ($^{187}Os/^{188}Os$ ~1.06, Sharma et al. 1997; Levasseur et al. 1998). Nonetheless, Re abundances in three of the five samples with greenschist-facies retrogression are very low (25, 41 and 75 ppt, Table 6.1) and fall below the entire field of gabbros and gabbroic eclogites, strongly suggesting the loss of Re during retrograde metamorphism. One of the two samples which contain the lowest Re abundances is a strongly sheared leucogabbro, while the other is also a leucogabbro which has undergone less extensive deformation. As leucogabbros, they contain greater amounts of Al_2O_3 and lower abundances of S. Interestingly, five of the six greenschist-facies samples have S contents which are the same as, or lower than, the lowest value for an unaltered gabbro. The trend in Figure 6.5 illustrates that with low S contents, the samples are likely to have low Re concentrations, and this is consistent with high aluminium contents (Figure 6.6) and a limited abundance of olivine, which may be accompanied by only a limited amount of sulphide precipitation. Nonetheless, the deviation of the samples from the reference line necessitates the perturbation of the Re-Os system subsequent to igneous crystallisation. However, whether the post-magmatic depletion in Re (and possibly S) is a result of prograde or retrograde metamorphism is unclear, although the absence of Re loss from the eclogitic samples suggests that Re loss occurred during retrograde metamorphism.

6.2.2 Metabasaltic eclogites

A study by Becker (2000) concluded that basaltic samples which have undergone HP metamorphism have lost a significant proportion of their Re, thus lowering $^{187}Re/^{188}Os$ in subducted oceanic crust and limiting the radiogenic Os signatures

attained by old recycled crustal material in the mantle. The message from the gabbroic section of the crust, outlined above, is that Re loss may not be a significant process during HP metamorphism. In addition to the investigation of gabbroic lithologies, this study has also analysed a suite of basaltic eclogites from the ZSO, the results of which are presented in Figure 6.10 and Table 6.2.

None of the metabasaltic samples plot within error of the 164 Ma reference line (Figure 6.10). With the exception of two samples, one from Pfulwe and one from the Allalin, all the basalts have lower $^{187}Re/^{188}Os$ ratios than required to account for the radiogenic Os isotope signatures that they possess. This observation is most easily explained by the loss of Re from these samples during HP metamorphism, although the addition of Os to the samples would have the same effect of decreasing $^{187}Re/^{188}Os$ ratios. The evidence outlined below in Section 6.4 strongly suggests that Re has been lost from metabasalts at some point since their formation. The deviation of samples from the reference line precludes a model where the only loss of Re occurs during degassing (this would result in the evolution of lower $^{187}Os/^{188}Os$ ratios, but the samples should still possess the correct model age). If Os were added during metamorphism, then it may have an effect not only on the $^{187}Re/^{188}Os$ ratio, but also on the Os isotopic composition. If relatively Os-rich fluids were derived from the lithospheric mantle, their unradiogenic Os composition would have the effect of reducing $^{187}Os/^{188}Os$ as well as reducing $^{187}Re/^{188}Os$. The net result may be the movement of the point along a line close to the reference line, rather than away from it, although the exact movement of a sample on an isochron diagram would depend on the Os abundance and isotopic composition of the sample and of the infiltrating fluid. Addition of a fluid containing Os derived from within the mafic oceanic crust may not have the effect of decreasing the Os isotopic composition of the sample and may even result in an increase in $^{187}Os/^{188}Os$, as well as a decrease in $^{187}Re/^{188}Os$. However, it is unlikely that a fluid derived from the Os-poor oceanic crust would have an

abundance of Os high enough to strongly affect either the Os concentration of the sample or its isotopic composition.

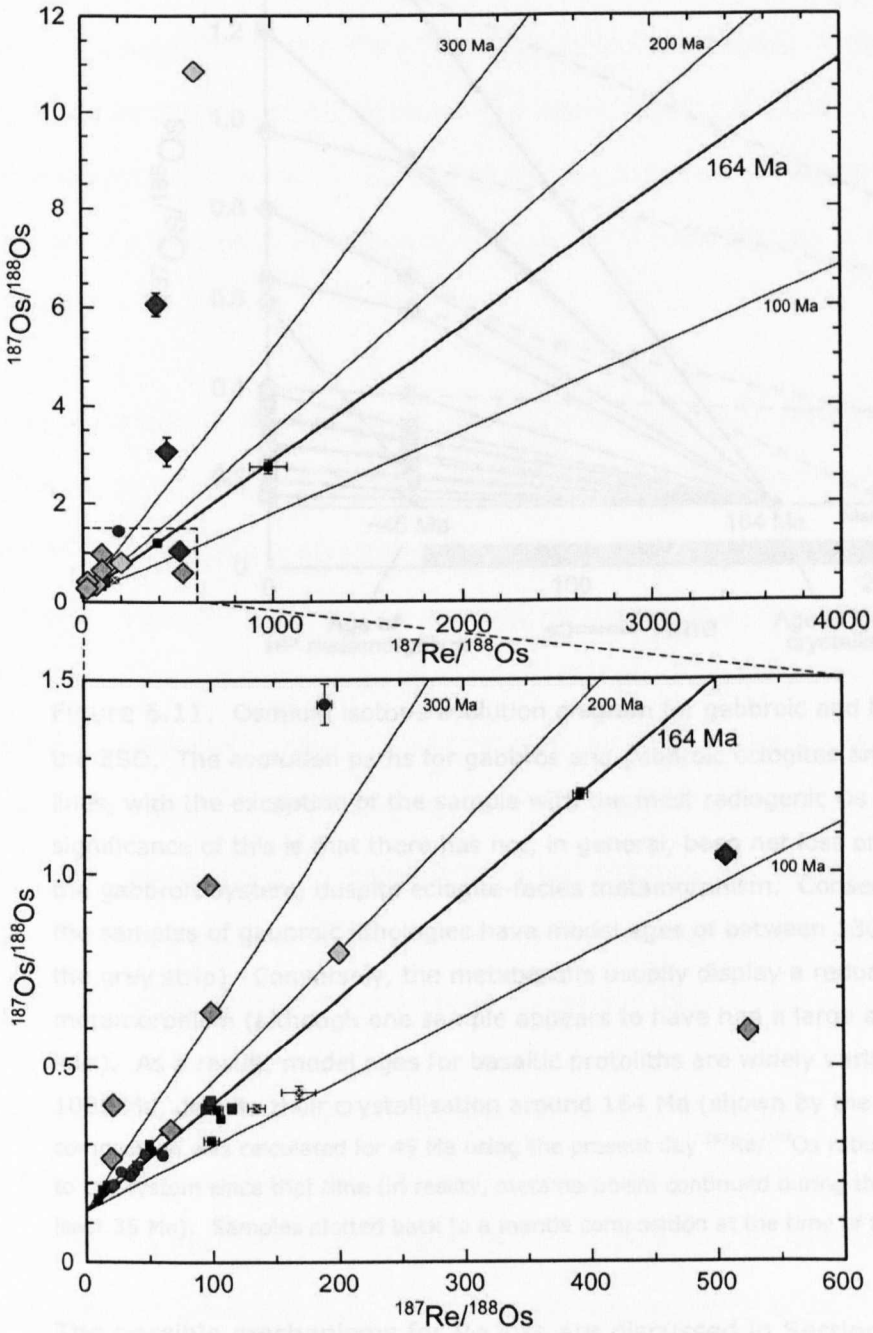

Figure 6.10. Re-Os isochron diagrams for basaltic eclogites, Zermatt-Saas ophiolite. Lightest green: undifferentiated metabasalts from Pfulwe, mid-green: metapillows from Pfulwe, dark green: metabasalts from the Allalin unit. The gabbro and gabbroic eclogite data (from Figure 6.9) are shown as small navy squares, red circles and red squares. The metabasalts do not plot close to the 164 Ma reference line, illustrating that their Re or Os (or both) budgets have been perturbed. In particular, most samples plot with more radiogenic Os signatures than can be explained through radiogenic ingrowth over 164 million years, given their current, measured $^{187}Re/^{188}Os$ ratios (i.e. they plot to the upper left of the 164 Ma reference line). Assuming the age is correct, this can be explained by Re loss or Os gain subsequent to crystallisation.

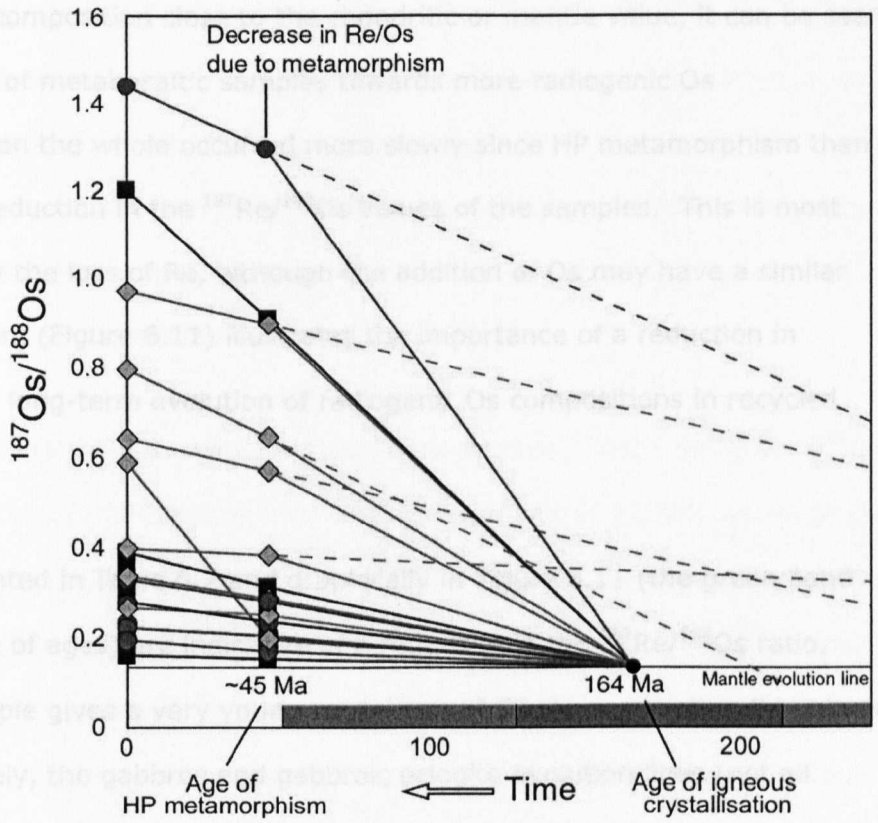

Figure 6.11. Osmium isotope evolution diagram for gabbroic and basaltic lithologies from the ZSO. The evolution paths for gabbros and gabbroic eclogites are approximately straight lines, with the exception of the sample with the most radiogenic Os signature. The significance of this is that there has not, in general, been net loss or gain of Re or Os within the gabbroic system, despite eclogite-facies metamorphism. Consequently, all but two of the samples of gabbroic lithologies have model ages of between 130 and 210 Ma (shown by the grey strip). Conversely, the metabasalts usually display a reduction in Re/Os ratio after metamorphism (although one sample appears to have had a large addition of Re (or Os loss). As a result, model ages for basaltic protoliths are widely variable, from 40 Ma to over 1000 Ma, despite their crystallisation around 164 Ma (shown by the green strip). Os isotopic composition was calculated for 45 Ma using the present day $^{187}Re/^{188}Os$ ratios, assuming no disturbance to the system since that time (in reality, metamorphism continued during the exhumation path to at least 35 Ma). Samples plotted back to a mantle composition at the time of their crystallisation, 164 Ma.

The possible mechanisms for Re loss are discussed in Section 6.4, together with estimates of the magnitude of Re loss taken from different sources.

An alternative way to present the isotope evolution of samples from the ZSO is shown in Figure 6.11. The present day $^{187}Re/^{188}Os$ and $^{187}Os/^{188}Os$ ratios for each sample were used to calculate the Os isotopic composition at 45 Ma. By inferring

an initial isotopic composition close to the chondritic or mantle value, it can be seen that the evolution of metabasaltic samples towards more radiogenic Os compositions has on the whole occurred more slowly since HP metamorphism than before, due to a reduction in the $^{187}Re/^{188}Os$ values of the samples. This is most likely explained by the loss of Re, although the addition of Os may have a similar effect. The diagram (Figure 6.11) illustrates the importance of a reduction in $^{187}Re/^{188}Os$ on the long-term evolution of radiogenic Os compositions in recycled oceanic basalts.

Model ages presented in Table 6.2 and graphically in Figure 6.11 (the green band denotes the range of ages) are indicative of a reduction in the $^{187}Re/^{188}Os$ ratio, although one sample gives a very young model age of 52 Ma, suggesting Re gain or Os loss. Conversely, the gabbros and gabbroic eclogite evolution lines (not all shown for the sake of clarity) are approximately straight indicating that no significant net movement of Re or Os has occurred (except in the one gabbroic eclogite with the highest $^{187}Os/^{188}Os$). Either geological disturbance or analytical problems due to sample powder heterogeneity has resulted in a variety of model ages from 110 Ma to 220 Ma, but in comparison with the range of model ages for metabasalts (52 to 1065 Ma) this is a relatively narrow field.

It seems very likely that the internal structure of basaltic lithologies, particularly the pillow units, strongly influences the extent of deformation and fluid flow experienced during both seafloor hydrothermal alteration and HP metamorphism (this is discussed in Section 3.3.3). Furthermore, the proximity of the basaltic units to the seafloor (relative to the gabbroic bodies) affects the extent to which they are hydrated. These factors probably exert a controlling role on the loss, or otherwise, of Re from the down-going slab. Basaltic units will be more hydrated prior to subduction, and therefore more likely to experience extensive fluid flow and consequently greater Re loss. However, the eclogitic parts of the Allalin unit have

also undergone hydration during hydrothermal alteration, as illustrated by their hydrous mineralogy, their sulphide mineralogy (see Section 3.3.1.2) and lower average $\delta^{18}O$, compared to the gabbros (Barnicoat and Cartwright 1997). This makes the lack of Re loss perhaps more surprising and points to an important role for deformation, in facilitating the extraction of fluids from hydrous units. These issues will be expanded upon in Chapter 8.

An important point to note is that given parent (^{187}Re) – daughter (^{187}Os) ratios of approximately 8000 in typical MORB ($^{187}Re/^{188}Os$ = ~1000) (average calculated from Schiano et al. (1997) excluding very Os-poor samples), it would be expected that basaltic samples would evolve to $^{187}Os/^{188}Os$ ratios of approximately 2.5-3.0 in 164 million years, even allowing for 60% Re loss at 45 Ma. Only three of the samples possess radiogenic signatures which are higher than this value, and all others are considerably lower. It is possible, therefore, that Re loss occurred at some point prior to HP metamorphism, either during volcanic degassing (despite the samples being submarine), seafloor hydrothermal alteration, or at the onset of subduction. However, it cannot be conclusively proven from this evidence, that the loss of Re was not confined to the HP event, due to highly variable Re/Os ratios in MORB, and in the samples analysed. To investigate this issue further, a suite of metabasalts from the Sulitjelma ophiolite was analysed. These samples have experienced regional metamorphism at biotite to kyanite grades, and thus may indicate if Re loss from basaltic oceanic crust occurs at lower metamorphic grades than those seen in the Zermatt-Saas ophiolite.

6.3 Sulitjelma ophiolite

A suite of regionally metamorphosed basalts from the Sulitjelma ophiolite (SO) has been analysed in order to constrain the P-T conditions at which Re begins to be lost from basaltic lithologies. The metabasalts from the SO have been subjected to P-T conditions equivalent to the biotite to kyanite Barrovian metamorphic grades. In addition, a suite of metagabbros from the same ophiolite have been studied to investigate Re-Os systematics in a different gabbroic body.

6.3.1 Re and Os abundances and systematics in metabasalts and metagabbros

Whole rock Re and Os abundances and isotope data for samples from the Sulitjelma ophiolite are presented in Table 6.3. The Re/Os elemental ratios of the Sulitjelma samples are plotted against Os concentration in Figure 6.1. The samples plot with lower Re/Os ratios (or lower Os), compared to the MORB field, and have similarities with the field of ocean island basalts, although this type of basalt defines a very broad field (probably due to loss of Re during volcanic degassing). In general, Os abundances are lower in the Sulitjelma metabasalts (0.7–9.4 ppt, mean = 7) than in the ZSO basalts (mean = 15 ppt). The same is true of the Sulitjelma gabbros which have a range of Os from 1.1-29.4 ppt (mean = 9.5) compared to an average of approximately 25 ppt for the Allalin gabbroic lithologies. Rhenium concentrations are similar in the Otervann metabasalts of the SO (mean = 404 ppt) and the ZSO metabasalts (385 ppt). Rhenium abundances in gabbroic lithologies are somewhat lower in the SO (181 ppt mean) than in the Allalin gabbros (~250 ppt mean). Figure 6.12 compares the abundances of Re and Os in both metabasalts and metagabbros. In contrast to the Allalin gabbros (shown as small black squares, and in Figure 6.2), which define a positive correlation between Os and Re abundances, the analyses of the Sulitjelma Gabbro display a weak negative correlation between the two elements. The metabasaltic samples, as is the case with the ZSO, do not exhibit any correlation between Re and Os.

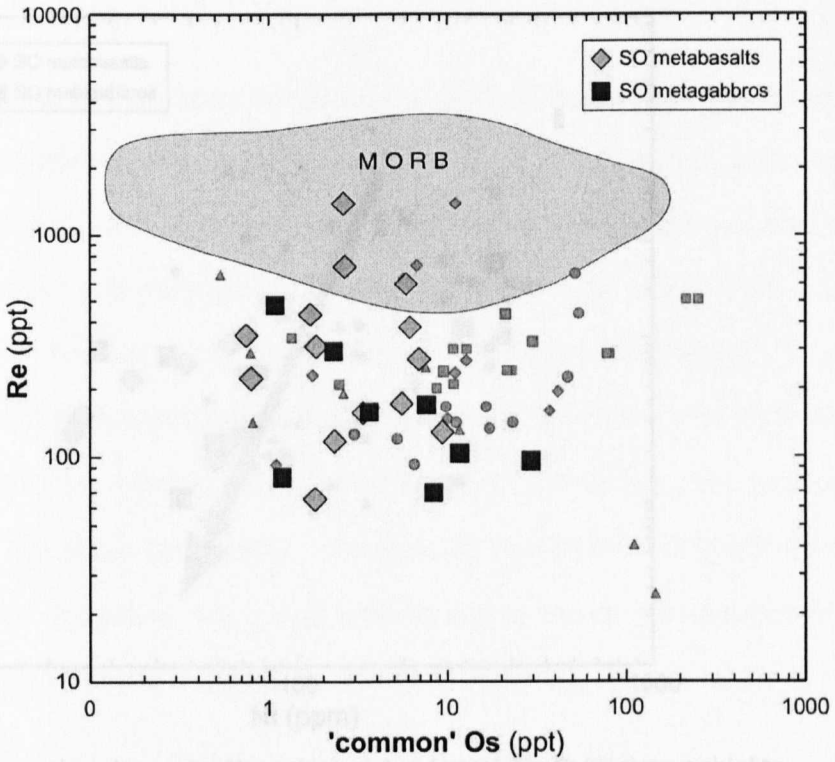

Figure 6.12. Os (ppt) against Re (ppt) for Sulitjelma ophiolite samples. Unlike the ZSO, there is a weak negative correlation between Re and Os abundances in the metagabbroic samples, while no correlation is evident in the metabasaltic samples. Small grey symbols: ZSO samples. MORB field after Schiano et al. (1997) and unpublished data from A. Gannoun.

	Mmorphic grade	Sample mass (g)	[Re] (ppt)	[Os] (ppt)	$^{187}Os/^{188}Os$	$^{187}Re/^{188}Os$	"Common" Os (ppt)	Blank contr.(%) Os	Re	Model age
Metabasalts										
Giles 1	Biotite	0.4751	157	5.45	4.885 ± 0.201	222 ± 11	3.37	2.1	1.9	1271
Giles 5	Biotite	0.4627	720	6.11	10.24 ± 0.07	1303 ± 65	2.65	1.9	0.4	464
Giles 7	Biotite	0.4896	172	7.78	3.228 ± 0.055	148 ± 7	5.55	1.5	1.7	1247
A77	Garnet	0.4907	597	6.89	1.654 ± 0.015	415 ± 24	5.88	1.7	0.5	164
A78	Garnet	0.4636	435	5.54	17.78 ± 0.29	1237 ± 62	1.70	2.1	0.7	851
A162	Kyanite	0.4895	118	2.84	1.840 ± 0.040	242 ± 5	2.32	4.0	2.5	424
B75	Garnet	0.4908	348	2.39	17.29 ± 0.76	2256 ± 135	0.74	4.7	0.9	455
B76	Garnet	0.4699	223	1.17	3.936 ± 0.148	1076 ± 108	0.79	9.1	1.3	165
B77	Garnet	0.4773	310	5.43	15.45 ± 0.21	818 ± 41	1.83	2.1	1.0	1114
B89	Garnet	0.4815	128	11.88	2.166 ± 0.044	65 ± 3	9.39	1.0	2.3	1856
B90	Garnet	0.4740	1392	17.23	44.69 ± 0.39	2627 ± 184	2.60	0.7	0.2	1010
D1	Biotite	0.4752	377	8.31	2.783 ± 0.220	292 ± 15	6.18	1.4	0.8	545
A163	Kyanite	0.4708	269	10.62	4.217 ± 0.155	186 ± 6	6.94	1.1	1.1	1309
Metagabbros										
B58	Kyanite	0.4203	82	2.07	5.855 ± 0.411	330 ± 20	1.19	6.3	4.6	1032
B84	Kyanite	0.4208	69	10.05	1.646 ± 0.010	39.4 ± 1.6	8.39	1.4	5.4	2272
B109	Kyanite	0.4198	169	9.36	1.841 ± 0.010	105 ± 2	7.66	1.5	2.4	972
B112	Ky/Gt	0.4363	480	2.06	7.815 ± 0.537	1510 ± 170	1.08	6.4	0.9	198
M3	Garnet	0.4128	158	3.97	0.829 ± 0.009	207 ± 21	3.63	3.4	2.5	203
T158	Garnet	0.4661	96	31.47	0.664 ± 0.002	15.5 ± 1.2	29.40	0.4	4.1	2046
V34	Garnet	0.4418	295	4.01	5.907 ± 0.220	614 ± 37	2.30	3.4	1.4	562
V39	Garnet	0.3200	103	12.70	0.763 ± 0.005	42.1 ± 1.3	11.73	1.1	3.6	902

Table 6.3. Rhenium and osmium abundance and isotopic data for analyses of Sulitjelma ophiolite metabasalts and metagabbros. Errors quoted (2 σ) have been propagated from the standard error, assuming 20% uncertainty in blank composition. Model ages have been calculated with a calculated chondritic initial composition for 437Ma, of $^{187}Os/^{188}Os = 0.1255$.

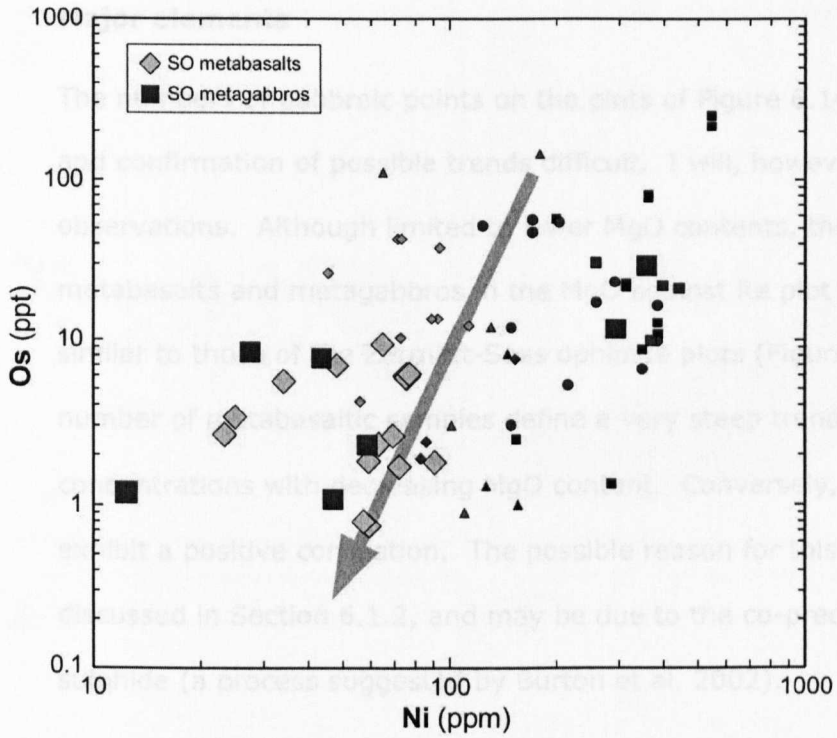

Figure 6.13. Osmium abundance (ppt) against nickel (ppm) for Sulitjelma ophiolite samples. Generally lower nickel abundances compared to ZSO suggest more evolved magmas in the generation of the gabbroic suite, than in the Allalin gabbro. There is a broad positive correlation between Ni and Os, with a suggestion of two discrete positive trends (two different magmas?). Small grey symbols: ZSO samples. The grey arrow corresponds to a 'best-fit' line for MORB data (Schiano et al. (1997) and A. Gannoun - unpubl.), orientated with the arrow towards more differentiated samples.

Nickel is commonly found to correlate positively with Os abundance in oceanic basalts (e.g. Burton et al. 2002). In the metabasalts and metagabbros of the SO the trend is not well-defined, but there does appear to be co-variation. With the exception of two data points, the metagabbroic samples contain almost an order-of-magnitude less nickel and more often than not, lower Os concentrations than the ZSO gabbros. The correlation is broad and there is the suggestion of two discrete trends, although the number of points is insufficient to confirm this. The fractional crystallisation of two different magmas with varying initial Os and Ni abundances could perhaps lead to two trends.

Major elements

The numbers of gabbroic points on the plots of Figure 6.14 make the recognition and confirmation of possible trends difficult. I will, however, offer some tentative observations. Although limited to lower MgO contents, the patterns of SO metabasalts and metagabbros in the MgO against Re plot (Figure 6.14 a) are very similar to those of the Zermatt-Saas ophiolite plots (Figure 6.6). The greater number of metabasaltic samples define a very steep trend of increasing Re concentrations with decreasing MgO content. Conversely, the gabbros appear to exhibit a positive correlation. The possible reason for this positive trend has been discussed in Section 6.1.2, and may be due to the co-precipitation of olivine and sulphide (a process suggested by Burton et al. 2002).

In contrast to the analyses of Allalin gabbros, Figure 6.14 (b) and (c) display weak positive correlations between Al_2O_3 and Re and CaO and Re for gabbroic samples. The basaltic suite scatters over a broad area in these two plots and does not define obvious trends. Osmium does not appear to be correlated with MgO or Al_2O_3 content in either the basaltic or gabbroic lithologies. There is, however, a crude negative correlation between CaO and Os abundance in the metagabbroic samples, but not in the basaltic suite. The reason behind the correlation of CaO with Os is not clear; particularly considering Os is not correlated with MgO or Al_2O_3.

Figure 6.14. Os and Re concentrations as a function of MgO, Al_2O_3 and CaO content in Sulitjelma metabasalts and metagabbros. See text for detailed discussion. Rhenium and particularly osmium are not well correlated with any of the major elements, reflecting their incompatibility in silicate phases. Grey fields outline trends within unaltered gabbro data. MORB data from Schiano et al. (1997) and A. Gannoun (unpublished data).

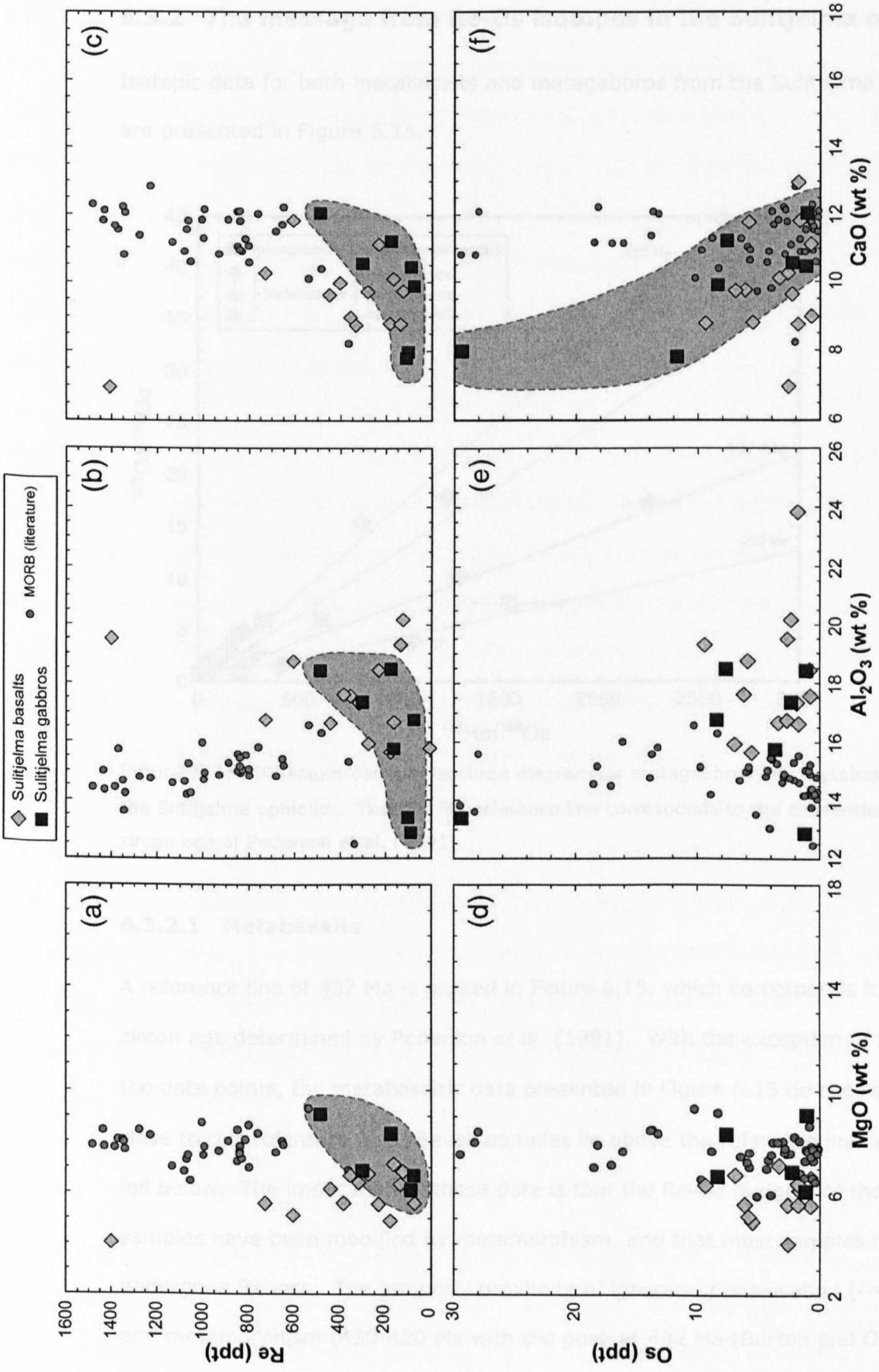
Sulitjelma basalts
Sulitjelma gabbros
MORB (literature)
(a)
(b)
(c)
(d)
(e)
(f)
Re (ppt)
Os (ppt)
MgO (wt %)
Al2O3 (wt %)
CaO (wt %)

6.3.2 The message from Re-Os isotopes in the Sulitjelma ophiolite

Isotopic data for both metabasalts and metagabbros from the Sulitjelma ophiolite are presented in Figure 6.15.

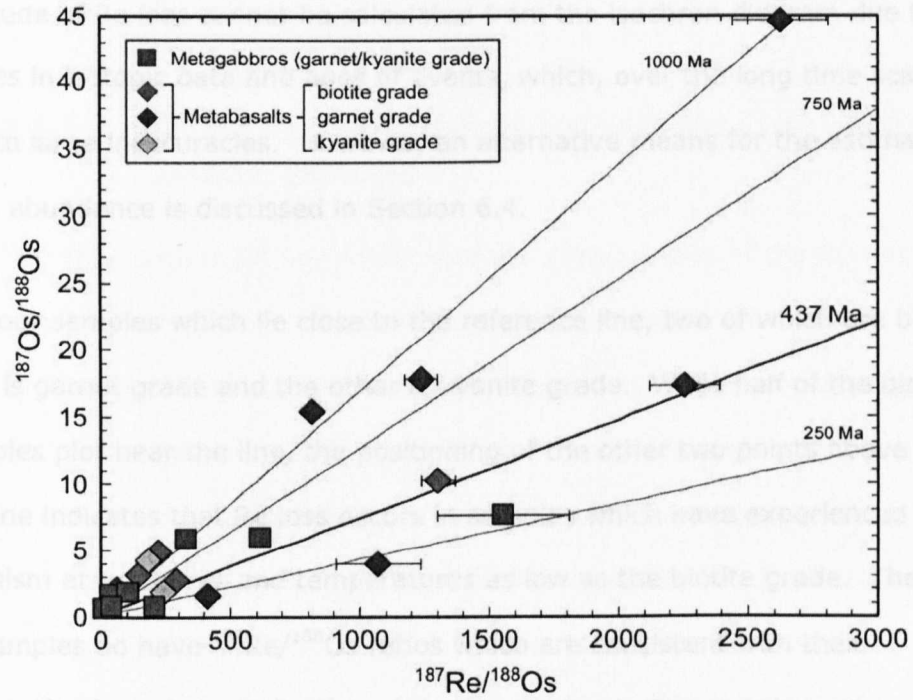

Figure 6.15. Rhenium-osmium isochron diagram for metagabbros and metabasalts from the Sulitjelma ophiolite. The 437 Ma reference line corresponds to the conventional U-Pb zircon age of Pederson et al. (1991).

6.3.2.1 Metabasalts

A reference line of 437 Ma is plotted in Figure 6.15, which corresponds to the U-Pb zircon age determined by Pederson et al. (1991). With the exception of three of the data points, the metabasaltic data presented in Figure 6.15 do not lie on or close to this reference line. Seven samples lie above the reference line and three fall below. The implication of these data is that the Re-Os budgets of these samples have been modified by metamorphism, and that most samples have undergone Re loss. The temporal proximity of igneous crystallisation (~437 Ma) and metamorphism (430-420 Ma with the peak at 432 Ma (Burton and O'Nions 1992)), means that considerable ingrowth must have occurred in the short interval

prior to metamorphism, and that substantial Re and/or Os loss must have occurred during metamorphism to create the observed variations in model ages. Given the extreme $^{187}Re/^{188}Os$ ratios of modern MORB, (up to 15,000, Schiano et al. 1997), $^{187}Os/^{188}Os$ ratios of up to 2.7 can be generated over as little as 10 million years. The magnitude of Re loss cannot be calculated from the isochron diagram due to uncertainties in isotopic data and ages of events, which, over the long time scale could lead to large inaccuracies. However, an alternative means for the estimation of initial Re abundance is discussed in Section 6.4.

There are four samples which lie close to the reference line, two of which are biotite grade, one is garnet grade and the other is kyanite grade. While half of the biotite grade samples plot near the line, the positioning of the other two points above the reference line indicates that Re loss occurs in samples which have experienced metamorphism at pressures and temperatures as low as the biotite grade. The fact that four samples do have $^{187}Re/^{188}Os$ ratios which are consistent with their $^{187}Os/^{188}Os$ ratios is perhaps indicative of the very heterogeneous nature of elemental loss from metamorphic samples. Thus, gabbroic samples from the ZSO which have experienced very HP metamorphism have not lost significant quantities of Re, whereas metabasalts from the SO, which have undergone lower grade metamorphism, have. Samples which have undergone greater deformation and fluid flow are more likely to suffer from elemental loss or gain than samples where fluids and deformation have been limited. These issues will be discussed further in Chapter 8.

6.3.2.2 Metagabbros

All the metagabbroic samples were collected from within the garnet and kyanite metamorphic zones. The data are presented in Figure 6.15. It appears that in contrast to the data from the Allalin gabbros, the Sulitjelma metagabbros exhibit open system behaviour of Re (and possibly osmium, although assuming the

mobility of Re it is not possible to determine net loss or gain of Os from the isotope diagram). None of the samples plot within error of the 437 Ma reference line. Most have $^{187}Os/^{188}Os$ ratios which are higher than the time-integrated result of their $^{187}Re/^{188}Os$ ratios, for the given age of 437 Ma – i.e. they appear to have undergone Re loss.

6.3.2.3 Conflicting messages from the Sulitjelma and Zermatt-Saas ophiolitic gabbros?

The difference in Re behaviour between metagabbros of the SO and the Allalin unit may be controlled by variations in the extent of deformation and related fluid flow, as discussed previously. Hence, Allalin samples which have undergone rehydration during retrogression, in the form of amphibole formation at the expense of omphacite, appear to have lost Re whereas those eclogites which underwent hydration, probably as a result of seafloor alteration, and subsequent dehydration during subduction do not display Re loss. Furthermore, the type of metamorphism may well have a control on Re mobility. The Sulitjelma ophiolite was very young and therefore still relatively warm when metamorphism took place. This, and the type of metamorphic setting, led to considerably higher temperatures for a given pressure during metamorphism of the SO, than in the case of the ZSO. The latter reached peak P-T conditions of approximately 600°C at >2.0 GPa. In contrast, the SO metamorphic peak was around 550°C at 0.8 GPa. The mineralogical transformations in the two settings will be different and this may have a control on some of the elemental budgets.

As a result of the differences between the two ophiolite suites, the assessment of the composition of subducted material becomes more difficult. If the type of metamorphism is the major control on Re mobility, then most samples which have undergone HP prograde metamorphism may not experience Re loss. However, the main controlling factor is likely to be the presence, and movement, of a free fluid

phase, in order to facilitate the transfer of Re (and other elements). Factors such as temperature and pressure conditions and the extent of deformation are also likely to play a role. Indeed, fluid was present during the eclogitisation of the Allalin Gabbro (as a result of dehydration reactions), but without pervasive deformation, it is plausible that the free fluid phase did not escape from the body, and thus the transfer of elements occurred only on a small scale and resulted in the redistribution of elements locally. However, a reduction in the budgets of some fluid mobile elements has been documented in the gabbroic eclogites in Chapter 4, and this will be discussed further, in the light of all the available data, in Chapter 8.

6.4 The rhenium budget in ZSO metabasalts and metagabbros

Gabbroic eclogites. The gabbroic eclogites have a slightly lower mean Re abundance than unaltered gabbros, and span a broader compositional range. The mean rhenium abundance in the Allalin gabbroic eclogites is 225 ppt. This value is considerably lower than the average (585 ppt) for the published ODP core gabbro data of Blusztajn et al. (2000). This apparent disparity may be explained by the non-cumulate nature of the gabbros analysed by Blusztajn and co-authors and the lower Os and higher Re concentrations that isotropic gabbros may have, due to their slightly more evolved nature.

A comparison of Re and Yb concentrations is presented in Figure 6.16. These two elements are thought to behave similarly in processes of mantle melting and fractional crystallisation, hence the broad correlation evident in MORB samples. While there is not a good correlation for abundances in gabbroic samples there is no clear evidence for depletion of Re in gabbroic eclogites (as illustrated by a comparison of Re and Os abundances, and the isochron diagram in Figure 6.8), except in several samples with pervasive greenschist retrogression that have been discussed in Section 6.2.1. However, it is possible that the gabbroic eclogites experienced a small degree of Re loss during an earlier stage in their history (so as

not to affect the isotope evolution and model age) most likely in the form of hydrothermal alteration. Peucker-Ehrenbrink et al. (2003) performed a study of Re and Os abundances in upper oceanic crust affected by an hydrothermal system. The authors concluded that Re gain, rather than loss, may be the predominant process, although neither affect the budget in a significant way. However, the reworking and redistribution of elements during hydrothermal alteration has been commonly documented (e.g. Staudigel et al. 1996), and the larger range of Re concentrations in the gabbroic eclogites may be consistent with this process.

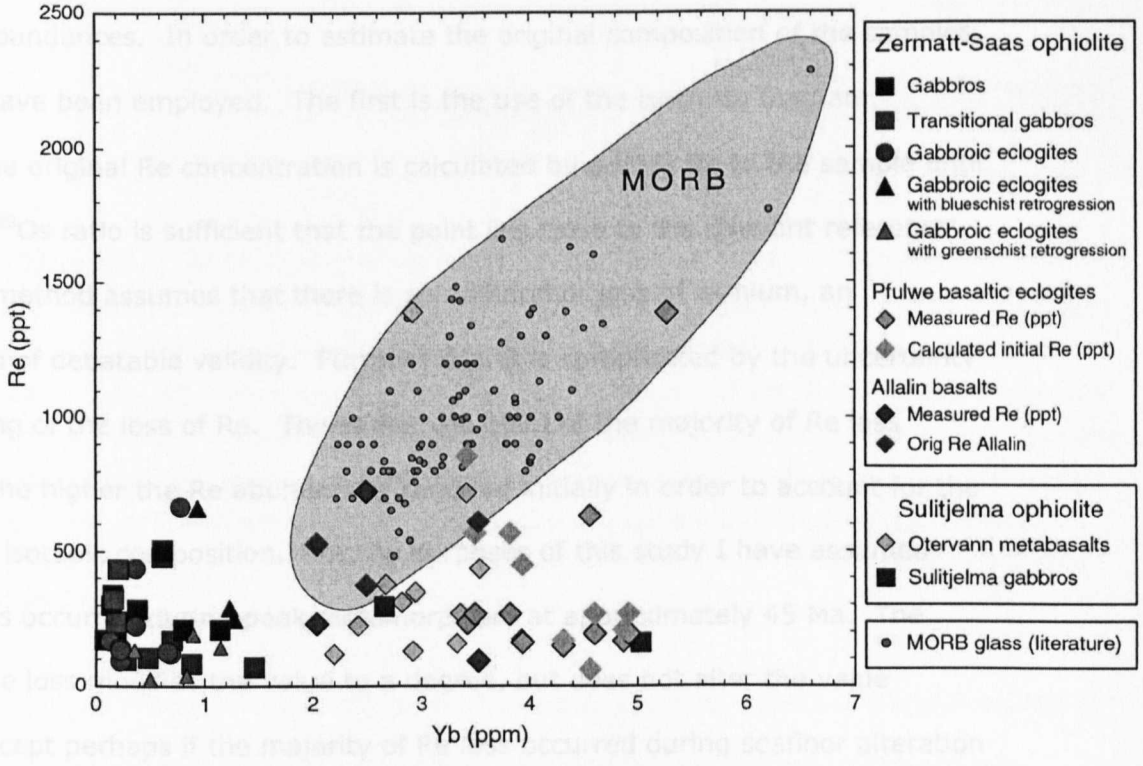

Figure 6.16. Rhenium against Ytterbium for Zermatt-Saas and Sulitjelma ophiolite samples. Gabbroic samples possess both lower Yb and lower, but variable, Re concentrations. Basaltic samples have Yb concentrations which are comparable to MORB, but contain much lower Re concentrations than expected. Some loss of Re has occurred during HP metamorphism, but calculations of initial Re concentrations have been made using the isochron diagram (assuming no net loss or gain of Os) and initial Re abundances (marked by plain green diamonds) are, for the most part, lower than the range for MORB. MORB field from Schiano et al. (1997) (Yb calculated from Tb data), Sun et al. (2003c) and A. Gannoun (unpublished).

Basaltic eclogites. In contrast to the eclogitic gabbros, basaltic eclogites display reduced $^{187}Re/^{188}Os$ ratios on an isochron diagram (Figure 6.10 and Figure 6.11), while also displaying unexpectedly low Re concentrations when compared to the similarly compatible, but immobile element, Yb (Figure 6.16). MORB defines a good positive correlation between Re and Yb, which is determined by their relatively similar compatibility. The data for Sulitjelma metabasalts, and particularly for Zermatt-Saas basaltic eclogites, reveal Re concentrations which are significantly lower than the field for MORB. In order to estimate the extent of Re loss from metabasaltic samples during HP metamorphism, it is necessary to constrain the initial Re abundances. In order to estimate the original composition of the samples, two tools have been employed. The first is the use of the isochron diagram, whereby the original Re concentration is calculated by adding Re to the sample until the $^{187}Re/^{188}Os$ ratio is sufficient that the point lies close to the relevant reference line. This method assumes that there is no addition or loss of osmium, an assumption of debatable validity. Furthermore, it is complicated by the uncertainty in the timing of the loss of Re. The earlier the point of the majority of Re loss occurred, the higher the Re abundances required initially in order to account for the current Os isotopic composition. For the purposes of this study I have assumed that Re loss occurred during peak metamorphism at approximately 45 Ma. The timing of Re loss modifies the value to a degree, but does not alter the value greatly, except perhaps if the majority of Re loss occurred during seafloor alteration (i.e. early in their evolution). The second method is to assume that Re/Yb is constant for all MORB and similar lithologies. In this case the original Re concentrations can be calculated using the slope and intercept of a best-fit line through the MORB data. Using the Yb method, a sample would plot in the MORB field in Figure 6.16, at a point along a line corresponding to its specific Yb content. Even using the lower side of the MORB field as a reference, the calculation from Yb contents results in much higher initial Re concentrations than the isochron diagram

method, as illustrated in Figure 6.16, where isochron calculated initial Re abundances are plotted alongside the measured Re abundances.

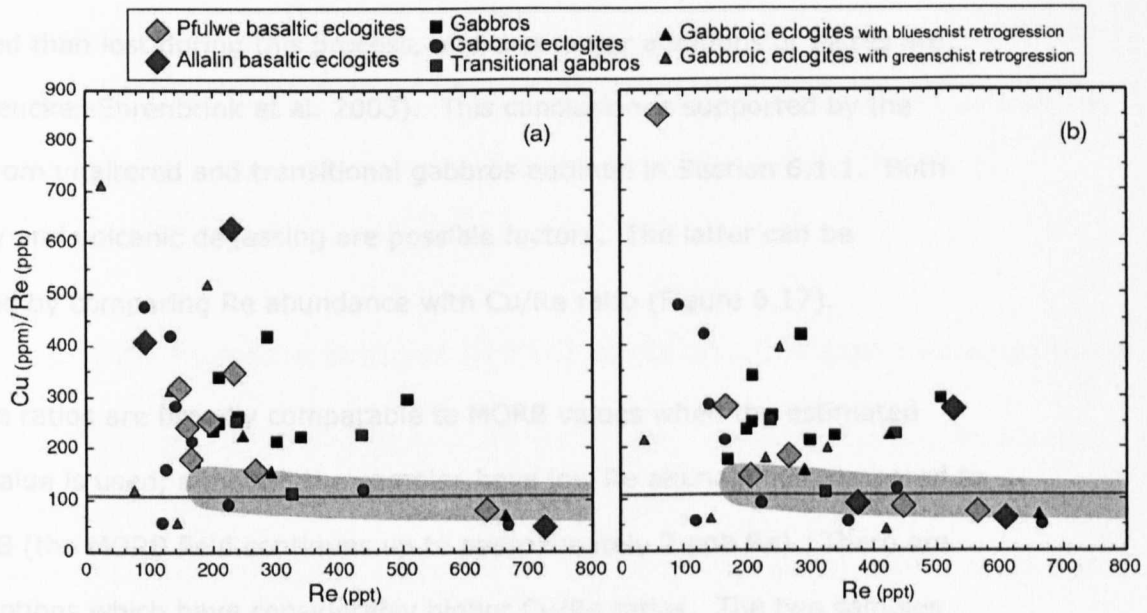

Figure 6.17. Re (ppt) plotted against Cu (ppm)/Re (ppb) ratio for ZSO samples. Copper and rhenium are thought to be similarly incompatible elements, and thus large increases in Cu/Re ratio are suggestive of volatile loss of Re during volcanic degassing (see Lassiter 2003). The left-hand graph (a) in Figure 6.17 is plotted with measured Re abundances and so also contains the effects of Re loss during metamorphism, which may increase the Cu/Re ratio. Graph (b) uses the Re values which have been calculated from the isochron diagram. The primitive mantle average is marked as the grey line, and MORB compositions are defined by the grey field. The MORB field has a negative slope due to the fact that Re is slightly more incompatible than Cu.

Possible reasons for the discrepancy in estimated initial Re concentrations may include the following: (1) that Yb and Re do not display similarly compatible behaviour in all settings, thus estimates of Re from Yb concentrations may be false, (2) the coincident loss of Os, as well as Re, from these samples would result in an increase in the $^{187}Re/^{188}Os$ ratio and an underestimate of the Re loss, (3) Re may have been lost through volatile loss during volcanic degassing, or (4) very early loss of Re may have occurred during seafloor hydrothermal alteration. Given the similarity of the Zermatt-Saas ophiolite composition to MORB (see Chapter 4) it seems unlikely that Yb and Re behaved differently in the formation of these

ophiolites than they do in MORB. Although hydrothermal alteration appears to have had a strong influence on the composition of both the ZSO and SO metabasalts (see Chapter 4), the limited data published thus far suggest that Re is more likely to be gained than lost during this process, and that major additions or losses are unlikely (Peucker-Ehrenbrink et al. 2003). This conclusion is supported by the evidence from unaltered and transitional gabbros outlined in Section 6.1.1. Both Os mobility and volcanic degassing are possible factors. The latter can be investigated by comparing Re abundance with Cu/Re ratio (Figure 6.17).

Most Cu/Re ratios are broadly comparable to MORB values when the estimated initial Re value is used, although the samples have low Re abundances compared to most MORB (the MORB field continues up to approximately 2 ppb Re). There are three exceptions which have considerably higher Cu/Re ratios. The two samples from Pfulwe are pillows and may have undergone a degree of degassing despite their submarine eruption, whereas the sample from the Allalin was collected from a dyke and so is unlikely to have experienced degassing (it instead appears to have an unusually high Cu abundance). Lassiter (2003) documented extensive volatile Re loss during sub-aerial eruptions in Hawaii, but he also identified an increase in Re abundance with water depth in the submarine samples, suggesting that significant Re loss may occur through degassing even in water depths up to 1000m. The depth of the Piemonte-Liguria Tethys is not well-constrained, but given its nature as a marginal basin, the water depth could have been relatively shallow (<<2km, by comparison with present day examples).

Calculated Re losses from metabasaltic eclogites using the isochron method range from 12 to 90% of their likely protolith compositions, with a mean of 51%, excluding the two samples which plot below the reference line. However, including the two samples which lie below the isochron (i.e. those that have gained Re), estimated loss from all the samples combined falls to 17%. Estimates from a

comparison with Yb data are between 41 and 90%, with a somewhat higher mean of 63%. These estimates are comparable to those published by Becker (2000), who concluded average Re loss of approximately 60% from basaltic samples subjected to HP metamorphism, using a comparison of Re concentrations in the metabasites and MORB (the likely protolith). Subduction-related Re loss from the slab has implications for mantle recycling of oceanic crust, and this will be discussed, with the use of modelling, in Chapter 8.

6.5 The osmium budget in ZSO metabasalts and metagabbros

The difficulty in assessing Os budgets within oceanic basalts is that comparison cannot be made with a suitable, similarly compatible element. Conversely, the analysis of isochron diagrams combined with comparisons with elements such as Yb, Y and Cu can provide insight into the behaviour and abundance of Re. The problem for Os is compounded by the very heterogeneous nature of its distribution. For this reason, the measured Os abundances in the gabbros and gabbroic eclogites of this study can be considered identical. The metabasalts contain levels of osmium that are typical for basaltic rocks, but the broad range in global MORB, and within individual sample suites, means that it is not possible to determine whether an individual sample is likely to have lost or gained Os.

One factor that would suggest only limited mobility of Os is its compatibility. During mantle melting Os tends to be partitioned into and retained predominantly in the sulphide phases (Hart and Ravizza 1996; Burton et al. 2002), even when substantial amounts of sulphur are added to the melt (800-1500 ppm for MORB, Mathez 1976; Schiano et al. 1997). The same may be true during fluid transfer of elements, with the loss of sulphur but little or no corresponding loss of Os, except perhaps when the point of sulphide-out is reached. However, this observation is not borne out by the PGE data from sulphides presented in Section 7.2, whereby Os

abundances appear to be lower in sulphides from gabbroic eclogites rather than those from unaltered gabbros.

It is probable that some of the increased $^{187}Re/^{188}Os$ ratios observed (samples plotting below the reference lines) are the result of a decrease in Os abundance rather than an increase in Re. However, it is plausible that in an area where many samples are losing a significant proportion of their Re contents, there will be beneficiaries, resulting in increased Re/Os ratios in some samples.

If Os mobility had been significant during HP metamorphism, the calculation of original Re content by the isochron method would be inherently inaccurate (due to Os variations controlling the position of points on the isochron diagram, rather than only Re variations). However, the Cu/Re data fit the expected trend reasonably well after the initial Re abundance has been estimated by the isochron method (previous section). Therefore, it is plausible, although by no means definite, that Os loss has not occurred on a significant scale during HP metamorphism. If Os is not significantly mobile during the process of subduction, then alternative mechanisms are required to explain the elevated osmium isotope compositions in some arc settings.

7 Re-Os, PGE and trace elements at the mineral scale in the Allalin metagabbros and Pfulwe metabasalts

In this chapter, Re-Os abundances and isotopic data are presented for all significant mineral phases in both unaltered gabbro and completely eclogitised metagabbro. The concentration data have been used in a mass balance calculation in order to investigate the redistribution of Re and Os during HP metamorphism.

Platinum-group element (PGE) data, acquired by laser-ablation (LA)-ICP-MS, are also presented for sulphide phases from unaltered gabbros and gabbroic eclogites. Trace element data for silicate phases have been obtained by LA-ICP-MS and are used both qualitatively and quantitatively in a discussion of petrogenetic processes and the redistribution of trace elements during HP metamorphism, with particular reference to those elements which are considered to be 'fluid-mobile' in subduction zone environments (see Section 2.2 for an introduction to the chemistry of subduction zones).

7.1 Re-Os abundances in minerals from gabbroic lithologies of the Allalin Gabbro, ZSO

Mineral Separation

Gabbro (S01/39iiix). Olivine, augite and plagioclase were all hand-picked from a gabbro which displays very little recrystallisation. Inclusion-free olivine proved difficult to separate as nearly all olivine contained numerous, tiny opaque inclusions. The opaque inclusions were too small to analyse using available methods, but are probably ilmenite and/or Al-chromite, which are both present as larger crystals that have been identified by electron probe microanalysis. The presence of sulphide inclusions cannot be ruled out. All phases picked were primary magmatic minerals and largely free from the effects of metamorphism. However, a small fraction of the selected plagioclase displayed the initial stages of

recrystallisation with moderate turbidity due to the incipient crystallisation of zoisite. Sulphide forms small composite intra- and inter-granular grains. All sulphide grains proved very difficult to separate from other phases in sufficient quantities to analyse. However, two sulphides weighing 9 and 28 µg were successfully separated, dissolved and prepared for N-TIMS analysis (see Section 5.3.3 for methods), although one of these did not produce a reliable Re analysis. An oxide mineral fraction was picked and analysed which, on the basis of electron probe microanalysis of sections from the same sample, consisted of a mixture of ilmenite and chromite, although the precise proportions are not known.

Augite and olivine (both a 'clean' and an inclusion-rich fraction) were analysed from sample S02/83vix. The 'clean' olivine was not entirely inclusion-free, but contained as few inclusions as possible, and therefore represents a maximum abundance for pure olivine, although the actual value could be significantly lower (assuming the inclusions are richer in Os and Re). The inclusion-rich fraction contained numerous opaque inclusions of undetermined composition (see above).

Gabbroic eclogite (S01/3iix). This gabbroic eclogite, from which mineral phases were separated, is mineralogically complex and, in some parts, very fine grained. It was therefore not possible to separate individual phases from the matrix that constitutes the recrystallised plagioclase domain. Instead, a mineral fraction termed 'saussurite' has been analysed; this consists of a fine-grained assemblage of predominantly clinozoisite but also subordinate omphacite, kyanite, paragonite and probably quartz (although the latter was not actually observed, due to its minute grain-size, in this particular sample). Sulphide, garnet, glaucophane, talc and omphacite were all successfully separated and analysed. Omphacite constitutes only a very small proportion of this sample (<2% modal proportion) and was therefore difficult to separate in sufficient quantities. Furthermore, omphacite crystals in the Allalin gabbroic eclogites contain a significant number of rutile

inclusions and this, combined with its low modal abundance, made it impossible to separate a fraction of inclusion-free omphacite which was large enough to analyse. However, care was taken to ensure that the least inclusion-rich omphacite was separated.

Sulphide, Cr-omphacite, talc, chloritoid and garnet were analysed from sample S01/39ix. This sample does not lie on the 164 Ma reference line on an isochron diagram (see Section 6.2) and was omitted from the diagrams in Chapter 6 due to its very low osmium abundance and the high blank contribution to the analysis. However, some of the constituent phases have been analysed in order to elucidate possible compatibility differences between the mineral phases.

7.1.1 Re and Os abundances

Due to the siderophile and chalcophile nature of Os, concentrations are typically low in silicate minerals. The abundances of Os were measured in mantle phases by Burton et al. (1999; 2000; 2002), and found to be as low as 10 ppt in clinopyroxene and garnet and up to 150 ppt in olivine. Abundances in silicate phases in basaltic systems are considerably lower still, due to the much lower bulk Os content of such lithologies. Gannoun et al. (2004b) found that a clinopyroxene separate from MORB carried as little as 1 ppt Os, while olivine contained 2 and 12 ppt in the two fractions analysed. In contrast, sulphides can contain very high concentrations of Os, particularly in mantle rocks (4 ppm, Burton et al. (2000), up to 10 ppm, Pearson et al. (1998)). Sulphides in MORB systems are also known to contain relatively high abundances of Os although typically they are an order of magnitude lower than mantle sulphides (e.g. <1ppm and <0.7 ppm, Roy-Barman et al. 1998; Gannoun et al. 2004b, respectively).

Re abundances in mantle silicate phases are typically as low as 10 ppt in olivine and clinopyroxene, while garnet may contain up to 250 ppt (Burton et al. 1999; 2000;

2002), indicating that it is moderately incompatible in silicate phases. Pearson et al. (1998) determined the Re concentrations of numerous mantle sulphides, and concluded their Re contents ranged from 50 to 2500 ppb.

The data of Gannoun et al. (2004b) indicate that Re abundances in basaltic sulphides can be higher (700 and 3500 ppb) than those in mantle lithologies, probably reflecting the greater whole rock Re content of basaltic systems, which is a result of its moderately incompatible behaviour. Silicate minerals within basaltic systems can also possess significantly higher Re abundances than mantle silicate phases; e.g. 270 ppt in plagioclase and 4000 ppt in olivine (Gannoun et al. 2004b).

Gabbros. The Re and Os abundance data for mineral phases from unaltered gabbro samples are plotted in Figure 7.1 and presented in Table 7.1 together with isotopic data. There is a positive correlation between Re and Os abundances when Os = ~5 ppt or greater. However, the plagioclase analysis, and possibly the pyroxene data, display considerably higher Re abundances for their given Os content, on the basis of the trend in Figure 7.1.

The range of Os abundances in gabbroic minerals spans six orders of magnitude, while Re concentrations vary by five orders of magnitude. Sulphides are by far the most Os-rich phase, with concentrations typically 10 to 100 ppb. Rhenium is also most concentrated in sulphides, although the difference between sulphide and silicate concentrations of Re is less dramatic than in the case of Os. This may be due to the lower sulphide-silicate partition coefficient for Re compared to Os (e.g. 43, Roy-Barman et al. 1998), although the data of Gannoun et al. (2004b) gives a much higher $^{\text{sulphide-silicate}}D$ of ~1000 for Re. The concentrations of Re and Os within the group of sulphides spans a very large range, from ~2 ppb to over 300 ppb. An explanation for the large range of abundances may lie in the major element

	Sample mass (mg)	[Os] (ppt)	[Re] (ppt)	$^{187}Os/^{188}Os$	$^{187}Re/^{188}Os$	"Common" Os (ppt)	Blank contr.(%) Os	Blank contr.(%) Re	Model age
Gabbros									
S01/39iiix									
Whole rock	460.05	11.2	145	0.334 ± 0.004	63 ± 3	10.9	6.9	21.0	189
dupl.	406.55	19.9	208	0.301 ± 0.003	50 ± 1	19.5	0.7	5.4	199
Silicates									
Olivine[1]	380.80	6.7	25	0.217 ± 0.007	17.1 ± 0.5	6.6	2.4	11.5	288
Olivine[2]	2.00	45.0	1410	0.275 ± 0.021	127 ± 10	44.1	12.2	31.0	66
Olivine[3]	45.39	23.6	360		70 ± 9	23.7	4.5	7.0	-19
Plagioclase[4]	64.75	<0.5	174			<0.5	80.0	9.8	-
Augite	44.26	1.3	125	1.414 ± 0.174	618 ± 124	1.1	47.3	18.1	154
Oxides									
Opaque fraction (Ilmenite & Al-chromite)	1.83	127.5	1803	0.167 ± 0.006	51 ± 11	126.8	5.3	39.5	37
Sulphides	(µg)	(ppb)	(ppb)			(ppb)			
Sulphide[5]	27.30	9.32	715.6	0.678 ± 0.012	352 ± 21	8.69	3.8	23.8	93
Sulphide[5]	9.00	19.05		0.340 ± 0.010		18.53	5.5		
S01/83vix									
Whole rock	411.02	81.4	292	0.193 ± 0.001	16.4 ± 0.2	80.7	0.9	11.6	210
dupl.	2092.87	78.8	315	0.194 ± 0.000	19.1 ± 0.3	78.0	0.1	1.4	185
dupl.	305.36	79.1	279	0.194 ± 0.001	16.2 ± 0.3	78.4	0.2	8.2	216
Silicates									
Olivine[6]	10.36	18.6	498	0.184 ± 0.006	108 ± 11	18.5	6.3	29.5	27
Augite	24.34	2.8	81	0.411 ± 0.041	84 ± 38	2.7	15.8	52.1	197
Olivine[7] with inclusions	1.52	362.8	1201	0.161 ± 0.015	12 ± 3	360.9	2.3	41.0	134

Table 7.1. Re and Os abundances and isotopic data for mineral phases from two unaltered gabbros. Data from ID N-TIMS analysis. Model age: assumes elevated initial of $^{187}Os/^{188}Os$ = 0.135 (see Chapter 6). Three olivine separates were analysed from S01/39iiix: [1] very coarse grains and inclusion content not known, [2] very small quantity with minimal inclusions, [3] separated with unavoidable, but limited inclusions. [4] The Os abundance in plagioclase was too low to allow a meaningful measurement of isotopic ratios. [5] sulphides dissolved and purified by microdistillation only (Os) and the residue used for Re chemistry. [6] few opaque inclusions, [7] oxide phases could not be separated in sufficient quantities to analyse, and so olivine with most opaque inclusions was separated. Major and trace element compositions for the phases are presented in Appendix C, Table C.1.

composition of the sulphide analysed (e.g. chalcopyrite, pyrrhotite or pentlandite) – this possibility is discussed further in Section 7.4 below.

Most of the sulphide analyses displayed in Figure 7.1 were obtained by laser ablation (LA)-ICP-MS (small symbols). The sections cut from sample S01/39iiix (from which all phases were separated by hand-picking) did not contain any sulphides large enough to analyse by laser ablation. For this reason, all the LA-ICP-MS analyses plotted are from samples S02/83vix and S01/36ix. The large symbol

denotes a sulphide which was separated, dissolved and analysed through negative thermal ionisation mass spectrometry (N-TIMS). There is a discrepancy between the Re concentration obtained by TIMS analysis (the large symbol) and those obtained by LA-ICP-MS. It is possible that this discrepancy is due to greater Re concentrations in sulphides from S01/39iiix. However, while there is a large spread of Re concentrations for both groups of sulphides analysed by LA-ICP-MS, the range between the two groups is comparable, suggesting that average concentrations do not vary significantly from sample to sample. The explanation for the discrepancy is as yet unconfirmed, although difficulty obtaining accurate Re data through the micro-distillation procedure for sulphides (described in Section 5.3.3) is a possibility.

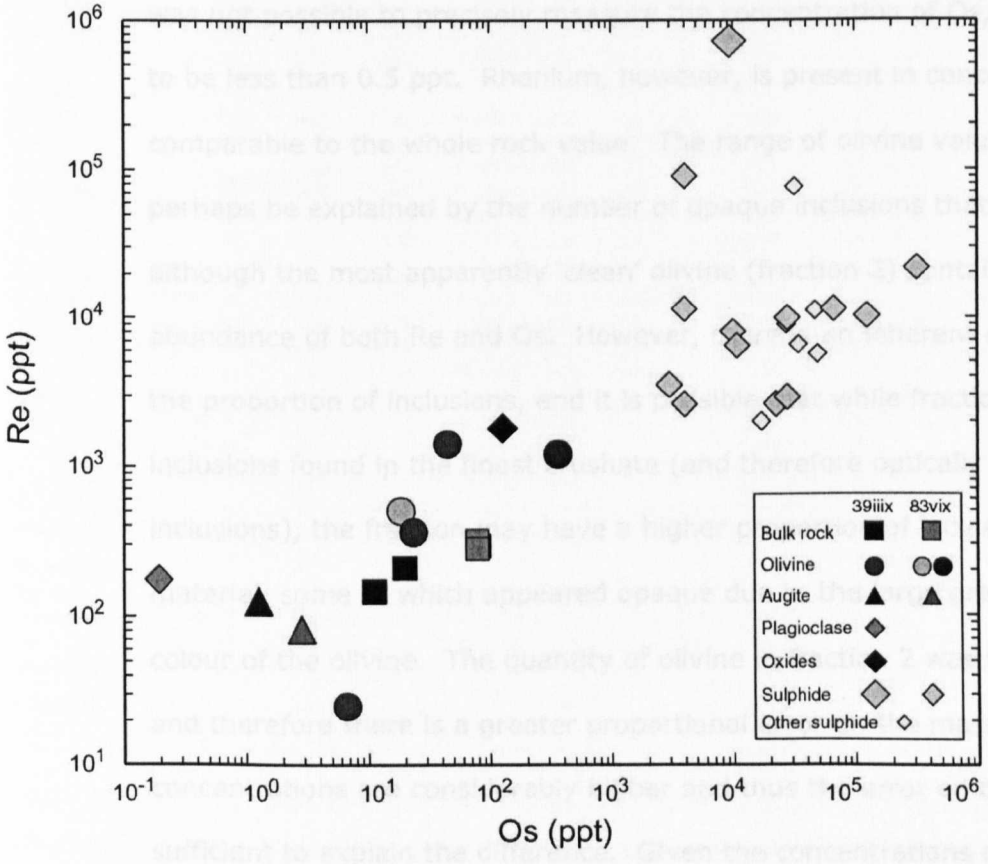

Figure 7.1. Os against Re for mineral phases from two unaltered gabbro samples. All three major phases (plagioclase, olivine and augite), an oxide fraction consisting of ilmenite/Al-chromite, and a single sulphide grain have been analysed from Sample S01/39iiix. All silicate and oxide analyses were obtained by ID N-TIMS. All except one (the largest symbol) of the sulphide data were measured by LA-ICP-MS.

The oxide fraction from S01/39iiix and the opaque-rich olivine separate from S02/83vix both have high Re and Os abundances (Os = 127.5 and 363 ppt respectively, Re = 1803 and 1201 ppt). Righter et al. (1998) proposed that Re was compatible in magnetite and Walker et al. (1996) found Os concentrations to be very high in mantle chromite (16-67 ppb). The evidence for the compatibility of Re and Os in Al-chromite and ilmenite from the gabbro analysed in this study is purely qualitative (due to both being present in the separate), but suggests abundances of the two elements which are nearly an order of magnitude higher than bulk rock values.

All silicate phases contain low abundances of Os. Plagioclase contains virtually no Os. Despite low blank levels and a relatively large mass of separate (64 mg), it was not possible to precisely measure the concentration of Os, although it is known to be less than 0.5 ppt. Rhenium, however, is present in concentrations which are comparable to the whole rock value. The range of olivine values observed could perhaps be explained by the number of opaque inclusions that they contained, although the most apparently 'clean' olivine (fraction 2) contains the highest abundance of both Re and Os. However, there is an inherent difficulty in estimating the proportion of inclusions, and it is possible that while fraction 2 had the fewest inclusions found in the finest crushate (and therefore optically possible to see the inclusions), the fraction may have a higher proportion of inclusions than the coarser material, some of which appeared opaque due to the large grain-size and strong colour of the olivine. The quantity of olivine in fraction 2 was very small (2 mg) and therefore there is a greater proportional error on the mass. Nonetheless, the concentrations are considerably higher and thus the error on the mass is not sufficient to explain the difference. Given the concentrations of Os and Re in the oxide fraction, and the proportion of opaque inclusions (<0.05%) within the picked olivine, it is not possible to explain the range of Re and Os concentrations in olivine (Os = 6.7–45 ppt, Re = 25–1410 ppt) through mixing of 'clean' olivine and oxide

phases. Therefore, the olivine crystals must contain some sulphide, or actually possess variable Os concentrations themselves. In this case, it is possible that fraction 2, despite containing fewer inclusions, contains a tiny, but very Os-rich, proportion of sulphide. Pyroxene does not contain high abundances of either Os (1.3 and 2.8 ppt) or Re (81 and 125 ppt). The contribution of the various phases to the whole rock budget of Re and Os will be discussed below in Section 7.2.

Gabbroic eclogites. The Re and Os abundance data for mineral phases from two gabbroic eclogites are plotted in Figure 7.2 and presented in Table 7.2 together with isotopic data.

	Sample mass (mg)	[Os] (ppt)	[Re] (ppt)	$^{187}Os/^{188}Os$	$^{187}Re/^{188}Os$	"Common" Os (ppt)	Blank contr. (%) Os	Blank contr. (%) Re	Model age[a]	Model age[b]
Gabbroic eclogites										
S01/3iix										
Whole rock	419.93	47.7	224	0.194 ± 0.001	22.2 ± 0.3	47.3	0.3	4.5	161	-
dupl.	398.22	57.0	366	0.189 ± 0.001	20.6 ± 2.1	56.5	0.6	15.4	157	-
Silicates										
Garnet	24.53	48.3	7223	0.168 ± 0.002	715 ± 21	48.0	1.1	0.7	3	-1
Saussurite[1]	21.75	5.4	111	0.210 ± 0.011	67 ± 20	5.4	10.0	8.3	67	31
Saussurite[2]	95.04	10.4	142	0.446 ± 0.003	65 ± 2	10.4	4.8	47.0	285	248
Glaucophane	88.12	91.3	157	0.175 ± 0.001	8.0 ± 0.2	90.7	0.6	6.8	298	-3
Omphacite	16.38	33.0	332	0.214 ± 0.003	44 ± 3	32.6	2.3	18.9	107	52
Talc	6.36	151.0	560	0.177 ± 0.004	15 ± 2	149.9	1.3	26.3	162	7
Sulphides	(µg)	(ppb)	(ppb)			(ppb)				
Sulphide	1793.40	31.50	14.92	0.184 ± 0.001	2.2 ± 0.1	31.25	0.6	3.9	1306	248
Sulphide	2750.20	0.49	28.35	0.367 ± 0.010	282 ± 17	0.48	21.2	1.4	49	41
Sulphide	1134.70	2.23	101.5	0.181 ± 0.001	218 ± 7	2.21	12.6	0.9	13	2
Sulphide	620.00	0.41	54.44	0.718 ± 0.021	665 ± 20	0.41	4.8	3.9	53	49
Sulphide	200.00	0.37	73.94	1.212 ± 0.135	1104 ± 132	0.36	14.9	8.4	59	56
Sulphide[3]	69.80	15.32		0.204 ± 0.003		15.15	0.9			
Sulphide[3]	59.60	1.30		0.380 ± 0.033		1.26	11.4			
S01/39ix										
Whole rock	2118.41	5.3	120	0.219 ± 0.014	70 ± 1	5.2	3.9	68.9	72	50
Silicates										
Garnet	24.53	8.4	1022	0.157 ± 0.003	574 ± 17	8.4	3.2	2.6	2	0
Cr-omphacite	35.32	12.5	30	0.148 ± 0.003	6.5 ± 3.0	12.5	2.9	54.2	116	-115
Talc	16.52	19.6	648	0.197 ± 0.005	147 ± 24	19.4	3.9	16.7	25	15
Chloritoid	14.62	4.5	203	0.491 ± 0.034	204 ± 41	4.3	16.4	19.2	105	98
Sulphides	(µg)	(ppb)	(ppb)			(ppb)				
Sulphide	930.00	0.41	96.43	0.974 ± 0.010	1224 ± 37	0.374	3.3	1.4	41	40

Table 7.2. Re and Os abundances and isotopic data for mineral phases from two gabbroic eclogites. Data from ID N-TIMS analysis. Model ages: [a] assumes elevated initial of $^{187}Os/^{188}Os$ = 0.135 (see Chapter 6), [b] calculated from whole rock initial at ~45 Ma (peak metamorphic age –see Chapter 3). [1] very coarse grains and inclusion content not known, [2] smaller grains, free of opaque inclusions. [3] sulphides - see [5] from Table 7.1. Major and trace element compositions for the phases are presented in Appendix C, Table C.5.

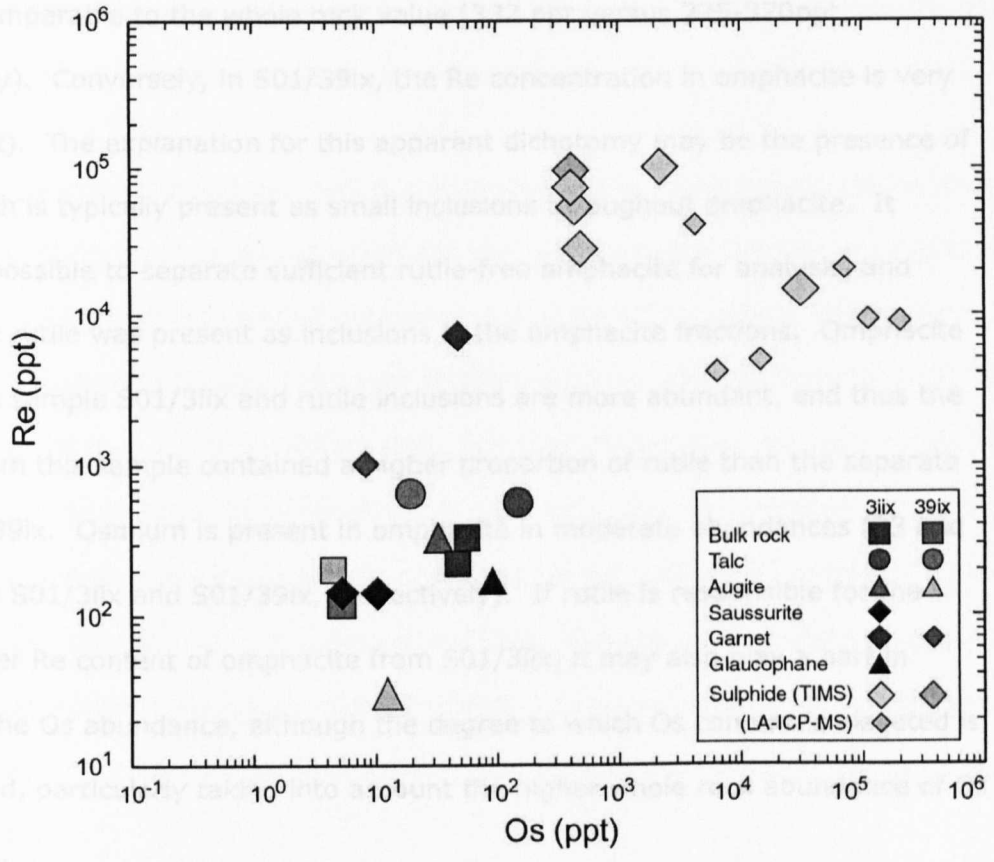

Figure 7.2. Os against Re for mineral phases from two gabbroic eclogites. All the major phases from S01/3iix have been analysed.

On average, sulphides from the gabbroic eclogite S01/3iix contain lower Os and higher Re abundances than sulphides from unaltered gabbros. This observation will be discussed further in Section 7.4, together with other PGE data. Sulphides still retain by far the highest abundances of Os and the highest Re concentrations (>4 ppb). Garnet contains high levels of Re (~8 and 1 ppb), and being far more abundant than sulphide, is likely to be a major carrier of Re in metamorphosed mafic rocks. This observation is in agreement with experimental data by Righter and Hauri (1998) performed at higher temperatures, comparable to the uppermost mantle (approximately 1300°C), which concluded that Re is compatible in garnet.

Omphacite is an important constituent of eclogite-facies mafic rocks. In sample S01/3iix, omphacite (which has pseudomorphed augite, as opposed to the very fine-grained omphacite in the saussurite) has a relatively high Re concentration,

which is comparable to the whole rock value (332 ppt versus 225-370ppt, respectively). Conversely, in S01/39ix, the Re concentration in omphacite is very low (30 ppt). The explanation for this apparent dichotomy may be the presence of rutile, which is typically present as small inclusions throughout omphacite. It proved impossible to separate sufficient rutile-free omphacite for analysis, and thus, some rutile was present as inclusions in the omphacite fractions. Omphacite is scarce in sample S01/3iix and rutile inclusions are more abundant, and thus the fraction from this sample contained a higher proportion of rutile than the separate from S01/39ix. Osmium is present in omphacite in moderate abundances (33 and 12.5 ppt in S01/3iix and S01/39ix, respectively). If rutile is responsible for the much higher Re content of omphacite from S01/3iix, it may also play a part in elevating the Os abundance, although the degree to which Os content is elevated is less marked, particularly taking into account the higher whole rock abundance of Os in S01/3iix.

Saussurite is the HP recrystallisation product of plagioclase (zoisite + omphacite + kyanite ± paragonite ± quartz). It contains osmium at higher concentrations (5.4 and 10.4 ppt) than the plagioclase from which it was formed (by comparison with plagioclase from a different sample, S01/39iiix). It is possible that Os from inclusions within the original plagioclase has been incorporated into the saussurite. Due to the extremely fine grained nature of the saussurite, it has not been possible to separate individual phases and so it is not known in which of the saussurite phases most Os or Re resides. The Re abundances measured are somewhat lower than that of plagioclase, although at the resolution possible, this difference may not be significant. The contribution of saussurite and plagioclase to the whole rock budget of Re and Os will be discussed below in Section 7.2. The lower Re abundances, if real, suggest that Re may be less compatible in zoisite than in plagioclase, although the uncertainty on all measurements and the two very

different omphacite analyses (another saussurite constituent) make it impossible to confirm such a conclusion.

Glaucophane and talc, which are present in the recrystallised olivine domain, contain Os abundances which are vastly in excess of the precursor olivine (by comparison with olivine measured in a sample S01/39iiix). Both glaucophane and talc contain Os concentrations of approximately 100 ppt in sample S01/3iix – twice as high as the whole rock value. Rhenium abundances are high in talc (~500 ppt) but much lower in glaucophane (~150 ppt). The incorporation of Os from the numerous opaque inclusions contained within olivine may explain the higher Os concentrations in glaucophane and talc. The opaque inclusions have not been preserved through HP metamorphism, and their major element components (Fe, Al?, Ti?) have probably also been consumed in the formation of glaucophane and talc.

Os, Re and Ni. Figure 7.3 presents Re and Os abundances in minerals plotted against Ni content which has been independently analysed by LA-ICP-MS of a thick-section. While the Ni data do not correspond to the exact same crystals as the Os and Re data, the average value for a given phase has been plotted, and this is likely to match closely the true composition of the fraction.

The co-variation of Os and Ni found in suites of MORB (see Section 5.2.2.1), is also evident at a mineral scale in Figure 7.3 (c). This plot displays minerals and whole rock abundances from the two gabbroic samples: S01/39iiix and S02/83vix. Sulphides contain very high Ni abundances and correspondingly high Os concentrations. Olivine is considerably richer in both nickel and osmium than augite. Plagioclase contains very little Ni (<3 ppm) or Os (<0.5 ppt). The trend for Ni versus Re (Figure 7.3 a) is less pronounced, with olivine, augite and sulphide less disparate in terms of Re content, while variations within the group of olivine analyses is greater. Nevertheless, there is a broad correlation between Ni and Re

for sulphide, olivine and augite. However, plagioclase, on the basis of the only available analysis, appears to contain higher Re concentrations than its Ni content would predict (as indeed it contains high Re for its given Os, as discussed previously). There are no good correlations for the gabbroic eclogites (Figure 7.3 b & d). In the case of Ni v Os (d), this is in part due to the loss of Ni and Os from sulphides in gabbroic eclogites (see Section 7.4 below) and a degree of homogenisation of Ni and Os abundances between the phases, with the plagioclase domain (saussurite) gaining Os with respect to unaltered plagioclase.

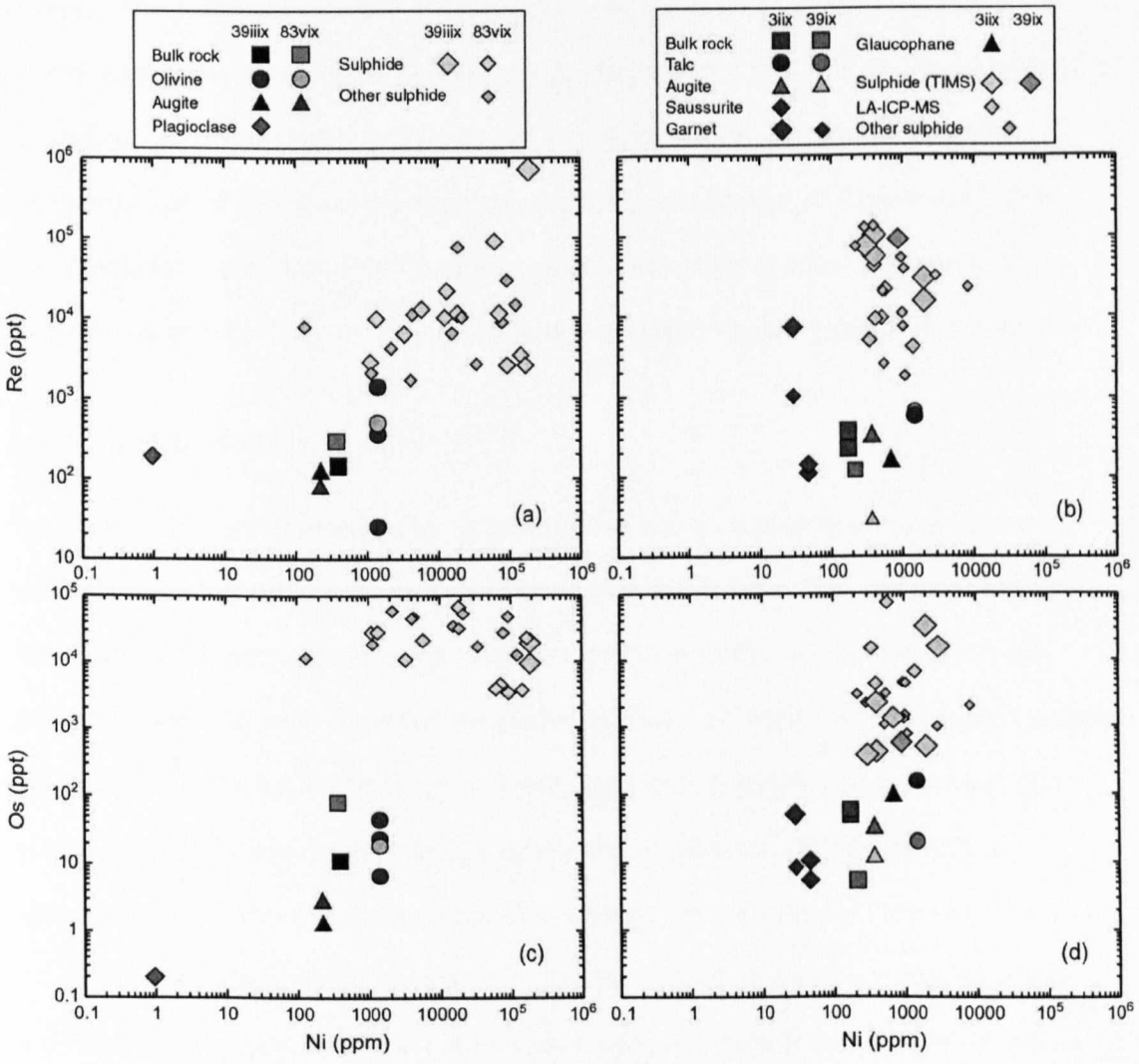

Figure 7.3. Re and Os abundances (ppt) versus Ni (ppm) for mineral phases and whole rock from unaltered gabbro (a & c) and gabbroic eclogite (b & d). Most sulphide data (all the small points) were determined by LA-ICP-MS. Large sulphide symbols denote N-TIMS analysis. The Os and Re data have been plotted against the average Ni content for that phase, determined by LA-ICP-MS of a thick-section.

Rhenium concentrations in minerals were also plotted against Cu, which is known to be similarly compatible (e.g. Lassiter 2003). The data (not shown) do not form a correlation that is as well-defined as that illustrated for Os versus Ni in Figure 7.3, although a very broad positive correlation can be identified.

7.2 Mass balance for Re and Os in gabbroic lithologies

Mineral separates representing all the major phases from one gabbro and one gabbroic eclogite have been analysed for Re and Os. These data have been quantitatively assessed in order to establish which phases are the significant carriers of Re and Os in gabbroic lithologies. While some of the mineral fractions contained impurities in the form of inclusions (which was inevitable given the inclusion-rich nature of olivine and omphacite, see Section 7.1) the data presented in Section 7.1.1 provide upper limits for the concentrations of Re and Os in silicate phases. The estimated modal abundances, and Re and Os concentrations for gabbro and gabbroic eclogite phases are presented in Table 7.3, together with their percentage contribution to the whole rock budgets of Re and Os. A graphic representation of the mass balance calculation is presented in Figure 7.4. The modal abundance of sulphide has been calculated using S data, and the modal abundances of the other phases have been estimated by petrographic observation.

7.2.1 Gabbro (S01/39iiix).

The Re and Os concentrations for sulphide that were used in the mass balance calculation for the gabbro were determined by LA-ICP-MS. This is because it is clear from the preceding sections that Re and Os abundances in sulphides are extremely variable both between sulphides of different major element compositions and between different sulphide grains with similar compositions, even from the same sample. By assuming that the analyses obtained by TIMS (n=2) are representative of the sulphide composition, large errors may be incurred. However, as LA-ICP-MS data was not collected from the sample in question (due to a lack of sulphides of sufficient size in the sections available), data from sample S02/36ix have been used in the calculation. While this too is unsatisfactory, this sample was chosen because it has Re and Os abundances that are most similar to sample S01/39iiix. The whole rock Os concentration of S02/36ix (average = 22.6 ppt) is

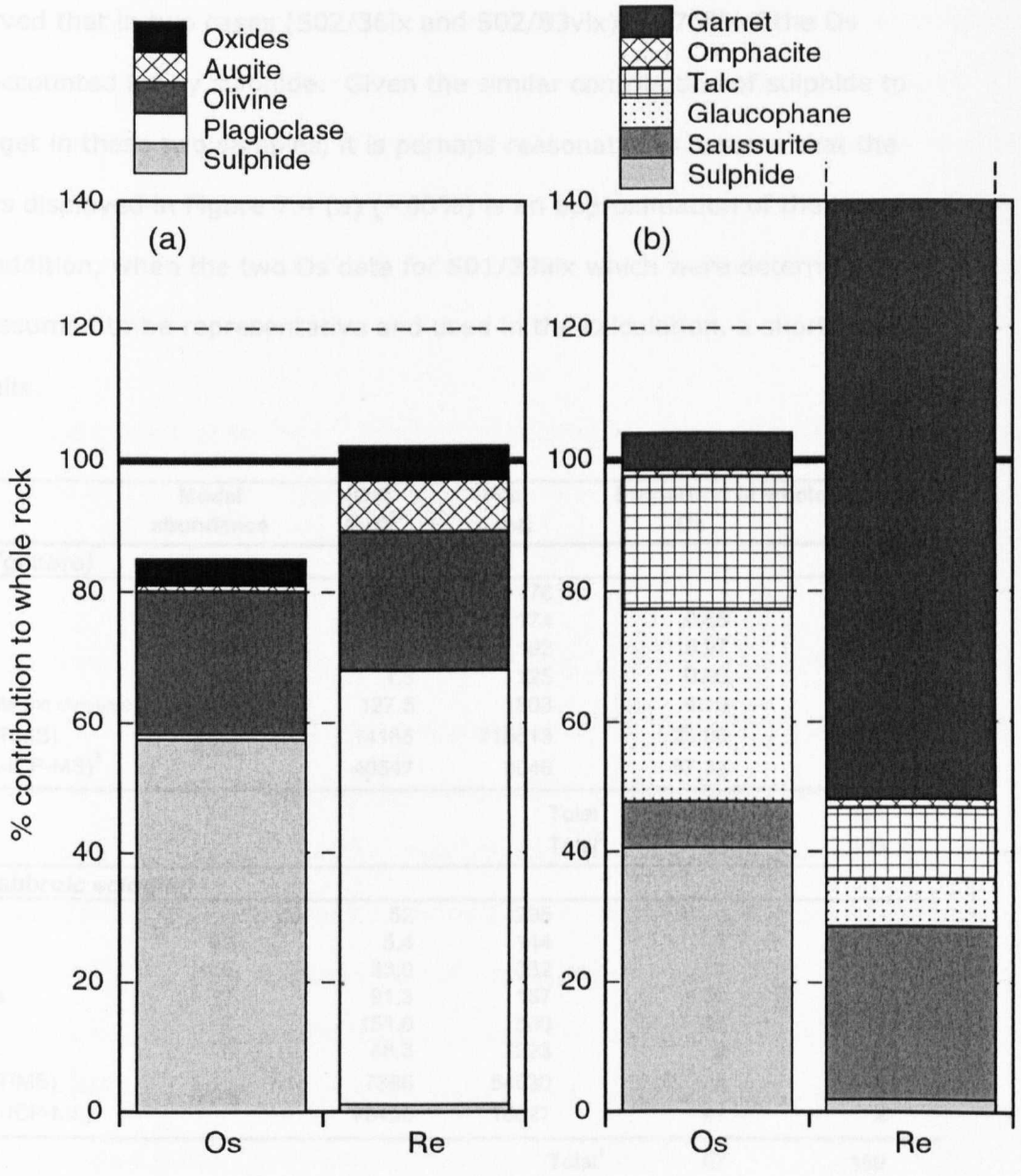

Figure 7.4. Comparison of the contribution of individual mineral phases to the whole rock budget of Re and Os in (a) an unaltered gabbro sample (S01/39iiix) and (b) a gabbroic eclogite (S01/3iix). Due to uncertainties involving the estimation of modal abundances and the errors inherent in analysis of such small quantities of sample, a total of 70-130% should be considered well balanced.

actually approximately 50% higher than the average of the two rather disparate measurements of S01/39iiix (11 and 20 ppt). However, the modal proportion of sulphide is larger by roughly the same proportion in S01/36ix (~70%, 0.038% compared to 0.022%). Furthermore, by calculating the contribution of sulphides to the Os whole rock abundances of the three samples analysed by LA-ICP-MS, it has

been observed that in two cases (S02/36ix and S02/83vix) 60-70% of the Os budget is accounted for by sulphide. Given the similar contribution of sulphide to the Os budget in these two samples, it is perhaps reasonable to assume that the value for Os displayed in Figure 7.4 (a) (~60%) is an approximation of the true value. In addition, when the two Os data for S01/39iiix which were determined by TIMS are assumed to be representative and used in the calculation, a shortfall of ~40% results.

	Modal abundance	[Os] (ppt)	[Re] (ppt)	Proportion of whole rock (%) Os	Re
S01/39iiix (gabbro)					
Whole rock	-	15.5	176	-	-
Plagioclase	68	<0.5	174	0.85	66.93
Olivine	20	15.2	192	19.97	22.32
Augite	11	1.3	125	0.90	7.81
Oxides (ilmenite and chromite)	0.5	127.5	1803	4.10	5.11
Sulphide (N-TIMS)	0.02	14185	715613	20.06	89.17
Sulphide (LA-ICP-MS)[3]		40547	9046	57.33	1.13
			Total[1]	46	191
			Total[2]	83	103
S01/3iix (gabbroic eclogite)					
Whole rock	-	52	295	-	-
Saussurite	69	5.4	144	7	27
Omphacite	1.5	33.0	332	1	1
Glaucophane	17	91.3	157	30	7
Talc	7	151.0	560	20	11
Garnet	6	48.3	7223	6	118
Sulphide (N-TIMS)	0.03	7386	54630	4	4
Sulphide (LA-ICP-MS)		73466	18927	41	2
			Total[1]	67	169
			Total[2]	104	166

Table 7.3. Modal abundances, Os and Re abundances and the contribution of the different phases to the whole rock budget of Os and Re for S01/39iiix (gabbro) and S01/3iix (gabbroic eclogite). Total[1] includes sulphide measured by N-TIMS, total[2] uses the average from LA-ICP-MS analyses ([3] in the case of S01/39iiix, the LA-ICP-MS values used are those obtained from sample S02/36ix, as discussed in the text). The difference between the sulphide data from N-TIMS and from LA-ICP-MS is almost certainly a result of the analysis of different types of sulphide. Modal abundances were estimated by petrographic observation, except sulphide which was calculated from the S content of the sample.

The other sample (S02/6ix) analysed by LA-ICP-MS differed significantly from the two others, with only 13% of the Os budget housed by sulphide. However, this

sample contains a very high Os abundance (>200 ppt) and possesses atypical, elevated trace element patterns as well as very high Ti and Nb contents (it consistently plots below the gabbro field in the 'M'/Yb vs. Nb/Yb diagrams in Figure 4.7). The elevation of Ti and Nb is due to a high modal abundance of ilmenite, which may house a significant proportion of the Os budget. Therefore, this gabbro is not considered to be representative of the samples in general.

In stark contrast to the contribution of sulphide to the Os budget, sulphide is not a major carrier of Re. Less than 2% of the whole rock budget of Re is hosted in sulphide.

The other major phase to house Os is olivine, although its precise contribution cannot be confirmed due to the large range of Os abundances measured in the olivine fractions analysed. An average of the two lower abundances obtained has been used in Figure 7.4. The presence of micro-inclusions in the olivine probably contributes to the apparent Os abundance in olivine, and therefore moderate compatibility of Os in olivine cannot necessarily be concluded. If the lowest Os concentration measured in olivine is used for the mass balance calculation, then the total Os accounted for by all phases is only 72%, which suggests that the inclusions may house a significant proportion of the total Os.

Olivine also contains a significant proportion of the Re budget (~20%) if an average of the two lower values is employed. If the lowest value is used, as little as 3% of the whole rock is accounted for in olivine. Again, this suggests the influence of inclusions, and their Re-rich nature (compared to Os) indicates that the majority probably do not consist of sulphide. However, it is equally possible that Re abundances are simply variable in olivine.

Plagioclase contains an abundance of Re that is comparable to the whole rock value, and is by far the most abundant phase (almost 70% by modal proportion).

The combination of these factors makes it the most important carrier of Re in this sample. The Os abundance of plagioclase is the lowest of all the phases measured, being too low to measure precisely (<0.5 ppt), and consequently plagioclase does not play a significant role in housing Os.

Augite contains very low Os abundances (1.3 ppt) and Re concentrations which are lower than the whole rock (125 ppt compared to ~175 ppt). Due to its moderate modal abundance (~11%), augite is a significant carrier of Re but contains less than 1% of the total Os in the sample.

The abundances of Os and Re in the oxide fraction (~125 ppt and ~1800 ppt respectively) are both highly elevated with respect to whole rock values (~15 ppt and 175 ppt). The exact contribution of oxides to the whole rock budget is very difficult to constrain due to the inaccuracies of estimating the modal proportion of oxides, particularly given the fact that olivine contains numerous tiny opaque inclusions. In this case, a value of 0.5% has been used and this is unlikely to be an underestimate. Consequently, oxides contribute approximately 5% to the whole rock budget of both Os and Re. In the case of sample S02/6ix, which has been discussed previously regarding the low contribution of sulphide to the Os budget, oxides are likely to house a large proportion of the Os. In particular, ilmenite is very abundant and must contribute significantly to the whole rock budget, given the low contribution from sulphide.

7.2.2 Gabbroic eclogite (S01/3iix)

Sulphide in this gabbroic eclogite (S01/3iix) houses a lower proportion of the Os budget than in unaltered gabbros. The proportion of whole rock Os which is accounted for by sulphide in the four gabbroic eclogites studied by LA-ICP-MS (see Section 7.4.1.1) ranges from 5 to 80%, but for three of the samples the proportion

is 40% or lower. Re concentrations are slightly higher but the contribution to the whole rock from sulphide remains insignificant (<3%).

Garnet is a major host of Re in the gabbroic eclogite, and probably housed over 50% of the Re, despite only constituting 6% of the rock by modal abundance. The measured concentration is likely to be somewhat elevated compared to the true average value, given the over-calculation of the Re budget for S01/3iix (160-170% of the whole rock value - Figure 7.4 and Table 7.3). However, there may have been an over-estimation of the modal abundance of garnet, although the whole rock budget remains over-accounted for with lower abundances of garnet (4%). Despite relatively high Os abundances in garnet (48 ppt) which approach the whole rock concentration (52 ppt), the low modal proportion limits its role in the Os budget.

Glaucophane and talc, which pseudomorph olivine, contain a higher proportion of the budget of Os (than the precursor olivine). This is probably a reflection of the incorporation of Os from the inclusions in olivine into glaucophane and talc, as discussed in Section 7.1.1. However, the proportion of the Re budget is not increased which, if the inclusions were also Re-rich as concluded in Section 7.2.1, suggests that Re has been lost from the olivine domain, and therefore has been mobile at least on a mineral domain scale. The evidence from the isochron plot for this gabbroic eclogite (Figure 7.7 and related text) indicates that there was a degree of homogenisation of Os isotopes during metamorphism and thus Os must have been mobile on a domainal scale. Nevertheless, talc and glaucophane both possess low $^{187}Re/^{188}Os$ ratios, which is characteristic of the olivine from which they have grown, suggesting that homogenisation was incomplete.

The modal abundance of omphacite (1.5%) means that this phase is negligible in terms of the Os and Re budget of the whole rock, despite a relatively high Re concentration (330 ppt). This Re abundance is considerably greater than augite

from S01/39iiix, although omphacite from S01/39ix contained very little Re (30 ppt) indicating that Re abundances can be very disparate and also suggesting that rutile inclusions in omphacite from S01/3iix may house a significant quantity of Re, as discussed in Section 7.1.1. Nevertheless, it is possible that in samples with a greater modal proportion of omphacite, that this phase will play an important role in carrying Re.

Saussurite contains a lower proportion of the Re budget than plagioclase which it pseudomorphs (by comparison with plagioclase from a different sample). The Os content of Saussurite is higher than plagioclase, and accounts for approximately 5-10% of the whole rock budget.

7.3 Isotopic data for minerals from gabbro and gabbroic eclogite

Rhenium and Os isotopic data are presented in this section for the two gabbros and two gabbroic eclogites for which Re and Os abundance data has been determined.

Re-Os isochron diagrams are shown for gabbros in Figure 7.5 and Figure 7.6, and for gabbroic eclogites in Figure 7.7 and Figure 7.8. In each case a reference line for 164 Ma has been included, which corresponds to the age of igneous crystallisation of the gabbro (Rubatto et al. 1998) (see Section 3.2.1.3). In addition, a reference line of 45 Ma is also displayed, which corresponds to the approximate timing of peak metamorphic conditions (Rubatto et al. 1998; Amato et al. 1999). This latter reference line has been forced through the present day bulk rock isotopic composition.

Gabbros. The high $^{187}Re/^{188}Os$ ratios of augite (due to its very low Os content) and gabbroic sulphide are evident in Figure 7.5. Conversely, olivine and the oxide mineral fraction have low $^{187}Re/^{188}Os$ ratios. The bulk rock isotopic composition is shown by the navy blue squares. The bulk rock data plot approximately on the 164 Ma reference line, illustrating that no significant perturbation of the Re-Os system occurred at a whole rock scale during metamorphism. This observation has been discussed in Chapter 6. The mineral data are more difficult to interpret, although regression of bulk rock, olivine[1], and augite gives an age of 152 ± 12 Ma with a MSWD of less than 1 and an elevated initial isotopic ratio of $^{187}Os/^{188}Os = 0.174$. This is just in agreement with the age of crystallisation of the gabbro body determined by Rubatto et al. (1998), and suggests that Re and Os has not been perturbed on a mineral scale through HP metamorphism at >2.0 GPa and 600°C. However, the sulphide, oxide fraction and one olivine analysis plot at significantly younger ages. If some mineral phases have been partially reset during metamorphism, and plot below the 164 Ma isochron, the retention of a 164 Ma age

for the bulk rock requires the presence of a phase, or phases, which plot above and to the left of the 164 Ma reference line (i.e. with older apparent ages). This putative phase must also have been perturbed during HP metamorphism. Such a phase has not been found thus far. Plagioclase, which is not plotted due to an extremely high blank contribution, would plot to the lower right of the line if the blank-corrected value is correct, and thus is unlikely to be the 'missing' phase. Alternatively, the bulk rock age could be explained by a phase plotting close to the bulk rock composition which is very Os-rich, and therefore controls the Os budget. It is possible that some sulphide may have the necessary $^{187}Re/^{188}Os$ ratio, but given that this phase only accounts for 60% of the Os budget, and that Re/Os ratios in sulphides are very heterogeneous, this explanation seems unlikely.

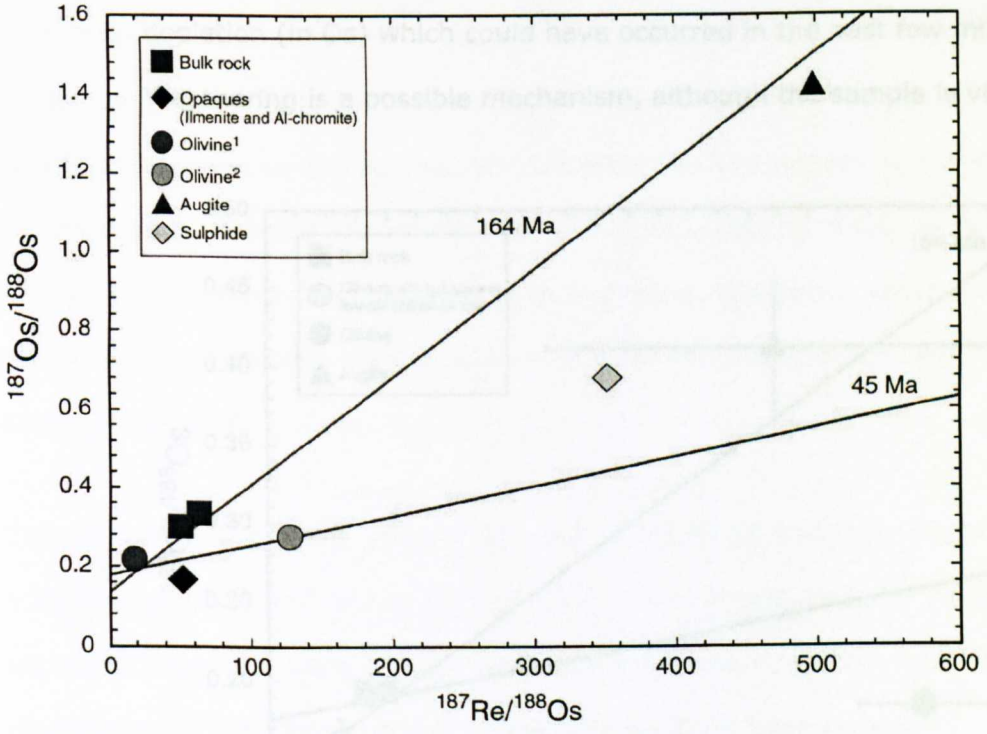

Figure 7.5. Re-Os isochron diagram for gabbro S01/39iiix. Plagioclase has been omitted due to the extremely high contribution of the blank to the analysis (80%). The 164 Ma reference line corresponds to a U-Pb SHRIMP age of crystallisation of the Allalin Gabbro (Rubatto et al. 1998), and the 45 ma reference line refers to the approximate age of peak metamorphic conditions (Rubatto et al. 1998; Amato et al. 1999).

Augite, inclusion-rich olivine and bulk rock from sample S02/83vix lie approximately on the 164 Ma reference line (Figure 7.6), although the errors are considerable and thus no precise age estimate can be obtained by regression. The inclusions within olivine are Os-rich (whole fraction = 362 ppt) and almost certainly primary and so are likely to give the most accurate guide to the magmatic age. As is the case for two analyses from S01/39iiix, olivine plots at a very young age, suggesting a recent (past few million years) enrichment in Re, which has not allowed time for ingrowth of ^{187}Os. It is possible that a large degree of Os loss could account for the change, although >70% Os loss would be required, and again the modification would have had to occur recently (past 5 million years?), otherwise the $^{187}Os/^{188}Os$ ratio would have increased due to ingrowth of ^{187}Os. It is difficult however, to envisage a suitable process to enable such enrichment (in Re) or depletion (in Os) which could have occurred in the past few millions years. Weathering is a possible mechanism, although the sample is visibly unaltered.

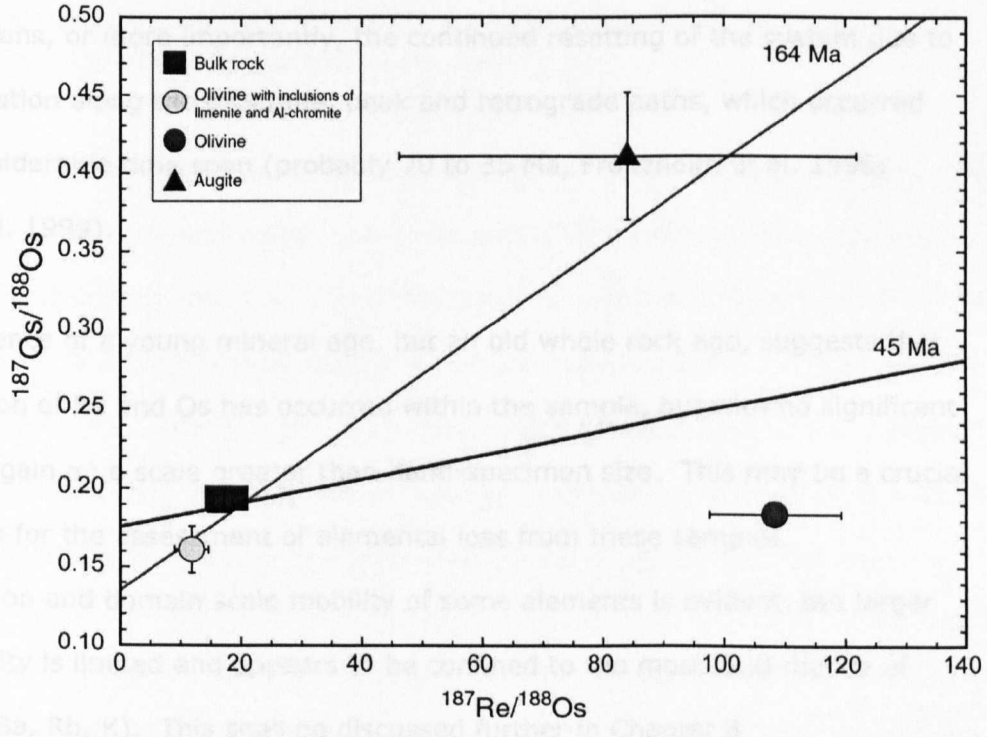

Figure 7.6. Re-Os isochron diagram for gabbro S01/83vix. As is the case for sample S01/39iiix, olivine has a young model age; a suitable explanation for such a young age is not apparent. Reference lines: see Figure 7.5.

Gabbroic eclogites. Figure 7.7 displays an isochron diagram for sample S01/3iix. This eclogite has undergone complete metamorphic recrystallisation (as has S01/39ix), yet approximately retains its igneous age of 164 Ma on a whole rock scale (shown on Figure 7.7) (This observation and its implications have been discussed in Chapter 6.) It is clear from Figure 7.7 that with the exception of one of the saussurite data, the mineral ages are much younger than the bulk rock age and typically correspond to ages which are consistent with resetting during metamorphism (a reference line for the peak metamorphic age is shown by the blue line). The calculation of an isochron for the data presented is not possible due to the large scatter of the points (even when some points are omitted); however, regression of all data gives an age of 52 ± 11 Ma, but with a very high MSWD of 1152. The presence of a good trend on the isochron plot, but with no precise age, is an indication that the osmium isotopic composition of the whole rock was largely, but not completely, homogenised during HP metamorphism. The lack of an isochron could also be due to analytical uncertainties of analyses at these concentrations, or more importantly, the continued resetting of the system due to recrystallisation along the prograde, peak and retrograde paths, which occurred over a considerable time span (probably 70 to 35 Ma, Froitzheim et al. 1996; Amato et al. 1999).

The occurrence of a young mineral age, but an old whole rock age, suggests that redistribution of Re and Os has occurred within the sample, but with no significant net loss or gain on a scale greater than hand-specimen size. This may be a crucial observation for the assessment of elemental loss from these samples. Redistribution and domain scale mobility of some elements is evident, but larger scale mobility is limited and appears to be confined to the most fluid-mobile of elements (Ba, Rb, K). This shall be discussed further in Chapter 8.

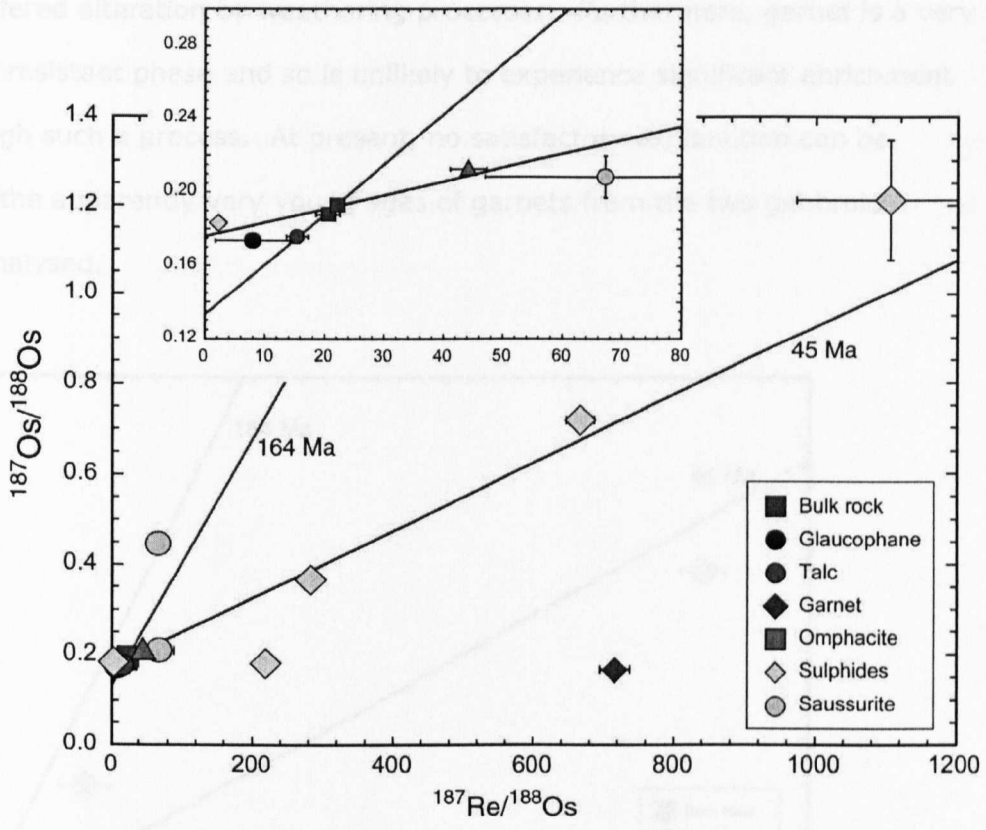

Figure 7.7. Re-Os isochron diagram for gabbroic eclogite S01/3iix. With the exception of garnet, one sulphide and one saussurite data point, the minerals define a good trend corresponding approximately to the age of metamorphism (shown by the 45 Ma reference line). 164 Ma reference line: see Figure 7.5.

The saussurite data point which plots to the upper left of the 164 Ma reference line can be explained by the loss of Re during HP metamorphism, without the concomitant resetting of the Os isotopic composition. This again emphasises the lack of complete equilibration within an individual sample. In addition, it is possible from this evidence, that the measurement of plagioclase in the unaltered gabbro was not indicative of the true average, and that some plagioclase could be the 'missing' phase from the gabbro which has a higher apparent age.

Garnet has a $^{187}Re/^{188}Os$ ratio that is much too high given the unradiogenic $^{187}Os/^{188}Os$ signature that it possesses, unless the garnet has been recently enriched in Re. The same is true for the garnet analysed from S01/39ix (Figure 7.8). A recent enrichment in Re is unlikely as the samples are well-preserved and do not appear

to have suffered alteration by weathering processes. Furthermore, garnet is a very weathering resistant phase and so is unlikely to experience significant enrichment of Re through such a process. At present, no satisfactory explanation can be offered for the apparently very young ages of garnets from the two gabbroic eclogites analysed.

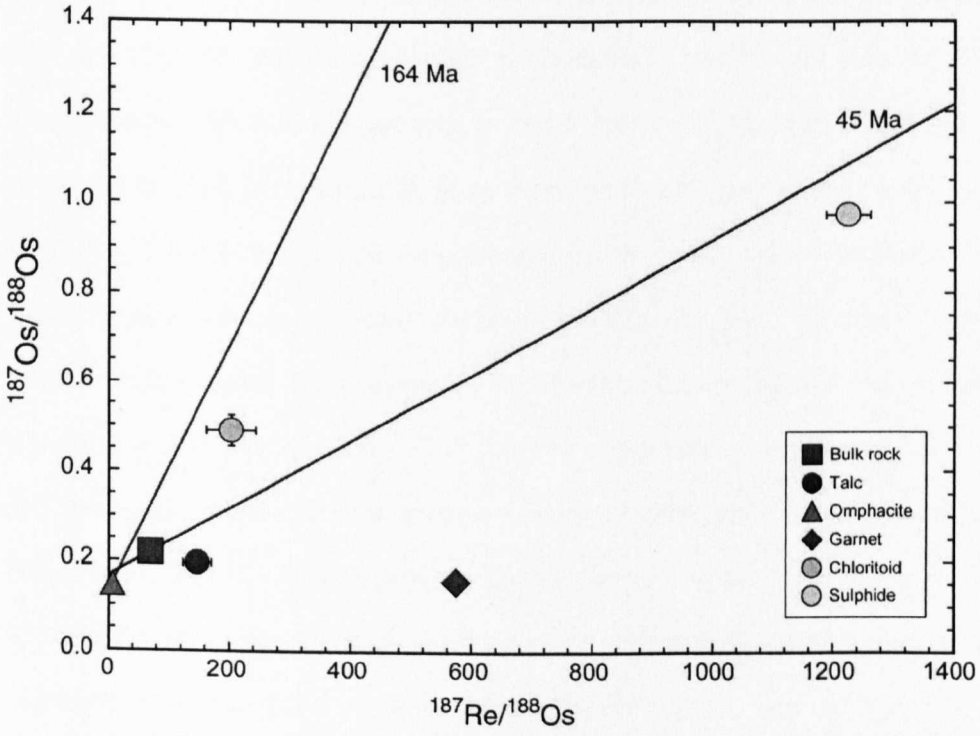

Figure 7.8. Re-Os isochron diagram for gabbroic eclogite S01/39ix. In this case, the whole rock analysis gives a model age (see Table 7.2) which is considerably younger than the igneous crystallisation age (which is 164 Ma), although the very high blank contribution to the Re whole rock analysis (~65%) precluded its entry in the isochron diagram in Chapter 6 (Figure 6.8). The minerals ages, however, are also relatively young (see Table 7.2) and largely correspond to the age of metamorphism. Reference lines: see Figure 7.5.

The gabbroic eclogite S01/39ix is unusual in that the bulk rock age appears to have been reset by metamorphism (Figure 7.8 and Table 7.2), although there was a very large contribution to the Re analysis from the blank (~65%) and thus the $^{187}Re/^{188}Os$ ratio must be treated with extreme caution. If the whole rock value is real, then it would suggest a larger scale resetting of the isotope system. However, given the unradiogenic $^{187}Os/^{188}Os$ signature of the bulk rock, the sample must

have been enriched in Re or experienced significant Os loss during metamorphism. The mineral data typically have model ages which are even younger than the bulk rock age (with the exception of chloritoid). Three of the five phases measured possess ages that are approximately consistent with resetting of the system around the time of peak metamorphism.

7.4 Platinum group elements and Re in sulphides from gabbroic lithologies: insights from LA-ICP-MS

The platinum group elements (PGE) can be sub-divided into two groups: the I-PGE (iridium group) which comprises Os, Ir and Ru, and the P-PGE (platinum group) which consists of Rh, Pt and Pd. These elements are all highly siderophile and, together with Au and Re, constitute the HSE (highly siderophile elements). As such, the PGE, Au and Re have been preferentially partitioned into the Earth's core. Consequently, the PGE are present in much lower abundances in the silicate Earth compared to chondritic samples (e.g. average Pt concentrations: 1.01 ppm in CI chondrite, 0.0071 ppm in the bulk silicate Earth – values from McDonough and Sun (1995)). However, as has been discussed in Chapter 5 for Re and Os, the HSE are present (i) in greater abundances in the Earth's silicate mantle than models of core formation would suggest and (ii) in roughly chondritic proportions, not consistent with the large range of metal/silicate partition coefficients for those elements (e.g. O'Neill et al. 1995). This paradox between measured concentrations and those estimated from experimentally derived partition coefficients has been explained by a late influx of chondritic material, after core formation, termed the 'late veneer' (e.g. Wanke et al. 1984; Morgan 1985; 1986). However, several authors have found non-chondritic ratios within mantle samples (e.g. Snow and Schmidt 1998; Rehkämper et al. 1999), and this is difficult to reconcile with the late addition of chondritic material. It has been suggested that these non-chondritic ratios are evidence of core-mantle transfer or the late addition of non-chondritic material to the Earth (Snow and Schmidt 1998; Morgan et al. 2001).

It has long been recognised that sulphides are the major host of HSE in the mantle (e.g. Mitchell and Keays 1981). Alard et al. (2000) analysed sulphides from mantle xenoliths and found two distinct types (intra-silicate and interstitial), which comprise different mineralogy and possess different chemical signatures. Those enclosed by silicate minerals typically have high Os and Ir abundances and low

Pd/Ir, and are considered to be the residues after melting. Conversely, interstitial sulphides, which are richer in Cu and Ni, generally have high Pd/Ir and are interpreted as the *in situ* crystallisation of percolating 'metasomatic' melts (Alard et al. 2000). Similarly, Bockrath et al. (2004) confirmed, experimentally, that two types of sulphides may co-exist in the upper mantle. Therefore, the presence of chemical heterogeneity on a mineral scale and between samples, due to fluid/melt processes, circumvents the need for addition of core or non-chondritic material to the mantle, and demonstrates that HSE can be fractionated, relative to each other, by magmatic processes.

A more relevant application of these findings to the study at hand is that they offer a new mechanism for the partitioning of HSE between the mantle and basaltic melts. Indeed, P-PGE/Ir ratios are often elevated in melts. This can be seen in the chondrite-normalised PGE patterns of MORB glasses published by Bezos et al. (in press). Nonetheless, such fractionation has been difficult to explain either quantitatively or qualitatively within the framework of a simple melting model using known sulphide/silicate partition coefficients. However, the occurrence of two sulphide populations described by Alard et al. (2000) and Bockrath et al. (2004) may offer an alternative mechanism. Crystalline monosulphides, enriched in Os-Ir-Ru, remain in the residue because of their tendency to adhere to silicates (Bockrath et al. 2004). Immiscible sulphide droplets, moderately depleted in Os, Ir and Ru but enriched in Rh, Pt and Pd, are dispersed in silicate melt and can be segregated from the melting region together with the silicate melt. Thus, these processes, which have been identified in many mantle samples from various tectonic settings (e.g. Archaean and Proterozoic SCLM (Alard et al. 2000; Lorand and Alard 2001; Alard et al. 2002; Pearson et al. 2002) and oceanic mantle (Rehkämper et al. 1999; Luguet et al. 2001; Luguet et al. 2004)) offer a way to significantly fractionate P-PGE relative to I-PGE during melting, by a combination of mechanical extraction and PGE partitioning between two sulphide melts which possess contrasting

physical and chemical properties. In the presence of entrained sulphide, the PGE abundances of basalts and gabbros would be mainly controlled by the amount of sulphide incorporated into the melt and the concentrations of PGE in that sulphide. The PGE ratios in mafic samples should therefore reflect partitioning between monosulphide and sulphide melt (see Ballhaus et al. 2001), rather than between sulphide and silicate (Fleet et al. 1996).

There is a comparative paucity of data on sulphides from gabbros and basalts, but it is extremely plausible that sulphide represents the main carrier of HSE in mafic oceanic crust. Although, during the past two decades, garnet (Righter and Hauri 1998), olivine (Brugmann et al. 1987) and chromite (Walker et al. 1996) have all been suggested as significant repository phases for HSE in these lithologies.

	Gabbro			*Gabbroic eclogite*		
	Po	**Pn**	**Cp**	**Py**	**Po**	**Cp**
S	36.53	32.48	34.81	53.18	38.92	34.99
Fe	63.29	40.51	30.82	46.55	60.06	30.71
Co	0.04	1.62	0.01	0.66	0.06	0.02
Ni	0.03	25.69	0.02	0.00	0.65	0.01
Cu	0.00	0.07	32.70	0.00	0.16	32.55
Total	99.88	100.37	98.37	100.39	99.85	98.27
No.of S	**8**	**8**	**2**	**2**	**8**	**2**
S	8.03	7.82	2.02	1.99	7.91	2.03
Fe	7.98	5.60	1.03	1.00	7.00	1.02
Co	0.00	0.21	0.00	0.01	0.01	0.00
Ni	0.00	3.38	0.00	0.00	0.07	0.00
Cu	0.00	0.01	0.96	0.00	0.02	0.95
Total	16.02	17.02	4.01	3.00	15.01	4.00

Table 7.4. Representative major element sulphide compositions, for unaltered gabbros and gabbroic eclogites.

In the following sections, PGE, Re, Au, Ag and Pb data and preliminary findings are presented for sulphides from gabbros and gabbroic eclogites of the Allalin Gabbro, Zermatt-Saas ophiolite, Switzerland. Sulphides within gabbros range between several μm to 500 μm in diameter and occur both in intra-silicate sites and interstitial sites between all the major phases. Olivine typically contains many tiny

(~1μm) opaque inclusions (see Figure 3.12) which are present along planes (fractures or dislocations) within the crystals. These have proved too small for their composition to be determined using the analytical methods available. It is possible that they are sulphide grains, although Al-chromite and ilmenite are also both present in the gabbros. Representative sulphide compositions for gabbros and corresponding gabbroic eclogites are given in Table 7.4. The modal proportions of the different types vary from sample to sample. Pyrrhotite accounts for the majority of the sulphide present in gabbros, while pentlandite and chalcopyrite are also significant. Conversely, gabbroic eclogite sulphides are often considerably larger (800 x 1000 μm in one case) and are dominated by pyrite, reflecting their modification, or origin, during a hydrothermal alteration episode (see Section 3.3.1.2). Pyrrhotite is less abundant and chalcopyrite is rare (usually <<5%). Pentlandite has not been found in the samples investigated. Despite the larger size of the sulphides in gabbroic eclogites, the lower sulphur content of such samples (average: ~100 ppm) compared to unaltered gabbro (~200 ppm) indicates that sulphide is less abundant. The major element chemistry of the sulphides, combined with lower sulphide contents, suggests that there has been post-magmatic loss (probably during hydrothermal alteration) of nickel, copper and sulphur during the recrystallisation of the sulphide grains.

7.4.1 PGE in gabbroic sulphides

The abundances of PGE, Re, Au, Ag, Pb, Mo, Se and major elements in sulphides from unaltered gabbros are presented in Table 7.5 and Table 7.6. Primitive mantle-normalised abundances of the HSE, Ag and Pb in sulphides from three gabbros (a - c) and four gabbroic eclogites (d – f) are presented in Figure 7.9. The patterns are characterised by strong depletions in Pt and Au, particularly in purely magmatic sulphides (the unaltered gabbro samples). The PGE patterns of the gabbros display broad similarities with the interstitial, magmatic/fluid derived sulphides from peridotite samples measured by Alard et al. (2000) and Luguet et al. (2004),

although the actual abundances are lower by one to four orders of magnitude in the gabbroic sulphides of this study. In particular, negative Pt anomalies are apparent in both, while Rh and Ru appear to be enriched with respect to Os and Ir in the gabbroic samples. The reason for very low Pt concentrations, despite the lower mantle melting compatibility of Pt (compared to Os and Ir), lies in the fact that Pt-rich nuggets have been found to be associated with sulphides (Alard et al. 2000; Luguet et al. 2001), particularly located at the interfaces of sulphide and silicate phases. It is likely that these phases account for a significant proportion of the Pt whole-rock budget. The presence of another phase housing a significant proportion of the Pt budget is consistent with data from MORB whole rock and glass samples which possess normalised Pt concentrations considerably in excess of Ir or Ru (e.g. Bezos et al. in press). The gabbroic eclogites do not display such strong depletions in Pt and Au and in some cases appear to be enriched in these elements compared to Ru and Rh. Alard et al. (2000) postulate that the development of Pt nuggets may be the result of serpentinisation with an accompanying lowering of oxygen fugacity. The evidence from Pt concentrations in gabbroic eclogites which have undergone seafloor alteration suggests that, in the case of gabbros at least, water-rock interaction does not facilitate the development of Pt nuggets, and may instead serve to homogenise the Pt content throughout the sulphide. Handler and Bennett (1999) suggested the possibility that micro-nuggets may form upon low-temperature exsolution of monosulphide solid-solutions. The smaller Pt anomalies in the eclogitic sulphides are similar to those with a hydrothermal source analysed by Luguet et al. (2004).

The strongly chalcophile nature of Rh and Pd (Luguet et al. 2001) results in some enrichment of these elements in chalcopyrite, together with Ag, although it has been necessary to correct Rh concentrations for interference with a ^{63}CuAr compound and thus the Rh values are not reliable and are often negative due to an over-correction. Palladium is also more abundant in pentlandite than pyrrhotite,

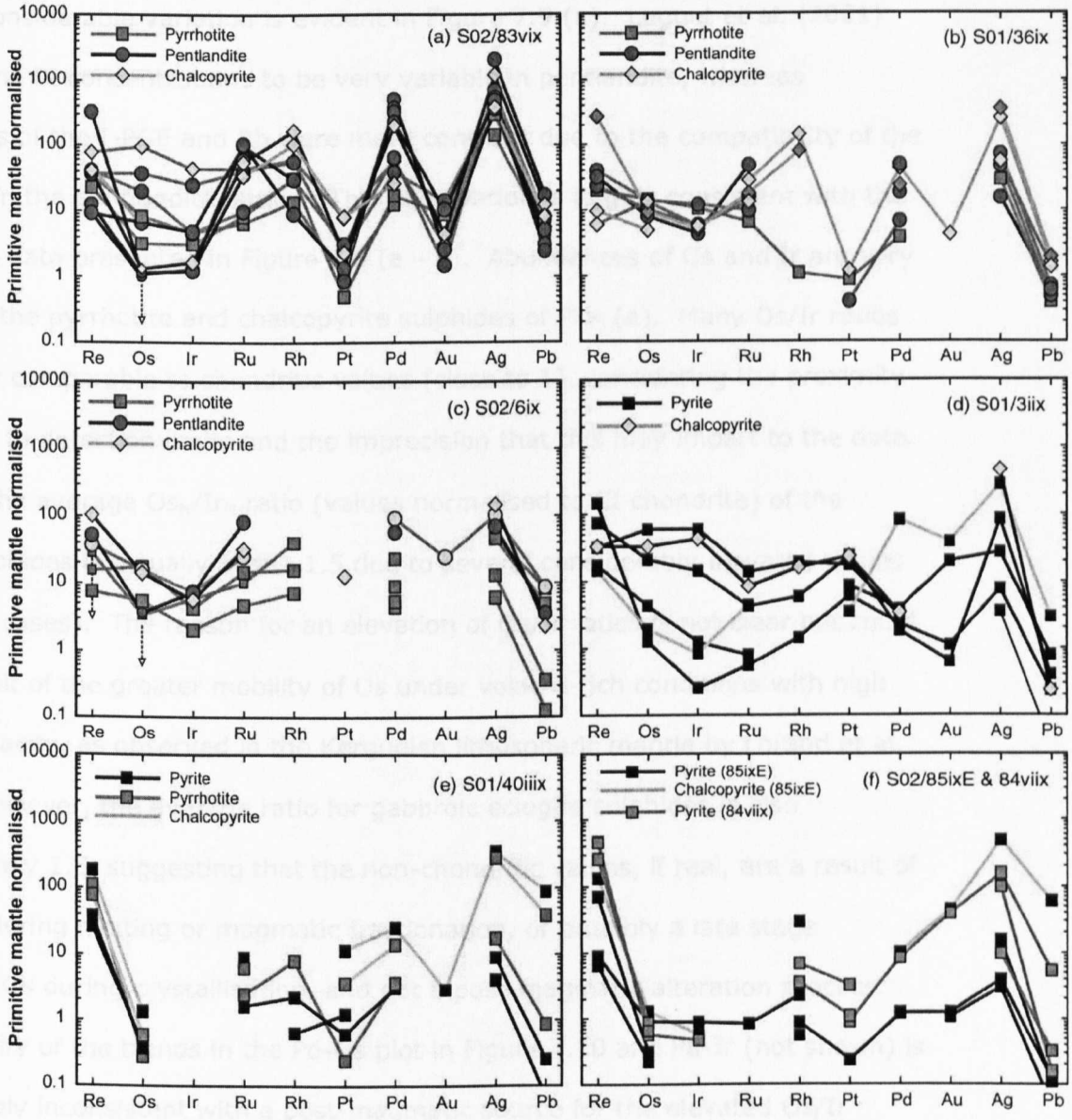

Figure 7.9. Primitive mantle-normalised patterns for PGE, Re, Au, Ag and Pb concentrations in gabbros (a, b and c) and gabbroic eclogites (d, e and f). See text for discussion. Note the presence of pyrite in eclogitic samples and the lack of pentlandite. Data presented using combinations of line colours and symbols denoting different sulphide types represent composite sulphide grains. Primitive mantle values from McDonough and Sun (1995). Values for Rh have been corrected for interference by the ^{63}CuAr complex; as a result, Rh concentrations in Cu-rich sulphides are poorly constrained and are often negative after correction. Ruthenium also has interferences from ^{59}CoAr (^{99}Ru) and from the minor Ni isotope ^{61}NiAr (^{101}Ru), consequently, the ^{101}Ru values were used and are probably falsely elevated in pentlandite due to the high nickel content of these sulphides. ^{108}Pd values were used to avoid interference of ^{65}CuAr with ^{105}Pd. The smaller symbols with dashed arrows denote that the measured value was below detection limits, and thus these represent an upper limit concentration. Errors are presented in Appendix C (Table C.16).

although considerable variation is evident in Figure 7.9 (a). Luguet et al. (2001) found Pd and Pt concentrations to be very variable in pentlandite, whereas abundances of the I-PGE and Rh were more constant due to the compatibility of the I-PGE within the pentlandite lattice. This observation is largely consistent with the pentlandite data presented in Figure 7.9 (a – c). Abundances of Os and Ir are very variable in the pyrrhotite and chalcopyrite sulphides of Plot (a). Many Os/Ir ratios are broadly comparable to chondritic values (close to 1), considering the proximity of the data to detection limits and the imprecision that this may impart to the data. However, the average Os_N/Ir_N ratio (values normalised to CI chondrite) of the gabbro sulphides is actually over ~1.5 due to several considerably elevated values (~3 in two cases). The reason for an elevation of Os/Ir ratios is not clear but could be the result of the greater mobility of Os under volatile-rich conditions with high oxygen fugacity, as observed in the Kerguelen lithospheric mantle by Lorand et al. (2004). However, the average ratio for gabbroic eclogite sulphides is also approximately 1.5, suggesting that the non-chondritic values, if real, are a result of a process during melting or magmatic fractionation, or possibly a late stage addition of Os during crystallisation, and not a post-magmatic alteration process. The similarity of the trends in the Pd-Os plot in Figure 7.10 and Pd-Ir (not shown) is also probably inconsistent with a post-magmatic source for the elevated Os/Ir ratios.

Osmium. A striking feature of the PGE patterns in Figure 7.9 is the large variability of Os (and Ir) concentrations in the sulphides of samples S02/83vix and S01/3iix (Os varies from 1 to 100 times the primitive mantle value for S02/83vix). Both samples are comparatively rich in Os (79 and 52 ppt, respectively), and this seems qualitatively at least, to be due to enrichment within some sulphide grains (up to 100 times primitive mantle value in the case of S02/83vix). However, the gabbro S02/6ix is far richer in Os (235 ppt) and yet the highest Os value measured in a sulphide from this rock was approximately 20 times the primitive mantle value.

	S01/36lx S1a Cp	S1b Po/Pn	S2a Po	S2b Po (Pn)	S3a Pn	S3b Po/Cp (Pn)	S4 Cp/Pn/Po
S	240163	240163	223485	236827	235493	220816	254839
Fe	651433	856138	943238	926813	667827	1002217	731817
Co	127	46	0	15	208	4	24
Ni	34251	15570	1	4292	78398	4048	18853
Cu	41949	935	3	509	9	3273	35315
Se	61.8	61.0	61.4	61.0	54.8	65.7	84.3
Pb	0.242	0.105	0.060	0.074	0.090	0.206	0.289
Au	0.0043	<0.0021	<0.0011	<0.0013	<0.0028	<0.0014	<0.0018
Re	0.0027	0.0065	0.0056	0.0111	0.0089	0.0017	0.0758
Ag	2.0480	0.5710	0.2315	0.3770	0.1213	0.4460	2.8450
PGE							
Os	0.0170	0.0344	0.0496	0.0474	0.0274	0.0452	0.0319
Ir	<0.0025	0.0191	0.0340	0.0385	0.0141	0.0184	0.0166
Ru	0.0334	0.0492	0.1420	0.0810	0.0900	0.2430	0.0670
Rh (corr.)	0.1293	-	0.0010	-	-	-	0.0718
Pt	0.0086	<0.0032	0.0062	0.0029	<0.0044	<0.0022	<0.0026
Pd	0.1690	0.0720	0.0151	0.0262	0.1920	<0.0048	0.0924

	S02/6lx S1 Po/Pn/Cp	S2a Pn	S2a Pn/Cp	S2b Po	S2b Po	S3 Po	S4 Po
S	232157	220149	220149	239162	239162	242164	240830
Fe	732091	652420	642668	882083	891351	987518	962528
Co	36	275	165	0	2	6	19
Ni	21424	121633	91488	28	1140	132	2149
Cu	14341	3184	22860	8	539	729	258
Se	67.4	58.3	60.6	62.5	58.6	35.6	55.1
Pb	1.291	0.525	0.339	0.054	0.019	1.213	0.720
Au	0.0246	<0.0115	<0.022	<0.0013	<0.0013	<0.0104	<0.0059
Re	0.0103	0.0145	0.0420	0.0026	0.0021	<0.0079	<0.0043
Ag	0.8300	0.5610	1.1960	0.1055	0.0483	0.4040	0.3720
PGE							
Os	0.0531	<0.0125	0.0480	0.0180	0.0184	<0.0114	0.0589
Ir	0.0239	0.0232	0.0180	0.0088	0.0064	0.0185	0.0135
Ru	0.1250	0.4110	0.1600	0.0156	0.0233	<0.051	0.0730
Rh (corr.)	-	-	-	0.0013	0.0064	0.0362	0.0142
Pt	<0.0066	<0.017	0.0900	<0.0019	<0.0019	<0.0156	<0.0092
Pd	0.3640	0.2260	<0.083	0.0172	0.0208	0.0900	0.0350

	S02/83vlx S1a Pn	S1b(1) Po	S1b(2) Po	S2a(1) Pn	S2a(2) Pn/Cp	S2b Cp	S2c(1) Po	S2c(2) Po (Pn)	S3a(1) Pn	S3a(2) Pn	S3b(1) Po (Pn)	S3b(2) Po/Cp
S	221483	221483	230156	240830	240830	220816	220816	242164	242164	221483	242831	242831
Fe	590201	1022429	1006637	536458	520040	493736	929622	892136	698622	721216	961728	882589
Co	440	4	4	273	131	9	5	21	157	106	36	24
Ni	168688	1101	1352	144071	71729	5816	3285	12270	92522	61948	18634	13134
Cu	2027	30	7771	10594	57247	105317	2889	7234	3365	6598	843	22262
Se	54.6	57.1	56.4	50.4	52.9	75.4	61.6	56.7	75.5	75.1	14.8	34.3
Pb	0.771	0.579	0.697	2.570	1.840	1.225	0.796	1.207	0.466	0.368	1.075	0.849
Au	0.0026	<0.0015	<0.0019	<0.0030	0.0045	<0.019	0.0088	0.0143	<0.0031	0.0106	0.0015	0.0031
Re	0.0026	0.0029	0.0099	0.0035	0.0114	<0.0129	0.0064	0.0102	0.0026	0.0900	0.0114	0.0215
Ag	2.9700	0.9150	1.1400	16.3200	9.6500	3.0500	2.3910	3.4000	4.3300	3.9000	5.6300	5.9100
PGE												
Os	0.0226	0.0278	0.0280	<0.0037	<0.0045	<0.021	0.0108	0.1256	<0.0034	<0.0039	0.0671	0.3210
Ir	0.0156	0.0136	0.0151	0.0041	0.0053	<0.0134	0.0100	0.0798	<0.0022	0.0039	0.0151	0.1400
Ru	0.4950	0.0341	0.0327	0.5240	0.2750	0.1710	0.0415	0.2040	0.3010	0.1780	0.0495	0.2200
Rh (corr.)	0.0271	0.0022	0.0124	0.0082	0.1494	0.0921	0.0280	0.0501	-	-	0.0272	0.0540
Pt	<0.0024	0.0034	0.0070	0.0096	0.0165	0.0580	0.0035	0.0174	0.0061	<0.0051	0.0221	0.0565
Pd	1.9820	0.0303	0.0487	1.4530	0.7830	0.1020	0.0667	0.1501	1.2660	0.8860	0.2530	0.2240

Table 7.5. Concentrations of the HSE, Ag, Se, Pb and major metals in sulphides from unaltered gabbro samples. All values in ppm. Rh abundances have been corrected for interference from ^{63}CuAr resulting in some negative values, hence the absence of some Rh data. Errors are quoted in Appendix C, Table C.16.

	S01/40IIIx					S02/85IxE			
	S1a	S1b	S1c	S1d	S1e	S1a	S1b	S1c	S2
	Cp/Py	Py	Po	Py	Cp/Po	Py	Cp/Py	Py	Py
S	296868	357576	266848	356909	246834	355574	355574	313546	355574
Fe	775560	864895	1056516	900611	596749	773382	1249969	870105	734826
Co	164	395	101	389	699	227	14	211	263
Ni	951	1014	2892	985	8198	546	1036	523	1081
Cu	53993	9	327	121	27209	1	13085	6	1
Se	29.2	21.4	23.1	21.6	17.8	5.9	55.5	62.6	20.1
Pb	13.140	0.010	0.128	0.038	5.760	0.018	8.980	0.017	0.007
Au	0.0029	<0.0009	<0.0009	<0.0012	<0.0018	0.0012	0.0437	<0.0010	0.0011
Re	0.0520	0.0072	0.0307	0.0106	0.0219	0.0024	0.0358	0.0194	0.0016
Ag	2.8300	0.0327	0.1397	0.0711	2.3130	0.0310	3.8300	0.1210	0.0235
PGE									
Os	0.0045	0.0015	<0.0010	<0.0013	0.0020	0.0025	0.0036	<0.0011	<0.0007
Ir	<0.0015	<0.0007	<0.0006	<0.0008	<0.0013	0.0028	0.0018	<0.0008	<0.0006
Ru	0.0446	0.0080	0.0121	<0.0055	0.0309	0.0042	<0.0096	<0.0048	<0.0031
Rh (corr.)	3.4900	0.0020	0.0191	0.0099	1.7400	0.0020	0.8500	0.0008	0.0005
Pt	0.0810	0.0043	0.0017	0.0086	0.0256	<0.0010	<0.0030	0.0017	<0.0010
Pd	0.0984	0.0121	<0.0144	<0.0038	0.0542	0.0048	0.0392	0.0047	<0.0023

	S01/3IIx						S02/84vIIx		
	S1a	S1b	S1c	S2a	S2b	S2c	S1a	S2a	S2b
	Py	Py	Cp/Po	Py	Py/Cp	Py	Py	Py	Py
S	356241	355574	230156	356241	293532	293532	358576	348236	356909
Fe	907455	928936	783228	928578	695587	694293	839694	1037509	866061
Co	214	173	76	265	305	320	232	250	213
Ni	395	341	1392	573	507	415	218	389	291
Cu	3	873	22037	188	3340	19	74	1717	49
Se	101.1	59.7	230.6	102.8	44.3	32.0	42.9	59.7	56.1
Pb	0.036	0.119	0.440	0.061	0.036	0.006	0.024	0.790	0.048
Au	0.0011	0.0199	0.0389	0.0006	<0.0031	<0.0034	<0.0025	0.0383	<0.0019
Re	0.0414	0.0049	0.0041	0.0208	0.0156	0.0116	0.0730	0.1310	0.1270
Ag	0.0618	0.2170	2.2100	0.6800	3.6200	0.0283	0.7790	1.2420	0.0771
PGE									
Os	0.0043	0.0147	0.0065	0.0720	0.1120	0.2040	<0.0030	0.0019	<0.0022
Ir	0.0008	0.0039	0.0027	0.0460	0.1370	0.1920	<0.0020	0.0015	<0.0013
Ru	0.0028	0.0040	0.0221	0.0212	0.0420	0.0700	<0.0122	<0.0050	<0.0083
Rh (corr.)	0.0013	0.0580	1.3150	0.0135	0.2740	0.0224	0.0075	0.1081	0.0039
Pt	0.0433	0.0615	0.0248	0.1700	0.1670	0.1250	0.0225	0.0064	0.0078
Pd	0.0090	0.0151	0.3220	0.0071	0.0133	0.0119	<0.0093	0.0324	<0.0068

Table 7.6. Concentrations of the HSE, Ag, Se, Pb, S and major metals in sulphides from gabbroic eclogites. All values in ppm. Rh abundances have been corrected for interference from $^{63}CuAr$ resulting in some negative values, hence the absence of some Rh data. Errors are quoted in Appendix C, Table C.17.

S02/6ix does have a 50% greater modal abundance of sulphide, but on the basis of the data presented, the proportion of the Os budget accounted for by sulphide in this sample is considerably lower than S02/83vix. This has been developed further and more quantitatively in Section 7.2.

Rhenium. Rhenium concentrations vary by an order of magnitude or more (when normalised to primitive mantle) in both gabbros and gabbroic eclogites. The greater affinity of Re for Cu- and Ni-rich sulphides has been suggested in the preceding section (7.4.1.1), and this is largely evident in the PGE patterns of Figure

7.9, although there are exceptions such as the Re-poor chalcopyrite in plot (b). One factor which adds to the variability of Re concentration is the presence of molybdenite nuggets adjacent to, or within the sulphide grains, which are evident through the sharp, well-defined Mo and Re peaks during the laser ablation run, similar to those observed by Alard et al. (2000) and Luguet et al. (2001) for Pt nuggets. Rhenium-Mo peaks were observed in several analyses, and in one case the peak was accompanied by markedly elevated counts of Ir, and to a lesser extent Os, suggesting the presence of a micro-grain of osmiridium. Concentrations of Re in these micro-phases can be much higher than the sulphide itself (as high as 0.7 ppm in one case from S02/83vix). In general, however, most HSE displayed fairly constant count intensities in the time-resolved signals of the laser ablation analysis.

The concentrations of Os, Re, Pt and Ru are plotted against Pd in Figure 7.10. Ru and Pd (plot d) are very well correlated in both gabbros and eclogites, with the exception of one gabbroic sulphide which is either depleted in Pd or enriched in Ru, and perhaps one eclogitic sulphide which has higher Pd for a given Ru content. The fact that eclogitic samples contain generally lower abundances of both Pd and Ru, but maintain a trend in Ru-Pd space, is intriguing. This observation indicates that the systematic difference in concentrations could be the result of one of two processes. Either the sulphides had different original magmatic concentrations (which is possible considering the lower Os abundances of the eclogites analysed), or less likely, Pd and Ru may be equally mobile and housed in the same sulphide phase(s) which has been affected by hydrothermal alteration, thus depleting both elements roughly equally. The cluster of Pd-rich gabbroic sulphides, which is particularly evident in Figure 7.10 (a) (b) and (c) (from S02/83vix), are pentlandite-type sulphides. Plot (d) illustrates that Ru is also most highly concentrated in these sulphides. It is possible then that the depletion of Ru and Pd observed in eclogitic sulphides is the result, at least in part, of the loss of

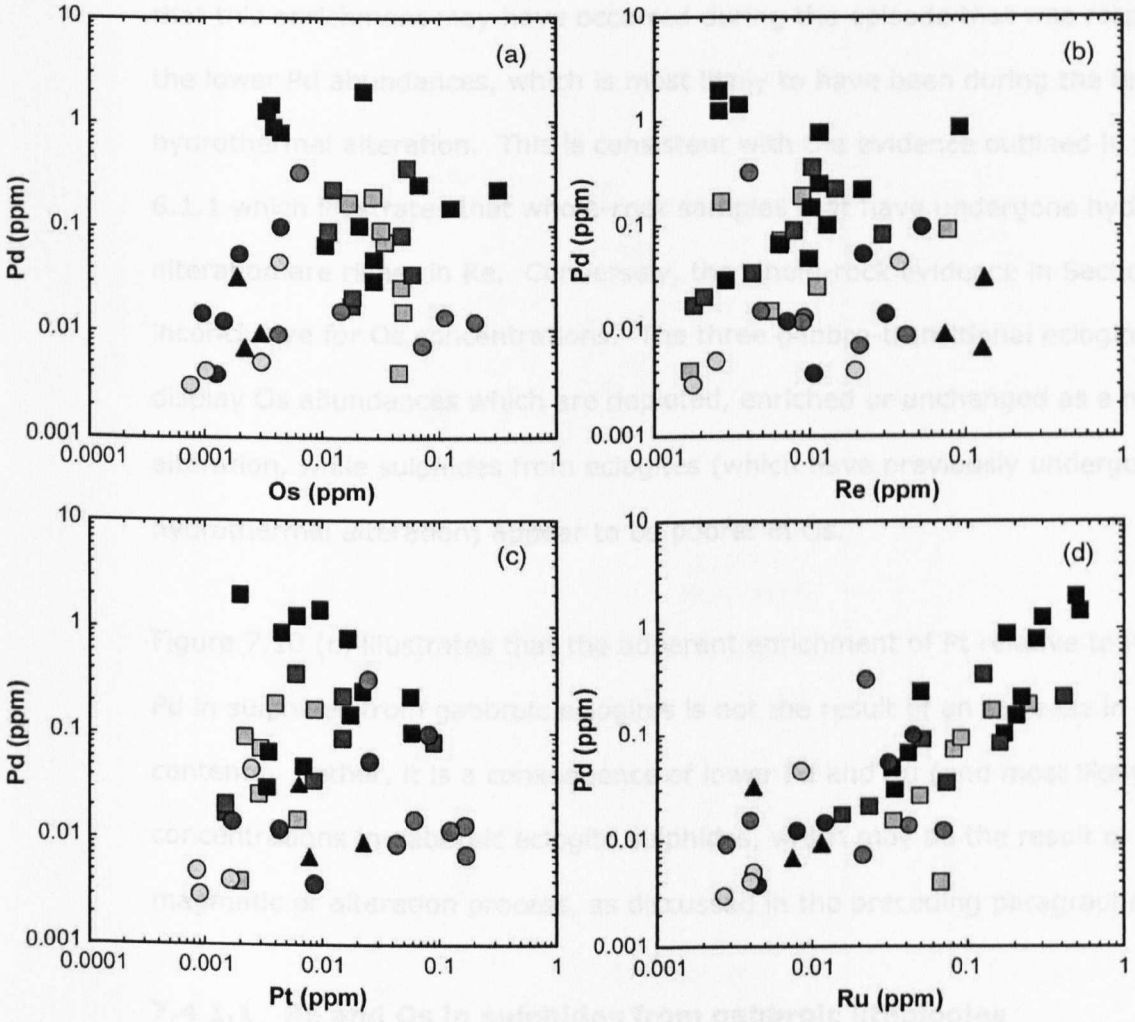

Figure 7.10. Binary plots of Pd abundance against Os, Re, Pt and Ru for sulphides from gabbros and gabbroic eclogites. Key to symbols as for Figure 7.11.

pentlandite from such samples. These pentlandite grains do not contain very high abundances of Os, Re or Pt and so the loss of pentlandite would not necessarily result in the same systematic change in plots (a), (b) and (c).

The gabbroic sulphide field in the Figure 7.10 (a) defines a weak negative correlation between Pd and Os (and Pd-Ir, not shown). The gabbroic eclogites do not define any trend, but plot to lower average Os contents as previously discussed. Whether this is a result of the loss of Os concomitantly (or otherwise) with Pd is not clear. Unlike the PGE, the average Re concentration of sulphides from the metamorphosed samples is slightly elevated with respect to the gabbros. It seems

that this enrichment may have occurred during the episode that was responsible for the lower Pd abundances, which is most likely to have been during the time of hydrothermal alteration. This is consistent with the evidence outlined in Section 6.1.1 which illustrates that whole-rock samples that have undergone hydrothermal alteration are richer in Re. Conversely, the whole-rock evidence in Section 6.1.1 is inconclusive for Os concentrations. The three gabbro-transitional eclogite pairs display Os abundances which are depleted, enriched or unchanged as a result of alteration, while sulphides from eclogites (which have previously undergone hydrothermal alteration) appear to be poorer in Os.

Figure 7.10 (c) illustrates that the apparent enrichment of Pt relative to Rh, Ru and Pd in sulphides from gabbroic eclogites is not the result of an increase in Pt contents. Rather, it is a consequence of lower Pd and Ru (and most likely Rh) concentrations in gabbroic eclogite sulphides, which may be the result of a magmatic or alteration process, as discussed in the preceding paragraphs.

7.4.1.1 Re and Os in sulphides from gabbroic lithologies

Rhenium is plotted against Os for both unaltered gabbros and gabbroic eclogites in Figure 7.11. There is no clear overall correlation between Re and Os abundances in either gabbroic or eclogitic sulphides. The sulphides from gabbros S01/36ix and S02/6ix delineate a fairly well defined field, its steep positive attitude suggests Re contents increase rapidly as Os increases. In contrast, the sulphides from S02/83vix do not generally lie within this field, although by excluding two sulphides (both with Os concentration below detection limits) the data do suggest an overall positive correlation between Re and Os, although with a much shallower slope than for the other two gabbros. If the concentrations of Re and Os are controlled by the same process, the ratio of the respective D values should give a slope for a correlation between the two elements. The lack of correlation suggests that different processes control the abundances of the two elements in sulphide, or

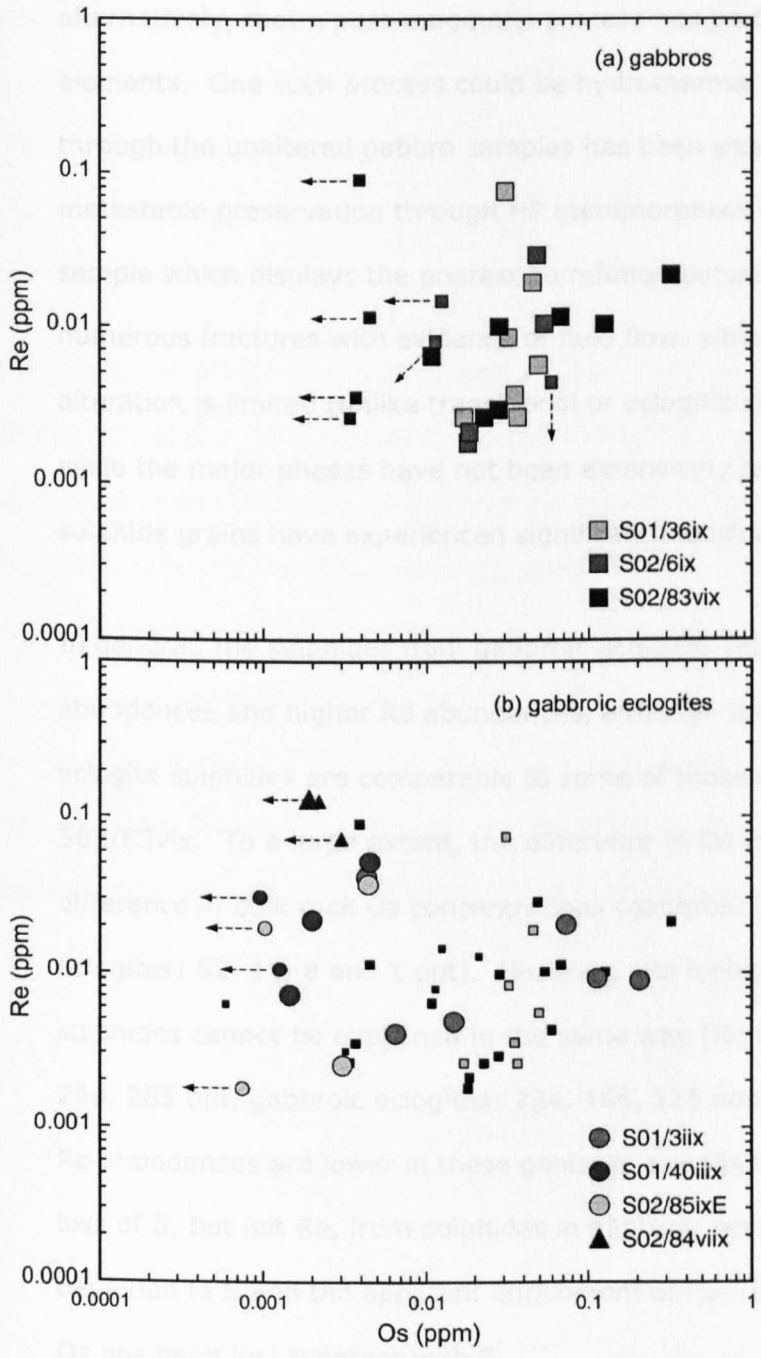

Figure 7.11. Os (ppm) versus Re (ppm) for sulphides from (a) largely unaltered gabbros and (b) gabbroic eclogites. Note that average Re contents of sulphides from gabbroic eclogites are somewhat higher than for gabbros, while Os abundances are generally lower. Some of the variability in Os contents can be reconciled with different whole rock concentrations (see end of this caption), but Re concentrations cannot be. Symbols, with whole rock Os and Re abundances (ppt) in brackets: (a) mid-blue squares – sample S02/6ix (Os:235ppt, Re:507ppt), light blue – S01/36ix (22.5, 240), navy – S02/83vix (79, 285), (b) orange circles – S01/3iix (52, 224), red circles – S01/40iiix (14, 166), yellow circles – S02/85ixE (8, 125) and blue triangles – S02/84viix (1, 290) (this sample has recrystallised under blueschist-facies conditions). Small symbols with arrows represent data below detection limits. The arrow denotes that the actual value will plot at a lower concentration. Gabbro samples shown as small grey/black squares in (b).

alternatively, that a post-magmatic process has perturbed one or both of the elements. One such process could be hydrothermal alteration, although fluid flow through the unaltered gabbro samples has been extremely limited (hence their metastable preservation through HP metamorphism). Nonetheless, the gabbroic sample which displays the poorest correlation between Os and Re (S02/83vix) has numerous fractures with evidence of fluid flow, although the extent of visible alteration is limited (unlike transitional or eclogitic samples). It is plausible that while the major phases have not been extensively recrystallised, the intergranular sulphide grains have experienced significant modification.

In general, the sulphides from gabbroic eclogites (Figure 7.11 b) have lower Os abundances and higher Re abundances, although the Os concentrations of gabbroic eclogite sulphides are comparable to some of those analysed in the gabbro S02/83vix. To a large extent, the difference in Os content may simply reflect the difference in bulk rock Os concentrations (gabbros: 235, 79 and 22.5 ppt, gabbroic eclogites: 52, 14, 8 and 1 ppt). However, the higher Re abundances of the eclogitic sulphides cannot be explained in the same way (Re concentrations, gabbros: 507, 240, 285 ppt, gabbroic eclogites: 224, 166, 125 and 290 ppt); in fact the bulk rock Re abundances are lower in these gabbroic eclogites than in these gabbros. The loss of S, but not Re, from sulphides in gabbroic eclogites could explain the depletion in S and the apparent enrichment of Re. In this case, it is possible that Os has been lost together with S.

A comparison of Os and Re abundances with major element composition of the analysed sulphide does not produce any clear trends. Luguet et al. (2001) found that Os is more compatible in pentlandite. Sample S01/36ix displays slightly lower Os in sulphides with higher Cu and Ni, suggesting that in this case Os is not more compatible in pentlandite. However, sulphides from sample S01/83vix define a broad field with a steep positive slope on a Ni vs. Os plot (not shown), which is

consistent with the findings of Luguet et al. (2001). Rhenium appears to be broadly correlated, in a positive sense, with both Ni and Cu, suggesting a greater affinity for pentlandite and chalcopyrite. Given the strongly siderophile nature of Os and its compatibility in sulphide, the first precipitates of sulphide should contain the highest levels of Os.

Most of the gabbroic eclogites do not contain enough sulphide grains, or compositional variability, to establish patterns between Re and Os and Ni and Cu. Analyses from sample S01/3iix possess lower Re concentrations for a given Ni and Cu content, whereas the two other eclogites (excluding the blueschist sample) display a weak positive correlation between Re, and Cu and Ni. The absence of any trends between Cu and Os is perhaps a result of the hydrothermal redistribution of sulphide. It is interesting to note that while Cu is (no longer?) correlated with Os, the same is not true for Re. This is again suggestive of mobilisation of Os during the hydrothermal phase, while Re remained largely immobile.

7.5 The distribution of trace elements in gabbroic lithologies and basaltic eclogites.

A large range of silicate phase trace element concentrations has been determined by *in situ* laser-ablation-ICP-MS, for metastably preserved gabbros, and gabbroic and basaltic eclogites. Oxide phases have not been analysed because of difficulties calibrating the data, due to the lack of an oxide standard. However, oxide phases (e.g. rutile and ilmenite) have previously been found to contain a large proportion of the Nb, Ta and Ti budgets and may also contain considerable amounts of Zr and Hf, while they do not contain significant abundances of REE or LILE (e.g. Zack et al. 2002b).

It has only been in the past decade that routine *in situ* analysis of trace element concentrations has become established through the use of laser-ablation-ICP-MS. In that time, there have been several studies of trace element concentrations in subduction-related metamorphosed basic rocks. Most notably, work published by Spandler et al. (2003) sought to investigate the redistribution of trace elements during HP metamorphism of both mafic and pelitic rock types from New Caledonia. The data from that study will be referred to throughout this section and also discussed, together with findings from this work, in Chapter 8.

Whole rock data are presented on various figures in this chapter. For actual trace element concentrations (and errors/reproducibility) for whole rock powders (XRF and ICP-MS) and mineral phases (electron microprobe and LA-ICP-MS), I refer the reader to Appendix C.

7.5.1 Gabbroic lithologies

7.5.1.1 Gabbros

All major silicate mineral phases have been analysed from two Allalin gabbros which display minimal metamorphic recrystallisation. In the case of S01/5G, the plagioclase is so well-preserved that twinning is still observed despite subduction to >60 km depth. The three major phases are olivine (Fo_{80-85}), plagioclase ($\sim An_{60}$) and augite. The modal proportions vary markedly due to the cumulate nature of the Allalin body. Figure 7.12 displays the concentrations of a selection of trace elements, for gabbroic minerals, normalised to chondrite. REE abundances are presented, normalised to chondrite, in Figure 7.13.

Augite contains by far the highest concentrations of most trace elements (over 100 times greater than plagioclase for the HREE). Notable exceptions are Sr, Ba and Li (Figure 7.12). The latter is most concentrated in olivine (up to 4 ppm in some cases), while Sr and Ba are partitioned strongly into plagioclase. The lack of Li in augite is unusual, as it is thought that Li is compatible in clinopyroxene in mantle peridotites (Seitz and Woodland 2000) (although compositionally these may be somewhat different – diopside with Na substitution due to the pressures involved). However, the unpublished data of S. Hammond shows high concentrations of Li (>2 ppm) in augitic pyroxenes from arc magmas. Lithium is known to be concentrated in Mg-silicates (Tomascak et al. 2002), and particularly into olivine in mantle lithologies (Seitz and Woodland 2000). The scarcity of Li in augite in the Allalin gabbros may, in part, be due to the later crystallisation of augite and its formation, in many cases, from an isolated intergranular fluid between the major cumulate phases of plagioclase and olivine, which may already be depleted in Li due to olivine crystallisation.

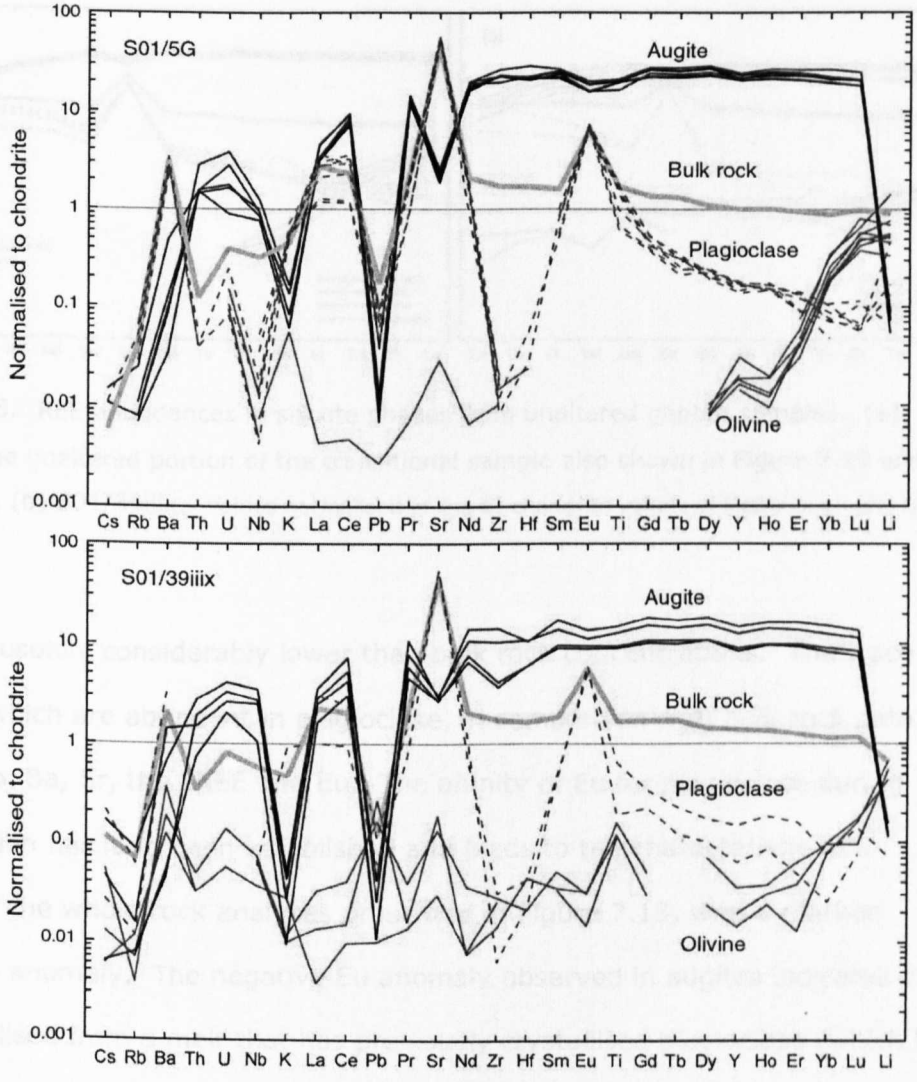

Figure 7.12. Mixed element spidergrams normalised to chondrite for two gabbroic samples from the Allalin unit. Sample S01/5G is the unaltered half of a transitional sample, the other half of which is presented in *Transitional samples* below (in Figure 7.19 and Figure 7.20). Major and trace element abundances and errors for the phases are presented in Appendix C, Tables C.1-14. Chondrite values from McDonough and Sun (1995).

However, the calculation of a mass balance for Li in the two gabbros analysed leaves a shortfall of nearly 40% in one sample (S01/5G) and over 70% in the other (S01/39iiix - Figure 7.14). Given that Li concentrations vary from 0.5 to 2.2 ppm in olivine, and to a large degree in plagioclase, it may be possible that Li is concentrated in small fluid or melt inclusions which have been trapped in the cumulate phases or that it is very heterogeneously distributed within the mineral structure itself. With the exception of Li, olivine contains low abundances of all the

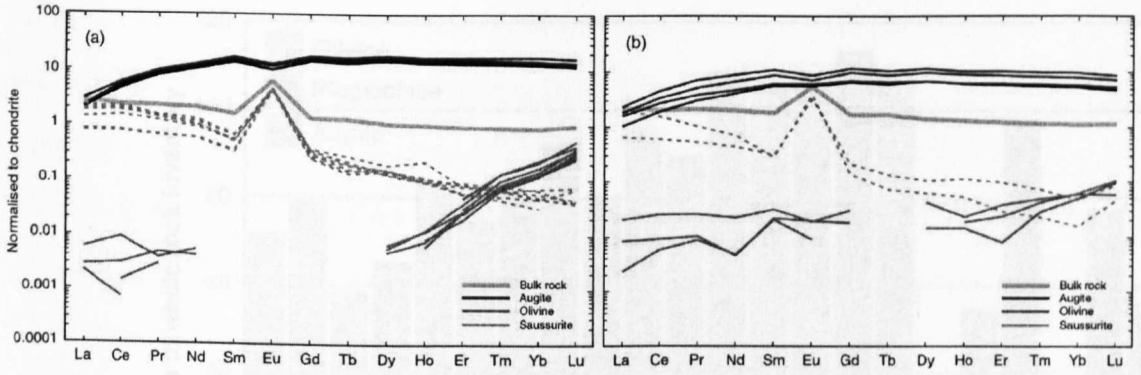

Figure 7.13. REE abundances in silicate phases from unaltered gabbro samples. (a) S01/5G – the unaltered portion of the transitional sample also shown in Figure 7.19 and Figure 7.20, (b) S01/39iiix. Values normalised to the CI chondrite values of McDonough and Sun (1995).

elements; usually considerably lower than bulk rock concentrations. The trace elements which are abundant in plagioclase, in comparison with bulk rock data, are: Cs, Rb, Ba, Sr, the LREE and Eu. The affinity of Eu for plagioclase during crystallisation has long been established and leads to the characteristic REE patterns of the whole rock analyses presented in Figure 7.13, with a marked positive Eu anomaly. The negative Eu anomaly observed in augites indicates that it has crystallised from a melt that has previously crystallised plagioclase (which has a positive Eu anomaly). This is consistent with the petrographic observation that pyroxene is anhedral and interstitial to olivine and plagioclase and therefore was the last of the major phases to crystallise.

By taking into account the modal proportions of the minerals, it can be seen that clinopyroxene, while containing the highest abundances of nearly all trace elements presented, does not house the majority of the budget of many elements, including Cs, Rb, Ba, the light REE (LREE), Sr, Eu and Li (Figure 7.14).

Olivine does not contain a significant proportion of any of the elements presented except Li. One sample (S01/5G - Figure 7.13) contains olivine which houses a considerable quantity of HREE, although conversely, olivine from the other gabbroic

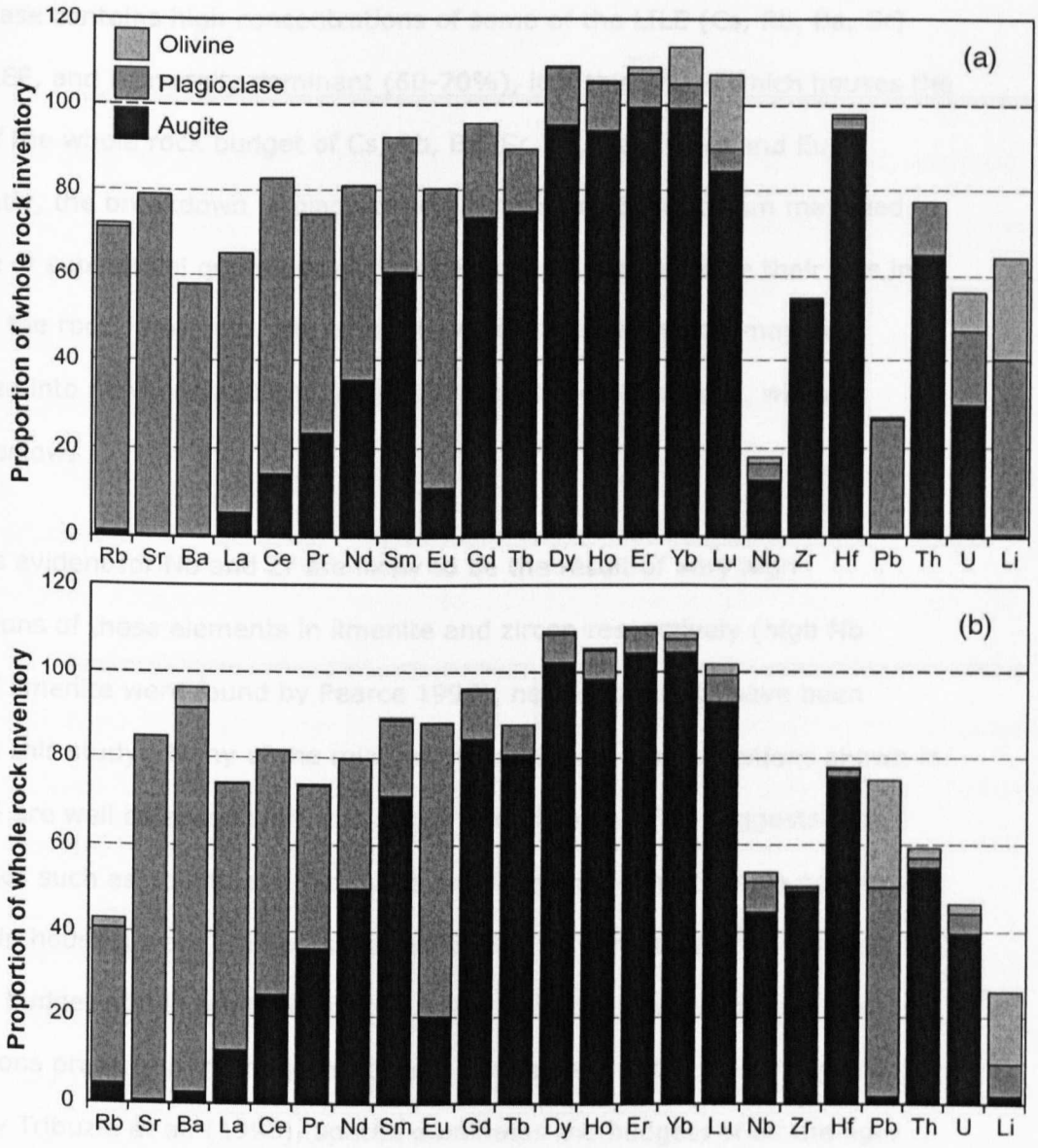

Figure 7.14. Trace element distribution within two unaltered gabbros. (a) S01/5G, (b) S01/39iiix. Modal abundances estimated from thin section observation. While few of the mineral concentrations can be precisely balanced with the whole rock budget (i.e. 100% accounted for), the inaccuracies of the estimation of modal abundance and the heterogeneous distribution of trace elements in some cases means that elements where 80-120% of the budget has been accounted for are considered well balanced. Modal proportions in the two gabbros are approximately: (a) Plagioclase – 63%, olivine – 33%, pyroxene – 4%, oxides – 0.2%, (b) Plagioclase – 68%, olivine – 21%, pyroxene – 11%, opaques – 0.2%. Major and trace element abundances and errors for the phases are presented in Appendix C, Tables C.1-14.

sample contains very low abundances of these elements. Variable contributions from olivine to the whole rock budget of U, Pb and Ta (not shown due to very low abundances in most phases) suggests the unavoidable sampling of opaque inclusions within the olivine (as mentioned under *Mineral Separates* - Section 7.1).

As plagioclase contains high concentrations of some of the LILE (Cs, Rb, Ba, Sr) and the LREE, and is modally dominant (60-70%), it is this phase which houses the majority of the whole rock budget of Cs, Rb, Ba, Sr, La, Ce, Pr, Nd and Eu. Consequently, the breakdown of plagioclase during HP metamorphism may lead to the release of substantial quantities of these elements, and facilitate their loss in fluids from the rock. However, the extent to which these elements may be incorporated into newly crystallising phases, such as epidote/zoisite, will be discussed below.

The deficits evident for Nb and Zr are likely to be the result of very high concentrations of these elements in ilmenite and zircon respectively (high Nb contents of ilmenite were found by Pearce 1990), neither of which have been analysed in this study. Many of the mineral trace element concentrations shown in Figure 7.14 are well balanced with whole rock abundances. This suggests that minor phases such as apatite and monazite are uncommon and thus do not play a major role in housing trace elements (except perhaps Th in monazite). Indeed, the whole-rock budget of P in both gabbroic samples can be accounted for by the concentrations present in the major silicates. Conversely, in the Fe-Ti-gabbros analysed by Tribuzio et al. (1996), apatite dominates the budgets of all the light and middle REE. The difference in trace element distribution between gabbroic bodies of different composition could have important implications for the release of elements during subduction, due to the variable stability fields of different minerals and assemblages.

7.5.1.2 Gabbroic eclogites

The main silicate mineral phases from two gabbroic eclogite samples have been analysed for a variety of trace elements. These data are presented, normalised to chondritic values, in Figure 7.15 and Figure 7.16. The REE concentrations have also been plotted separately in Figure 7.17. The two samples are both coronitic eclogites which have undergone complete recrystallisation but do still retain a broadly domainal structure based upon the original igneous mineralogy. One point to note is that omphacite is used here to refer to the metamorphic replacement product of augite. Omphacite is also present in the saussurite assemblage, and has slightly different major (and probably trace) element chemistry, although the individual phases of the saussurite assemblage were too fine-grained to permit individual analyses by LA-ICP-MS. Therefore, in this work the term saussurite will be used to refer to the analysis of the saussuritic assemblage: zoisite, omphacite, kyanite, paragonite and quartz.

Pyroxene domain. Sample S01/40viix contains a small quantity of metastably preserved augite (1% modal abundance), while the majority has undergone high-pressure recrystallisation to omphacite. Omphacite does not possess trace element concentrations which are as high as those present in igneous augite (with the exception of Cs, Rb, Sr and Ba) (Figure 7.15 a). The positive anomalies of Nb, Ti and possibly Zr and Hf in Figure 7.15 and Figure 7.16 are a result of the unavoidable sampling of rutile inclusions within the omphacite (Nb and Ta are strongly compatible in rutile, Zr and Hf are also typically moderately abundant; e.g. Zack et al. 2002b). These inclusions are common and occur due to the incompatibility of high abundances of Ti in the omphacite structure. The transformation from augite to omphacite clearly permits the release of some trace elements from the mineral structure (particularly LREE and MREE - Figure 7.17 and Figure 7.18). This is important, as these elements will either be incorporated into another stable phase, or they may be lost from the sample, if there is a medium of

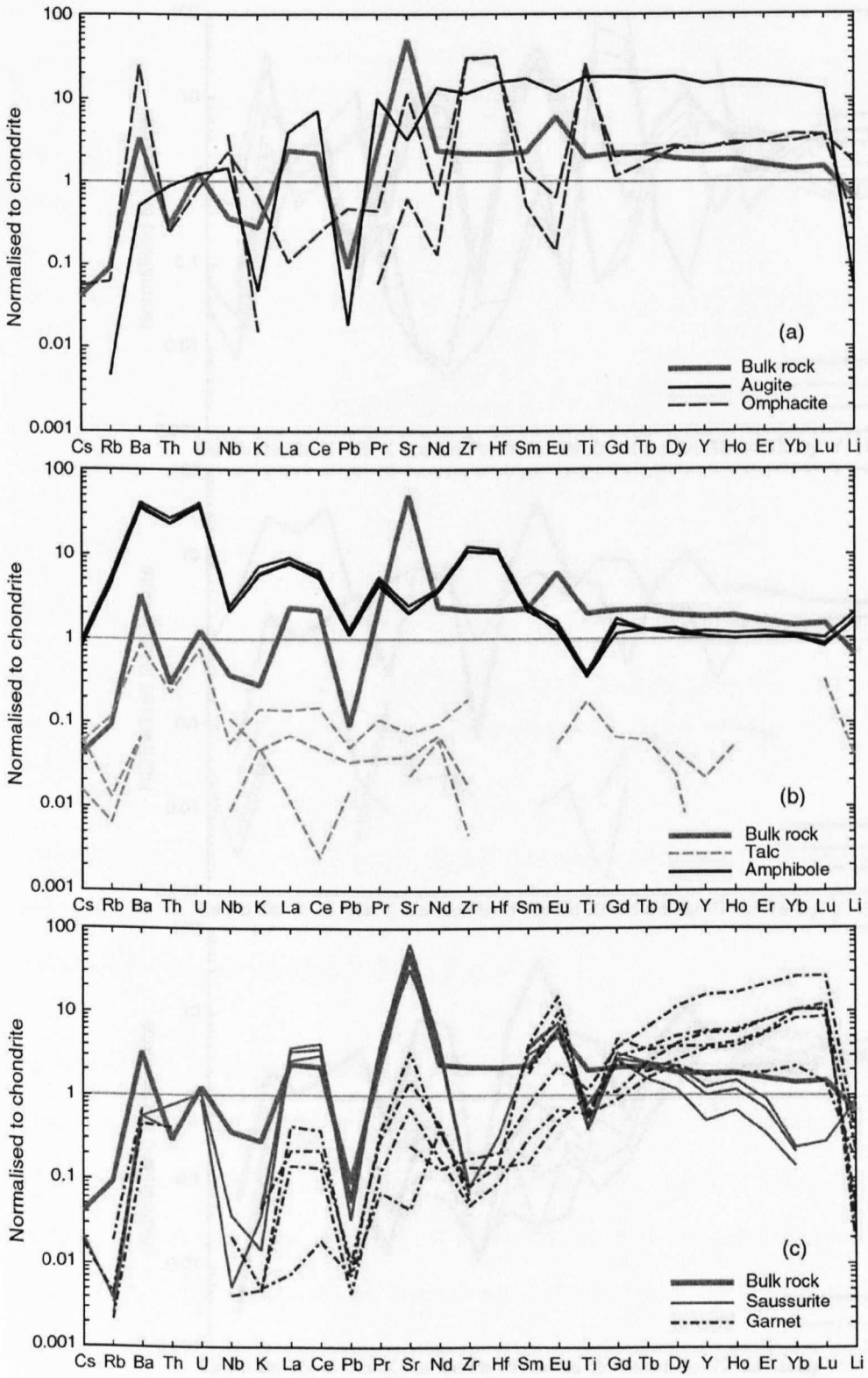

Figure 7.15. Mixed element spidergrams normalised to chondrite for silicate phases from a gabbroic eclogite (S01/40viix) from the Allalin unit. (a) igneous augite and its HP replacement product, omphacite, (b) amphibole (actinolite) and talc which have replaced olivine, (c) garnet and saussurite, which is the fine-grained HP recrystallisation product of plagioclase (zoisite + omphacite + kyanite ± paragonite ± quartz – see Section 3.3.1.2). Values normalised to the CI chondrite values of McDonough and Sun (1995).

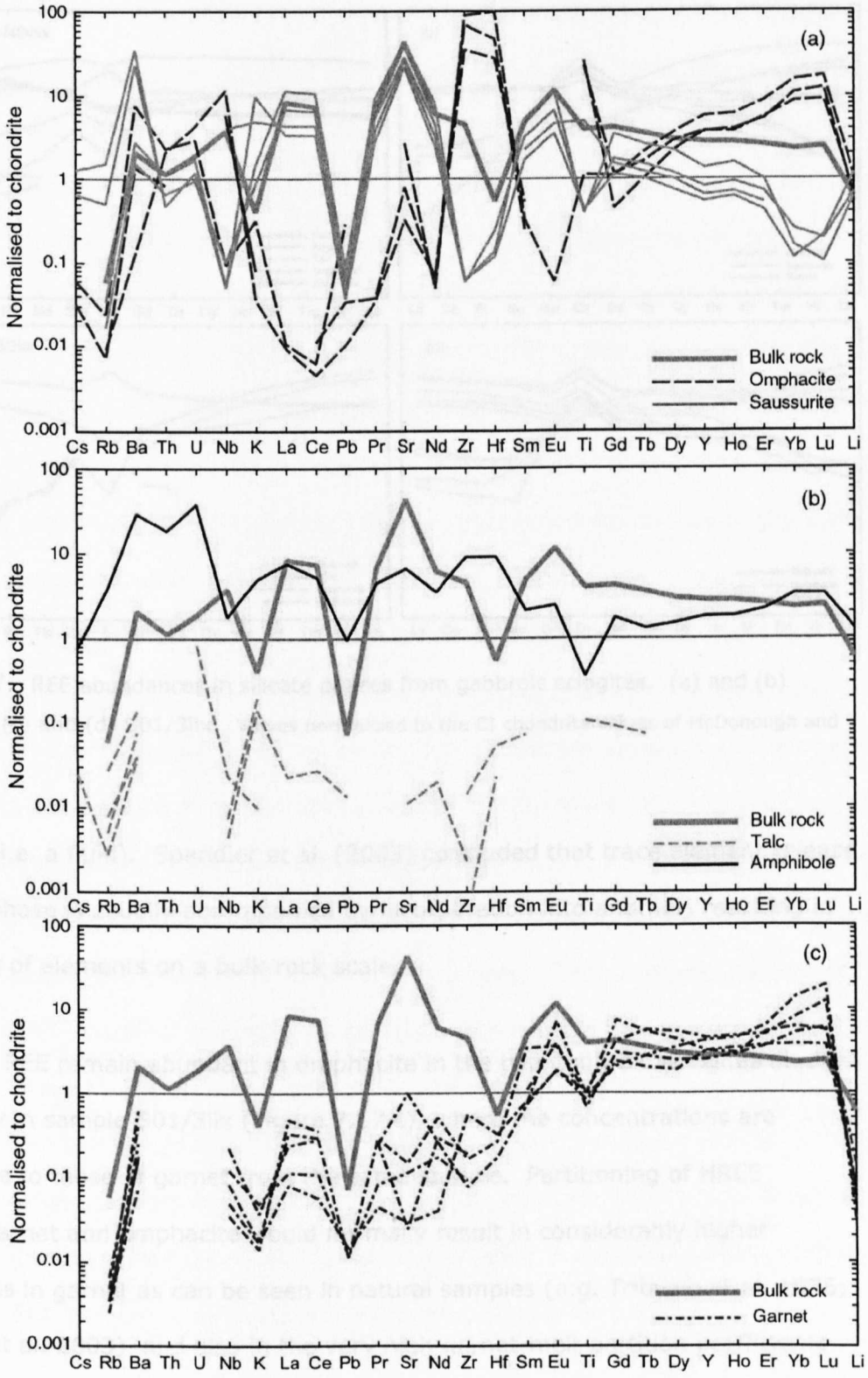

Figure 7.16. Mixed element spidergrams for silicate mineral phases from a gabbroic eclogite (S01/3iix). (a) omphacite from the augite domain and saussurite, which is the fine-grained HP recrystallisation product of plagioclase (zoisite + omphacite + kyanite ± paragonite ± quartz – see Section 3.3.1.2). Values normalised to the CI chondrite values of McDonough and Sun (1995). Major and trace element abundances and errors for the phases are presented in Appendix C, Tables C.1-14.

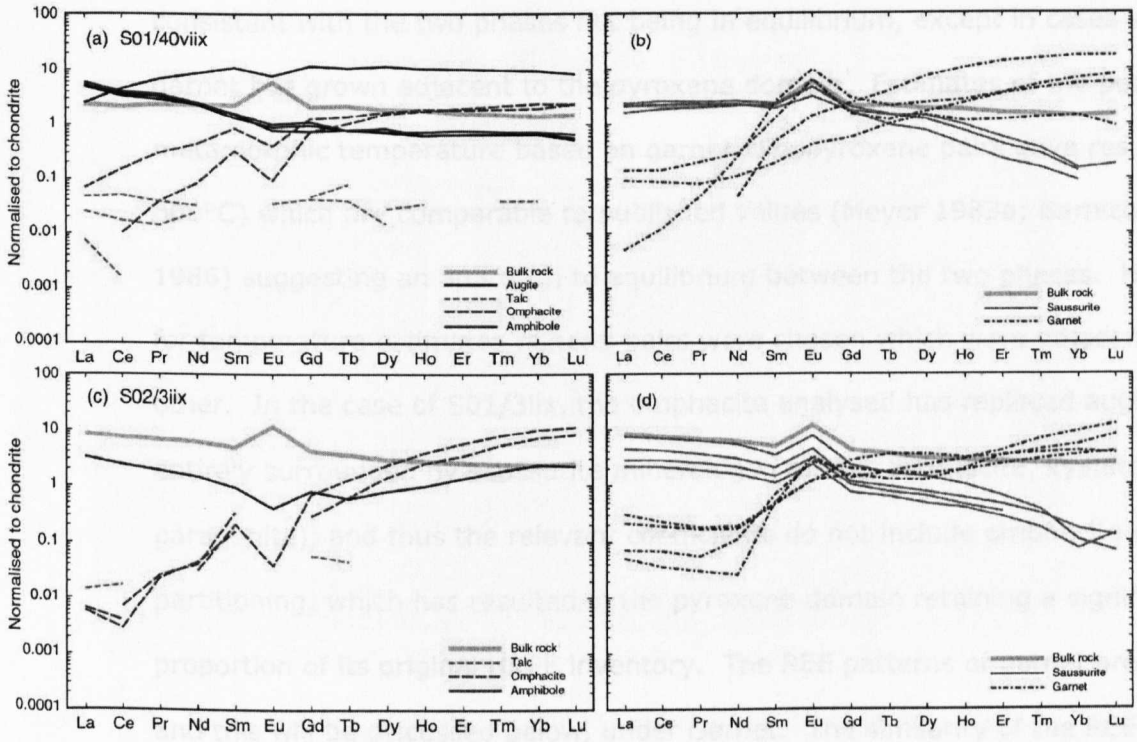

Figure 7.17. REE abundances in silicate phases from gabbroic eclogites. (a) and (b) S01/40viix, (c) and (d) S01/3iix. Values normalised to the CI chondrite values of McDonough and Sun (1995).

transport (i.e. a fluid). Spandler et al. (2003) concluded that trace element release from one phase is usually accompanied by incorporation into another, resulting in no net loss of elements on a bulk-rock scale.

The heavy REE remain abundant in omphacite in the two gabbroic eclogites studied, particularly in sample S01/3iix (Figure 7.17 c), where the concentrations are comparable to those of garnet from the same sample. Partitioning of HREE between garnet and omphacite would normally result in considerably higher abundances in garnet as can be seen in natural samples (e.g. Tribuzio et al. 1996; Spandler et al. 2003) and also in the very high garnet-melt partition coefficients for the HREE (see van Westrenen et al. 2000; 2001), thus, the minerals analysed here do not appear to have attained equilibrium. As omphacite pseudomorphs igneous augite, whereas garnet has grown at the interface of different mineral domains (particularly between olivine and plagioclase), the petrographic evidence is

consistent with the two phases not being in equilibrium, except in cases where garnet has grown adjacent to the pyroxene domain. Estimates of the peak metamorphic temperature based on garnet-clinopyroxene pairs gave results (500-600°C) which are comparable to published values (Meyer 1983a; Barnicoat and Fry 1986) suggesting an approach to equilibrium between the two phases. However, for temperature estimates mineral pairs were chosen which were adjacent to each other. In the case of S01/3iix, the omphacite analysed has replaced augite which is entirely surrounded by saussurite mineralogy (zoisite, omphacite, kyanite, paragonite), and thus the relevant coefficients do not include omphacite-garnet partitioning, which has resulted in the pyroxene domain retaining a significant proportion of its original HREE inventory. The REE patterns of garnet are unusual, and this will be discussed below, under *Garnet*. The similarity of the REE chondrite-normalised patterns for omphacite and augite (but with the latter containing much greater abundances) is consistent with omphacite compositions being controlled to a large extent by the precursor augite. Furthermore, the negative Eu anomalies of omphacite analyses are probably inherited from the igneous augite, combined with the retention of anomalously high Eu in the mineralogy which has replaced the plagioclase (saussurite minerals and garnet). The lower abundances of LREE and MREE retained in omphacite (compared to HREE) may be a result of the lower compatibility of these elements in omphacite, and may also be due to the partitioning of the LREE into zoisite in the surrounding saussurite. From the evidence of subduction zone magmatism, the LREE are thought to be more mobile than the HREE, and this may also be a factor in determining the fractionation of REE between omphacite and the surrounding phases.

In contrast, the concentrations of REE presented for omphacite and garnet from basaltic eclogites (see Section 7.5.2 below) display more conventional partitioning between the two phases, with garnet more enriched in the HREE by three orders of magnitude. The metabasaltic samples clearly show at least an approach to large

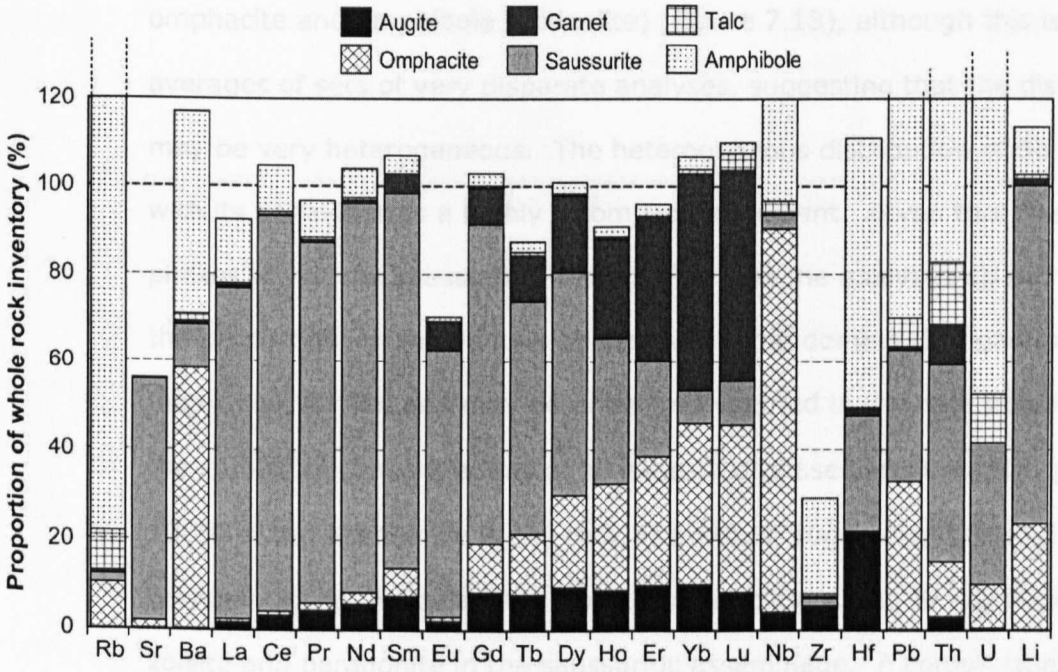

Figure 7.18. Trace element distribution within a coronitic gabbroic eclogite (S01/40viix). When 80-120% of the whole rock budget is accounted for, the element is considered to be well balanced. Modal proportions in S01/40viix are approximately: (a) Saussurite – 50% (of which ~70% is zoisite, 20% is omphacite and the remainder is kyanite, paragonite and quartz), talc – 18%, actinolite – 7%, omphacite – 15%, garnet – 9%, opaques – 0.5%. Major and trace element abundances and errors for the phases are presented in Appendix C, Tables C.1-14.

scale equilibrium due to the greater degree of deformation which they have experienced.

Plagioclase domain. Due to the very fine grained nature of the saussurite assemblage, it was not possible to obtain analyses which solely represent an individual phase from within the assemblage. Consequently, the application of precise major element data for internal calibration was not possible (although care was taken to apply the most accurate major element data) and therefore the data is quantitatively subject to a greater error than analyses of the other phases.

The composition of the saussurite domain retains its diagnostic plagioclase enrichments of Sr, Eu and the LREE (Figure 7.15 c and Figure 7.16 a). Barium, however, is much less abundant in saussurite than in the plagioclase of the unaltered gabbroic samples. The majority of the Ba budget is contained in

omphacite and amphibole (actinolite) (Figure 7.18), although this is based on the averages of sets of very disparate analyses, suggesting that the distribution of Ba may be very heterogeneous. The heterogeneous distribution of Ba is consistent with its behaviour as a highly incompatible element. Given that there are several phases within the saussurite, it is possible that the analyses do not fully represent the proportions of the various phases within the domain (i.e. paragonite is usually a major host for Ba, and may be under-represented in the data obtained), although the combined concentrations of all measured phases accounts for approximately 100% of the abundance in the rock as a whole, suggesting the analyses are representative. Following the breakdown of plagioclase, Sr will be incorporated into zoisite and paragonite in the saussuritic assemblage. A comparison of the data from Figure 7.17 with that of the unaltered gabbros in Figure 7.13 suggests that there has been a degree of enrichment of the MREE, and possibly the LREE, in the saussurite. This observation is confirmed by the greater relative contribution of saussurite than plagioclase to the whole rock budget of the MREE (Figure 7.14 and Figure 7.18). The loss of LREE from the clinopyroxene domain may have resulted in the supply of LREE to the plagioclase domain during recrystallisation.

Olivine domain. Whereas olivine is a major contributor to the whole rock budget of Li, the recrystallised olivine domain (predominantly talc) contains very little Li (Figure 7.15 and Figure 7.16), and the majority of the Li budget is housed in the saussurite domain in gabbroic eclogites, probably in the fine-grained omphacite (Figure 7.18). The omphacite which pseudomorphs augite also contains a significant proportion of the whole-rock Li budget (~25%). Actinolite, tremolite or glaucophane (actinolite in S01/40viix, glaucophane in S01/3iix) which also forms a part of the olivine domain assemblage contains high concentrations of Li (2.5 ppm) but is volumetrically inferior to talc. Talc contains very low concentrations of all elements presented, with the possible exception of Ba, Th and U in two analyses

(Figure 7.15 and Figure 7.16). The redistribution of Li throughout the sample (even into the omphacite which pseudomorphs augite) suggests significant mobility of Li.

The most striking feature of the olivine domain mineral chemistry is the high abundance of the LILE, Cs, Rb, Ba, Th and U, as well as the LREE contained in amphibole (Figure 7.15, Figure 7.16 and Figure 7.17). Actinolite, despite accounting for only ~5% of the rock by modal proportion, is a major repository for Rb, Ba, Hf, Pb, Th and U (Figure 7.18). The presence of high concentrations of these elements, compared to the original olivine composition, is evidence of the transfer of these elements at least on a domain scale. It may be possible that much of the Ba, U and Th are derived from the plagioclase domain as a result of the breakdown of plagioclase. However, another possibility is that some of the enrichment of these elements occurred during the hydrothermal alteration episode witnessed by the eclogitic samples in the Allalin unit. The fact that most of these elements are fluid-mobile serves to add weight to the latter theory.

Garnet. The REE profiles of garnets from the two gabbroic eclogite samples are presented in Figure 7.17. REE abundances in garnets are usually characterised by extreme enrichment in the HREE (10-1000 times greater than chondrite, e.g. Tribuzio et al. 1996; Spandler et al. 2003) and depletion in the LREE (~0.001 to 0.01 of average chondrite). The garnets from the samples analysed in this study display less extreme fractionation of the REE, with surprisingly high concentrations of the LREE, given the low abundances in the whole rock. Strong positive Eu anomalies are also found in some of the garnets analysed. The existence of Eu anomalies is indicative of growth from plagioclase without extensive influx or outflux of elements (i.e. approaching isochemical). The patterns observed are good indicators that garnet compositions are not in equilibrium with the compositions of other phases within the sample.

Many garnets are strongly enriched in Sr and Ba which is also a reflection of their growth from a plagioclase precursor. Garnet possesses a significant amount of the middle and heavy REE, and in the case of sample S01/40viix, contains approximately 50% of the whole rock budget of Yb and Lu, despite constituting less than 10% of the rock by modal abundance, and also without the classic extreme enrichment in the HREE which is displayed in the basaltic eclogite samples presented in Section 7.5.2.

Transitional eclogites

Detailed petrographic information on transitional samples is presented in Section 3.3.1.2. Transitional eclogites are characterised by the pervasive recrystallisation of plagioclase and the partial recrystallisation of olivine. Augite has been largely preserved metastably, although it sometimes develops narrow coronas of garnet. Plagioclase has been pseudomorphed by saussurite: a fine grained assemblage of zoisite, omphacite, kyanite, paragonite and quartz. Olivine develops coronas of enstatite, chlorite and garnet from the interior to exterior of the domain. Mixed element and REE concentrations of the major silicate phases are presented in Figure 7.19 and Figure 7.20.

Olivine domain. Chlorite and enstatite have both crystallised in the olivine domain as a result of the infiltration of water and of various major elements (see Section 3.3.1.2). As well as increases in major elements (e.g. Al), the abundances of trace elements in chlorite and enstatite (both marked as 'chlorite' in Figure 7.19 and Figure 7.20) display enrichment with respect to olivine. The REE profiles of chlorite and enstatite are remarkably flat, but more elevated than olivine. On the mixed element plot, enrichment in Ba and negative Pb anomalies are evident. The enrichment of Rb, Ba, Th and U in amphibole in the olivine domain of gabbroic eclogites could be due to influx of these elements during hydrothermal alteration or high-pressure fluid flow (and therefore enrichment by an externally derived fluid),

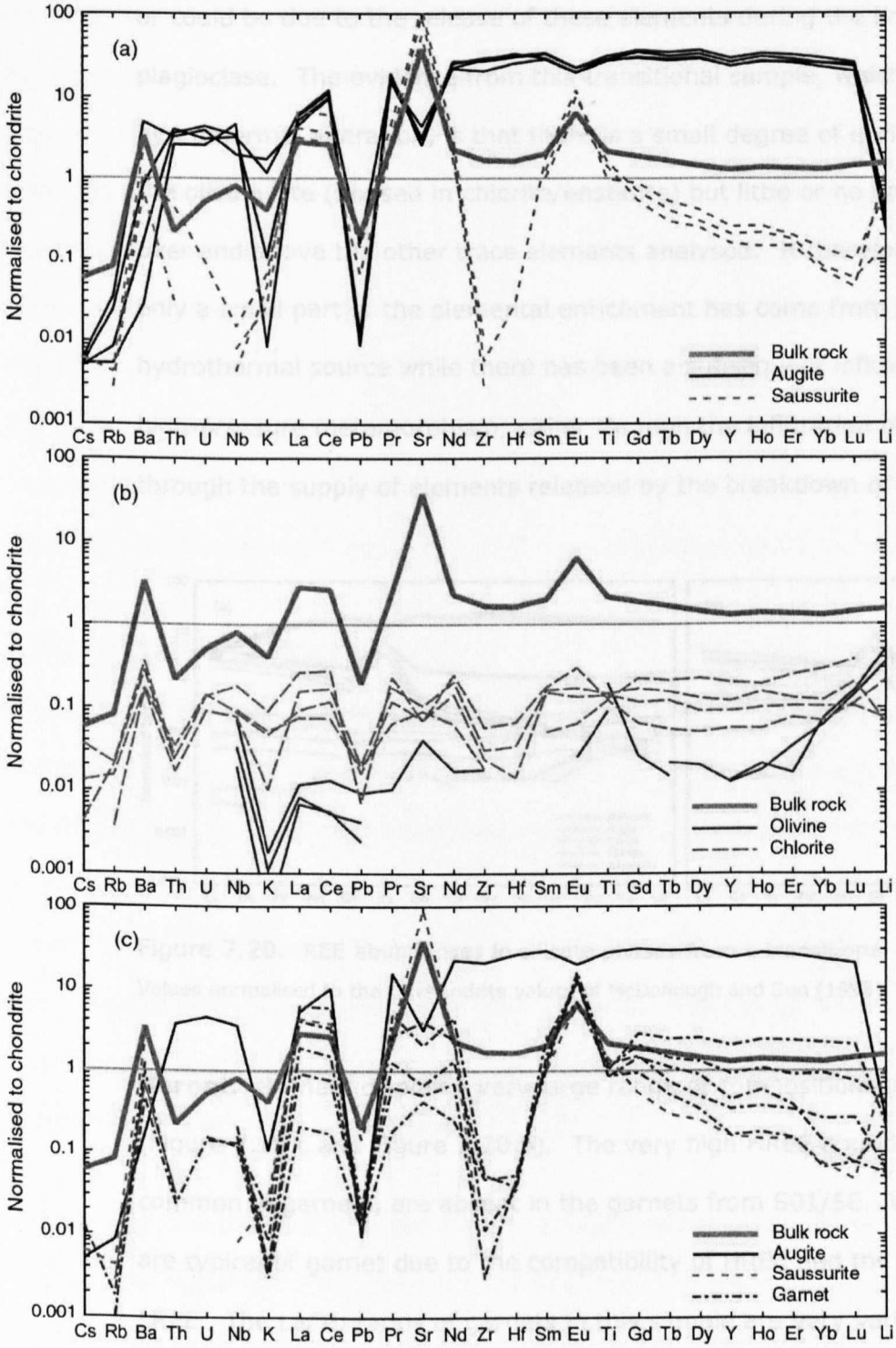

Figure 7.19. Mixed element spidergrams for silicate mineral phases from a transitional eclogite sample (S01/5E). This sample is part of the transitional sample S01/5, the other part, S01/5G, is unaltered gabbro and has been presented in Section 7.5.1.1. (a) igneous augite and saussurite, which is the fine-grained HP recrystallisation product of plagioclase (zoisite + omphacite + kyanite ± paragonite ± quartz – see Section 3.3.1.2). (b) olivine domain mineralogy, 'chlorite' includes data from analysis of enstatite. (c) garnet, note the large range of compositions. Major and trace element abundances and errors for the phases are presented in Appendix C, Tables C.1-14.

or could be due to the release of these elements during the breakdown of plagioclase. The evidence from this transitional sample, which has undergone some hydrothermal alteration, is that there is a small degree of enrichment in Ba within the olivine site (housed in chlorite/enstatite) but little or no enrichment in U and Th over and above the other trace elements analysed. It therefore seems likely that only a small part of the elemental enrichment has come from an externally derived hydrothermal source while there has been a subsequent influx of elements during high-pressure metamorphism, either through the infiltration of an external fluid or through the supply of elements released by the breakdown of plagioclase.

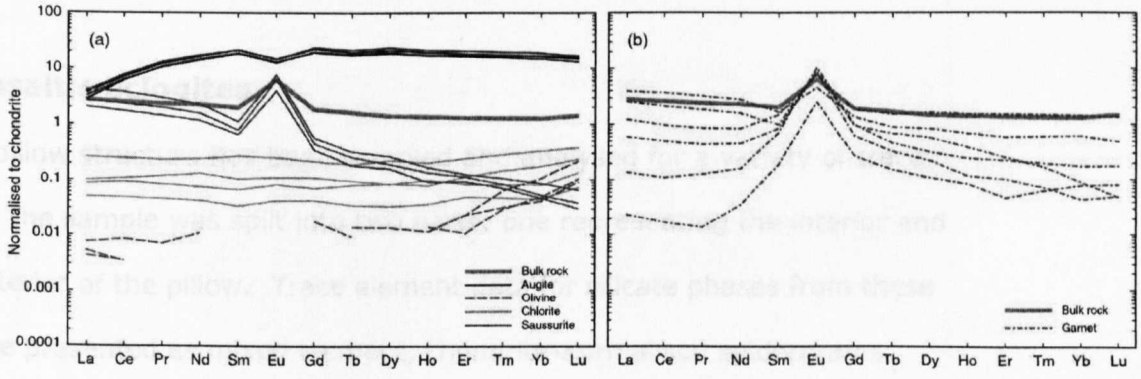

Figure 7.20. REE abundances in silicate phases from a transitional eclogite (S01/5E). Values normalised to the CI chondrite values of McDonough and Sun (1995).

Garnet. Garnets display a very large range of compositions in terms of REE and Sr (Figure 7.19 c and Figure 7.20 b). The very high HREE abundances which are common in garnets, are absent in the garnets from S01/5E. Very low La/Yb ratios are typical of garnet due to the compatibility of HREE and the incompatibility of the LREE. The La/Yb ratios of garnets in this sample are very variable and much higher than is normally the case (0.07 to 43). In contrast, La/Yb ratios from the gabbroic eclogite, S01/40viix, are typically around 0.006. The garnet analyses from the basaltic eclogites presented in the following section have even lower La/Yb ratios with an average of ~0.003. The unusual REE patterns observed in the transitional eclogite are a result of the limited availability of certain elements. The LREE appear to have been abundantly available due to the breakdown of plagioclase, whereas

the HREE are retained in the metastably preserved augite and thus have not been available for incorporation into garnet (augite contains 80-90% of the HREE whole rock budget in S01/5G). Consequently, the REE profiles of garnets bear a clear resemblance to the saussurite REE profiles, including a very marked positive Eu anomaly (Figure 7.20). This is an extreme example of disequilibrium between garnet and clinopyroxene. The garnet compositions of the gabbroic eclogites exhibit an approach to equilibrium in some cases. The control by augite, on the mid to heavy REE budget, is also evident in the lack of an increased MREE composition of the saussurite when compared to the plagioclase of the unaltered portion of this transitional sample (S01/5G – see previously under Section 7.5.1.1).

7.5.2 Basaltic eclogites

A basaltic pillow structure has been sampled and analysed for a variety of trace elements. The sample was split into two parts: one representing the interior and one the exterior of the pillow. Trace element data for silicate phases from these portions are presented as mixed element, chondrite-normalised spidergrams (interior: Figure 7.21 and exterior: Figure 7.22), and REE patterns (Figure 7.23). The trace element data obtained have been combined with modal abundance estimates of the phases, in order to assess the relative contributions of the different phases to the whole rock budget (Figure 7.24).

The cores of garnets from both parts of the eclogitic basalt pillow possess considerably higher concentrations of the HREE and LREE than the garnet rims. This feature can be explained by growth zoning. The compatibility of the HREE in garnet leads to strong partitioning of these elements into garnet. The abundances of HREE outside the garnet core are lower due to prior depletion of these elements after strong partitioning into garnet, during the initial stages of growth. The trace element abundances in phases from the interior and exterior of the pillow are very similar, as would be expected from their crystallisation from the same bulk rock

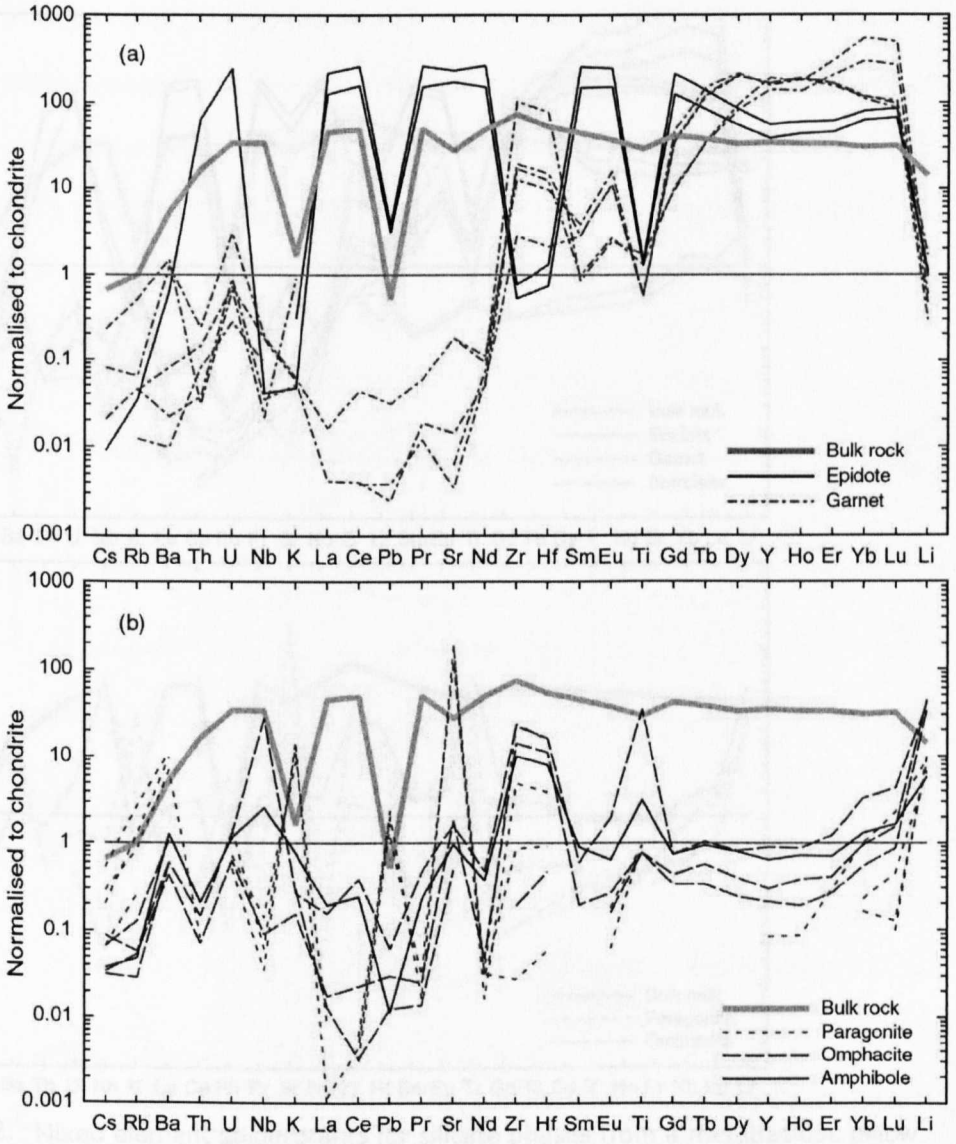

Figure 7.21. Mixed element spidergrams for silicate phases from a metabasaltic pillow interior. Concentrations normalised to the CI chondrite values of McDonough and Sun (1995)

composition. However, there are differences in the REE abundances of garnet cores from the two portions of the pillow, with somewhat higher HREE abundances in the cores of garnets from the pillow interior. A possible explanation could be that the measured cores of the garnets of the pillow interior represent the initial stage of garnet growth whereas those measured from the pillow exterior grew somewhat later, although the comparable size of the garnets analysed makes this explanation less plausible. An alternative possibility does not clearly present itself. The HREE abundances of epidote are also different between the pillow interior and exterior, with the most HREE-rich epidote in the central portion of the pillow.

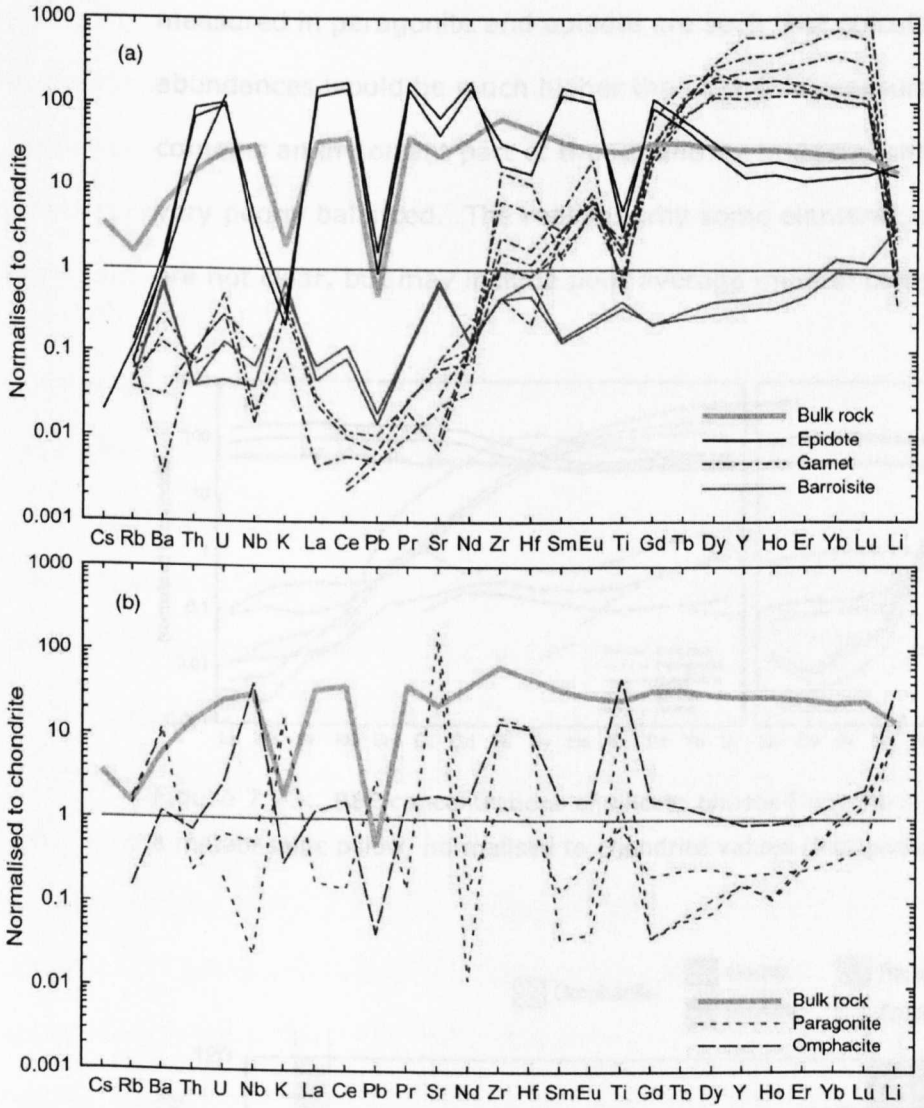

Figure 7.22. Mixed element spidergrams for silicate phases from a metabasaltic pillow exterior. Major and trace element abundances and errors for the phases are presented in Appendix C, Tables C.1-14.

Although Figure 7.24 shows that the whole rock concentrations of several elements are poorly balanced by the abundances in the minerals analysed, the REE, Li and U are well balanced. Two phases account for the majority of the budget of all the REE, Pb, Sr, Th and U in sample S01/75iiiC. Garnet contains a significant proportion of the mid to heavy REE (60-70% for Yb and Lu) and epidote houses almost all the LREE and MREE budget and contributes greatly to the HREE. In addition, epidote dominates the budgets of U and Th, and together with paragonite, accounts for almost all of the Sr and Pb in the whole rock. The concentrations

measured in paragonite and epidote are such that calculated whole rock abundances would be much higher than the true measured values. Paragonite also contains an important part of the Rb and Ba budgets, although these elements are very poorly balanced. The reasons why some elements are poorly accounted for are not clear, but may include poor average mineral compositions due to a limited

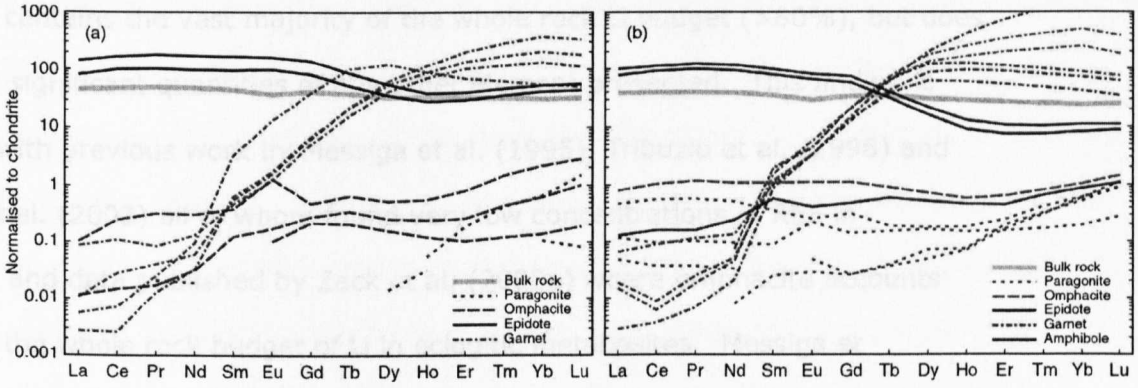

Figure 7.23. REE concentrations of silicate phases from the interior (a) and exterior (b) of a metabasaltic pillow, normalised to chondrite values (McDonough and Sun 1995).

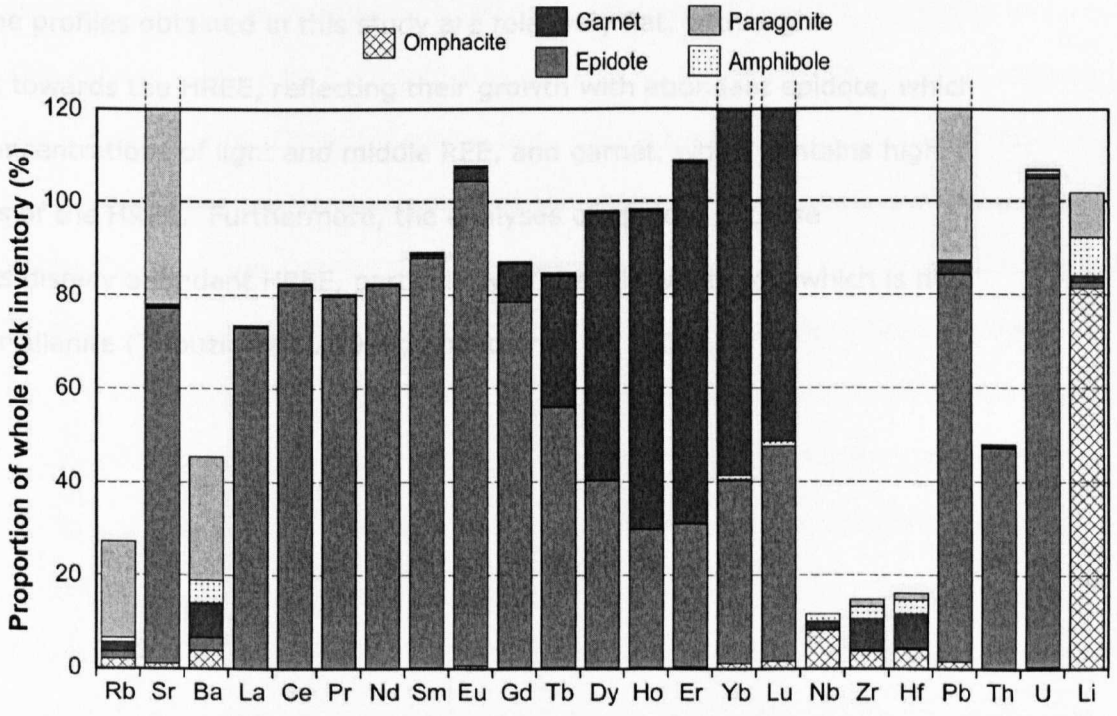

Figure 7.24. Trace element distribution within a basaltic eclogite (S02/75iiiC). When 80-120% of the whole rock budget is accounted for, the element is considered to be well balanced. Modal proportions in S01/75iiiC are approximately: (a) Omphacite – 32%, garnet – 17%, epidote – 20%, paragonite (and minor phengite): 16%, retrogressive amphibole (barroisite) – 15%, oxides – 0.1%.

number of analyses (and heterogeneity), and/or errors in the estimation of modal abundances. The budgets of Nb, Zr and Hf will be dominated by rutile and zircon, neither of which were analysed in this study, although the minor contribution of omphacite to the budgets of Nb, Zr and Hf is almost certainly due to the unavoidable sampling of small rutile inclusions within the omphacite crystals.

Omphacite contains the vast majority of the whole rock Li budget (>80%), but does not contain significant quantities of any other element presented. This finding is consistent with previous work by Messiga et al. (1995), Tribuzio et al. (1996) and Spandler et al. (2003) all of whom found very low concentrations of REE in omphacite, and data published by Zack et al. (2002a) where omphacite accounts for 80% of the whole rock budget of Li in eclogitic metabasites. Messiga et al.(1995) and Tribuzio et al. (1996) found that the REE patterns of omphacite were bell-shaped and richest in the MREE due to their growth with allanite (which strongly partitions the LREE) and garnet (which is enriched in the HREE). In contrast, the profiles obtained in this study are relatively flat, with slight enrichment towards the HREE, reflecting their growth with abundant epidote, which has high concentrations of light *and* middle REE, and garnet, which contains high abundances of the HREE. Furthermore, the analyses of epidote in these metabasalts display abundant HREE, particularly in the pillow interior, which is not the case for allanite (Tribuzio et al. 1996; Spandler et al. 2003).

8 Discussion and consequences

This chapter will first discuss possible mechanisms and conditions which promote chemical modification of the down-going slab, including deformation, fluid flow and mineralogical reactions. Secondly, I will assess whether losses of mobile elements in the ZSO mafic samples are systematic, with loss of one element being accompanied by loss of another, and also attempt to relate losses to deformation, fluids or mineralogical transformations. In the third section of this chapter, the implications of the findings of this study for fluxes from mafic crust will be outlined. In the last section, a quantitative assessment of the effects of subducting oceanic crust on the Os isotopic signature of mantle reservoirs is presented, in the light of new data for gabbroic and basaltic oceanic crust presented in this work.

Are the samples studied typical of subducted oceanic crust?

When inferring possible processes and outcomes from relatively small suites of samples, it must be considered whether or not the samples are representative. This is particularly true for subduction settings where the whole rock composition, the P-T conditions of metamorphism and the extent of deformation and fluid flow must be assessed. The apparent difference in Re behaviour between the metagabbros of the Zermatt-Saas and Sulitjelma ophiolites, which have undergone different metamorphic histories, illustrates this point well (see Chapter 6 and Section 6.3.2.3 in particular). Moreover, across-arc variations in trace element compositions have been observed (e.g. Ishikawa and Nakamura 1994; Ryan et al. 1995) and it is possible that these variations result from changes in trace element mobility with increasing depth of the slab. Indeed, decreasing mobile element concentrations have been correlated with increasing metamorphic grade by Moran et al. (1992), Bebout et al. (1993) and Bebout (1995). Both of these conclusions emphasise that the data from the suites of samples analysed in this study may only be representative of rocks which have experienced similar P-T conditions,

deformation and fluid flow. That said, the following conclusions in this chapter will be based upon the assumption that the behaviour of elements in the rocks analysed can be applied to similar lithologies which have undergone subduction.

Gabbros. The Allalin unit is a gabbroic body that remains largely intact despite subduction and subsequent exhumation. Consequently, the degree of deformation in some parts of the body is low. The unit experienced partial infiltration by hydrothermal fluids on the seafloor, and has undergone fluid loss during high-pressure (HP) metamorphism, although the presence of numerous hydrous phases (particularly amphibole and talc, but also zoisite and chloritoid) has facilitated the retention of <1.5 % water. Therefore, further dehydration upon subduction to greater depths cannot be ruled out. Nonetheless, parts of the gabbro which had undergone pervasive hydrothermal alteration (as evidenced by oxygen isotopes and mineralogy - see Section 3.3.1.2) are likely to have lost a significant proportion of their water content (chlorite is abundant in samples which retain some of their seafloor metamorphic assemblage). However, the lack of deformation would have hindered the transport and escape of fluids from the body. Nevertheless, veins containing garnet, chlorite, amphibole and carbonate are evidence of fluid flow under HP conditions in the Allalin unit.

The presence of almost pristine gabbro, despite having experienced P-T conditions > 2.0 GPa and 600°C, would at first appear to be atypical. However, there are numerous examples of gabbroic bodies that retain their igneous structure and some of their mineralogy despite HP metamorphism (e.g. Monviso, western Alps (Nisio et al. 1986; Messiga et al. 1999), Rocciavrè, Western Alps (Pognante 1982a; b) and Flemsøy, western Norway (Mørk 1985; 1986). Moreover, the units in the Alps have also experienced a strong compressive regime during mountain building, which is in addition to the stresses experienced during subduction itself. Therefore, it is possible that the igneous structure of these units was even better preserved prior

to their incorporation in the orogenic event. The coherent nature of gabbroic bodies and their intrusion into the lower crust, away from the slab margin and the main zone of strain, is probably a major factor controlling the extent (or lack of) deformation.

The spreading regime under which the oceanic crust was formed could have a control on the extent of deformation and hydration and therefore on the processes occurring during subduction. In Section 2.2.1 the structure of oceanic crust at slow and fast spreading centres is compared. Fast spreading ridges generate crust which is largely coherent and not extensively faulted, whereas oceanic crust at slow spreading ridges tends to be deeply faulted. The presence of tectonic structures in the crust will encourage the flow of fluid and thus may result in a greater extent of hydration and probably greater deformation and fluid loss during subduction. However, it is difficult to quantify what proportion of the slab passes deep into subduction zones without extensive deformation.

Basaltic eclogites. The basaltic eclogites of the ZSO have undergone seafloor alteration (see major element data in Chapter 4) and have subsequently been completely recrystallised during eclogite facies metamorphism. In contrast to the gabbros, no igneous mineralogy or texture is preserved. However, the retention of (elongated) pillow structures in many samples precludes intense deformation. The pillows also retain a broad similarity with unaltered pillows in that they are finer grained towards the exterior. The other metabasaltic samples are devoid of any structural evidence of their prior existence as basaltic material, and thus the samples chosen cover a range of deformation and should be fairly representative of the basaltic upper portion of the subducted slab.

Most samples, with the exception of the Allalin basalts, were chosen for their well-preserved eclogite facies assemblages, and thus should only represent the process of burial and not subsequent modification during exhumation.

8.1 Factors controlling the extent of chemical modification

In order to facilitate significant fluxes of elements over distances greater than the sample scale, it is necessary to invoke a free fluid phase and to permit its movement through the rock. While fluids do not require deformation in order to infiltrate samples, the processes involved in deformation result in lines of structural weakness which may be exploited by fluids and may allow considerably higher fluid fluxes to pass through the rock. The establishment of fluid flow along shear zones has been long established, as has the observation that this flow results in chemical modification of the rock. The *extent* to which the chemistry is modified has been a source of debate and appears to be dependent on many factors, discussed in the following section.

Chemical modifications along fluid pathways: evidence from the literature

Whether or not geochemical modifications are evident in subduction-related rocks probably depends to a large degree on the presence of fluid pathways along which elements can be transported. It seems likely that the loss of elements from the slab during HP metamorphism will be focussed along shear zones with accompanying fluid flow. Evidence from shear zones under P conditions of approximately 1.5 GPa, from Tinos island, Greece showed that fluid flow occurred in a broad zone of up to 100m, but with the highest fluid-rock ratios at the tectonic contact (Matthews et al. 1999).

The chemical changes produced by fluid-rock interaction depend on many factors such as the P-T conditions, protolith chemistry, composition of the fluid and the fluid-rock ratio (Selverstone et al. 1991). Selverstone et al. (1992) identified variations in the activity of water between layers within banded mafic eclogites from the Tauern Window, Austria. Thus, differences in fluid-rock interaction may occur over relatively small scales and may result in variable elemental depletions.

High-pressure fluids can contain very high concentrations of dissolved solute (Philippot and Selverstone 1991; Scambelluri and Philippot 2001) and are often of NaCl-rich composition. From this evidence, it would appear likely that high-pressure vein conduits and shear zones provide a mechanism of transporting significant fluxes of elements into the mantle wedge. However, largely on the basis of oxygen isotope data, Nadeau et al. (1993) and van Wyk et al. (1996) concluded that the length-scale and chemical modification of fluids at HP may be small. Conversely, evidence from lower pressure shear zones which developed during exhumation, indicates considerable chemical modification due to much greater fluid-rock ratios, suggesting this is the dominant controlling factor (McCaig et al. 1990; Selverstone et al. 1991; Cartwright and Buick 1999).

This observation may explain the mobility of Re in the metagabbroic samples from the Allalin unit which have undergone fluid flow and concomitant recrystallisation at greenschist-facies conditions. The lack of modification observed along HP fluid pathways may be a result of low fluid-rock ratios, combined with the local derivation of the fluid. Long length-scale fluid flow at lower pressures juxtaposes rocks with fluids that are exotically derived, and thus are likely to carry a different geochemical signature.

Poli and Schmidt (2002) concluded that fluids leaving the slab would in general be water-rich, and CO_2- and trace element-poor, and this has been reaffirmed by the modelling of Manning (2004). This is hard to reconcile with the hypothesis for large scale elemental fluxes from the slab into the mantle wedge, unless the fluid flux is high. It is possible that a considerable amount of flux into the mantle wedge occurs at shallower levels and is then transported in the mantle wedge by means of 'corner flow'. An alternative mechanism for some of the trace element enrichments observed in arc magmas could be the stripping of elements from the mantle wedge as proposed by Arculus and Powell (1986) and discussed in Chapter 2.

It is clear that fluid-rock interactions are highly variable and preclude the determination of precise processes which may control the flux of particular elements, without a greater knowledge of the effects of P, T and fluid and rock composition.

Mineral reactions and mineral-fluid interactions

Several examples of the decomposition of minerals are proposed in Section 8.2 as possible mechanisms to allow the release of some elements from ZSO samples. However, the evidence from Section 7.5 suggests that metamorphic phases form in the slab which strongly partition some of the more fluid-mobile elements (e.g. LILE in paragonite, LREE, Sr, U and Pb in epidote). Zoisite is stable to approximately 3.0 GPa, while lawsonite, present in relatively cold subduction settings (originally present in ZSO metabasalts, but pseudomorphed by zoisite) remains stable up to pressures of 9 GPa (Poli and Schmidt 2002). The stability field for paragonite is beyond 2.5 GPa, though not as great as the K-rich mica - phengite. The stability of these minerals to approximately sub-arc depths suggests the possibility that they are the source of some of the elemental flux from the slab. However, Poli and Schmidt (2002) emphasise the continuous nature of mineral reactions and do not envisage mineral breakdown being associated with a particular depth. Spandler et al. (2003) also conclude that mineral breakdown alone is unlikely to cause elemental release due to the incorporation of elements into newly crystallising phases. However, if fluid flow and mineral breakdown occur concurrently, it is plausible that elements which have an affinity for the fluid phase will be partially fractionated into the fluid and thus may be transported out of the rock. Perhaps a requirement for such loss of elements is the textural isolation of a phase into which the element in question would be strongly partitioned.

Available data on mineral-fluid partitioning is limited. Brenan et al. (1995) performed experiments at 900°C and 2.0 GPa to obtain garnet- and clinopyroxene-

fluid partition coefficients. Strontium, Th and Pb are effectively retained in clinopyroxene, whereas these elements will be more readily partitioned into fluid relative to garnet. Conversely, U will be retained to a greater extent in garnet than in clinopyroxene. Barium is incompatible in both phases and will be strongly partitioned into the fluid, although neither garnet nor omphacite are likely to control the majority of the Ba budget, which tends to be concentrated in mica phases. An important conclusion of this work is that U, Th and Nb are all more strongly partitioned into silicate melts than aqueous fluids. The greater mobility of Th and Nb in melts has previously been proposed to explain the signatures of some arc magmas (e.g. Hawkesworth et al. 1997). Conversely, U is usually considered mobile in fluids. The experimental evidence is, however, consistent with the whole rock data presented in Section 4.3 and the data of Becker, Arculus and Spandler cited above (from which the authors concluded that U is not significantly mobile in mafic lithologies). Keppler (1996) determined a strong control of partitioning by the fluid composition, particularly for U, which is discussed further in Section 8.3. In contrast, Stalder et al. (1998) concluded that temperature, pressure and crystal chemistry had a greater control on partitioning, than fluid composition.

A final point is that the composition of minerals and their tendency to house trace elements can be strongly influenced by fluid composition. In the case of phengites from the Franciscan complex, California, and two massifs in the Alps (Voltri and Monviso), Brouwer and Sorenson (2002) concluded that Ba, Ti and K contents of the mica varied according to fluid flow, and apparently independently of the P-T conditions or the bulk rock composition. Selverstone et al. (1992) and Austrheim (1987) also recognised that fluid composition may affect mineral-fluid partitioning, based on investigations of naturally occurring minerals in HP shear zones. Furthermore, different mineral phases exhibit variable responses to fluids. Matthews et al. (1999) noted that calcite, within a HP ductile shear zone, displayed an oxygen-isotope signature which had been affected by the infiltrating externally

derived fluid, whereas the signature of quartz and dolomite had not been significantly altered.

Thermal regime

The Zermatt-Saas ophiolite has undergone subduction in a relatively cool, mature subduction system as illustrated by the P-T path in Section 3.2.1.4 and the stability of lawsonite during prograde metamorphism *and* the early exhumation history (Barnicoat and Fry 1986). The thermal regime may play an important role in determining the trace element flux from the slab. Certainly, the temperatures present in this subduction zone were insufficient to cause melting. However, the geothermal structure will affect the mineralogical changes that occur. For example, the presence of lawsonite in mafic lithologies from cool subduction zones will transport larger volumes of water to great depth than is the case for zoisite-bearing mafic crust from subduction zones with warmer thermal structures. Furthermore, the thermal structure may affect partition coefficients between fluids and minerals (Stalder et al. 1998). However, Keppler (1996) and Brenan et al. (1995) concluded that partitioning is more dependent on fluid composition.

A discussion of elemental loss and transport, determined by previous work on HP terranes, has been presented in Section 2.2.4.

8.2 Comparison of geochemical changes between different monitors/systems in the ZSO

In order to build a picture of elemental behaviour during HP metamorphism of the gabbros and basalts of the ZSO, this section brings together data from Chapters 4 and 6. The magnitude of elemental loss or gain from samples has been estimated by means of the non-conservative element discrimination diagrams of Pearce (1983) which are used in Chapter 4 (Section 4.3.3) to assess which elements have been lost from samples and those which have not. As the ZSO has MORB affinities

(Chapter 4), by assuming that neither Nb nor Yb are significantly mobile, the original concentration of an element can be estimated using a best-fit line through the MORB data. The difference between the measured value and the estimated initial concentration is assumed to have been lost (or gained) either during seafloor metamorphism or, more likely, during HP metamorphism as the ophiolite was being subducted. Strontium losses have been particularly difficult to estimate due to the strong effect of plagioclase crystallisation and accumulation. As discussed in Section 4.3.3 the 'M'/Yb vs. Nb/Yb diagram (Figure 4.7) suggests that Sr has not been lost from metabasalts. The Sr losses quoted here have been estimated from the Sr/Sr* diagram in the same chapter (Figure 4.8), but the estimates are not conclusive. In Section 6.4, there is a discussion on the Re budget of the ZSO samples. It was tentatively suggested in that section, that the estimation of Re loss by comparison with a given Yb content was not a robust means of assessing the true Re loss occurring during metamorphism, due to the possibility that Re was initially lost through degassing. Thus, the estimates quoted have been calculated using the isochron method discussed in Section 6.4, although it is worth bearing in mind that this method assumes no mobility of Os during metamorphism.

The estimates of elemental flux lost or gained by the metabasalts are quoted as a percentage of the postulated initial composition and are presented in Table 8.1 and Figure 8.1. Thus, those samples with the highest negative values have lost the greatest amount of the element in question, whereas those with positive values have higher abundances than those estimated for the original sample.

The original compositions of the gabbroic eclogites have been estimated using a best-fit line through the unaltered gabbro data. In the case of Sr, the suite of unaltered gabbros forms a moderately well defined trend in the Sr/Yb vs. Nb/Yb plot (Figure 4.7 d) and therefore deviation from this trend was used to estimate Sr loss from the gabbroic eclogites in the same way as for other elements.

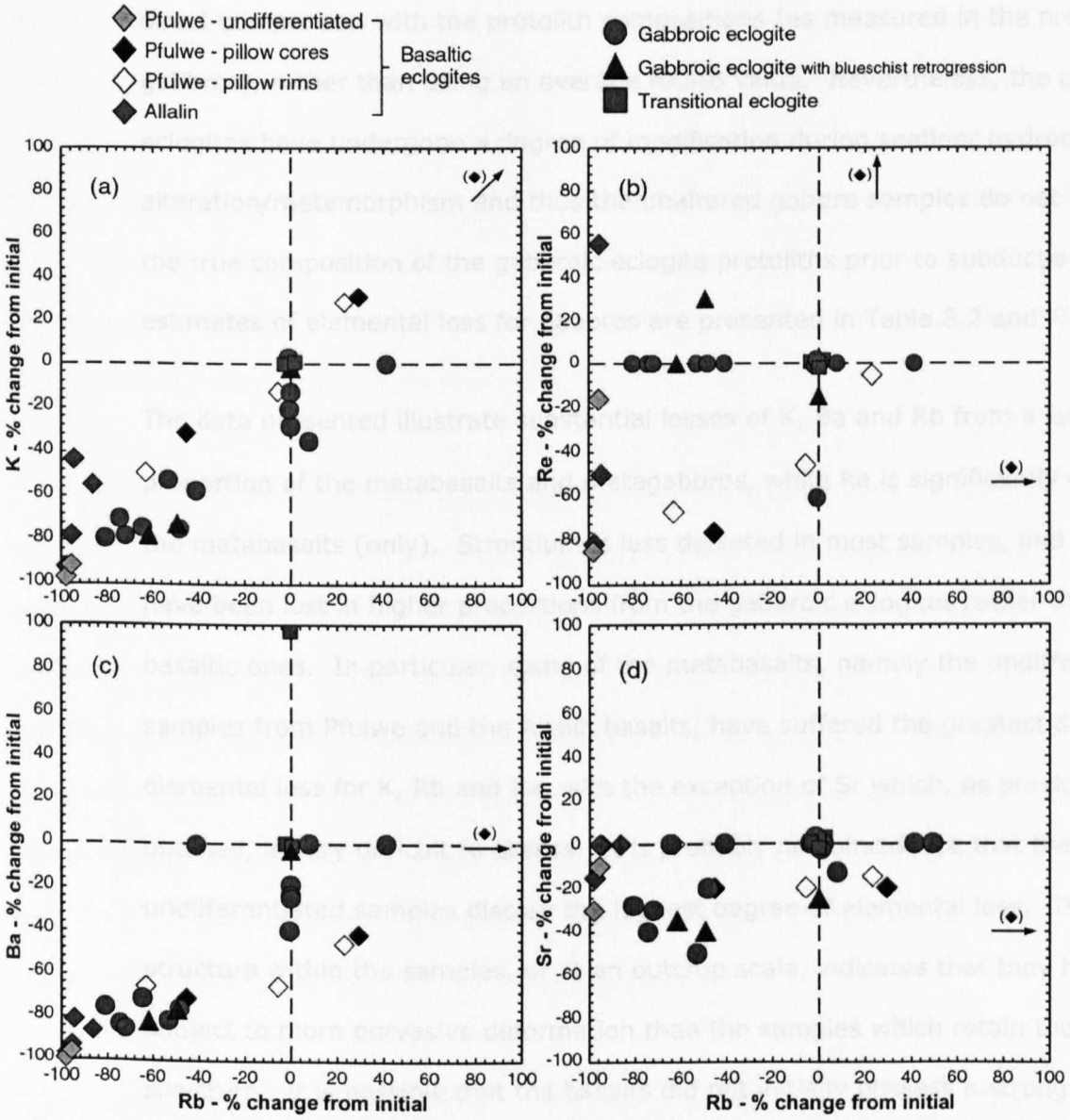

Figure 8.1. Comparison of the estimated modifications to the budgets of Rb, Sr, K, Ba and Re in basaltic and gabbroic eclogites. A net loss from an individual sample is quoted as a negative percentage of the estimated initial composition (see text), thus a sample plotting at -95% on the x-axis, contains only 5% of its original concentration of Rb. Some samples have been enriched in the LILE (plotted with positive % change), possibly as a result of seafloor alteration. The lack of gabbroic eclogites which have lost 10-30% Rb is an artefact of the estimation, whereby those samples with small losses are not clearly differentiated from the field of gabbros. In reality, the trend may be more continuous.

Rhenium, as concluded in Chapter 6, has not been significantly mobile in the gabbroic eclogites. The scatter and limited quantity of the gabbro data makes the estimation of original composition, and therefore elemental loss, subject to a greater degree of error. However, estimates for gabbroic lithologies benefit from a

direct comparison with the protolith compositions (as measured in the preserved gabbros), rather than using an average MORB value. Nevertheless, the gabbroic eclogites have undergone a degree of modification during seafloor hydrothermal alteration/metamorphism and thus the unaltered gabbro samples do not represent the true composition of the gabbroic eclogite protoliths prior to subduction. The estimates of elemental loss for gabbros are presented in Table 8.2 and Figure 8.1.

The data presented illustrate substantial losses of K, Ba and Rb from a large proportion of the metabasalts and metagabbros, while Re is significantly depleted in the metabasalts (only). Strontium is less depleted in most samples, and appears to have been lost in higher proportions from the gabbroic eclogites rather than the basaltic ones. In particular, some of the metabasalts, namely the undifferentiated samples from Pfulwe and the Allalin basalts, have suffered the greatest degree of elemental loss for K, Rb and Ba, with the exception of Sr which, as previously outlined, is very difficult to assess. It is probably no coincidence that the undifferentiated samples display the highest degree of elemental loss. The lack of structure within the samples, or at an outcrop scale, indicates that they have been subject to more pervasive deformation than the samples which retain their pillow structure. It is possible that the basalts did not initially possess a strong structure, but it is more likely that the structure that was present has been obliterated by recrystallisation accompanied by deformation.

There is a well-defined positive correlation between samples which have lost substantial amounts of K and those from which Rb has been lost. Equally, the samples which contain concentrations of K which are greater than their estimated protolith, also contain higher Rb. The correlation between Rb and Ba (and therefore also K and Ba) is well defined, although differs from Rb and K in that only one sample (transitional eclogite) displays enrichment in Ba despite an apparently high degree of enrichment of Rb and K in some metabasaltic samples (>100% in one sample). Broadly speaking there is a correlation between the degree of

deformation and the extent of elemental loss. The undifferentiated metabasaltic samples exhibit the highest levels of loss, while the Allalin metabasalts also display large losses. The latter were sampled from the edges of the Allalin body which have been more strongly deformed, particularly during exhumation (see Section 3.3.2), and thus the assemblage contains a significant proportion of barroisite. Consequently, the losses observed may be the partly the result of retrogressive processes and accompanying fluid flow.

In the case of gabbroic eclogites, K, Ba and Rb all appear to have been mobile and lost from approximately half of the samples analysed. Strontium appears to be significantly depleted in approximately one third of the gabbroic eclogites, as illustrated in Figure 4.7 d (Chapter 4). Unlike the basaltic samples, the extent of elemental loss in the gabbroic eclogites does not appear to be clearly correlated with deformation. While none of the samples exhibit intense deformation of the degree displayed by the undifferentiated metabasalts, there are examples of samples which have apparently experienced the same degree of deformation, but display very different depletions of the LILE (Figure 8.2).

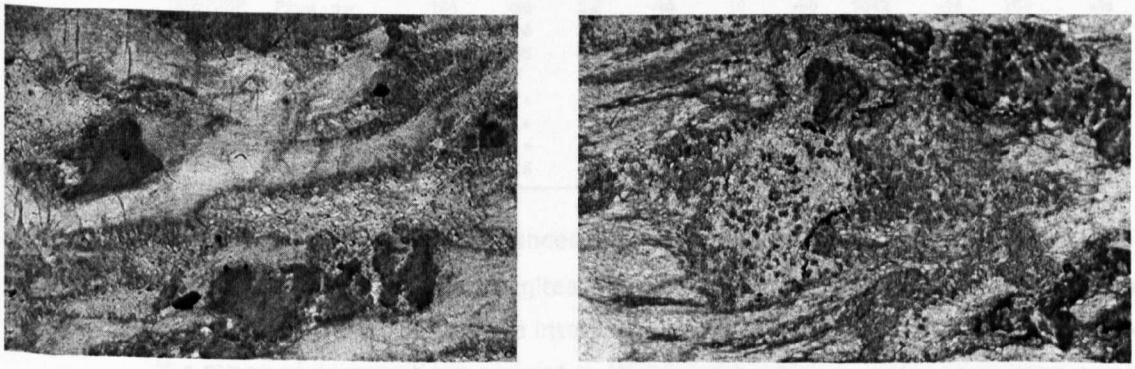

Figure 8.2. Thin section photographs of two gabbroic eclogites with blueschist retrogression which have experienced starkly different elemental loss. S02/84viix (left) has lost ~60% of its original Rb and ~80% of its Ba. S02/84viiix, despite displaying comparable deformation (elongation and joining of mineral domains), has not experienced depletion in Rb or Ba. Both photos approximately 2.5cm across.

The apparent lack of large scale Sr loss from the basaltic samples is interesting when compared to the 80-90% losses of Ba, Rb and K. The good correlation between losses of K and Rb (and to a lesser degree Ba), and the lack of correlation between losses of Sr and K and Rb suggests that two different processes control the losses of these elements. Barium, Sr, K and Rb are usually considered to be 'fluid-mobile' due to their LIL nature, although their respective compatibilities vary significantly. Strontium is the most compatible of the elements during mantle melting and is clearly very compatible in plagioclase. When plagioclase breaks down, Sr is largely incorporated into zoisite/epidote (and probably paragonite in the case of metabasaltic samples), as demonstrated in Section 7.5, and previously observed by Spandler et al. (2003). Barium, Rb and K are all accommodated in paragonite (and presumably phengite where present) but are not compatible in epidote. It is possible that this is an important factor in limiting the loss of Sr

		Sr		Rb		Ba		K		Re			Nb/Yb
		ppm	% change	ppm	% change	ppm	% change	ppm	% change	ppt	% change (isochron)	% change (from Yb)	
Pfulwe													
S02/41ii	Undifferentiated	220	**-30**	0.1	**-98**	0.7	**-99**	63	**-97**	1385	**-85**	**-8**	2.45
S02/41v	Undifferentiated	267	**-10**	0.3	**-96**	3.4	**-96**	187	**-91**	165	**-16**	**-86**	2.79
S02/75iC	Pillow - core	221	**-20**	5.3	**29**	26	**-42**	1702	**31**	632	**201**	**-53**	1.77
S02/75ivC	Pillow - core	133	**-40**	9.3	**138**	43	**-**	3036	**145**	159	**-55**	**-81**	1.77
S02/75iiiC	Pillow - core	201	**-20**	2.3	**-46**	13	**-71**	904	**-31**	194	**-76**	**-82**	1.66
S02/75iiiR	Pillow - rim	165	**-20**	3.6	**-10**	14	**-66**	1042	**-14**	267	**-46**	**-67**	1.93
S02/74ii	Pillow - rim	250	**0**	1.3	**-63**	14	**-66**	581	**-49**	233	**-67**	**-68**	2.07
S02/75iiR	Pillow - rim	217	**-15**	4.8	**23**	23	**-46**	1577	**28**	147	**-5**	**-85**	1.95
Allalin													
S02/4i	Dyke	253	**+**	0.1	**-95**	2.6	**-81**	249	**-43**	230	**-50**	**-8**	1.35
S02/4iiix	Dyke	223	**+**	0.1	**-96**	1.1	**-93**	115	**-78**	725	**56**	**21**	1.29
S02/4iiii	Dyke	237	**+**	0.8	**-86**	10	**-86**	833	**-55**				5.07
S02/7i	Dyke	159	**-15**	0.1	**-98**	1.2	**-97**	83	**-92**	93	**-81**	**-88**	1.89

Table 8.1. Elemental abundances and estimated percentage losses of some 'fluid-mobile' LILE and Re from basaltic eclogites from the ZSO. See text for explanation of method of calculation. The estimates are intended as a guide only, and are inherently imprecise due to the range of compositions present in MORB (with which samples have been compared). A space denotes that the concentration of the element was not determined. A dash denotes no significant loss. The + sign denotes basalts which have Sr/Sr* ratios >1 and therefore have either gained Sr or more likely had initially elevated concentrations and thus it is impossible to establish whether subsequent loss has occurred. Nb/Yb ratio is included as a guide to the extent of differentiation of the individual sample – the higher the ratio, the higher the predicted initial concentrations of Sr, Rb, Ba, K and probably Re.

	Sr		Rb		Ba		K		Re			Nb/Yb
	ppm	% change	ppm	% change	ppm	% change	ppm	% change	ppt	% change (isochron)	% change (from Yb)	
Gabbroic eclogites												
S01/35iix	206	**-50**	0.3	**-55**	5.9	**-80**	442	**-50**	437	-	-	2.36
S01/36iix	534	**-30**	0.1	**-80**	3.9	**-75**	116	**-80**				0.79
S01/36iiix	280	**-10**	0.2	-	7.4	-	196	**-35**				0.24
S01/39ix	309	-	0.0	**-65**	1.5	**-70**	42	**-75**	120	**166**	-70	0.25
S01/40ix	272	-	0.1	**-40**	5.1	-	74	**-55**				0.58
S01/40iix	307	-	0.2	-	6.5	-	280	-				0.91
S01/40iiix	250	-	0.0	-	1.5	**-20**	62	**-30**	166	-	-	0.60
S01/40vx	321	-	0.1	-	2.2	**-25**	105	**-15**	141	-	-30	0.49
S01/40vix	255	**-20**	0.1	**-45**	1.3	**-75**	59	**-75**				0.40
S01/40viix	369	-	0.2	**40**	7.9	-	153	-	92	-	-55	0.38
S01/40viix	364	-	0.2	**50**	7.7	-	153	-	92	-	-	0.37
S01/3iix	312	**-40**	0.1	**-70**	5.0	**-85**	221	**-70**	224	-	-	2.44
S02/33i	387	**-30**	0.1	**-70**	2.0	**-85**	83	**-75**	133	-	-35	1.93
S02/85ixE	461	-	0.1	-	4.0	**-40**	166	**-20**	126	**-65**	-70	0.23
Gabbroic eclogites *with blueschist retrogression*												
S01/40iiiix	301	**-40**	0.1	**-60**	2.2	**-85**	108	**-80**	247	**-30**	-65	0.34
S02/84viix	298	**-35**	0.1	**-70**	1.3	**-90**	83	**-90**	291	-	-60	0.39
S02/84viiix	333	**-25**	0.3	-	11.5	-	540	-	662	**15**	-	0.42
Transitional eclogites												
S01H/5a	274	-	0.2	-	8.0	-	225	-	435	-	-	0.94
S02/10iiixE	341	-	0.2	-	6.7	-	291	-	324	-	-	1.21
S02/83viiixE	398	-	0.1	-	35	**95**	208	-	237	-	-	0.46

Table 8.2. Elemental abundances and estimated percentage losses of some 'fluid-mobile' LILE and Re from gabbroic eclogites from the ZSO. The estimates are intended as a guide only and have been rounded to the nearest 5%, although in reality the precision is much lower due to the difficulty in defining a precise field for unaltered gabbro (with which gabbroic eclogites have been compared). Nb/Yb ratio is included as a guide to the extent of differentiation of the individual sample.

and the LREE (which are also strongly partitioned into epidote (e.g. Bowtell et al. 1994)), as oppose to Rb, Ba and K. However, the pitfalls of estimating Sr loss have already been outlined and thus the lack of correlation in the Sr vs. Rb plot (Figure 8.1 d) may simply be due to an error in the estimation of losses.

It has been observed that Sr is more obviously depleted in metamorphosed gabbroic samples, while the message for metabasaltic samples is unclear. One possible explanation for this is the greater enrichment of the gabbroic protoliths in Sr, due to the accumulation of plagioclase. Thus, when plagioclase breaks down, zoisite may not be capable of housing quantities of Sr which are as high as in the plagioclase. It is difficult to determine whether this conclusion is valid because there are considerable uncertainties on the measurements of saussurite, due to the lack of an accurate internal standard with which to calibrate the data.

Nevertheless, it is possible that the breakdown of plagioclase could liberate Sr and result in its loss in greater amounts from gabbroic lithologies than from basaltic ones. In the latter samples, Sr abundances are lower, and thus all the Sr may be incorporated into zoisite/epidote. However, without the more precise determination of Sr abundances in the saussurite mineralogy, it is not possible to conclude that this is a controlling factor.

The lack of a good correlation between LILE losses and those estimated for Re, illustrates that Re loss is not necessarily coupled with the depletion of other elements known to be mobile. This suggests different behaviour of Re during fluid-rock partitioning. Given the chalcophile nature of Re, its *moderate* incompatibility, and the different ionic radius and valency (Ertel et al. 2001) compared to the LILE, different behaviour of Re and the LILE is not surprising. However, despite the chalcophile nature of Re, its budget in gabbroic samples is almost entirely controlled by silicate phases (see Section 7.2). The degree of LILE loss appears to be partly dependent on the extent of deformation, whereas Re loss is not clearly correlated with deformation and may be dependent on complex fluid-rock interactions not yet understood.

I would suggest that in order to confirm the lack of mobility of Re and Os in subducted gabbroic material, a study of gabbroic bodies which have experienced different degrees/styles of deformation should be undertaken. This is particularly important given the apparently heterogeneous nature of Re loss from the basaltic eclogites outlined previously (Section 8.2). Conversely, the evidence of Re mobility in subduction zones (Becker 2000; this study) derives largely from samples which have experienced considerable deformation and fluid flow. While this is probably more typical of the upper parts of the subducting slab due to their proximity to the seafloor and then the slab-mantle interface, the evidence from lawsonite blueschists from New Caledonia (Spandler et al. 2003) is that finer grained

lithologies (as well as coarser ones) can retain their igneous mineralogy deep into subduction zones (30-40 km). Therefore, Re loss from basalts may be confined to those which have undergone extensive hydration during seafloor processes and/or deformation during subduction.

8.3 Implications of variable elemental loss

The enrichment of ^{238}U observed in many arc lavas is thought to be derived from fluids which transfer elements from the down-going slab (Elliott et al. 1997; Hawkesworth et al. 1997). Paradoxically, recent data from mafic rocks which have undergone subduction-related HP metamorphism indicate that U is not significantly mobilised up to the P-T conditions experienced by those samples (Arculus et al. 1999; Becker et al. 2000; Spandler et al. 2004). The U whole-rock data presented in Section 4.3 are consistent with the findings of these recent studies and indicates that neither basaltic nor gabbroic lithologies have been depleted in U. If this apparent immobility of U is typical of mafic crust which has been subducted, then alternative sources are required for the enrichment in U that is observed in many arc lavas.

However, it has been discussed in Section 2.2.4 that U (and Pb) depletion in HP metamorphic terranes appears to increase with increasing grade and therefore may be dependent on pressure and particularly temperature (Becker et al. 2000). In this case, it is possible that the samples analysed in this study and by Arculus et al. (1999) and Spandler et al. (2004) had not experienced sufficient temperatures to facilitate significant loss of U. Becker (2000) concluded that most U loss occurs at temperatures higher than 600°C. Well-established subduction zones which consume old oceanic crust may remain at temperatures below 600°C until pressures greater than 3.0 Ga (even with slow subducting slabs) (Peacock 1993; Poli and Schmidt 2002), and thus may not undergo U loss. This is particularly true of the lower parts of the subducting oceanic crust which remain cooler than the

upper section due to shear heating and conduction of heat into the upper crust from the mantle wedge (e.g. Peacock 1993).

The experimental determination of fluid-mineral partition coefficients by Keppler (1996) has provided an alternative explanation for the U 'paradox'. By varying the composition of the fluid from a chloride-free hydrous fluid to a 5M (Na,K)Cl solution, a large increase in fluid-mineral partitioning for U was observed (from <0.3 to 36). The partitioning of La into the fluid phase is also encouraged by the presence of a chloride-rich fluid. Thus, the lack of U loss from the samples of the Allalin Gabbro and Pfulwe area may be due to the presence of a primarily water-rich fluid. If the HP metamorphic fluids in this part of the ZSO were largely derived from internal dehydration reactions (as suggested by the oxygen isotope work of Barnicoat and Cartwright 1995; Barnicoat and Cartwright 1997; Cartwright and Barnicoat 1999), the lack of chloride-rich fluids is consistent with electron microprobe data for hydrous minerals, where very low concentrations of Cl have been measured (below detection limits: <150ppm). Furthermore, chlorite and amphibole from a vein in the Allalin also contain similarly low Cl concentrations.

The experimental data for Rb, Ba and K all reveal fluid-mineral coefficients which are greater than 1 for both water- and saline-rich fluids, although the mobility of K increases greatly in the latter. This experimental data may provide an explanation for the apparent mobility and loss of K, Rb, Ba and Sr from the Allalin Gabbro, while U, La have remained immobile. In addition, the derivation of HP fluid from within the Allalin Gabbro (after infiltration of fluids on the seafloor, Barnicoat and Cartwright 1997) may also limit the amount of elemental loss from these gabbros. In contrast, John et al. (2004) found that fluid induced eclogitisation in Zambian gabbros resulted in significant chemical modification (largely depletion), including LREE abundances. The latter authors suggest that the fluids must have been derived from the underlying serpentinised lithospheric mantle. Given the exotic

nature of the fluids, this perhaps provides an explanation for the different elemental behaviour in these two settings, despite similar protoliths and P-T conditions.

Unfortunately there is no fluid-mineral data available for Re, although the loss of Re from basaltic lithologies suggests that its mobility is not dependent on the presence of a chloride-rich fluid.

Models for the derivation and transport of fluids from the slab to the mantle wedge, such as those of Peacock (1990), rely on estimates of the extent of hydration of the subducting slab, and thus the probable loss of fluid from the different slab sections. On the basis of the data presented for the Allalin lithologies, it is important to recognise that not all hydrated rocks entering subduction zones will experience 'typical' elemental losses, and that many elements considered 'fluid-mobile' have not been depleted.

In Section 5.2.3, an introduction to the current state of knowledge about Re and Os in subduction zones is presented. Alves et al. (1999; 2002) found radiogenic Os isotope signatures in arc magmas and invoked a slab-derived flux in order to explain these elevations. Brandon et al. (1996) and Widom et al. (2003), through the analysis of mantle xenoliths, both concluded that Os is mobile in Cl-rich fluids derived from the slab, thus elevating the $^{187}Os/^{188}Os$ signature of the mantle wedge. Widom et al. (2003) also suggested, from evidence in the Kamchatka region, that melts efficiently transport both Re and Os into the mantle wedge in the hotter parts of subduction zones (e.g. where the slab is tearing). However, on the basis of mixing calculations, Borg et al. (2000) and Chesley et al. (2004) concluded that Os concentrations in slab fluids would need to be unreasonably enriched in Os compared to the slab itself in order to explain the radiogenic Os values observed in arcs. Moreover, Woodhead and Brauns (2004) cast doubt on the existence of an Os 'arc signature' altogether, and point to crustal contamination as being a possible mechanism for enriching the radiogenic component of arc magmas. In intra-

oceanic settings, these authors emphasised the need to more accurately constrain the composition of the regional upper mantle before conclusions about arc fluxes can be reached.

From the evidence of subducted rocks, like those of the ZSO, it is difficult to ascertain whether Os is mobile, due to a lack of suitable elements with which to compare Os abundances. By comparison of unaltered and eclogitic gabbroic lithologies from the Allalin Gabbro, Os does not appear to have been lost, at least not in significant quantities. Another mechanism to explain the radiogenic Os signatures of arc rocks, is the addition of a Re flux from the down-going slab into the mantle wedge, assuming sufficient time for ^{187}Re decay in the wedge. The loss of Re during HP metamorphism of basaltic crust (Section 6.2.2) is consistent with this theory, although quantitative modelling is required in order to determine whether the flux is of sufficient magnitude to create the observed Os signature. A problem with this hypothesis may be the timescale required, as U-series studies indicate that the slab to arc transfer of elements may occur over short timescales (probably <100,000 years, e.g. Turner et al. 2000). Re was not found to be elevated in the mantle xenoliths studied by Widom et al. (2003) and thus these authors concluded Re to be immobile, or to be transported over limited distances due to reaction with the mantle wedge (although clearly it is extremely plausible that Re enrichment would be strongly heterogeneous and therefore they may have simply analysed non-enriched samples). By integrating these findings with the data in Chapter 6 and from Becker (2000), Re is likely to be lost from the basaltic portion of the slab but is perhaps not transported efficiently into the source region for arc magmatism.

A suite of metabasaltic samples has been analysed which were collected from the Sulitjelma ophiolite. This ophiolite has been metamorphosed at biotite to kyanite grades, during regional Barrovian-type metamorphism. The data suggest that Re

loss has occurred at biotite grade or lower. This finding leads to an alternative hypothesis, for the lack of Re enrichment in mantle xenoliths from arc settings. If loss occurs to a large extent at low metamorphic grades, the postulated flux of Re from the slab will not necessarily be transferred to the mantle wedge, and thus will not be sampled by arc magmatism. While having an important effect on the likely fluxes into the mantle source of arc melts, this observation does not affect the conclusion that Re depleted basaltic crust is recycled into the mantle.

8.4 Modelling recycled oceanic crust in the mantle: insights from Re-Os isotope systematics

Hofmann and White (1982) first proposed that ancient recycled oceanic crust in the mantle could account for some of the isotopic variations observed in OIB basalts. Since that time, the development of Re-Os analytical procedures has permitted the investigation of Re-Os isotope systematics in oceanic basalts. As discussed in Chapter 1 and Chapter 5, Re/Os ratios in oceanic crust are extremely elevated with respect to mantle values, leading to very radiogenic $^{187}Os/^{188}Os$ ratios; thus, the system should be a valuable tool for identifying recycled oceanic crust in the mantle. Consequently, many authors have proposed recycled oceanic crust as a means of explaining the elevated $^{187}Os/^{188}Os$ signatures of some OIB (Hauri and Hart 1993; Reisberg et al. 1993; Marcantonio et al. 1995; Roy-Barman and Allegre 1995; Widom and Shirey 1996; Widom et al. 1999). The coupling of elevated $^{206}Pb/^{204}Pb$ and $^{187}Os/^{188}Os$ in HIMU-type OIB is consistent with the presence of recycled oceanic crustal material in the mantle source of these magmas. However, constraining and quantifying the precise nature of recycling is fraught with difficulty, due to many unknowns such as the behaviour of elements during seafloor and subduction-related fluid flow, the exact proportions of different lithologies in the crust, the extent to which they are hydrated by hydrothermal processes and the precise composition of both the unaltered oceanic crust and the mantle with which it is mixed.

After investigating Re concentrations in basaltic samples metamorphosed in palaeo-subduction zones, Becker (2000) concluded that Re loss occurred during subduction, resulting in lower $^{187}Re/^{188}Os$ ratios in recycled mafic crust. Consequently, less radiogenic Os isotope ratios would evolve over time, requiring the mantle sources of HIMU basalts to contain unrealistic quantities of recycled material (80-90%), given a recycling timescale of ~500 Ma which is imposed (according to Becker) by the Pb isotope compositions observed in OIB.

In this section, the effects of recycled oceanic crust on the Os isotopic signature of mantle reservoirs is reassessed, taking into account the data presented in this thesis, and other data from the literature. The discussion will primarily focus on Os isotopes, although calculations for Pb have also been performed, using the Excel spreadsheet (basalt+sedrecycling) of Stracke et al. (2003). This spreadsheet has proved very useful in rapidly assessing the effects of changing various parameters. However, the calculations therein do not include the mixing of ancient oceanic crustal material with the mantle. This mixing calculation, together with the evolution and mixing of Os isotopes, has been completed independently. Subducted sediments have been omitted from this assessment, due to the extra uncertainty that it entails and because this discussion is primarily concerned with the formation of HIMU-type signatures which are not considered to include a component of subducted sediment (Hofmann 1997). Rhenium and Os concentrations in gabbros and gabbroic eclogites have been measured in this study, providing much needed data on the Re-Os composition of the lower oceanic crust. The only published data currently available for the lower portion of the crust are those of Blusztajn et al. (2000) for strip samples from a gabbroic section at ODP site 735B.

There are several ways in which the calculations presented here differ from those of Becker (2000). Firstly, the gabbroic portion of the crust has been included in this assessment, and is elementally distinct from the basaltic part of the crust, resulting

in a different isotopic signature over time. Secondly, the basalt data obtained in this thesis have not been used as representative of the Re-Os composition of subducted basaltic material. This is because I have concluded, in Chapter 6, that some of the basalts may have lost Re during volcanic degassing, rather than subduction (a process which may have occurred due to the shallowness of the basin in which the ZSO formed). Furthermore, the Os concentrations of the metabasalts are relatively high for MORB (mean: 20 ppt), and the basalts are somewhat differentiated and have lower than average Mg numbers, and thus may not be representative of MORB in general. Instead, the conclusion of approximately 60% Re loss, found in this work and in the paper of Becker (2000), has been applied to the global MORB glass datasets of Schiano et al. (1997) and A. Gannoun (unpublished data). The effect of using the ZSO values would slightly lower the evolved $^{187}Os/^{188}Os$ values of the basaltic portion of the crust. Whether MORB glass is precisely representative of MORB as a whole is also a matter of debate. In terms of the Re-Os system, it is possible that glass is not fully representative of MORB (pillow rims tend to have higher Re/Os ratios than pillow cores, Gannoun et al. 2004b). It is also possible that MORB is not fully representative of subducted material as a whole (e.g. Spandler et al. 2004). However, for the purpose of this modelling, MORB glass has been considered representative of the basaltic portion of the crust. The third way in which this assessment differs is the treatment of Pb isotopes. One conclusion by Becker (2000), is that the $^{238}U/^{204}Pb$ (μ) ratio of subducted crust is elevated to such an extent (~37) that young recycling ages are required in order to limit the radiogenic ingrowth of ^{206}Pb. A ratio of 37 for μ is reasonable for altered MORB (μ = 40 is used here), but (as Becker (2000) pointed out) MORB will be partly altered and partly unaltered, and thus a lower value should be used (unaltered MORB, μ = 11.5, (Stracke et al. 2003 and references therein)). Furthermore, the mixing calculation of Becker (2000) was performed with a low mantle Pb abundance (20 ppb). While it is unclear whether HIMU-type OIB source a reservoir in the upper or lower mantle, or indeed whether these

geochemically distinct zones occur at all, it is likely that the Pb abundance for the mantle component should be higher than the value used by Becker and closer to that of the primitive mantle. The effect of using a low value accentuates the radiogenic component of the recycled crust, upon mixing with the mantle. For the calculations presented here I have utilised a value of 30 ppb used by Shirey and Walker (1998), although this may possibly still be an underestimate (Chauvel et al. (1992) estimated that the depleted mantle contains 58 ppb Pb). Finally, it has been assumed for the Os calculation that subducting oceanic crust is, on average, 100 Myr old, and therefore has evolved with original magmatic $^{187}Re/^{188}Os$ ratios for that time, prior to modification by subduction. This is twice the length of time allowed by Becker (2000), but is probably a reasonable estimate given the average age of *all* oceanic crust of about 55-65 Ma. An unknown factor however, is the average age of crust that was subducted *2 billion years ago*, although modelling by Davies (1992) suggests it may be considerably younger (30-40 Ma).

Representative values. One difficulty in assessing the effects of recycling is accurately constraining the composition of the various components. The abundances and ratios used in these calculations are presented in Table 8.3.

Component	U (ppm)	Pb (ppm)	$^{238}U/^{204}Pb$	References
Unaltered MORB	0.017	0.09	11	Hofmann 1988
Altered MORB	0.072	0.05	98	Staudigel et al. 1996
MOR Gabbro	0.009	0.10	6	Hart et al. 1999, Zimmer et al. 1995
Combined MORB	0.045	0.09	40	Stracke et al. 2003 and references therein
Complete crust	0.022	0.07	15	Stracke et al. 2003 and references therein
			$^{206}Pb/^{204}Pb$	
Mantle		0.030	18.300	Shirey and Walker 1998

	Re (ppt)	Os (ppt)	$^{187}Re/^{188}Os$	References
Unaltered MORB	1150	8	675	Schiano et al. 1997, Gannoun (unpubl.), Sun et al. 2003
Altered MORB	1150	8	675	No Re or Os loss assumed
MOR Gabbro	450	36	58	This work, Blustjahn et al. 2000
MORB (Re loss)	460	8	262	MORB data less 60% Re (Becker 2000, this study)
Complete crust (Re loss basalt)	453	27	~90	(depending on proportions within crust and extent of Re loss)
			$^{187}Os/^{188}Os$	
Mantle	-	3100	0.129	Meisel et al. 1996

Table 8.3. Data used in calculations, with references. Re and Os have been assumed to be unaffected by hydrothermal alteration although relatively small changes may occur (see Sharma et al. 2000; and Peucker-Ehrenbrink et al. 2003).

Despite the ever-growing Re-Os dataset, there remains only a relatively small amount of data on low-abundance samples such as basalts and gabbros. Furthermore, the extremely heterogeneous distribution of Re and Os makes establishing an 'average' whole rock composition problematic. If median values are used for Os and Re abundances in gabbros and MORB, they are lower than the mean. However, Os is proportionally lower than Re and therefore the median gives a higher $^{187}Re/^{188}Os$ ratio. The effect of this is to increase the radiogenic signature of evolved median MORB, with respect to the mean; but the lower Os abundance means that its impact within the mantle is more diluted. Consequently, mean values consistently produce slightly more radiogenic mantle reservoirs.

Figure 8.3 illustrates the evolution of oceanic crust through time. Half of the basaltic portion of the crust is assumed to have been modified during hydrothermal alteration (U and Pb values from Staudigel et al. 1996), while the other half is unaltered MORB (Hofmann 1988). Slightly more radiogenic Pb signatures are generated if the unaltered N-MORB values of Sun and McDonough (1989) are used, but the difference is insignificant for basaltic crust which has undergone partial alteration. Significant net fluxes of Re and Os during hydrothermal alteration do not appear to occur, and so the abundances have not been altered in this model, although redistribution may be a significant process that could affect Re and Os behaviour during subduction (Sharma et al. 2000; Peucker-Ehrenbrink et al. 2003). For the average complete crust, gabbros constitute 65%, while altered and unaltered MORB comprise 17.5% each. All calculations include subduction modification of Pb and U (Stracke et al. 2003 and references therein).

The effect of alteration and subduction on the U-Pb system is considerable. Without alteration, MORB evolves to $^{206}Pb/^{204}Pb$ ratios of approximately 19.2 (19.65 for Sun and McDonough (1989) values) over a time period of 2500 Ma. With alteration, values of >20 can be generated in less than 500 Ma. As previously

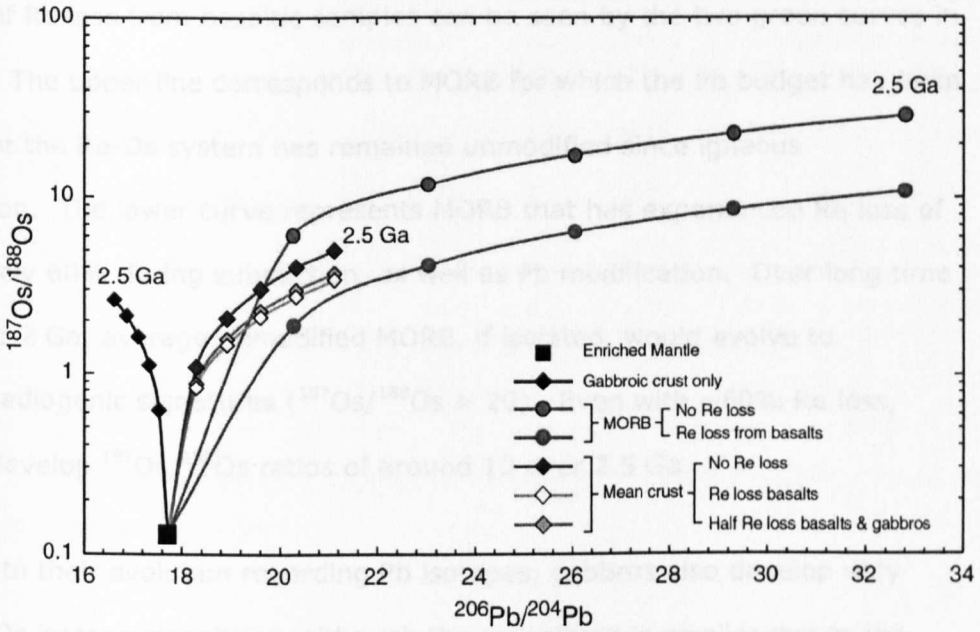

Figure 8.3. Isotope evolution for oceanic crustal material. All curves calculated assuming modification of U and Pb through hydrothermal alteration and subduction. MORB has much higher $^{187}Re/^{188}Os$ ratios than MOR gabbro. Thus, over time, MORB evolves to much more radiogenic Os isotope compositions. However, average MORB contains less Os than average MOR gabbro and therefore it has a lesser impact when mixed with the mantle. The points are spaced at 500 Ma. Note the log scale for Os isotopes.

mentioned, Becker (2000) made the point that oceanic crust recycled into the HIMU source must be young, otherwise more radiogenic Pb signatures would be present in HIMU-type OIB. However, gabbro contains low concentrations of U while Pb is relatively abundant and thus does not produce radiogenic signatures, unless perhaps it has been extensively altered, and in fact it develops *lower* $^{206}Pb/^{204}Pb$ ratios than the mantle. This has a strong influence on the evolution of the crust as a whole, and significantly limits the development of high $^{206}Pb/^{204}Pb$ ratios. In addition, independent evidence from Pb isotope studies by Thirlwall (1997) suggests that young recycled crust will impart a negative $\Delta\ ^{207}Pb/^{204}Pb$ (compared to the Northern Hemisphere reference line) to the source of OIB. Thus, the lack of a significant negative $\Delta\ ^{207}Pb/^{204}Pb$ value in extreme HIMU OIB (e.g. Mangaia) argues for an older recycled component in the source of these OIB.

The effect of Re loss from basaltic samples can be seen by the two green curves in Figure 8.3. The upper line corresponds to MORB for which the Pb budget has been modified but the Re-Os system has remained unmodified since igneous crystallisation. The lower curve represents MORB that has experienced Re loss of approximately 60% during subduction, as well as Pb modification. Over long time periods of ≥ 2 Ga, average unmodified MORB, if isolated, would evolve to extremely radiogenic signatures ($^{187}Os/^{188}Os > 20$). Even with ~60% Re loss, MORB will develop $^{187}Os/^{188}Os$ ratios of around 10 over 2.5 Ga.

In contrast to their evolution regarding Pb isotopes, gabbros also develop very radiogenic Os isotope signatures, although the magnitude is smaller due to the lower Re contents of MOR gabbros, compared to MORB. The limiting effect of gabbros on the isotope evolution of the whole crust can be seen clearly in Figure 8.3. However, this diagram does not take into account the greater abundance of Os within gabbros. Figure 8.4 illustrates the isotopic compositions that result when gabbroic, basaltic and combined crustal material are mixed with mantle over a time period of 2 Ga. This timescale has been inferred by several authors who deem the correlations between ^{206}Pb and ^{207}Pb to have age significance (e.g. Hofmann and White 1982). It can be seen in Table 8.4 that relatively old ages (≥ 2.0 Ga) of recycled material are required to approach the radiogenic signatures of HIMU-type OIB, given the estimated Os isotope composition of subducted oceanic crust. This is consistent with the Pb age.

Figure 8.4 emphasises the effect of incorporated gabbro into the oceanic crust which is recycled. As Pb is relatively abundant in gabbros, the unradiogenic $^{206}Pb/^{204}Pb$ ratios that they possess exert a strong influence on the isotope evolution of the oceanic crust as a whole. Thus, a complete section of oceanic crust, if homogenised, will generate considerably lower $^{206}Pb/^{204}Pb$ ratios than MORB that has been altered. The calculation of Pb isotope evolution for the gabbroic part of the crust (and the combined crustal section) used values from

	Re lost during subduction?		Age	Evolved	Proportion of oceanic crust in source				
	Gabbro	Basalt	Ga	$^{187}Os/^{188}Os$	10%	20%	30%	40%	50%
Complete oceanic crust									
Mean	NO	NO	1	2.21	0.131	0.134	0.138	0.142	0.149
Mean	NO	YES	1	1.56	0.131	0.132	0.135	0.138	0.143
with 10% higher initial Re	NO	YES	1	1.70	0.131	0.133	0.136	0.139	0.144
Median	NO	YES	1	2.11	0.130	0.131	0.133	0.135	0.139
Mean	HALF	YES	1	1.36	0.130	0.132	0.134	0.137	0.141
Mean	NO	NO	2	4.32	0.134	0.139	0.146	0.156	0.169
Mean	NO	YES	2	2.94	0.132	0.136	0.141	0.147	0.156
with 10% higher initial Re	NO	YES	2	3.22	0.132	0.136	0.142	0.149	0.159
Median	NO	YES	2	4.10	0.131	0.134	0.137	0.142	0.149
Mean	HALF	YES	2	2.52	0.132	0.135	0.139	0.144	0.152

Table 8.4. The effect of changing parameters on the Os isotope evolution of a complete section of oceanic crust.

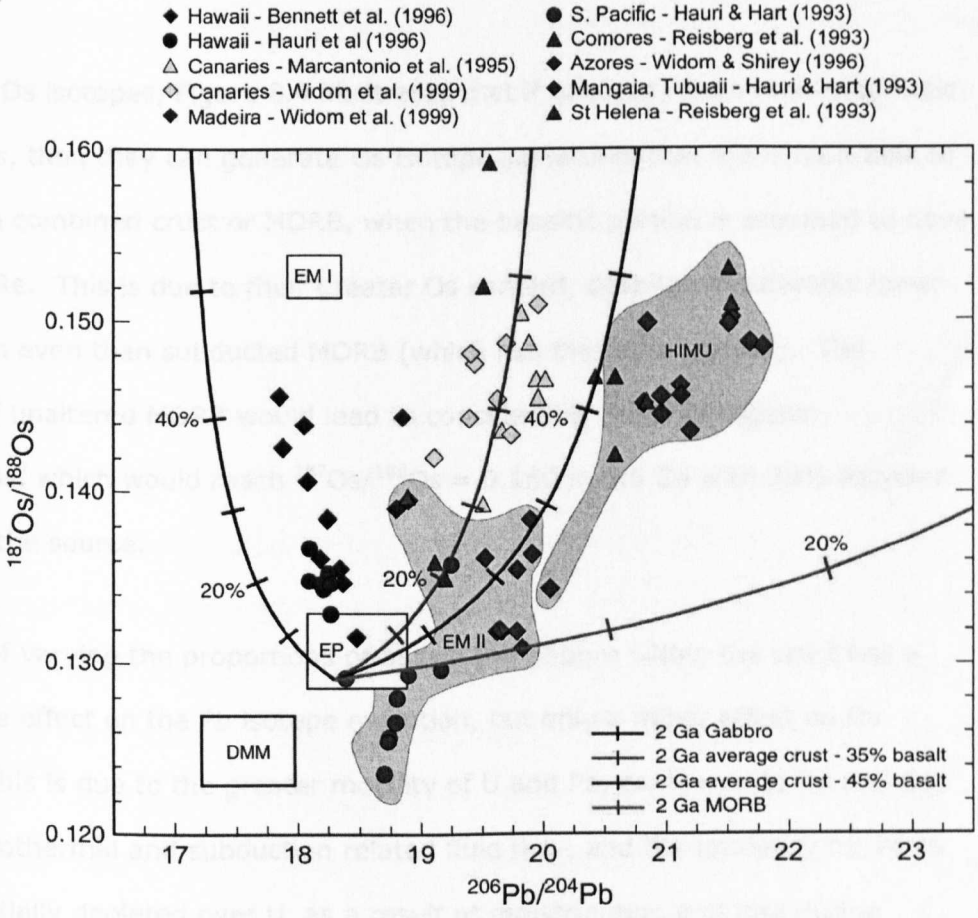

Figure 8.4. Mixing of oceanic crust with mantle, in ^{187}Os-^{206}Pb isotope space. All mixing lines calculated assuming Re loss of ~60% from basaltic units, and no loss from gabbroic units. Also shown are data for various OIB. With the exception of the green circles (South Pacific, data from Hauri and Hart 1993), all OIB have elevated $^{187}Os/^{188}Os$ ratios compared to the primitive or depleted MORB mantle values. Red symbols refer to HIMU-type OIB. Blue symbols plot between the enriched plume (EP) component, and the EMI reservoir. The data from the Canaries has a radiogenic Os signature but does not possess $^{206}Pb/^{204}Pb$ comparable to HIMU. Tick marks at 10% mixing intervals.

Hart et al. (1999) and thus included the geochemical effects of a degree of seawater circulation. Moreover, subduction modification was assumed although perhaps unlikely from those parts of the gabbro section that do not undergo deformation and/or fluid flow. Without modification during subduction, gabbros evolve to even less radiogenic Pb compositions. Due to the high Pb concentrations in sediments, the addition of ~2% sediment also drastically decreases the Pb isotopic evolution of recycled crust (Chauvel et al. 1992). Sediment, like gabbro, only has a small effect on the Os isotope evolution (Roy-Barman and Allegre 1995), thus addition of sediment and gabbro cannot easily be differentiated in terms of Pb or Os isotopes, but will produce different signatures for other tracers such as Sr.

In terms of Os isotopes, Figure 8.4 illustrates that if gabbros retain their magmatic Re/Os ratios, then they can generate Os isotope signatures that are comparable to those of the combined crust or MORB, when the basaltic portion is assumed to have lost ~60% Re. This is due to their greater Os content, despite considerably lower Re/Os ratios even than subducted MORB (which has therefore lost Re). The evolution of unaltered MORB would lead to considerably more radiogenic compositions, which would reach $^{187}Os/^{188}Os = 0.150$ in 1.5 Ga with 30% recycled material in the source.

The effect of varying the proportions of basalt and gabbro within the crust has a considerable effect on the Pb isotope evolution, but only a minor effect on Os isotopes. This is due to the greater mobility of U and Pb, compared to Re and Os, during hydrothermal and subduction related fluid flow, and the tendency for Pb to be preferentially depleted over U, as a result of redistribution and loss during hydrothermal alteration and further depletion during subduction.

It is possible that the OIB that plot with high Os isotopic ratios, but relatively low $^{206}Pb/^{204}Pb$ values (particularly those of the Canaries (Marcantonio et al. 1995; Widom et al. 1999)), could be the result of a greater input from gabbroic material

into the source reservoir, thus lowering the $^{206}Pb/^{204}Pb$ ratio, but not affecting the Os signature to a significant degree. However, this theory requires testing against other isotope systems and trace elements to confirm this hypothesis. Currently, the favoured explanations for OIB with this signature are either the recycling of oceanic crust with lower U/Pb ratios, or a relatively young age (1.2 Ga) for the recycled component (Marcantonio et al. 1995; Widom et al. 1999).

The theory that individual recycled components may give rise to isotopic variations within a single plume has been put forward by several authors. Chauvel (1992) suggested that the variety of OIB signatures in the French Polynesian islands are the result of sampling of various parts of recycled lithosphere (HIMU: altered mafic crust, EMI and II: the addition of entrained sedimentary material). Lassiter and Hauri (1998) concluded that Os, O and Pb data from Hawaii are consistent with some islands having a source which has a significant component of recycled oceanic crust (plus sediment), whereas other islands display unradiogenic Os isotope signatures and light oxygen isotopes which suggest a lithospheric component. The Hawaiian plume has also been the subject of a trace element study (Sobolev et al. 2000), which indicated, through the occurrence of positive Eu anomalies, the presence of a plagioclase-rich source, postulated to be recycled oceanic crust, and in particular, the gabbroic portion. Finally, the presence of the gabbroic portion of recycled crust in the source of Icelandic picritic lavas has been proposed by Chauvel and Hémond on the basis of strong positive Sr and Pb anomalies. The authors suggest that alkali basalts contain a component derived from the basaltic crust (as illustrated by higher $^{206}Pb/^{204}Pb$). Given the very unradiogenic Pb isotope evolution of gabbros, the magmas produced by the postulated lower oceanic crust section should have very low Pb isotope compositions, particularly for an old age for the recycled material.

Summary. Becker (2000) concluded that 80-90% oceanic crust in the mantle source was necessary to explain the extremely radiogenic Os signatures observed in OIB samples from Mangaia (end-member HIMU) and the Canaries, given an age of ~1 Ga imposed by Pb isotopes. Even with an older recycling age (2 Ga) and less Re loss from the basalts, Becker calculated that at least 60% of the mantle source must consist of oceanic crust. Using slightly different parameters, but ones which are equally valid given current understanding of the processes involved, the calculations presented here allow HIMU-type signatures to evolve over timescales of 2–2.5 Ga, with mixing of 45% oceanic crust and 55% mantle. Despite the conclusion that little or no Re is lost from gabbroic lithologies during subduction, the lower Re/Os ratios of gabbros result in similar estimates of Os isotope signatures for the whole crust and for MORB which has lost ~60% of its Re. However, the presence of gabbro in the source significantly limits the generation of radiogenic Pb signatures and thus, on the basis of Pb isotopes, permits greater ages of recycling. Consequently, Pb isotope evolution can be modified, while Os isotopes are largely unaffected.

A value of ≥40% for the recycled component in the mantle source is higher than previous estimates (Hauri and Hart 1993; Reisberg et al. 1993; Roy-Barman and Allegre 1995; Widom 1997) and is probably unlikely given current knowledge of mantle processes. However, as Re and Os abundances in oceanic crust are heterogeneous and poorly constrained, particularly for the gabbroic portion, it is plausible that the estimates of Re/Os ratios are conservative. If so, HIMU signatures may be generated with lower proportions of crust.

An alternative mechanism of generating more radiogenic signatures with low proportions of recycled crust is to invoke incongruent melting of host peridotite and enclosed pyroxenite layers. Pyroxenite layers in orogenic massifs (e.g. Rhonda) have been found to possess variable and very radiogenic Os isotope signatures and

are often thought as representing ancient recycled oceanic crustal material (e.g. Reisberg et al. 1991; Roy-Barman et al. 1996). The work of Hirschmann and Stolper (1996) demonstrates that preferential melting of enclosed pyroxenite over the host peridotite occurs. This is due to the solidi of the former being at lower temperatures than peridotite solidi, thus melting commences at higher pressure during decompression, and continues to a greater degree. Approximately 20% of the resulting melt may be sourced from the pyroxenite despite only constituting ~5% of the source by volume. However, one commonly held belief is that OIB major element compositions cannot be produced by the melting of pyroxenite layers thought to represent recycled oceanic crust (e.g. Becker 2000 and references therein). The high silica content of pyroxenites is thought to preclude the derivation of silica-deficient melts of the type seen in some OIB. However, the recent experimental work of Kogiso et al. (2003) has suggested that it is possible to produce silica-poor magmas from the melting of garnet pyroxenite. On the basis of this evidence, it may not be necessary to place an upper limit on the proportion of oceanic crust in the mantle source of OIB nor to exclude the possibility of incongruent melting. The latter remains a likely mechanism which would lead to more radiogenic compositions in OIB than in their bulk source.

PAGE
MISSING
IN
ORIGINAL

9 Conclusions

9.1 Re and Os in subducted mafic lithologies

9.1.1 Whole rock data

Oceanic crust has high Re/Os ratios (relative to mantle) and thus, over time, develops elevated $^{187}Os/^{188}Os$ ratios; therefore the Re-Os system is an excellent tracer for recycled crust in the mantle. However, the available data from basalts suggest that up to 60% of Re may be lost during high-pressure metamorphism, resulting in lower Re/Os ratios in the subducted slab (Becker 2000). In this case, large quantities of oceanic crust or very long residence times in the mantle source would be required to generate the observed Os isotope compositions of HIMU-type OIB.

In order to provide a more complete understanding of the Re-Os composition of subducted crust, a suite of gabbroic eclogites and metastable gabbros from the Allalin Gabbro, ZSO, has been analysed. In addition, a suite of basaltic eclogites from the same ophiolite have been analysed. The ZSO has experienced metamorphism at very high-pressure (>2.0 GPa) during partial subduction prior to incorporation into the Alpine orogenic belt.

The key observations are:

- Basaltic eclogites from the Zermatt-Saas ophiolite (ZSO) display significant depletion of Re, thought to be the result of loss during HP metamorphism. This is in agreement with data for HP metabasalts documented by Becker (2000).
- Metastable gabbros and gabbroic eclogites of the Allalin unit yield a best-fit regression line (on a Re-Os isochron plot) that is consistent with a U-Pb zircon age of 164 Ma, considered to be the age of igneous crystallisation (Rubatto et al. 1998). This indicates that low-strain gabbroic bodies may remain closed, with respect to the Re-Os system, during subduction.

- Loss of Re from subducted basaltic crust would significantly affect the isotopic evolution of recycled oceanic crust. Equally, the retention of primarily magmatic Re/Os ratios in subducted gabbroic crust may have important implications for the recycling of oceanic crustal material in the mantle (see Section 9.1.2).
- In addition to assessing the behaviour of Re and Os during the process of subduction, the analysis of gabbroic lithologies has also provided vital new Re and Os data for the lower oceanic crust.

The recognition that Re is depleted in eclogite-facies rocks raises the question of the conditions under which Re loss commences. A suite of metabasaltic samples has been analysed from the Sulitjelma ophiolite, which has been metamorphosed at biotite to kyanite grade conditions.

- These data suggest that some Re loss has occurred in all samples, including those at biotite grade. If this is the case, much of the observed Re loss in the ZSO metabasalts may take place during the initial stages of burial and thus may not be transferred into the source region of arc magmatism.

However, the Sulitjelma ophiolite has experienced a Barrovian-type thermal regime and thus, the Re loss observed may not be representative of subduction-related metamorphism, particularly if Re mobility is dependent on temperature.

The retention of magmatic Re/Os ratios during subduction may depend on various factors including the extent of hydration of the crust, the structure of the oceanic crust prior to subduction (which itself is dependent on the rate of spreading), the degree of HP fluid flow through the rock, and also the composition of fluid. It is probable that the lack of Re loss from the Allalin Gabbro is a result of lower fluid-rock ratios in the unit during subduction (as illustrated by oxygen isotope values which remain consistent with seafloor hydrothermal alteration; Barnicoat and

Cartwright 1997), and a lack of pervasive deformation which would inhibit the flow of large volumes of fluid through the unit.

9.1.2 Implications for mantle recycling

The retention of magmatic Re/Os ratios through metamorphism of the Allalin Gabbro (see Section 6.2) may have important consequences for the recycling of oceanic crust in the mantle. It has previously been established that *basaltic* oceanic crust may lose a significant proportion of its Re during subduction and therefore evolve to less radiogenic Os isotope values during storage in the mantle (Becker 2000). The data for basaltic eclogites from the Zermatt-Saas ophiolite (presented in Chapter 6) also reveal modification of the Re-Os system and the likely loss of approximately 50-60% of the original magmatic budget of Re.

The Os isotopic evolution of a complete section of mafic oceanic crust has been calculated, while the spreadsheets of Stracke et al. (2003) have been used to model $^{206}Pb/^{204}Pb$ isotope evolution. Different quantities of oceanic crust were then mixed with the mantle in order to determine whether the Os and Pb signatures of HIMU-type OIB can be generated within well-constrained geological parameters.

The following conclusions can be drawn from the modelling:

- Despite the lower initial Re/Os ratios of gabbros, upon mixing with mantle a complete section of oceanic crust will generate similarly high Os isotope signatures as subducted MORB alone.
- Complete oceanic crust will evolve to much lower $^{206}Pb/^{204}Pb$ ratios than MORB alone.
- These observations provide a means of allowing long residence timescales for ^{187}Os ingrowth without producing $^{206}Pb/^{204}Pb$ signatures which are more elevated than any known OIB.

- Timescales of 2 to 2.5 Ga are required to generate the observed $^{187}Os/^{188}Os$ signature of some OIB (~0.150).
- High proportions of oceanic crust (>40%) are required in the mantle source of HIMU-type OIB to produce sufficiently elevated Os isotope signatures.

The estimated proportion of oceanic crust in the mantle (>40%) is high in comparison with previous models (20-30%, e.g. Hauri and Hart 1993; Reisberg et al. 1993; Roy-Barman and Allegre 1995). Furthermore, until recently, melting of such high proportions of crustal material was expected to result in silica-rich, rather than silica-undersaturated melts of the type displayed by HIMU OIB. However, new data from Kogiso et al. (2003) suggest that OIB magmas could be produced from melting of garnet pyroxenite, which may result from interactions between recycled crust and mantle.

Given the current limitations to the knowledge of Re and Os in oceanic crust, it is possible that lower (or higher) quantities of crust would be required to produce the necessary Os isotope signatures.

9.1.3 Re and Os in mineral phases

Osmium isotope data and Re and Os abundances have been determined by ID N-TIMS analysis for mineral separates from two gabbros and two gabbroic eclogites. Silicate mineral phases typically contain very low concentrations of Re and Os, thus their analysis can be problematic. However, using the chemical separation procedure of Birck et al. (1997), it has been possible to achieve extremely low Os blanks (~15 femtograms) and low Re blanks (<2 picograms) and thus to obtain precise abundance and isotopic data for silicate, oxide and sulphide phases. Re and Os abundances in sulphide, together with PGE elements, have also be determined by LA-ICP-MS.

The key findings for the cumulate gabbros are as follows:

- Sulphide phases contain Os abundances which are highly variable but are 1 to 3 orders-of-magnitude greater than any silicate phases (0.4 – 325 ppb). Re abundances also vary (2 – 135 ppb) and are typically 1 to 2 orders-of-magnitude greater than silicates.
- Sulphides account for 50-70% of the Os budget in the samples analysed, but only contain 2-4% of the whole rock budget of Re.
- Plagioclase contains a Re abundance (174 ppt) which is comparable to the whole-rock value and given its high modal abundance, hosts nearly 70% of the total Re. Os, however, is virtually absent (<0.5 ppt).
- Olivine is an important carrier of both Re and Os (190 and 15 ppt, respectively) although tiny opaque inclusions may account for some of the Re and Os present.

The conclusions from the gabbroic eclogites are as follows:

- Sulphides generally contain lower Os and higher Re abundances than in unaltered gabbros, although they remain an important host of Os and an insignificant host of Re. The difference probably reflects modification during the hydrothermal episode.
- Garnet contains high concentrations of Re (1.0 and 7.2 ppb in the two fractions analysed), and thus is likely to control the Re budget in subducted oceanic crust.
- Talc and glaucophane have both been found to contain considerable abundances of Os (151 and 91 ppt, respectively), while talc, particularly, also hosts Re in high abundances (561 ppt).

The isotopic data for the minerals reveal:

- Some gabbroic phases yield a best-fit age of ~152 ± 12 Ma, indicating that the Re-Os system has not been significantly perturbed at a mineral grain scale for these phases.
- Most phases from a gabbroic eclogite lie close to a 50 Ma reference line, while the whole rock gives a model age close to 164 Ma. This demonstrates that the Re-Os system has been reset at a mineral scale as a result of metamorphism, while the sample as a whole has retained its igneous age (i.e. has remained closed-system on a whole-rock scale).

9.2 Trace elements in silicate phases

Trace element concentrations have been determined for silicate phases from unaltered gabbros and gabbroic and basaltic eclogites from the ZSO. The rationale behind these measurements was to gain a greater understanding of the phases which control the budget of key arc-related elements (those elements which are commonly discussed with respect to arc genesis, e.g. LILE, LREE, Nb). The most important phases hosting trace elements are outlined here:

- In gabbros, clinopyroxene (augite) contains almost the entire budget of M- and H-REE, as well as being a significant repository for Nb, Zr, Hf, U and Th. Plagioclase contains the highest abundances of the LILE and the highest proportion of the LILE and LREE budget.
- In gabbroic eclogites, saussurite (which pseudomorphs plagioclase - predominantly consists of zoisite) dominates the budgets of LREE, Li and Sr, while the other LILE and Pb are hosted primarily in amphibole. Omphacite contains abundant Ba, Li, Nb, Zr and Hf, although the elevations of Nb, Zr and Hf may be explained by small inclusions of rutile. Garnet contains a significant proportion of the HREE despite being volumetrically subordinate (modal proportion ~6%).

- In basaltic eclogites, paragonite contains the highest abundances (and proportions) of LILE. Epidote hosts the majority of the LREE and Sr, Pb. Garnet contains the majority of the HREE. Omphacite contains almost all the whole-rock Li budget.
- Trace element patterns in garnet and omphacite from some gabbroic eclogites indicate a lack of equilibrium within these samples. Garnet possesses positive Eu anomalies inherited from the plagioclase from which it has grown.

If mineral reactions exert a control on the loss of elements from the down-going slab (a matter of debate, see Spandler et al. 2003), the most important phase breakdown reactions in gabbroic rocks will include clinopyroxene (for M- to H-REE) and plagioclase (for LILE and the LREE). Regardless of whether the release of elements from the slab is primarily controlled by mineral breakdown or by mineral-fluid interactions, plagioclase is the most important phase controlling the release of 'fluid-mobile' elements from the slab. At pressures above the stability of plagioclase, epidote/zoisite and a mica phase (usually paragonite in mafic lithologies) will be the phases which carry the majority of the LREE and LILE. The breakdown of these phases at approximately sub-arc depths (~3 GPa, Poli and Schmidt 2002) may provide a flux of elements into the source region of arc magmas. However, mineral reactions are likely to be continuous and so the elemental release (if any) would occur over a longer depth range (Poli and Schmidt 2002).

9.3 Mobility of trace elements in subducted mafic crust and implications for arc magmatism

Unlike Re, some typically fluid-mobile elements are depleted in the gabbroic eclogites of the Allalin, suggesting that fluid loss/flow has occurred. Barium, K, Rb and Sr all display variable depletion from 0 to 85% of the postulated initial

composition. Basaltic eclogites have, in general, also been extensively depleted in the LILE, although Sr loss is less clearly displayed than in the gabbroic lithologies. The salient points from the study of whole rock trace element data are as follows:

- U and La are not depleted in either metabasaltic of metagabbroic samples. The mobility of U in fluids has been invoked to explain elevated abundances in arc magmas (Elliott et al. 1997). The lack of depletion in these samples suggests either immobility, or that mobility is strongly dependent on fluid composition and/or temperature (see Keppler 1996; and Becker et al. 2000).
- Rb and K have been depleted by an average of ~35% in the metabasalts. Barium has been more highly depleted (average ~70%) while Sr concentrations may be 20% lower than the proposed protolith. However, some samples are enriched in LILE suggesting redistribution, as opposed to net loss, of some of the mobile elements.
- In the gabbroic samples displaying LILE depletion, Sr losses appear to be higher than in many metabasaltic samples. This may be due to the considerably higher initial Sr abundance which may not be adequately incorporated into newly crystallising phases, following the breakdown of plagioclase.
- It is difficult to ascertain whether Os is lost from the subducting slab due to a lack of similarly compatible elements with which to compare abundances, although a comparison of the unaltered and eclogitic gabbros from the Allalin suggests no Os loss from the gabbroic section of the crust.
- Re loss from the basaltic crust may explain some of the elevated Os isotope signatures of arc magmas, although the magnitude of Os isotope elevations in arcs is a matter of debate as many of these elevations have been ascribed to crustal contamination (Woodhead and Brauns 2004).

References

Ahrens, T. J., Schubert, G. (1975). "Gabbro-eclogite reaction rate and its geophysical significance." Reviews of Geophysics and Space Physics 13: 383-400.

Alard, O., W. L. Griffin, J. P. Lorand, S. E. Jackson and S. Y. O'Reilly (2000). "Non-chondritic distribution of the highly siderophile elements in mantle sulphides." Nature 407(6806): 891-894.

Alard, O., W. L. Griffin, N. J. Pearson, J. P. Lorand and S. Y. O'Reilly (2002). "New insights into the Re-Os systematics of sub-continental lithospheric mantle from in situ analysis of sulphides." Earth and Planetary Science Letters 203(2): 651-663.

Allegre, C. J. and J. M. Luck (1980). "Osmium isotopes as petrogenetic and geological tracers." Earth and Planetary Science Letters 48(1): 148-154.

Allegre, C. J. and D. L. Turcotte (1986). "Implications of a 2-Component Marble-Cake Mantle." Nature 323(6084): 123-127.

Alt, J. C. (1995). Sub-seafloor processes in mid-ocean ridge hydrothermal systems. In: Seafloor hydrothermal systems: Physical, chemical, biological and geological interactions. S. E. Humphris, R. A. Zierenberg et al. American Geophysical Union, Washington, DC: 85-114.

Alves, S., P. Schiano and C. J. Allegre (1999). "Rhenium-osmium isotopic investigation of Java subduction zone lavas." Earth and Planetary Science Letters 168(1-2): 65-77.

Alves, S., P. Schiano, F. Capmas and C. J. Allegre (2002). "Osmium isotope binary mixing arrays in arc volcanism." Earth and Planetary Science Letters 198(3-4): 355-369.

Amato, J. M., C. M. Johnson, L. P. Baumgartner and B. L. Beard (1999). "Rapid exhumation of the Zermatt-Saas ophiolite deduced from high-precision Sm-Nd and Rb-Sr geochronology." Earth and Planetary Science Letters 171(3): 425-438.

Arculus, R. J. and R. Powell (1986). "Source Component Mixing in the Regions of Arc Magma Generation." Journal of Geophysical Research-Solid Earth and Planets 91(B6): 5913-5926.

Arculus, R. J., H. Lapierre and E. Jaillard (1999). "Geochemical window into subduction and accretion processes: Raspas metamorphic complex, Ecuador." Geology 27(6): 547-550.

Arnaud, N. O. and S. P. Kelley (1995). "Evidence for Excess Argon During High-Pressure Metamorphism in the Dora-Maira Massif (Western Alps, Italy), Using an Ultra- Violet Laser-Ablation Microprobe Ar-40-Ar-39 Technique." Contributions to Mineralogy and Petrology 121(1): 1-11.

Austrheim, H. (1987). "Eclogitization of Lower Crustal Granulites by Fluid Migration through Shear Zones." Earth and Planetary Science Letters 81(2-3): 221-232.

Avigad, D., C. Chopin, B. Goffe and A. Michard (1993). "Tectonic Model for the Evolution of the Western Alps." Geology 21(7): 659-662.

Ballhaus, C., M. Tredoux and A. Spath (2001). "Phase relations in the Fe-Ni-Cu-PGE-S system at magmatic temperature and application to massive sulphide ores of the Sudbury Igneous Complex." Journal of Petrology 42(10): 1911-1926.

Barnes, S. J., A. J. Naldrett and M. P. Gorton (1985). "The Origin of the Fractionation of Platinum-Group Elements in Terrestrial Magmas." Chemical Geology 53(3-4): 303-323.

Barnicoat, A. C. and N. Fry (1986). "High-Pressure Metamorphism of the Zermatt-Saas Ophiolite Zone, Switzerland." Journal of the Geological Society 143: 607-618.

Barnicoat, A. C. (1988). "Zoned high-pressure assemblages in pillow lavas of the Zermatt-Saas ophiolite zone, Switzerland." Lithos 21(3): 227-236.

Barnicoat, A. C. and I. Cartwright (1995). "Focused fluid flow during subduction: Oxygen isotope data from high-pressure ophiolites of the western Alps." Earth and Planetary Science Letters 132(1-4): 53-61.

Barnicoat, A. C. (1996). "V71C-07: Dolomite breakdown under ultra-high pressure conditions in the Allalin Gabbro of SW Switzerland." American Geophysical Union 77, no. 46: No. 762.

Barnicoat, A. C. and I. Cartwright (1997). "The gabbro-eclogite transformation: An oxygen isotope and petrographic study of west Alpine ophiolites." Journal of Metamorphic Geology 15(1): 93-104.

Baumgartner, P. O. (1987). "Age and Genesis of Tethyan Jurassic Radiolarites." Eclogae Geologicae Helvetiae 80(3): 831-&.

Bearth, P. (1959). "Über Eklogite, Glaucophanschiefer, und metamorphe Pillowlaven." Schweizerische Mineralogische und Petrographische Mitteilungen 39: 267-286.

Bearth, P. (1963). "Chloritoid und Paragonit aus der Ophiolith-Zone von Zermatt-Saas Fee." Schweizerische Mineralogische und Petrographische Mitteilungen = Bulletin Suisse de Mineralogie et Petrographie 43(1): 269-286.

Bearth, P. (1967a). Die Ophiolithe der Zone von Zermatt-Saas Fee. In: Beitraege zur Geologischen Karte der Schweiz N.F. Bern Kuemmerly & Frey, 132.

Bearth, P. and H. Schwandler (1967b). "Mineralogie und Petrographie." Verhandlungen der Naturforschenden Gesellschaft in Basel 78(1): 80-84.

Bearth, P. (1971). "Investigations on the ophiolites of the Alps." Upper Mantle Project; Final Report of Switzerland Schweizerische Mineralogische und Petrographische Mitteilungen = Bulletin Suisse de Mineralogie et Petrographie 51(2-3): 578.

Bearth, P. and W. Stern (1971). "Zum Chemismus der Eklogite und Glaukophanite von Zermatt." Schweizerische Mineralogische und Petrographische Mitteilungen = Bulletin Suisse de Mineralogie et Petrographie 51(2-3): 349-359.

Bearth, P. and W. Stern (1979). "Zur Geochemie von Metapillows der Region Zermatt-Saas." Schweizerische Mineralogische und Petrographische Mitteilungen = Bulletin Suisse de Mineralogie et Petrographie 59(3): 349-373.

Bebout, G. E., J. G. Ryan and W. P. Leeman (1993). "B-Be Systematics in Subduction-Related Metamorphic Rocks - Characterization of the Subducted Component." Geochimica Et Cosmochimica Acta 57(10): 2227-2237.

Bebout, G. E. (1995). "The impact of subduction-zone metamorphism on mantle-ocean chemical cycling." Chemical Geology 126(2): 191-218.

Beccaluva, L., G. V. Dal Piaz and G. Macciotta (1984). "Transitional to normal MORB affinities in ophiolitic metabasites from the Zermatt-Saas, Combin and Antrona units, Western Alps; implications for the paleogeographic evolution of the western Tethyan Basin." Ophiolites and ultramafic rocks; a tribute to Emile den Tex Geologie en Mijnbouw 63(2): 165-177.

Becker, H. (1993). "Garnet peridotite and eclogite Sm-Nd mineral ages from the Lepontine Dome (Swiss Alps) - New evidence for Eocene high-pressure metamorphism in the Central Alps." Geology 21(7): 599-602.

Becker, H., K. P. Jochum and R. W. Carlson (1999). "Constraints from high-pressure veins in eclogites on the composition of hydrous fluids in subduction zones." Chemical Geology 160(4): 291-308.

Becker, H. (2000). "Re-Os fractionation in eclogites and blueschists and the implications for recycling of oceanic crust into the mantle." Earth and Planetary Science Letters 177(3-4): 287-300.

Becker, H., K. P. Jochum and R. W. Carlson (2000). "Trace element fractionation during dehydration of eclogites from high-pressure terranes and the implications for element fluxes in subduction zones." Chemical Geology 163(1-4): 65-99.

Ben Othman, D., W. M. White and J. Patchett (1989). "The Geochemistry of Marine-Sediments, Island-Arc Magma Genesis, and Crust Mantle Recycling." Earth and Planetary Science Letters 94(1-2): 1-21.

Bennett, V. C., T. M. Esat and M. D. Norman (1996). "Two mantle-plume components in Hawaiian picrites inferred from correlated Os-Pb isotopes." Nature 381(6579): 221-224.

Bezos, A., J. P. Lorand, E. Humler and M. Gros (in press). "Platinum-group element systematics in mid-oceanic ridge basaltic glasses from the Pacific, Atlantic and Indian oceans." Geochimica et Cosmochimica Acta.

Birck, J. L. and C. J. Allegre (1994). "Contrasting Re/Os magmatic fractionation in planetary basalts." Earth and Planetary Science Letters 124(1-4): 139-148.

Birck, J. L., M. R. Barman and F. Capmas (1997). "Re-Os isotopic measurements at the femtomole level in natural samples." Geostandards Newsletter-the Journal of Geostandards and Geoanalysis 21(1): 19-27.

Blusztajn, J., S. R. Hart, G. Ravizza and H. J. B. Dick (2000). "Platinum-group elements and Os isotopic characteristics of the lower oceanic crust." Chemical Geology 168(1-2): 113-122.

Bockrath, C., C. Ballhaus and A. Holzheid (2004). "Fractionation of the platinum-group elements during mantle melting." Science 305(5692): 1951-1953.

Bocquet, J., M. Delaloye, J. C. Hunziker and D. Krummenacher (1974). "K-Ar and Rb-Sr Dating of Blue Amphiboles, Micas, and Associated Minerals from the Western Alps." Contributions to Mineralogy and Petrology 47(1): 7-26.

Borg, L. E., A. D. Brandon, M. A. Clynne and R. J. Walker (2000). "Re-Os isotopic systematics of primitive lavas from the Lassen region of the Cascade arc, California." Earth and Planetary Science Letters 177(3-4): 301-317.

Boudier, F. and A. Nicolas (1995). "Nature of the Moho transition zone in the Oman ophiolite." Journal of Petrology 36(3): 777-796.

Bourdon, E., J. P. Eissen, M. Monzier, C. Robin, H. Martin, J. Cotten and M. L. Hall (2002). "Adakite-like lavas from Antisana volcano (Ecuador): Evidence for slab melt metasomatism beneath the Andean Northern volcanic zone." Journal of Petrology 43(2): 199-217.

Bowtell, S. A. (1991). Geochronological and geochemical studies of the Zermatt - Saas Fee Ophiolite, Western Alps. Earth Sciences. Leeds, University of Leeds: 240.

Bowtell, S. A., R. A. Cliff and A. C. Barnicoat (1994). "Sm-Nd Isotopic Evidence on the Age of Eclogitization in the Zermatt-Saas Ophiolite." Journal of Metamorphic Geology 12(2): 187-196.

Boyle, A. P. (1980). "The Sulitjelma amphibolites, Norway: Part of a Lower Palaeozoic ophiolite complex?" Proceedings of the International Ophiolite Symposium, Nicosia 1979: 567-75.

Boyle, A. P. (1982). Structure, petrology and ophiolitic affinities of the Sulitjelma amphibolites, Central Scandinavian Caledonides. PhD thesis. Department of Geological Sciences, University College London.

Boyle, A. P. (1989). The geochemistry of the Sulitjelma ophiolite and associated basic volcanics: tectonic implications. In: The Caledonide Geology of Scandinavia. R. A. Gayer. Graham & Trotman Limited, London: 153-163.

Boyle, A. P. and R. K. Westhead (1992). "Metamorphic Peak Geothermobarometry in the Furulund Group, Sulitjelma, Scandinavian Caledonides - Implications for Uplift." Journal of Metamorphic Geology 10(5): 615-626.

Brady, J. B. and R. H. McCallister (1983). "Diffusion Data for Clinopyroxenes from Homogenization and Self- Diffusion Experiments." American Mineralogist 68(1-2): 95-105.

Brandon, A. D., R. A. Creaser, S. B. Shirey and R. W. Carlson (1996). "Osmium recycling in subduction zones." Science 272(5263): 861-864.

Brandon, A. D., H. Becker, R. W. Carlson and S. B. Shirey (1999). "Isotopic constraints on time scales and mechanisms of slab material transport in the mantle wedge: evidence from the Simcoe mantle xenoliths, Washington, USA." Chemical Geology 160(4): 387-407.

Brenan, J. M., H. F. Shaw, F. J. Ryerson and D. L. Phinney (1995). "Mineral-aqueous fluid partitioning of trace elements at 900°C and 2.0 GPa: Constraints on the trace element chemistry of mantle and deep crustal fluids." Geochimica et Cosmochimica Acta 59(16): 3331-3350.

Brouwer, F. and S. Sorenson (2002). "Goldschmidt Abstracts: Whole-rock and mineral trace element distributions in Alpine and Franciscan eclogites." Geochimica et Cosmochimica Acta 66(Supplement 1): 105.

Brugmann, G. E., N. T. Arndt, A. W. Hofmann and H. J. Tobschall (1987). "Noble-Metal Abundances in Komatiite Suites from Alexo, Ontario, and Gorgona-Island, Colombia." Geochimica Et Cosmochimica Acta 51(8): 2159-2169.

Burton, K. W., A. P. Boyle, W. L. Kirk and R. Mason (1989). Pressure, temperature and structural evolution of the Sulitjelma fold-nappe, central Scandinavian Caledonides. In: Evolution of Metamorphic Belts. J. S. Daly, R. A. Cliff and B. W. D. Yardley. Geological Society of London, London: 391-411.

Burton, K. W. and R. K. O'Nions (1992). "The Timing of Mineral Growth across a Regional Metamorphic Sequence." Nature 357(6375): 235-238.

Burton, K. W., P. Schiano, J. L. Birck and C. J. Allegre (1999). "Osmium isotope disequilibrium between mantle minerals in a spinel-lherzolite." Earth and Planetary Science Letters 172(3-4): 311-322.

Burton, K. W., P. Schiano, J.-L. Birck, C. J. Allegre, M. Rehkämper, A. N. Halliday and J. B. Dawson (2000). "The distribution and behaviour of rhenium and osmium amongst mantle minerals and the age of the lithospheric mantle beneath Tanzania." Earth and Planetary Science Letters 183(1-2): 93-106.

Burton, K. W., A. Gannoun, J.-L. Birck, C. J. Allegre, P. Schiano, R. Clocchiatti and O. Alard (2002). "The compatibility of rhenium and osmium in natural olivine and their behaviour during mantle melting and basalt genesis." Earth and Planetary Science Letters 198(1-2): 63-76.

Caron, M., R. Doessegger, R. Steiger and R. Truempy (1982). "Das Alter der juengsten Sedimente der Ortler-Decke (oberostalpin) in der Val Trupchun (Schweizerischer Nationalpark, Graubuenden)." Eclogae Geologicae Helvetiae 75(1): 159-169.

Carson, C. J., R. Powell and G. L. Clarke (1999). "Calculated mineral equilibria for eclogites in CaO-Na2O-FeO- MgO-Al2O3-SiO2-H2O: application to the Pouebo Terrane, Pam Peninsula, New Caledonia." Journal of Metamorphic Geology 17(1): 9-24.

Cartwright, I. and A. C. Barnicoat (1999). "Stable isotope geochemistry of Alpine ophiolites: a window to ocean-floor hydrothermal alteration and constraints on fluid- rock interaction during high-pressure metamorphism." International Journal of Earth Sciences 88(2): 219-235.

Cartwright, I. and I. S. Buick (1999). "The flow of surface-derived fluids through Alice Springs age middle-crustal ductile shear zones, Reynolds Range, central Australia." Journal of Metamorphic Geology 17(4): 397-414.

Cartwright, I. and A. C. Barnicoat (2002). "Petrology, geochronology, and tectonics of shear zones in the Zermatt-Saas and Combin zones of the Western Alps." Journal of Metamorphic Geology 20(2): 263-281.

Chakraborty, S. and J. Ganguly (1991). Compositional zoning and cation diffusion in garnets. In: Diffusion, atomic ordering, and mass transport; selected topics in geochemistry. Advances in Physical Geochemistry. Springer, New York, NY, 8: 120-175.

Chauvel, C., A. W. Hofmann and P. Vidal (1992). "HIMU-EM: the French-Polynesian Connection." Earth and Planetary Science Letters 110(1-4): 99-119.

Chauvel, C., S. L. Goldstein and A. W. Hofmann (1995). "Hydration and Dehydration of Oceanic-Crust Controls Pb Evolution in the Mantle." Chemical Geology 126(1): 65-75.

Chesley, J., J. Ruiz, K. Righter, L. Ferrari and A. Gomez-Tuena (2002). "Source contamination versus assimilation: an example from the Trans-Mexican Volcanic Arc." Earth and Planetary Science Letters 195(3-4): 211-221.

Chesley, J., K. Righter and J. Ruiz (2004). "Large-scale mantle metasomatism: a Re-Os perspective." Earth and Planetary Science Letters 219(1-2): 49-60.

Chinner, G. A. and J. E. Dixon (1973). "Some High-pressure Parageneses of the Allalin Gabbro, Valais, Switzerland." Journal of Petrology 14(2): 185-202.

Chopin, C. and P. Monié (1984). "A Unique Magnesiochloritoid-Bearing, High-Pressure Assemblage from the Monte-Rosa, Western Alps - Petrologic and Ar-40-Ar-39 Radiometric Study." Contributions to Mineralogy and Petrology 87(4): 388-398.

Cohen, A. S. and F. G. Waters (1996). "Separation of osmium from geological materials by solvent extraction for analysis by thermal ionisation mass spectrometry." Analytica Chimica Acta 332(2-3): 269-275.

Coleman, R. G. and X. Wang (1995). Overview of the geology and tectonics of UHPM. In: Ultra-high-pressure metamorphism. R. G. Coleman and X. Wang. Cambridge University Press: 1-32.

Constantin, M. (1999). "Gabbroic intrusions and magmatic metasomatism in harzburgites from the Garrett transform fault; implications for the nature of the mantle-crust transition at fast-spreading ridges." Contributions to Mineralogy and Petrology 136(1-2): 111-130.

Cooper, M. A., G. M. Bliss, I. L. Ferriday and C. Halls (1979). "The Geology of the Sorjusdalen area, Nordland, Norway." Norges Geologiske Undersokelse 351: 31-50.

Creaser, R. A., D. A. Papanastassiou and G. J. Wasserburg (1991). "Negative Thermal Ion Mass-Spectrometry of Osmium, Rhenium, and Iridium." Geochimica Et Cosmochimica Acta 55(1): 397-401.

Crocket, J. H. and W. E. Macrae (1986). "Platinum-Group Element Distribution in Komatiitic and Tholeiitic Volcanic-Rocks from Munro Township, Ontario." Economic Geology 81(5): 1242-1251.

Dal Piaz, G. V. and W. G. Ernst (1978). "Areal Geology and Petrology of Eclogites and associated metabasites of the Piemonte Ophiolite Nappe, Breuil-St. Jacques area, Italian Western Alps." Tectonophysics 51: 99-126.

Dal Piaz, G. V. (2001). "Geology of the Monte Rosa massif: historical review and personal comments." Schweizerische Mineralogische Und Petrographische Mitteilungen 81(3): 275-303.

Davies, G. F. (1992). "On the Emergence of Plate-Tectonics." Geology 20(11): 963-966.

Davies, J. H. and M. J. Bickle (1991). "A Physical Model for the Volume and Composition of Melt Produced by Hydrous Fluxing above Subduction Zones." Philosophical Transactions of the Royal Society of London Series A-Mathematical Physical and Engineering Sciences 335(1638): 355-364.

Davies, J. H. and D. J. Stevenson (1992). "Physical Model of Source Region of Subduction Zone Volcanics." Journal of Geophysical Research-Solid Earth 97(B2): 2037-2070.

Deer, W. A., R. A. Howie and J. Zussman (1992). An introduction to the rock-forming minerals. Longman, Harlow, United Kingdom. p.696

Dewey, J. F., W. C. Pitman, III, W. B. F. Ryan and J. Bonnin (1973). "Plate Tectonics and the Evolution of the Alpine System." Geological Society of America Bulletin 84(10): 3137-3180.

Domanik, K. J. and J. R. Holloway (1996). "The stability and composition of phengitic muscovite and associated phases from 5.5 to 11 GPa: Implications for deeply subducted sediments." Geochimica Et Cosmochimica Acta 60(21): 4133-4150.

Dunning, G. R. and R. B. Pedersen (1988). "U/Pb Ages of Ophiolites and Arc-Related Plutons of the Norwegian Caledonides - Implications for the Development of Iapetus." Contributions to Mineralogy and Petrology 98(1): 13-23.

Dupre, B. and C. J. Allegre (1983). "Pb-Sr Isotope Variation in Indian-Ocean Basalts and Mixing Phenomena." Nature 303(5913): 142-146.

Elliott, T., T. Plank, A. Zindler, W. White and B. Bourdon (1997). "Element transport from slab to volcanic front at the Mariana arc." Journal of Geophysical Research-Solid Earth 102(B7): 14991-15019.

Ellis, D. J. and D. H. Green (1979). "An experimental study of the effect of Ca upon garnet-clinopyroxene Fe-Mg exchange equilibria." Contributions to Mineralogy and Petrology 71(1): 13-22.

Ernst, W. G. (1973). "Interpretative Synthesis of Metamorphism in the Alps." Geological Society of America Bulletin 84(6): 2053-2078.

Ernst, W. G. and G. V. Dal Piaz (1978). "Mineral Parageneses of eclogitic rocks and related mafic schists of the Piemonte ophiolite nappe, Breuil-St.Jacques area, Italian Western Alps." American Mineralogist 63: 621-640.

Ertel, W., H. S. C. O'Neill, P. J. Sylvester, D. B. Dingwell and B. Spettel (2001). "The solubility of rhenium in silicate melts: Implications for the geochemical properties of rhenium at high temperatures." Geochimica et Cosmochimica Acta 65(13): 2161-2170.

Esser, B. K. and K. K. Turekian (1993). "The osmium isotopic composition of the continental crust." Geochimica et Cosmochimica Acta 57(13): 3093-3104.

Falloon, T. J., A. Malahoff, L. P. Zonenshain and Y. Bogdanov (1992). "Petrology and Geochemistry of Back-Arc Basin Basalts from Lau Basin Spreading Ridges at 15-Degrees, 18-Degrees and 19- Degrees-S." Mineralogy and Petrology 47(1): 1-35.

Fehn, U., R. Teng, D. Elmore and P. W. Kubik (1986). "Isotopic Composition of Osmium in Terrestrial Samples Determined by Accelerator Mass-Spectrometry." Nature 323(6090): 707-710.

Fleet, M. E., J. H. Crocket and W. E. Stone (1996). "Partitioning of platinum-group elements (Os, Ir, Ru, Pt, Pd) and gold between sulfide liquid and basalt melt." Geochimica Et Cosmochimica Acta 60(13): 2397-2412.

Florineth, D. and N. Froitzheim (1994). "Transition from Continental to Oceanic Basement in the Tasna Nappe (Engadine Window, Graubunden, Switzerland) - Evidence for Early Cretaceous Opening of the Valais Ocean." Schweizerische Mineralogische Und Petrographische Mitteilungen 74(3): 437-448.

Freer, R., M. A. Carpenter, J. V. P. Long and S. J. B. Reed (1982). "Null Result Diffusion Experiments with Diopside - Implications for Pyroxene Equilibria." Earth and Planetary Science Letters 58(2): 285-292.

Frisch, W. (1979). "Tectonic progradation and plate tectonic evolution of the Alps." Tectonophysics 60(3-4): 121-139.

Froitzheim, N., S. M. Schmid and M. Frey (1996). "Mesozoic paleogeography and the timing of eclogite-facies metamorphism in the Alps: A working hypothesis." Eclogae Geologicae Helvetiae 89(1): 81-.

Fumagalli, P., L. Stixrude, S. Poli and D. Snyder (2001). "The 10 angstrom phase: a high-pressure expandable sheet silicate stable during subduction of hydrated lithosphere." Earth and Planetary Science Letters 186(2): 125-141.

Ganguly, J., W. J. Cheng and S. Chakraborty (1998). "Cation diffusion in aluminosilicate garnets: experimental determination in pyrope-almandine diffusion couples." Contributions to Mineralogy and Petrology 131(2-3): 171-180.

Gannoun, A., K. W. Burton, O. Alard, I. J. Parkinson and L. E. Thomas (2004a). "Assessing the scale of osmium isotope heterogeneity in Mid-Ocean Ridge Basalts." Geochimica Et Cosmochimica Acta 68(11): A703-A703.

Gannoun, A., K. W. Burton, L. E. Thomas, I. J. Parkinson, P. van Calsteren and P. Schiano (2004b). "Osmium isotope heterogeneity in the constituent phases of mid- ocean ridge basalts." Science 303(5654): 70-72.

Gardien, V., E. Reusser and D. Marquer (1994). "Pre-Alpine Metamorphic Evolution of the Gneisses from the Valpelline Series (Western Alps, Italy)." Schweizerische Mineralogische Und Petrographische Mitteilungen 74(3): 489-502.

Gente, P., R. A. Pockalny, C. Durand, C. Deplus, M. Maia, G. Ceuleneer, C. Mevel, M. Cannat and C. Laverne (1995). "Characteristics and evolution of the segmentation of the Mid-Atlantic Ridge between 20 degrees N and 24 degrees N during the last 10 million years." Earth and Planetary Science Letters 129(1-4): 55-71.

Gramlich, J. W., T. J. Murphy and E. L. Garner (1973). "The atomic weight of rhenium." J. Res. Nat. Bur. Stand. Sect. A 77: 691-698.

Handler, M. R. and V. C. Bennett (1999). "Behaviour of Platinum-group elements in the subcontinental mantle of eastern Australia during variable metasomatism and melt depletion." Geochimica Et Cosmochimica Acta 63(21): 3597-3618.

Hart, S. R. and H. Staudigel (1982). "The control of alkalies and uranium in seawater by ocean crust alteration." Earth and Planetary Science Letters 58: 202-212.

Hart, S. R. (1984). "A Large-Scale Isotope Anomaly in the Southern-Hemisphere Mantle." Nature 309(5971): 753-757.

Hart, S. R., J. Blusztajn, H. J. B. Dick and J. R. Lawrence (1994). "Fluid Circulation in the Oceanic-Crust - Contrast between Volcanic and Plutonic Regimes." Journal of Geophysical Research-Solid Earth 99(B2): 3163-3173.

Hart, S. R. and G. Ravizza (1996). Os partitioning between phases in lherzolite and basalt. In: Earth processes: reading the isotopic code. A. Basu and S. R. Hart. American Geophysical Union: 123-134.

Hart, S. R., J. Blusztajn, H. J. B. Dick, P. S. Meyer and K. Muehlenbachs (1999). "The fingerprint of seawater circulation in a 500-meter section of ocean crust gabbros." Geochimica et Cosmochimica Acta 63(23-24): 4059-4080.

Hauri, E. H. and S. R. Hart (1993). "Re-Os Isotope Systematics of HIMU and EM-II Oceanic Island Basalts from the South-Pacific Ocean." Earth and Planetary Science Letters 114(2-3): 353-371.

Hauri, E. H., J. C. Lassiter and D. J. DePaolo (1996). "Osmium isotope systematics of drilled lavas from Mauna Loa, Hawaii." Journal of Geophysical Research-Solid Earth 101(B5): 11793-11806.

Hawkesworth, C. and R. Ellam (1989). "Chemical Fluxes and Wedge Replenishment Rates Along Recent Destructive Plate Margins." Geology 17(1): 46-49.

Hawkesworth, C. J., K. Gallagher, J. M. Hergt and F. McDermott (1993). "Mantle and Slab Contributions in Arc Magmas." Annual Review of Earth and Planetary Sciences 21: 175-204.

Hawkesworth, C. J., S. P. Turner, F. McDermott, D. W. Peate and P. van Calsteren (1997). "U-Th isotopes in arc magmas: Implications for element transfer from the subducted crust." Science 276(5312): 551-555.

Hekinian, R., D. Bideau, J. Francheteau, J. L. Cheminee, R. Armijo, P. Lonsdale and N. Blum (1993). "Petrology of the East Pacific Rise crust and upper mantle exposed in Hess Deep (eastern Equatorial Pacific)." Journal of Geophysical Research, B, Solid Earth and Planets 98(5): 8069-8094.

Henry, D. J. and C. V. Guidott (2002). "Titanium in biotite from metapelitic rocks: Temperature effects, crystal-chemical controls, and petrologic applications." American Mineralogist 87(4): 375-382.

Herr, W., W. Hoffmeister, B. Hirt, J. Geiss and F. G. Houtermans (1961). "Versuch zur datiering von eisenmeteoriten nach der rhenium-osmium-methode." Z. Naturforsch. Teil A 16: 1053-1058.

Herzberg, C. and J. Z. Zhang (1998). "Melting experiments in the systems CaO-MgO-Al2O3-SiO2 and MgO- SiO2 at 3 to 15 GPa." American Mineralogist 83(5-6): 491-500.

Hirschmann, M. M. and E. M. Stolper (1996). "A possible role for garnet pyroxenite in the origin of the "garnet signature" in MORB." Contributions to Mineralogy and Petrology 124(2): 185-208.

Hirt, B., W. Herr and W. Hoffmeister (1963). Age determination by the rhenium-osmium method. In: Radioactive dating. Internat. Atomic Energy Agency, Vienna: 35-44.

Hofmann, A. W. and W. M. White (1982). "Mantle Plumes from Ancient Oceanic-Crust." Earth and Planetary Science Letters 57(2): 421-436.

Hofmann, A. W. (1988). "Chemical Differentiation of the Earth - the Relationship between Mantle, Continental-Crust, and Oceanic-Crust." Earth and Planetary Science Letters 90(3): 297-314.

Hofmann, A. W. (1997). "Mantle geochemistry: The message from oceanic volcanism." Nature 385(6613): 219-229.

Holland, T. J. B. and R. Powell (1985). "An Internally Consistent Thermodynamic Dataset with Uncertainties and Correlations .2. Data and Results." Journal of Metamorphic Geology 3(4): 343-370.

Holland, T. J. B. and R. Powell (1990). "An Enlarged and Updated Internally Consistent Thermodynamic Dataset with Uncertainties and Correlations - the System K2o- Na2o-Cao-Mgo-Mno-Feo-Fe2o3-Al2o3-Tio2-Sio2-C-H2-O2." Journal of Metamorphic Geology 8(1): 89-124.

Holland, T. J. B. and R. Powell (1998). "An internally consistent thermodynamic data set for phases of petrological interest." Journal of Metamorphic Geology 16(3): 309-343.

Horan, M. F., J. W. Morgan, R. J. Walker and J. N. Grossman (1992). "Rhenium-Osmium Isotope Constraints on the Age of Iron- Meteorites." Science 255(5048): 1118-1121.

Horan, M. F., J. W. Morgan, R. I. Grauch, R. M. Coveney, J. B. Murowchick and L. J. Hulbert (1994). "Rhenium and Osmium Isotopes in Black Shales and Ni-Mo-PGE-rich Sulfide Layers, Yukon-Territory, Canada, and Hunan and Guizhou Provinces, China." Geochimica Et Cosmochimica Acta 58(1): 257-265.

Ida, Y. (1983). "Convection in the Mantle Wedge above the Slab and Tectonic Processes in Subduction Zones." Journal of Geophysical Research 88(NB9): 7449-7456.

Inger, S., W. Ramsbotham, R. A. Cliff and D. C. Rex (1996). "Metamorphic evolution of the Sesia-Lanzo Zone, Western Alps: Time constraints from multi-system geochronology." Contributions to Mineralogy and Petrology 126(1-2): 152-168.

Ishikawa, T. and E. Nakamura (1994). "Origin of the Slab Component in Arc Lavas from across-Arc Variation of B and Pb Isotopes." Nature 370(6486): 205-208.

John, T., E. E. Scherer, K. Haase and V. Schenk (2004). "Trace element fractionation during fluid-induced eclogitization in a subducting slab: trace element and Lu-Hf-Sm-Nd isotope systematics." Earth and Planetary Science Letters 227(3-4): 441-456.

Jones, J. H. and M. J. Drake (1986). "Geochemical Constraints on Core Formation in the Earth." Nature 322(6076): 221-228.

Kay, R. W. (1980). "Volcanic arc magmas; implications of a melting-mixing model for element recycling in the crust-upper mantle system." Journal of Geology 88(5): 497-522.

Keays, R. R. (1995). "The Role of Komatiitic and Picritic Magmatism and S-Saturation in the Formation of Ore-Deposits." Lithos 34(1-3): 1-18.

Keppler, H. (1996). "Constraints from partitioning experiments on the composition of subduction-zone fluids." Nature 380(6571): 237-240.

Kienast, J. R. (1973). "Sur l'existence de deux séries différentes au sein de l'ensemble "schistes lustrés-ophiolites" du Val d'Aoste: quelques arguments fondés sur l'étude des roches métamorphiques." Comptes Rendus Hebdomadaires des Seances de l'Academie des Sciences, Serie D: Sciences Naturelles 276(19): 2621-2624.

Kienast, J. R. and B. Messiga (1987). "Cr-Rich Mg-Chloritoid, a 1st Record in High-Pressure Metagabbros from Monviso (Cottian Alps), Italy." Mineralogical Magazine 51(363): 681-687.

Kogiso, T., M. M. Hirschmann and D. J. Frost (2003). "High-pressure partial melting of garnet pyroxenite: possible mafic lithologies in the source of ocean island basalts." Earth and Planetary Science Letters 216(4): 603-617.

Kollung, S. (1989). "Sulitjemafeltat." Norges Geologiske Undersokelse Skrifter 93: 47.

Koons, P. O., D. C. Rubie and G. Fruehgreen (1987). "The Effects of Disequilibrium and Deformation on the Mineralogical Evolution of Quartz Diorite During Metamorphism in the Eclogite Facies." Journal of Petrology 28(4): 679-700.

Kozur, H. (1991). "The Evolution of the Meliata-Hallstatt Ocean and Its Significance for the Early Evolution of the Eastern Alps and Western Carpathians." Palaeogeography Palaeoclimatology Palaeoecology 87(1-4): 109-135.

Kretz, R. (1983). "Symbols for Rock-Forming Minerals." American Mineralogist 68(1-2): 277-279.

Krogh, E. J. (1988). "The Garnet-Clinopyroxene Fe-Mg Geothermometer - a reinterpretation of existing experimental data." Contributions to Mineralogy and Petrology 99(1): 44-48.

Krogh Ravna, E., J. G. Liou and D. A. Carswell, Eds. (2000). The garnet-clinopyroxene Fe2+-Mg geothermometer; an updated calibration. Blackwell, Oxford, United Kingdom. 211-219

Kumar, N., L. Reisberg and A. Zindler (1996). "A major and trace element and strontium, neodymium, and osmium isotopic study of a thick pyroxenite layer from the Beni Bousera Ultramafic Complex of northern Morocco." Geochimica Et Cosmochimica Acta 60(8): 1429-1444.

Lassiter, J. C. and E. H. Hauri (1998). "Osmium-isotope variations in Hawaiian lavas: evidence for recycled oceanic lithosphere in the Hawaiian plume." Earth and Planetary Science Letters 164(3-4): 483-496.

Lassiter, J. C. (2003). "Rhenium volatility in sub-aerial lavas: constraints from subaerial and submarine portions of the HSDP-2 Mauna Kea drillcore." Earth and Planetary Science Letters 6766: 1-15.

Levasseur, S., J. L. Birck and C. J. Allegre (1998). "Direct measurement of femtomoles of osmium and the Os-187/Os- 186 ratio in seawater." Science 282(5387): 272-274.

Liati, A., D. Gebauer, N. Froitzheim and C. M. Fanning (2001). "U-Pb SHRIMP geochronology of an amphibolitized eclogite and an orthogneiss from the Furgg zone (Western Alps) and implications for its geodynamic evolution." Schweizerische Mineralogische Und Petrographische Mitteilungen 81(3): 379-393.

Lindner, M., D. A. Leich, R. J. Borg, G. P. Russ, J. M. Bazan, D. S. Simons and A. R. Date (1986). "Direct Laboratory Determination of the ^{187}Re Half-Life." Nature 320(6059): 246-248.

Lindner, M., D. A. Leich, G. P. Russ, J. M. Bazan and R. J. Borg (1989). "Direct Determination of the Half-Life of Re-187." Geochimica et Cosmochimica Acta 53(7): 1597-1606.

Loomis, T. P. (1978). "Multicomponent diffusion in garnet; II, Comparison of models with natural data." American Journal of Science 278(8): 1119-1137.

Lorand, J. P. and O. Alard (2001). "Platinum-group element abundances in the upper mantle: New constraints from in situ and whole-rock analyses of Massif Central xenoliths (France)." Geochimica Et Cosmochimica Acta 65(16): 2789-2806.

Lorand, J. P., G. Delpech, M. Gregoire, B. Moine, S. Y. O'Reilly and J. Y. Cottin (2004). "Platinum-group elements and the multistage metasomatic history of Kerguelen lithospheric mantle (South Indian Ocean)." Chemical Geology 208(1-4): 195-215.

Luck, J. M., J. L. Birck and C. J. Allegre (1980). "^{187}Re-^{187}Os systematics in meteorites; early chronology of the solar system and age of the Galaxy." Nature 283(5744): 256-259.

Luck, J. M. and C. J. Allegre (1983). "^{187}Re-^{187}Os Systematics in Meteorites and Cosmochemical Consequences." Nature 302(5904): 130-132.

Lugmair, G. W. and S. J. G. Galer (1992). "Age and Isotopic Relationships among the Angrites Lewis Cliff- 86010 and Angra-Dos-Reis." Geochimica Et Cosmochimica Acta 56(4): 1673-1694.

Luguet, A., O. Alard, J. P. Lorand, N. J. Pearson, C. Ryan and S. Y. O'Reilly (2001). "Laser-ablation microprobe (LAM)-ICPMS unravels the highly siderophile element geochemistry of the oceanic mantle." Earth and Planetary Science Letters 189(3-4): 285-294.

Luguet, A., J.-P. Lorand, O. Alard and J.-Y. Cottin (2004). "A multi-technique study of platinum group element systematic in some Ligurian ophiolitic peridotites, Italy." Chemical Geology 208(1-4): 175-194.

Magenheim, A. J., A. J. Spivack, P. J. Michael and J. M. Gieskes (1995). "Chlorine stable isotope composition of the oceanic crust: Implications for Earth's distribution of chlorine." Earth and Planetary Science Letters 131(3-4): 427-432.

Manning, C. E. (2004). "The chemistry of subduction-zone fluids." Earth and Planetary Science Letters 223(1-2): 1-16.

Marcantonio, F., A. Zindler, T. Elliott and H. Staudigel (1995). "Os Isotope Systematics of La Palma, Canary-Islands - Evidence for Recycled Crust in the Mantle Source of HIMU Ocean Islands." Earth and Planetary Science Letters 133(3-4): 397-410.

Martin, C. E. (1991). "Osmium Isotopic Characteristics of Mantle-Derived Rocks." Geochimica et Cosmochimica Acta 55(5): 1421-1434.

Martin, C. E., R. W. Carlson, S. B. Shirey, F. A. Frey and C. Y. Chen (1994). "Os-Isotopic Variation in Basalts from Haleakala Volcano, Maui, Hawaii - a Record of Magmatic Processes in Oceanic Mantle and Crust." Earth and Planetary Science Letters 128(3-4): 287-301.

Mason, R. (1966). The Sulitjelma gabbro complex. Unplubl. PhD thesis. University of Cambridge.

Mason, R. (1971). "The chemistry and structure of the Sulitjelma gabbro." Norsk Geol. Unders. 269: 108-141.

Mathez, E. A. (1976). "Sulphur solubility and magmatic sulphides in submarine basalt glass." Journal of Geophysical Research 81: 4249-4275.

Matthews, A., J. Lieberman, D. Avigad and Z. Garfunkel (1999). "Fluid-rock interaction and thermal evolution during thrusting of an Alpine metamorphic complex (Tinos island, Greece)." Contributions to Mineralogy and Petrology 135(2-3): 212-224.

McCaig, A. M., S. M. Wickham and H. P. Taylor (1990). "Deep Fluid Circulation in Alpine Shear Zones, Pyrenees, France - Field and Oxygen Isotope Studies." Contributions to Mineralogy and Petrology 106(1): 41-60.

McCulloch, M. T. and J. A. Gamble (1991). "Geochemical and Geodynamical Constraints on Subduction Zone Magmatism." Earth and Planetary Science Letters 102(3-4): 358-374.

McDaniel, D. K., R. J. Walker, S. R. Hemming, M. F. Horan, H. Becker and R. I. Grauch (2004). "Sources of osmium to the modern oceans: New evidence from the Pt-190-(OS)-O-186 system." Geochimica Et Cosmochimica Acta 68(6): 1243-1252.

McDonough, W. F. and S.-s. Sun (1995). "The composition of the Earth." Chemical Geology 120(3-4): 223-253.

McInnes, B. I. A., J. S. McBride, N. J. Evans, D. D. Lambert and A. S. Andrew (1999). "Osmium isotope constraints on ore metal recycling in subduction zones." Science 286(5439): 512-516.

McKenzie, D. and M. J. Bickle (1988). "The Volume and Composition of Melt Generated by Extension of the Lithosphere." Journal of Petrology 29(3): 625-679.

Meisel, T., R. J. Walker and J. W. Morgan (1996). "The osmium isotopic composition of the Earth's primitive upper mantle." Nature 383(6600): 517-520.

Meisel, T., R. J. Walker, A. J. Irving and J. P. Lorand (2001). "Osmium isotopic compositions of mantle xenoliths: A global perspective." Geochimica Et Cosmochimica Acta 65(8): 1311-1323.

Messiga, B., R. Tribuzio, P. Bottazzi and L. Ottolini (1995). "An ion microprobe study of trace-element composition of clinopyroxenes from blueschist and eclogitized Fe-Ti-gabbros, Ligurian Alps, Northwestern Italy - Some petrologic considerations." Geochimica et Cosmochimica Acta 59(1): 59-75.

Messiga, B., J. R. Kienast, G. Rebay, M. P. Riccardi and R. Tribuzio (1999). "Cr-rich magnesiochloritoid eclogites from the Monviso ophiolites (Western Alps, Italy)." Journal of Metamorphic Geology 17(3): 287-299.

Meyer, J. (1983a). "The development of the high-pressure metamorphism in the Allalin metagabbro (Switzerland)." Terra Cognita 3: 187.

Meyer, J. (1983b). Mineralogie und Petrologie des Allalingabbros. Unpublished PhD thesis. Earth Sciences, Basel.

Michard, A. and F. Albarede (1985). "Hydrothermal Uranium Uptake at Ridge Crests." Nature 317(6034): 244-246.

Miller, D. M., S. L. Goldstein and C. H. Langmuir (1994). "Cerium Lead and Lead-Isotope Ratios in Arc Magmas and the Enrichment of Lead in the Continents." Nature 368(6471): 514-520.

Miller, J. A., I. S. Buick, I. Cartwright and A. Barnicoat (2002). "Fluid processes during the exhumation of high-P metamorphic belts." Mineralogical Magazine 66(1): 93-119.

Mitchell, R. H. and R. R. Keays (1981). "Abundance and Distribution of Gold, Palladium and Iridium in Some Spinel and Garnet Iherzolites - Implications for the Nature and Origin of Precious Metal-Rich Intergranular Components in the Upper Mantle." Geochimica Et Cosmochimica Acta 45(12): 2425-2442.

Monié, P. and C. Chopin (1991). "^{40}Ar-^{39}Ar Dating in Coesite-Bearing and Associated Units of the Dora-Maira Massif, Western Alps." European Journal of Mineralogy 3(2): 239-262.

Moran, A. E., V. B. Sisson and W. P. Leeman (1992). "Boron depletion during progressive metamorphism: Implications for subduction processes." Earth and Planetary Science Letters 111(2-4): 331-349.

Morgan, J. W. and J. F. Lovering (1967). "Rhenium and osmium abundances in chondritic meteorites." Geochimica et Cosmochimica Acta 31(10): 1893-1909.

Morgan, J. W. (1985). "Osmium Isotope Constraints on Earths Late Accretionary History." Nature 317(6039): 703-705.

Morgan, J. W. (1986). "Ultramafic Xenoliths - Clues to Earths Late Accretionary History." Journal of Geophysical Research-Solid Earth and Planets 91(B12): 2375-2387.

Morgan, J. W., R. J. Walker and J. N. Grossman (1990). "Rhenium-osmium isotope systematics in enstatite chondrites." Abstracts of the 21st lunar and planetary science conference 21: 809-810.

Morgan, J. W., M. F. Horan, R. J. Walker and J. N. Grossman (1995). "Rhenium-osmium concentration and isotope systematics in Group IIAB Iron-Meteorites." Geochimica Et Cosmochimica Acta 59(11): 2331-2344.

Morgan, J. W. (1997a). Osmium. In: Encyclopaedia of Geochemistry. R. Fairbridge. New York: Chapman-Hall.

Morgan, J. W. (1997b). Rhenium. In: Encyclopaedia of Geochemistry. R. Fairbridge. New York: Chapman-Hall.

Morgan, J. W., R. J. Walker, A. D. Brandon and M. F. Horan (2001). "Siderophile elements in Earth's upper mantle and lunar breccias: Data synthesis suggests manifestations of the same late influx." Meteoritics & Planetary Science 36(9): 1257-1275.

Mørk, M. B. E. (1985). "A gabbro to eclogite transition on Flemsøy, Sunnmøre, Western Norway." Chemical Geology 50: 283-310.

Mørk, M. B. E. (1986). "Coronite and eclogite formation in olivine gabbro (Western Norway) - reaction paths and garnet zoning." Mineralogical Magazine 50(357): 417-426.

Morris, J. D., W. P. Leeman and F. Tera (1990). "The Subducted Component in Island-Arc Lavas - Constraints from Be Isotopes and B-Be Systematics." Nature 344(6261): 31-36.

Muhe, R., B. Peucker-Ehrenbrink, C. W. Devey and D. GarbeSchonberg (1997). "On the redistribution of Pb in the oceanic crust during hydrothermal alteration." Chemical Geology 137(1-2): 67-77.

Nadeau, S., P. Philippot and F. Pineau (1993). "Fluid Inclusion and Mineral Isotopic Compositions (H-C-O) in Eclogitic Rocks as Tracers of Local Fluid Migration During High-Pressure Metamorphism." Earth and Planetary Science Letters 114(4): 431-448.

Naldrett, A. J. (1989). Magmatic sulphide deposits. Oxford University Press, New York. p.186

Nisio, P., J. M. Lardeaux and H. Bertrand (1986). "Chemical and Mineralogical Relicts of Oceanic Metamorphism in Subducted Oceanic-Crust - Example from Monviso Eclogites (Italian Alps)." Comptes Rendus De L Academie Des Sciences Serie Ii 303(12): 1111-&.

Okamoto, K. and S. Maruyama (1999). "The high-pressure synthesis of lawsonite in the MORB+H2O system." American Mineralogist 84(3): 362-373.

O'Neill, H. S. C., D. B. Dingwell, A. Borisov, B. Spettel and H. Palme (1995). "Experimental petrochemistry of some highly siderophile elements at high temperatures, and some implications for core formation and the mantle's early history." Chemical Geology 120(3-4): 255-273.

Ono, S. (1998). "Stability limits of hydrous minerals in sediment and mid-ocean ridge basalt compositions: Implications for water transport in subduction zones." Journal of Geophysical Research-Solid Earth 103(B8): 18253-18267.

Otten, M. T. and P. R. Buseck (1987). "Tem Study of the Transformation of Augite to Sodic Pyroxene in Eclogitized Ferrogabbro." Contributions to Mineralogy and Petrology 96(4): 529-538.

Parkinson, I. J., C. J. Hawkesworth and A. S. Cohen (1998). "Ancient mantle in a modern arc: Osmium isotopes in Izu-Bonin- Mariana forearc peridotites." Science 281(5385): 2011-2013.

Pattison, D. R. M. and R. C. Newton (1989). "Reversed Experimental Calibration of the Garnet-Clinopyroxene Fe-Mg Exchange Thermometer." Contributions to Mineralogy and Petrology 101(1): 87-103.

Pawley, A. R. and J. R. Holloway (1993). "Water Sources for Subduction Zone Volcanism - New Experimental Constraints." Science 260(5108): 664-667.

Peacock, S. M. (1990). "Fluid Processes in Subduction Zones." Science 248(4953): 329-337.

Peacock, S. M. (1993). "The Importance of Blueschist - Eclogite Dehydration Reactions in Subducting Oceanic-Crust." Geological Society of America Bulletin 105(5): 684-694.

Peacock, S. M., T. Rushmer and A. B. Thompson (1994). "Partial melting of subducting oceanic crust." Earth and Planetary Science Letters 121(1-2): 227-244.

Pearce, J. A. (1983). Role of the sub-continental lithosphere in magma genesis at active continental margins. In: Continental Basalts and Mantle Xenoliths. C. J. Hawkesworth and M. J. Norry. Shiva, Nantwich, UK: 230-249.

Pearce, J. A., P. E. Baker, P. K. Harvey and I. W. Luff (1995). "Geochemical Evidence for Subduction Fluxes, Mantle Melting and Fractional Crystallization beneath the South Sandwich-Island Arc." Journal of Petrology 36(4): 1073-1109.

Pearce, J. A. and D. W. Peate (1995). "Tectonic Implications of the Composition of Volcanic Arc Magmas." Annual Review of Earth and Planetary Sciences 23: 251-285.

Pearce, N. J. G. (1990). "Zirconium and Niobium-Bearing Ilmenites from the Igaliko Dyke Swarm, South Greenland." Mineralogical Magazine 54: 585-588.

Pearson, D. G., R. W. Carlson, S. B. Shirey, F. R. Boyd and P. H. Nixon (1995). "Stabilization of Archean Lithospheric Mantle - a Re-Os Isotope Study of Peridotite Xenoliths from the Kaapvaal Craton." Earth and Planetary Science Letters 134(3-4): 341-357.

Pearson, D. G., S. B. Shirey, J. W. Harris and R. W. Carlson (1998). "Sulphide inclusions in diamonds from the Koffiefontein kimberlite, S Africa: constraints on diamond ages and mantle Re-Os systematics." Earth and Planetary Science Letters 160(3-4): 311-326.

Pearson, N. J., O. Alard, W. L. Griffin, S. E. Jackson and S. Y. O'Reilly (2002). "In situ measurement of Re-Os isotopes in mantle sulfides by laser ablation multicollector-inductively coupled plasma mass spectrometry: Analytical methods and preliminary results." Geochimica et Cosmochimica Acta 66(6): 1037-1050.

Pedersen, R.-B., H. Furnes and G. R. Dunning (1991). "A U/Pb age for the Sulitjelma Gabbro, North Norway; further evidence for the development of a Caledonian marginal basin in Ashgill-Llandovery time." Geological Magazine 128(2): 141-153.

Pegram, W. J. and C.-J. Allegre (1992). "Osmium isotopic compositions from oceanic basalts." Earth and Planetary Science Letters 111(1): 59-68.

Pennacchioni, G. (1996). "Progressive eclogitization under fluid-present conditions of pre-Alpine mafic granulites in the Austroalpine Mt Emilius Klippe (Italian Western Alps)." Journal of Structural Geology 18(5): 549-561.

Petrological database of the ocean floor (2004). http://www.petdb.org/.

Peucker-Ehrenbrink, B. (1996). "Accretion of extraterrestrial matter during the last 80 million years and its effect on the marine osmium isotope record." Geochimica Et Cosmochimica Acta 60(17): 3187-3196.

Peucker-Ehrenbrink, B., W. Bach, S. R. Hart, J. Blusztajn and T. Abbruzzese (2003). "Rhenium-osmium isotope systematics and platinum group element concentrations in oceanic crust from DSDP/ODP sites 504 and 417/418." Geochemistry Geophysics Geosystems 4(7): 10.1029/2002GC000414.

Philippot, P. and J. Selverstone (1991). "Trace-Element-Rich Brines in Eclogitic Veins - Implications for Fluid Composition and Transport During Subduction." Contributions to Mineralogy and Petrology 106(4): 417-430.

Philippot, P. and H. L. M. van Roermund (1992). "Deformation Processes in Eclogitic Rocks - Evidence for the Rheological Delamination of the Oceanic-Crust in Deeper Levels of Subduction Zones." Journal of Structural Geology 14(8-9): 1059-1077.

Plank, T. and C. H. Langmuir (1993). "Tracing Trace-Elements from Sediment Input to Volcanic Output at Subduction Zones." Nature 362(6422): 739-743.

Platt, J. P. (1986). "Dynamics of Orogenic Wedges and the Uplift of High-Pressure Metamorphic Rocks." Geological Society of America Bulletin 97(9): 1037-1053.

Platt, J. P. (1993). "Exhumation of High-Pressure Rocks - a Review of Concepts and Processes." Terra Nova 5(2): 119-133.

Pognante, U. (1982a). "Coronitic reactions and ductile shear zones in eclogitic ophiolite metagabbros, western Italian Alps." Terra Cognita 2: 308.

Pognante, U. (1985). "Coronitic Reactions and Ductile Shear Zones in Eclogitized Ophiolite Metagabbro, Western Alps, North Italy." Chemical Geology 50: 99-109.

Pognante, U., F. Talarico, N. Rastelli and N. Ferrati (1987). "High-Pressure Metamorphism in the Nappes of the Valle Dell Orco Traverse (Western Alps Collisional Belt)." Journal of Metamorphic Geology 5(3): 397-414.

Pognante, U., Lombardo, B. and Venturelli, G.P. (1982b). "Petrology and geochemistry of Fe-Ti gabbros and plagiogranites from the Western Alps ophiolites." Schweiz. Mineral. Petrogr. Mitt. 62: 457-472.

Poli, S. (1993). "The Amphibolite-Eclogite Transformation - an Experimental-Study on Basalt." American Journal of Science 293(10): 1061-1107.

Poli, S. and M. W. Schmidt (1995). "H_2O Transport and Release in Subduction Zones - Experimental Constraints on Basaltic and Andesitic Systems." Journal of Geophysical Research-Solid Earth 100(B11): 22299-22314.

Poli, S. and M. W. Schmidt (2002). "Petrology of subducted slabs." Annual Review of Earth and Planetary Sciences 30: 207-235.

Potts, P. J., P. C. Webb and J. S. Watson (1984). "Energy-Dispersive X-Ray-Fluorescence Analysis of Silicate Rocks for Major and Trace-Elements." X-Ray Spectrometry 13(1): 2-15.

Powell, R. and T. J. B. Holland (1985). "An Internally Consistent Thermodynamic Dataset with Uncertainties and Correlations .1. Methods and a Worked Example." Journal of Metamorphic Geology 3(4): 327-342.

Powell, R. and T. J. B. Holland (1988). "An Internally Consistent Dataset with Uncertainties and Correlations .3. Applications to Geobarometry, Worked Examples and a Computer-Program." Journal of Metamorphic Geology 6(2): 173-204.

Ramsbotham, W., S. Inger, B. Cliff, D. Rex and A. Barnicoat (1994). "Time constraints on the metamorphic and structural evolution of the southern Sesia-Lanzo Zone, western Italian Alps." Mineralogical Magazine 58A: 758-759.

Ramsey, M. H., P. J. Potts, P. C. Webb, P. Watkins, J. S. Watson and B. J. Coles (1995). "An Objective Assessment of Analytical Method Precision - Comparison of Icp-Aes and Xrf for the Analysis of Silicate Rocks." Chemical Geology 124(1-2): 1-19.

Rebay, G. and R. Powell (2002). "The formation of eclogite facies metatroctolites and a general petrogenetic grid in Na2O-CaO-FeO-MgO-Al2O3-SiO2-H2O (NCFMASH)." Journal of Metamorphic Geology 20(9): 813-826.

Reed, S. J. B. (1995). Electron probe microanalysis. In: Microprobe techniques in the Earth Sciences. P. J. Potts, J. F. W. Bowles et al. Chapman and Hall, London: 49-89.

Rehkämper, M., A. N. Halliday, J. Alt, J. G. Fitton, J. Zipfel and E. Takazawa (1999). "Non-chondritic platinum-group element ratios in oceanic mantle lithosphere: petrogenetic signature of melt percolation?" Earth and Planetary Science Letters 172(1-2): 65-81.

Reinecke, T. (1991). "Very-High-Pressure Metamorphism and Uplift of Coesite-bearing Metasediments from the Zermatt-Saas Zone, Western Alps." European Journal of Mineralogy 3 (1): 7-17.

Reinecke, T. (1998). "Prograde high- to ultrahigh-pressure metamorphism and exhumation of oceanic sediments at Lago di Cignana, Zermatt- Saas Zone, western Alps." Lithos 42(3-4): 147-189.

Reisberg, L., A. Zindler, F. Marcantonio, W. White, D. Wyman and B. Weaver (1993). "Os Isotope Systematics in Ocean Island Basalts." Earth and Planetary Science Letters 120(3-4): 149-167.

Reisberg, L. C., C. J. Allegre and J. M. Luck (1991). "The Re-Os Systematics of the Ronda Ultramafic Complex of Southern Spain." Earth and Planetary Science Letters 105(1-3): 196-213.

Reisberg, L. C., X. Zhi and L. Zheng (2004). "Re-Os systematics of the UHP Dabie-Sulu terrain, China: Results from Qinglongshan." Geochimica Et Cosmochimica Acta 68(11): A604-A604.

Righter, K., J. T. Chesley, D. Geist and J. Ruiz (1998). "Behavior of Re during magma fractionation: an example from Volcan Alcedo, Galapagos." Journal of Petrology 39(4): 785-795.

Righter, K. and E. H. Hauri (1998). "Compatibility of rhenium in garnet during mantle melting and magma genesis." Science 280(5370): 1737-1741.

Roberts, D. and B. A. Sturt (1980). "Caledonian deformation in Norway." Journal of the Geological Society, London 137: 241-250.

Rosenberg, N. D., F. J. Spera and R. M. Haymon (1993). "The Relationship between Flow and Permeability Field in Sea- Floor Hydrothermal Systems." Earth and Planetary Science Letters 116(1-4): 135-153.

Roy-Barman, M. and C. J. Allegre (1994). "^{187}Os-^{186}Os Ratios of Midocean Ridge Basalts and Abyssal Peridotites." Geochimica et Cosmochimica Acta 58(22): 5043-5054.

Roy-Barman, M. and C. J. Allegre (1995). "$^{187}Os/^{186}Os$ in Oceanic Island Basalts - Tracing Oceanic-Crust Recycling in the Mantle." Earth and Planetary Science Letters 129(1-4): 145-161.

Roy-Barman, M., J.-M. Luck and C. J. Allegre (1996). "Os isotopes in orogenic lherzolite massifs and mantle heterogeneities." Chemical Geology 130(1-2): 55-64.

Roy-Barman, M., G. J. Wasserburg, D. A. Papanastassiou and M. Chaussidon (1998). "Osmium isotopic compositions and Re-Os concentrations in sulfide globules from basaltic glasses." Earth and Planetary Science Letters 154(1-4): 331-347.

Rubatto, D., D. Gebauer and M. Fanning (1998). "Jurassic formation and Eocene subduction of the Zermatt-Saas- Fee ophiolites: implications for the geodynamic evolution of the Central and Western Alps." Contributions to Mineralogy and Petrology 132(3): 269-287.

Rubatto, D. and D. Gebauer (1999). "Eo/Oligocene (35 Ma) high-pressure metamorphism in the Gornergrat Zone (Monte Rosa, Western Alps): implications for paleogeography." Schweizerische Mineralogische Und Petrographische Mitteilungen 79(3): 353-362.

Rubatto, D., D. Gebauer and R. Compagnoni (1999). "Dating of eclogite-facies zircons; the age of Alpine metamorphism in the Sesia-Lanzo Zone (Western Alps)." Earth and Planetary Science Letters 167(3-4): 141-158.

Rubie, D. C. (1990). Role of kinetics in the formation and preservation of eclogites. In: Eclogite facies rocks. D. A. Carswell. Blackie, Glasgow | Chapman and Hall: 111-140.

Rubie, D. C. (1998). Disequilibrium during metamorphism: the role of nucleation kinetics. In: What Drives Metamorphism and Metamorphic Reactions? P. J. Treloar, O'Brien, P. J. The Geological Society, London 138: 199-214.

Ryan, J. G., J. Morris, F. Tera, W. P. Leeman and A. Tsvetkov (1995). "Cross-Arc Geochemical Variations in the Kurile Arc as a Function of Slab Depth." Science 270(5236): 625-627.

Scambelluri, M., G. B. Piccardo, P. Philippot, A. Robbiano and L. Negretti (1997). "High salinity fluid inclusions formed from recycled seawater in deeply subducted alpine serpentinite." Earth and Planetary Science Letters 148(3-4): 485-499.

Scambelluri, M., G. Pennacchioni and P. Philippot (1998). "Salt-rich aqueous fluids formed during eclogitization of metabasites in the Alpine continental crust (Austroalpine Mt. Emilius unit, Italian western Alps)." Lithos 43(3): 151-167.

Scambelluri, M. and P. Philippot (2001). "Deep fluids in subduction zones." Lithos 55(1-4): 213-227.

Schiano, P., J. L. Birck and C. J. Allegre (1997). "Osmium-strontium-neodymium-lead isotopic covariations in mid- ocean ridge basalt glasses and the heterogeneity of the upper mantle." Earth and Planetary Science Letters 150(3-4): 363-379.

Schmid, S. M., O. A. Pfiffner, N. Froitzheim, G. Schonborn and E. Kissling (1996). "Geophysical-geological transect and tectonic evolution of the Swiss-Italian Alps." Tectonics 15(5): 1036-1064.

Schmid, S. M. and E. Kissling (2000). "The arc of the western Alps in the light of geophysical data on deep crustal structure." Tectonics 19(1): 62-85.

Schmidt, M. W. and S. Poli (1998). "Experimentally based water budgets for dehydrating slabs and consequences for arc magma generation." Earth and Planetary Science Letters 163(1-4): 361-379.

Seitz, H. M. and A. B. Woodland (2000). "The distribution of lithium in peridotitic and pyroxenitic mantle lithologies - an indicator of magmatic and metasomatic processes." Chemical Geology 166(1-2): 47-64.

Selverstone, J., G. Morteani and J. M. Staude (1991). "Fluid Channeling During Ductile Shearing - Transformation of Granodiorite into Aluminous Schist in the Tauern Window, Eastern Alps." Journal of Metamorphic Geology 9(4): 419-431.

Selverstone, J., G. Franz, S. Thomas and S. Getty (1992). "Fluid Variability in 2-GPa Eclogites as an Indicator of Fluid Behavior During Subduction." Contributions to Mineralogy and Petrology 112(2-3): 341-357.

Sharma, M., D. A. Papanastassiou and G. J. Wasserburg (1997). "The concentration and isotopic composition of osmium in the oceans." Geochimica Et Cosmochimica Acta 61(16): 3287-3299.

Sharma, M., G. J. Wasserburg, A. W. Hofmann and D. A. Butterfield (2000). "Osmium isotopes in hydrothermal fluids from the Juan de Fuca Ridge." Earth and Planetary Science Letters 179(1): 139-152.

Shen, J. J., D. A. Papanastassiou and G. J. Wasserburg (1996). "Precise Re-Os determinations and systematics of iron meteorites." Geochimica et Cosmochimica Acta 60(15): 2887-2900.

Shirey, S. B. and R. J. Walker (1995). "Carius Tube Digestion for Low-Blank Rhenium-Osmium Analysis." Analytical Chemistry 67(13): 2136-2141.

Shirey, S. B. and R. J. Walker (1998). "The Re-Os isotope system in cosmochemistry and high-temperature geochemistry." Annual Review of Earth and Planetary Sciences 26: 423-500.

Smoliar, M. I., R. J. Walker and J. W. Morgan (1996). "Re-Os ages of group IIA, IIIA, IVA, and IVB iron meteorites." Science 271(5252): 1099-1102.

Snow, J. E. and L. Reisberg (1995). "Os isotopic systematics of the MORB mantle: results from altered abyssal peridotites." Earth and Planetary Science Letters 133(3-4): 411-421.

Snow, J. E. and G. Schmidt (1998). "Constraints on Earth accretion deduced from noble metals in the oceanic mantle." Nature 391(6663): 166-169.

Sobolev, A. V., A. W. Hofmann and I. K. Nikogosian (2000). "Recycled oceanic crust observed in 'ghost plagioclase' within the source of Mauna Loa lavas." Nature 404(6781): 986-990.

Sobolev, N. V. and V. S. Shatsky (1990). "Diamond Inclusions in Garnets from Metamorphic Rocks - a New Environment for Diamond Formation." Nature 343(6260): 742-746.

Spandler, C., J. Hermann, R. Arculus and J. Mavrogenes (2003). "Redistribution of trace elements during prograde metamorphism from lawsonite blueschist to eclogite facies; implications for deep subduction-zone processes." Contributions to Mineralogy and Petrology 146(2): 205-222.

Spandler, C., J. Hermann, R. Arculus and J. Mavrogenes (2004). "Geochemical heterogeneity and element mobility in deeply subducted oceanic crust; insights from high-pressure mafic rocks from New Caledonia." Chemical Geology 206(1-2): 21-42.

Spiegelman, M. and D. McKenzie (1987). "Simple 2-D Models for Melt Extraction at Mid-Ocean Ridges and Island Arcs." Earth and Planetary Science Letters 83(1-4): 137-152.

Stakes, D. (1993). Oxygen and hydrogen isotope compositions of oceanic plutonic rocks: high temperature deformation and metamorphism of oceanic layer 3. In: Stable Isotope Geochemistry: A Tribute to Samuel Epstein. H. P. Taylor, J. R. O'Neil and I. Kaplan. Geochemical Society Special Publication No. 3: 77-90.

Stakes, D. S., C. Mevel, M. Cannat and T. Chaput (1991). Metamorphic stratigraphy of Hole 735B. In: Proceedings of the ODP, Scientific results. R. P. Von Herzen, P. T. Robinson et al. College Station, TX (Ocean Drilling Program), 118: 153-180.

Stalder, R., S. F. Foley, G. P. Brey and I. Horn (1998). "Mineral aqueous fluid partitioning of trace elements at 900- 1200 degrees C and 3.0-5.7 GPa: New experimental data for garnet, clinopyroxene, and rutile, and implications for mantle metasomatism." Geochimica et Cosmochimica Acta 62(10): 1781-1801.

Stampfli, G. M. (1993). "The Briançonnais, Exotic Terrane in the Alps." Eclogae Geologicae Helvetiae 86(1): 1-45.

Staudigel, H., T. Plank, B. White and H.-U. Schmincke (1996). Geochemical fluxes during seafloor alteration of the basaltic upper oceanic crust; DSDP sites 417 and 418. In: Subduction, Top to Bottom. G. E. Bebout, D. W. Scholl et al. American Geophysical Union, Washington, DC 96:19-38: pp.384.

Stephens, M. B., M. Gustavson, I. B. Ramberg and E. Zachrisson (1985). The Caledonides of Central-North Scandinavia - a tectonostratigraphic overview. In: The Caledonide Orogen - Scandinavia and Related Areas. D. G. Gee and B. A. Sturt. John Wiley & Sons Ltd: 135-162.

Stephens, M. B. (1986). "Terrane analysis of Sulitjelma, Upper Allochthon, Scandinavian Caledonides." Geol. Fören. Stockh. Förh 108: 303-304.

Stracke, A., M. Bizimis and V. J. M. Salters (2003). "Recycling oceanic crust: Quantitative constraints." Geochemistry Geophysics Geosystems 4: art. no.-8003.

Sun, S.-s. and W. F. McDonough (1989). Chemical and isotopic systematics of oceanic basalts: implications for mantle composition and processes. In: Magmatism in the ocean basins. A. D. Saunders and M. J. Norry. Geological Society Special Publication, London 42: 313-345.

Sun, W., V. C. Bennett, S. M. Eggins, R. J. Arculus and M. R. Perfit (2003c). "Rhenium systematics in submarine MORB and back-arc basin glasses: laser ablation ICP-MS results." Chemical Geology 196(1-4): 259-281.

Sun, W., V. C. Bennett and V. S. Kamenetsky (2004). "The mechanism of Re enrichment in arc magmas: evidence from Lau Basin basaltic glasses and primitive melt inclusions." Earth and Planetary Science Letters 222(1): 101-114.

Sun, W. D., V. C. Bennett, S. M. Eggins, V. S. Kamenetsky and R. J. Arculus (2003a). "Enhanced mantle-to-crust rhenium transfer in undegassed arc magmas." Nature 422(6929): 294-297.

Sun, W. D., R. J. Arculus, V. C. Bennett, S. M. Eggins and R. A. Binns (2003b). "Evidence for rhenium enrichment in the mantle wedge from submarine arc-like volcanic glasses (Papua New Guinea)." Geology 31(10): 845-848.

Suzuki, K., H. Shimizu and A. Masuda (1996). "Re-Os dating of molybdenites from ore deposits in Japan: Implication for the closure temperature of the Re-Os system for molybdenite and the cooling history of molybdenum ore deposits." Geochimica Et Cosmochimica Acta 60(16): 3151-3159.

Tatsumi, Y., M. Sakuyama, H. Fukuyama and I. Kushiro (1983). "Generation of Arc Basalt Magmas and Thermal Structure of the Mantle Wedge in Subduction Zones." Journal of Geophysical Research 88(NB7): 5815-5825.

Tatsumi, Y. (1986). "Formation of the Volcanic Front in Subduction Zones." Geophysical Research Letters 13(8): 717-720.

Thirlwall, M. F. (1997). "Pb isotopic and elemental evidence for OIB derivation from young HIMU mantle." Chemical Geology 139(1-4): 51-74.

Thompson, J. B., J. Laird and A. B. Thompson (1982). "Reactions in Amphibolite, Greenschist and Blueschist." Journal of Petrology 23(1): 1-27.

Thoni, M. and E. Jagoutz (1993). "Isotopic Constraints for Eo-Alpine High-P Metamorphism in the Austroalpine Nappes of the Eastern Alps - Bearing on Alpine Orogenesis." Schweizerische Mineralogische Und Petrographische Mitteilungen 73(2): 177-189.

Tomascak, P. B., E. Widom, L. D. Benton, S. L. Goldstein and J. G. Ryan (2002). "The control of lithium budgets in island arcs." Earth and Planetary Science Letters 196(3-4): 227-238.

Treiman, A. H., M. J. Drake, M. J. Janssens, R. Wolf and M. Ebihara (1986). "Core Formation in the Earth and Shergottite Parent Body (SPB) - Chemical Evidence from Basalts." Geochimica Et Cosmochimica Acta 50(6): 1071-1091.

Tribuzio, R., B. Messiga, R. Vannucci and P. Bottazzi (1996). "Rare earth element redistribution during high-pressure-low- temperature metamorphism in ophiolitic Fe-gabbros (Liguria, northwestern Italy): Implications for light REE mobility in subduction zones." Geology 24(8): 711-714.

Turner, S., B. Bourdon, C. Hawkesworth and P. Evans (2000). "Case studies of plagioclase growth and residence times in island arc lavas from Tonga and the Lesser Antilles, and a model to reconcile discordant age information." Earth and Planetary Science Letters 179: 581-593.

van der Klauw, S. N. G. C., T. Reinecke and B. Stockhert (1997). "Exhumation of ultrahigh-pressure metamorphic oceanic crust from Lago di Cignana, Piemontese zone, western Alps: the structural record in metabasites." Lithos 41(1-3): 79-102.

van Westrenen, W., N. L. Allan, J. D. Blundy, J. A. Purton and B. J. Wood (2000). "Atomistic simulation of trace element incorporation into garnets - comparison with experimental garnet-melt partitioning data." Geochimica Et Cosmochimica Acta 64(9): 1629-1639.

van Westrenen, W., B. J. Wood and J. D. Blundy (2001). "A predictive thermodynamic model of garnet-melt trace element partitioning." Contributions to Mineralogy and Petrology 142(2): 219-234.

van Wyck, N., J. W. Valley and H. Austrheim (1996). "Oxygen and carbon isotopic constraints on the development of eclogites, Holsnoy, Norway." Lithos 38(3-4): 129-145.

Vielzeuf, D. and M. W. Schmidt (2001). "Melting relations in hydrous systems revisited: application to metapelites, metagreywackes and metabasalts." Contributions to Mineralogy and Petrology 141(3): 251-267.

Volkening, J., T. Walczyk and K. G. Heumann (1991). "Osmium Isotope Ratio Determinations by Negative Thermal Ionization Mass-Spectrometry." International Journal of Mass Spectrometry and Ion Processes 105(2): 147-159.

Walczyk, T., E. H. Hebeda and K. G. Heumann (1991). "Osmium isotope ratio measurements by negative thermal ionization mass spectrometry (NTI-MS)." Fresenius' Journal of Analytical Chemistry 341: 537-541.

Walker, R. J. and J. D. Fassett (1986). "Isotopic Measurement of Subnanogram Quantities of Rhenium and Osmium by Resonance Ionization Mass-Spectrometry." Analytical Chemistry 58(14): 2923-2927.

Walker, R. J., S. B. Shirey and O. Stecher (1988). "Comparative Re-Os, Sm-Nd and Rb-Sr Isotope and Trace-Element Systematics for Archean Komatiite Flows from Munro-Township, Abitibi-Belt, Ontario." Earth and Planetary Science Letters 87(1-2): 1-12.

Walker, R. J. and J. W. Morgan (1989). "Rhenium-Osmium Isotope Systematics of Carbonaceous Chondrites." Science 243(4890): 519-522.

Walker, R. J., J. W. Morgan, A. J. Naldrett, C. Li and J. D. Fassett (1991b). "Re-Os Isotope Systematics of Ni-Cu Sulfide Ores, Sudbury Igneous Complex, Ontario - Evidence for a Major Crustal Component." Earth and Planetary Science Letters 105(4): 416-429.

Walker, R. J., J. W. Morgan and M. F. Horan (1995). "Os-187 Enrichment in Some Plumes - Evidence for Core-Mantle Interaction." Science 269(5225): 819-822.

Walker, R. J., E. Hanski, J. Vuollo and J. Lilpo (1996). "The Os isotopic composition of Proterozoic upper mantle: Evidence for chondritic upper mantle from the Outokumpu ophiolite, Finland." Earth and Planetary Science Letters 141(1-4): 161-173.

Wanke, H., G. Dreibus and E. Jagoutz (1984). Mantle chemistry and accretion history of the Earth. In: Archaean Geochemistry. A. Kroner, G. Hanson and H. Goodwin. Springer-Verlag, Berlin: 1-24.

Warren, P. H. and G. W. Kallemeyn (1996). "Siderophile trace elements in ALH84001, other SNC meteorites and eucrites: Evidence of heterogeneity, possibly time-linked, in the mantle of Mars." Meteoritics & Planetary Science 31(1): 97-105.

Wasson, J. T. (1985). Meteorites: their record of early solar-system history. W. H. Freeman and Co., New York p.267

Watson, J. S. (1996). "Fast, simple method of powder pellet preparation for X-ray fluorescence analysis." X-Ray Spectrometry 25(4): 173-174.

Wayte, G. J., R. H. Worden, D. C. Rubie and G. T. R. Droop (1989). "A Tem Study of Disequilibrium Plagioclase Breakdown at High- Pressure - the Role of Infiltrating Fluid." Contributions to Mineralogy and Petrology 101(4): 426-437.

Westhead, R. K. and A. P. Boyle (1995). "Petrographic evidence for diachronous metamorphism of the Skaiti Supergroup, Koli Nappe Complex, Arctic Scandinavian Caledonides." Geological Journal 30(3-4): 373-383.

Widom, E. and S. B. Shirey (1996). "Os isotope systematics in the Azores: Implications for mantle plume sources." Earth and Planetary Science Letters 142(3-4): 451-465.

Widom, E. (1997). "Sources of ocean island basalts: A review of the osmium isotope evidence." Physica A 244(1-4): 484-496.

Widom, E., K. A. Hoernle, S. B. Shirey and H. U. Schmincke (1999). "Os isotope systematics in the Canary Islands and Madeira: Lithospheric contamination and mantle plume signatures." Journal of Petrology 40(2): 279-296.

Widom, E., P. Kepezhinskas and M. Defant (2003). "The nature of metasomatism in the sub-arc mantle wedge: evidence from Re-Os isotopes in Kamchatka peridotite xenoliths." Chemical Geology 196(1-4): 283-306.

Woodhead, J. and M. Brauns (2004). "Current limitations to the understanding of Re-Os behaviour in subduction systems, with an example from New Britain." Earth and Planetary Science Letters 221(1-4): 309-323.

Woodland, S. J., D. G. Pearson and M. F. Thirlwall (2002). "A platinum group element and Re-Os isotope investigation of siderophile element recycling in subduction zones: Comparison of Grenada, Lesser Antilles arc, and the Izu-Bonin arc." Journal of Petrology 43(1): 171-198.

Yogodzinski, G. M., J. M. Lees, T. G. Churikova, F. Dorendorf, G. Woerner and O. N. Volynets (2001). "Geochemical evidence for the melting of subducting oceanic lithosphere at plate edges." Nature 409(6819): 500-504.

Yund, R. A. (1986). "Interdiffusion of NaSi-CaAl in peristerite." Physics and Chemistry of Minerals 13(1): 11-16.

Zack, T., S. F. Foley and T. Rivers (2002a). "Equilibrium and disequilibrium trace element partitioning in hydrous eclogites (Trescolmen, Central Alps)." Journal of Petrology 43(10): 1947-1974.

Zack, T., A. Kronz, S. F. Foley and T. Rivers (2002b). "Trace element abundances in rutiles from eclogites and associated garnet mica schists." Chemical Geology 184(1-2): 97-122.

Zeininger, H. and K. G. Heumann (1983). "Boron Isotope Ratio Measurement by Negative Thermal Ionization Mass-Spectrometry." International Journal of Mass Spectrometry and Ion Processes 48(FEB): 377-380.

Zindler, A., E. Jagoutz and S. Goldstein (1982). "Nd, Sr and Pb Isotopic Systematics in a 3-Component Mantle - a New Perspective." Nature 298(5874): 519-523.

Zindler, A. and S. Hart (1986). "Chemical Geodynamics." Annual Review of Earth and Planetary Sciences 14: 493-571.

BLANK PAGE
IN
ORIGINAL

A Appendix A - Analytical techniques

A.1 Sample preparation

Each sample was trimmed of any weathered edges that were present. The remainder was either split or cut into pieces which were suitable for crushing. At least one of these pieces was kept for section making and reference. A section of ~100μm thickness was made for both electron microprobe and subsequent laser ablation (LA-ICP-MS) analysis of trace elements. Another thinner section (30μm) was made for petrographic work.

The other pieces were crushed and ground for analytical chemistry. In order to minimise metal contamination, the rock fragments were placed inside at least two thick plastic bags and broken up with a lump hammer. Further bags were needed after several blows (!) The fragments were transferred to a pre-contaminated agate Tema or ball mill and ground for at least 10 minutes or 40 minutes respectively. In certain cases when the samples were particularly hard, a couple of the initial fragments were passed through the jaw-crusher and powdered for XRF analysis, while a smaller quantity was split, crushed by hammer, and ground for isotope work. It was important at this point to ensure sufficient quantities of sample were crushed to be confident that the powder was representative.

A.1.1 Mineral separation

A portion of the crushate (taken from the jaw-crusher for ease of preparation), was washed with water through a stack of several sieves, with various aperture sizes. Sieve apertures of 600, 150 and 63μm were used. The crushate was then dried ready for picking. With the exception of a metallic phase in the gabbro, all phases were separated by hand picking with the use of a binocular microscope. Both transmitted and incident light were used in order to ensure that the picked fraction was free from inclusions and did not have any other phases around the edges of the grains. The fraction alone was checked again in a clean Petri dish.

Leaching techniques were not applied to the mineral separates because the effects of leaching are not easily quantifiable and it may result in the loss of rhenium and osmium from the fraction to be analysed. However, thorough cleaning was performed. The mineral fraction was sonicated in a Pyrex beaker for 30 minutes, using the following reagents in turn: acetone, 2M TD HCl and Millipore water. The mineral fractions were then dried for several hours in an oven at 80 degrees C, and crushed and ground in an agate pestle and mortar. The pestle and mortar was pre-cleaned by the grinding of fine pure quartz powder and then rinsing with acetone followed by millipore water.

A.2 X-Ray Fluorescence Analysis (XRF)

Major and trace element analyses were performed on whole-rock powders following the standard XRF technique at the Open University (Potts et al. 1984).

A.2.1 Major element preparation – fused glass discs

Aliquots of powder were placed in porcelain crucibles and dried at 100°C, overnight in an oven. Lithium metaborate/tetraborate (Johnson-Matthey Spectroflux 100B), which acts as a flux, was weighed into platinum crucibles. The mass, which varied according to the batch of flux, was approximately 3.5g, and was weighed accurately to 4 decimal places. The dried and cooled rock powders were then weighed into the same platinum crucibles, to a mass of 0.7000g, and the two powders mixed with a polythene rod. The crucibles were placed in a muffle furnace at 1100°C for 15 minutes. To ensure homogeneity and allow gas bubbles to escape, the crucibles were swirled using tongs every five minutes. The melt was quenched by pouring onto, and pressing into, a preheated brass mould.

In order to determine the loss on ignition of each of the samples, approximately 1.2g of each dried powder was weighed accurately (to 4 decimal places) into alumina crucibles. Prior to weighing, the crucibles were placed in the muffle furnace at 1000°C for 15 minutes to ensure they were fully oxidised (i.e. maximum mass), and then allowed to cool. The alumina crucibles, with sample, were then ignited at 1000°C in the furnace for 45 minutes, allowed to cool, and then reweighed. The difference, as a percentage of the powder mass, is the loss on ignition value.

A.2.2 Trace elements – pressed pellets

Approximately 9-10g of whole rock powder was weighed out in a small plastic bag and ~0.9g of a binder consisting of polyvinylpyrollidinone (PVP) and methyl cellulose was added (Watson 1996). The two were thoroughly mixed, placed in a

hardened steel mould, and the mould placed in an hydraulic press at between 5 and 7 tons p.s.i. The pellets were dried overnight at ~100°C in order to increase their competence.

A.2.3 Analysis

Analyses were performed on an ARL 8420+ dual geniometer wavelength dispersive XRF spectrometer, which is equipped with a 3kW Rh anode end-window X-ray tube, and uses fully collimated flow proportional and scintillation counters. Elemental intensities are corrected for background and peak overlap interferences during each run. There is a drift normalisation monitor built into the software which performs a correction for medium-term instrumental drift. It is necessary to correct data for matrix effects. This was achieved for major elements by the Traill-Lachance procedure and for trace elements by calibrating against the Compton scattered tube lines for atomic numbers ≥27, and by a Lucas-Tooth correction and Compton scatter peak intensities method for atomic numbers <27. It has been estimated that major element concentrations can typically be determined to a precision of ~0.18-0.73%, with the exception of Cr for which precision is ~0.83% (Ramsey et al. 1995). In-house standards were included with batches of major and trace element analyses to monitor the quality of sample preparation and analysis.

A.3 Electron probe microanalysis

Analyses were performed on a wavelength dispersive (WD) Cameca SX100 electron microprobe. The technique followed the method outlined by Reed (1995), and all corrections (spectrometer angles, count times, crystal selection and PAP corrections) were performed automatically.

Polished thin sections were made to a thickness of 100-150μm, to allow subsequent analysis by laser ablation inductively-coupled plasma mass spectrometry (LA-ICP-MS). Sections were observed and categorised petrographically and photographed prior to analysis. A conductive carbon coating was applied to the sections, under a vacuum, to prevent the build up of charge in the sample and avoid potentially dangerous de-charging. Beam conditions during quantitative analysis were kept constant: an accelerating potential of 20kV, a current of 20nA, and a beam size of 10μm. Occasionally, the beam size was reduced to 5μm, to allow the accurate analysis of very small mineral grains. Calculations of H_2O contents were generally performed through an external Excel spreadsheet, although a software update made automatic water calculations possible. The WD spectrometers were also used to produce x-ray maps of sulphides. For this purpose, a 1μm beam diameter was used to achieve the greatest possible resolution.

A.4 Inductively-coupled plasma mass spectrometry (ICP-MS)

A.4.1 Sample preparation - dissolution and dilution

Whole rock powders (0.1g ± 0.001g, but recorded to 5 decimal places) were weighed and placed in 15ml Teflon vials and the following reagents were added: 1ml of 15M QD HNO_3 and 4ml of 29M Aristar HF. The vials were closed and placed in an ultrasonic bath for 20 minutes and then placed on a hotplate at 130°C for at least 36 hours. The sonication procedure was repeated at least once more during dissolution. If dissolution was not complete, a further 1ml of HF was added and the vial returned to the hotplate overnight. After dissolution, the samples were dried to incipient dryness on a hotplate at approximately 120°C. Over-drying (and the possibility of fluoride formation) was avoided by careful observation when close to dry.

Once dry, 2ml of 15M QD HNO_3 and 4ml of 18.4 M ohm Millipore water was added, and the vials were sonicated (for 20 minutes) and placed back on the hotplate at 130°C for at least 4 hours. The samples were dried again on a hotplate at 120°C. Subsequently, 3ml of 15M (70%) QD HNO_3 and 6ml of Millipore water was added. The vials were placed back on a hotplate for at least 4 hours at 120°C. One 125ml Nalgene bottle for every sample was cleaned using 2% HNO_3 and Millipore water, and then left to dry. The bottles were weighed without their tops, and then the samples were added. In order to achieve a yield which was as near as possible to 100%, the vials were rinsed 3 times with Millipore water and the water added to the bottle. The bottle containing solution was then weighed, and the mass of the sample solution calculated. Following this, water was added to attain a 100ml solution of approximately ~2.1% HNO_3. This procedure results in solutions with a dilution factor of 1000 times, compared to original rock values. While this reduces the concentrations of trace elements, sometimes to a point below detection limits, it is a necessary step in order to decrease the concentrations of major elements, as no chemical separation procedure is performed.

Due to very low Zr and Hf concentrations in some sample solutions, compared to XRF data, it seemed likely that full dissolution of acid resistant phases such as zircon was not being achieved at the temperatures and pressures achieved inside the 15ml Teflon vials. To test this theory, a set of five dissolutions was performed at around 200°C in Teflon vessels placed inside Monel metal jackets. The abundances of Zr and Hf from these dissolutions were comparable to the XRF data, confirming that the standard dissolution technique was not sufficient to dissolve zircons in some of the samples. However, the important point to note is that with the exception of Zr and Hf, there was very little difference in the concentrations of other elements from the Monel dissolutions. Uranium and some heavy rare earth element (HREE) abundances were slightly higher, but not to a significant degree.

A.4.2 Analysis

Samples were analysed on an Agilent 7500s ICP-MS, fitted with a Babington nebuliser (flow rate 0.4ml min^{-1}). A mixed spike (Be, ±Sc, Rh, In, Tm, Re, Bi) was added 'on line' during the run of analyses. At least two total procedural blanks were prepared for each batch of samples. Sample values were blank corrected, though these values were almost always negligible. Four or five dissolved rock standards were analysed which, together with the blank value, defined a calibration curve for the run of analyses. At least one of the standards was repeated every five to ten analyses in order to quantify drift and apply a correction. The correction was applied using the slope and intersect of a 'best fit' line (generated by Excel) for the repeated standard data.

Typical reproducibility of the standards over the three runs was as follows (quoted as 2 relative s.d.): BHVO-1: 5% (n=3), JB-2: 6% (n=3). Reproducibility of samples was slightly lower: Gabbroic origin: ~8% (2 s.d., n=2-3). Basaltic origin: ~7%. This is probably the result of lower abundances, particularly in the gabbro and possibly a lack of homogeneity due to the coarse grain size of the samples.

A.5 Laser ablation ICP-MS (LA-ICP-MS)

Laser ablation analysis was performed on thick-cut polished probe sections (100-150μm). This allowed initial petrographic work, analysis by microprobe, and then in situ analysis of trace elements and platinum group elements (PGEs). Prior to ablation, mineral phases were analysed by electron microprobe (see section A.3) to determine major element (Ca, Si, Mg) concentrations. These data were used to calibrate the laser ablation data. Prior to the ablation of sulphides, X-ray maps of elemental abundances were made with the electron microprobe along with quantitative analyses. Categorisation and analysis of sulphides prior to LA-ICP-MS is important because the laser ablation technique is particularly destructive to sulphides. The carbon coating, necessary for electron microprobe analysis, was removed from the sections before laser ablation analysis.

Sections were loaded into the housing of a New Wave 213 Nd:YAG deep UV (213 nm) laser system. Ablation was performed in a pure helium atmosphere. Prior to analysis, the helium flow was balanced with the argon flow in the ICP-mass spectrometer to ensure a stable beam. For the analysis of silicate materials, analytical conditions were as follows: 80 μm beam diameter with a 10 Hz laser frequency (0.8 mJ). The total duration of each analysis was 240 seconds: a warm-up period of 120 seconds, during which background levels were measured, a 60 second period during which the laser was fired and a further 60 seconds when levels fall after ablation has stopped. A wash-out period of 240 seconds was carried out between analyses. Detection limits are frequently in the 1-10ppb range.

For sulphide analyses beam conditions were as follows: 40-80 μm beam size (depending on size of sulphide), 10Hz laser frequency. The warm-up period was 150 seconds, the laser fired for 50 seconds, and the wash-out duration between analyses was at least 320 seconds.

Data processing and standards. The data were processed in time-resolved mode using Glitter software. This allows peaks and troughs to be smoothed, improving detection limits and precision. It also allows the user to choose a specific time segment of the analysis. This feature is particularly useful as the ablation process frequently samples inclusions or even a phase lying below (in a thick section) the one intended for analysis.

For silicate trace element analysis, an external NIST-612 glass standard was used to provide external calibration. This was analysed twice at the start of the run of analyses, then once every eight to ten samples, and finally twice at the end of the run. For sulphide analyses, two standards were used, the first was PGE-A, used for calibrating all PGE and other elements measured except Re, Pb and Tl which were calibrated using the other standard, ReOs#4. The electron microprobe major element data provided an internal calibration, and were entered into the Glitter processing software after analysis. Ca or Si was used for silicate analyses, while S was used for sulphides.

BLANK PAGE
IN
ORIGINAL

B Appendix B

B.1 Trace (LA-ICP-MS and XRF) and major element (XRF) whole rock data

N.B. Significant figures:

As a rule, trace element data determined by XRF are accurate to 2-3 significant figures. Trace element LA-ICP-MS data are accurate to at least 3 significant figures.

Table B.1. Major and trace element compositions of whole-rock samples from the Allalin Gabbro.

	Gabbros								
Unit	Allalin	Allalin	Allalin	Allalin	Allalin	Allalin	Allalin	Allalin	Allalin
Lithology	Gabbro	Gabbro	Gabbro	Gabbro	Gabbro	Gabbro	Gabbro	Gabbro	Gabbro
Mm. facies	-	-	-	-	-	-	-	-	-
Sample	S01/30IIIx	S01/35bx	S01/36bx	S01/39IIIx	S01/39IIIx	S01H/3bx	S01H/5b	S02/6bx	S02/10IIIxG
Protolith	Gabbro	Gabbro	Gabbro	Gabbro	Gabbro	Gabbro	Gabbro	Gabbro	Gabbro
XRF									
SiO2	49.78	49.52	48.94	48.02	48.02	49.98	47.47	46.49	49.46
TiO2	0.28	0.26	0.14	0.11	0.11	0.20	0.12	0.37	0.12
Al2O3	19.18	20.06	22.69	22.71	22.71	19.98	19.73	14.85	23.98
Fe2O3	5.02	5.77	4.38	4.20	4.20	4.94	6.29	8.27	4.33
MnO	0.09	0.10	0.07	0.07	0.07	0.08	0.10	0.13	0.07
MgO	9.83	9.17	9.17	10.29	10.29	9.93	14.14	17.67	6.65
CaO	11.66	10.87	10.46	10.96	10.96	11.05	9.14	8.73	10.00
Na2O	3.12	3.22	3.28	2.95	2.95	3.25	2.76	2.14	3.72
K2O	0.07	0.09	0.07	0.06	0.06	0.05	0.06	0.06	0.06
P2O5	0.02	0.03	0.02	0.02	0.02	0.02	0.02	0.06	0.02
CO2	-	-	-	-	-	-	-	-	-
LOI	0.81	1.25	1.13	1.07	1.07	0.82	0.23	0.69	0.66
Total	99.86	100.34	100.35	100.46	100.46	100.30	100.07	99.47	99.06
Sr	311.30	333.80	341.60	343.70	343.70	322.60	291.45	235.80	370.00
Y	6.30	5.80	2.30	2.20	2.20	4.80	2.10	6.30	2.00
Zr	13.00	15.10	6.30	6.50	6.50	8.20	6.45	21.10	8.00
Nb	0.80	1.50	1.10	0.60	0.60	0.60	1.30	1.50	1.00
Ba	12.30	3.80	13.00	65.30	65.30	11.30	8.05	12.20	9.00
Sc	25.20	20.10	9.70	8.40	8.40	24.90	7.75	19.70	5.00
V	79.70	69.00	28.10	24.70	24.70	71.00	22.35	73.70	6.00
Cr	827.20	179.20	292.10	218.00	218.00	319.30	155.10	941.60	10.00
Co	33.10	41.30	34.10	32.50	32.50	34.50	45.65	67.40	26.00
Ni	208.20	204.20	270.40	344.70	344.70	229.60	423.60	559.50	198.00
Cu	70.10	55.60	43.50	50.30	50.30	69.40	53.95	115.40	24.00
Zn	23.80	29.10	21.80	31.20	31.20	24.00	31.55	41.00	26.00
Ga	10.30	10.80	9.90	10.10	10.10	9.40	8.85	8.40	13.00
As	3.50	2.80	3.50	2.00	2.00	1.10	4.80	3.70	0.00
S	210.50	209.80	134.00	77.00	77.00	61.80	145.30	400.30	120.00
ICPMS									
Li	1.40	2.84	1.84	0.97	0.93	0.55	1.35	2.14	0.35
Sc	25.81	18.51	6.43	8.36	51.37	19.86	6.05	16.21	1.80
Ti	1604.00	1517.00	896.46	724.54	4951.00	1174.00	731.88	2422.80	733.04
V	82.08	66.64	26.08	28.65	165.35	62.10	18.77	75.95	8.24
Cr	867.70	323.70	271.60	400.28	616.10	304.55	143.29	944.62	7.68
Co	36.25	39.72	36.54	40.05	26.57	36.18	46.06	64.71	28.92
Ni	223.51	209.12	313.19	385.94	117.34	224.23	384.58	545.94	189.54
Cu	88.15	71.98	62.72	52.03	7.75	81.94	64.06	149.75	28.63
Zn	26.08	31.88	24.34	25.46	20.75	25.75	30.62	45.08	24.10
Rb	0.11	0.24	0.23	0.15	0.16	0.13	0.09	0.26	0.09
Sr	324.66	348.60	348.04	317.43	366.07	343.78	319.08	252.01	397.98
Y	5.99	5.68	2.37	2.15	13.82	3.98	1.58	7.39	0.88
Zr	9.93	9.16	6.47	4.93	2.00	5.59	3.27	14.42	1.86
Nb	0.18	0.29	0.18	0.13	2.14	0.13	0.08	1.41	0.11
Mo	0.25	0.93	0.13	0.07	0.07	0.18	0.07	0.17	0.03
Sn	0.21	0.42	0.19	0.11	0.47	0.12	0.12	0.35	0.12
Sb	0.01	0.07	0.02	0.00	0.00	0.01	0.01	0.01	0.01
Cs	0.01	0.10	0.02	0.02	0.00	0.00	0.00	0.03	0.00
Ba	6.74	8.96	6.40	12.28	4.10	6.56	7.56	7.94	7.83
La	0.89	1.11	0.74	0.52	2.06	0.67	0.64	1.38	0.87
Ce	2.27	2.73	1.70	1.24	5.43	1.64	1.41	3.65	1.84
Pr	0.37	0.42	0.26	0.19	0.86	0.26	0.21	0.59	0.24
Nd	1.96	2.12	1.17	0.92	4.43	1.35	0.94	2.84	1.00
Sm	0.68	0.69	0.32	0.27	1.50	0.46	0.23	0.86	0.20
Eu	0.51	0.53	0.35	0.31	0.75	0.44	0.36	0.43	0.45
Gd	0.95	0.92	0.38	0.33	2.07	0.64	0.27	1.12	0.20
Tb	0.16	0.16	0.07	0.06	0.36	0.11	0.05	0.20	0.03
Dy	0.99	0.94	0.39	0.35	2.19	0.65	0.27	1.18	0.15
Ho	0.21	0.20	0.08	0.07	0.47	0.14	0.06	0.25	0.03
Er	0.58	0.56	0.21	0.20	1.31	0.38	0.15	0.67	0.08
Tm	-	-	-	-	-	-	-	-	-
Yb	0.51	0.49	0.20	0.18	1.14	0.34	0.14	0.62	0.08
Lu	0.08	0.08	0.03	0.03	0.18	0.05	0.02	0.10	0.01
Hf	0.30	0.25	0.15	0.12	0.10	0.17	0.08	0.38	0.04
Ta	0.01	0.02	0.01	0.01	0.14	0.01	0.01	0.08	0.01
Pb	0.20	0.70	0.31	0.28	0.18	0.21	0.42	0.45	0.32
Th	0.01	0.02	0.01	0.01	0.08	0.01	0.00	0.07	0.01
U	0.00	0.01	0.01	0.01	0.03	0.01	0.00	0.03	0.00
TIMS and MC-ICP-MS									
Os (ppt)			22.0	19.9	19.9		12.4	253.4	58.1
Re (ppt)			240	208	208		322	507	186
$^{187}Os/^{188}Os$			0.2841	0.3005	0.3005		0.3744	0.1575	0.1824

Table B.1 contd. Major and trace element compositions of whole-rock samples from the Allalin Gabbro.

	Gabbros				Transitional		
Unit	Allalin	Allalin	Allalin	Allalin	Allalin	Allalin	Allalin
Lithology	Gabbro	Gabbro	Gabbro	Gabbro	Transitional	Transitional	Transitional
Mm. facies	-	-	-	-	none/ecl.	none/ecl.	none/ecl.
Sample	S02/83vix	S02/83viix	S02/83viiixG	S02/83viiiix	S01H/5a	S02/10iiixE	S02/83viiixE
Protolith	Gabbro	Gabbro	Gabbro	Gabbro	Gabbro	Gabbro	Gabbro
XRF							
SiO2	47.88	50.80	48.36	48.07	47.28	48.15	47.83
TiO2	0.22	0.42	0.14	0.12	0.12	0.14	0.14
Al2O3	17.85	16.88	21.18	20.33	20.73	21.42	20.58
Fe2O3	6.71	4.43	5.15	5.40	5.49	5.78	5.28
MnO	0.11	0.09	0.08	0.09	0.08	0.09	0.08
MgO	13.36	8.88	10.72	11.37	11.82	9.27	11.11
CaO	9.74	13.57	10.05	9.38	9.19	9.38	9.59
Na2O	2.71	3.01	2.99	2.92	3.13	3.24	3.00
K2O	0.06	0.07	0.06	0.06	0.05	0.07	0.05
P2O5	0.02	0.02	0.02	0.02	0.02	0.02	0.02
CO2	-	-	-	-	-	-	-
LOI	0.97	1.24	0.69	1.41	2.24	1.91	2.27
Total	99.64	99.40	99.44	99.17	100.15	99.47	99.93
Sr	279.90	286.40	328.00	317.00	277.70	325.00	356.00
Y	4.70	9.90	4.00	3.00	1.20	2.00	3.00
Zr	11.30	16.80	12.00	10.00	6.35	12.00	11.00
Nb	1.40	1.30	1.00	1.00	0.45	1.00	2.00
Ba	5.60	17.30	24.00	14.00	6.85	5.00	38.00
Sc	19.90	47.50	11.00	10.00	9.00	8.00	10.00
V	60.10	161.80	31.00	23.00	20.50	28.00	32.00
Cr	522.20	453.60	180.00	97.00	169.20	47.00	221.00
Co	52.00	28.20	40.00	44.00	43.05	41.00	42.00
Ni	359.50	141.70	357.00	304.00	407.45	282.00	382.00
Cu	90.10	56.60	41.00	64.00	49.75	31.00	49.00
Zn	33.70	21.80	30.00	32.00	32.15	34.00	34.00
Ga	8.90	11.20	11.00	11.00	9.10	11.00	10.00
As	1.00	3.70	1.00	1.00	0.00	0.00	4.00
S	248.60	158.80	204.00	353.00	147.00	291.00	231.00
ICPMS							
Li	2.23	1.55	1.01	1.42	2.05	1.89	1.99
Sc	14.63	51.06	5.95	5.72	7.05	1.07	7.11
Ti	1424.68	2688.34	893.94	769.60	927.24	848.90	849.35
V	59.39	163.16	28.39	23.06	24.31	16.70	26.61
Cr	522.24	470.55	195.72	97.95	124.87	43.51	224.79
Co	51.76	29.23	39.78	42.28	50.02	37.63	41.51
Ni	362.96	154.23	348.67	285.51	428.40	260.91	369.44
Cu	119.31	70.93	46.80	75.51	98.13	35.35	60.20
Zn	35.46	21.99	26.52	28.70	33.00	29.65	31.72
Rb	0.22	0.22	0.11	0.16	0.19	0.16	0.14
Sr	308.82	314.31	361.42	345.91	271.21	348.86	397.59
Y	4.59	10.37	2.28	1.82	2.12	1.60	2.15
Zr	9.84	14.28	4.74	3.96	5.68	4.96	3.28
Nb	0.20	0.15	0.09	0.14	0.19	0.19	0.08
Mo	0.11	0.11	0.06	0.11	0.07	0.15	0.07
Sn	0.19	0.26	0.10	0.15	0.18	0.12	0.10
Sb	0.01	0.01	0.00	0.02	0.01	0.01	0.03
Cs	0.01	0.02	0.00	0.01	0.01	0.01	0.01
Ba	5.97	9.39	17.42	5.81	8.09	6.64	34.66
La	0.84	0.84	0.62	0.68	0.68	0.83	0.62
Ce	2.08	2.49	1.45	1.48	1.60	1.88	1.43
Pr	0.34	0.49	0.23	0.21	0.23	0.25	0.22
Nd	1.71	2.73	1.03	0.96	1.07	1.11	0.99
Sm	0.53	1.06	0.29	0.25	0.29	0.27	0.28
Eu	0.42	0.61	0.38	0.36	0.36	0.42	0.35
Gd	0.69	1.52	0.36	0.29	0.36	0.31	0.34
Tb	0.12	0.29	0.06	0.05	0.06	0.05	0.06
Dy	0.74	1.71	0.37	0.30	0.36	0.26	0.35
Ho	0.16	0.36	0.08	0.06	0.08	0.06	0.07
Er	0.42	0.94	0.21	0.17	0.21	0.16	0.20
Tm	-	-	-	-	-	-	-
Yb	0.38	0.80	0.19	0.16	0.21	0.16	0.18
Lu	0.06	0.13	0.03	0.03	0.03	0.03	0.03
Hf	0.26	0.48	0.12	0.09	0.12	0.09	0.09
Ta	0.01	0.01	0.01	0.01	0.01	0.02	0.01
Pb	0.35	0.45	0.20	0.18	0.46	0.17	1.18
Th	0.01	0.01	0.00	0.01	0.01	0.01	0.00
U	0.01	0.01	0.00	0.01	0.00	0.01	0.00
TIMS							
Os (ppt)	79.1	2.9	9.0	1.7	21.2	30.5	9.9
Re (ppt)	281	209	215	417	435	324	237
$^{187}Os/^{188}Os$	0.1936	1.1825	0.3091	2.7437	0.4123	0.2452	0.3922

Table B.1 contd. Major and trace element compositions of whole-rock samples from the Allalin Gabbro.

	Gabbroic eclogites (mainly coronites)								
Unit	Allalin	Allalin	Allalin	Allalin	Allalin	Allalin	Allalin	Allalin	Allalin
Lithology	Gabbroic ecl.	Coronite	Coronite	Coronite	Gab. ecl.	Gab. ecl.	Coronite	Coronite	Gab. ecl.
Mm. facies	Eclogite	Eclogite	Eclogite	Eclogite	Eclogite	Eclogite	Eclogite	Eclogite	Eclogite
Sample	S01/31i	S01/35ibx	S01/35iibx	S01/36ibx	S01/36iibx	S01/39ibx	S01/40ibx	S01/40iibx	S01/40iibx
Protolith	Gabbro	Gabbro	Gabbro	Gabbro	Gabbro	Gabbro	Gabbro	Gabbro	Gabbro
XRF									
SiO2	48.68	49.33	48.85	49.92	50.51	48.91	48.88	50.36	46.26
TiO2	0.26	0.40	0.46	0.51	0.47	0.36	0.20	0.17	0.09
Al2O3	15.95	22.73	23.09	17.27	15.97	16.64	21.99	24.90	21.58
Fe2O3	6.99	5.11	4.72	5.62	4.27	5.42	3.90	3.44	5.01
MnO	0.17	0.08	0.07	0.09	0.08	0.11	0.07	0.05	0.10
MgO	16.01	8.35	7.03	9.11	8.39	10.76	9.20	5.83	12.33
CaO	7.45	10.21	10.67	13.39	15.46	12.85	11.63	10.53	9.87
Na2O	1.53	3.56	4.41	2.75	3.03	2.36	3.23	4.09	1.76
K2O	0.03	0.11	0.16	0.03	0.05	0.01	0.02	0.07	0.01
P2O5	0.02	0.04	0.11	0.05	0.02	0.02	0.02	0.02	0.01
CO2	-	-	-	-	-	-	-	-	-
LOI	3.58	0.55	0.70	1.30	1.17	2.07	1.17	1.12	3.26
Total	100.67	100.47	100.27	100.03	99.42	99.50	100.30	100.57	100.29
Sr	177.20	197.90	278.00	506.00	266.00	281.00	263.60	299.40	247.40
Y	5.60	5.30	9.90	12.20	11.10	8.00	3.60	3.10	2.00
Zr	15.40	22.80	29.20	37.00	22.10	20.00	12.40	10.20	7.00
Nb	1.30	1.90	1.60	2.80	0.60	2.00	1.80	1.50	1.10
Ba	7.50	9.50	27.10	9.90	16.70	11.00	6.60	9.10	5.30
Sc	21.40	8.00	13.30	37.80	53.00	36.00	16.10	10.70	6.90
V	78.10	41.90	85.80	151.20	189.50	128.00	55.70	31.70	21.30
Cr	827.60	117.70	189.80	605.40	1402.90	1426.00	991.90	82.00	149.40
Co	53.90	32.30	27.30	31.80	22.70	36.00	26.90	20.80	34.40
Ni	470.30	249.00	134.70	184.70	201.00	241.00	295.70	129.30	404.40
Cu	109.40	46.60	27.10	14.80	81.70	6.00	77.60	19.10	30.20
Zn	35.70	19.20	26.00	36.90	23.00	14.00	16.00	18.40	27.30
Ga	9.60	12.10	14.40	13.30	9.40	10.00	10.80	11.90	10.00
As	1.60	0.90	2.70	1.60	1.60	4	2.10	3.60	0.30
S	205.60	105.90	185.00	157.20	57.90	80.00	38.40	52.50	66.90
ICPMS									
Li	0.72	2.29	3.43	2.20	0.94	0.16	1.67	1.49	0.44
Sc	-	0.30	9.76	42.99	63.81	40.40	10.31		3.95
Ti	1576.50	2099.00	2526.50	2573.00	2749.50	2213.68	1128.50	1069.65	464.70
V	77.17	36.41	79.40	133.70	175.15	131.66	48.47	29.64	12.23
Cr	792.53	117.90	224.85	564.85	1346.50	1526.45	895.70	79.72	123.59
Co	56.35	33.56	31.05	35.22	25.26	37.16	26.50	23.37	39.38
Ni	386.50	203.87	124.04	159.94	188.14	216.05	248.85	105.39	384.71
Cu	150.51	52.50	34.10	19.50	98.23	6.81	80.13	22.73	35.50
Zn	36.65	18.71	26.33	35.65	20.34	10.80	15.37	18.99	28.69
Rb	0.09	0.30	0.45	0.07	0.16	0.04	0.10	0.16	0.05
Sr	183.43	205.84	285.39	533.85	280.22	309.26	271.65	306.64	250.22
Y	5.36	4.19	9.32	13.04	11.40	8.10	3.77	3.12	1.31
Zr	1.35	3.51	2.48	2.90	4.99	2.88	1.65	1.99	0.93
Nb	0.42	0.87	1.31	0.85	0.23	0.17	0.20	0.24	0.08
Mo	0.02	0.45	0.84	0.16	0.09	0.03	0.32	0.00	0.07
Sn	0.28	0.31	0.63	0.39	0.24	0.14	0.19	0.21	0.08
Sb	0.01	0.03	0.04	0.00	0.00	0.00	0.03	0.00	0.00
Cs	0.01	0.01	0.02	0.01	0.02	0.00	0.00	0.01	0.00
Ba	2.17	5.92	16.86	3.90	7.40	1.54	5.08	6.48	1.49
La	0.74	1.34	3.62	2.10	0.87	0.71	0.81	1.04	0.50
Ce	2.11	3.23	9.40	5.49	2.67	2.01	2.03	2.49	1.11
Pr	0.34	0.47	1.41	0.87	0.49	0.37	0.31	0.35	0.16
Nd	1.82	2.22	6.72	4.46	2.94	2.03	1.56	1.60	0.71
Sm	0.62	0.64	1.87	1.51	1.18	0.75	0.49	0.43	0.18
Eu	0.34	0.52	0.79	0.77	0.62	0.45	0.39	0.48	0.28
Gd	0.81	0.81	2.11	2.07	1.75	1.09	0.64	0.54	0.20
Tb	0.14	0.13	0.31	0.36	0.31	0.21	0.11	0.09	0.04
Dy	0.90	0.72	1.63	2.12	1.89	1.27	0.63	0.56	0.20
Ho	0.20	0.15	0.33	0.45	0.40	0.28	0.13	0.11	0.04
Er	0.55	0.40	0.88	1.24	1.12	0.75	0.37	0.30	0.12
Tm	-	-	-	-	-	-	-	-	-
Yb	0.55	0.37	0.78	1.07	0.96	0.69	0.34	0.26	0.13
Lu	0.09	0.06	0.13	0.17	0.15	0.11	0.05	0.04	0.02
Hf	0.05	0.06	0.10	0.09	0.26	0.11	0.06	0.05	0.02
Ta	0.02	0.07	0.08	0.06	0.02	0.01	0.01	0.02	0.01
Pb	0.31	0.08	0.30	0.45	0.27	0.13	0.17	0.19	0.18
Th	0.02	0.05	0.10	0.06	0.02	0.01	0.01	0.03	0.02
U	0.01	0.02	0.04	0.02	0.01	0.00	0.01	0.01	0.01
TIMS									
Os (ppt)		55.2	53.0			2.3			16.8
Re (ppt)		437	667			290			166
$^{187}Os/^{188}Os$		0.2279	0.2720			0.2164			0.2738

Table B.1 contd. Major and trace element compositions of whole-rock samples from the Allalin Gabbro.

	Gabbroic eclogites (mainly coronites)						Blueschist eclogites		
Unit	Allalin	Allalin	Allalin	Allalin	Allalin	Allalin	Allalin	Allalin	Allalin
Lithology	Gab. ecl.	Gab. ecl.	Coronite	Coronite	Coronite	Gab. ecl.	Bschist ecl.	Bschist ecl.	Bschist ecl.
Mm. facies	Eclogite	Eclogite	Eclogite	Eclogite	Eclogite	Eclogite	Ecl retro-bsch	Ecl retro-bsch	Ecl retro-bsch
Sample	S01/40vx	S01/40vix	S01/40vilx	S01H/3ilx	S02/33I	S02/85bE	S01/40iilx	S02/84vilx	S02/84viilx
Protolith	Gabbro	Gabbro	Gabbro	Gabbro	Gabbro	Gabbro	Gabbro	Gabbro	Gabbro
XRF									
SiO2	46.87	50.35	47.37	49.10	45.98	48.60	51.04	49.92	51.41
TiO2	0.16	0.40	0.13	0.26	0.16	0.35	0.63	0.69	0.58
Al2O3	20.36	14.64	20.17	22.78	22.99	20.73	16.30	16.25	16.86
Fe2O3	5.99	5.18	4.57	5.54	3.80	4.71	6.08	6.20	5.44
MnO	0.13	0.11	0.07	0.08	0.04	0.08	0.12	0.12	0.09
MgO	11.87	12.38	12.32	7.80	8.57	6.84	8.99	8.84	8.43
CaO	9.75	12.54	10.87	9.30	11.02	12.14	13.12	12.18	11.56
Na2O	2.45	2.47	2.21	3.83	2.91	4.19	3.29	3.62	3.28
K2O	0.03	0.01	0.04	0.05	0.02	0.04	0.03	0.02	0.13
P2O5	0.02	0.01	0.01	0.04	0.03	0.02	0.02	0.02	0.03
CO2	-	-	-	-	-	-	-	-	-
LOI	2.91	2.07	2.58	1.33	3.68	1.62	1.25	1.38	1.76
Total	100.53	100.16	100.35	100.11	99.21	99.31	100.87	99.24	99.58
Sr	326.50	240.00	310.90	263.70	358.00	413.00	285.20	266.00	301.00
Y	3.00	9.20	2.60	4.80	3.00	8.00	15.40	15.00	11.00
Zr	7.10	19.90	8.20	17.20	19.00	21.00	27.10	31.00	28.00
Nb	1.10	1.40	1.00	2.00	2.00	2.00	1.50	2.00	2.00
Ba	3.60	17.20	8.90	6.30	9.00	7.00	12.30	14.00	22.00
Sc	11.50	45.10	12.70	7.10	8.00	25.00	47.30	48.00	41.00
V	39.70	162.40	40.00	28.10	26.00	92.00	194.80	205.00	168.00
Cr	183.40	1142.30	608.40	22.60	195.00	418.00	189.60	125.00	118.00
Co	38.70	39.10	37.00	28.40	26.00	23.00	26.80	33.00	36.00
Ni	319.30	265.40	487.90	233.80	274.00	147.00	157.90	156.00	125.00
Cu	16.10	43.30	37.80	17.80	52.00	17.00	50.30	39.00	41.00
Zn	27.80	22.40	26.00	30.10	34.00	26.00	30.70	36.00	34.00
Ga	9.20	8.70	9.30	13.30	12.00	12.00	11.40	14.00	12.00
As	2.80	-0.20	0.80	-	0.00	0.00	3.60	0.00	0.00
S	45.60	196.10	47.90	137.70	119.00	161.00	102.70	219.00	608.00
ICPMS									
Li	1.12	1.10	1.01	0.89	1.44	3.93	2.53	1.54	1.27
Sc	8.05	58.16	6.03	2.46	0.32	25.53	57.11	57.27	50.37
Ti	941.47	2329.50	865.45	1735.50	987.35	2308.52	3586.50	4618.23	3719.07
V	31.99	151.10	42.65	34.62	22.05	97.46	182.10	207.40	171.45
Cr	204.04	1157.50	760.20	24.30	215.90	440.76	190.20	133.38	119.43
Co	41.18	43.92	36.03	31.16	27.99	25.36	29.95	34.32	41.57
Ni	292.30	252.97	348.20	171.52	259.50	149.13	145.29	155.77	126.49
Cu	39.91	55.27	42.73	20.58	55.77	20.15	55.75	45.41	46.68
Zn	28.62	22.58	20.48	26.40	29.71	24.12	30.25	31.39	31.27
Rb	0.13	0.08	0.22	0.13	0.07	0.12	0.10	0.09	0.25
Sr	320.88	254.86	366.46	311.51	386.86	460.62	300.70	298.04	332.98
Y	2.50	8.87	2.74	4.36	2.49	8.11	15.74	15.96	10.64
Zr	1.16	1.71	5.62	2.04	1.97	6.36	1.42	5.29	3.29
Nb	0.11	0.29	0.09	0.90	0.44	0.15	0.43	0.48	0.40
Mo	0.05	0.06	0.18	0.06	0.06	0.05	0.13	0.05	0.06
Sn	0.12	0.18	0.11	0.18	0.30	0.22	0.35	0.27	0.21
Sb	0.00	0.00	0.01	0.00	0.01	0.03	0.01	0.00	0.00
Cs	0.00	0.01	0.01	0.00	0.01	0.02	0.00	0.00	0.01
Ba	2.21	1.33	7.78	4.98	2.03	3.97	2.21	1.29	11.47
La	0.66	0.83	0.55	1.97	0.93	1.03	1.40	1.29	1.12
Ce	1.56	2.44	1.33	4.48	2.13	2.76	4.20	3.91	3.17
Pr	0.24	0.45	0.21	0.61	0.30	0.48	0.77	0.76	0.57
Nd	1.16	2.54	1.05	2.76	1.37	2.59	4.41	4.35	3.06
Sm	0.33	1.00	0.33	0.71	0.36	0.89	1.72	1.64	1.10
Eu	0.34	0.52	0.34	0.65	0.33	0.66	0.87	0.83	0.66
Gd	0.41	1.45	0.44	0.82	0.43	1.22	2.49	2.33	1.52
Tb	0.07	0.26	0.08	0.13	0.07	0.22	0.43	0.43	0.28
Dy	0.41	1.52	0.46	0.73	0.40	1.30	2.62	2.56	1.71
Ho	0.09	0.32	0.10	0.15	0.09	0.28	0.55	0.54	0.37
Er	0.23	0.86	0.26	0.41	0.24	0.73	1.51	1.43	1.02
Tm	-	-	-	-	-	-	-	-	-
Yb	0.23	0.73	0.23	0.37	0.23	0.66	1.27	1.23	0.94
Lu	0.04	0.11	0.04	0.06	0.04	0.10	0.20	0.19	0.15
Hf	0.04	0.10	0.11	0.06	0.06	0.20	0.09	0.23	0.13
Ta	0.01	0.02	0.05	0.06	0.03	0.01	0.03	0.04	0.03
Pb	0.66	0.13	0.23	0.17	0.38	0.60	0.26	0.16	0.30
Th	0.01	0.02	0.01	0.03	0.03	0.01	0.02	0.02	0.02
U	0.00	0.01	0.01	0.01	0.01	0.00	0.01	0.01	0.01
TIMS									
Os (ppt)	23.5		6.7	47.7	17.4	3.5	8.2	1.0	1.3
Re (ppt)	141		92	224	133	126	247	291	662
$^{187}Os/^{188}Os$	0.2281		0.3266	0.1944	0.2170	1.4365	0.7651	5.5811	11.2544

Table B.1 contd. Major and trace element compositions of whole-rock samples from the Allalin Gabbro.

	Metagabbro - Pervasive deformation and retrogressed									
Unit	Allalin	Allalin	Allalin	Allalin	Allalin	Allalin	Allalin	Allalin	Allalin	Allalin
Lithology	Metagabbro	Metagabbro	Metagabbro	Metagabbro	Metagabbro	Metagabbro	Metagabbro	Metagabbro	Metagabbro	Metagabbro
Mm. facies	retro eclogite	retro eclogite	retro eclogite	retro eclogite	retro eclogite	retro eclogite	retro eclogite	retro eclogite	retro eclogite	retro eclogite
Sample	S01/23i	S01/25x	S01/30i	S01/30ii	S01/31ii	S01/32iiix	S01/39iiix	S02/5i	S02/7i	S02/85aR
Protolith	Gabbro	Gabbro	Gabbro	Gabbro	Gabbro	Gabbro	Gabbro	Gabbro	Gabbro	Gabbro
XRF										
SiO2	50.87	48.92	50.85	49.35	47.00	45.93	49.80	48.01	47.81	44.94
TiO2	0.61	1.14	0.50	0.27	0.18	0.24	0.86	0.48	0.17	0.17
Al2O3	16.11	18.20	16.72	23.21	28.81	21.03	17.12	21.79	21.51	23.53
Fe2O3	6.12	7.38	5.98	2.69	1.21	5.81	5.03	4.99	6.89	5.47
MnO	0.11	0.13	0.10	0.04	0.03	0.04	0.09	0.05	0.15	0.06
MgO	9.16	7.42	9.23	4.09	1.59	9.89	8.48	7.35	6.94	7.66
CaO	11.76	10.60	12.47	16.41	16.08	11.08	13.32	10.45	11.31	10.72
Na2O	3.88	4.30	3.40	2.24	2.85	2.70	3.27	3.71	3.21	3.43
K2O	0.11	0.11	0.06	0.02	0.23	0.02	0.08	0.09	0.10	0.04
P2O5	0.06	0.18	0.03	0.02	0.03	0.02	0.06	0.02	0.02	0.02
CO2	-	-	-	-	-	-	-	-	-	-
LOI	1.55	1.58	1.46	1.60	2.04	2.90	1.51	2.73	1.73	3.03
Total	100.35	99.98	100.79	99.95	100.06	99.67	99.60	99.68	99.82	99.08
Sr	316.80	267.00	272.10	487.70	465.80		349.00	434.90	381.20	446.00
Y	12.10	22.00	10.20	8.70	2.70		13.80	7.20	8.50	3.00
Zr	37.60	103.80	23.90	40.00	11.20		41.50	23.80	6.60	10.00
Nb	2.00	8.30	2.00	1.10	0.90		2.90	1.50	1.70	2.00
Ba	21.90	16.20	7.30	3.00	9.40		14.50	14.30	8.70	6.00
Sc	43.90	29.30	46.50	32.20	7.30		46.90	18.20	13.50	7.00
V	157.60	175.00	171.80	94.70	27.60		179.90	112.10	55.40	23.00
Cr	901.90	258.50	231.90	1001.80	509.70		612.70	630.20	82.50	31.00
Co	29.70	26.60	27.60	10.80	6.40		22.30	33.00	31.10	33.00
Ni	98.40	115.60	105.40	70.40	51.60		119.60	186.50	139.70	185.00
Cu	20.00	42.30	80.10	59.90	5.20		8.10	15.50	39.30	9.00
Zn	33.80	42.30	30.60	10.50	6.00		21.40	33.00	25.00	48.00
Ga	11.50	14.10	11.10	12.60	10.80		11.60	11.00	14.80	12.00
As	5.60	1.80	5.40	1.90	2.10		0.00	0.00	0.00	1.00
S	23.90	140.40	119.90	21.80	27.00		17.50	28.00	65.60	75.00
ICPMS										
Li	10.06	3.92	1.42	0.10	0.47	1.65	0.78	1.70	2.39	7.40
Sc	-	-	-	-	-	12.94	-	18.06	7.93	1.41
Ti	3720.19	6902.13	3060.34	1621.24	1062.45	1400.50	5187.20	2859.50	985.20	1057.88
V	148.65	164.52	162.39	93.65	29.44	50.73	170.02	106.50	47.43	17.85
Cr	855.14	234.09	232.40	998.22	571.80	131.45	599.33	636.10	82.55	28.87
Co	32.30	28.75	31.97	13.10	5.30	73.40	25.43	34.94	32.56	32.22
Ni	92.66	105.20	101.04	64.84	46.33	300.36	109.74	179.24	130.74	187.14
Cu	23.77	49.25	99.55	65.08	6.78	585.70	8.16	17.53	41.26	8.98
Zn	35.51	44.57	32.24	9.66	4.97	35.85	21.58	34.80	24.97	43.58
Rb	0.56	0.29	0.13	0.04	0.61	0.04	0.16	0.37	0.39	0.25
Sr	328.46	276.28	284.72	497.72	489.65	347.36	358.95	465.40	395.14	495.16
Y	12.08	22.01	10.49	7.86	2.86	4.61	13.18	6.80	8.13	1.91
Zr	4.02	11.27	4.40	1.56	1.26	0.91	4.26	1.50	0.77	1.33
Nb	1.00	7.94	0.43	0.23	0.32	0.24	2.22	0.93	0.25	0.15
Mo	0.02	0.39	0.01	-0.01	0.00	0.17	0.01	0.04	0.07	0.04
Sn	0.52	1.20	0.34	0.30	0.16	0.21	0.51	0.34	0.30	0.13
Sb	0.00	0.00	0.00	0.00	0.01	0.01	0.00	0.00	0.00	0.12
Cs	0.03	0.00	0.00	0.00	0.00	0.00	0.00	0.01	0.01	0.21
Ba	11.98	6.78	2.98	0.83	10.77	1.66	3.60	9.60	6.14	2.97
La	1.90	6.20	1.16	0.75	0.78	0.91	2.01	1.29	2.21	0.96
Ce	5.40	15.41	3.49	2.12	2.02	2.16	5.54	3.32	5.12	2.03
Pr	0.88	2.18	0.61	0.35	0.29	0.33	0.87	0.53	0.75	0.29
Nd	4.69	10.33	3.50	1.98	1.37	1.62	4.54	2.70	3.59	1.22
Sm	1.55	2.84	1.24	0.69	0.37	0.52	1.50	0.89	1.21	0.29
Eu	0.84	1.14	0.71	0.60	0.45	0.49	0.74	0.55	1.18	0.49
Gd	2.00	3.41	1.68	1.00	0.46	0.71	1.96	1.19	1.78	0.33
Tb	0.33	0.56	0.29	0.18	0.08	0.12	0.34	0.20	0.32	0.06
Dy	2.09	3.49	1.83	1.24	0.48	0.75	2.18	1.17	1.72	0.31
Ho	0.44	0.77	0.39	0.28	0.10	0.16	0.47	0.24	0.29	0.07
Er	1.19	2.15	1.05	0.83	0.28	0.45	1.29	0.63	0.59	0.17
Tm	-	-	-	-	-	-	-	-	-	-
Yb	1.03	1.99	0.89	0.83	0.26	0.42	1.15	0.50	0.35	0.15
Lu	0.15	0.30	0.14	0.12	0.04	0.07	0.17	0.08	0.05	0.03
Hf	0.15	0.30	0.13	0.08	0.04	0.04	0.16	0.04	0.02	0.04
Ta	0.07	0.47	0.03	0.02	0.02	0.02	0.14	0.05	0.01	0.01
Pb	0.41	0.52	0.19	0.26	0.22	0.40	0.16	0.31	0.24	0.63
Th	0.04	0.43	0.02	0.02	0.02	0.01	0.08	0.03	0.01	0.00
U	0.02	0.14	0.01	0.01	0.01	0.01	0.03	0.02	0.03	0.00
TIMS										
Os (ppt)			3.0	110.7			0.9	145.7	12.0	2.7
Re (ppt)			192	41			143	25	132	75
$^{187}Os/^{188}Os$			1.2510	0.1569			0.9523	0.1575	0.3498	0.7568

Table B.2. Major and trace element compositions of whole-rock basaltic eclogite samples from the ZSO.

	Metabasalts - Pfulwe							
Unit	Zermatt-Saas	Zermatt-Saas	Zermatt-Saas	Zermatt-Saas	Zermatt-Saas	Zermatt-Saas	Zermatt-Saas	Zermatt-Saas
Lithology	Mafic Eclogite	Eclogite	Eclogite	Eclogite	Eclogite	Eclogite	Eclogite	Eclogite
Mm. facies	Eclogite	Eclogite	Eclogite with gechist retro		Eclogite with gechist retro		Eclogite	
Sample	S02/41ii	S02/41v	S02/74ii	S02/75iC	S02/75iiR	S02/75iiiC	S02/75iiiR	S02/75ivC
Protolith	Basalt	Basalt	Pillow basalt	Pillow basalt	Pillow basalt	Pillow basalt	Pillow basalt	Pillow basalt
XRF								
SiO2	47.14	49.04	48.41	49.83	49.99	50.71	50.35	50.86
TiO2	2.75	2.72	1.80	2.17	2.09	2.15	1.97	2.08
Al2O3	17.27	16.38	15.71	16.48	16.52	16.55	15.33	15.43
Fe2O3	9.99	10.68	9.00	9.69	9.79	9.72	10.06	10.24
MnO	0.22	0.17	0.15	0.17	0.17	0.17	0.16	0.16
MgO	5.20	5.51	6.17	5.40	5.31	5.63	6.46	6.40
CaO	11.83	8.28	10.69	7.97	8.09	7.83	7.11	7.35
Na2O	4.32	5.23	4.58	5.11	5.18	5.39	5.30	5.01
K2O	0.02	0.05	0.14	0.41	0.38	0.22	0.25	0.73
P2O5	0.26	0.39	0.31	0.41	0.38	0.37	0.34	0.24
CO2	-	-				-	-	-
LOI	0.91	1.04	1.94	1.38	1.29	0.99	1.97	0.94
Total	99.91	99.49	98.91	99.02	99.18	99.73	99.30	99.43
Sr	206.80	247.50	242.00	210.00	210.00	195.20	158.30	123.20
Y	58.00	56.30	37.00	49.00	47.00	49.20	42.30	46.30
Zr	321.20	326.90	173.00	245.00	240.00	257.60	234.90	242.90
Nb	12.20	13.10	7.00	9.00	9.00	8.50	8.00	7.30
Ba	19.80	26.20	19.00	27.00	23.00	38.00	36.20	60.10
Sc	28.60	30.10	33.00	27.00	28.00	28.40	26.00	26.10
V	279.40	294.30	236.00	265.00	278.00	265.00	237.40	258.70
Cr	70.10	58.50	226.00	144.00	139.00	144.60	137.70	135.00
Co	23.80	24.60	33.00	27.00	28.00	26.90	34.60	31.40
Ni	50.00	57.70	123.00	76.00	73.00	77.60	95.30	93.90
Cu	21.40	27.70	79.00	51.00	48.00	47.30	39.20	34.90
Zn	61.70	99.00	68.00	87.00	84.00	79.20	98.10	95.70
Ga	20.90	21.80	17.00	18.00	19.00	18.30	17.00	18.50
As	1.70	1.90	3.00	0.00	0.00	2.10	3.00	2.80
S	390.00	202.00	393.00	132.00	204.00	157.80	128.60	102.60
ICPMS								
Li	14.52	18.71	16.52	9.92	12.06	19.10	19.70	14.58
Sc	30.56	29.71	30.02	28.90	28.05	19.99	19.82	26.96
Tl	17173.79	17118.60	10660.00	12795.00	12180.00	13210.20	12139.92	13003.85
V	274.40	278.99	210.90	230.65	235.25	242.83	220.03	246.46
Cr	66.97	57.49	208.30	135.10	129.95	129.70	121.75	132.59
Co	25.91	30.33	32.42	26.02	27.29	28.32	33.72	33.50
Ni	45.53	55.99	112.92	75.76	72.82	72.30	90.82	93.69
Cu	21.79	29.67	81.11	51.00	46.63	49.80	42.56	38.41
Zn	60.91	96.86	60.52	81.62	79.21	75.98	96.56	92.08
Rb	0.13	0.30	1.34	5.34	4.81	2.21	3.48	9.34
Sr	219.70	266.96	250.06	220.64	217.32	201.55	168.06	133.42
Y	64.17	63.86	38.65	52.16	50.07	54.11	45.58	49.95
Zr	36.34	34.15	9.56	11.63	15.39	280.51	249.80	13.45
Nb	12.93	13.57	7.09	8.06	7.62	8.09	7.54	7.68
Mo	0.20	0.16	0.73	0.22	0.31	0.26	0.28	0.20
Sn	3.17	3.14	1.92	2.76	2.67	2.63	2.29	2.32
Sb	0.05	0.05	0.03	0.07	0.06	0.05	0.06	0.04
Cs	0.02	0.05	0.07	0.17	0.15	0.11	0.60	0.23
Ba	0.66	3.41	14.03	26.16	22.87	12.73	14.69	43.49
La	15.98	12.06	7.75	11.09	10.43	10.62	7.95	10.07
Ce	43.75	32.94	21.25	30.56	28.56	29.91	22.96	28.88
Pr	6.68	5.02	3.28	4.76	4.46	4.73	3.65	4.59
Nd	29.98	22.77	16.05	22.88	21.68	22.41	17.43	21.27
Sm	7.94	6.27	4.92	6.75	6.43	6.57	4.99	5.96
Eu	2.54	2.07	1.73	2.15	2.06	2.08	1.58	1.85
Gd	9.37	7.73	6.21	8.40	8.09	8.01	6.37	6.93
Tb	1.64	1.44	1.02	1.37	1.33	1.36	1.20	1.29
Dy	9.61	9.00	6.06	7.99	7.64	8.08	7.30	7.79
Ho	2.05	1.98	1.32	1.75	1.67	1.78	1.51	1.62
Er	5.65	5.51	3.77	5.07	4.80	5.10	4.10	4.31
Tm	-	-	-	-	-	-	-	-
Yb	5.27	4.87	3.43	4.56	4.31	4.76	3.66	3.94
Lu	0.79	0.73	0.52	0.68	0.64	0.73	0.57	0.60
Hf	1.24	0.79	0.27	0.27	0.34	3.14	2.76	0.45
Ta	0.78	0.80	0.44	0.53	0.51	0.58	0.48	0.48
Pb	1.37	1.61	1.82	1.24	1.20	1.33	1.20	1.10
Th	1.18	0.71	0.40	0.53	0.49	0.48	0.42	0.47
U	0.55	0.43	0.28	0.22	0.21	0.24	0.18	0.18
TIMS								
Os (ppt)	26.4	4.2	11.1	6.0	10.3	43.1	13.6	37.8
Re (ppt)	1385	165	233	687	147	194	267	159
$^{187}Os/^{188}Os$	10.8451	0.7947	0.9728	0.5905	0.3373	0.4004	0.6435	0.2638

Table B.2. contd. Major and trace element compositions of whole-rock basaltic eclogite samples from the ZSO.

	Metabasalts - Allalin				Other Zermatt-Saas metabasalts	
Unit	Allalin	Allalin	Allalin	Allalin	Zermatt-Saas	Zermatt-Saas
Lithology	Metabasalt	Metabasalt	Metabasalt	Metabasalt	Metabasalt	Metabasalt
Mm. facies	Eclogite with gschist retro		Eclogite with gschist retro		Eclogite	Eclogite
Sample	S02/4i	S02/4iiix	S02/4iii	S02/7i	S01/39iix	S01/39vx
Protolith	Basalt dyke	Basalt dyke	Basalt dyke	Basalt dyke		
XRF						
SiO2	50.43	49.21	49.77	49.23	52.03	46.19
TiO2	1.16	1.26	1.38	1.92	2.39	2.27
Al2O3	16.62	18.38	17.02	16.13	15.80	18.46
Fe2O3	6.28	8.76	7.82	8.44	10.35	12.79
MnO	0.12	0.21	0.13	0.18	0.13	0.23
MgO	8.30	7.98	7.94	7.74	5.30	4.86
CaO	11.64	8.34	9.89	10.36	7.04	10.92
Na2O	3.59	3.92	4.13	3.56	4.89	3.88
K2O	0.06	0.03	0.20	0.02	0.61	0.28
P2O5	0.11	0.15	0.21	0.29	0.50	0.33
CO2	-	-	-	-	-	-
LOI	1.73	1.50	1.26	1.60	1.36	0.54
Total	100.04	99.73	99.73	99.46	100.40	100.76
Sr	235.00	217.50	235.60	146.00	114.90	206.10
Y	20.00	26.00	25.60	36.00	43.60	58.00
Zr	86.00	102.70	124.10	140.00	289.40	237.10
Nb	3.00	3.20	11.70	7.00	10.50	8.30
Ba	4.00	12.10	25.30	8.00	37.90	37.60
Sc	36.00	28.80	30.10	37.00	24.30	37.90
V	193.00	161.30	205.40	272.00	265.10	305.10
Cr	182.00	241.70	273.00	149.00	69.60	189.30
Co	30.00	48.50	35.70	33.00	22.70	26.10
Ni	82.00	160.10	130.40	90.00	50.00	85.50
Cu	134.00	27.00	37.40	36.00	37.10	47.00
Zn	33.00	27.80	33.70	30.00	91.40	67.40
Ga	13.00	13.70	14.90	12.00	18.80	25.00
As	3.00	2.40	1.70	0.00	0.80	1.70
S	241.00	426.50	131.60	131.00	35.30	45.40
ICPMS						
Li	1.13	3.89	1.43	0.46	23.00	51.15
Sc	43.13	32.55	-	40.49	-	-
Ti	6761.00	7323.00	8384.43	11735.00	14299.74	13334.35
V	186.10	139.10	186.99	255.30	230.57	282.96
Cr	178.75	223.05	249.93	153.55	57.29	173.38
Co	30.76	48.80	30.60	29.59	27.10	29.71
Ni	85.64	153.28	117.50	82.64	42.14	71.68
Cu	144.52	34.25	42.13	37.96	46.18	49.35
Zn	31.27	27.20	34.23	27.61	94.10	66.36
Rb	0.08	0.07	0.77	0.08	8.90	4.56
Sr	252.72	222.70	236.51	159.06	114.33	197.84
Y	20.62	26.15	25.12	38.93	45.85	57.28
Zr	5.91	4.64	20.37	17.05	34.18	38.07
Nb	2.74	3.23	11.36	6.66	10.99	7.77
Mo	0.16	0.47	0.17	0.17	0.05	0.07
Sn	0.46	0.68	1.20	0.47	2.90	3.27
Sb	0.12	0.00	0.00	0.01	0.04	0.04
Cs	0.00	0.00	0.01	0.00	0.33	0.16
Ba	2.59	1.11	10.43	1.18	18.28	10.91
La	3.47	4.85	7.62	7.37	12.58	16.40
Ce	10.15	12.79	18.45	21.30	35.01	42.66
Pr	1.66	1.93	2.59	3.35	5.13	5.88
Nd	8.37	9.28	12.01	16.36	24.15	28.37
Sm	2.60	2.87	3.30	4.72	6.48	7.91
Eu	0.92	1.03	1.14	1.05	1.83	2.95
Gd	3.28	3.79	3.83	5.65	7.14	9.46
Tb	0.54	0.65	0.63	0.93	1.19	1.51
Dy	3.21	3.97	3.97	5.73	7.46	8.83
Ho	0.72	0.90	0.87	1.32	1.64	1.93
Er	2.14	2.64	2.40	3.88	4.53	5.48
Tm	-	-	-	-	-	-
Yb	2.03	2.49	2.24	3.53	4.35	5.29
Lu	0.32	0.39	0.34	0.56	0.64	0.78
Hf	0.18	0.09	0.44	0.49	0.70	0.75
Ta	0.19	0.23	0.66	0.42	0.70	0.53
Pb	0.33	0.12	0.28	0.32	0.63	1.97
Th	0.12	0.22	0.68	0.17	0.68	1.34
U	0.03	0.08	0.22	0.06	0.35	0.33
TIMS						
Os (ppt)	2.4	7.6		1.9		
Re (ppt)	238	785		93		
$^{187}Os/^{188}Os$	3.0553	1.1450		6.0613		

Table B.3. Major and trace element compositions of metabasalts from the Sulitjelma ophiolite (XRF data from Boyle 1982).

	SULITJELMA Pillows								
Unit	Lomivann	Lomivann	Lomivann	Otervann	Otervann	Otervann	Otervann	Otervann	Otervann
Lithology	Amphibolite	Amphibolite	Amphibolite	Amphibolite	Amphibolite	Amphibolite	Amphibolite	Amphibolite	Amphibolite
Mm. grade	Biotite	Biotite	Biotite	Garnet	Garnet	Garnet	Garnet	Garnet	Kyanite
Sample	Giles 1	Giles 5	Giles 7	A63	A64	A65	A77	A78	A162
Protolith	Pillow basalt	Pillow basalt	Pillow basalt	Pillow basalt	Pillow basalt	Pillow basalt	Pillow basalt	Pillow basalt	Pillow basalt
XRF									
SiO2	51.90	51.84	55.62	49.86	49.75	52.84	48.77	48.84	48.02
TiO2	1.10	1.11	1.01	1.29	1.41	1.55	1.02	1.41	1.13
Al2O3	16.67	16.75	15.64	17.74	16.86	16.93	18.73	16.63	20.17
Fe2O3	7.35	7.06	6.46	7.79	7.86	8.28	6.74	8.34	6.24
MnO	0.13	0.13	0.12	0.14	0.13	0.13	0.11	0.14	0.09
MgO	7.12	5.58	4.90	7.10	7.08	5.22	5.11	6.14	6.84
CaO	10.11	10.26	8.81	9.98	11.40	8.48	11.79	11.83	9.63
Na2O	3.46	4.03	4.54	3.71	3.26	4.76	3.96	3.32	4.20
K2O	0.83	0.91	0.95	0.19	0.17	0.24	0.46	0.21	0.14
P2O5	0.14	0.15	0.14	0.15	0.17	0.20	0.15	0.23	0.14
CO2	-	-	-	0.59	0.15	0.35	1.09	1.29	0.95
LOI	-	-	-	1.65	1.36	1.08	2.05	1.49	2.14
Total	98.81	97.82	98.19						
Sr	242.00	229.00	230.00	245.00	242.00	231.00	232.00	287.00	318.00
Y	36.00	40.00	45.00	31.00	30.00	44.00	29.00	38.00	22.00
Zr	175.00	197.00	230.00	104.00	108.00	185.00	121.00	142.00	99.00
Nb	-	-	-	2.00	2.00	5.00	3.00	4.00	2.00
Ba	168.00	211.00	144.00	-	-	-	-	-	-
Sc	37.00	33.00	30.00	-	-	-	-	-	-
V	179.00	167.00	157.00	-	-	-	-	-	-
Cr	223.00	193.00	182.00	294.00	298.00	196.00	234.00	229.00	203.00
Co	-	-	-	-	-	-	-	-	-
Ni	26.00	21.00	34.00	61.00	63.00	48.00	79.00	74.00	67.00
Cu	-	-	-	82.00	80.00	46.00	6.00	48.00	132.00
Zn	77.00	74.00	69.00	107.00	110.00	84.00	85.00	83.00	106.00
Ga	-	-	-	-	-	-	-	-	-
As	-	-	-	-	-	-	-	-	-
S	-	-	-	-	-	-	-	-	-
ICPMS									
Li	15.57	13.73	13.01	10.45	8.70	10.17	8.68	9.21	9.20
Sc	-	-	-	-	-	-	-	-	-
Ti	6982.14	6766.14	6077.23	7619.01	8362.90	9165.01	5941.51	8430.20	6684.11
V	179.42	174.93	153.31	206.40	222.00	209.78	151.51	175.92	162.85
Cr	217.04	201.88	179.99	268.34	273.23	183.00	222.33	210.89	196.04
Co	51.43	51.44	41.53	52.87	58.46	57.11	43.87	52.26	48.95
Ni	24.95	23.31	34.19	61.67	61.30	46.12	75.35	72.15	63.04
Cu	7.68	9.80	40.62	98.10	75.05	55.21	6.98	69.30	174.59
Zn	78.85	75.98	74.17	74.84	77.92	79.50	74.09	77.31	110.49
Rb	24.23	29.96	34.12	1.45	0.83	1.44	5.99	1.32	1.09
Sr	255.45	250.26	235.10	243.70	253.37	238.06	243.25	305.73	326.22
Y	37.23	37.49	42.50	30.48	32.88	45.38	30.89	39.36	24.83
Zr	182.32	146.07	171.19	56.28	75.69	124.54	108.56	121.31	60.63
Nb	5.48	5.69	6.79	2.46	2.72	4.61	3.16	5.47	3.16
Mo	0.32	0.30	0.21	0.18	0.25	0.46	0.14	0.22	0.18
Sn	3.39	2.45	2.95	1.33	1.47	2.26	1.60	1.93	1.31
Sb	0.66	0.97	1.13	0.20	0.29	0.13	0.25	0.23	0.44
Cs	0.96	1.21	1.68	0.06	0.03	0.08	0.16	0.06	0.24
Ba	166.15	161.14	150.82	28.02	30.74	47.07	60.05	25.58	46.99
La	15.54	15.92	18.94	4.47	4.79	8.66	5.73	7.64	5.10
Ce	35.81	36.75	42.43	13.21	14.29	23.98	15.95	21.18	13.94
Pr	4.79	4.89	5.66	2.15	2.33	3.67	2.45	3.26	2.13
Nd	20.87	21.24	24.22	11.25	12.19	18.32	12.16	16.19	10.54
Sm	5.27	5.35	6.01	3.54	3.81	5.37	3.61	4.78	3.05
Eu	1.52	1.50	1.48	1.14	1.27	1.65	1.20	1.62	1.15
Gd	5.79	5.83	6.49	4.47	4.81	6.56	4.43	5.86	3.73
Tb	0.96	0.97	1.08	0.76	0.83	1.13	0.75	1.00	0.62
Dy	5.96	6.05	6.75	4.89	5.29	7.17	4.86	6.27	3.94
Ho	1.30	1.31	1.47	1.08	1.16	1.60	1.09	1.38	0.86
Er	3.64	3.67	4.18	2.99	3.24	4.50	3.04	3.88	2.39
Tm	-	-	-	-	-	-	-	-	-
Yb	3.33	3.42	3.93	2.73	2.99	4.20	2.88	3.54	2.20
Lu	0.49	0.50	0.57	0.41	0.44	0.62	0.42	0.53	0.33
Hf	3.30	3.14	3.92	1.38	1.80	2.85	1.75	2.56	1.32
Ta	0.78	0.84	0.66	0.54	0.72	0.88	0.52	0.58	0.56
Pb	6.07	6.73	7.83	1.62	3.21	2.40	6.64	2.65	4.29
Th	3.83	3.93	5.06	0.38	0.43	1.25	0.70	0.67	0.65
U	1.27	1.40	1.92	0.15	0.17	0.48	0.35	0.26	0.29

Table B.3. contd. Major and trace element compositions of metabasalts from the Sulitjelma ophiolite (XRF data from Boyle 1982).

	SULITJELMA Pillows							
Unit	Otervann	Otervann	Otervann	Otervann	Otervann	Otervann	Otervann	Otervann
Lithology	Amphibolite	Amphibolite	Amphibolite	Amphibolite	Amphibolite	Amphibolite	Amphibolite	Amphibolite
Mm. grade	Garnet	Garnet	Garnet	Garnet	Garnet	Garnet	Garnet	Biotite
Sample	B11	B75	B76	B77	B89	B90	B90'	D1
Protolith	Pillow basalt	Pillow basalt	Pillow basalt	Pillow basalt	Pillow basalt	Pillow basalt	Pillow basalt	Pillow basalt
XRF								
SiO2	52.42	50.32	50.17	50.71	49.17	53.25	49.86	49.52
TiO2	1.75	1.37	1.09	1.29	1.40	1.49	0.36	1.38
Al2O3	15.78	17.56	18.43	17.33	19.29	19.49	16.40	17.61
Fe2O3	7.58	8.06	6.86	7.34	8.44	6.62	7.20	8.02
MnO	0.14	0.12	0.12	0.11	0.12	0.08	0.15	0.16
MgO	6.07	6.68	5.55	6.40	6.33	4.03	9.00	5.59
CaO	8.38	8.99	11.13	8.76	8.79	6.97	12.15	9.75
Na2O	5.20	4.54	4.46	5.09	4.30	5.78	2.27	4.25
K2O	0.18	0.14	0.10	0.11	0.16	0.12	0.15	0.52
P2O5	0.23	0.15	0.15	0.16	0.16	0.16	0.08	0.18
CO2	1.21	0.34	0.88	1.32	0.77	0.36	1.70	1.75
LOI	0.96	1.99	1.54	1.85	1.61	1.40	0.88	1.01
Total								
Sr	227.00	166.00	210.00	305.00	362.00	409.00	169.00	348.00
Y	41.00	29.00	24.00	30.00	30.00	31.00	27.00	25.00
Zr	215.00	132.00	96.00	114.00	118.00	119.00	84.00	116.00
Nb	6.00	4.00	5.00	5.00	5.00	6.00	0.00	7.00
Ba	-	-	-	-	-	-	-	-
Sc	-	-	-	-	-	-	-	-
V	-	-	-	-	-	-	-	-
Cr	174.00	282.00	260.00	280.00	293.00	289.00	315.00	-
Co	-	-	-	-	-	-	-	-
Ni	37.00	67.00	60.00	63.00	70.00	72.00	64.00	-
Cu	76.00	47.00	27.00	49.00	37.00	47.00	44.00	-
Zn	96.00	81.00	64.00	78.00	97.00	79.00	87.00	-
Ga	-	-	-	-	-	-	-	-
As	-	-	-	-	-	-	-	-
S	-	-	-	-	-	-	-	-
ICPMS								
Li	8.38	12.62	8.99	13.59	17.65	11.80	21.02	12.17
Sc	-	-	-	-	-	-	-	-
Ti	10522.85	7934.64	6460.96	7580.26	8176.35	8694.96	7631.23	8389.18
V	221.56	215.90	184.27	205.29	212.52	197.45	229.22	208.69
Cr	162.03	272.29	257.12	259.61	262.30	265.18	281.93	209.20
Co	52.01	49.68	40.60	41.49	42.67	43.03	45.46	50.68
Ni	33.62	59.35	57.27	59.07	64.76	69.20	56.14	76.99
Cu	69.58	48.17	24.65	48.45	43.57	46.26	39.75	78.96
Zn	85.66	83.62	61.39	67.72	73.94	84.71	76.01	62.78
Rb	0.68	0.62	0.48	0.31	0.46	0.43	0.98	11.30
Sr	229.22	161.42	212.34	299.15	365.02	420.54	180.69	362.84
Y	45.02	31.94	26.70	30.74	31.95	34.05	28.36	30.29
Zr	194.04	98.16	67.47	93.17	107.65	73.94	42.98	104.27
Nb	7.07	2.60	2.12	2.39	2.56	3.57	1.86	3.38
Mo	0.32	0.12	0.09	0.11	0.08	0.13	0.44	0.10
Sn	2.39	1.43	1.14	1.30	1.49	1.29	1.11	1.39
Sb	0.08	0.50	0.39	0.24	0.34	0.18	0.40	0.32
Cs	0.08	0.05	0.04	0.03	0.01	0.02	0.15	0.47
Ba	36.40	13.66	9.38	14.42	14.87	20.82	14.20	147.98
La	9.67	4.69	3.86	4.63	4.42	5.91	3.17	4.80
Ce	26.17	14.06	11.45	13.58	13.34	15.34	10.10	13.98
Pr	3.87	2.31	1.87	2.20	2.18	2.45	1.74	2.24
Nd	18.80	12.01	9.79	11.45	11.47	12.85	9.54	11.60
Sm	5.37	3.79	3.08	3.59	3.62	3.99	3.16	3.55
Eu	1.63	1.31	1.14	1.17	1.44	1.04	1.14	1.31
Gd	6.48	4.78	3.87	4.52	4.60	5.07	4.12	4.43
Tb	1.10	0.81	0.67	0.77	0.79	0.86	0.71	0.76
Dy	6.93	5.17	4.27	4.89	5.06	5.38	4.56	4.81
Ho	1.53	1.14	0.94	1.08	1.12	1.18	1.01	1.06
Er	4.28	3.17	2.62	3.00	3.11	3.24	2.76	2.93
Tm	-	-	-	-	-	-	-	-
Yb	3.99	2.95	2.42	2.82	2.92	2.92	2.44	2.67
Lu	0.59	0.43	0.36	0.42	0.45	0.42	0.35	0.40
Hf	3.76	2.23	1.32	2.11	2.53	1.89	1.09	2.22
Ta	0.74	0.44	0.33	0.30	0.27	0.34	0.28	0.33
Pb	4.45	4.35	3.71	5.36	3.24	4.38	4.17	6.80
Th	1.69	0.42	0.34	0.41	0.32	0.33	0.15	0.35
U	0.68	0.17	0.14	0.19	0.13	0.28	0.09	0.12

Table B.3. contd. Major and trace element compositions of metabasalts from the Sulitjelma ophiolite (XRF data from Boyle 1982).

	SULITJELMA Dykes								
Unit	Mietjerpakte	Mietjerpakte	Mietjerpakte	Mietjerpakte	Mietjerpakte	Mietjerpakte	Mietjerpakte	Mietjerpakte	Mietjerpakte
Lithology	Amphibolite	Amphibolite	Amphibolite	Amphibolite	Amphibolite	Amphibolite	Amphibolite	Amphibolite	Amphibolite
Mm. grade	Garnet	Garnet	Garnet	Kyanite	Grt/Ky	Grt/Ky	Garnet	Garnet	Garnet
Sample	A14	A24	A25	A163	B85	B98	B128	B129	B150
Protolith	Basalt dyke	Basalt dyke	Basalt dyke	Basalt dyke	Basalt dyke	Basalt dyke	Basalt dyke	Basalt dyke	Basalt dyke
XRF									
SiO2	48.29	49.71	49.59	49.70	47.37	48.56	45.98	48.38	48.46
TiO2	0.80	1.54	1.46	1.75	0.39	1.16	0.87	1.27	0.83
Al2O3	15.94	16.03	15.74	15.93	23.81	18.86	21.37	17.36	21.78
Fe2O3	6.88	8.52	9.15	9.20	4.15	6.70	5.38	7.46	6.92
MnO	0.14	0.15	0.14	0.31	0.08	0.11	0.09	0.13	0.13
MgO	10.64	7.34	7.39	6.74	5.59	5.60	4.11	7.44	6.31
CaO	11.63	10.35	9.35	9.73	12.97	12.21	12.17	12.03	11.35
Na2O	2.00	3.81	3.87	3.69	2.75	3.54	4.14	3.09	2.77
K2O	0.70	0.32	0.45	0.20	0.11	0.17	0.55	0.21	1.05
P2O5	0.11	0.17	0.17	0.20	0.09	0.18	0.14	0.17	0.11
CO2	0.52	0.42	0.63	0.49	0.61	1.12	2.68	0.66	0.27
LOI	2.25	1.35	1.72	1.70	1.87	1.85	3.01	1.87	1.75
Total									
Sr	178.00	213.00	212.00	189.00	258.00	246.00	382.00	236.00	244.00
Y	14.00	31.00	30.00	36.00	7.00	27.00	17.00	22.00	17.00
Zr	49.00	101.00	107.00	131.00	26.00	102.00	69.00	102.00	54.00
Nb	3.00	2.00	2.00	4.00	2.00	4.00	5.00	5.00	5.00
Ba	-	-	-	-	-	-	-	-	-
Sc	-	-	-	-	-	-	-	-	-
V	-	-	-	-	-	-	-	-	-
Cr	409.00	267.00	281.00	237.00	210.00	216.00	211.00	242.00	244.00
Co	-	-	-	-	-	-	-	-	-
Ni	170.00	59.00	60.00	50.00	97.00	96.00	69.00	72.00	80.00
Cu	20.00	62.00	32.00	170.00	17.00	17.00	50.00	107.00	4.00
Zn	91.00	81.00	66.00	233.00	41.00	63.00	42.00	63.00	49.00
Ga	-	-	-	-	-	-	-	-	-
As	-	-	-	-	-	-	-	-	-
S	-	-	-	-	-	-	-	-	-
ICPMS									
Li	18.42	6.13	7.14	7.71	6.38	7.15	21.52	7.16	11.88
Sc	-	-	-	-	-	-	-	-	-
Tl	4763.28	9373.35	8630.26	10660.64	2355.59	6751.63	5326.06	7552.97	4880.11
V	149.14	231.20	213.26	234.12	77.32	169.92	132.47	187.66	122.01
Cr	374.14	252.96	250.25	218.06	218.40	207.50	220.27	246.97	236.86
Co	61.81	62.09	63.00	60.31	34.41	38.08	40.97	49.86	41.49
Ni	147.39	59.70	55.73	48.13	90.71	88.03	62.11	67.73	73.01
Cu	28.46	61.01	38.12	180.53	18.64	20.04	46.60	83.22	4.46
Zn	76.69	60.89	42.73	186.10	34.49	67.61	44.90	58.71	41.60
Rb	8.63	2.18	8.58	1.18	1.54	0.68	12.75	1.98	27.68
Sr	191.48	225.96	221.42	200.17	274.83	251.23	400.09	252.71	487.81
Y	16.69	32.13	31.48	37.52	8.25	28.43	18.29	25.92	16.83
Zr	43.25	87.01	93.00	121.64	9.95	41.51	46.42	87.25	42.78
Nb	1.65	3.98	3.82	4.70	0.71	2.24	2.49	3.59	1.75
Mo	0.13	0.29	0.47	0.38	0.07	0.07	0.12	0.20	0.17
Sn	0.76	1.61	1.94	1.73	0.47	1.34	0.85	1.23	0.81
Sb	5.85	0.10	0.49	0.18	0.19	0.24	1.66	0.40	0.49
Cs	0.21	0.04	0.12	0.14	0.08	0.03	0.57	0.08	0.62
Ba	220.46	61.53	135.47	14.52	26.21	25.62	113.02	31.30	353.76
La	2.52	5.41	5.96	5.97	1.25	3.95	3.44	4.80	2.59
Ce	7.36	15.87	15.98	17.33	3.47	12.02	9.64	13.66	7.27
Pr	1.20	2.51	2.54	2.74	0.55	1.98	1.51	2.13	1.20
Nd	6.25	12.94	12.99	14.25	2.94	10.41	7.62	10.83	6.32
Sm	1.96	3.90	3.87	4.41	0.96	3.29	2.26	3.22	2.01
Eu	0.81	1.42	1.40	1.52	0.44	1.17	1.01	1.22	0.79
Gd	2.49	4.85	4.78	5.50	1.23	4.14	2.76	3.93	2.54
Tb	0.42	0.83	0.81	0.94	0.21	0.71	0.47	0.66	0.43
Dy	2.73	5.22	5.11	5.95	1.35	4.53	2.92	4.21	2.74
Ho	0.60	1.14	1.12	1.31	0.30	0.99	0.64	0.92	0.60
Er	1.67	3.14	3.12	3.61	0.82	2.77	1.76	2.53	1.67
Tm	-	-	-	-	-	-	-	-	-
Yb	1.53	2.83	2.84	3.36	0.76	2.53	1.61	2.31	1.55
Lu	0.23	0.43	0.43	0.51	0.12	0.38	0.24	0.34	0.24
Hf	1.44	2.17	2.13	2.67	0.31	1.14	1.04	1.91	0.99
Ta	0.52	0.70	1.67	0.75	0.26	0.26	0.36	0.49	0.41
Pb	1.91	0.66	0.89	4.62	1.12	3.84	1.12	0.92	1.29
Th	0.14	0.39	0.38	0.49	0.05	0.29	0.27	0.38	0.16
U	0.06	0.14	0.17	0.20	0.02	0.12	0.08	0.11	0.05

Table B.4. Major and trace element compositions of metagabbros from the Sulitjelma ophiolite (XRF data from Boyle 1982).

	SULITJELMA Gabbro						
Unit	Sulit. Gabbro	Sulit. Gabbro	Sulit. Gabbro	Sulit. Gabbro	Sulit. Gabbro	Sulit. Gabbro	Sulit. Gabbro
Lithology	Metagabbro	Metagabbro	Metagabbro	Metagabbro	Metagabbro	Metagabbro	Metagabbro
Mm. grade	Garnet	Kyanite	Kyanite	Kyanite	Kyanite	Kyanite	Garnet
Sample	A80	A146	B40	B56	B60	B68	B137
Protolith	Gabbro	Gabbro	Gabbro	Gabbro	Gabbro	Gabbro	Gabbro
XRF							
SiO2	42.99	50.56	48.78	49.26	50.95	53.85	50.50
TiO2	0.71	0.62	1.52	0.97	0.32	0.68	0.71
Al2O3	23.81	17.28	18.08	18.53	24.59	15.98	13.59
Fe2O3	4.00	7.69	8.33	7.45	3.75	5.56	11.08
MnO	0.07	0.16	0.15	0.15	0.06	0.10	0.13
MgO	3.88	8.68	6.85	7.22	3.92	7.50	7.96
CaO	15.73	8.23	10.71	11.08	10.97	11.79	9.66
Na2O	2.87	4.08	2.93	3.68	4.15	3.49	4.02
K2O	0.37	0.69	0.24	0.18	0.29	0.08	0.15
P2O5	0.12	0.06	0.08	0.14	0.06	0.07	0.37
CO2	3.00	0.02	0.62	0.44	0.54	0.32	0.25
LOI	2.22	1.65	0.90	1.18	0.77	1.14	1.36
Total							
Sr	316.00	213.00	285.00	265.00	407.00	276.00	245.00
Y	12.00	17.00	8.00	18.00	1.00	12.00	19.00
Zr	45.00	32.00	12.00	69.00	11.00	22.00	28.00
Nb	2.00	1.00	4.00	5.00	0.00	1.00	4.00
Ba	-	-	-	-	-	-	-
Sc	-	-	-	-	-	-	-
V	-	-	-	-	-	-	-
Cr	217.00	354.00	214.00	258.00	35.00	318.00	287.00
Co	-	-	-	-	-	-	-
Ni	86.00	112.00	88.00	68.00	105.00	60.00	71.00
Cu	150.00	6.00	21.00	7.00	10.00	3.00	tr.
Zn	120.00	45.00	61.00	68.00	34.00	30.00	53.00
Ga	-	-	-	-	-	-	-
As	-	-	-	-	-	-	-
S	-	-	-	-	-	-	-
ICPMS							
Li	11.84	11.81	7.69	7.65	3.80	6.14	1.51
Sc	-	-	-	-	-	-	-
Ti	4206.74	3472.44	1743.64	9358.12	5788.00	1809.26	3982.79
V	106.97	145.15	73.04	218.86	167.64	49.77	181.16
Cr	214.69	309.59	289.35	208.63	236.88	24.07	289.69
Co	44.20	49.19	47.95	41.74	49.42	35.25	44.15
Ni	83.22	96.85	69.77	22.01	63.40	12.74	57.79
Cu	145.55	4.49	151.98	20.02	5.18	9.79	3.66
Zn	86.69	40.23	139.08	50.74	57.77	26.28	33.09
Rb	2.92	10.84	1.17	1.79	0.73	6.31	0.82
Sr	336.17	211.24	368.01	294.90	276.82	425.03	268.57
Y	13.55	17.99	7.64	8.92	20.46	3.00	17.86
Zr	36.61	18.95	9.47	7.76	39.08	5.17	18.76
Nb	2.07	0.75	0.55	1.56	2.09	0.52	0.88
Mo	0.10	0.10	0.25	0.11	0.14	0.10	0.10
Sn	0.72	2.26	0.77	0.23	1.10	0.11	1.22
Sb	0.14	0.17	1.08	0.13	0.03	0.09	0.06
Cs	0.21	1.04	0.07	0.03	0.10	0.25	0.04
Ba	49.76	255.52	17.39	46.38	46.48	80.12	53.39
La	2.54	1.80	1.52	1.50	3.20	2.04	6.15
Ce	7.13	5.55	3.72	3.67	9.26	3.99	13.24
Pr	1.11	1.04	0.58	0.59	1.50	0.49	1.76
Nd	5.63	6.08	3.00	3.24	7.82	2.10	8.27
Sm	1.70	2.16	0.94	1.11	2.43	0.49	2.34
Eu	0.78	1.21	0.69	1.03	1.00	0.90	1.06
Gd	2.09	2.71	1.23	1.50	3.06	0.55	2.93
Tb	0.35	0.46	0.20	0.26	0.52	0.09	0.48
Dy	2.26	2.92	1.24	1.59	3.31	0.53	2.98
Ho	0.49	0.64	0.27	0.34	0.72	0.11	0.64
Er	1.38	1.75	0.71	0.91	2.00	0.29	1.73
Tm	-	-	-	-	-	-	-
Yb	1.28	1.60	0.64	0.80	1.84	0.26	1.47
Lu	0.19	0.24	0.10	0.12	0.28	0.04	0.22
Hf	0.81	0.63	0.28	0.33	1.02	0.15	0.64
Ta	0.40	0.32	0.73	0.46	0.51	0.46	0.32
Pb	1.18	12.76	14.16	1.47	1.24	1.63	1.23
Th	0.15	0.10	0.08	0.06	0.20	0.11	0.72
U	0.27	0.06	0.03	0.04	0.06	0.04	0.25

Table B.4. contd. Major and trace element compositions of metagabbros from the Sulitjelma ophiolite (XRF data from Boyle 1982).

	SULITJELMA Gabbro								
Unit	Sulit. Gabbro	Sulit. Gabbro	Sulit. Gabbro	Sulit. Gabbro	Sulit. Gabbro	Sulit. Gabbro	Sulit. Gabbro	Sulit. Gabbro	Sulit. Gabbro
Lithology	**Metagabbro**	**Metagabbro**	**Metagabbro**	**Metagabbro**	**Metagabbro**	**Metagabbro**	**Metagabbro**	**Metagabbro**	**Metagabbro**
Mm. grade	Kyanite	Kyanite	Kyanite	Ky/Gt	Ky/Gt	?	?	?	?
Sample	B58	B84	B109	B112	B115	M3	T158	V34	V39
Protolith	Gabbro	Gabbro	Gabbro	Gabbro	Gabbro	Gabbro	Gabbro	Gabbro	Gabbro
XRF									
SiO2	40.18	50.15	49.78	48.58	49.53	61.63	44.53	50.91	45.75
TiO2	4.92	3.16	0.41	0.31	0.37	1.58	0.15	1.37	0.24
Al2O3	12.89	16.76	18.47	18.42	16.31	15.76	13.41	17.36	10.72
Fe2O3	11.16	8.72	7.32	6.97	7.28	7.49	9.89	7.61	10.91
MnO	0.25	0.16	0.14	0.12	0.15	0.08	0.16	0.14	0.18
MgO	6.11	6.68	8.32	9.07	9.07	1.63	21.92	6.88	22.26
CaO	10.46	9.90	11.23	12.06	12.40	2.27	8.00	10.56	7.82
Na2O	2.16	3.38	2.84	1.98	2.24	7.07	1.36	3.08	1.62
K2O	0.31	0.19	0.20	0.21	0.15	0.11	0.08	0.71	0.06
P2O5	0.07	0.17	0.08	0.07	0.06	0.54	0.05	0.16	0.05
CO2	6.78	0.15	0.30	0.38	0.61	0.36	0.20	0.30	0.17
LOI	4.75	1.20	1.29	1.52	2.03	1.59	0.35	1.11	0.62
Total									
Sr	152.00	289.00	292.00	253.00	237.00	205.00	196.00	265.00	181.00
Y	10.00	15.00	6.00	5.00	9.00	51.00	2.00	27.00	6.00
Zr	29.00	59.00	12.00	8.00	6.00	273.00	1.00	106.00	0.00
Nb	9.00	7.00	2.00	2.00	4.00	17.00	2.00	1.00	3.00
Ba	-	-	-	-	-	-	-	-	-
Sc	-	-	-	-	-	-	-	-	-
V	-	-	-	-	-	-	-	-	-
Cr	109.00	393.00	227.00	388.00	190.00	-	333.00	379.00	322.00
Co	-	-	-	-	-	-	-	-	-
Ni	20.00	32.00	51.00	51.00	30.00	-	428.00	63.00	341.00
Cu	7.00	17.00	54.00	34.00	32.00	-	74.00	42.00	68.00
Zn	77.00	67.00	43.00	48.00	55.00	-	84.00	85.00	126.00
Ga	-	-	-	-	-	-	-	-	-
As	-	-	-	-	-	-	-	-	-
S	-	-	-	-	-	-	-	-	-
ICPMS									
Li	20.53	8.69	6.47	10.08	8.87	5.30	3.78	9.70	2.16
Sc	-	-	-	-	-	-	-	-	-
Ti	29121.55	18587.06	2308.80	1779.40	2128.01	8660.79	798.20	8151.09	1382.83
V	541.32	341.48	164.85	154.62	215.95	69.34	43.42	202.29	89.60
Cr	82.08	377.47	220.38	362.20	199.04	1.28	318.08	367.17	314.89
Co	35.96	63.52	69.07	54.53	49.32	26.73	105.11	71.16	110.04
Ni	12.38	27.55	43.59	46.96	25.65	2.49	358.62	58.59	293.46
Cu	7.63	18.80	50.64	35.47	35.78	95.76	74.74	46.30	67.55
Zn	73.08	60.43	50.93	46.02	46.96	23.75	66.19	66.49	86.61
Rb	9.23	1.46	2.64	2.92	2.88	3.46	1.12	21.54	0.68
Sr	153.86	304.84	300.13	262.76	246.15	191.87	197.47	274.80	186.29
Y	9.09	15.69	7.50	6.81	10.66	50.77	2.84	29.60	5.11
Zr	17.20	38.57	8.77	6.63	10.72	266.52	6.35	102.10	5.96
Nb	5.99	4.56	0.46	0.14	0.15	15.09	0.22	2.75	0.15
Mo	0.08	0.17	0.12	0.11	0.06	0.26	0.17	0.32	0.22
Sn	0.15	0.49	0.15	0.07	0.11	1.65	0.12	1.42	0.15
Sb	0.56	0.13	0.13	0.11	0.19	0.08	0.01	0.10	0.01
Cs	0.31	0.10	0.12	0.15	0.17	0.82	0.03	1.38	0.05
Ba	56.67	50.09	33.72	35.78	39.75	32.62	24.52	174.81	26.46
La	1.04	7.14	1.90	1.29	1.35	22.91	0.78	8.28	0.55
Ce	2.80	14.94	4.40	3.05	3.61	54.42	1.82	21.05	1.49
Pr	0.50	2.11	0.64	0.47	0.61	7.17	0.26	3.00	0.26
Nd	2.90	9.45	3.19	2.49	3.51	30.70	1.26	14.16	1.48
Sm	1.05	2.40	0.97	0.82	1.27	7.44	0.36	3.93	0.54
Eu	0.40	1.28	0.88	0.79	0.90	1.79	0.31	1.31	0.36
Gd	1.43	2.73	1.21	1.10	1.71	7.95	0.45	4.62	0.75
Tb	0.24	0.43	0.21	0.19	0.30	1.31	0.08	0.77	0.13
Dy	1.59	2.67	1.32	1.18	1.87	8.22	0.49	4.78	0.86
Ho	0.35	0.57	0.28	0.26	0.41	1.83	0.10	1.04	0.19
Er	0.96	1.57	0.76	0.69	1.08	5.16	0.28	2.85	0.52
Tm	-	-	-	-	-	-	-	-	-
Yb	0.88	1.46	0.70	0.61	0.96	5.03	0.27	2.66	0.48
Lu	0.14	0.23	0.11	0.09	0.14	0.76	0.04	0.40	0.07
Hf	0.64	0.98	0.29	0.25	0.38	6.32	0.16	2.53	0.21
Ta	0.53	0.94	0.33	0.27	0.16	1.30	0.61	0.82	0.79
Pb	2.37	3.46	1.32	0.82	0.62	1.47	0.76	3.21	0.42
Th	0.03	0.70	0.16	0.05	0.06	7.09	0.09	1.28	0.02
U	0.01	0.23	0.05	0.02	0.02	1.88	0.02	0.43	0.00

B.2 Reproducibility of ICP-MS and XRF measurements

Table B.5. Reproducibility of ICP-MS trace element analysis of known standards.

BHVO-1	Li	Tl	Rb	Sr	Y	Zr	Nb	Cs	Ba	Hf	Ta	Pb	Th	U
Pref value	4.9	16610	9.5	390.0	26.0	180.0	19.5	0.1	133.0	4.3	1.2	2.1	1.3	0.4
BHVO-1	5.088	16340	9.480	400.876	27.980	180.612	19.533	0.1094	127.15	4.261	1.240	2.030	1.248	0.417
BHVO-1	4.701	16650	9.686	391.2	27.47	178.7	18.970	0.1134	128.10	4.261	1.2	1.929	1.235	0.4214
BHVO-1	4.909	16950	8.976	419.2	29.07	195.7	19.040	0.0875	132.40	4.314	1.191	2.05	1.203	0.4125
Mean	4.899	16647	9.381	403.76	28.173	185.00	19.181	0.103	129.22	4.279	1.210	2.003	1.229	0.417
2 SD	0.387	610	0.731	28.44	1.635	18.62	0.613	0.028	5.594	0.061	0.052	0.130	0.046	0.009
rel 2sd	7.906	3.665	7.788	7.044	5.802	10.067	3.198	26.973	4.329	1.424	4.313	6.477	3.754	2.137
Average/accepted	1.000	1.002	0.987	1.035	1.006	1.028	0.984	1.034	0.972	0.995	1.009	0.954	0.975	0.992
BIR-1														
Pref value	3.4	5755	0.2	110.0	16.5	14.5	0.6	0.0	6.4	0.6	0.1	3.0	0.0	0.0
BIR-1	3.421	5752	0.214	108.935	16.748	14.690	0.546	0.006	6.439	0.553	0.040	3.252	0.030	0.010
BIR-1	3.245	5774	0.231	107.100	15.950	14.880	0.758	0.012	7.945	0.557	0.054	2.960	0.015	0.007
BIR-1	2.924	5381	0.232	101.500	15.560	14.460	0.816	0.006	5.975	0.496	0.058	2.632	0.027	0.009
Mean	3.197	5636	0.226	105.845	16.086	14.743	0.706	0.008	6.786	0.535	0.051	2.948	0.024	0.009
St dev	0.504	442	0.020	7.746	1.211	0.491	0.284	0.007	2.060	0.068	0.019	0.620	0.016	0.003
rel 2sd	15.779	7.837	8.654	7.319	7.530	3.331	40.200	88.601	30.349	12.771	36.793	21.039	67.037	32.465
Average/accepted	0.940	0.979	0.940	0.962	0.975	1.017	1.284	1.601	1.060	0.956	0.844	0.983	0.795	0.896
JB-2														
Pref value	8.0	7132	6.2	178.0	26.0	52.0	0.8	0.9	208.0	1.4	0.2	5.4	0.3	0.2
JB-2	8.719	6875	6.343	176.929	24.852	49.128	0.503	0.903	209.214	1.412	0.042	5.329	0.257	0.159
JB-2	8.236	7019	6.718	180.000	25.200	50.480	0.671	0.911	213.800	1.433	0.044	4.452	0.246	0.153
JB-2	8.479	7299	6.066	187.500	26.190	51.840	0.522	0.729	215.400	1.427	0.042	4.963	0.250	0.146
Mean	8.478	7064	6.376	181.476	25.414	50.483	0.565	0.848	212.805	1.424	0.043	4.915	0.251	0.153
St dev	0.483	431	0.654	10.876	1.388	2.712	0.184	0.206	6.421	0.022	0.003	0.881	0.011	0.013
rel 2sd	5.692	6.104	10.265	5.993	5.462	5.372	32.494	24.282	3.018	1.542	6.925	17.926	4.439	8.196
Average/accepted	1.060	0.991	1.028	1.020	0.977	0.971	0.707	0.942	1.023	1.017	0.213	0.910	0.760	0.954

BHVO-1	La	Ce	Pr	Nd	Sm	Eu	Gd	Tb	Dy	Ho	Er	Yb	Lu
Pref value	15.5	38.0	5.5	24.7	6.2	2.1	6.2	1.0	5.3	1.0	2.6	2.0	0.3
BHVO-1	15.42	35.93	5.177	23.767	6.066	2.041	6.424	0.966	5.036	0.953	2.463	1.882	0.279
BHVO-1	15.46	38.44	5.442	25.07	6.226	2.062	6.316	0.944	5.189	1	2.507	1.99	0.2833
BHVO-1	15.66	38.03	5.61	25.55	6.271	2.119	6.474	1.021	5.435	0.9956	2.457	1.984	0.2849
Mean	15.513	37.47	5.410	24.796	6.188	2.074	6.405	0.977	5.220	0.983	2.476	1.952	0.282
2 SD	0.257	2.693	0.437	1.846	0.216	0.081	0.162	0.079	0.403	0.052	0.055	0.121	0.006
rel 2sd	1.658	7.188	8.071	7.443	3.492	3.898	2.522	8.093	7.712	5.297	2.208	6.220	2.076
Average/accepted	1.001	0.986	0.993	1.004	1.003	1.007	1.030	1.029	0.994	0.983	0.967	0.986	1.016
BIR-1													
Pref value	0.6	1.9	0.4	2.4	1.1	0.5	2.0	0.4	2.5	0.6	1.7	1.6	0.3
BIR-1	0.623	1.884	0.372	2.405	1.143	0.540	1.954	0.382	2.538	0.576	1.733	1.632	0.268
BIR-1	0.527	1.601	0.346	2.253	1.060	0.516	1.843	0.363	2.470	0.569	1.675	1.621	0.250
BIR-1	0.543	1.657	0.341	2.231	0.994	0.476	1.709	0.351	2.327	0.513	1.476	1.487	0.230
Mean	0.564	1.714	0.353	2.296	1.065	0.510	1.835	0.365	2.445	0.553	1.628	1.580	0.249
St dev	0.102	0.300	0.033	0.189	0.149	0.065	0.245	0.031	0.216	0.069	0.269	0.162	0.038
rel 2sd	18.122	17.487	9.353	8.252	13.994	12.700	13.344	8.526	8.818	12.450	16.545	10.224	15.442
Average/accepted	0.973	0.926	0.954	0.977	0.969	0.982	0.932	0.961	0.978	0.970	0.958	0.988	0.997
JB-2													
Pref value	2.4	6.5	1.2	6.5	2.3	0.9	3.3	0.6	3.9	0.8	2.4	2.5	0.4
JB-2	2.311	6.430	1.124	6.188	2.353	0.833	3.361	0.598	3.857	0.865	2.523	2.472	0.412
JB-2	2.202	6.402	1.147	6.343	2.294	0.834	3.231	0.591	3.905	0.885	2.567	2.531	0.396
JB-2	2.244	6.343	1.172	6.440	2.254	0.839	3.252	0.615	3.952	0.852	2.472	2.429	0.391
Mean	2.252	6.392	1.148	6.324	2.300	0.835	3.281	0.601	3.905	0.867	2.521	2.477	0.400
St dev	0.110	0.089	0.048	0.254	0.099	0.006	0.140	0.025	0.095	0.033	0.095	0.102	0.022
rel 2sd	4.882	1.390	4.184	4.014	4.307	0.755	4.254	4.136	2.428	3.810	3.772	4.133	5.622
Average/accepted	0.938	0.983	0.956	0.973	1.000	0.982	0.994	0.970	1.014	1.045	1.050	0.991	0.999

Table B.6. Reproducibility of trace element abundance analysis of gabbros, gabbroic eclogites and basaltic eclogites (ICP-MS).

Sample duplicates

	Gabbro					Relative	Transitional					Relative
	S02/10iiixG	dupl.	dupl.	Mean	2 SD	2 SD (%)	S01H/5a	duplicate	duplicate	Mean	2 SD	2 SD (%)
ICPMS												
Li	0.35	0.41	0.28	0.35	0.1	37.2	2.05	2.28	1.82	2.05	0.5	22.8
Sc	1.80						7.05					
Ti	748.3	722.8	728.0	733.0	27.0	3.7	930.2	932.6	919.0	927.2	14.5	1.6
V	8.41	8.21	8.11	8.24	0.3	3.8	24.59	24.19	24.16	24.31	0.5	2.0
Cr	8.29	7.99	6.77	7.68	1.6	20.9	130.20	118.85	125.56	124.87	11.4	9.1
Co	30.16	29.48	27.12	28.92	3.2	11.0	50.95	50.03	49.08	50.02	1.9	3.7
Ni	194.81	199.99	173.82	189.54	27.7	14.6	444.88	442.73	397.57	428.40	53.4	12.5
Cu	28.21	29.95	27.74	28.63	2.3	8.2	103.82	98.42	92.16	98.13	11.7	11.9
Zn	23.74	24.30	24.27	24.10	0.6	2.6	32.71	32.41	33.90	33.00	1.6	4.8
Rb	0.10	0.10	0.08	0.09	0.0	19.5	0.20	0.19	0.19	0.19	0.0	3.3
Sr	414.0	400.4	379.5	398.0	34.7	8.7	280.7	273.7	259.3	271.2	21.8	8.0
Y	0.91	0.89	0.85	0.88	0.1	7.6	2.25	2.01	2.10	2.12	0.2	11.7
Zr	1.96	1.81	1.82	1.86	0.2	9.2	4.23	5.68	3.60	4.50	2.1	47.4
Nb	0.11	0.11	0.11	0.11	0.0	4.8	0.19	0.19	0.18	0.19	0.0	8.5
Mo	0.04	0.05	0.00	0.03	0.1	190.1	0.09	0.10	0.01	0.07	0.1	148.4
Sn	0.10	0.13	0.12	0.12	0.0	23.1	0.18	0.19	0.19	0.18	0.0	19.1
Sb	0.01	0.01	0.00	0.01	0.0	104.4	0.01	0.01	0.01	0.01	0.0	35.0
Cs	0.00	0.00	0.00	0.00	0.0	78.6	0.01	0.01	0.01	0.01	0.0	29.2
Ba	8.16	8.11	7.23	7.83	1.0	13.4	8.49	7.98	7.78	8.09	0.7	9.1
La	0.87	0.90	0.84	0.87	0.1	6.8	0.69	0.68	0.68	0.68	0.0	5.6
Ce	1.82	1.85	1.84	1.84	0.0	1.5	1.61	1.57	1.62	1.60	0.1	3.6
Pr	0.25	0.24	0.23	0.24	0.0	6.0	0.24	0.22	0.23	0.23	0.0	8.2
Nd	1.04	1.00	0.96	1.00	0.1	7.9	1.11	1.03	1.06	1.07	0.1	7.6
Sm	0.21	0.21	0.19	0.20	0.0	11.0	0.30	0.29	0.29	0.29	0.0	4.5
Eu	0.46	0.46	0.44	0.45	0.0	5.0	0.37	0.36	0.35	0.36	0.0	6.0
Gd	0.20	0.21	0.19	0.20	0.0	8.4	0.37	0.37	0.35	0.36	0.0	4.2
Tb	0.03	0.03	0.03	0.03	0.0	11.1	0.06	0.06	0.06	0.06	0.0	7.7
Dy	0.16	0.15	0.16	0.15	0.0	4.9	0.37	0.35	0.37	0.36	0.0	7.2
Ho	0.03	0.03	0.03	0.03	0.0	4.4	0.08	0.07	0.08	0.08	0.0	2.4
Er	0.08	0.08	0.08	0.08	0.0	7.0	0.21	0.21	0.21	0.21	0.0	2.8
Tm												
Yb	0.08	0.08	0.08	0.08	0.0	3.9	0.21	0.21	0.20	0.21	0.0	3.6
Lu	0.01	0.01	0.02	0.01	0.0	9.3	0.03	0.03	0.03	0.03	0.0	4.9
Hf	0.04	0.04	0.04	0.04	0.0	4.8	0.10	0.15	0.11	0.12	0.0	39.3
Ta	0.01	0.01	0.01	0.01	0.0	19.5	0.01	0.02	0.01	0.01	0.0	23.5
Pb	0.33	0.33	0.30	0.32	0.0	12.6	0.48	0.49	0.40	0.46	0.1	21.6
Th	0.01	0.01	0.01	0.01	0.0	7.7	0.01	0.01	0.01	0.01	0.0	44.1
U	0.002	0.002	0.002	0.002	0.0	41.8	0.004	0.004	0.004	0.004	0.0	12.0
Y/Ho	30.58	29.30	29.28	29.72	1.5	5.0	29.59	27.00	27.87	28.16	2.6	9.4

	Transitional				Relative	Coronite				Relative
	S02/10iiixE	duplicate	Mean	2 SD	2 SD (%)	S01/40viix	duplicate	Mean	2 SD	2 SD (%)
ICPMS										
Li	1.81	1.97	1.89	0.2	11.6	0.95	1.06	1.01	0.2	15.7
Sc	1.07					11.04	1.02	6.03	14.2	235.2
Ti	831.0	866.8	848.9	50.6	6.0	868.5	862.4	865.4	8.6	1.0
V	16.37	17.04	16.70	0.9	5.6	43.32	41.98	42.65	1.9	4.5
Cr	45.11	41.92	43.51	4.5	10.4	816.85	703.55	760.20	160.2	21.1
Co	38.49	36.77	37.63	2.4	6.4	37.31	34.75	36.03	3.6	10.1
Ni	263.29	258.53	260.91	6.7	2.6	349.39	347.02	348.20	3.3	1.0
Cu	34.18	36.52	35.35	3.3	9.3	44.02	41.44	42.73	3.6	8.5
Zn	30.57	28.74	29.65	2.6	8.7	20.93	20.03	20.48	1.3	6.2
Rb	0.16	0.16	0.16	0.0	1.1	0.21	0.23	0.22	0.0	14.8
Sr	341.3	356.4	348.9	21.3	6.1	369.1	363.9	366.5	7.3	2.0
Y	1.60	1.61	1.60	0.0	0.7	2.82	2.66	2.74	0.2	8.1
Zr	2.26	4.96	3.61	3.8	105.5	2.17	5.62	3.89	4.9	125.4
Nb	0.19	0.20	0.19	0.0	7.5	0.09	0.09	0.09	0.0	2.1
Mo	0.09	0.21	0.15	0.2	111.9	0.06	0.30	0.18	0.3	182.0
Sn	0.12	0.12	0.12	0.0	5.2	0.10	0.12	0.11	0.0	15.9
Sb	0.01	0.01	0.01	0.0	11.4	0.00	0.02	0.01	0.0	188.6
Cs	0.01	0.01	0.01	0.0	6.6	0.01	0.01	0.01	0.0	41.8
Ba	6.67	6.61	6.64	0.1	1.2	7.87	7.68	7.78	0.3	3.6
La	0.84	0.82	0.83	0.0	4.6	0.55	0.55	0.55	0.0	0.2
Ce	1.84	1.91	1.88	0.1	5.1	1.32	1.35	1.33	0.0	2.6
Pr	0.25	0.25	0.25	0.0	2.8	0.21	0.21	0.21	0.0	5.4
Nd	1.10	1.12	1.11	0.0	3.7	1.06	1.04	1.05	0.0	3.0
Sm	0.27	0.28	0.27	0.0	4.7	0.33	0.33	0.33	0.0	1.7
Eu	0.42	0.43	0.42	0.0	2.5	0.33	0.34	0.34	0.0	2.2
Gd	0.30	0.31	0.31	0.0	6.1	0.43	0.45	0.44	0.0	6.6
Tb	0.05	0.05	0.05	0.0	4.6	0.08	0.08	0.08	0.0	3.0
Dy	0.26	0.27	0.26	0.0	6.8	0.46	0.45	0.46	0.0	2.9
Ho	0.05	0.06	0.06	0.0	6.2	0.10	0.10	0.10	0.0	3.0
Er	0.15	0.16	0.16	0.0	7.6	0.25	0.27	0.26	0.0	8.3
Tm										
Yb	0.15	0.16	0.16	0.0	7.3	0.23	0.24	0.23	0.0	6.5
Lu	0.03	0.03	0.03	0.0	9.4	0.04	0.04	0.04	0.0	7.8
Hf	0.06	0.11	0.09	0.1	92.1	0.07	0.16	0.11	0.1	104.5
Ta	0.01	0.02	0.02	0.0	43.9	0.01	0.09	0.05	0.1	239.1
Pb	0.16	0.17	0.17	0.0	9.7	0.22	0.23	0.23	0.0	7.4
Th	0.01	0.01	0.01	0.0	2.2	0.01	0.01	0.01	0.0	15.9
U	0.005	0.006	0.006	0.0	18.4	0.009	0.010	0.010	0.0	10.7
Y/Ho	29.54	28.42	28.98	1.6	5.5	28.31	27.31	27.81	1.4	5.1

Table B.6 contd. Reproducibility of trace element abundance analysis of gabbros, gabbroic eclogites and basaltic eclogites (ICP-MS).

	Pillow S02/75iiiC	duplicate	Mean	2 SD	Relative 2 SD (%)	Pillow S02/75iiiR	duplicate	Mean	2 SD	Relative 2 SD (%)
ICPMS										
Li	17.24	20.96	19.10	5.3	27.6	18.00	21.40	19.70	4.8	24.4
Sc	27.68	12.29	19.99	21.8	108.9	26.59	13.05	19.82	19.1	96.6
Ti	13570	12850	13210	1018.8	7.7	12795	11485	12140	1852.4	15.3
V	249.61	236.05	242.83	19.2	7.9	231.62	208.45	220.03	32.8	14.9
Cr	135.80	123.60	129.70	17.3	13.3	128.90	114.60	121.75	20.2	16.6
Co	29.33	27.32	28.32	2.9	10.1	35.22	32.22	33.72	4.2	12.5
Ni	71.47	73.14	72.30	2.4	3.3	92.73	88.91	90.82	5.4	5.9
Cu	50.68	48.92	49.80	2.5	5.0	43.12	42.00	42.56	1.6	3.7
Zn	76.49	75.48	75.98	1.4	1.9	96.99	96.12	96.56	1.2	1.3
Rb	2.14	2.28	2.21	0.2	8.8	3.40	3.56	3.48	0.2	6.6
Sr	202.3	200.8	201.5	2.1	1.0	171.3	164.8	168.1	9.3	5.5
Y	54.51	53.70	54.11	1.2	2.1	46.80	44.36	45.58	3.5	7.6
Zr	17.01	280.51	148.76	372.6	250.5	23.82	249.80	136.81	319.6	233.6
Nb	8.05	8.14	8.09	0.1	1.6	7.70	7.38	7.54	0.4	5.9
Mo	0.22	0.31	0.26	0.1	52.1	0.22	0.34	0.28	0.2	63.1
Sn	2.44	2.81	2.63	0.5	20.3	2.19	2.40	2.29	0.3	13.1
Sb	0.06	0.05	0.05	0.0	30.9	0.06	0.05	0.06	0.0	20.9
Cs	0.10	0.12	0.11	0.0	36.5	0.54	0.67	0.60	0.2	31.0
Ba	12.71	12.76	12.73	0.1	0.6	14.89	14.48	14.69	0.6	4.0
La	10.55	10.69	10.62	0.2	1.7	7.84	8.05	7.95	0.3	3.8
Ce	30.02	29.80	29.91	0.3	1.1	22.65	23.27	22.96	0.9	3.8
Pr	4.85	4.60	4.73	0.3	7.3	3.71	3.59	3.65	0.2	4.7
Nd	22.55	22.28	22.41	0.4	1.7	17.59	17.28	17.43	0.4	2.5
Sm	6.55	6.59	6.57	0.1	1.0	4.92	5.06	4.99	0.2	4.1
Eu	2.07	2.08	2.08	0.0	0.9	1.57	1.60	1.58	0.0	2.5
Gd	7.80	8.23	8.01	0.6	7.5	6.21	6.53	6.37	0.5	7.1
Tb	1.35	1.36	1.36	0.0	0.7	1.21	1.20	1.20	0.0	0.5
Dy	8.04	8.12	8.08	0.1	1.4	7.27	7.33	7.30	0.1	1.0
Ho	1.75	1.81	1.78	0.1	4.8	1.49	1.53	1.51	0.1	3.6
Er	4.91	5.28	5.10	0.5	10.2	3.97	4.23	4.10	0.4	9.1
Tm										
Yb	4.60	4.92	4.76	0.4	9.4	3.50	3.82	3.66	0.5	12.5
Lu	0.69	0.78	0.73	0.1	17.8	0.53	0.60	0.57	0.1	18.7
Hf	0.85	5.44	3.14	6.5	206.6	0.62	4.91	2.76	6.1	219.5
Ta	0.50	0.65	0.58	0.2	36.5	0.47	0.49	0.48	0.0	4.4
Pb	1.38	1.28	1.33	0.1	11.0	1.25	1.16	1.20	0.1	10.8
Th	0.48	0.48	0.48	0.0	0.2	0.41	0.42	0.42	0.0	2.7
U	0.23	0.25	0.24	0.0	15.6	0.16	0.19	0.18	0.0	19.5
Y/Ho	31.09	29.59	30.34	2.1	7.0	31.35	28.96	30.16	3.4	11.2

Table B.6 contd. Reproducibility of trace element abundance analysis of gabbros, gabbroic eclogites and basaltic eclogites (ICP-MS).

	SO gabbro				Relative
	B137	duplicate	Mean	2 SD	2 SD (%)
ICPMS					
Li	1.96	1.07	1.51	1.3	83.4
Sc					
Ti	4003	3963	3983	57.4	1.4
V	176.68	185.64	181.16	12.7	7.0
Cr	302.48	276.90	289.69	36.2	12.5
Co	39.19	49.12	44.15	14.1	31.8
Ni	53.64	61.95	57.79	11.8	20.3
Cu	3.08	4.25	3.66	1.7	45.3
Zn	22.99	43.18	33.09	28.6	86.3
Rb	0.50	1.14	0.82	0.9	111.4
Sr	289.9	247.2	268.6	60.4	22.5
Y	14.36	21.36	17.86	9.9	55.4
Zr	16.06	21.47	18.76	7.7	40.8
Nb	0.93	0.84	0.88	0.1	15.8
Mo	0.13	0.07	0.10	0.1	79.1
Sn	0.54	1.91	1.22	1.9	158.1
Sb	0.04	0.08	0.06	0.1	87.2
Cs	0.03	0.05	0.04	0.0	65.8
Ba	77.62	29.16	53.39	68.5	128.4
La	2.84	9.46	6.15	9.4	152.1
Ce	6.53	19.94	13.24	19.0	143.4
Pr	0.97	2.54	1.76	2.2	126.0
Nd	4.94	11.59	8.27	9.4	113.8
Sm	1.62	3.06	2.34	2.0	86.9
Eu	0.86	1.27	1.06	0.6	54.3
Gd	2.17	3.68	2.93	2.1	72.7
Tb	0.38	0.59	0.48	0.3	60.5
Dy	2.42	3.55	2.98	1.6	53.3
Ho	0.53	0.76	0.64	0.3	49.9
Er	1.42	2.03	1.73	0.9	49.9
Tm					
Yb	1.25	1.69	1.47	0.6	41.9
Lu	0.19	0.25	0.22	0.1	36.6
Hf	0.58	0.71	0.64	0.2	29.1
Ta	0.38	0.26	0.32	0.2	51.6
Pb	1.29	1.18	1.23	0.2	13.1
Th	0.68	0.76	0.72	0.1	16.4
U	0.28	0.22	0.25	0.1	33.5
Y/Ho	27.09	28.21	27.65	1.6	5.8

Table B.7. Reproducibility of major element abundances for XRF standards WS-E and OUG94.

All values in wt. %	SiO2	TiO2	Al2O3	Fe2O3	MnO	MgO	CaO	Na2O	K2O	P2O5	Total
WS-E	51.08	2.40	13.86	13.11	0.17	5.57	8.95	2.44	1.00	0.30	99.72
WS-E	51.05	2.40	13.85	13.12	0.17	5.57	8.96	2.44	1.00	0.30	99.71
WS-E	51.13	2.41	13.97	13.16	0.17	5.68	9.05	2.50	1.00	0.31	100.23
WS-E	51.12	2.42	13.92	13.15	0.17	5.65	9.00	2.49	1.00	0.31	100.08
WS-E	51.22	2.41	13.89	13.17	0.17	5.70	9.03	2.50	0.99	0.31	100.25
WS-E	51.19	2.42	13.95	13.15	0.17	5.68	9.03	2.47	1.00	0.31	100.22
WS-E	51.21	2.44	13.91	13.19	0.17	5.60	9.02	2.46	1.00	0.30	100.18
WS-E	51.11	2.42	13.92	13.20	0.17	5.61	9.00	2.49	1.00	0.31	100.06
Average	51.14	2.42	13.91	13.16	0.17	5.63	9.01	2.47	1.00	0.31	100.06
2 SD	0.13	0.03	0.08	0.06	0.00	0.11	0.07	0.05	0.01	0.01	0.44
% 2 SD	0.25	1.18	0.57	0.48	2.67	1.89	0.76	2.14	0.71	1.77	0.44
Recommended	51.10	2.40	13.78	13.15	0.17	5.55	8.95	2.47	1.00	0.30	99.72
Average/recomm.	1.001	1.007	1.009	1.000	0.998	1.015	1.006	1.001	0.999	1.011	1.003
OUG94	69.65	0.32	14.52	3.05	0.08	1.04	1.37	4.59	2.98	0.17	99.73
OUG94	69.66	0.32	14.56	3.05	0.08	1.04	1.36	4.55	2.96	0.16	99.73
OUG94	69.53	0.31	14.56	3.04	0.08	1.05	1.36	4.65	2.97	0.17	99.69
OUG94	69.50	0.32	14.61	3.04	0.08	1.03	1.35	4.69	2.97	0.16	99.72
OUG94	69.78	0.32	14.59	3.04	0.08	1.05	1.37	4.71	2.97	0.17	100.03
OUG94	69.66	0.31	14.60	3.05	0.07	1.06	1.36	4.68	2.96	0.17	99.89
OUG94	69.91	0.32	14.63	3.05	0.08	1.07	1.35	4.69	3.00	0.17	100.23
OUG94	69.82	0.32	14.62	3.06	0.08	1.05	1.35	4.66	3.00	0.16	100.08
Average	69.69	0.32	14.59	3.05	0.08	1.05	1.36	4.65	2.98	0.17	99.89
SD	0.14	0.00	0.04	0.01	0.00	0.01	0.01	0.06	0.02	0.00	0.21
% SD	0.20	1.23	0.24	0.23	2.05	1.06	0.57	1.23	0.50	1.50	0.21
Recommended	69.95	0.31	14.66	3.05	0.08	1.04	1.34	4.60	2.96	0.17	100.12
Average/recomm.	0.996	1.011	0.995	0.999	1.026	1.008	1.014	1.011	1.005	1.006	0.998

Table B.8. Reproducibility of trace element abundances determined for XRF standards

	Rb	Sr	Y	Zr	Nb	Ba	Pb	Th	U	Cr	Co	Ni	Cu	Zn	S
Expected	11	403	28	179	19	139	3	1	0	289	45	121	136	105	102
BHVO-1	10	403	29	178	18	146	1	5	2	290	46	119	139	109	172
BHVO-1	9	406	28	178	19	152	2	1	0	290	43	122	140	109	179
BHVO-1	10	403	28	174	20	139	3	3	2	293	38	120	136	108	170
BHVO-1	10	402	29	177	19	145	3	3	1	293	37	122	138	107	173
BHVO-1	9	407	29	179	19	149	6	0	0	289	47	122	139	108	178
BHVO-1	10	405	29	179	20	151	4	0	0	291	48	118	139	110	174
BHVO-1	9	407	29	179	19	149	6	0	0	289	47	122	139	108	178
BHVO-1	10	405	29	179	20	151	4	0	0	291	48	118	139	110	174
Mean	10	405	29	178	19	147	4	2	1	291	44	120	139	109	175
2 SD	0.9	4.2	0.6	3.2	1.6	8.6	3.7	4.2	1.7	3.2	8.7	3.7	2.2	1.8	6.5
Relative 2 SD	8.0	1.0	2.3	1.8	8.6	6.2	141.4	384.9	414.9	1.1	19.3	3.0	1.6	1.7	6.3
Average/expected	0.875	1.004	1.036	0.993	1.008	1.060	1.466	1.412	1.845	1.007	0.986	0.994	1.020	1.033	1.712
Expected	74	336	24	185	10	1370	20	5	2	3	7	6	29	61	30
QLO-1	74	332	25	189	10	1366	20	5	2	5	9	6	29	61	83
QLO-1	75	335	25	190	11	1376	19	6	1	4	11	6	29	61	86
QLO-1	74	334	25	192	10	1358	19	4	2	5	15	6	27	60	86
QLO-1	74	336	24	192	11	1374	19	4	0	5	14	5	28	61	86
QLO-1	74	334	25	192	10	1358	19	4	2	5	15	6	27	60	86
QLO-1	74	336	24	192	11	1374	19	4	0	5	14	5	28	61	86
QLO-1	74	334	25	191	11	1390	18	5	1	5	12	6	30	60	90
QLO-1	75	338	26	193	11	1392	18	4	3	5	14	4	29	60	87
Mean	74	335	25	191	11	1373	19	4	1	5	13	5	28	61	86
2 SD	0.9	3.6	1.3	2.3	0.9	25.4	1.5	1.5	1.9	0.8	4.0	1.1	1.8	1.4	3.7
Relative 2 SD	1.2	1.1	5.3	1.2	9.0	1.9	7.4	33.7	99.2	26.3	55.6	18.9	6.2	2.3	12.3
Average/expected	1.002	0.996	1.043	1.035	1.040	1.003	0.909	0.994	0.689	1.516	1.818	0.914	0.981	0.993	2.874
Expected	5	145	18	41	3	114	6	0	0	285	55	247	96	66	392
DNC-1	4	148	19	41	3	111	10	1	3	279	58	247	95	67	426
DNC-1	5	147	18	41	3	106	8	3	1	274	57	250	94	68	422
DNC-1	4	146	19	41	3	109	7	2	1	275	49	248	96	67	422
DNC-1	4	148	19	42	3	110	6	1	1	276	50	253	97	69	424
DNC-1	4	148	19	41	3	111	11	0	1	272	58	249	94	70	427
DNC-1	4	148	19	41	2	110	10	2	0	276	57	250	93	69	421
DNC-1	4	148	19	41	3	111	11	0	1	272	58	249	94	70	427
DNC-1	4	148	19	41	2	110	10	2	0	276	57	250	93	69	421
Mean	4	148	19	41	3	110	9	1	1	275	55	249	95	68	424
2 SD	0.8	1.9	0.7	0.5	1.0	3.3	3.5	1.9	1.9	4.4	7.4	3.8	3.1	2.3	4.7
Relative 2 SD	18.8	1.3	4.0	1.2	32.7	2.9	55.9	950.1	1913.7	1.6	13.5	1.5	3.2	3.4	1.2
Average/expected	0.914	1.018	1.053	1.005	0.917	0.961	1.433	6.688	11.125	0.966	1.012	1.010	0.985	1.038	1.081
Expected	20	194	24	94	8	182	9	2	1	93	44	70	103	77	79
W-2	20	200	23	95	8	189	8	4	0	99	44	69	104	79	221
W-2	21	201	23	93	8	182	10	4	1	97	47	71	105	80	228
W-2	20	200	23	94	8	180	6	2	0	97	45	70	106	81	227
W-2	20	201	23	95	8	173	9	2	0	94	44	70	104	81	233
W-2	20	200	23	94	8	180	6	2	0	97	45	70	106	81	227
W-2	20	201	23	95	8	173	9	2	0	94	44	70	104	81	233
W-2	20	198	23	93	7	182	9	2	2	96	39	66	105	81	212
W-2	21	199	23	94	8	173	8	1	1	95	40	71	105	79	217
Mean	20	200	23	94	8	179	8	2	0	96	44	70	105	81	225
2 SD	0.6	1.9	0.4	2.0	0.6	11.4	2.5	2.2	1.6	3.9	5.8	3.0	1.7	2.0	15.0
Relative 2 SD	3.0	1.0	1.5	2.1	7.6	6.2	27.4	98.6	306.4	4.2	13.1	4.3	1.7	2.6	19.0
Average/expected	1.016	1.030	0.959	1.003	0.997	0.983	0.843	1.063	0.802	1.033	0.989	0.994	1.018	1.046	2.843

C Appendix C

Trace (LA-ICP-MS) and major elements (electron microprobe) in silicate phases and PGE in sulphides (LA-ICP-MS)

C.1 Silicate phase trace element data (LA-ICP-MS)

N.B. Significant figures:

Major element data determined by electron microprobe are accurate to 2 decimal places. In general, trace element LA-ICP-MS data are known to 3 significant figures.

Table C.1. Trace and major element concentrations in silicates from sample S01/39iiix – determined by LA-ICP-MS and electron microprobe respectively. *bulk rock majors analysed by XRF.

Concentrations

All values in ppm	S01/39iiix									
	*Bulk rock**	*Olivine*			*Plagioclase*		*Augite*			
Element		OL1	OL2	OL3	PL1	PL2	PX1	PX2	PX3	PX4
Li	0.966	0.992	0.644	0.812	<0.0165	0.105	0.182	0.165	0.225	0.164
Be	8.356	0.021	<0.024	<0.026	0.098	0.124	0.05	0.068	0.052	0.09
B		1.35	17.6	1.38	0.836	0.647	1.42	1.14	1	2.52
Mg		367477	359911.5	359153.9	615.86	394.66	131738.6	136108.2	132264.9	130492.5
Si		186508.3	186508.3	186508.3	229045.3	229045.3	239796.4	239796.4	239796.4	239796.3
P		47.91	45.8	46.65	37.89	33.15	46.16	40.77	41.02	51.35
K	249.042	5.25	14.67	6.12	17.62	495.15	23.1	4.92	14.14	27.06
Ca		98.57	311.88	623.88	165984.8	79366.38	162016.1	156755.6	157299.8	165598.1
Sc		3.01	4.58	3.1	0.573	0.934	113.92	107.65	109.03	117.53
Ti	724.544	51.22	48.03	67.23	79.75	277.65	5628.23	3980.84	4161.16	6485.47
V	28.649	0.554	1.234	8.16	0.395	3.65	326.41	288.4	304.87	319.04
Cr	400.280	7.5	12.97	15.23	0.8	0.36	6707.05	7529.97	8041.15	9444.62
Ni	385.938	1325.85	1497.18	1396.43	0.945	2.86	203.45	219.53	235.3	208.68
Cu	52.034	0.453	0.205	5.14	0.231	8.88	4.3	0.449	15.97	1.282
Zn	25.458	90.57	106.13	69.48	1.501	3.78	19.89	18.59	20.52	23.15
Rb	0.150	0.0083	0.0257	0.0154	0.0259	0.1341	0.0343	0.0153	0.0173	0.192
Sr	317.426	1.299	0.209	0.93	389.63	399.08	22	19.44	19.1	20.77
Y	2.147	0.0215	0.0293	0.0531	0.0949	0.222	19.57	13.2	14.21	23.08
Zr	6.500	0.0517	0.0945	0.1035	0.0231	0.115	39.39	13.98	15.7	54.25
Nb	0.135	0.0154	0.0086	0.0171	<0.00085	0.0136	0.588	0.246	0.641	0.828
Mo	0.067	0.285	0.338	0.281	0.0427	0.0067	0.18	0.15	0.184	0.193
Cs	0.021	0.01	0.00108	0.00234	0.00488	0.0385	0.00863	<0.00043	0.00115	0.03
Ba	5.000	2.92	0.289	0.432	3.07	8.01	3.36	0.124	0.1056	1.54
La	0.519	0.00308	0.00085	0.00747	0.709	0.234	0.663	0.381	0.58	0.844
Ce	1.240	0.0089	0.00569	0.0244	1.487	0.567	3.22	1.84	2.58	4.38
Pr	0.193	0.00142	0.00122	0.00356	0.1418	0.0719	0.719	0.42	0.533	0.991
Nd	0.919	0.0033	0.0035	0.016	0.49	0.311	4.84	2.96	3.42	6.36
Sm	0.268	0.005	0.0048	0.0073	0.0666	0.0729	2.03	1.325	1.42	2.52
Eu	0.312	0.00173	0.0008	0.00167	0.338	0.285	0.629	0.5	0.535	0.764
Gd	0.334	0.0056	<0.0034	0.0095	0.0431	0.0664	3.01	2.02	2.15	3.6
Tb	0.061	<0.00038	<0.00044	<0.00052	0.00424	0.008	0.516	0.358	0.387	0.618
Dy	0.347	0.0056	<0.0019	0.0167	0.0241	0.0404	3.77	2.64	2.65	4.47
Ho	0.073	0.00125	0.00158	0.00197	0.00453	0.0096	0.775	0.528	0.537	0.89
Er	0.197	0.002	0.0059	0.0097	0.0074	0.0244	2.18	1.49	1.56	2.6
Yb	0.181	0.0123	0.0154	0.0149	0.0039	0.012	1.99	1.33	1.45	2.42
Lu	0.028	0.00378	0.00408	0.00226	0.0018	0.0033	0.279	0.184	0.206	0.332
Hf	0.118	0.0044	<0.0016	0.0021	0.0022	0.0042	1.107	0.618	0.611	1.084
Ta	0.010	0.00108	<0.00050	0.00072	<0.00051	0.00055	0.047	0.00285	0.0194	0.0917
Re		<0.00042	<0.00042	<0.00044	<0.00043	<0.00048	<0.00036	<0.00038	<0.00038	<0.00040
Pb	0.285	0.641	0.0236	0.39	0.263	0.1439	0.1007	0.0254	0.0262	0.061
Th	0.009	0.00089	0.0009	0.00139	<0.00062	<0.00061	0.0429	0.0211	0.0548	0.0789
U	0.006	<0.00033	0.00041	0.00098	0.00039	<0.00052	0.019	0.0149	0.0241	0.0302
***Majors** (electron microprobe)*										
weight %										
SiO2	48.02	40.277	40.183	39.943	48.038	47.593	51.039	51.083	51.479	51.773
TiO2	0.114	0.018	0.008	0	0.063	0.078	1.203	0.701	0.643	0.583
Al2O3	22.71	0	0	0	31.65	29.582	4.376	4.103	4.03	3.878
Cr2O3		0	0	0	0	0	1.107	1.302	1.132	1.036
MgO	10.29	45.564	44.993	45.161	0	0.126	15.397	15.347	15.146	16.925
CaO	10.96	0.061	0	0.021	16.404	17.587	21.699	21.773	22.666	20.441
MnO	0.07	0.155	0.205	0.159	0.014	0	0.141	0.141	0.13	0.121
FeO	3.78	13.86	14.647	14.324	0.499	0.495	4.897	4.548	4.283	4.726
Na2O	2.95	0.004	0	0.008	1.784	3.35	0.016	0.024	0.026	0.037
K2O	0.06				0.028	0.01	0.554	0.593	0.571	0.505
Total	-	100.133	100.233	99.851	98.537	98.825	100.429	99.615	100.106	100.025

Table C.2. Analytical errors (1 sigma) for LA-ICP-MS determination of trace elements in silicates from sample S01/39iiix. Errors calculated by GLITTER.

1 sigma error

	S01/39iiix								
	Olivine			*Plagioclase*		*Augite*			
Element	OL1	OL2	OL3	PL1	PL2	PX1	PX2	PX3	PX4
Li	0.041	0.027	0.034	0.0095	0.014	0.012	0.012	0.014	0.012
Be	0.016	0.012	0.015	0.021	0.026	0.016	0.016	0.016	0.018
B	0.13	1.39	0.13	0.086	0.082	0.13	0.11	0.1	0.24
Mg	20946.87	20820.62	21085.4	36.72	23.9	8082.18	8472.84	8353.96	8361.95
Si	5898.45	5898.25	5898.32	7243.44	7243.6	7583.37	7583.37	7583.39	7583.38
P	5.65	5.5	5.7	4.72	4.21	5.96	5.36	5.48	6.98
K	0.28	0.76	0.33	0.94	26.66	1.26	0.28	0.79	1.53
Ca	5.88	15.13	29.82	7744.71	3740.86	7710.42	7533.91	7634.63	8116.21
Sc	0.16	0.25	0.17	0.033	0.055	6.5	6.21	6.37	6.95
Ti	2.21	2.08	2.93	3.5	12.25	249.77	178.23	187.96	295.51
V	0.026	0.056	0.37	0.019	0.17	15.02	13.39	14.29	15.1
Cr	0.36	0.58	0.68	0.11	0.13	296.12	335.68	361.95	429.26
Ni	62.04	70.85	66.83	0.052	0.15	10.08	11	11.92	10.69
Cu	0.02	0.01	0.21	0.011	0.36	0.18	0.02	0.66	0.055
Zn	3.72	4.4	2.91	0.071	0.17	0.86	0.81	0.9	1.02
Rb	0.0014	0.0021	0.0016	0.0022	0.0085	0.0026	0.0015	0.0017	0.012
Sr	0.079	0.013	0.058	24.27	25.16	1.4	1.26	1.25	1.37
Y	0.0024	0.0028	0.0048	0.0083	0.019	1.64	1.12	1.22	2.01
Zr	0.0052	0.0079	0.0089	0.0027	0.01	3.08	1.11	1.26	4.41
Nb	0.0017	0.001	0.0017	0.0005	0.0016	0.038	0.016	0.043	0.055
Mo	0.019	0.022	0.019	0.0041	0.0025	0.013	0.011	0.013	0.014
Cs	0.00099	0.00035	0.00044	0.00062	0.0026	0.00078	0.00027	0.00034	0.002
Ba	0.18	0.021	0.03	0.19	0.5	0.21	0.011	0.0097	0.1
La	0.00063	0.00034	0.00093	0.051	0.017	0.049	0.029	0.044	0.064
Ce	0.001	0.00066	0.0019	0.095	0.037	0.21	0.12	0.17	0.29
Pr	0.00045	0.00033	0.00056	0.0084	0.0046	0.042	0.025	0.032	0.059
Nd	0.0023	0.0018	0.0031	0.035	0.024	0.33	0.21	0.24	0.45
Sm	0.0024	0.0021	0.0026	0.0068	0.0079	0.14	0.094	0.1	0.18
Eu	0.00061	0.00047	0.00061	0.021	0.019	0.04	0.032	0.035	0.05
Gd	0.0025	0.002	0.0026	0.0054	0.0081	0.24	0.16	0.18	0.3
Tb	0.0003	0.00029	0.00034	0.00062	0.001	0.039	0.027	0.03	0.048
Dy	0.0019	0.0011	0.0026	0.0032	0.005	0.31	0.22	0.22	0.38
Ho	0.00042	0.00041	0.00047	0.00065	0.0012	0.06	0.042	0.043	0.072
Er	0.0011	0.0014	0.0017	0.0015	0.0032	0.18	0.12	0.13	0.22
Yb	0.0025	0.0025	0.0026	0.0015	0.0027	0.16	0.11	0.12	0.21
Lu	0.00072	0.00061	0.00051	0.00043	0.00066	0.024	0.016	0.018	0.03
Hf	0.0015	0.0011	0.0011	0.0011	0.0016	0.098	0.056	0.056	0.1
Ta	0.0004	0.00029	0.00032	0.0003	0.00038	0.0041	0.00045	0.0018	0.0081
Re	0.00027	0.00023	0.00027	0.00026	0.00031	0.0002	0.00021	0.00022	0.00023
Pb	0.039	0.0024	0.024	0.017	0.0099	0.0069	0.0024	0.0026	0.0046
Th	0.00048	0.00037	0.00045	0.00033	0.00043	0.0037	0.002	0.0048	0.0068
U	0.0002	0.00026	0.0003	0.00021	0.00029	0.0015	0.0012	0.0019	0.0023

Table C.3. Trace and major element concentrations in silicates from sample S01/5G - determined by LA-ICP-MS and electron microprobe respectively. * bulk rock majors analysed by XRF.

Concentrations

All values in ppm	**Sample S01/5G**									
	Bulk rock*	***Olivine***								
		OL1	**OL2**	**OL3**	**OL4**	**OL5**	**OL6**	**OL7**	**OL8**	**OL9**
Trace elements										
Li	1.347	0.792	2.14	3.68	1.135	0.837	1.027	0.687	0.507	0.761
Be		<0.0030	0.00072	0.169	<0.0061	<0.0032	<0.0028	0.0048	<0.0029	<0.0031
B		1.12	1.055	1.13	1.13	0.93	0.64	0.45	0.408	0.552
Mg		258255.5	258074.6	33067.06	258255.6	260523.2	265185.2	260782.6	257706.7	258189.2
Si		154524.5	154331	219764.4	153900.5	154827.9	164580.3	156313.6	153360.9	150546.2
P		53.17	90.32	68.16	63.34	65.35	51.6	51.14	45.15	44.78
Ca		140.85	206.38	89337.63	169.77	212.31	225.51	190.97	176.57	211.74
Sc	6.047	3.52	4.6	0.943	4	3.61	4.3	4.18	4.46	4.06
Ti	731.879	69.27	94.87	587.47	54.86	24.88	33.38	39.33	43.91	63.49
V	18.769	1.908	2.426	1.223	0.959	1.055	1.059	0.973	1.137	1.54
Cr	143.290	12.09	14.06	0.88	6.7	8.54	7.02	8.67	9.87	11.22
Ni	384.578	1025.02	1029.72	28.67	984.01	1015.9	1038.76	987.29	954.71	983.9
Cu	64.059	0.891	0.318	3.94	0.05	0.0301	6.94	0.435	0.0457	0.991
Zn	30.621	95.68	102.37	55.05	104.87	100.65	91.31	103.57	99.55	103.62
Ga		0.2159	0.2216	12.09	0.218	0.2092	0.262	0.2197	0.2059	0.2238
Ge		0.935	0.838	0.625	0.844	0.793	0.918	0.807	0.743	0.772
Rb	0.093	<0.0024	0.0027	0.0804	<0.0045	<0.0033	<0.0034	<0.0025	0.0027	0.0028
Sr	319.079	0.0223	0.0202	465.5	0.0578	0.206	0.1473	0.0038	0.00245	0.0293
Y	1.578	0.0222	0.0475	0.245	0.0428	0.0286	0.0435	0.0277	0.0253	0.0312
Zr	6.450	0.1206	0.1378	0.0086	0.0748	0.0393	0.0276	0.0247	0.0361	0.0558
Nb	0.076	0.0091	0.00543	<0.0011	0.00163	0.00177	0.003	0.00117	0.00079	0.00378
Mo	0.067	0.533	0.518	0.062	0.506	0.517	0.53	0.485	0.537	0.526
Cs	0.001	<0.00116	<0.00137	<0.0029	<0.0024	<0.0018	<0.0019	<0.0013	<0.00129	<0.00141
Ba	7.563	0.0174	0.0828	6.61	0.0079	0.0043	0.102	0.0062	<0.0030	0.0656
La	0.638	<0.00058	0.0008	0.965	<0.00056	0.00102	0.00218	<0.00036	<0.00041	<0.00045
Ce	1.408	0.00139	0.00068	2.064	0.00071	0.00288	0.0087	<0.00027	<0.00031	<0.00025
Pr	0.206	0.0004	<0.00011	0.231	<0.00029	0.00065	0.00052	<0.00030	<0.00032	<0.00033
Nd	0.938	<0.0017	<0.0021	0.919	0.0038	0.003	0.0039	<0.0021	<0.0017	<0.0019
Sm	0.234	<0.0026	<0.0029	0.135	<0.0037	<0.0034	<0.0028	<0.0015	<0.0023	<0.0022
Eu	0.356	<0.00030	<0.00083	0.401	<0.00115	<0.00086	0.0039	<0.00076	<0.00050	<0.00072
Gd	0.269	<0.0023	<0.0029	0.11	<0.0051	<0.0034	0.0037	<0.0026	<0.0028	<0.0030
Tb	0.047	<0.00071	<0.00073	0.0091	<0.0015	<0.00105	<0.00105	<0.00080	<0.00087	<0.00102
Dy	0.265	<0.0012	0.0022	0.048	0.0037	0.0025	0.0038	<0.0017	0.0019	0.002
Ho	0.055	0.00052	0.00104	0.0079	<0.00074	0.00101	<0.00078	0.00072	0.00066	<0.00063
Er	0.148	0.0064	0.0093	0.0145	0.0075	0.0067	0.0119	0.0048	0.0065	0.0061
Yb		0.00167	0.00298	0.002	0.0026	0.00191	0.0042	0.00264	0.00136	0.00259
Lu	0.141	0.0313	0.0566	0.0062	0.0418	0.0311	0.0528	0.029	0.0304	0.0353
Hf	0.024	0.0104	0.0159	<0.00118	0.0136	0.0117	0.0195	0.0124	0.0093	0.0142
Ta	0.079	<0.0017	<0.0024	<0.0049	<0.0031	<0.0026	<0.0023	<0.0020	<0.0019	0.0024
Re	0.006	0.00103	<0.00090	<0.0019	<0.00134	<0.00098	<0.00111	<0.00069	<0.00047	<0.00052
Pb	0.425	0.007	0.0047	1.219	0.0083	0.0066	0.0132	0.0074	0.006	0.0077
Th	0.004	<0.00106	<0.00113	0.0014	<0.00173	<0.00116	<0.0012	<0.00109	<0.00076	<0.00090
U	0.003	<0.00051	0.00106	<0.0012	<0.00102	<0.00090	0.00112	0.0007	<0.00046	0.00068
***Majors** (electron microprobe)*										
weight %										
SiO2	48.02	39.684	39.85	39.336	39.744	39.818	40.079	39.659	39.626	39.733
TiO2	0.114	0.017	0.01	0.001	0	0	0	0.016	0.009	0
Al2O3	22.71	0	0	0.006	0.005	0	0	0.005	0.011	0
Cr2O3		0	0.02	0	0.008	0.013	0	0	0.001	0
MgO	10.29	43.177	43.723	42.734	42.791	43.197	43.971	43.287	43.851	43.39
CaO	10.96	0.003	0.01	0.225	0.016	0.021	0.008	0.033	0.028	0.026
MnO	0.07	0.262	0.265	0.288	0.284	0.269	0.244	0.28	0.239	0.269
FeO	5.66	16.075	15.847	16.551	17.144	16.24	15.528	16.189	15.766	15.964
Na2O	2.95	0	0.011	0.004	0.008	0.004	0.01	0.015	0.025	0.008
K2O	0.06									
Total	-	99.387	99.894	99.309	100.176	99.734	100	99.645	99.722	99.566

Table C.3. contd. Trace and major element concentrations in silicates from sample S01/5G – determined by LA-ICP-MS and electron microprobe respectively. * bulk rock majors analysed by XRF.

Concentrations	All values in ppm													
	Sample S01/5G						**Sample S01/5G**							
	Clinopyroxene						***Plagioclase***							
	CPX1	CPX2	CPX3	CPX4	CPX5	CPX6	FSP1	FSP2	FSP3	FSP4	FSP5	FSP6	FSP7	FSP8
Trace elements														
Li	0.129	0.138	0.114	0.081	0.137	0.108	0.256	<0.048	0.199	0.706	<0.091	0.102	0.18	<0.143
Be	0.262	0.277	0.215	0.218	0.239	0.225	0.165	0.155	0.166	0.152	0.177	0.133	0.215	0.149
B	0.94	0.82	0.78	0.72	0.603	0.394	0.547	0.537	0.344	0.493	0.65	0.343	1.16	0.66
Mg	90038	109403	109475	109879	90345	90454	264	293	263	400	216	221	226	324
Si	184014	225492	221330	225683	184569	180534	329985	321611	269432	255494	250207	215476	228085	249850
P	44.97	49.98	49.51	52.06	41.42	38.58	42.35	42.81	35.9	35.42	45.85	36.37	68.95	64.45
Ca	132111	156763	153661	151438	133373	131364	89359	90738	91553	92911	98629	90846	90931	92196
Sc	117.69	160.27	141.98	140.9	127.42	123.01	1.633	1.537	1.231	1.14	1.025	0.841	0.804	0.884
Ti	7226.9	9303.7	8933.3	9258.9	8773.1	8634.1	758.16	683.47	624.71	429.04	299.44	269.31	769.61	745.8
V	415.1	545.03	496.99	499.29	426.47	434.81	2.74	3.67	2.47	2.81	2.66	2.35	1.68	1.69
Cr	2797.33	3598.46	4137.84	3846.01	3968.89	4117.81	0.92	0.88	1.03	1.21	1.11	0.91	1.33	1.13
Ni	115.72	152.98	143.03	154.84	116.51	116.24	2.64	1.87	1.34	1.56	0.786	0.727	1.71	1.61
Cu	0.567	2.32	0.713	1.47	1.87	0.792	6.53	5.71	4.52	4.88	3.52	2.96	3.85	4.04
Zn	16.78	21.46	43.97	23.33	16.71	16.72	1.615	1.718	1.523	1.439	1.146	0.925	0.997	1.289
Ga	4.8	6.33	6.43	6.26	5.12	5.01	18.69	17.98	13.79	12.23	10.91	9.14	12.24	13.35
Ge	1.796	2.304	2.272	2.32	1.627	1.827	1.053	1.027	0.795	0.695	0.609	0.579	0.682	0.721
Rb	0.0157	0.018	0.0166	0.0176	0.0549	0.0245	0.144	0.148	0.0928	0.1156	0.0731	0.0634	0.074	0.113
Sr	13.19	16.71	17.84	18.6	15.28	14.86	416.13	393.73	391.5	401.19	406.44	383.83	404.33	415.9
Y	34.15	38.16	34.02	36.37	32.45	32.64	0.217	0.231	0.26	0.284	0.268	0.266	0.295	0.275
Zr	85.3	99.92	74.45	86.03	88.39	88.15	0.032	0.0373	0.0354	0.0592	0.076	0.0455	0.0266	0.068
Nb	0.1032	0.183	0.414	0.299	0.223	0.239	0.00101	0.0033	0.00335	0.0042	0.0122	0.0083	0.0019	0.0026
Mo	0.249	0.305	0.293	0.336	0.246	0.26	0.077	0.0056	<0.0042	0.0037	<0.0055	0.0065	<0.0090	<0.0089
Cs	<0.00122	0.002	0.003	<0.0020	0.0027	<0.00121	<0.0015	<0.0015	<0.00168	0.002	<0.0026	<0.0025	0.0067	<0.0041
Ba	0.081	0.237	0.276	0.21	1.183	0.313	8.25	7.53	6.56	6.72	6.11	5.54	7.15	7.42
La	0.769	0.798	1.081	1.05	0.743	0.749	0.703	0.65	0.661	0.497	0.304	0.281	0.886	0.855
Ce	4.78	5.22	5.62	5.75	4.33	4.52	2.167	1.971	1.78	1.406	0.745	0.711	1.731	1.732
Pr	1.175	1.3	1.28	1.338	1.097	1.079	0.201	0.1889	0.1884	0.1665	0.0892	0.0877	0.205	0.203
Nd	8.13	9.06	8.73	9	7.64	7.37	0.751	0.725	0.716	0.648	0.413	0.404	0.924	0.835
Sm	3.51	3.93	3.65	3.78	3.29	3.18	0.114	0.123	0.124	0.12	0.081	0.074	0.154	0.146
Eu	0.9	1.127	1.039	1.058	0.899	0.884	0.412	0.376	0.386	0.407	0.41	0.363	0.371	0.411
Gd	4.82	5.49	5.2	5.32	4.49	4.43	0.105	0.091	0.0845	0.095	0.079	0.076	0.111	0.106
Tb	0.849	0.989	0.915	0.929	0.81	0.79	0.0126	0.0093	0.0112	0.0108	0.0086	0.0077	0.0157	0.0114
Dy	6.09	7.06	6.6	6.78	5.74	5.63	0.0478	0.0532	0.0492	0.0582	0.0608	0.0556	0.072	0.058
Ho	1.261	1.462	1.33	1.378	1.175	1.166	0.008	0.0093	0.0083	0.0091	0.0084	0.0096	0.0185	0.0079
Er	3.65	4.22	3.71	3.91	3.35	3.3	0.0193	0.0216	0.0227	0.0209	0.0142	0.0145	0.0195	0.0146
Yb	0.519	0.616	0.524	0.545	0.484	0.455	0.00295	0.00161	0.00312	0.00232	0.0029	0.0024	0.0022	0.0019
Lu	3.55	4.25	3.39	3.58	3.15	3.11	0.014	0.0113	0.0165	0.0121	0.0172	0.0114	<0.0070	0.0076
Hf	0.497	0.608	0.508	0.511	0.445	0.444	0.00166	0.00156	0.00143	0.00139	0.0028	0.0026	0.0023	<0.0016
Ta	2.13	2.94	2.32	2.3	2.26	2.22	0.0028	<0.0020	<0.0023	<0.0028	<0.0034	0.0057	<0.0051	<0.0064
Re	0.026	0.0352	0.045	0.0683	0.0499	0.0503	<0.00066	<0.00069	<0.00099	<0.00102	<0.00154	<0.00162	<0.0030	<0.0024
Pb	0.0215	0.0902	0.0311	0.0219	0.0244	0.0168	0.226	0.235	0.217	0.194	0.152	0.1115	0.115	0.16
Th	0.0456	0.0439	0.0857	0.0821	0.045	0.0424	0.00112	<0.00093	0.00158	0.00114	<0.0017	<0.0017	0.117	<0.0028
U	0.0131	0.0066	0.0506	0.0281	0.0208	0.0122	0.0006	0.00078	<0.00081	0.00182	<0.00130	<0.00106	0.0021	<0.00123
Majors *(electron microprobe)*														
weight %														
SiO2	50.024	50.07	49.811	49.729	49.646	50.025	52.947	52.503	52.628	51.991	52.11	52.139	52.454	51.244
TiO2	1.581	1.646	1.703	1.578	1.552	1.513	0.082	0.082	0.09	0.057	0.084	0.092	0.086	0.046
Al2O3	4.746	4.9	4.73	4.814	4.51	4.624	29.619	29.999	29.647	30.203	29.742	29.632	29.996	30.982
Cr2O3	0.656	0.915	0.901	0.949	0.622	0.773								
MgO	14.934	15.21	15.031	14.977	14.929	15.072								
CaO	21.934	21.216	21.607	21.623	22.221	21.779	12.503	12.696	12.726	12.644	12.568	12.723	11.568	12.209
MnO	0.113	0.147	0.14	0.123	0.146	0.152								
FeO	4.488	4.4	4.574	4.822	4.702	4.518	0.207	0.244	0.238	0.128	0.228	0.248	0.18	0.066
Na2O	0.629	0.809	0.768	0.695	0.693	0.63	4.707	4.582	4.834	4.536	4.62	4.551	5.133	4.406
K2O							0.076	0.087	0.074	0.096	0.077	0.073	0.076	0.052
Total	99.125	99.338	99.293	99.336	99.045	99.11	100.141	100.217	100.237	99.68	99.429	99.46	99.494	99.005

Table C.4. Analytical errors (1 sigma) for LA-ICP-MS determination of trace elements in silicates from sample S01/5G. Errors calculated by GLITTER.

1 sigma error

	Sample S01/5G								
	Olivine								
Element	OL1	OL2	OL3	OL4	OL5	OL6	OL7	OL8	OL9
Li	0.045	0.11	0.24	0.077	0.057	0.071	0.051	0.04	0.055
Be	0.0021	0.00088	0.034	0.0033	0.0019	0.002	0.0038	0.0019	0.0022
B	0.1	0.096	0.21	0.16	0.11	0.11	0.08	0.066	0.076
Mg	8166.83	8161.1	1253.45	8166.96	8238.59	8386.09	8246.8	8149.5	8164.75
Si	5706.94	5702.02	11152.12	5703.11	5751.29	6132.67	5846.04	5760.07	5681.72
P	3.81	6.51	7.79	4.77	5.05	4.13	4.22	3.85	3.95
Ca	5.92	7.85	2835.21	8.92	9.15	10.55	8.52	7.53	8.8
Sc	0.13	0.17	0.044	0.15	0.14	0.17	0.17	0.18	0.17
Ti	2.33	3.19	20.04	1.95	0.91	1.24	1.44	1.6	2.33
V	0.069	0.088	0.058	0.04	0.042	0.045	0.041	0.047	0.065
Cr	0.56	0.65	0.35	0.43	0.47	0.44	0.51	0.57	0.67
Ni	36.09	36.55	1.31	35.87	37.66	39.28	38.14	37.74	39.86
Cu	0.038	0.015	0.21	0.011	0.0076	0.33	0.024	0.0064	0.053
Zn	3.28	3.53	1.92	3.7	3.59	3.32	3.82	3.73	3.96
Ga	0.0085	0.0085	0.38	0.011	0.0093	0.012	0.0098	0.0086	0.0092
Ge	0.04	0.037	0.061	0.053	0.042	0.051	0.042	0.037	0.038
Rb	0.0013	0.0014	0.0078	0.0029	0.002	0.0024	0.0018	0.0016	0.0017
Sr	0.0017	0.0015	14.47	0.0044	0.009	0.0079	0.00084	0.00058	0.0022
Y	0.0019	0.0031	0.015	0.0043	0.0028	0.0043	0.0029	0.0024	0.0028
Zr	0.0083	0.009	0.003	0.0083	0.0047	0.0046	0.0037	0.0042	0.0058
Nb	0.0012	0.00086	0.001	0.00097	0.00075	0.0012	0.00059	0.00049	0.00085
Mo	0.027	0.025	0.014	0.036	0.031	0.036	0.03	0.028	0.028
Cs	0.00067	0.00072	0.002	0.0016	0.0012	0.0013	0.001	0.0008	0.00086
Ba	0.0042	0.0086	0.26	0.0049	0.003	0.016	0.0037	0.0018	0.0087
La	0.00038	0.00038	0.042	0.00044	0.00054	0.00094	0.00029	0.00032	0.00023
Ce	0.00049	0.00033	0.074	0.00056	0.00076	0.0016	0.00029	0.00027	0.00021
Pr	0.00029	0.0001	0.012	0.00023	0.00037	0.00043	0.00016	0.00018	0.0002
Nd	0.0012	0.0012	0.056	0.003	0.0023	0.003	0.0013	0.0012	0.0014
Sm	0.0017	0.0016	0.02	0.003	0.0023	0.0026	0.0016	0.0017	0.0011
Eu	0.00029	0.0004	0.021	0.00088	0.00062	0.0014	0.00057	0.00032	0.00041
Gd	0.0016	0.002	0.019	0.0037	0.0024	0.0033	0.0022	0.0017	0.0019
Tb	0.00044	0.00045	0.0024	0.0011	0.00068	0.00085	0.00058	0.00058	0.00063
Dy	0.0011	0.0013	0.011	0.0033	0.0019	0.0029	0.0016	0.0015	0.0016
Ho	0.0003	0.00047	0.0021	0.00069	0.00065	0.00073	0.00051	0.00043	0.00048
Er	0.0017	0.002	0.0055	0.003	0.0024	0.0038	0.0021	0.0021	0.002
Yb	0.00051	0.00062	0.0013	0.0012	0.00069	0.0013	0.00085	0.0006	0.00075
Lu	0.0047	0.0059	0.0043	0.0086	0.0058	0.0095	0.0059	0.005	0.0054
Hf	0.0014	0.0016	0.00099	0.0024	0.0018	0.0029	0.0019	0.0014	0.0017
Ta	0.0013	0.0014	0.0029	0.0024	0.0015	0.0021	0.0016	0.0013	0.0018
Re	0.00065	0.00038	0.0014	0.00062	0.00054	0.00063	0.00059	0.00036	0.00026
Pb	0.0026	0.0022	0.057	0.0043	0.0028	0.004	0.0027	0.0021	0.0023
Th	0.00066	0.0006	0.0014	0.00092	0.00086	0.0011	0.0008	0.00055	0.00062
U	0.00039	0.00057	0.001	0.00094	0.00064	0.00098	0.00064	0.00033	0.00049

Table C.4. contd. Analytical errors (1 sigma) for LA-ICP-MS determination of trace elements in silicates from sample S01/5G. Errors calculated by GLITTER.

1 sigma error

	Sample S01/5G						Sample S01/5G							
	Clinopyroxene						*Plagioclase*							
Element	CPX1	CPX2	CPX3	CPX4	CPX5	CPX6	FSP1	FSP2	FSP3	FSP4	FSP5	FSP6	FSP7	FSP8
Li	0.031	0.035	0.042	0.042	0.034	0.028	0.045	0.033	0.039	0.09	0.055	0.055	0.12	0.088
Be	0.027	0.037	0.034	0.033	0.025	0.023	0.027	0.025	0.024	0.023	0.031	0.026	0.051	0.033
B	0.1	0.11	0.12	0.12	0.079	0.057	0.094	0.091	0.066	0.081	0.12	0.098	0.26	0.16
Mg	2847.36	4567.08	4635.7	4721.64	2857.08	2860.49	11.57	13.06	11.86	18.34	10.12	10.56	11.13	16.05
Si	7067.23	11479	11282.4	11520.2	7837.98	7741.17	16872.6	16471.4	13822.3	13133.2	12891.1	11127.5	11817.4	12967.8
P	4.37	6.4	6.46	6.91	5.28	5	5.72	5.88	5.01	5.02	6.6	5.32	10.24	9.69
Ca	4666.93	4960.8	4865.1	4794.49	5731.72	5743.02	2831.29	2874.46	2898.29	2941.62	3125.98	2880.66	2896.71	2926.89
Sc	5.38	6.62	5.98	6.06	8.44	8.39	0.076	0.073	0.059	0.056	0.055	0.047	0.056	0.054
Ti	274.87	322.62	311.08	323.73	425.04	426.82	26.7	24.18	22.18	15.33	10.82	9.8	28.19	27.32
V	18.42	31.57	29.81	30.98	25.76	26.86	0.18	0.25	0.17	0.2	0.2	0.18	0.14	0.14
Cr	180.38	312.51	375.58	364.4	390.52	417	0.19	0.19	0.2	0.22	0.31	0.29	0.63	0.46
Ni	5.09	9.61	9.34	10.5	7.07	7.23	0.2	0.15	0.11	0.13	0.08	0.078	0.19	0.17
Cu	0.035	0.19	0.062	0.13	0.16	0.069	0.59	0.54	0.44	0.49	0.37	0.32	0.43	0.46
Zn	0.69	0.78	1.59	0.86	0.86	0.87	0.073	0.076	0.064	0.063	0.06	0.052	0.078	0.074
Ga	0.16	0.21	0.21	0.21	0.18	0.18	0.61	0.59	0.46	0.41	0.37	0.31	0.42	0.46
Ge	0.078	0.093	0.098	0.1	0.083	0.083	0.053	0.051	0.041	0.038	0.047	0.046	0.087	0.067
Rb	0.0024	0.0027	0.0032	0.0032	0.0043	0.0025	0.01	0.011	0.007	0.0088	0.0073	0.0068	0.012	0.012
Sr	0.48	0.53	0.56	0.59	0.67	0.66	13.13	12.45	12.4	12.74	12.94	11.62	12.98	13.35
Y	2.14	2.11	1.95	2.16	3.17	3.28	0.015	0.017	0.018	0.021	0.021	0.022	0.028	0.025
Zr	6.73	7.38	5.74	6.93	11.28	11.62	0.005	0.0055	0.0047	0.0073	0.01	0.0077	0.0083	0.012
Nb	0.0074	0.011	0.023	0.018	0.019	0.021	0.00056	0.00098	0.00089	0.001	0.0024	0.002	0.0015	0.0016
Mo	0.019	0.022	0.026	0.028	0.018	0.017	0.012	0.0032	0.0029	0.0026	0.0046	0.0048	0.0054	0.0062
Cs	0.00092	0.0011	0.0014	0.0013	0.001	0.00075	0.0011	0.001	0.00091	0.001	0.0016	0.0016	0.004	0.0027
Ba	0.011	0.018	0.025	0.021	0.063	0.022	0.31	0.28	0.24	0.25	0.24	0.23	0.33	0.31
La	0.042	0.038	0.053	0.053	0.057	0.058	0.037	0.035	0.035	0.028	0.019	0.019	0.058	0.054
Ce	0.15	0.18	0.2	0.21	0.15	0.15	0.081	0.074	0.067	0.054	0.031	0.031	0.076	0.073
Pr	0.041	0.043	0.043	0.045	0.043	0.043	0.0088	0.0082	0.0074	0.0069	0.0054	0.0055	0.014	0.011
Nd	0.36	0.34	0.34	0.36	0.45	0.44	0.042	0.04	0.036	0.034	0.03	0.031	0.076	0.058
Sm	0.17	0.16	0.16	0.17	0.21	0.2	0.014	0.014	0.011	0.012	0.013	0.013	0.03	0.022
Eu	0.036	0.04	0.039	0.04	0.041	0.04	0.018	0.017	0.015	0.016	0.019	0.018	0.026	0.022
Gd	0.23	0.23	0.23	0.24	0.27	0.27	0.014	0.012	0.0096	0.011	0.013	0.014	0.027	0.02
Tb	0.043	0.044	0.043	0.044	0.056	0.055	0.0019	0.0016	0.0014	0.0015	0.002	0.002	0.0045	0.003
Dy	0.3	0.33	0.32	0.34	0.39	0.39	0.0076	0.0079	0.0061	0.0072	0.01	0.0099	0.018	0.012
Ho	0.061	0.064	0.061	0.064	0.077	0.078	0.0015	0.0016	0.0012	0.0014	0.0019	0.0021	0.0046	0.0022
Er	0.17	0.18	0.17	0.18	0.21	0.21	0.0041	0.0043	0.0036	0.0036	0.0043	0.0045	0.0087	0.0057
Yb	0.025	0.027	0.025	0.026	0.03	0.029	0.00092	0.00073	0.00077	0.00073	0.0011	0.0011	0.002	0.0011
Lu	0.16	0.18	0.15	0.16	0.17	0.17	0.0045	0.004	0.0037	0.0035	0.0058	0.0052	0.0073	0.0058
Hf	0.025	0.027	0.025	0.025	0.029	0.029	0.00075	0.00066	0.00053	0.00066	0.0011	0.0013	0.002	0.0013
Ta	0.12	0.14	0.12	0.12	0.17	0.17	0.002	0.0011	0.0013	0.002	0.0023	0.0034	0.0053	0.0049
Re	0.0032	0.0035	0.005	0.0063	0.0051	0.0048	0.00062	0.00062	0.00054	0.00059	0.00088	0.0009	0.0026	0.0017
Pb	0.0033	0.0067	0.0048	0.004	0.0031	0.0024	0.014	0.014	0.012	0.012	0.012	0.01	0.016	0.014
Th	0.0046	0.0042	0.0078	0.0074	0.0047	0.0042	0.00097	0.00082	0.00086	0.00076	0.0012	0.0013	0.016	0.0019
U	0.0019	0.0013	0.0057	0.0037	0.0025	0.0016	0.00058	0.00062	0.00045	0.00072	0.00069	0.00084	0.0017	0.00095

Table C.5. Trace and major element concentrations in silicates from sample S01/3iix – determined by LA-ICP-MS and electron microprobe respectively. *bulk rock majors analysed by XRF.

Concentrations

All values in ppm	**Sample S01/3iix**							
	Bulk rock*	***Saussurite** (no precise internal calibration)*				***Talc***		***Glaucophane***
		PL1	**PL2**	**PL3**	**PL4**	**TC1**	**TC2**	**GL1**
Trace elements								
Li	0.892	1.38	0.916	1.038	1.77	0.026	0.035	1.94
Be		0.448	0.479	0.402	0.606	<0.0081	<0.0081	0.056
B		17.7	1.38	1.32	59.35	0.88	0.97	4.65
Mg		23776.38	24854.18	27871.09	38638.73	214022	220640.5	97625.76
Si		252417.3	176224.6	176224.6	210347.7	286540.3	286540.3	286540.31
P		53.78	34.84	31.56	33.55	56.25	43.02	46.47
K	220.610	2684.15	813.92	476.08	5406.77	5.35	15.49	2697.15
Ca		49885.25	81779.77	75217.31	59676.75	94.41	37.58	34156.38
Sc	2.457	1.88	2.06	2.12	3.12	0.435	0.473	1.88
Ti	1735.50	2182.83	170.82	186.03	186.15	33.25	47.06	155.96
V	34.620	20.4	19.02	19.15	23.03	0.296	2.52	2.76
Cr	24.300	6.68	3.48	2.97	5.43	1.59	5.6	3.11
Ni	171.522	53.38	28.36	33.22	77.98	1170.42	1796.95	447.55
Cu	20.576	143.54	5.95	4.79	313.88	3.62	5.28	11.7
Zn	26.399	9.92	10.33	11.27	16.03	137.43	163.85	49.48
Rb	0.132	1.161	0.0772	0.0379	3.5	0.0063	0.0116	8.6
Sr	311.514	190.5	320.3	207.2	159.39	0.149	0.0792	47.61
Y	4.355	1.005	2.138	1.263	0.85	<0.00109	0.0025	2.83
Zr	17.200	0.243	0.228	0.22	0.234	0.0012	0.0088	34.59
Nb	0.896	0.962	0.0125	0.0243	0.0119	0.0055	<0.00064	0.427
Mo	0.064	0.0101	0.01	0.0075	0.0136	<0.0043	0.007	0.136
Cs	0.003	0.1225	<0.0034	<0.0031	0.239	0.0046	<0.0036	0.142
Ba	4.976	55.96	6.62	3.71	84.95	0.09	0.178	70.84
La	1.973	1.023	2.707	1.604	0.799	<0.00127	<0.00137	1.773
Ce	4.477	2.645	6.51	3.93	2.026	0.0034	<0.00123	3.17
Pr	0.612	0.342	0.838	0.49	0.254	<0.00120	<0.0012	0.411
Nd	2.763	1.49	3.76	2.09	1.122	<0.0071	0.009	1.59
Sm	0.714	0.332	0.779	0.471	0.251	<0.0095	<0.0097	0.314
Eu	0.648	0.259	0.648	0.375	0.199	<0.0030	<0.0029	0.137
Gd	0.824	0.306	0.687	0.346	0.226	<0.0110	0.018	0.347
Tb	0.128	0.0437	0.0938	0.0541	0.0363	<0.0023	0.0026	0.0476
Dy	0.726	0.242	0.535	0.286	0.179	<0.0083	<0.0102	0.373
Ho	0.150	0.0381	0.0858	0.0501	0.0335	<0.0018	<0.0023	0.1
Er	0.408	0.084	0.158	0.113	0.067	0.0123	<0.0082	0.35
Yb	0.368	<0.021	0.026	0.041	0.0184	<0.0106	<0.0118	0.536
Lu	0.060	<0.0049	0.0025	0.0048	0.0052	<0.0021	<0.0028	0.081
Hf	0.056	<0.018	0.0141	0.0251	0.0122	0.0123	<0.011	0.939
Ta	0.063	0.0419	<0.0029	<0.0024	<0.0029	0.0033	0.0037	0.0423
Re		<0.0058	<0.0029	<0.0028	<0.0032	<0.0029	<0.0033	<0.0034
Pb	0.175	0.148	0.205	0.11	0.091	0.015	0.015	2.36
Th	0.033	0.0141	0.0317	0.019	0.0136	<0.0068	<0.0062	0.531
U	0.014	<0.0108	0.0125	0.007	0.0088	0.0062	<0.0057	0.281
***Majors** (electron microprobe)*								
weight %		zoisite	zoisite	paragonite	omphacite			
SiO2	49.10	37.533	37.689	45.87	55.636	61.463	61.603	58.587
TiO2	0.26	0.047	0.018	0.024	0.025	0	0	0.016
Al2O3	22.78	31.656	31.631	38.861	10.348	0.257	0.222	12.271
Cr2O3		0.017	0.008	0.011	0.021	0	0	0.016
MgO	7.80	0.039	0.03	0.108	10.055	29.407	29.605	13.798
CaO	9.30	24.592	24.448	0.298	14.589	0.004	0.016	0.722
MnO	0.08	0.004	0.017	0	0.022	0.01	0.006	0.005
FeO	4.98	1.127	1.272	0.171	2.894	3.156	3.165	3.932
Na2O	3.83	0.026	0.018	7.511	6.669	0.045	0.055	7.326
K2O	0.05	0	0	0.509	0	0.008	0	0.009
Total	-	95.044	95.148	93.394	100.273	94.361	94.726	96.695

Table C.5. contd. Trace and major element concentrations in silicates from sample S01/3iix – determined by LA-ICP-MS and electron microprobe respectively. *bulk rock majors analysed by XRF.

Concentrations

All values in ppm	**Sample S01/3iix**								
	Omphacite			***Garnet***					
Element	CPX1	CPX2	CPX3	GT1	GT2	GT3	GT4	GT5	GT6
Li	0.986	1.58	0.855	0.104	0.119	0.077	0.215	0.48	0.044
Be	0.418	0.614	0.342	0.012	0.025	<0.0096	0.041	0.139	0.0079
B	0.8	0.92	0.98	0.88	0.85	1.36	1.31	0.89	0.86
Mg	121659.5	75103.13	137844.2	46068.52	50827.04	53298.14	48944.86	51925.11	47515.88
Si	260130	260130	260130	175757.2	175757.2	175757.2	175757.2	175757.2	175757.2
P	37.42	31.95	36.8	51.14	52.6	59.37	63.04	36.71	48.01
K	43.88	174.99	19.5	26.61	20.4	9.41	9.86	99.75	7.85
Ca	59341.12	95283.23	47048.55	56764.23	43660.25	42709.12	51275.3	34430.54	50648.48
Sc	134.95	197.98	104.15	5.26	5.59	26.24	3.59	2.91	8
Ti	9962.07	498.82	11638.22	296.59	431.2	466.95	359.28	195.46	412.18
V	561.32	844.35	441.05	3.46	15.05	33.07	5.43	9.28	11.17
Cr	725.78	624.44	661.63	1	0.81	2.11	1.31	8.36	1.96
Ni	582.38	156.86	593.02	21.2	3.09	5.46	16.84	123.96	3.67
Cu	8.36	36.82	6.7	5.31	1.82	5.76	3.44	5.43	1.66
Zn	82.6	50.9	82.46	24.3	19.92	22.07	23.96	30.55	21.63
Rb	0.0164	0.0546	0.0209	0.0112	0.0058	0.0081	0.0079	0.0152	0.008
Sr	5.72	19.49	2.37	0.823	1.064	0.213	7.24	12.98	0.179
Y	5.91	8.95	5.88	3.91	4.99	7.11	4.97	4.24	6.67
Zr	135.08	341.83	265.47	0.348	0.627	2.13	0.294	0.208	0.729
Nb	1.399	0.0226	2.79	0.0293	0.0539	0.0119	0.0197	0.0035	0.0085
Mo	0.0153	0.0198	0.0136	0.599	0.61	0.699	0.546	0.212	0.699
Cs	0.006	0.0113	<0.0035	<0.0039	<0.0036	<0.0041	<0.0039	<0.0029	<0.0036
Ba	3.27	18.4	0.31	1.48	0.43	0.604	0.405	0.971	0.18
La	<0.0018	0.0025	0.0022	0.0268	0.0568	0.0189	0.0778	0.1045	0.1135
Ce	0.0067	0.0038	0.0028	0.0662	0.172	0.0342	0.18	0.297	0.216
Pr	0.0035	<0.00140	0.0032	0.0077	0.0272	0.0041	0.0227	0.0408	0.0245
Nd	0.029	0.0221	0.032	0.079	0.233	0.0183	0.12	0.18	0.134
Sm	0.079	0.049	0.037	0.16	0.506	0.118	0.108	0.053	0.111
Eu	<0.0034	0.0033	<0.0027	0.22	0.201	0.102	0.105	0.0469	0.398
Gd	0.232	0.218	0.089	0.594	1.45	0.825	0.47	0.093	0.413
Tb	0.0594	0.0767	0.037	0.0986	0.194	0.202	0.0729	0.0246	0.0998
Dy	0.715	0.902	0.549	0.603	1.074	1.328	0.466	0.351	0.664
Ho	0.205	0.33	0.217	0.157	0.186	0.259	0.163	0.146	0.246
Er	0.883	1.404	0.847	0.583	0.59	0.801	0.847	0.702	1.013
Yb	1.39	2.48	1.75	0.839	0.614	1.29	0.985	1.099	2.23
Lu	0.222	0.422	0.307	0.148	0.092	0.299	0.137	0.163	0.466
Hf	2.9	10.12	4.87	<0.0102	0.027	0.033	0.0176	<0.0104	<0.0093
Ta	0.0552	<0.0031	0.087	<0.0030	0.0034	<0.0038	<0.0036	<0.0023	<0.0029
Re	<0.0040	<0.0033	0.0046	<0.0035	<0.0033	<0.0042	<0.0036	<0.0027	<0.0034
Pb	0.084	0.716	0.025	0.029	0.028	0.036	<0.016	0.021	<0.0123
Th	0.024	0.0669	0.06	<0.0077	<0.0068	<0.0079	<0.0069	0.0106	<0.0068
U	<0.0098	0.0215	0.032	<0.0064	<0.0064	<0.0073	<0.0063	<0.0049	<0.0054
Majors *(electron microprobe)*									
SiO2	55.849	55.503	55.503	37.771	37.775	37.509	37.771	37.462	37.535
TiO2	0.04	0.073	0.073	0.09	0.045	0.064	0.09	0.048	0.055
Al2O3	10.975	10.506	10.506	21.57	21.547	21.471	21.57	21.401	21.432
Cr2O3	0.158	0.165	0.165	0.002	0	0	0.002	0.015	0.005
MgO	9.221	9.675	9.675	6.562	6.362	6.324	6.562	5.964	6.097
CaO	13.672	14.052	14.052	8.222	8.508	7.996	8.222	9.306	8.161
MnO	0.017	0.013	0.013	0.621	0.694	0.659	0.621	0.598	0.691
FeO (Fe2O3)	2.436	2.63	2.63	23.916	23.748	24.284	23.916	23.467	24.325
Na2O	7.112	6.868	6.868	0.034	0.032	0.021	0.034	0.019	0.03
K2O	0.002	0.004	0.004	0	0	0	0	0	0.003
Total	99.512	99.517	99.517	98.79	98.738	98.339	98.79	98.284	98.341

Table C.6. Analytical errors (1 sigma) for LA-ICP-MS determination of trace elements in silicates from sample S01/3iix. Errors calculated by GLITTER.

1 sigma error

	Sample S01/3iix						
	Saussurite (no precise internal calibration)				*Talc*		*Glaucophane*
Element	PL1	PL2	PL3	PL4	TC1	TC2	GL1
Li	0.1	0.069	0.08	0.13	0.016	0.025	0.087
Be	0.043	0.034	0.034	0.043	0.0049	0.0025	0.014
B	3.07	0.25	0.25	10.99	0.18	0.22	0.22
Mg	1154	1220	1384	1941	10874	11341	5239
Si	7983	5573	5573	6852	9062	9063	8648
P	7.11	4.67	4.3	4.64	7.9	6.15	6.04
K	221.6	68.22	40.51	467.02	0.48	1.39	7.09
Ca	2601.54	4313.84	4015.6	3224.29	7.55	6.7	264.89
Sc	0.1	0.11	0.12	0.17	0.028	0.035	0.06
Ti	122.81	9.75	10.75	10.89	2.02	2.93	5.48
V	1.2	1.13	1.15	1.41	0.021	0.16	1
Cr	0.37	0.19	0.19	0.27	0.19	0.42	0.39
Ni	2.48	1.33	1.58	3.73	56.59	87.97	34.71
Cu	11.36	0.48	0.39	26.14	0.31	0.46	0.53
Zn	0.55	0.57	0.63	0.9	7.76	9.39	4.74
Rb	0.049	0.0049	0.0038	0.14	0.0033	0.0054	0.0055
Sr	7.87	13.34	8.71	6.76	0.01	0.0091	0.0072
Y	0.038	0.076	0.046	0.032	0.00081	0.0017	0.0016
Zr	0.016	0.013	0.013	0.014	0.0012	0.004	0.0087
Nb	0.043	0.0015	0.0025	0.0016	0.0017	0.0002	0.00072
Mo	0.0046	0.0027	0.0029	0.0033	0.0036	0.0062	0.0038
Cs	0.0086	0.0017	0.0018	0.012	0.0028	0.0037	0.0026
Ba	2.54	0.32	0.19	3.94	0.022	0.045	0.035
La	0.041	0.097	0.06	0.031	0.00071	0.00042	0.0016
Ce	0.099	0.23	0.14	0.076	0.0017	0.00038	0.0027
Pr	0.018	0.036	0.023	0.013	0.00099	0.0016	0.0011
Nd	0.093	0.19	0.12	0.068	0.007	0.011	0.0047
Sm	0.036	0.048	0.037	0.024	0.0077	0.0097	0.007
Eu	0.018	0.032	0.022	0.013	0.0026	0.0034	0.0023
Gd	0.036	0.048	0.033	0.024	0.0099	0.02	0.0082
Tb	0.0054	0.0066	0.0051	0.0039	0.0018	0.0029	0.0015
Dy	0.027	0.036	0.025	0.019	0.0055	0.0066	0.0055
Ho	0.0056	0.0066	0.0052	0.0039	0.0017	0.0029	0.0014
Er	0.014	0.014	0.013	0.0096	0.0066	0.006	0.0055
Yb	0.013	0.0081	0.01	0.008	0.0077	0.0064	0.0069
Lu	0.0029	0.0015	0.0019	0.0018	0.002	0.0029	0.0017
Hf	0.011	0.0056	0.0081	0.0069	0.0077	0.015	0.0078
Ta	0.0056	0.0015	0.0014	0.0017	0.0024	0.0036	0.0021
Re	0.0047	0.0023	0.0025	0.0028	0.0034	0.0049	0.0036
Pb	0.0029	0.0014	0.0016	0.0017	0.0022	0.0029	0.0022
Th	0.022	0.019	0.015	0.014	0.011	0.017	0.012
U	0.0082	0.0052	0.0053	0.0044	0.0043	0.0078	0.0043

Table C.6. contd. Analytical errors (1 sigma) for LA-ICP-MS determination of trace elements in silicates from sample S01/3iix. Errors calculated by GLITTER.

1 sigma error

	Sample S01/3iix								
	Omphacite			*Garnet*					
Element	CPX1	CPX2	CPX3	GT1	GT2	GT3	GT4	GT5	GT6
Li	0.091	0.14	0.082	0.021	0.02	0.02	0.027	0.047	0.014
Be	0.055	0.048	0.05	0.01	0.01	0.0069	0.013	0.018	0.0057
B	0.2	0.22	0.25	0.22	0.22	0.35	0.34	0.24	0.23
Mg	6704	4187	7774	2628	2933	3111	2890	3101	2869
Si	8227	8227	8227	5559	5559	5559	5559	5558	5558
P	5.82	5.04	5.89	8.28	8.63	9.87	10.62	6.26	8.29
K	4.26	17.2	1.95	2.69	2.09	0.98	1.04	10.61	0.85
Ca	3528.55	5728.91	2864.2	3494.3	2718.75	2690.25	3266.14	2217.84	3298.81
Sc	8.21	12.19	6.49	0.33	0.36	1.7	0.24	0.19	0.54
Ti	642.78	32.6	769.32	19.88	29.22	32.02	24.93	13.72	29.25
V	38.09	58.04	30.71	0.25	1.08	2.39	0.4	0.69	0.84
Cr	32.32	28.03	30.04	0.18	0.16	0.22	0.18	0.43	0.17
Ni	30.75	8.39	32.12	1.18	0.19	0.32	0.97	7.16	0.22
Cu	0.8	3.57	0.66	0.53	0.19	0.6	0.36	0.58	0.18
Zn	5.11	3.18	5.23	1.57	1.3	1.46	1.6	2.06	1.48
Rb	0.0051	0.005	0.0052	0.0038	0.003	0.0036	0.0032	0.0027	0.0027
Sr	0.27	0.9	0.12	0.042	0.053	0.013	0.35	0.63	0.011
Y	0.22	0.33	0.22	0.15	0.19	0.27	0.19	0.16	0.25
Zr	6.73	17.19	13.49	0.024	0.037	0.12	0.02	0.014	0.043
Nb	0.07	0.0026	0.14	0.0037	0.0049	0.0022	0.0028	0.001	0.0015
Mo	0.0063	0.0043	0.006	0.035	0.034	0.04	0.032	0.014	0.037
Cs	0.0039	0.0026	0.0029	0.0025	0.0025	0.0026	0.0024	0.0016	0.002
Ba	0.22	0.96	0.049	0.11	0.045	0.058	0.044	0.069	0.023
La	0.0013	0.0011	0.0017	0.0041	0.0055	0.0033	0.0066	0.0066	0.0072
Ce	0.0028	0.0014	0.0019	0.0066	0.011	0.0043	0.011	0.015	0.012
Pr	0.002	0.00095	0.002	0.0021	0.0036	0.0017	0.0033	0.0037	0.003
Nd	0.015	0.0079	0.014	0.018	0.028	0.0095	0.02	0.02	0.018
Sm	0.024	0.012	0.017	0.027	0.048	0.022	0.02	0.011	0.017
Eu	0.0028	0.002	0.003	0.019	0.016	0.011	0.011	0.0057	0.025
Gd	0.043	0.028	0.026	0.063	0.11	0.077	0.051	0.016	0.041
Tb	0.0086	0.007	0.0067	0.01	0.015	0.016	0.0077	0.0033	0.0086
Dy	0.071	0.065	0.06	0.055	0.081	0.1	0.044	0.031	0.065
Ho	0.02	0.023	0.021	0.015	0.016	0.021	0.015	0.012	0.019
Er	0.079	0.098	0.077	0.052	0.051	0.067	0.069	0.055	0.078
Yb	0.13	0.18	0.16	0.081	0.061	0.11	0.09	0.092	0.18
Lu	0.022	0.03	0.028	0.015	0.01	0.025	0.013	0.014	0.035
Hf	0.2	0.58	0.31	0.0072	0.01	0.013	0.0089	0.0061	0.0064
Ta	0.0085	0.0019	0.011	0.0023	0.0024	0.0025	0.0022	0.0013	0.0016
Re	0.0053	0.0033	0.0047	0.0038	0.0035	0.004	0.0039	0.0025	0.0031
Pb	0.003	0.0019	0.0031	0.0024	0.002	0.0024	0.0024	0.0016	0.0018
Th	0.022	0.061	0.015	0.013	0.012	0.014	0.011	0.0081	0.0077
U	0.01	0.0099	0.014	0.0061	0.0041	0.0039	0.0048	0.0043	0.004

Table C.7. Trace and major element concentrations in silicates from S01/40vilx – determined by LA-ICP-MS and electron microprobe respectively. *bulk rock majors analysed by XRF.

Concentrations	All values in ppm									
		Section S01/40vilx								
	*Bulk rock**	*Augite*	*Omph.*	*Omph.*	*Saussurite*			*Amphibole (trem-actinolite)*		
		CPX1	CPX2	CPX3	PL1	PL2	PL3	AM1	AM2	AM3
Trace elements					Data poorly calibrated					
Li	0.952	0.085	0.478	2.51	1.277	1.061	1.71	2.49	2.33	2.94
Be		0.596	0.583	0.457	0.134	0.104	0.18	0.056	0.071	0.069
B		1.38	2.43	1.2	0.748	1.02	1.11	5.12	5.24	6.32
Mg		118914	88704	72617	30373	23313	43132	83389	82336	50734
Si		234187	248210	257559	177627	177627	210348	273452	273452	273452
P		41.33	47.84	40.04	30.4	31.09	41.11	48.61	53.01	49.06
K	153.202	25.99	354.52	8.23	24.15	19.66	7.96	3193.09	3100.06	3942.85
Ca		158499	123130	105683	100952	99852	99142	23452	22865	29471
Sc	11.038	135.5	138.24	112.7	2.5	2.25	5.02	0.701	0.72	0.762
Ti	868.494	7875.6	9281.28	11654.58	188.65	169.38	342.23	155.34	152.3	173.56
V	43.325	417.05	483.37	380.08	10.05	9.43	15.75	1.84	3.84	1.71
Cr	816.847	3336.91	4221.76	3253.91	17.58	27.83	30.8	26.53	53.41	33.72
Ni	349.386	214.25	242.19	189.98	115.59	173.58	59.18	191.72	205.51	162.2
Cu	44.021	1.42	9.79	5.69	12.61	16.62	4.53	8.77	7.91	9.34
Zn	20.934	23.75	53.45	19.4	6.44	6.99	10.09	39.97	38.69	38.33
Rb	0.210	0.0104	0.1431	<0.0040	0.0087	0.0078	0.0057	10.4	10.12	12.5
Sr	369.052	22.91	82.76	4.46	387.54	484.16	233.05	14.86	14.42	17.69
Y	2.815	23.43	3.83	3.93	1.946	1.569	0.775	1.653	1.671	1.907
Zr	8.200	43.95	116.62	110.7	0.244	0.249	0.307	41.87	41.39	47.22
Nb	0.087	0.347	0.532	0.893	<0.00107	0.00126	0.009	0.499	0.499	0.58
Mo	0.065	0.1192	0.0269	0.0292	0.0183	0.0113	0.0139	0.0433	0.0423	0.047
Cs	0.008	<0.0020	0.0103	<0.0031	0.0039	<0.0031	<0.0030	0.175	0.151	0.179
Ba	7.875	1.225	60.65	0.469	1.35	1.665	1.342	89.77	84.41	96.7
La	0.547	0.919	0.0251	<0.0020	0.603	0.868	0.786	1.929	1.835	2.173
Ce	1.321	4.3	0.143	0.0096	1.816	2.529	2.162	3.48	3.16	3.85
Pr	0.214	0.928	0.0408	0.0053	0.28	0.363	0.323	0.448	0.397	0.496
Nd	1.059	6.11	0.318	0.059	1.564	1.933	1.649	1.72	1.67	1.81
Sm	0.331	2.53	0.197	0.075	0.529	0.567	0.456	0.364	0.312	0.372
Eu	0.333	0.678	0.0357	0.0082	0.408	0.415	0.28	0.069	0.079	0.089
Gd	0.426	3.59	0.395	0.229	0.636	0.544	0.523	0.229	0.297	0.343
Tb	0.079	0.624	0.0815	0.0608	0.0874	0.0851	0.0561	0.0462	0.046	0.0484
Dy	0.461	4.41	0.657	0.605	0.542	0.462	0.288	0.324	0.276	0.284
Ho	0.099	0.889	0.164	0.151	0.0813	0.0634	0.0357	0.0543	0.0538	0.0632
Er	0.254	2.55	0.469	0.499	0.142	0.108	0.055	0.165	0.167	0.191
Yb	0.228	2.34	0.489	0.6	0.038	0.0335	0.023	0.163	0.168	0.179
Lu	0.037	0.312	0.0906	0.0896	0.0068	<0.0029	<0.0023	0.0197	0.0213	0.0251
Hf	0.072	1.573	3.2	3.29	<0.0084	<0.0097	0.034	1.085	1.055	1.172
Ta	0.007	0.0176	0.0647	0.0884	<0.0023	<0.0025	<0.0029	0.0506	0.0557	0.0617
Re		<0.0021	<0.0022	<0.0029	<0.0025	<0.0028	<0.0028	<0.0039	<0.0036	<0.0032
Pb	0.221	0.0446	1.156	0.0133	0.131	0.15	0.062	2.79	2.76	3.19
Th	0.008	0.025	0.0069	<0.0059	0.0108	0.004	0.0218	0.683	0.671	0.781
U	0.009	<0.0041	0.006	<0.0051	0.002	0.0065	0.0076	0.302	0.269	0.293
Majors *(electron microprobe)*										
weight %					zoisite	zoisite	zoisite			
SiO2	47.37	51.06	55.48	55.44	38.77	39.83	39.30	55.69	53.80	54.74
TiO2	0.13	1.09	0.03	0.05	0.07	0.02	0.04	0.05	0.09	0.07
Al2O3	20.17	4.04	10.05	10.05	31.98	31.46	31.72	3.29	4.87	4.12
Cr2O3		0.50	0.39	0.24	0.02	0.00	0.01	0.03	0.00	0.01
MgO	4.57	15.31	10.61	10.74	0.20	0.62	0.41	19.99	18.59	19.26
CaO	0.07	22.87	15.15	15.28	24.43	24.01	24.27	11.86	11.04	11.46
MnO	12.32	0.09	0.00	0.01	0.01	0.00	0.00	0.12	0.13	0.13
FeO	10.87	3.08	1.57	1.35	0.63	0.67	0.65	5.11	6.35	5.73
Na2O	2.21	1.19	6.32	6.10	0.07	0.61	0.34	1.13	1.64	1.39
K2O	0.04	0.00	0.01	0.01	0.01	0.00	0.00	0.00	0.03	0.02
Total	100.35	99.34	99.63	99.31	96.19	97.22	96.76	97.30	96.56	96.94

Table C.7. contd. Trace and major element concentrations in silicates from S01/40viix – determined by LA-ICP-MS and electron microprobe respectively. *bulk rock majors analysed by XRF.

Concentrations	All values in ppm											
	Section S01/40vilx											
	Garnet									*Talc*		
	GT1	GT2	GT3	GT4	GT5	GT6	GT7	GT8	GT9	TC1	TC2	TC3
Trace elements												
Li	0.492	0.328	0.156	0.045	0.242	1.02	0.041	0.071	0.026	0.025	0.067	0.059
Be	0.044	0.019	0.0231	0.026	0.083	0.163	0.021	0.018	0.0231	<0.0056	<0.0072	0.024
B	3.5	1.64	1.72	0.79	0.51	1.34	0.79	1.59	0.92	1.22	1.43	2.04
Mg	69027	53168	70790	55003	60808	232635	48597	42903	43094	215240	228704	258430
Si	222088	171690	189340	191548	185294	416981	171747	178603	145063	290415	290415	290415
P	72.86	59.51	70.69	35.65	37.25	88.21	44.86	41.01	38.42	35.44	38.7	38.86
K	112.55	8.78	2.55	5.26	2.67	35.88	4.82	24.15	2.81	26.81	78.81	25.29
Ca	84235	61779	70477	91453	62894	56447	103667	102917	75758	68.22	556.38	179.97
Sc	21.52	7.89	2.549	24.76	3.36	8.8	1.73	11.8	21.32	0.574	0.644	0.704
Ti	512.73	428.61	260.77	253.14	260.35	142.95	321.89	289.13	223.44	80.51	66.96	401.43
V	13.78	6.68	8.27	6.11	4.44	156.68	2.85	4.23	5.96	3.58	4.51	6.19
Cr	86.16	23.23	5.52	26.62	3.68	1510.06	28.99	49.6	86.13	175.57	420.29	462.57
Ni	521.61	63.47	14.87	1.61	8.57	610.65	84.55	264.46	6.06	1083.45	1014.45	1152.26
Cu	17.78	2.69	0.344	0.0353	0.491	10.03	2.69	9.7	0.494	11.45	12.88	19.76
Zn	20.06	14.44	16.63	13.73	14.16	212.44	15.52	21.98	10.1	62.37	67.72	82.09
Rb	0.0424	<0.0039	<0.0044	<0.0043	<0.0034	<0.0110	<0.0037	0.0101	0.0049	0.0147	0.27	0.0293
Sr	1.801	4.04	23.83	0.1129	5.01	98.93	0.783	10.61	0.1469	0.163	0.537	0.276
Y	24.38	8.7	3.13	9.11	2.65	0.439	1.008	5.63	5.99	0.001	0.0334	0.0114
Zr	1.004	0.524	0.284	0.473	0.182	0.237	0.171	0.209	0.317	0.0173	0.736	0.0653
Nb	0.0017	0.00116	<0.00092	0.0038	0.001	0.0099	0.0047	<0.00080	0.005	0.0021	0.0132	0.0266
Mo	0.542	0.389	0.401	0.573	0.372	0.151	0.556	0.49	0.421	0.0113	0.0117	0.0205
Cs	<0.0045	<0.0034	<0.0036	0.0041	<0.0027	<0.0085	<0.0031	0.0033	<0.0027	0.0029	0.0103	0.0122
Ba	1.66	0.496	0.205	0.641	0.132	1.87	0.242	1.1	0.381	0.163	2.07	0.158
La	0.0016	0.0016	0.0996	0.00155	0.034	0.472	0.0015	0.0514	0.0018	0.0028	0.0329	0.0162
Ce	0.0045	0.0044	0.229	0.0037	0.0832	1.626	0.0045	0.135	0.0114	0.0015	0.092	0.0287
Pr	<0.0017	<0.00108	0.0331	0.0052	0.0112	0.269	<0.0012	0.0275	0.0064	<0.00083	0.01	0.0034
Nd	0.033	<0.0095	0.167	0.107	0.08	1.37	0.018	0.205	0.176	0.027	0.044	0.031
Sm	0.114	0.023	0.074	0.269	0.045	0.398	0.041	0.299	0.596	<0.0071	<0.0093	<0.010
Eu	0.124	0.0279	0.0641	0.353	0.0378	0.163	0.11	0.557	0.858	0.003	0.0038	<0.0028
Gd	0.744	0.222	0.28	0.583	0.176	0.387	0.119	0.485	0.938	0.013	<0.0129	0.014
Tb	0.23	0.0883	0.0846	0.133	0.0577	0.0392	0.0256	0.0689	0.126	0.0022	<0.0017	0.0046
Dy	2.79	1.003	0.732	1.24	0.553	0.167	0.174	0.643	0.939	0.0059	0.0106	<0.0074
Ho	0.898	0.308	0.125	0.329	0.097	0.0291	0.0446	0.206	0.235	<0.0022	0.0029	<0.0022
Er	3.39	1.25	0.271	1.27	0.299	0.042	0.119	0.872	0.904	<0.0047	<0.0062	<0.0070
Yb	4.26	1.71	0.17	1.69	0.354	0.046	0.099	1.32	1.66	0.01	0.014	<0.0131
Lu	0.658	0.254	0.0191	0.259	0.0346	<0.0074	0.0191	0.213	0.299	<0.0020	<0.0029	0.0079
Hf	0.021	0.0142	<0.0092	<0.0100	0.0095	0.025	<0.0082	<0.0095	0.0149	<0.0078	<0.0100	<0.0078
Ta	<0.0035	<0.0028	<0.0031	0.0046	<0.0024	0.007	0.0027	<0.0026	<0.0022	<0.0023	0.003	0.0056
Re	<0.0042	<0.0028	<0.0032	<0.0033	<0.0025	<0.0083	<0.0029	<0.0029	<0.0025	<0.0025	<0.0028	<0.0034
Pb	<0.018	<0.0124	0.0192	0.048	0.011	0.039	0.021	0.026	0.018	0.038	0.121	0.082
Th	<0.0089	<0.0074	0.0073	<0.0073	<0.0052	<0.0135	<0.0065	0.0118	<0.0045	<0.0049	0.0066	<0.0053
U	<0.0070	<0.0063	<0.0054	<0.0053	<0.0043	<0.0146	<0.0057	<0.0051	<0.0044	<0.0042	0.0056	<0.0060
Majors (electron microprobe) weight %												
SiO2	39.21	38.96	38.38	38.95	38.78	38.83	38.85	38.47	39.46	62.07	62.59	62.13
TiO2	0.03	0.02	0.08	0.03	0.09	0.04	0.04	0.03	0.08	0.02	0.00	0.00
Al2O3	22.17	22.03	21.96	22.21	22.59	22.18	22.20	22.13	21.92	0.73	0.24	0.44
Cr2O3	0.00	0.03	0.00	0.00	0.03	0.03	0.00	0.01	0.00	0.21	0.00	0.00
MgO	7.31	6.69	5.98	8.15	7.82	8.89	8.05	5.65	8.40	30.43	30.58	30.52
CaO	11.74	12.99	13.54	9.79	9.58	8.55	9.58	13.57	10.09	0.03	0.13	0.01
MnO	0.49	0.47	0.62	0.58	0.64	0.44	0.62	0.50	0.43	0.01	0.01	0.00
FeO	18.84	18.38	18.94	19.94	20.05	20.43	20.36	18.93	19.14	1.82	1.80	1.85
Na2O	0.02	0.01	0.02	0.01	0.03	0.02	0.03	0.01	0.35	0.05	0.09	0.03
K2O	0.01	0.01	0.00	0.00	0.00	0.00	0.00	0.00	0.00	0.02	0.01	0.01
Total	99.84	99.59	99.51	99.67	99.61	99.43	99.76	99.32	99.89	95.43	95.47	95.04

Table C.8. Analytical errors (1 sigma) for LA-ICP-MS determination of trace elements in silicates from sample S01/40viix. Errors calculated by GLITTER.

1 sigma error

	Section S01/40viix								
	*Bulk rock**	*Augite*	*Omph.*	*Omph.*	*Saussurite*			*Amphibole (actinolite)*	
		CPX1	CPX2	CPX3	PL1	PL2	PL3	AM1	AM2	AM3
Trace elements										
Li		0.011	0.031	0.14	0.076	0.064	0.1	0.17	0.17	0.21
Be		0.041	0.043	0.037	0.018	0.015	0.026	0.018	0.022	0.02
B		0.16	0.28	0.15	0.098	0.13	0.15	0.81	0.85	1.04
Mg		4774.1	3564.63	2929.7	1229.05	946.79	1759.06	3833.66	3825.48	2382.67
Si		7406.01	7849.55	8145.18	5617.54	5617.49	6652.48	8648.35	8648.68	8648.46
P		4.1	4.75	3.99	3.04	3.13	4.16	5.95	6.59	6.19
K		1.62	22.04	0.52	1.52	1.25	0.52	244.34	240.84	311
Ca		6735.2	5235.75	4510.4	4321.76	4290.71	4280.39	1156.18	1140.94	1485.87
Sc		5.84	5.96	4.88	0.11	0.1	0.22	0.04	0.043	0.044
Ti		355.83	419.54	528.8	8.62	7.77	15.77	8.28	8.24	9.48
V		19.34	22.44	17.73	0.47	0.45	0.75	0.1	0.22	0.1
Cr		117.23	148.45	114.77	0.67	1.03	1.15	1.11	2.18	1.41
Ni		8.15	9.23	7.28	4.45	6.7	2.31	8.38	9.09	7.25
Cu		0.084	0.57	0.33	0.74	0.98	0.27	0.64	0.59	0.71
Zn		1.04	2.32	0.86	0.3	0.32	0.47	2.04	2.01	2.01
Rb		0.0022	0.0078	0.0024	0.0025	0.0025	0.0029	0.4	0.39	0.48
Sr		0.83	2.98	0.16	14.02	17.56	8.48	0.59	0.58	0.72
Y		0.76	0.13	0.13	0.066	0.054	0.03	0.062	0.065	0.072
Zr		1.67	4.44	4.22	0.014	0.014	0.018	1.79	1.79	2.06
Nb		0.015	0.022	0.035	0.00074	0.00067	0.0019	0.025	0.027	0.029
Mo		0.0082	0.0043	0.0046	0.0037	0.0033	0.0041	0.008	0.0091	0.0084
Cs		0.0012	0.002	0.0017	0.0018	0.0017	0.0022	0.012	0.012	0.013
Ba		0.068	2.34	0.038	0.078	0.089	0.087	3.89	3.72	4.36
La		0.033	0.0029	0.0011	0.024	0.032	0.032	0.075	0.074	0.084
Ce		0.14	0.008	0.0018	0.064	0.088	0.079	0.13	0.12	0.14
Pr		0.036	0.0036	0.0013	0.013	0.016	0.016	0.024	0.023	0.027
Nd		0.26	0.026	0.012	0.062	0.095	0.093	0.11	0.12	0.12
Sm		0.12	0.021	0.014	0.04	0.04	0.042	0.044	0.046	0.047
Eu		0.03	0.0048	0.0026	0.022	0.021	0.019	0.01	0.012	0.012
Gd		0.17	0.034	0.025	0.048	0.041	0.048	0.037	0.048	0.047
Tb		0.028	0.0062	0.0053	0.0067	0.0064	0.006	0.0065	0.0074	0.0067
Dy		0.19	0.042	0.04	0.038	0.033	0.03	0.037	0.039	0.036
Ho		0.041	0.011	0.01	0.0069	0.0057	0.0051	0.0077	0.0066	0.0067
Er		0.12	0.031	0.033	0.015	0.012	0.011	0.023	0.026	0.026
Yb		0.12	0.038	0.044	0.01	0.0094	0.01	0.03	0.034	0.032
Lu		0.017	0.0076	0.0077	0.0023	0.0018	0.0016	0.0065	0.0062	0.006
Hf		0.078	0.15	0.15	0.0055	0.0059	0.01	0.081	0.087	0.068
Ta		0.0025	0.0054	0.0067	0.0014	0.0015	0.0018	0.0069	0.0062	0.0079
Re		0.002	0.0023	0.0024	0.0024	0.0027	0.0028	0.0045	0.0052	0.0044
Pb		0.0092	0.066	0.008	0.016	0.017	0.016	0.18	0.19	0.21
Th		0.005	0.0037	0.004	0.004	0.0032	0.0067	0.051	0.055	0.059
U		0.0029	0.0032	0.0031	0.0029	0.0036	0.0044	0.03	0.031	0.031

Table C.8. contd. Analytical errors (1 sigma) for LA-ICP-MS determination of trace elements in silicates from sample S01/40viix. Errors calculated by GLITTER.

1 sigma error

	Section S01/40viix											
	Garnet									*Talc*		
	GT1	GT2	GT3	GT4	GT5	GT6	GT7	GT8	GT9	TC1	TC2	TC3
Trace elements												
Li	0.036	0.026	0.017	0.016	0.025	0.072	0.018	0.018	0.011	0.018	0.018	0.023
Be	0.016	0.01	0.0088	0.012	0.025	0.044	0.013	0.011	0.0085	0.0089	0.0057	0.014
B	0.63	0.3	0.32	0.16	0.12	0.29	0.17	0.33	0.19	0.2	0.23	0.34
Mg	2687.85	2075.06	2768.17	2162.35	2399.88	9225.64	1928.79	1708.32	1721.37	9699.51	10301.09	11758.59
Si	14246.15	11079.3	12293.53	12608.12	10963.99	27879.76	11568.69	12129.77	9935.53	9185.23	9184.92	9186.38
P	6.82	5.6	6.7	3.44	3.63	8.66	4.45	4.1	3.88	4.15	4.6	4.69
K	5.28	0.43	0.16	0.28	0.18	1.79	0.28	1.22	0.17	1.97	5.86	1.92
Ca	2671.93	1959.99	2232.9	2897.74	1998.84	1799.19	3288.13	3262.97	2399.6	6.98	29.9	13.01
Sc	0.76	0.28	0.093	0.87	0.13	0.32	0.069	0.43	0.76	0.034	0.037	0.042
Ti	18.75	15.71	9.58	9.37	9.72	5.46	12.06	10.87	8.4	4.21	3.54	21.09
V	0.5	0.24	0.3	0.22	0.17	5.71	0.11	0.16	0.22	0.19	0.25	0.34
Cr	4.22	1.18	0.33	1.38	0.29	77.15	1.57	2.64	4.56	6.74	16.07	17.84
Ni	38.73	4.78	1.14	0.14	0.7	49.24	6.94	22.01	0.52	45.86	43.36	49.75
Cu	1.66	0.26	0.035	0.0097	0.054	1.03	0.28	1.03	0.055	0.8	0.91	1.42
Zn	1	0.72	0.83	0.7	0.74	10.74	0.82	1.15	0.53	3.06	3.37	4.13
Rb	0.0061	0.0029	0.0026	0.0029	0.0028	0.0068	0.0034	0.0039	0.0022	0.0046	0.016	0.0062
Sr	0.07	0.15	0.86	0.0072	0.19	3.64	0.035	0.4	0.0078	0.012	0.027	0.018
Y	1.04	0.37	0.14	0.4	0.12	0.027	0.05	0.26	0.27	0.001	0.0043	0.003
Zr	0.046	0.026	0.015	0.024	0.015	0.021	0.015	0.015	0.016	0.0048	0.041	0.0089
Nb	0.001	0.00074	0.00061	0.0013	0.0011	0.0032	0.0018	0.00075	0.0012	0.0014	0.0028	0.0047
Mo	0.033	0.024	0.023	0.032	0.027	0.02	0.037	0.032	0.024	0.0053	0.0049	0.0073
Cs	0.0031	0.0023	0.0019	0.0024	0.0024	0.0058	0.003	0.0027	0.0017	0.0028	0.0035	0.0045
Ba	0.11	0.049	0.025	0.054	0.03	0.15	0.041	0.088	0.034	0.035	0.14	0.038
La	0.0013	0.0012	0.0074	0.00099	0.0055	0.032	0.0015	0.0064	0.0011	0.0018	0.0052	0.0043
Ce	0.0019	0.0018	0.014	0.0015	0.0091	0.09	0.0023	0.012	0.0021	0.0015	0.0089	0.0058
Pr	0.0015	0.00066	0.0038	0.0016	0.003	0.024	0.0011	0.0045	0.0015	0.00074	0.0028	0.0021
Nd	0.013	0.0075	0.021	0.019	0.021	0.13	0.011	0.032	0.022	0.013	0.015	0.015
Sm	0.025	0.011	0.015	0.034	0.017	0.063	0.017	0.043	0.055	0.0058	0.0029	0.012
Eu	0.015	0.0059	0.0078	0.029	0.0083	0.023	0.015	0.047	0.065	0.0032	0.0032	0.003
Gd	0.079	0.033	0.034	0.061	0.035	0.065	0.029	0.062	0.065	0.013	0.0089	0.014
Tb	0.021	0.0095	0.0084	0.013	0.0086	0.0086	0.0054	0.0091	0.012	0.0021	0.0017	0.003
Dy	0.22	0.088	0.064	0.11	0.063	0.037	0.031	0.069	0.083	0.0079	0.0089	0.006
Ho	0.072	0.027	0.012	0.029	0.013	0.0077	0.008	0.022	0.022	0.0018	0.0025	0.0018
Er	0.26	0.1	0.028	0.11	0.039	0.019	0.022	0.085	0.081	0.0015	0.003	0.008
Yb	0.37	0.16	0.025	0.16	0.053	0.024	0.026	0.14	0.16	0.011	0.012	0.0099
Lu	0.057	0.024	0.0038	0.025	0.0075	0.0043	0.0057	0.024	0.028	0.0014	0.0026	0.0042
Hf	0.012	0.0085	0.005	0.0071	0.0095	0.018	0.0088	0.0083	0.0066	0.0079	0.0089	0.0071
Ta	0.0025	0.0016	0.0017	0.0024	0.0018	0.0049	0.0027	0.002	0.0014	0.0023	0.0025	0.0036
Re	0.0048	0.0034	0.003	0.0034	0.0041	0.0082	0.0036	0.004	0.0023	0.0041	0.0043	0.0048
Pb	0.011	0.0096	0.0098	0.013	0.011	0.026	0.014	0.013	0.0078	0.016	0.023	0.023
Th	0.0058	0.0047	0.0041	0.0046	0.0026	0.0088	0.0047	0.0066	0.0029	0.005	0.0059	0.0031
U	0.0049	0.0036	0.0035	0.0039	0.0047	0.0093	0.0053	0.0036	0.003	0.0033	0.0053	0.0041

Table C.9. Trace and major element concentrations in silicates from S01/5E – determined by LA-ICP-MS and electron microprobe respectively. *bulk rock majors analysed by XRF.

Concentrations	All values in ppm										
	Sample S01/5E										
	*Bulk rock**	*Olivine*			*Pyroxene*				*Saussurite*		
		OL1	OL2	OL3	PX1	PX2	PX3	PX4	PL1	PL2	PL3
Trace elements											
Li	2.282377	0.527	0.762	0.753	0.406	0.35	0.577	1.844	0.962	0.216	1.844
Be		0.03	<0.017	<0.021	0.23	0.236	0.515	1.487	0.176	0.063	0.123
B		1.466	1.394	0.92	1.362	1.457	1.502	1.414	0.793	0.811	0.776
Mg		356371	352404.8	357536.5	121042.8	119489.4	117842.7	107040	1750.31	549.06	1165.37
Si		186975.7	186975.7	186975.7	231382.5	231382.5	231382.5	231382.5	182301.3	182301.3	182301.3
P		60.85	72.82	77.48	65.09	57.45	61.16	57.67	38.35	56.03	48.03
K	224.9679	0.603	0.98	0.159	4.55	57.46	641.06	940.32	26.04	14.92	37.43
Ca		226.87	199.66	276.16	176823.6	179597.1	165072.3	161542.7	132214.2	150692.6	82993.83
Sc		3.87	4.24	5.68	166.45	152.17	162.02	155.57	0.562	0.51	0.577
Ti	932.55	40.29	88.27	71.02	13745.94	11963.52	12604.48	12396.89	433.81	707.66	619.14
V	24.185	1.299	2.676	1.734	557.17	540.32	540.2	516.27	1.661	1.531	1.692
Cr	118.85	11.61	13.58	12.21	8029.85	7655.97	7304.24	4589.41	0.53	0.602	0.534
Ni	442.7343	1338.83	1358.84	1290.85	187.46	174.14	196.09	158.44	1.466	0.932	3.63
Cu	98.42107	0.0049	2.582	<0.0047	0.637	0.766	4.77	2.11	1.749	0.535	2.479
Zn	32.40825	106.04	105.91	107.65	56.29	73.88	44.98	45.62	2.378	0.722	2.33
Rb	0.188793	<0.00137	<0.00120	<0.00143	0.0121	0.0191	0.0555	0.0796	0.0096	0.00631	0.00637
Sr	273.6532	0.0603	0.3	0.0825	23.47	21.92	18.44	31.48	847.52	672.71	396.16
Y	2.00883	0.0195	0.0205	0.0321	46.22	37.01	41.36	37.34	0.396	0.324	0.25
Zr	6.35	0.0525	0.0665	0.0833	111.77	77.66	103.18	107.89	0.0215	0.0106	0.0417
Nb	0.193333	0.00811	0.0179	0.0046	1.125	0.825	0.779	0.472	0.00102	0.0019	0.0036
Mo	0.100801	0.264	0.254	0.27	0.205	0.209	0.1816	0.1915	0.0233	0.0202	0.0066
Cs	0.011064	<0.00057	0.0006	<0.00056	0.00099	0.00092	0.00095	0.00112	0.00117	<0.00058	<0.00046
Ba	7.982585	0.0048	0.0907	0.0053	0.0672	0.409	2.013	11.75	5.69	1.638	2.74
La	0.6563	0.00196	0.00276	0.00159	1.375	1.21	1.457	1.049	1.579	0.983	0.751
Ce	1.568	0.00321	0.00804	0.00335	6.85	6.07	7.43	5.9	3.67	2.23	1.669
Pr	0.2197	<0.00048	0.00096	<0.00050	1.664	1.435	1.773	1.467	0.417	0.273	0.1974
Nd	1.030517	<0.0033	0.0077	<0.0033	11.58	9.98	12.26	10.29	1.623	1.126	0.827
Sm	0.293525	<0.0027	<0.0029	0.004	5	4.2	4.89	4.32	0.259	0.183	0.1517
Eu	0.3559	0.00143	<0.00080	<0.00088	1.271	1.091	1.257	1.116	0.672	0.567	0.354
Gd	0.36975	<0.0041	0.0053	<0.0039	7.27	6.08	6.94	5.9	0.173	0.1372	0.1057
Tb	0.05925	0.00079	0.00053	<0.00055	1.253	1.042	1.134	1.005	0.0187	0.0147	0.01057
Dy	0.349366	0.005	<0.0019	<0.0022	9	7.38	8.16	7.12	0.1007	0.0727	0.061
Ho	0.074389	0.00096	0.00115	0.00094	1.823	1.477	1.666	1.456	0.0141	0.01159	0.00796
Er	0.211893	0.0056	0.0026	0.0057	5.13	4.13	4.58	4.23	0.0317	0.0286	0.0236
Yb	0.206722	0.0102	0.0122	0.0267	4.69	3.85	4.08	4.13	0.0216	0.0131	0.0117
Lu	0.034888	0.00358	0.00401	0.00831	0.638	0.498	0.573	0.611	0.00247	0.00146	0.00114
Hf	0.145394	<0.0018	<0.0019	<0.0022	3.25	2.62	3.1	3.42	0.0029	<0.00177	<0.00142
Ta	0.015184	0.00066	<0.00051	<0.00053	0.1507	0.0788	0.1148	0.0942	<0.00	<0.00047	<0.00039
Re		<0.00043	<0.00040	<0.00044	0.00051	<0.00043	<0.00040	<0.00043	0.00037	<0.00041	<0.00037
Pb	0.487099	0.0102	0.023	0.0059	0.0212	0.0225	0.0298	0.399	0.496	0.353	0.1642
Th	0.006419	<0.00056	<0.00057	<0.00066	0.0744	0.1044	0.1164	0.0939	<0.00034	0.0009	0.013
U	0.003807	<0.00041	<0.00035	<0.00042	0.0188	0.0324	0.0228	0.029	<0.00026	<0.00036	0.0007
***Majors** (electron microprobe)*											
weight %											
SiO2	47.42	40.369	39.922	40.022	50.07	49.811	50.217	50.03	56.826	52.176	46.073
TiO2	0.12	0	0.005	0.013	1.646	1.703	1.27	1.54	0.014	0.066	0.025
Al2O3	20.16	0	0.004	0	4.9	4.73	4.53	4.72	26.557	31.693	29.536
Cr2O3		0.005	0	0	0.915	0.901	0.756	0.857			
MgO	5.89	45.717	44.849	45.146	15.21	15.031	15.002	15.061			
CaO	0.09	0.003	0	0	21.216	21.607	22.065	21.629	3.209	6.124	22.304
MnO	13.45	0.093	0.112	0.085	0.147	0.14	0.137	0.14			
FeO	9.41	13.536	14.274	14.037	4.4	4.574	4.471	4.482	1.278	0.567	0.525
Na2O	2.78	0.01	0.041	0	0.809	0.768	0.629	0.735	12.539	9.41	0.045
K2O	0.05	0.004	0.024	0					0.025	0.093	0.002
Total	100.11	99.737	99.262	99.313	99.338	99.293	99.091	99.241	99.45	100.139	98.51

Table C.9. contd. Trace and major element concentrations in silicates from S01/5E – determined by LA-ICP-MS and electron microprobe respectively. *bulk rock majors analysed by XRF.

Concentrations	All values in ppm							
	Sample S01/5E							
	Garnet							
	GT1	**GT2**	**GT3**	**GT4**	**GT6**	**GT7**	**GT8**	**GT9**
Trace elements								
LI	0.071	0.091	0.123	0.041	0.316	0.0813	0.296	0.613
Be	0.095	0.151	<0.019	<0.022	0.406	0.838	0.137	0.83
B	1.004	0.961	0.827	1.044	0.683	0.696	0.78	0.593
Mg	40198.05	38329.41	52828.68	56192.2	50780.46	35348.25	39235.7	49570.89
Si	186508.3	186882.2	185573.4	186975.7	186975.7	186975.7	186975.7	186975.7
P	56.65	50.49	55.86	50.68	50.48	46.55	45.59	43.4
K	1.536	1.668	38.38	8.61	2.2	1.954	10.65	4.46
Ca	138879.7	128829.8	84441.55	123446.5	109040.7	116746	106711.5	93201.91
Sc	0.544	0.623	0.586	0.717	4.91	0.539	0.595	4.69
Ti	540.31	524.24	410.59	670.9	442.92	378.51	370.88	473.36
V	1.847	2.131	1.826	11.41	2.587	0.899	1.33	3.55
Cr	1	1.44	0.77	77.34	0.94	0.9	0.84	1.19
Ni	8.92	9.11	3.23	2.88	43.86	6.47	6.1	31.07
Cu	0.11	0.1451	0.1453	0.1174	0.111	0.0692	0.1276	0.1889
Zn	20.57	62.1	21.81	18.83	946.9	113.16	98.18	403.94
Rb	<0.0017	<0.00160	0.02	0.0066	0.002	<0.00143	0.00416	0.00237
Sr	5.17	3.02	52.63	10.97	4.83	3.64	27.39	14.69
Y	0.344	0.538	0.198	0.184	3.14	0.258	0.693	1.432
Zr	0.091	0.176	0.16	0.742	0.178	0.0118	0.0427	0.198
Nb	0.0201	0.0287	0.0122	0.009	0.0505	0.0377	0.0281	0.0309
Mo	0.533	0.675	0.558	0.452	0.911	0.963	0.954	0.625
Cs	0.00156	<0.00058	0.0309	0.00822	<0.00073	<0.00056	0.00235	<0.00063
Ba	5.51	0.854	316.65	38.82	2.31	2.42	2.96	1.095
La	0.0497	0.0496	0.00859	0.00166	0.446	0.218	0.927	1.417
Ce	0.104	0.1036	0.0159	0.00238	0.908	0.468	1.974	3.48
Pr	0.0144	0.0172	0.00185	<0.00047	0.1155	0.0588	0.246	0.434
Nd	0.0966	0.1124	0.0251	<0.0035	0.59	0.318	1.095	1.95
Sm	0.1026	0.162	0.0429	0.0077	0.335	0.193	0.227	0.373
Eu	0.516	0.885	0.215	0.0262	0.661	0.712	0.758	0.389
Gd	0.186	0.296	0.0813	0.0194	0.552	0.188	0.283	0.405
Tb	0.0195	0.0263	0.00872	0.00395	0.0863	0.0184	0.0393	0.0508
Dy	0.0736	0.1176	0.0408	0.0307	0.605	0.0831	0.217	0.313
Ho	0.0142	0.0202	0.00705	0.00681	0.1274	0.00974	0.032	0.0576
Er	0.0414	0.0539	0.0115	0.025	0.365	0.0246	0.0609	0.143
Yb	0.0181	0.0423	0.0191	0.0231	0.348	0.0106	0.0216	0.149
Lu	0.00304	0.00658	0.00303	0.00268	0.0497	0.00187	0.00182	0.0184
Hf	0.0034	0.0053	0.0069	0.0061	<0.0025	0.0046	0.0035	0.0039
Ta	0.00125	0.00089	<0.00058	<0.00051	0.00118	<0.00058	<0.00059	<0.00058
Re	<0.00056	0.00062	<0.00049	<0.00052	<0.00056	0.00045	<0.00045	0.00084
Pb	0.1417	0.0283	2.64	1.272	0.0374	0.043	0.0495	0.0241
Th	<0.00059	0.00237	<0.00052	<0.00046	0.00077	<0.00062	<0.00068	0.00068
U	0.00163	<0.00038	<0.00045	<0.00044	<0.00054	<0.00039	0.00113	0.00103
Majors *(electron microprobe)*								
weight %								
SiO2	40.4	40.807	38.818	38.508	39.387	39.847	38.244	39.25
TiO2	0.037	0.096	0.06	0.074	0.044	0.052	0.05	0.023
Al2O3	22.075	21.021	21.726	22.067	21.511	22.505	22.63	22.095
Cr2O3	0	0	0.015	0.007	0			
MgO	7.896	5.544	5.008	4.788	5.731	7.072	4.094	5.26
CaO	12.208	14.391	12.436	11.845	13.865	12.977	9.144	14.941
MnO	0.383	0.212	0.397	0.431	0.542	0.641	0.748	0.603
FeO	17.436	17.584	21.036	22.09	18.249	18.548	26.274	18.751
Na2O	0.021	0.611	0.03	0.023	0.012			
K2O	0	0	0	0	0.005			
Total	100.525	100.336	99.548	99.866	99.378	101.642	101.184	100.923

Table C.9. contd. Trace and major element concentrations in silicates from S01/5E – determined by LA-ICP-MS and electron microprobe respectively. *bulk rock majors analysed by XRF.

Concentrations	All values in ppm								
	Sample S01/5E								
	Ex-Olivine - chlorite and enstatite						***Olivine corona - chlorite***		
	EXOL1	**EXOL2**	**EXOL3**	**EXOL4**	**EXOL5**	**EXOL6**	**OLCOR**	**OLCOR**	**OLCOR**
Trace elements									
Li	0.528	0.0969	<0.0110	<0.0092	0.1111	0.322	0.0151	0.0201	0.0778
Be	<0.0170	0.0134	<0.0167	0.0276	0.0218	<0.0161	0.047	0.026	0.026
B	0.834	0.715	1.336	1.87	1.34	3.45	1.37	2.23	5.5
Mg	225753.1	154509.7	197907.7	143012.4	138649.2	206571	148260.2	237564.4	215309.9
Si	140231.8	140231.8	140231.8	140231.8	140231.8	140231.8	142569	142569	142569
P	50.11	37.75	37.57	39.35	30.77	42.63	33.84	39.93	38.99
K	7.76	5.58	49.5	7.34	26.09	29.27	14.88	87.42	352.75
Ca	115.9	159.88	338.56	241.45	227.04	286.18	476.06	734.64	1693.93
Sc	2.069	2.55	5.86	3.39	3.91	2.43	6.34	7.38	7.72
Ti	93.06	65.35	56.45	245.58	62.12	54.15	2729.97	339.42	90.08
V	0.792	2.61	27.38	12.44	2.96	2.5	37.01	84.73	28.26
Cr	2.38	11.78	51.01	20.03	7.45	8.51	697.57	592.66	172.19
Ni	2136.35	365.18	600.35	193.73	163.53	730.21	420.99	874.29	717.97
Cu	131.04	1.984	0.251	0.312	1.629	0.613	15.28	1.251	0.279
Zn	52.17	37.58	33.51	37.91	35.32	45.41	41.73	35.98	34.8
Rb	0.00486	0.0082	0.0489	0.00713	0.034	0.0452	0.0284	0.1391	0.486
Sr	7.68	0.765	0.498	0.893	0.523	0.654	0.825	0.328	0.885
Y	0.188	0.188	0.318	0.0881	0.144	0.0896	0.495	0.1024	0.222
Zr	0.1404	0.1181	0.223	0.0766	0.0907	0.068	0.954	0.444	0.289
Nb	0.0459	0.0191	0.0444	0.0218	0.0212	0.0227	0.1693	0.0282	0.026
Mo	0.1052	0.0641	0.0348	0.0649	0.0694	0.0822	0.0784	0.022	0.0262
Cs	<0.00044	<0.00029	0.00687	0.00037	0.0024	0.00079	0.00214	0.024	0.0686
Ba	56.42	0.395	0.868	0.324	0.418	0.686	0.647	2.63	13.87
La	0.0397	0.0372	0.0633	0.0215	0.0222	0.0181	0.0941	0.0124	0.0316
Ce	0.1287	0.1043	0.1722	0.0513	0.0726	0.0461	0.237	0.0469	0.0891
Pr	0.0179	0.01634	0.022	0.00566	0.01113	0.00611	0.0318	0.00585	0.01148
Nd	0.1118	0.0944	0.1152	0.0362	0.0659	0.0296	0.169	0.0255	0.0529
Sm	0.0261	0.0243	0.0266	0.0063	0.0226	0.0076	0.0612	0.0076	0.0153
Eu	0.0129	0.00975	0.0169	0.00402	0.00758	0.00364	0.0217	0.00316	0.00713
Gd	0.0439	0.0341	0.0451	0.015	0.0234	0.013	0.0659	0.014	0.0217
Tb	0.00564	0.00563	0.00769	0.00208	0.00439	0.00201	0.01095	0.00152	0.00467
Dy	0.0331	0.0322	0.0563	0.0167	0.0226	0.0126	0.0851	0.0121	0.0328
Ho	0.00733	0.00853	0.01058	0.00302	0.00546	0.00308	0.0172	0.0033	0.00673
Er	0.022	0.021	0.0398	0.0087	0.0168	0.0122	0.0603	0.0097	0.0292
Yb	0.021	0.02	0.0467	0.018	0.0168	0.0113	0.0818	0.0202	0.043
Lu	0.00428	0.00507	0.00937	0.00286	0.00255	0.00278	0.0144	0.00477	0.00697
Hf	0.004	0.00353	0.0069	0.00404	0.00144	<0.00130	0.0326	0.0132	0.0133
Ta	0.00106	0.0006	0.00254	0.00166	0.00121	0.00125	0.0121	0.00094	0.00282
Re	0.00089	<0.00024	0.00046	<0.00025	<0.00020	0.00043	<0.00025	<0.00033	<0.00031
Pb	0.849	0.0501	0.0172	0.017	0.0386	0.0465	0.0388	0.0183	0.0294
Th	0.0008	0.00048	0.00072	<0.00030	0.00101	0.00062	0.01061	<0.00049	0.00215
U	0.00065	0.00068	0.00102	0.00049	0.00107	<0.00027	0.00176	0.00038	0.00141
Majors *(electron microprobe)*									
weight %									
SiO2	31.44	56.499	35.402	57.318	57.994	35.402	57.671	31.945	32.258
TiO2	0	0	0.001	0.009	0	0.001	0.005	0.015	0.032
Al2O3	19.31	0.085	16.172	0.065	0.151	16.172	0.04	19.006	19.136
Cr2O3	0.015	0.008	0.024	0	0.008	0.024	0	0.013	0
MgO	30.832	32.421	30.789	31.685	33.716	30.789	33.222	31.411	31.3
CaO	0.004	0.067	0.197	0.059	0.049	0.197	0.048	0.009	0.02
MnO	0.014	0.096	0.011	0.267	0.07	0.011	0.075	0.01	0.005
FeO	3.689	10.077	4.777	10.07	8.327	4.777	8.615	3.684	3.837
Na2O	0.024	0.002	0.048	0.014	0.007	0.048	0.026	0.021	0.008
K2O	0.033	0	0.098	0	0.002	0.098	0.014	0.012	0.016
Total	85.403	99.31	87.611	99.505	100.348	87.611	99.755	86.264	86.736

Table C.10. Analytical errors (1 sigma) for LA-ICP-MS determination of trace elements in silicates from sample S01/5E. Errors calculated by GLITTER.

1 sigma error

	Sample S01/5E									
	*Bulk rock**	*Olivine*			*Pyroxene*				*Saussurite*		
		OL1	OL2	OL3	PX1	PX2	PX3	PX4	PL1	PL2	PL3
Trace elements											
Li		0.021	0.028	0.029	0.017	0.015	0.022	0.062	0.039	0.012	0.063
Be		0.012	0.011	0.012	0.023	0.023	0.038	0.095	0.028	0.014	0.016
B		0.086	0.085	0.066	0.082	0.085	0.088	0.084	0.071	0.059	0.056
Mg		14000.9	13875.94	14120.81	4798.88	4759.19	4718.89	4312.58	71.62	22.65	48.47
Si		5912.98	5913.02	5913.06	7317.23	7317.2	7317.21	7317.2	5765.6	5765.14	5765.12
P		4.11	4.93	5.28	4.46	3.97	4.27	4.07	2.76	4.04	3.58
K		0.051	0.059	0.052	0.18	2.19	24.53	36.16	1.02	0.59	1.48
Ca		9.11	8.26	11.14	6317.72	6432.53	5930.35	5824.36	4810.47	5508.68	3061.04
Sc		0.15	0.17	0.23	6.55	6.01	6.43	6.2	0.026	0.022	0.025
Ti		1.42	3.08	2.49	476.2	415.29	438.64	432.66	15.31	25	21.98
V		0.047	0.095	0.062	19.56	19.02	19.07	18.28	0.063	0.056	0.062
Cr		0.42	0.49	0.45	273.91	261.74	250.38	157.8	0.11	0.094	0.081
Ni		47.82	48.6	46.25	6.74	6.28	7.09	5.75	0.067	0.04	0.14
Cu		0.0025	0.087	0.0028	0.023	0.027	0.16	0.072	0.063	0.02	0.086
Zn		3.6	3.6	3.66	1.92	2.52	1.54	1.57	0.098	0.033	0.087
Rb		0.00078	0.00074	0.00084	0.0012	0.0015	0.0029	0.0039	0.0016	0.00093	0.00091
Sr		0.0033	0.014	0.0044	1.01	0.94	0.8	1.37	37.38	29.91	17.77
Y		0.0017	0.0018	0.0025	2.41	1.94	2.18	1.98	0.023	0.018	0.014
Zr		0.0038	0.0047	0.0057	5.56	3.88	5.19	5.46	0.0031	0.0015	0.0032
Nb		0.00096	0.0015	0.00082	0.049	0.036	0.034	0.021	0.00064	0.00057	0.00058
Mo		0.013	0.012	0.013	0.01	0.01	0.0091	0.0095	0.0035	0.0024	0.0017
Cs		0.0003	0.00033	0.00028	0.00036	0.00032	0.00031	0.0003	0.00046	0.00028	0.00022
Ba		0.0029	0.0079	0.0033	0.0061	0.021	0.09	0.51	0.26	0.076	0.13
La		0.00044	0.00054	0.00048	0.066	0.058	0.07	0.051	0.078	0.049	0.038
Ce		0.00051	0.00076	0.00054	0.3	0.26	0.33	0.26	0.16	0.1	0.076
Pr		0.00029	0.00036	0.00034	0.067	0.058	0.072	0.06	0.018	0.012	0.0087
Nd		0.002	0.0021	0.0021	0.52	0.45	0.56	0.47	0.082	0.055	0.041
Sm		0.0014	0.0015	0.0024	0.23	0.19	0.23	0.2	0.018	0.011	0.0095
Eu		0.00054	0.00044	0.00048	0.055	0.047	0.055	0.049	0.031	0.026	0.016
Gd		0.002	0.0024	0.0023	0.37	0.31	0.36	0.31	0.015	0.0095	0.0078
Tb		0.00032	0.00033	0.0003	0.061	0.051	0.056	0.05	0.0017	0.0011	0.00086
Dy		0.0015	0.0013	0.0014	0.47	0.38	0.43	0.38	0.0088	0.0054	0.0046
Ho		0.00036	0.00039	0.00038	0.091	0.074	0.084	0.074	0.0015	0.00095	0.00073
Er		0.0012	0.0011	0.0014	0.27	0.22	0.24	0.22	0.0038	0.0025	0.0022
Yb		0.0021	0.0023	0.0032	0.24	0.19	0.21	0.22	0.0038	0.0021	0.0019
Lu		0.00054	0.00063	0.00091	0.035	0.027	0.032	0.034	0.00065	0.00039	0.00037
Hf		0.001	0.001	0.0014	0.18	0.15	0.17	0.19	0.0014	0.00076	0.00071
Ta		0.00029	0.0003	0.00032	0.0082	0.0044	0.0063	0.0053	<0.00	0.00026	0.00021
Re		0.00024	0.00025	0.00028	0.00024	0.00022	0.00021	0.00023	0.00027	0.00023	0.00021
Pb		0.0017	0.0022	0.0018	0.002	0.002	0.0023	0.018	0.023	0.016	0.008
Th		0.00032	0.00032	0.00038	0.0042	0.0057	0.0063	0.0052	0.00035	0.00034	0.001
U		0.00024	0.00022	0.00023	0.0012	0.0017	0.0013	0.0016	0.00026	0.00021	0.0002

Table C.10 contd. Analytical errors (1 sigma) for LA-ICP-MS determination of trace elements in silicates from sample S01/5E. Errors calculated by GLITTER.

1 sigma error	Sample S01/5E							
	Garnet							
	GT1	GT2	GT3	GT4	GT6	GT7	GT8	GT9
Li	0.013	0.011	0.012	0.012	0.017	0.01	0.015	0.026
Be	0.022	0.022	0.012	0.014	0.038	0.064	0.02	0.068
B	0.085	0.072	0.068	0.083	0.063	0.059	0.063	0.058
Mg	1686.85	1624.46	2262.49	2433.05	2250.34	1585.7	1782.32	2281.01
Si	5898.49	5910.08	5868.72	5913.19	5913.03	5912.97	5912.96	5913.05
P	4.3	3.89	4.38	4.05	4.18	3.93	3.93	3.81
K	0.092	0.085	1.55	0.36	0.11	0.096	0.46	0.2
Ca	5136.6	4794.57	3164.25	4658.58	4177.14	4507.87	4154.5	3659.76
Sc	0.026	0.028	0.027	0.033	0.21	0.025	0.028	0.21
Ti	19.31	18.81	14.83	24.36	16.29	14.01	13.83	17.78
V	0.069	0.079	0.069	0.42	0.098	0.035	0.052	0.14
Cr	0.15	0.13	0.12	2.79	0.13	0.11	0.11	0.12
Ni	0.34	0.35	0.13	0.12	1.71	0.26	0.25	1.24
Cu	0.0073	0.0073	0.0075	0.0071	0.0064	0.0046	0.0063	0.0089
Zn	0.73	2.18	0.78	0.68	33.94	4.09	3.57	14.76
Rb	0.0011	0.00087	0.0018	0.0013	0.00093	0.00076	0.0009	0.00097
Sr	0.24	0.14	2.43	0.51	0.23	0.18	1.34	0.73
Y	0.02	0.031	0.012	0.012	0.19	0.016	0.043	0.09
Zr	0.007	0.011	0.01	0.043	0.011	0.0016	0.0034	0.013
Nb	0.002	0.0021	0.0013	0.0012	0.0031	0.0024	0.0019	0.0022
Mo	0.027	0.032	0.027	0.023	0.045	0.047	0.047	0.032
Cs	0.00059	0.00034	0.0018	0.00092	0.00036	0.00031	0.0004	0.00034
Ba	0.26	0.044	14.53	1.81	0.11	0.12	0.15	0.058
La	0.0034	0.0031	0.00092	0.00052	0.024	0.012	0.051	0.079
Ce	0.0057	0.0053	0.0012	0.00058	0.044	0.023	0.098	0.18
Pr	0.0013	0.0012	0.00042	0.00033	0.0056	0.003	0.012	0.02
Nd	0.0085	0.008	0.0036	0.0019	0.032	0.018	0.059	0.1
Sm	0.0094	0.011	0.0051	0.0026	0.02	0.012	0.014	0.023
Eu	0.025	0.041	0.011	0.0022	0.032	0.035	0.037	0.02
Gd	0.015	0.019	0.0074	0.0039	0.035	0.013	0.019	0.027
Tb	0.0017	0.0018	0.00088	0.00066	0.0051	0.0013	0.0025	0.0033
Dy	0.0068	0.0084	0.004	0.0037	0.037	0.0063	0.014	0.021
Ho	0.0014	0.0015	0.00081	0.0009	0.0076	0.0009	0.0022	0.0038
Er	0.0042	0.0043	0.0018	0.003	0.023	0.0024	0.0047	0.01
Yb	0.0035	0.0041	0.0028	0.0035	0.022	0.0019	0.0026	0.011
Lu	0.00067	0.00079	0.00056	0.00062	0.0035	0.00038	0.00037	0.0016
Hf	0.0016	0.0014	0.0015	0.002	0.0013	0.0011	0.0011	0.0015
Ta	0.00046	0.00035	0.00035	0.0003	0.00039	0.00029	0.0003	0.00034
Re	0.00038	0.00027	0.00028	0.00033	0.00028	0.00024	0.00023	0.00029
Pb	0.008	0.0026	0.12	0.059	0.003	0.003	0.0032	0.0024
Th	0.0003	0.00052	0.00027	0.00026	0.00038	0.00032	0.00034	0.00039
U	0.00044	0.00023	0.00028	0.0003	0.00028	0.0002	0.00029	0.0003

Table C.10 contd. Analytical errors (1 sigma) for LA-ICP-MS determination of trace elements in silicates from sample S01/5E. Errors calculated by GLITTER.

	1 sigma error								
	Sample S01/5E								
	Ex-Olivine - chlorite and enstatite						*Olivine corona - chlorite*		
	EXOL1	EXOL2	EXOL3	EXOL4	EXOL5	EXOL6	OLCOR	OLCOR	OLCOR
Li	0.021	0.0064	0.0062	0.0049	0.0065	0.014	0.0055	0.0074	0.0073
Be	0.0096	0.0075	0.0096	0.0082	0.007	0.0088	0.011	0.011	0.01
B	0.066	0.053	0.094	0.13	0.094	0.24	0.1	0.17	0.39
Mg	10668	7401.82	9613.28	7045.07	6927.89	10470.9	7624.66	12396.51	11400.76
Si	4434.78	4434.68	4434.74	4434.69	4434.67	4434.71	4508.64	4508.73	4508.64
P	4.58	3.52	3.57	3.81	3.04	4.3	3.48	4.19	4.17
K	0.34	0.25	2.22	0.34	1.2	1.36	0.7	4.17	17.03
Ca	5.53	6.94	14.43	10.4	9.83	12.51	20.7	32.17	73.57
Sc	0.096	0.12	0.28	0.16	0.19	0.12	0.31	0.37	0.39
Ti	3.56	2.52	2.2	9.58	2.45	2.16	109.1	13.7	3.68
V	0.032	0.1	1.09	0.5	0.12	0.1	1.52	3.51	1.18
Cr	0.17	0.46	1.96	0.78	0.3	0.35	27.54	23.61	6.93
Ni	86.83	14.99	24.9	8.12	6.93	31.26	18.22	38.25	31.76
Cu	4.68	0.072	0.01	0.012	0.061	0.024	0.57	0.048	0.012
Zn	1.94	1.4	1.26	1.44	1.35	1.75	1.62	1.41	1.37
Rb	0.00084	0.00075	0.0028	0.00076	0.002	0.0026	0.0019	0.0076	0.025
Sr	0.39	0.04	0.026	0.048	0.028	0.036	0.046	0.019	0.05
Y	0.013	0.013	0.022	0.0062	0.01	0.0065	0.035	0.0078	0.017
Zr	0.0095	0.0079	0.015	0.0054	0.0063	0.0051	0.064	0.031	0.02
Nb	0.0029	0.0013	0.0028	0.0015	0.0014	0.0016	0.0097	0.0021	0.002
Mo	0.0064	0.004	0.0028	0.0041	0.0043	0.0052	0.0051	0.0024	0.0024
Cs	0.00026	0.00018	0.00057	0.00021	0.00028	0.00022	0.00033	0.0015	0.0045
Ba	2.85	0.022	0.048	0.019	0.024	0.039	0.038	0.15	0.78
La	0.0026	0.0024	0.004	0.0015	0.0015	0.0014	0.0061	0.0011	0.0023
Ce	0.007	0.0057	0.0094	0.003	0.0041	0.0028	0.014	0.003	0.0054
Pr	0.0012	0.00098	0.0013	0.00047	0.00072	0.00051	0.0019	0.00059	0.00083
Nd	0.0078	0.0063	0.0079	0.0031	0.0048	0.0029	0.011	0.0031	0.0045
Sm	0.0032	0.0025	0.003	0.0015	0.0024	0.0017	0.0051	0.0022	0.0024
Eu	0.0011	0.00083	0.0013	0.00053	0.00069	0.00052	0.0016	0.00061	0.00077
Gd	0.0045	0.0033	0.0045	0.0021	0.0025	0.0021	0.0059	0.0026	0.0029
Tb	0.0006	0.00052	0.0007	0.00029	0.00042	0.0003	0.00092	0.00035	0.00051
Dy	0.0033	0.0028	0.0047	0.0018	0.0022	0.0016	0.0068	0.0019	0.0032
Ho	0.00073	0.00071	0.00091	0.00036	0.00051	0.00039	0.0014	0.00052	0.00069
Er	0.0022	0.0019	0.0033	0.0011	0.0016	0.0014	0.0048	0.0015	0.0027
Yb	0.0025	0.002	0.0041	0.0019	0.0018	0.0016	0.0066	0.0026	0.004
Lu	0.00056	0.00051	0.00088	0.00038	0.00033	0.00038	0.0013	0.00063	0.00087
Hf	0.001	0.00079	0.0013	0.00075	0.00065	0.00072	0.0031	0.0019	0.0017
Ta	0.00026	0.00018	0.00035	0.00024	0.0002	0.00023	0.001	0.00029	0.00036
Re	0.00022	0.00013	0.00018	0.00013	0.00011	0.00015	0.00015	0.0002	0.00016
Pb	0.043	0.003	0.0016	0.0014	0.0024	0.003	0.0026	0.0019	0.0022
Th	0.00028	0.00021	0.00033	0.00017	0.00023	0.00024	0.00095	0.00031	0.00036
U	0.00021	0.00018	0.00021	0.00016	0.00017	0.00016	0.00026	0.00022	0.00025

Table C.11. Trace and major element concentrations in silicates from S02/75iiiC - determined by LA-ICP-MS and electron microprobe respectively. *bulk rock majors analysed by XRF.

Concentrations	All values are reported in ppm											
	Sample S02/75iiiC											
	*Bulk rock**	*Garnet*										
		Gt1	Gt2	Gt3	Gt4	Gt5	Gt6	Gt7	Gt8	Gt9	Gt10	Gt11	Gt12
Trace Elements													
Li	20.96	2.5	1.061	6.46	1.389	3.07	0.684	0.593	0.684	1.079	0.674	0.877	0.442
Be		0.027	<0.017	0.233	0.064	0.033	<0.0203	0.016	<0.018	<0.0161	<0.021	<0.0166	<0.0166
B		1.3	2.14	2.19	1.63	1.28	1.37	1.25	1.22	1.4	1.17	1.25	1.16
Mg		28404.28	19935.38	15912.02	14000.1	32316.19	24938.65	17618.93	12918.26	11359.35	11024.66	15189.67	24726.58
Si		184091.6	179651	172013	179651	184091.6	173556.6	171657.8	170634.1	170003	183381.1	171821.4	172336.6
P		46.53	179.06	94.67	145.06	47.12	48.48	101.24	59.62	55.44	1932.8	48.37	41.62
K	903.69	500.27	169.44	198.13	33.7	588.01	28.13	14.44	2.83	71.21	17.63	30.9	<0.29
Ca		47304.29	54145.71	48841.73	63544.31	46792.02	45583.42	48436.43	59549.81	66289.56	90268.51	54486.53	45619.32
Sc	12.29	103.97	89.42	47.49	40.93	83.31	89.96	53.94	24.33	16.97	21.32	45.59	86.13
Ti	12850.00	247.54	3612.17	439.95	754.51	3329.3	250.55	12156.76	915.12	2404.47	1958.47	577.13	259.99
V	236.05	38	100	99.72	78.77	42.2	36.96	68.45	75.46	74.22	70.66	69.02	37.07
Cr	123.60	70.79	168.46	125.56	120.63	74.42	82.15	98.22	107.23	115.64	121.84	95.1	92.54
Ni	73.14	0.55	0.721	116.1	5.7	0.898	0.407	0.62	1.139	1.029	0.853	0.951	0.387
Cu	48.92	3.02	8.08	1456.85	81.35	8.2	0.375	1.828	8.17	7.71	21.37	1.089	0.101
Zn	75.48	64.74	54.7	62.64	46.66	64.8	54.89	53.45	36.39	31.69	30.23	39.6	54.94
Rb	2.28	1.186	0.222	0.388	0.148	0.72	0.106	0.0371	0.0451	0.142	0.0645	0.1007	0.0284
Sr	200.82	1.306	2.7	8.15	1.303	1.52	0.0457	0.413	27.15	0.821	23.02	0.1048	0.025
Y	53.70	246.63	314.72	178.4	299.67	191.06	260	260.19	143.61	61.56	136.75	219.41	262.17
Zr	280.51	48.11	151.01	87.47	395.56	26.88	73.01	45.58	77.71	374.17	67.77	64.67	10.89
Nb	8.14	0.0052	1.4	0.0572	0.0454	1.56	0.0062	6.4	0.192	0.887	0.475	0.0425	0.0222
Mo	0.31	0.1249	0.233	8.16	0.709	0.182	0.1243	0.275	0.449	0.892	1.382	0.299	0.1261
Cs	0.12	0.0426	0.0292	0.0853	0.0151	0.0315	0.0039	0.00216	0.00202	0.007	0.0113	<0.00094	<0.00104
Ba	12.76	3.64	0.707	54.51	3.03	5.7	0.0534	0.0491	0.41	2.02	0.479	0.194	0.0238
La	10.69	<0.00083	0.304	0.0317	0.0039	0.00203	<0.00072	<0.00088	1.177	0.0083	0.0616	0.00099	<0.00103
Ce	29.80	<0.00102	0.962	0.105	0.0264	0.0068	0.00197	0.00542	3.8	0.0695	0.232	0.00247	0.00233
Pr	4.60	<0.00079	0.159	0.0115	0.0055	0.00334	<0.00074	0.00101	0.574	0.00557	0.0355	0.00174	0.00111
Nd	22.28	0.0512	0.764	0.093	0.0428	0.068	0.0338	0.0131	2.96	0.0537	0.21	0.0229	0.0255
Sm	6.59	0.565	0.434	0.106	0.126	0.759	0.418	0.129	0.977	0.0478	0.087	0.145	0.417
Eu	2.08	0.892	0.314	0.1063	0.137	1.148	0.639	0.161	0.358	0.032	0.0455	0.15	0.636
Gd	8.23	9.67	3.67	1.55	1.95	12	7.08	1.97	2.39	0.406	0.483	2.09	7.3
Tb	1.36	5.44	2.3	0.931	1.29	5.83	4.32	1.46	0.979	0.246	0.249	1.25	4.51
Dy	8.12	53.75	37.42	15.76	23.39	46.21	49.47	25.93	13.5	4.06	5.87	20.31	50.64
Ho	1.81	10.05	11.32	5.92	9.75	7.44	10.25	9.17	4.67	1.75	3.88	7.38	10.49
Er	5.28	24.63	33.05	25.09	48.45	16.94	26.55	36.44	20.89	10.97	33.93	33.11	26.42
Yb	4.92	18.67	21.69	32.17	89.57	13.14	19.04	41.87	37.21	39.47	173.54	49.12	17 8
Lu	0.78	2.57	2.34	4.2	12.43	1.88	2.38	5.24	5.16	6.33	30.06	6.99	2.11
Hf	5.44	1.001	3.29	1.81	8	0.565	1.54	1.011	1.67	8.33	1.31	1.28	0.216
Ta	0.65	0.00164	0.0915	0.00145	0.00317	0.0924	0.00043	0.385	0.0103	0.0488	0.029	0.00201	0.00198
Re		0.00057	0.00098	0.00084	0.0004	<0.00033	0.00121	<0.00029	0.0015	<0.00029	0.0012	0.00087	<0.00034
Pb	1.28	0.0154	0.0616	1.91	0.0762	0.0348	<0.0035	0.0239	0.268	0.0181	0.0709	0.0061	0.0086
Th	0.48	0.00088	0.0283	0.0083	0.0069	<0.00091	0.00107	0.00134	0.0665	0.0145	0.0138	0.00422	0.00233
U	0.25	0.00484	0.0259	0.0156	0.0226	0.0042	0.00667	0.00426	0.0447	0.0245	0.0117	0.00534	0.00206
Majors (electron microprobe) weight %													
SiO2	50.70751	36.80	39.27	39.81	38.21	36.54	38.57	38.60	39.02	39.19	38.43	38.40	39.36
TiO2	2.15	4.14	0.17	0.05	0.03	0.08	0.06	0.03	0.04	0.02	0.07	0.06	0.03
Al2O3	16.55	20.10	20.26	21.80	21.06	20.92	21.18	21.17	21.33	21.61	21.05	21.19	21.66
Cr2O3		0.03	0.00	0.01	0.00	0.02	0.00	0.02	0.00	0.03	0.01	0.02	0.03
MgO	9.72	2.31	2.40	2.67	2.91	3.02	3.97	4.32	5.48	6.36	3.11	3.31	6.70
CaO	0.17	8.21	7.76	7.09	7.51	7.88	6.70	6.96	6.44	6.06	7.19	6.93	5.80
MnO	5.63	1.68	1.88	1.62	1.50	1.20	1.06	0.89	0.45	0.40	1.06	0.94	0.37
FeO	7.83	27.21	26.64	26.85	29.50	29.06	29.41	29.10	28.12	27.35	30.06	30.17	27.23
Na2O	5.39	0.01	0.93	0.67	0.01	0.04	0.03	0.04	0.03	0.00	0.02	0.02	0.02
K2O	0.22	0.00	0.02	0.05	0.00	0.00	0.01	0.00	0.00	0.00	0.00	0.00	0.00
Total	99.73	100.48	99.34	100.62	100.74	100.78	100.98	100.82	100.92	101.01	101.00	101.03	101.22

Table C.11. contd. Trace and major element concentrations in silicates from S02/75iiiC – determined by LA-ICP-MS and electron microprobe respectively. *bulk rock majors analysed by XRF.

Concentrations

	Sample S02/75IIIC											
	Omphacite				***Am + Rut Amph***		***Paragonite***				***Epidote/Zoisite***	
	Om1	**Om2**	**Om3**	**Om4**	**Am1**	**Am2**	**Mc1**	**Mc2**	**Mc3**	**Mc4**	**Ep1**	**Ep2**
Trace Elements												
Li	50.12	52.15	65.58	59.32	6.76	8.68	10.23	13.28	13.79	15.13	1.48	1.64
Be	1.73	2.1	1.76	1.52	1.1	1.01	6.98	5.27	7.29	7.39	0.061	0.071
B	2	2.19	4.41	4.26	3.09	1.88	15.74	12.21	25.45	17.68	3.76	2.06
Mg	45801	39376.6	42694.5	43538.6	34091.1	38089.2	1304.69	3383.39	2562.48	2091.63	1347.01	1106.7
Si	268441	267782	267913	267862	228358	228358	214330	217303	223530	222763	181479	181479
P	36.22	34.87	50.19	267.59	71.53	33.83	50.73	47.22	35.2	60.42	105.71	88.68
K	121.77	166.24	85.82	148.67	557.49	421.74	7563.64	6047.92	4906.41	6789.7	25.76	167.04
Ca	86026.3	79191.3	84859.8	91924.1	68368.4	53713.3	2968.65	6700.95	4876.35	2994.55	184292	179063
Sc	29.5	31.83	24.17	26.14	24.17	20.84	0.556	1.58	1.127	1.109	53.97	41.74
Ti	332.01	333.58	333.61	15382.2	747536	1399.04	402.55	373.87	405.21	409.16	629.96	561.82
V	457.75	475.98	403.08	450.67	1262.54	290.42	83.11	100.68	101.03	93.06	553.74	486.68
Cr	82.03	28.68	182.59	198.73	480.78	128.81	100.34	103.49	131.46	79.5	136.03	139.62
Ni	72.44	42.06	60.28	63.08	88.51	71.33	2.41	7	3.17	7.94	1.345	1.82
Cu	21.43	10.14	10.29	24.32	18.11	18.01	1.515	11.12	2.54	6.55	2.37	2.94
Zn	113.53	83.94	93	104	94.91	95.27	1.75	12.73	5.81	6.04	10.14	8.82
Rb	0.0656	0.297	0.124	0.134	0.127	0.1106	2.94	1.94	0.603	6.34	0.0791	0.257
Sr	9.23	3.58	13.33	11.88	11.32	6.91	1352.6	883.19	844.33	1304.3	1708.48	1247.28
Y	0.33	0.288	0.464	1.39	8.91	0.96	0.0356	0.0296	0.132	0.0069	87.5	60.67
Zr	0.728	0.611	54.21	85.53	3359.53	38.61	18.85	3.24	90.44	0.105	2.92	2.02
Nb	0.0034	<0.0024	0.022	6.77	321.64	0.629	0.0151	<0.0029	0.034	0.0084	0.0096	<0.0019
Mo	0.0084	0.013	<0.0043	0.144	7.86	0.0266	<0.0143	<0.0056	<0.0072	0.0122	0.0148	0.0193
Cs	0.0059	0.0126	0.0063	0.0167	0.0117	0.007	0.0378	0.0543	0.0125	0.0967	0.0017	0.0036
Ba	1.41	2.57	1.05	1.45	3.95	3.04	23.59	16.83	****	26.93	1.54	2.45
La	<0.0014	0.0031	0.0042	0.0375	1.042	0.0467	0.00027	0.0019	<0.0018	<0.0016	52.28	29.67
Ce	<0.00106	0.00199	0.014	0.237	4.47	0.15	0.0027	<0.0016	0.0019	0.0037	161.36	96.04
Pr	0.00179	0.00129	0.00232	0.0437	0.864	0.0214	0.00149	0.0028	<0.00113	<0.0015	24.56	14.03
Nd	<0.0041	<0.0049	0.0222	0.216	4.03	0.171	0.0074	0.0132	0.0158	0.0145	122.9	69.27
Sm	<0.0062	<0.0063	0.0287	0.087	1.07	0.131	<0.0153	<0.0069	<0.0104	<0.0100	38.76	22.01
Eu	0.0089	<0.00132	0.0149	0.112	1.36	0.0353	<0.0047	<0.0018	0.0101	0.0035	14.12	8.56
Gd	0.066	<0.0062	0.085	0.145	1.87	0.144	<0.0182	<0.0069	<0.0076	<0.0060	42.8	24.79
Tb	0.012	0.0061	0.0201	0.0374	0.276	0.0336	<0.0037	<0.0012	0.0021	<0.00135	4.94	3
Dy	0.0596	0.0425	0.097	0.197	1.61	0.194	<0.0169	0.0053	<0.0061	<0.0059	20.75	13.52
Ho	0.0104	0.0104	0.0206	0.0469	0.304	0.0385	<0.0042	0.0027	0.0047	<0.00159	3.28	2.36
Er	0.0258	0.0419	0.0647	0.197	1.25	0.11	<0.0138	<0.0033	0.046	<0.0036	9.79	7.28
Yb	0.0343	0.085	0.152	0.531	4	0.212	0.0364	0.0262	0.161	<0.0082	12.83	10.13
Lu	0.0072	0.0212	0.0382	0.107	1.11	0.0411	0.0106	0.0031	0.0664	0.0024	2.1	1.65
Hf	0.0478	0.0552	1.16	1.67	77.96	0.825	0.402	0.093	1.6	0.0061	0.135	0.076
Ta	<0.00069	0.0015	<0.00056	0.45	21	0.0347	<0.00255	<0.00058	0.00257	0.00451	0.00271	<0.00063
Re	0.00077	0.00099	<0.00044	0.00073	0.0062	0.0005	<0.00175	0.00065	<0.00073	0.00317	<0.00049	0.00146
Pb	0.0386	0.0308	0.0743	0.156	0.183	0.0282	5.12	2.85	4.25	5.99	9.34	7.65
Th	<0.00145	<0.00113	0.0021	0.0043	0.324	0.0061	<0.0036	0.0024	<0.00226	<0.0024	1.88	0.486
U	0.002	0.00347	0.0047	0.0097	0.251	0.0085	0.0108	<0.00144	0.0063	0.0038	1.84	0.918
Majors (electron microprobe)												
weight %												
SiO2	57.315	57.065	57.304	57.488	57.34	57.34	47.51	48.00	47.66	47.82	38.82	38.96
TiO2	0.02	0.03	0.038	0.036	0.00	0.00	0.02	0.04	0.06	0.06	0.07	0.12
Al2O3	11.85	11.39	11.076	12.507	2.09	2.09	38.99	39.12	38.73	39.33	26.31	25.78
Cr2O3	0.02	0.03	0.044	0.031	0.00	0.00	0.01	0.00	0.02	0.01	0.04	0.01
MgO	7.17	7.64	7.897	6.967	19.65	19.65	0.15	0.25	0.19	0.12	0.08	0.06
CaO	11.05	11.95	12.287	10.574	11.66	11.66	0.19	0.29	0.22	0.29	22.74	22.68
MnO	0.02	0.01	0.005	0.012	0.11	0.11	0.02	0.00	0.00	0.00	0.06	0.07
FeO	4.95	4.58	4.632	4.388	6.82	6.82	1.29	0.58	0.60	0.42	8.34	8.83
Na2O	8.31	7.77	7.573	8.526	0.61	0.61	6.55	6.96	6.90	7.35	0.00	0.00
K2O	0.00	0.01	0	0	0.03	0.03	1.41	0.81	0.99	0.53	0.02	0.00
Total	100.70	100.47	100.856	100.529	98.32	98.32	96.14	96.09	95.28	96.90	96.50	96.52

Table C.12. Analytical errors (1 sigma) for LA-ICP-MS determination of trace elements in silicates from sample S01/75iiiC. Errors calculated by GLITTER.

1 sigma error

	Sample S02/75iiiC											
	Garnet											
	Gt1	Gt2	Gt3	Gt4	Gt5	Gt6	Gt7	Gt8	Gt9	Gt10	Gt11	Gt12
Li	0.15	0.069	0.38	0.084	0.18	0.042	0.037	0.043	0.067	0.046	0.056	0.03
Be	0.012	0.017	0.036	0.017	0.018	0.009	0.012	0.012	0.0096	0.02	0.0096	0.0082
B	0.13	0.24	0.18	0.15	0.16	0.11	0.12	0.13	0.12	0.19	0.12	0.13
Mg	1206.86	848.52	678.5	598.53	1386.03	1073.63	761.91	561.43	496.4	484.82	672.15	1101.86
Si	5822.31	5684.75	5441.1	5682.28	5823.06	5488.87	5429.24	5396.93	5376.79	5801.55	5434.2	5460.75
P	4.38	16.87	8.96	13.73	4.5	4.64	9.76	5.82	5.44	191.21	4.85	4.23
K	29.94	10.16	11.9	2.04	35.54	1.72	0.9	0.24	4.42	1.14	1.96	0.36
Ca	2569.98	2950.66	2664.68	3476.44	2571.37	2515.42	2688.64	3326.27	3728.59	5119.4	3114.81	2632.19
Sc	6.86	5.91	3.15	2.72	5.55	6.02	3.64	1.65	1.3	1.47	3.17	6.19
Ti	14.72	214.66	26.24	45.08	199.54	15.11	736.06	55.8	147.62	121.27	36.05	16.42
V	2.03	5.36	5.35	4.24	2.28	2.01	3.74	4.14	4.1	3.94	3.88	2.1
Cr	4.06	9.75	7.25	6.98	4.35	4.79	5.78	6.35	6.9	7.38	5.78	5.88
Ni	0.04	0.078	5.22	0.28	0.065	0.03	0.044	0.069	0.062	0.075	0.057	0.036
Cu	0.14	0.37	62.56	3.51	0.36	0.022	0.086	0.36	0.34	0.96	0.064	0.016
Zn	3.81	3.27	3.7	2.77	5.03	3.26	3.2	2.19	1.92	1.87	2.43	3.4
Rb	0.072	0.019	0.026	0.011	0.046	0.0074	0.0038	0.0045	0.01	0.0077	0.0076	0.0036
Sr	0.093	0.2	0.58	0.094	0.11	0.0041	0.031	1.97	0.061	1.7	0.0087	0.003
Y	23.07	29.45	16.72	28.15	16.02	24.64	24.8	13.79	5.96	13.25	21.62	26.1
Zr	4.51	14.16	8.21	37.21	2.54	6.93	4.35	7.47	36.22	8.62	6.36	1.07
Nb	0.0012	0.11	0.0061	0.0048	0.12	0.0014	0.47	0.016	0.067	0.039	0.0041	0.0028
Mo	0.0081	0.017	0.46	0.041	0.012	0.0078	0.017	0.027	0.052	0.083	0.018	0.0089
Cs	0.0034	0.0044	0.0067	0.0019	0.0033	0.00075	0.00069	0.00073	0.0011	0.0022	0.00063	0.00051
Ba	0.27	0.077	4	0.23	0.43	0.0081	0.0089	0.038	0.16	0.053	0.02	0.0063
La	0.0005	0.027	0.0037	0.0011	0.00089	0.00038	0.00061	0.093	0.0013	0.0089	0.0004	0.00057
Ce	0.00066	0.068	0.0085	0.0028	0.0014	0.00057	0.00096	0.26	0.0056	0.018	0.00084	0.00071
Pr	0.00052	0.015	0.0018	0.001	0.00097	0.00033	0.0005	0.045	0.00091	0.0043	0.00049	0.00049
Nd	0.007	0.073	0.013	0.0072	0.01	0.0048	0.0033	0.23	0.0072	0.025	0.0042	0.0052
Sm	0.05	0.051	0.015	0.015	0.069	0.037	0.015	0.065	0.0071	0.015	0.015	0.04
Eu	0.069	0.028	0.01	0.012	0.089	0.049	0.013	0.029	0.0034	0.008	0.013	0.052
Gd	0.77	0.31	0.13	0.16	0.96	0.57	0.16	0.2	0.037	0.048	0.18	0.61
Tb	0.43	0.18	0.075	0.1	0.47	0.35	0.12	0.08	0.021	0.022	0.1	0.38
Dy	4.3	3	1.26	1.87	3.7	3.97	2.09	1.1	0.33	0.49	1.89	4.26
Ho	0.84	0.95	0.5	0.82	0.62	0.86	0.77	0.4	0.15	0.34	0.64	0.92
Er	2.07	2.78	2.1	4.06	1.43	2.24	3.09	1.78	0.94	2.93	2.88	2.32
Yb	1.5	1.75	2.58	7.19	1.06	1.54	3.4	3.04	3.24	14.35	4.09	1.5
Lu	0.22	0.2	0.36	1.06	0.16	0.2	0.45	0.45	0.56	2.64	0.69	0.19
Hf	0.087	0.29	0.16	0.68	0.052	0.13	0.069	0.15	0.73	0.12	0.11	0.021
Ta	0.00036	0.0079	0.00044	0.00051	0.0076	0.00023	0.031	0.001	0.0041	0.0026	0.00036	0.00041
Re	0.00028	0.00053	0.00043	0.00034	0.00036	0.00024	0.00029	0.0003	0.00025	0.00042	0.00029	0.00034
Pb	0.00019	0.00037	0.00025	0.00021	0.00024	0.00017	0.00018	0.00022	0.00017	0.0003	0.00018	0.0002
Th	0.0028	0.0068	0.1	0.0065	0.0048	0.0019	0.0033	0.016	0.0027	0.0079	0.0022	0.0026
U	0.0006	0.0043	0.0016	0.0013	0.00065	0.00064	0.0006	0.0068	0.0017	0.0024	0.00069	0.00078

Table C.12. contd. Analytical errors (1 sigma) for LA-ICP-MS determination of trace elements in silicates from sample S01/75iiiC. Errors calculated by GLITTER.

1 sigma error

	Sample S02/75iiiC											
	Omphacite				*Am + Rut Amph*		*Paragonite*				*Epidote/Zoisite*	
	Om1	Om2	Om3	Om4	Am1	Am2	Mc1	Mc2	Mc3	Mc4	Ep1	Ep2
Li	3.18	3.34	4.74	4.35	0.46	0.57	0.68	0.9	0.97	1.08	0.1	0.12
Be	0.14	0.15	0.14	0.15	0.18	0.086	0.46	0.39	0.51	0.52	0.026	0.026
B	0.23	0.19	0.29	0.35	0.58	0.18	0.85	0.7	1.31	0.96	0.28	0.25
Mg	2072.59	1796.66	2130.35	2197.03	1569.98	1769.08	61.26	160.37	125.23	103.37	64.5	53.6
Si	8490.9	8469.2	8473.62	8473.62	7231.05	7222.73	6779.65	6875.5	7071.1	7047.28	5740.64	5741.57
P	3.79	3.69	6.07	32.81	7.77	3.68	5.63	5.32	4.15	7.21	11.99	10.23
K	7.93	10.93	6.35	11.16	37.12	28.4	515.72	417.72	352.75	640.7	1.83	11.86
Ca	5062.52	4708.79	5638.62	6192.97	4123.81	3267.37	185.6	422.63	318.84	200.28	11621.7	11438
Sc	2.12	2.31	1.98	2.17	1.8	1.55	0.047	0.13	0.095	0.095	4.17	3.27
Ti	21.42	21.72	24.34	1135.75	49142.2	93.1	27.17	25.61	28.8	29.49	43.55	39.39
V	26.44	27.77	26.24	29.73	74.5	17.33	5.02	6.16	6.41	5.98	34.24	30.49
Cr	5.19	1.85	13.06	14.46	31.03	8.38	6.64	6.99	9.18	5.67	9.21	9.61
Ni	3.48	2.04	3.2	3.41	4.45	3.51	0.16	0.41	0.2	0.46	0.097	0.13
Cu	0.99	0.47	0.52	1.24	0.9	0.85	0.09	0.55	0.14	0.34	0.13	0.16
Zn	7.16	5.34	6.57	7.46	6.22	6.19	0.15	0.89	0.43	0.46	0.7	0.63
Rb	0.0074	0.021	0.011	0.014	0.02	0.0096	0.2	0.14	0.046	0.46	0.0081	0.022
Sr	0.71	0.28	1.16	1.05	0.9	0.55	108.68	71.89	71.56	112.09	140.92	104.28
Y	0.035	0.031	0.055	0.17	0.94	0.1	0.0063	0.0062	0.017	0.0034	9.64	6.78
Zr	0.078	0.065	6.32	10.12	350.54	4.08	2.02	0.36	10.25	0.017	0.32	0.23
Nb	0.0017	0.0013	0.0033	0.62	25.76	0.053	0.0034	0.0024	0.0053	0.0029	0.0025	0.0017
Mo	0.0038	0.003	0.0026	0.013	0.49	0.0037	0.0055	0.0037	0.0044	0.0051	0.0037	0.0041
Cs	0.0017	0.0018	0.0014	0.003	0.0044	0.0013	0.004	0.0065	0.0025	0.0093	0.0011	0.0014
Ba	0.13	0.21	0.1	0.15	0.38	0.26	1.95	1.43	0.88	2.38	0.14	0.23
La	0.001	0.001	0.0011	0.0054	0.096	0.0051	0.00027	0.0017	0.0012	0.001	4.62	2.66
Ce	0.00089	0.00084	0.0021	0.022	0.34	0.012	0.0011	0.0015	0.0012	0.0016	12.48	7.53
Pr	0.00077	0.00073	0.00078	0.0057	0.078	0.0026	0.00058	0.0013	0.00065	0.0011	2.16	1.25
Nd	0.0033	0.0033	0.0058	0.029	0.37	0.019	0.0031	0.0067	0.0061	0.0069	10.67	6.1
Sm	0.0048	0.0039	0.0068	0.017	0.13	0.017	0.0065	0.0023	0.0042	0.0044	3.62	2.09
Eu	0.0023	0.00092	0.0026	0.013	0.12	0.0043	0.0021	0.0018	0.0027	0.002	1.23	0.76
Gd	0.012	0.0031	0.013	0.023	0.2	0.018	0.0061	0.0044	0.0039	0.005	3.91	2.3
Tb	0.0021	0.0011	0.0027	0.0051	0.029	0.0037	0.0014	0.0011	0.0011	0.0006	0.45	0.28
Dy	0.0093	0.0064	0.012	0.025	0.16	0.02	0.0057	0.0038	0.004	0.0038	1.9	1.26
Ho	0.0019	0.0016	0.0028	0.0062	0.033	0.0043	0.0015	0.0014	0.0014	0.001	0.32	0.23
Er	0.0052	0.0057	0.0086	0.025	0.13	0.013	0.0053	0.0029	0.0076	0.0025	0.95	0.71
Yb	0.007	0.01	0.018	0.059	0.38	0.022	0.0066	0.0081	0.021	0.0036	1.18	0.95
Lu	0.0016	0.0026	0.0047	0.013	0.11	0.0047	0.0018	0.0014	0.0069	0.0012	0.21	0.17
Hf	0.0076	0.0072	0.12	0.18	7.28	0.08	0.042	0.015	0.16	0.0032	0.016	0.012
Ta	0.00039	0.00046	0.00037	0.044	1.81	0.0033	0.00095	0.00035	0.00075	0.00092	0.00061	0.0004
Re	0.00061	0.00041	0.00041	0.00051	0.0014	0.00033	0.00088	0.00068	0.00062	0.0007	0.00045	0.00052
Pb	0.00034	0.00026	0.00026	0.00039	0.001	0.00024	0.00065	0.00046	0.00043	0.00053	0.0003	0.00036
Th	0.0057	0.0042	0.0072	0.014	0.024	0.0041	0.3	0.17	0.26	0.37	0.55	0.46
U	0.00086	0.0007	0.001	0.0017	0.031	0.0013	0.0013	0.0018	0.00094	0.0016	0.15	0.04

Table C.13. Trace and major element concentrations in silicates from S02/75iiiR - determined by LA-ICP-MS and electron microprobe respectively. *bulk rock majors analysed by XRF.

Concentrations	All values reported in ppm									
	Sample S02/75iiiR									
	*Bulk rock**	*Garnet*								
		Gt1	Gt2	Gt3	Gt4	Gt5	Gt6	Gt7	Gt8	Gt9	Gt10
Trace Elements											
Li	21.40	0.852	1.012	1.241	0.562	1.554	3.09	3.85	0.75	1.432	0.759
Be											
B		3.39	2.75	2.75	2.33	1.86	1.71	1.93	1.32	1.36	1.38
Mg											
Si		187753.6	168649.5	223880.5	169578.3	159503.4	161608.6	168241.9	179964.1	179964.1	179964.1
P		63.2	54.37	82.1	50.26	44.45	43.02	46.72	47.28	46.68	48.47
K	1042	51.06	52.02	112.36	<0.26	17.1	240.55	176.65	<0.25	<0.25	<0.24
Ca		51187	48078	59256	60514	58555	54818	47535	52580	66977	54164
Sc	13.05	92.49	71.62	52.27	39.03	34.34	42.75	77.12	89.51	38.6	102.99
Ti	11485	220.19	367.75	495.15	785.49	745.12	626.79	289.48	10224.92	1007.97	328.09
V	208.45	39.14	41.25	63.9	55.21	58.7	66.69	38.88	59.32	66.97	45.11
Cr	114.60	69.26	75.14	113.61	95.38	81.03	95.36	65.28	131.23	92.45	91.4
Ni	88.91	1.55	1.51	3.55	0.317	1.377	4.81	4.84	0.694	1.126	0.899
Cu	42.00	0.786	1.503	4.18	0.0537	1.318	6.65	10.01	0.123	0.254	0.484
Zn	96.12	79.25	42.3	50.71	30.49	51.37	43.6	56.07	65.66	43.94	63.91
Rb	3.56	0.1354	0.184	0.298	0.0848	0.0962	0.325	0.648	0.0302	0.1758	0.0395
Sr	164.77	0.0499	0.1556	0.488	0.0734	0.2112	0.53	0.448	0.651	0.56	0.179
Y	44.36	273.27	214.23	143.76	572.84	379.83	182.46	282.96	286.02	975.21	356.16
Zr	249.80	9.19	56.34	34.37	25	1.774	6.02	4.13	138.96	4.17	628.55
Nb	7.38	<0.0018	0.0046	0.005	0.0034	<0.00121	<0.00141	0.0035	4.89	0.0276	0.0141
Mo	0.34	0.0896	0.196	0.245	0.655	0.586	0.384	0.1228	0.271	0.762	0.1266
Cs	0.67										
Ba	14.48	0.296	0.649	8.42	0.0705	0.388	3.98	3.82	<0.0064	0.0086	0.064
La	8.05	<0.00082	0.00105	0.007	<0.00093	<0.00088	0.00676	0.0056	0.0588	0.0247	0.0101
Ce	23.27	0.00142	0.00357	0.0084	<0.00074	0.00172	0.00682	0.00584	0.2247	0.0856	0.0488
Pr	3.59	0.00178	0.00093	0.00341	<0.00075	<0.00067	0.0023	0.00249	0.0381	0.0156	0.00514
Nd	17.28	0.0502	0.0151	0.0378	0.0549	0.0528	0.0509	0.0333	0.155	0.0952	0.0393
Sm	5.06	0.737	0.198	0.268	0.433	0.448	0.436	0.341	0.25	0.235	0.364
Eu	1.60	1.151	0.284	0.284	0.362	0.385	0.346	0.494	0.341	0.283	0.536
Gd	6.53	13.01	3.82	4.09	6.39	6.26	5.21	6.21	4.41	4.51	6.84
Tb	1.20	6.49	2.45	2.149	4.17	3.66	2.608	3.78	2.94	3.52	4.25
Dy	7.33	58.41	32.67	23.6	66.68	50.64	29.42	45.64	40.47	75.95	53.53
Ho	1.53	10.42	8.06	5.07	21.16	13.96	6.83	10.5	10.38	34.41	12.92
Er	4.23	24.4	22.43	13.46	83.43	49.3	19.82	28.01	29.81	182.46	35.14
Yb	3.82	17.59	17.78	10.28	119.66	60.9	18.39	21.74	23.91	389.42	28.61
Lu	0.60	2.43	2.343	1.294	14.14	6.91	2.343	2.85	3.04	45.17	3.88
Hf	4.91	0.1723	1.089	0.681	0.492	0.022	0.1197	0.0857	2.75	0.0874	13.03
Ta	0.49	<0.00058	<0.00046	0.00094	0.00067	0.00109	<0.00047	<0.00054	0.3	0.00271	0.00084
Re											
Pb	1.16	0.0113	0.0123	0.0234	0.014	0.0164	0.0253	0.016	0.0307	0.0482	0.0322
Th	0.42	0.00195	0.00208	0.00099	0.00287	<0.00060	<0.00056	<0.00063	0.0314	0.00284	0.0612
U	0.19	0.00085	0.00369	0.00235	0.00205	<0.00045	<0.00045	<0.00053	0.0245	0.00206	0.0578
***Majors** (electron microprobe) weight %*											
SiO2	50.34761	37.862	37.591	37.862	37.591	37.862	37.591	37.862	37.591	37.862	37.591
TiO2	1.96504	0.038	0.035	0.038	0.035	0.038	0.035	0.038	0.035	0.038	0.035
Al2O3	15.33438	20.799	20.93	20.799	20.93	20.799	20.93	20.799	20.93	20.799	20.93
Cr2O3		0.007	0.028	0.007	0.028	0.007	0.028	0.007	0.028	0.007	0.028
MgO	10.05779	4.648	4.546	4.648	4.546	4.648	4.546	4.648	4.546	4.648	4.546
CaO	0.16044	6.407	6.468	6.407	6.468	6.407	6.468	6.407	6.468	6.407	6.468
MnO	6.46315	0.478	0.504	0.478	0.504	0.478	0.504	0.478	0.504	0.478	0.504
FeO	7.11199	28.995	28.668	28.995	28.668	28.995	28.668	28.995	28.668	28.995	28.668
Na2O	5.3019	0.022	0.042	0.022	0.042	0.022	0.042	0.022	0.042	0.022	0.042
K2O	0.25111	0.001	0	0.001	0	0.001	0	0.001	0	0.001	0
Total	99.3049	99.298	98.87	99.298	98.87	99.298	98.87	99.298	98.87	99.298	98.87

Table C.13. contd. Trace and major element concentrations in silicates from S02/75iiiR – determined by LA-ICP-MS and electron microprobe respectively. *bulk rock majors analysed by XRF.

Concentrations All values reported in ppm

	Sample S02/75iiiR								
	Epidote/Zoisite		***Omphacite***	***Paragonite***				***Amphibole (glaucophane)***	
	EP1	**EP2**	**CPX1**	**MC1**	**MC2**	**MC3**	**MC4**	**AM1**	**AM2**
Trace Elements									
Li	27.03	19.78	51.69	20.22	15.91	10.84	15.6	1.065	4.78
Be									
B	1.464	1.83	2.74	30.16	21.3	24.8	17.53	0.978	1.153
Mg									
Si	179964.2	179964.2	267889.5	223884.7	241095.8	224370.9	240731.3	179964.13	179964.14
P	35.01	44.84	39.08	48.44	48.66	41.96	48.38	19.77	22.77
K	176.4	113.23	163.25	8863.56	8017.3	5766.55	8381.93	396.19	285.08
Ca	76158	87535	88281	3330	2664	2264	3059	25963	29177
Sc	25.96	24.72	27.39	0.637	0.732	0.803	0.974	12.82	13.81
Ti	2198.01	1289.16	20838.47	358.01	5839.2	1029.03	690.64	150.36	179.81
V	339.6	325.22	436.44	75.72	104.22	108.23	102.8	194.99	207.12
Cr	136.76	136.61	181.18	98.31	132.82	122.57	115.13	96.51	97.06
Ni	24.38	20.47	50.15	18.88	6.52	3.93	3.46	87.79	68.88
Cu	5.78	4.29	6.18	6.58	2.98	4.09	2.88	7.29	6.67
Zn	47.6	43.67	89.3	9.43	5.47	2.66	6.67	92.25	79.47
Rb	0.308	0.1637	0.35	4.01	3.24	0.665	3.34	0.0953	0.0942
Sr	297.74	489.15	14.31	1240.73	738.14	473.3	828.39	4.55	5.33
Y	20.49	28.92	1.36	0.335	0.251	0.466	0.273	0.511	0.699
Zr	126.49	68.1	54.17	5.92	112.57	75.6	63.28	1.66	1.71
Nb	0.924	0.48	9.7	0.0058	2.63	0.357	0.1239	0.0091	0.0158
Mo	0.0164	0.0119	0.1701	0.01	0.0466	0.0161	<0.0060	0.0048	0.0081
Cs									
Ba	3.6	2.543	2.89	24.95	23.91	48.91	28.98	1.465	1.721
La	28.69	36.68	0.292	0.043	0.0182	0.1713	<0.00128	0.01069	0.0156
Ce	88.4	107.3	0.991	0.0909	0.0358	0.53	<0.00120	0.0498	0.072
Pr	13.6	16.61	0.1609	0.014	0.0051	0.0774	<0.00091	0.00981	0.01043
Nd	66.6	82.22	0.772	0.0677	0.0239	0.362	0.0056	0.0623	0.0586
Sm	18.25	22.59	0.25	0.0203	<0.0054	0.0819	0.0057	0.0196	0.0215
Eu	5.71	7.02	0.0966	0.0192	0.0043	0.0221	0.00249	0.01181	0.0136
Gd	17.54	22.47	0.339	0.0424	0.008	0.0961	0.0079	0.0438	0.0424
Tb	1.803	2.29	0.0521	0.00879	0.00232	0.0109	0.00215	0.00913	0.0111
Dy	6.13	8.25	0.274	0.0629	0.0275	0.0679	0.0191	0.0711	0.1014
Ho	0.767	1.09	0.0486	0.0126	0.00642	0.0153	0.00604	0.0191	0.0281
Er	1.88	2.66	0.158	0.0388	0.0491	0.0614	0.0415	0.0752	0.1099
Yb	2.05	2.73	0.258	0.0481	0.128	0.148	0.146	0.149	0.216
Lu	0.338	0.422	0.055	0.0107	0.0352	0.0356	0.0431	0.022	0.0294
Hf	2.53	1.45	1.248	0.1026	2.56	1.59	1.33	0.049	0.0751
Ta	0.0618	0.0298	0.587	0.00177	0.1734	0.0301	0.00646	<0.00026	0.00105
Re									
Pb	2.19	3.95	0.1076	7.52	2.49	1.55	2.4	0.034	0.0456
Th	1.958	2.53	0.021	<0.00080	0.0041	0.0122	0.00691	0.00113	0.0011
U	0.692	0.754	0.0192	0.00153	0.0145	0.0069	0.00488	0.00033	0.00096
Majors *(electron microprobe)* weight %									
SiO2	39.301	39.155	57.31	47.896	48.13	49.428	48.485	59.774	59.512
TiO2	0.069	0.08	0.04	0.027	0.042	0.076	0.048	0.015	0.018
Al2O3	27.698	27.448	11.671	39.569	39.121	39.882	39.524	11.152	11.138
Cr2O3	0	0.003	0.014	0.009	0.016	0.061	0.029	0.005	0.02
MgO	0.128	0.11	7.694	0.094	0.193	0.179	0.155	11.897	12.108
CaO	23.112	23.071	11.677	0.24	0.248	0.115	0.201	0.657	0.644
MnO	0.001	0.016	0	0	0	0.002	0	0.021	0.036
FeO	6.48	7.004	4.44	0.502	0.482	0.542	0.509	7.896	7.453
Na2O	0	0	7.97	7.221	7.247	6.534	7.001	7.379	7.403
K2O	0.002	0	0	0.524	0.474	0.791	0.596	0.021	0.012
Total	96.872	96.943	100.868	96.144	95.972	97.645	96.587	98.927	98.398

Table C.14. Analytical errors (1 sigma) for LA-ICP-MS determination of trace elements in silicates from sample S01/75iiiR. Errors calculated by GLITTER.

1 sigma error

	Sample S02/75IIIR									
	*Bulk rock**	*Garnet*								
		Gt1	Gt2	Gt3	Gt4	Gt5	Gt6	Gt7	Gt8	Gt9	Gt10
Trace Elements										
Li		0.045	0.054	0.066	0.031	0.085	0.17	0.22	0.028	0.05	0.029
Be		0.29	0.25	0.25	0.22	0.18	0.17	0.19	0.12	0.11	0.13
B		13270.36	11986.21	16013.47	12219.43	11590.83	11853.96	12468.82	5691.81	5691.66	5692.17
Mg		5.96	5.13	7.75	4.75	4.21	4.08	4.45	2.85	2.88	3.07
Si		2.29	2.35	5.1	0.28	0.81	11.28	8.42	0.2	0.19	0.2
P		1623.42	1525.79	1879.03	1917.74	1855.99	1737.18	1507.7	3254.03	4252.41	3528.63
K		3.57	2.78	2.04	1.53	1.36	1.71	3.11	7.89	3.51	9.63
Ca		9.45	15.86	21.5	34.4	33.02	28.16	13.23	878.95	89.33	29.99
Sc		1.65	1.74	2.72	2.37	2.55	2.93	1.74	3.21	3.71	2.56
Ti		3.01	3.29	4.98	4.22	3.63	4.32	3.02	6.58	4.74	4.81
V		2.74	1.4	1.28	0.82	0.99	0.98	2.04	1.9	0.84	2.03
Cr		0.1	0.1	0.23	0.03	0.096	0.31	0.32	0.047	0.063	0.063
Ni		0.046	0.085	0.23	0.0083	0.078	0.39	0.6	0.012	0.018	0.034
Cu		0.056	0.094	0.26	0.014	0.082	0.41	0.64	0.023	0.021	0.038
Zn		4.53	2.45	2.96	1.8	3.08	2.66	3.49	2.44	1.65	2.43
Rb		0.38	0.32	0.4	0.32	0.34	0.38	0.41	0.31	0.27	0.34
Sr		0.015	0.018	0.017	0.013	0.013	0.012	0.015	0.014	0.011	0.014
Y		0.7	0.53	0.52	0.88	0.67	0.44	0.59	0.54	0.83	0.66
Zr		0.0089	0.012	0.018	0.0061	0.0068	0.02	0.039	0.0028	0.0082	0.0038
Nb		0.0035	0.0081	0.021	0.0044	0.01	0.022	0.02	0.029	0.025	0.01
Mo		11.5	9.07	6.14	24.7	16.59	8.08	12.74	24.62	86.46	32.51
Cs		0.38	2.35	1.45	1.06	0.079	0.26	0.19	11.65	0.36	55.83
Ba		0.001	0.0013	0.0013	0.001	0.00071	0.00069	0.0013	0.29	0.0027	0.0022
La		0.0071	0.013	0.015	0.035	0.032	0.022	0.0089	0.012	0.027	0.0082
Ce		0.022	0.039	0.36	0.0091	0.025	0.18	0.18	0.0036	0.0045	0.01
Pr		0.00055	0.00058	0.0011	0.00046	0.00059	0.00095	0.001	0.0038	0.002	0.0015
Nd		0.00064	0.00088	0.0012	0.00029	0.00058	0.00093	0.00096	0.01	0.0044	0.0034
Sm		0.00073	0.00048	0.00071	0.00046	0.00042	0.00051	0.00063	0.0024	0.0013	0.00096
Eu		0.0062	0.0042	0.006	0.0062	0.0062	0.0057	0.0053	0.012	0.0081	0.0066
Gd		0.034	0.015	0.017	0.022	0.023	0.022	0.019	0.017	0.016	0.025
Tb		0.042	0.011	0.011	0.014	0.015	0.013	0.019	0.019	0.016	0.031
Dy		0.45	0.14	0.14	0.22	0.22	0.18	0.22	0.27	0.28	0.43
Ho		0.22	0.085	0.075	0.15	0.13	0.093	0.14	0.19	0.24	0.29
Er		1.94	1.09	0.79	2.23	1.7	1	1.56	2.44	4.69	3.39
Yb		0.34	0.26	0.16	0.69	0.45	0.22	0.35	0.6	2.03	0.78
Lu		0.82	0.76	0.46	2.83	1.68	0.68	0.97	2.08	13.04	2.58
Hf		0.098	0.098	0.059	0.52	0.28	0.096	0.12	0.24	2.72	0.31
Ta		0.57	0.58	0.34	3.88	1.98	0.6	0.72	1.64	27.43	2.07
Re		0.085	0.083	0.046	0.5	0.25	0.084	0.1	0.24	3.74	0.33
Pb		0.0099	0.044	0.029	0.021	0.003	0.0072	0.0063	0.22	0.0086	1.07
Th		0.00033	0.00031	0.00039	0.0003	0.00031	0.00026	0.0003	0.016	0.00039	0.00036
U		0.00086	0.00084	0.00095	0.00085	0.00074	0.00067	0.00078	0.00077	0.00077	0.00088

Table C.14. contd. Analytical errors (1 sigma) for LA-ICP-MS determination of trace elements in silicates from sample S01/75iiiR. Errors calculated by GLITTER.

1 sigma error

	Sample S02/75iiiR							*Amphibole (glaucophane)*	
	Epidote/Zoisite		*Omphacite*	*Paragonite*					
	EP1	EP2	CPX1	MC1	MC2	MC3	MC4	AM1	AM2
Li	0.86	0.64	1.65	0.65	0.52	0.36	0.51	0.037	0.16
Be	0.082	0.12	0.14	1.11	0.81	0.94	0.68	0.07	0.086
B	5691.36	5691.83	8472.06	7080.89	7625.47	7096.41	7613.64	5691.35	5691.56
Mg	1.81	2.43	2.07	2.68	2.76	2.44	2.86	1.28	1.51
Si	5.48	3.54	5.08	276.85	251.05	181.05	263.89	12.63	9.12
P	3945.03	4763.09	4685.35	187.48	154.65	134.81	186	1734.39	1998.53
K	1.85	1.87	2.01	0.052	0.062	0.069	0.085	1.23	1.37
Ca	152.31	94.95	1488.01	27.22	457.52	83.2	57.6	14.15	17.42
Sc	15.76	15.74	20.68	3.75	5.27	5.6	5.44	11.28	12.25
Ti	5.92	6.17	8	4.55	6.27	5.9	5.66	5.15	5.3
V	0.41	0.37	0.8	0.1	0.046	0.082	0.047	1.13	1
Cr	0.94	0.83	1.97	0.78	0.29	0.19	0.17	4	3.2
Ni	0.29	0.23	0.32	0.36	0.17	0.23	0.17	0.47	0.44
Cu	0.24	0.19	0.24	0.27	0.094	0.15	0.084	0.4	0.37
Zn	1.65	1.55	3.12	0.36	0.23	0.12	0.27	3.52	3.07
Rb	1.16	1.61	1.07	1.87	1.91	1.9	2.03	0.65	0.72
Sr	0.02	0.026	0.011	0.014	0.015	0.014	0.015	0.0064	0.0078
Y	0.21	0.3	0.29	0.4	0.43	0.4	0.43	0.18	0.21
Zr	0.012	0.008	0.014	0.14	0.12	0.027	0.12	0.0045	0.005
Nb	11.26	19.02	0.55	48.94	29.56	19.25	34.22	0.2	0.24
Mo	1.43	2.14	0.099	0.027	0.021	0.039	0.024	0.048	0.068
Cs	8.62	4.92	3.8	0.44	8.64	5.98	5.16	0.15	0.16
Ba	0.047	0.027	0.5	0.0015	0.15	0.022	0.0089	0.0011	0.0018
La	0.0021	0.0027	0.0081	0.0033	0.0055	0.0037	0.0035	0.0015	0.0021
Ce	0.12	0.099	0.11	0.85	0.83	1.68	1.01	0.057	0.07
Pr	1.15	1.52	0.013	0.0032	0.0021	0.0093	0.00078	0.00096	0.0014
Nd	3.14	3.89	0.037	0.0049	0.0029	0.022	0.0005	0.0026	0.0037
Sm	0.46	0.56	0.0065	0.0014	0.001	0.0042	0.0006	0.00076	0.00094
Eu	2.59	3.3	0.036	0.0079	0.0053	0.023	0.0033	0.0051	0.0058
Gd	0.74	0.94	0.015	0.0051	0.0029	0.0098	0.0037	0.0029	0.0036
Tb	0.26	0.33	0.0052	0.0018	0.001	0.002	0.00089	0.00099	0.0012
Dy	0.88	1.19	0.02	0.0055	0.0033	0.0091	0.0032	0.004	0.0044
Ho	0.099	0.13	0.0032	0.00097	0.00059	0.0012	0.00055	0.00081	0.001
Er	0.31	0.44	0.016	0.0055	0.0037	0.006	0.0031	0.0053	0.0077
Yb	0.038	0.056	0.0028	0.0012	0.0009	0.0014	0.00084	0.0014	0.002
Lu	0.11	0.16	0.01	0.0037	0.0048	0.0055	0.0041	0.0061	0.0091
Hf	0.015	0.021	0.0019	0.00078	0.0012	0.0014	0.0011	0.0012	0.002
Ta	0.12	0.17	0.017	0.0049	0.011	0.012	0.012	0.012	0.017
Re	0.023	0.03	0.004	0.0012	0.0031	0.0032	0.0038	0.002	0.0028
Pb	0.16	0.1	0.084	0.0099	0.19	0.12	0.1	0.005	0.0077
Th	0.0029	0.0017	0.027	0.00043	0.0089	0.0019	0.00068	0.00015	0.00023
U	0.00046	0.00063	0.00068	0.00097	0.00096	0.00088	0.001	0.00039	0.00049

Table C.15. NIST-612 standard data for LA-ICP-MS analysis of trace elements in silicates.

	Li	P	K	Ti	Rb	Sr	Y	Zr	Nb	Mo	Cs	Ba	Pb	Th	U
NIST612 - 1	41.46	55.73		47.95	31.62	75.98	38.31	36.15	38.18	38.44	41.97	37.59	39.08	37.55	37.29
NIST612 - 2	41.49	54.98		48.36	31.58	76.42	38.24	35.87	37.94	38.03	40.99	37.98	38.73	36.79	36.81
NIST612 - 3	43.05	51.8		48.15	32.28	76.21	37.64	35.18	37.6	38.74	43.16	37.85	39.41	36.89	38.35
NIST612 - 4	39.24	58.17		48.02	30.62	76.02	39.44	37.66	38.96	37.6	39.56	37.52	38.23	37.93	35.41
NIST612 - 5	40.92	50.73	65.2	47.77	31.88	76.49	38.78	36.12	38.26	38.85	42.46	38.06	40.63	39.45	39.69
NIST612 - 6	42.33	56.21	66.12	49.06	31.99	77.24	38.68	36.22	38.42	38.44	41.32	37.54	39.27	37.36	37.31
NIST612 - 7	42.46	57.79	68.38	48.41	31.24	75.37	37.33	35.94	37.91	37.75	41.04	37.52	37	35.15	34.63
NIST612 - 8	41.01	57.33	66.91	47.58	31.07	75.62	37.72	35.42	37.27	37.65	40.82	37.71	37.66	36.15	35.54
NIST612 - 9	42.11	56.09	66.66	48.02	30.84	74.72	37.46	35.71	37.36	37.45	40.14	36.92	37.27	36.11	36.25
NIST612 - 10	42.54	56.53	68.55	48.88	32.37	76.33	38.16	35.73	38.48	37.55	41.98	37.66	37.7	37.8	38.41
NIST612 - 11	40.61	53.23	65.14	48.04	31.68	76.36	39.19	36.42	38.18	39.19	41.8	38.05	40.69	37.79	37.44
NIST612 - 12	41.3	53.1	63.73	47.75	32.16	77.7	38.77	36.44	38.77	39.53	43.44	38.24	42.13	38.05	38.38
NIST612 - 13	43.03	55.69	68.48	47.96	31.75	75.08	37.04	34.82	37.38	38.4	41.58	36.85	39.45	36.69	37.67
NIST612 - 14	41.36	56.94	63.98	48	31.27	76.3	39.31	36.94	38.48	38.13	41.41	38.04	38.55	37.61	36.51
NIST612 - 15	38.65	60.27	63.87	49.31	33.02	80.27	42.11	39.55	40.34	39.55	43.54	39.68	40	39.74	37.62
NIST612 - 16	40.03	54.95	66.54	47.57	31.4	77.26	38.67	36.48	38.19	38.31	41.67	37.82	38.64	36.97	36.57
NIST612 - 17	39.99	55.56	67.8	48.54	32	77.67	39.3	37.16	38.79	38.47	41.78	38.38	38.07	36.87	36.67
NIST612 - 18	44.51	48.54	68.02	47.54	31.61	73.83	34.84	32.88	36.1	37.79	41.5	37.47	39	35.68	39.37
NIST612 - 19	42.62	50.6	65.57	48.41	31.17	74.86	37.43	34.97	37.53	37.38	40.64	37.06	38.99	37.2	37.18
NIST612 - 20	42.73	58.58	67.74	48.55	31.66	76.89	39.61	37.04	38.92	39.07	42.39	38.68	40.24	38.65	37.76
NIST612 - 21	41.4	58.92	64.3	48.92	32.24	77.14	38.97	36.83	38.33	38.76	41.96	37.86	39.31	37.37	36.44
NIST612 - 22	41.78	57.26	64.57	47.04	30.99	74.62	38.66	36.16	38.06	38	41.1	36.57	38.52	37.49	36.64
NIST612 - 23	42.8	55.13	66.5	48.3	31.67	75.64	37.42	35.41	37.69	38.53	41.61	37.45	38.79	36.61	37.13
NIST612 - 24	41.19	53.81	65.86	48.09	31.53	75.74	38.48	35.94	38.02	37.8	41.45	37.72	38.75	37.28	36.88
NIST612 - 25	40.71	55.35	66.98	47.73	31.71	77.7	39.1	36.96	38.68	38.88	41.92	38.14	39.67	38.2	37.68
NIST612 - 26	40.72	58	65.52	48.46	31.87	76.5	38.74	36.29	38.31	38.4	42.03	38.11	38.94	37.35	37.4
NIST612 - 27	41.23	59.32	64.86	47.75	30.88	76.1	38.99	36.54	38.14	37.68	41.03	37.75	38.99	37.67	36.07
NIST612 - 28	42.4	54.02	67.09	48.49	31.67	75.55	37.54	35.28	37.74	38	41.97	37.13	38.65	36.35	36.92
NIST612 - 29	41.95	53.27	67.1	47.85	31.8	75.68	37.61	35.7	37.79	38.31	41.4	37.88	38.67	37.19	38.02
NIST612 - 30	41.56	52.36	66.6	48.25	32.21	76.59	38.23	35.91	38.2	39.27	41.85	37.91	39.39	37.41	37.68
NIST612 - 31	43.03	57.01	67.72	48.43	32.77	77.75	38.66	36.3	38.76	39.54		38.88	41.14	37.54	38.03
NIST612 - 32	40.1	53.8	64.44	48.24	30.53	74.61	38.13	35.87	37.65	36.91		36.79	36.85	36.98	36.11
NIST612 - 33	40.81	55.23	65.18	48.35	30.95	75.53	38.84	36.45	38.05	37.91		37.28	37.78	36.79	35.9
NIST612 - 34	42.93	54.12	67.92	47	32.85	77.04	37.06	35.08	37.58	39.48		38.13	41.94	37.71	40.27
NIST612 - 35	40.99	55.64	65.47	50.01	31.24	77.17	39.32	37.2	38.61	37.85		37.59	38.09	37.75	36.86
NIST612 - 36	41.83	55.19	66.53	47.27	31.83	75.46	37.85	35.42	37.94	38.4		37.96	39.23	36.9	37.01
Mean	41.58	55.31	66.23	48.17	31.67	76.26	38.38	36.11	38.13	38.33	41.65	37.77	39.04	37.31	37.22
2 S D	2.39	5.17	2.89	1.21	1.19	2.40	2.26	2.09	1.36	1.36	1.71	1.20	2.44	1.80	2.33
Relative 2 S D	5.74	9.35	4.36	2.52	3.76	3.15	5.88	5.78	3.57	3.56	4.10	3.18	6.25	4.83	6.25

	La	Ce	Pr	Nd	Sm	Eu	Gd	Tb	Dy	Ho	Er	Yb	Lu	Hf	Ta
NIST612 - 1	35.86	38.34	37.22	35.33	36.86	34.54	37.16	36.07	36.31	38.08	37.74	40.23	37.92	34.93	40.02
NIST612 - 2	35.69	38.33	37.06	35.14	36.53	34.29	36.67	35.73	35.5	37.59	37	39.54	37.42	34.57	39.43
NIST612 - 3	35.35	38.61	37.18	34.99	36.44	34.37	36.69	35.56	35.67	37.53	37.17	39.74	37.4	34.37	39.39
NIST612 - 4	36.59	37.92	37.14	35.7	37.26	34.58	37.46	36.62	36.58	38.54	37.97	40.37	38.33	35.55	40.52
NIST612 - 5	36.38	39.1	38.48	36.65	38.15	35.74	38.59	37.48	37.5	39.59	39.13	41.9	39.42	36.14	41.81
NIST612 - 6	35.71	38.14	36.71	34.51	35.96	34.16	35.93	35.49	35.5	37.61	36.84	39.9	37.65	35.04	39.72
NIST612 - 7	35.02	37.66	35.78	33.56	35.29	32.76	35.26	33.92	34.03	35.51	35.17	37.28	35.23	32.68	36.93
NIST612 - 8	34.91	37.39	35.83	34.05	35.38	33.23	35.54	34.77	34.61	36.57	36.11	38.13	36.39	33.21	38.15
NIST612 - 9	35.29	37.22	36.14	34.76	35.79	33.71	36.17	35.18	35.45	37.13	36.93	38.98	36.91	34.02	38.95
NIST612 - 10	35.81	38.9	37.42	35.52	36.76	34.78	37.27	36.19	35.98	38.4	37.93	40.76	38.38	35.74	40.68
NIST612 - 11	36.02	38.74	37.97	36.01	37.77	35.35	37.86	36.98	37.16	38.97	38.6	41.24	38.88	35.84	40.98
NIST612 - 12	36.96	39.42	38.65	36.35	38.1	35.55	38.34	37.09	37.23	39.07	38.32	41.46	38.84	35.65	41.12
NIST612 - 13	34.9	37.88	36.18	34.37	35.65	33.49	36.08	35.05	35.29	36.86	36.54	38.97	36.64	33.91	39.01
NIST612 - 14	36.24	38.3	37.58	35.57	37.05	34.91	37.37	36.38	36.2	38.5	38	40.53	38.45	35.21	40.29
NIST612 - 15	38.17	39.7	39.06	37.44	39.65	36.47	40.12	38.95	39.23	41.11	40.69	42.94	40.95	38.21	43
NIST612 - 16	36.26	38.92	37.85	35.89	37.43	34.83	37.37	36.44	36.63	38.73	37.94	40.41	38.27	35.23	40.06
NIST612 - 17	36.35	38.63	37.73	35.65	37.29	34.91	37.63	36.67	36.76	38.46	38.43	41.08	38.66	35.7	40.64
NIST612 - 18	34.31	38.18	36.45	34.44	35.77	33.71	35.01	34.21	33.88	35.57	34.73	37.68	35.22	32.39	37.12
NIST612 - 19	35.07	38.16	36.61	34.52	36.14	33.84	36.04	34.93	34.93	37	36.43	38.64	36.74	33.83	39.19
NIST612 - 20	36.47	38.87	37.85	35.75	37.38	35.14	37.94	36.81	36.85	39.22	38.76	41.45	39.25	36.05	41.33
NIST612 - 21	35.9	37.86	36.71	34.96	35.95	34.16	36.95	35.93	35.96	37.86	37.61	40.24	37.96	34.84	39.93
NIST612 - 22	35.49	37.64	36.55	34.92	36.44	33.99	36.99	35.88	36.13	37.9	37.69	39.67	37.61	34.83	40.07
NIST612 - 23	35.16	38.11	36.92	34.84	36.17	34.2	36.28	35.35	35.28	37.22	36.74	39.13	36.91	34.06	39.07
NIST612 - 24	35.93	38.3	37.1	35.18	36.84	34.38	36.97	36.01	36.16	37.93	37.54	40.17	37.89	34.85	40.01
NIST612 - 25	36.49	38.84	37.67	35.99	37.4	34.96	38	36.84	36.74	38.88	38.49	40.93	38.8	35.79	40.65
NIST612 - 26	35.97	38.57	37.2	35.39	36.83	34.46	37.18	35.79	36.2	38.05	37.36	40.17	37.82	35.05	39.79
NIST612 - 27	35.98	37.74	37.09	35.11	36.98	34.58	37.27	36.26	36.46	38.37	37.99	40.32	38.46	35.42	40.16
NIST612 - 28	35.27	37.88	36.91	34.76	36.23	33.9	36.08	35.21	34.89	37.06	36.44	38.95	36.61	33.56	38.38
NIST612 - 29	35.52	38.78	37.36	35.38	36.85	34.55	37.3	36.16	36.43	37.82	37.55	40.06	37.82	34.99	40.48
NIST612 - 30	35.95	38.96	37.11	35.45	36.5	34.63	36.72	35.91	35.84	37.81	37.57	40.09	37.63	34.73	40.14
NIST612 - 31	36.28	38.98	37.79	35.93	36.95	34.41	36.98	35.84	36.18	38.11	37.67	39.97	37.52	34.83	40.14
NIST612 - 32	35.24	37.29	36.38	34.56	36.29	34.21	36.76	35.85	35.59	37.5	37.45	40.03	38.08	34.94	39.46
NIST612 - 33	35.65	37.97	36.77	34.67	36.45	34.15	36.81	35.84	36.23	38.05	37.43	39.98	37.85	34.95	39.46
NIST612 - 34	35.99	39.98	38.11	36.03	37.46	35.38	37.39	36.27	35.92	37.86	36.93	39.69	37.22	34.12	40.05
NIST612 - 35	35.93	37.57	36.99	35.87	36.64	34.45	37.61	36.72	36.48	38.3	38.22	40.64	38.59	35.53	40.25
NIST612 - 36	35.65	38.52	37.12	34.79	36.61	34.19	36.39	35.29	35.54	37.51	37.14	39.58	37.29	34.47	39.49
Mean	35.83	38.37	37.19	35.28	36.76	34.47	37.01	35.99	36.04	37.95	37.51	40.02	37.81	34.87	39.89
2 S D	1.38	1.31	1.49	1.53	1.72	1.43	1.95	1.86	1.97	2.08	2.15	2.26	2.21	2.12	2.31
Relative 2 S D	3.85	3.42	4.02	4.35	4.67	4.14	5.27	5.17	5.47	5.49	5.72	5.64	5.85	6.09	5.80

C.2 LA-ICP-MS analysis of sulphides

Table C.16. Standard error (1 sigma) for LA-ICP-MS analysis of sulphides. Concentration data is presented in Section 7.4. Errors calculated by GLITTER.

1 sigma error

	S01/36lx S1a Cp	S1b Po/Pn	S2a Po	S2b Po (Pn)	S3a Pn	S3b Po/Cp (Pn)	S4 Cp/Pn/Po
S	7596	7596	7070	7491	7449	6985	8062
Fe	32546	31977	22815	30512	26625	24885	38374
Co	0.01	0.88	8.11	3.16	1.76	16.85	0.34
Ni	0.10	151.80	1236.91	576.54	718.65	3088.78	165.64
Cu	0.10	15.90	1332.18	31.07	1129.66	0.29	109.97
Se	2.37	2.33	2.5	2.5200	3.59	2.49	3.11
Pb	0.01	0.012	0.042	0.0200	0.06	0.021	0.052
Au	0.00088	0.00077	0.0022	0.0014	0.0013	0.002	0.0015
Re	0.00095	0.00091	0.0018	0.0012	0.0031	0.0017	0.0011
Ag	0.009	0.013	0.066	0.0200	0.09	0.0068	0.018
Os	0.0045	0.0041	0.003	0.0039	0.0038	0.0041	0.006
Ir	0.0027	0.0028	0.0017	0.0020	0.0019	0.0022	0.0025
Ru	0.0062	0.0056	0.016	0.0100	0.01	0.022	0.011
Rh	0.00084	0.0022	0.14	0.0043	0.14	0.002	0.017
Pt	0.0016	0.0013	0.0032	0.0021	0.0018	0.003	0.0023
Pd	0.0037	0.0034	0.013	0.0074	0.008	0.015	0.0051

	S02/6lx S1 Po/Pn/Cp	S2a Pn	S2a Pn/Cp	S2b Po	S2b Po	S3 Po	S4 Po
S	7350	6974	7012	7564	7564	7665	7626
Fe	24494	21945	21717	29779	30091	33539	32890
Co	1.08	8.27	4.99	0.01	0.06	0.19	0.58
Ni	672.37	3820.29	2884.27	0.99	35.89	4.70	68.52
Cu	444.90	91.88	694.12	0.41	15.53	20.56	8.83
Se	2.36	2.49	4.57	1.93	1.8	1.65	2.16
Pb	0.045	0.025	0.039	0.0027	0.0015	0.043	0.03
Au	0.0051	0.0084	0.019	0.00095	0.00081	0.0062	0.0056
Re	0.0031	0.0062	0.017	0.00076	0.00068	0.0048	0.0038
Ag	0.037	0.034	0.093	0.0053	0.0031	0.024	0.025
Os	0.006	0.0096	0.027	0.0016	0.0015	0.007	0.0078
Ir	0.0035	0.0066	0.016	0.00096	0.00081	0.0051	0.0045
Ru	0.025	0.056	0.12	0.0053	0.005	0.032	0.03
Rh	0.033	0.016	0.08	0.001	0.002	0.0078	0.0064
Pt	0.0055	0.013	0.037	0.0014	0.0013	0.0098	0.0081
Pd	0.031	0.041	0.081	0.0042	0.0039	0.026	0.022

	S02/83vlx S1a Pn	S1b(1) Po	S1b(2) Po	S2a(1) Pn	S2a(2) Pn/Cp	S2b Cp	S2c(1) Po	S2c(2) Po (Pn)	S3a(1) Pn	S3a(2) Pn	S3b(1) Po (Pn)	S3b(2) Po/Cp
S	7014	7007	7289	7617	7617	6988	6985	7661	7661	7006	7681	7680
Fe	25465	24674	23820	45703	43859	35145	36275	49643	45559	31355	56056	55188
Co	11.41	5.46	0.37	0.23	0.92	6.89	4.67	1.63	1.07	20.28	0.18	0.21
Ni	11225.23	5588.16	461.91	267.06	997.23	7738.10	5180.85	1610.25	1134.97	15110.44	102.55	125.90
Cu	712.68	4306.97	7909.28	221.31	551.20	252.65	510.56	67.15	1835.24	171.19	3.07	693.53
Se	3.13	3.11	4.81	3.68	3.38	4.68	4.59	0.99	2.2	3.53	3.81	3.74
Pb	0.17	0.12	0.086	0.055	0.082	0.034	0.026	0.078	0.062	0.057	0.045	0.053
Au	0.0037	0.0025	0.01	0.0015	0.0016	0.0029	0.0025	0.0015	0.0019	0.0013	0.0012	0.0011
Re	0.003	0.0026	0.0069	0.0013	0.0017	0.002	0.014	0.0023	0.0039	0.001	0.0011	0.002
Ag	0.55	0.32	0.12	0.082	0.11	0.15	0.13	0.19	0.2	0.1	0.034	0.041
Os	0.0042	0.0029	0.012	0.0017	0.01	0.003	0.0022	0.0064	0.027	0.0027	0.0032	0.003
Ir	0.0031	0.002	0.0074	0.0014	0.0076	0.002	0.0016	0.0022	0.014	0.002	0.0019	0.0019
Ru	0.049	0.022	0.051	0.0066	0.012	0.028	0.015	0.0094	0.019	0.028	0.0075	0.0063
Rh	0.036	0.16	0.31	0.011	0.024	0.013	0.02	0.0047	0.072	0.0081	0.0013	0.025
Pt	0.0062	0.0042	0.017	0.0017	0.0023	0.0041	0.0029	0.0036	0.0071	0.0017	0.0019	0.0019
Pd	0.074	0.034	0.035	0.0062	0.0076	0.056	0.035	0.015	0.015	0.07	0.0054	0.0051

Table C.16 contd. Standard error (1 sigma) for LA-ICP-MS analysis of sulphides. Concentration data is presented in Section 7.4. Errors calculated by GLITTER.

1 sigma error

	S01/40IIIx					S02/85IxE			
	S1a	K40xS1b	K40xS1c	K40xS1d	K40xS1e	C85IxeS2	D85xeS1a	E85xeS1b	E85xeS1c
	Cp/Py	Py	Po	Py	Cp/Po	Py	Py	Py(Cp)	Py
S	9389.42	11307.98	8439.02	11286.87	7806.44	11245.12	11244.86	9917.09	11244.91
Fe	51361.34	59752.43	76224.46	67911.12	47063.38	23787.85	25281.72	41348	29192.82
Co	9.21	22.99	6.12	24.51	45.8	7.9	6.82	0.44	6.33
Ni	109.51	122.02	363.41	129.18	1121.72	33.43	16.95	32.27	16.34
Cu	5804.11	1.06	38.45	14.88	3489.94	0.023	0.023	392.92	0.17
Se	2.34	1.76	1.98	1.91	1.64	0.64	0.21	1.74	1.9
Pb	1.21	0.0012	0.013	0.0041	0.62	0.00085	0.001	0.27	0.0011
Au	0.0015	0.00047	0.00057	0.00053	0.00094	0.00051	0.00045	0.0028	0.00052
Re	0.012	0.0017	0.0075	0.0028	0.0059	0.00047	0.0004	0.0021	0.00096
Ag	0.11	0.0019	0.0062	0.0035	0.095	0.0016	0.0016	0.12	0.0045
Os	0.0018	0.00056	0.00061	0.00062	0.0011	0.00053	0.00049	0.0015	0.00055
Ir	0.001	0.00035	0.00042	0.00037	0.00066	0.00038	0.00039	0.001	0.00039
Ru	0.0082	0.0023	0.0031	0.0024	0.0054	0.0023	0.002	0.0064	0.0025
Rh	0.19	0.00051	0.0015	0.00094	0.11	0.00047	0.00046	0.027	0.00053
Pt	0.011	0.00096	0.00091	0.0016	0.0045	0.00067	0.00062	0.0019	0.0008
Pd	0.0087	0.0019	0.0024	0.0018	0.005	0.0017	0.0016	0.006	0.0019

	3IIx						S02/84vIIx		
	S1a	C3IIxS1b	C3IIxS1c	C3IIxS2a	C3IIxS2b	C3IIxS2b	J84xS2a	K84xS1a	L84xS2b
	Py	Py	Cp/Po	Py	Py(Cp)	Py	Py	Py	Py
S	11265.64	11244.56	7279.22	11265.67	9285.43	9285.71	11339.9	11013.87	11287.74
Fe	115363.6	119494.6	102365.6	123766.2	94863.17	94686.98	164134.2	137384.6	151775.1
Co	32.06	26.41	11.83	42.1	49.86	52.33	48.23	46.41	46.07
Ni	30.94	26.99	111.39	46.56	41.99	34.36	36.15	20.9	29.45
Cu	0.22	64.54	1653.49	14.34	260.58	1.47	153.88	6.87	4.8
Se	3.77	2.24	8.69	3.89	1.81	1.36	2.45	1.83	2.43
Pb	0.0087	0.03	0.11	0.016	0.01	0.0031	0.25	0.008	0.017
Au	0.00035	0.0012	0.0028	0.00033	0.0021	0.0023	0.0027	0.0017	0.0011
Re	0.0052	0.00069	0.00097	0.0027	0.0028	0.0025	0.02	0.012	0.021
Ag	0.0042	0.014	0.14	0.045	0.25	0.0049	0.095	0.063	0.0075
Os	0.00071	0.0021	0.0016	0.01	0.017	0.03	0.00088	0.002	0.0013
Ir	0.00027	0.0005	0.00084	0.0047	0.015	0.02	0.00058	0.0013	0.00079
Ru	0.0015	0.0017	0.0057	0.0026	0.011	0.014	0.0034	0.0078	0.0051
Rh	0.00035	0.0041	0.092	0.0011	0.021	0.0036	0.0092	0.0021	0.0013
Pt	0.0034	0.0048	0.0028	0.013	0.015	0.012	0.0013	0.0037	0.0019
Pd	0.0015	0.0018	0.021	0.0014	0.0077	0.0083	0.0041	0.0061	0.0037

Table C.17. Standard data for PGE analysis of sulphides. Standard PGE-A was used for the calibration of all elements except Re and Pb which were calibrated using the ReOs#4 standard. The concentrations in the standard are much higher than the sulphides analysed and thus the reproducibility of the samples will be considerably lower. ^{34}S was used as an external calibration.

Reproducibility Standards	S	Fe	Co	Ni	Cu	Se
PGE1	278000	930.57	0.135	705928	244.04	223.22
PGE2	278000	914.90	0.146	724979	243.96	231.22
PGE3	278000	923.25	0.140	714543	244.00	226.64
PGE4	278000	907.05	0.138	709598	241.98	224.16
PGE5	278000	952.44	0.144	688529	234.42	223.76
PGE6	278000	934.81	0.141	763779	259.66	237.49
PGE7	278000	907.06	0.138	698070	239.18	221.95
PGE8	278000	953.43	0.158	736599	254.68	228.82
PGE9	278000	857.11	0.126	686890	229.87	227.62
PGE10	278000	923.34	0.133	694816	246.13	221.70
PGE11	278000	912.82	0.142	695169	238.80	230.02
PGE12	278000	1135.37	0.163	771070	259.44	230.03
PGE13	278000	885.39	0.140	705456	245.45	226.43
PGE14	278000	922.70	0.140	715000	244.00	227.00
PGE15	278000	922.70	0.140	715000	244.00	227.00
PGE16	278000	1209.45	0.177	821796	285.27	228.84
PGE17	278000	800.54	0.122	647339	221.91	225.45
Average		940.76	0.143	717327	245.69	227.14
SD		95.27	0.013	39340	13.90	3.89
% SD		10.13	9.23	5.48	5.66	1.71

Reproducibility Standards	Ag	Au	Os	Ir	Ru	Rh	Pt	Pd		Re	Pb
PGE1	227.99	209.74	185.01	199.82	197.80	214.00	197.32	266.14	ReOs1	59.29	1823.88
PGE2	230.05	214.44	207.43	218.99	209.05	227.14	214.04	276.42	ReOs2	58.79	2242.53
PGE3	228.94	211.84	193.43	207.35	202.59	219.58	204.15	270.66	ReOs3	59.03	1991.60
PGE4	229.26	209.12	189.28	203.62	203.34	217.51	201.38	272.31	ReOs4	61.99	2044.78
PGE5	225.88	206.52	199.28	204.12	197.43	220.74	197.51	268.46	ReOs5	53.01	2008.77
PGE6	231.18	226.05	205.77	227.11	207.43	225.95	223.77	270.21	ReOs6	62.80	1920.41
PGE7	228.75	206.79	186.79	200.63	202.35	216.35	198.19	272.37	ReOs7	60.27	2055.57
PGE8	238.13	212.61	210.52	222.03	212.40	227.54	213.31	278.27	ReOs8	53.54	2381.43
PGE9	224.23	209.92	186.98	199.95	195.02	216.54	197.14	259.35	ReOs9	61.96	1920.02
PGE10	220.15	210.50	177.11	196.07	194.97	209.57	197.67	268.57	ReOs10	60.84	2111.08
PGE11	227.58	210.01	205.57	211.24	207.65	222.63	205.64	278.96	ReOs11	64.64	2333.13
PGE12	243.52	226.67	226.26	230.70	216.20	236.33	223.81	281.27	ReOs12	67.71	1624.96
PGE13	230.07	208.21	191.61	208.19	202.22	218.71	203.50	267.87	ReOs13	54.83	2375.27
PGE14	229.00	212.00	194.30	208.00	203.00	220.00	204.70	271.00	ReOs14	59.00	2000.00
PGE15	229.00	212.00	194.30	208.00	203.00	220.00	204.70	271.00	ReOs15	59.00	2000.00
PGE16	262.26	239.64	207.75	221.26	216.58	241.69	230.51	306.70	ReOs16	66.63	2087.55
PGE17	210.95	196.59	185.15	198.93	193.10	206.57	190.16	250.04	ReOs17	56.70	1968.92
Average	230.41	213.10	196.86	209.77	203.77	221.23	206.32	272.33		60.00	2052.35
SD	10.65	9.67	12.30	10.54	7.07	8.73	11.16	11.51		4.14	196.87
% SD	4.62	4.54	6.25	5.02	3.47	3.95	5.41	4.23		6.90	9.59

BLANK PAGE
IN
ORIGINAL

D Appendix D – Sample details

ZSO sample details.

For Sulitjelma sample details I refer the reader to Boyle (1982).

Table D.1. Localities, sample type and mineral assemblages for ZSO samples. Abbreviations after Kretz (1983), except Phen: phengite, Barr: barroisite (though refers to any retrogressive amphibole composition. The mineral lists are not all exhaustive.

Sample No	Location	Grid ref. Easting	Grid ref. Northing	Unit	Lithology	Protolith	Mineralogy
SO1/23I	Hohlaub moraine	631 592	098 105	Zermatt-Saas	Flaser gabbro	Gabbro	Grt, Omp, Act, Zo, Pg, Rt
SO1/36I	Allalinhorn crags	637 682	100 130	Allalin Gabbro	Metagabbro	Gabbro	Grt, Tr, Hbl, Prg, Zo, Ttn, Qtz, Rt, Ab, Chl, Ilm
SO1/36II	Allalinhorn crags	637 682	100 130	Allalin Gabbro	Leuco-metagabbro	Leucogabbro	Grt, Tr, Hbl, Prg, Zo, Ttn, Qtz, Rt, Ab, Chl, Ilm
SO1/36IIIx	Allalinhorn crags	637 682	100 130	Allalin Gabbro	Olivine Gabbro	Gabbro	Ign - Ol, Aug, Labr, Chr, Ilm, Po, Pn, Cp MM - Zo
SO1/31I	Allalinhorn ridge to N	637 488	100 417	Allalin Gabbro	Tc-rich metagabbro	Gabbro	Grt, Omp, Ctd, Tlc, Zo, Tr
SO1/31II	Allalinhorn ridge to N	637 488	100 417	Allalin Gabbro	Leuco-metagabbro	Leucogabbro	Grt, Omp, Ctd, Chl, Zo, Tlc, Act, Barr
SO1/32IIIx	Hohlaub moraine	637 857	100 319	Allalin Gabbro	Leuco-metagabbro	Leucogabbro	Omp, Ctd, Chl, Tlc, Zo, Act
SO1/33ix	Moraine at Mattmark	640 091	100 623	Allalin Gabbro	Olivine Gabbro	Gabbro	Ign - Ol, Di-Aug, Byt, Chr, Ilm MM - Grt, Chl, Zo
SO1/35ix	Moraine at Mattmark	640 091	100 623	Allalin Gabbro	Leucocratic coronite	Gabbro	Grt, Gln, Tlc, Zo, Omp, Pg, Ky, Rt
SO1/35iix	Moraine at Mattmark	640 091	100 623	Allalin Gabbro	Leucocratic coronite	Gabbro	Grt, Gln, Tlc, Zo, Omp, Pg, Rt
SO1/36ix	Moraine at Mattmark	640 252	100 487	Allalin Gabbro	Leucogabbro	Gabbro	Ign - Ol, Di-Aug, Byt, Chr, Ilm, Po, Pn, Cp MM - Zo, Chl
SO1/36iix	Moraine at Mattmark	640 252	100 487	Allalin Gabbro	Coarse coronite	Gabbro	Grt, Omp, Tlc, Zo, Gln
SO1/36iiix	Moraine at Mattmark	640 252	100 487	Allalin Gabbro	Very coarse coronite	Gabbro	Ign - Aug MM - Grt, Omp, Tr, Tlc, Zo, Qtz, Ab, Rt
SO1/39ix	Moraine at Mattmark	640 106	100 698	Allalin Gabbro	Non-coronitic eclogite	Gabbro	Grt, Omp, Tlc, Act, Ctd, Zo, Py
SO1/39iix	Moraine at Mattmark	640 106	100 698	Zermatt-Saas	Mafic eclogite	Basalt	Grt, Omp, Gln, Zo, Rt, Qtz, Barr
SO1/39iiix	Moraine at Mattmark	640 106	100 698	Allalin Gabbro	Olivine Gabbro	Gabbro	Ign - Ol, Di-Aug, Pl (Byt), Chr, Ilm MM - En, Tr, Chl, Zo, Grt, Rt, Qtz
SO1/39iiiix	Moraine at Mattmark	640 106	100 698	Allalin Gabbro	Retrogressed metagabbro	Gabbro	Omp, Act, Tlc, Zo, Pg, Chl
SO1/39vx	Moraine at Mattmark	640 106	100 698	Zermatt-Saas	Mafic eclogite	Basalt	Grt, Omp, Gln, Zo, Rt, Qtz, Barr
SO1/40ix	Moraine at Mattmark	640 106	100 698	Allalin Gabbro	Leucocratic coronite	Gabbro	Omp, Gt, Tlc, Tr, Zo, Ky, Rt
SO1/40iix	Moraine at Mattmark	640 106	100 698	Allalin Gabbro	Leucocratic coronite	Gabbro	Omp, Gt, Tlc, Tr, Zo, Pg, Ky
SO1/40iiix	Moraine at Mattmark	640 106	100 698	Allalin Gabbro	Ctd-gabbroic eclogite	Gabbro	Ctd, Zo, Tlc, Grt, Omp, Act, Py, Po, Cp
SO1/40iiiix	Moraine at Mattmark	640 106	100 698	Allalin Gabbro	Blueschist gabbroic eclogite	Gabbro	Omp, Act, Gt, Tlc, Zo, Pg, Chl, Rt
SO1/40vx	Moraine at Mattmark	640 106	100 698	Allalin Gabbro	Ctd-gabbroic eclogite	Gabbro	Grt, Omp, Ctd, Zo, Tlc, Act
SO1/40vix	Moraine at Mattmark	640 106	100 698	Allalin Gabbro	Gabbroic eclogite	Gabbro	Grt, Omp, Tlc, Tr, Zo, Pg, Chl, Rt
SO1/40viix	Moraine at Mattmark	640 106	100 698	Allalin Gabbro	Gabbroic eclogite	Gabbro	Grt, Omp, Act, Ctd, Tlc, Zo, Chl
SO1/3ix	Moraine at Mattmark	640 106	100 698	Allalin Gabbro	Coarse gabbro	Gabbro	Ign - Ol, Aug, Lab/Byt, MM - Gt, En, Zo
SO1/3iix	Moraine at Mattmark	640 106	100 698	Allalin Gabbro	Leucocratic coronite	Gabbro	Grt, Omp, Ctd, Tlc, Zo, Gln, Pg, Ky
SO1/5G	Moraine at Mattmark	640 106	100 698	Allalin Gabbro	Olivine Gabbro	Gabbro	Ign - Ol, Di-Aug, Pl (Lab), Chr, Ilm, Po, Pn, Cp MM - Zo
SO1/5E	Moraine at Mattmark	640 106	100 698	Allalin Gabbro	Transitional eclogite	Gabbro	Ign - Ol, Aug, Chr, Ilm, Pl (?) MM - Grt, En, Ath, Tr, Zo, Chl

Table D.1 contd.

Sample No	Location	Grid ref. Easting	Grid ref. Northing	Unit	Lithology	Protolith	Mineralogy
S02/4i	Allalin lower cliff	637599	100101	Allalin Gabbro	Metabasaltic dyke	Mafic Dyke	Grt, Omp, Zo, Pg, Barr, Ab, Chl, Py, Cp
S02/4iiix	Allalin lower cliff	637599	100101	Allalin Gabbro	Metabasaltic dyke	Mafic Dyke	Grt, Omp, Pg, Zo, Qtz, Barr
S02/4iiii	Allalin lower cliff	637599	100101	Allalin Gabbro	Metabasaltic dyke	Mafic Dyke	Grt, Omp, Zo, Qtz, Barr
S02/5i	Allalin lower cliff	637577	100032	Allalin Gabbro	Sheared Leucogabbro	Gabbro	Grt, Omp, Zo, Barr, Ab, Chl
S02/5ii	Allalin lower cliff	637577	100032	Allalin Gabbro	Flaser gabbro	Gabbro	Grt, Omp, Zo, Pg, Barr, Ab, Chl
S02/6ix	Allalin lower cliff	637510	100006	Allalin Gabbro	Olivine Gabbro	Gabbro	Ign. Ol, Aug, Pl (Lab), Ilm, Po, Pn, Cp MM - Zo, Grt
S02/7i	Allalin lower cliff	637560	100020	Allalin Gabbro	Metabasaltic dyke	Mafic dyke	Grt, Omp, Zo, Pg, Barr, Ab, Chl
S02/7ii	Allalin lower cliff	637560	100020	Allalin Gabbro	Amph. Gabbro	Gabbro	Grt, Omp, Zo, Pg, Barr, Ab, Chl
S02/10iiixG	Allalin rear cliff	636052	099164	Allalin Gabbro	Olivine Gabbro	Gabbro	Ign - Ol, Di-Aug, Pl (Lab), Chr, Ilm MM - Zo
S02/10iiixE	Allalin rear cliff	636052	099164	Allalin Gabbro	Transitional eclogite	Gabbro	Ign - Ol, Aug, Pl (Lab), Chr, Ilm MM - Grt, Chl, Zo, En
S02/33i	Allalin minor peak	637289	100133	Allalin Gabbro	Mafic coronite	Gabbro + vein?	Grt, Omph, Act, Zo, Pg, Barr, Rt,
S02/41ii	Pfulwe pass	631323	096239	ZSO - Mafics	Mafic eclogite	Basalt	Grt, Omp, Ep, Gln, Pg, Phen, Barr, Rt
S02/41v	Pfulwe pass	631323	096239	ZSO - Mafics	Gl-eclogite	Basalt	Grt, Omp, Ep, Gln, Pg, Phen, Barr, Rt
S02/74ii	Pfulwe pass	631367	096082	ZSO - Mafics	Rim of pillow	Pillow Basalt	Grt, Omp, Ep, Gln, Pg, Barr, Phen, Rt
S02/75iC	Pfulwe pass	631358	096175	ZSO - Mafics	Core of eclogitic pillow	Pillow Basalt	Grt, Omp, Ep, Gln, Pg, Barr, Phen, Rt
S02/75iiR	Pfulwe pass	631358	096175	ZSO - Mafics	Rim of (75i) eclogitic pillow	Pillow Basalt	Grt, Omp, Ep, Gln, Pg, Barr, Phen, Rt
S02/75iiiC	Pfulwe pass	631358	096175	ZSO - Mafics	Core of pillow	Pillow Basalt	Grt, Omp, Ep, Gln, Pg, Barr, Phen, Rt
S02/75iiiR	Pfulwe pass	631358	096175	ZSO - Mafics	Rim of pillow	Pillow Basalt	Grt, Omp, Ep, Gln, Pg, Barr, Phen, Rt
S02/75ivC	Pfulwe pass	631358	096175	ZSO - Mafics	Core of pillow	Pillow Basalt	Grt, Omp, Ep, Gln, Pg, Barr, Phen, Rt
S02/83vix	Mattmark Moraine	—	—	Allalin Gabbro	Gabbro	Gabbro	Ign - Ol, Di-Aug, Pl (Lab), Chr, Ilm
S02/83viix	Mattmark Moraine	—	—	Allalin Gabbro	Gabbro + slight coronitisation	Gabbro	Ign - Ol, Di-Aug, Pl (Lab), Chr, Ilm
S02/83viiixG	Mattmark Moraine	—	—	Allalin Gabbro	Gabbro	Gabbro	Ign - Ol, Aug, Pl (Lab), Chr, Ilm
S02/83viiixE	Mattmark Moraine	—	—	Allalin Gabbro	Transitional eclogite	Gabbro	Ign - Ol, Aug, Pl (Lab), Chr, Ilm MM - Grt, Chl, Zo, En, Ath
S02/83viiiix	Mattmark Moraine	—	—	Allalin Gabbro	Gabbro + slight coronitisation	Gabbro	Ign - Ol, Aug, Pl (Lab), Chr, Ilm MM - Grt, Chl, Zo
S02/84viix	Mattmark Moraine	—	—	Allalin Gabbro	Blueschist gabbroic eclogite	Gabbro	Gln, Grt, Omp, Tlc, Zo, Chl, Py
S02/84viiix	Mattmark Moraine	—	—	Allalin Gabbro	Blueschist gabbroic eclogite	Gabbro	Gln, Grt, Omp, Tlc, Zo, Chl, Py
S02/85ixE	Mattmark Moraine	—	—	Allalin Gabbro	Gabbroic eclogite	Gabbro	Grt, Omp, Tlc, Zo, Chl, Act, Py, Cp
S02/85ixR	Mattmark Moraine	—	—	Allalin Gabbro	Gabbroic eclogite with retrogression	Gabbro	Grt, Barr, Tlc, Zo, Chl